DEPARTMENT OF MECHANICAL ENGINEERING

NUMERICAL AND EXPERIMENTAL ANALYSIS
OF SPUR GEARS IN MESH

JIANDE WANG

September 2003

STATEMENT OF ORIGINALITY

This thesis contains no material which has been accepted for the award of any other degree or diploma in any university.

To the best of my knowledge and belief this thesis contains no material previously published by any other person except where due acknowledgment has been made.

Signature: ....

Date: ....….

ACKNOWLEDGMENTS

I would like to express my deep gratitude and indebtedness to Dr. I. Howard for his initial encouragement to start this project and his valuable guidance and support throughout the course of my research. I would also like to express my sincere thanks to Senior Lecturers L. Morgan and K. Teh for their valuable suggestions in my PhD study. I also wish to thank all the members of the Mechanical Engineering School/Laboratory for their help during my research.

I also very much appreciated the Curtin University Postgraduate Scholarship (CUPS) provided for my doctoral study.

Finally, I would especially like to thank my wife, Grace - for all the love and practical help that made this thesis possible.

ABSTRACT

The investigation of numerical methods for modelling the mechanism properties of involute spur gears in mesh, over the mesh cycle, forms the major part of this thesis.

Gearing is perhaps one of the most critical components in power transmission systems and the transmission error of gears in mesh is considered to be one of the main causes of gear noise and vibration. Numerous papers have been published on gear transmission error measurement and many investigations have been devoted to gear vibration analysis. There still, however, remains to be developed a general Finite Element Model capable of predicting the effect of variations in rigid body gear tooth position, in which the critical stage is the prediction of gear behaviour with profile modifications (including tip-relief). In this thesis, FEA results have been obtained by using various techniques including: (a) adaptive re-mesh with contacts using quad (2D) and brick (3D) elements and (b) the element birth and death option. Tooth profile modifications can affect the behaviour of the gear meshing including the T.E., ratio of local deformation and load-sharing ratio results, etc, providing an alternative method for gear design. In the high order end, the elastic strains of the gear-shaft system have also been investigated. The results in this thesis have shown the potential for using strain-vibration relationships to monitor or control the transmission system.

The investigations have also included some analysis with non-metallic gears, an application area that is rapidly growing. The results achieved here are at a fundamental stage, and further research would necessitate applying a coupled field analysis (structural and thermal).

TABLE OF CONTENTS

LIST OF FIGURES

viii

ix

xiii

CHAPTER 1

INTRODUCTION

1.1   General Introduction

Gear transmission systems are an important aspect in many industries. The knowledge and understanding of the behaviour of gears in mesh including Transmission Error (T.E.), load sharing ratio, distortion field variation etc., is vitally important for condition monitoring and system control of gear transmission systems. A large range of literature on the topic of gear transmissions exists, as demonstrated by the review by Ozguven (Ozguven 1988). Fundamental publications on gears in mesh can be found in particular by Walker (Walker 1938), Harris (Harris 1958), Niemann (Niemann 1970) and Munro (Munro 1994). However, the fundamental study of the basic gear transmission unit still needs to be finalised and with recent software (FEA) advances and fast and cheap PC technology, many research studies are now aimed at furthering the basic understanding of gears in mesh. The improved understanding of gear behaviour will increase our capability to monitor gear transmission systems using measured parameters such as the gear case vibration signal.

The research into the elastic behaviour of gears in mesh has also highlighted the use of the gear strain variation as a new method of measuring gear transmission error and the effects of modified tooth profiles.

The range of non-metallic gear applications continues to grow fast due to the low cost (injection moulding), environmental benefits (without external lubrications) and many advanced features (White 1997; Walton 1998; Walton 1998; Luscher et al. 2000). Recent developments have sought to minimise the disadvantages of non-metallic gears, for example, using long-fiber reinforced composite materials (Alagoz 2002). The research has concentrated on the fundamental mechanism properties of non-metallic gears in mesh using both numerical analysis and experimental tests.

1.2   Basic Transmission Unit

The basic transmission unit is illustrated in Fig 1.2.1 with parallel shaft involute gears since this type of drive dominates the field of power transmission.
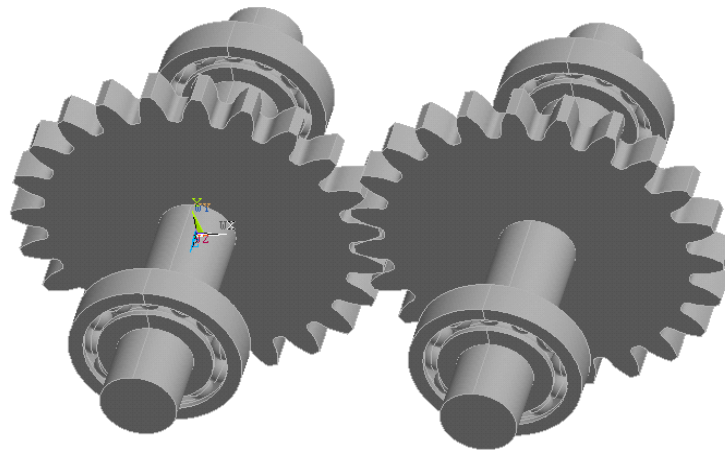
Figure 1.2.1   The basic transmission unit.

If the bearing supports are rigid enough (in many cases, the gearbox casing was ignored in the study of transmission error), the model shown here can be taken as the simplest unit for defining gear transmission error.

In this research, the model for the test rig was build according to Figure 1.2.1, with different gear materials being used in an attempt to measure accurate data. Numerical modelling has shown that the use of different spline or keyway methods for coupling the gear onto the shaft may influence the experimental data.

One of the complicating factors in the numerical study of gears in mesh is the large number of assumptions, which must be understood and documented. One of the simplest models developed in this work involved just a single tooth drive gear in contact with a rigid surface. In general, the less assumptions made in the model, the more complicated and difficult the FEA model.

1.3   Torsional Mesh Stiffness

The torsional mesh stiffness of gears in mesh was first defined by Sirichai (Sirichai 1997; Sirichai et al. 1998; Sirichai 1999). He defined it as the ratio between the torsional load and the total elastic angular rotation of the input gear hub, where both gears were of pure involute form. Because the shafts were not taken into account, the nodes on the input gear hub were coupled torsionally so that the FEA solution obtained the unique displacement value of the input gear hub which was the total elastic angular rotation. In the general case, the total angular rotation of the input gear hub will consist of elastic deformation and "rigid body motion" due to the tooth geometry, run out errors or profile modifications. This illustrates that accounting for the total angular rotation can be a complex task.

The combined torsional mesh stiffness as defined here is the ratio between the torsional load and the total angular rotation of the input gear (hub or the shaft). With a constant input load M, the combined torsional mesh stiffness K_m varies as the driven gear rotates and it has significant variability in a small region between the single-tooth-pair contact and the double-tooth-pair contact. The development of a torsional mesh stiffness model of gears in mesh can be used to determine the transmission error throughout the mesh cycle.

1.4   Non-linear problem

As mentioned above, the total angular rotation of the drive gear (pinion) hub represents the magnitude of angular rotation under a load (torque), mainly due to bulk tooth movements such as tooth bending and shearing with some rotation occurring at the tooth root. It also includes gear body distortions. The other part of the rotation amplitude would be that due to localised Hertzian contact deflection, which is non-linear. This component can be as

3

much as 25 percent of the total tooth deformation (Coy 1982). In FEA solutions, this non-linear problem can be solved by applying various types of contact elements to simulate different types of contact problems in ANSYS® or by definition of contact bodies (groups of element) in MSC/MARC®. However, obtaining unique results in the mesh cycle can be difficult and in some situations solutions will not converge due to the chaotic condition at the contact(s). Adaptive mesh with contact(s) using quad or brick elements has been found to be particularly useful in h-method finite element analysis of gears in mesh, where it has been found to significantly improve the quality of the solution data.

1.5   Solving the Unconstrained Structure

Solving unconstrained body motion is one of the critical stages in numerical simulation of tooth profile modifications (including tooth tip-relief) of gears in mesh. For example, FEA solutions for tip-relieved gears in mesh will be subject to unconstrained body motion when the mesh position is near the centre of the double contact zone. A few options can be applied to overcome this problem, such as adding weak spring(s) or solving the problem dynamically. However, when considering avoiding numerical errors and the accuracy of the final results, the element birth and death option was found to be one of the best methods for producing consistent results.

1.6   Transmission Error

Transmission error, according to most authors, is considered to be one of the main contributions to noise and vibration in a geared transmission system. Harris (Harris 1958) was the first to identify transmission error as a significant contributor to gear dynamics and the measurement of transmission error was first performed in the 1960's by the National Engineering Laboratory and by Gregory, Harris and Munro (Gregory 1963; Gregory 1963; Gregory 1963). Many others have performed measurements of transmission errors since that time.

In general, the main components of the total transmission error can be classified into three parts,

1. First order components: including profile, spacing and run out errors from the manufacturing process. Geometrical errors in alignment and tooth profile

modifications are also included here and the long modifications typically add "rigid body motion" into the total transmission error.

2. Higher order components: including the elastic deformation of the local contact tooth pair, tooth bending, shearing, some rotation about the tooth root and the deflection of the gear body due to the transmitted load through and transverse to the gear rotational axis.

3. Higher order dependent components: the relative sliding at the contact(s) truly is the first order component, however, this component is dependent on the variation of the higher order components. This special component can also be classified into the *loaded transmission error,* in contrast with the other first order components that can be counted as the *unloaded transmission error.* These components also include geometrical errors that may be introduced by static and dynamic elastic deflections in the supporting bearings and shafts.

The total transmission error always consists of the first and higher order components so that the relationships between transmission error and noise and vibration are complex.

Gear transmission error is the special case of the total transmission error. For gear transmission error, the relative model is just a pair of meshing gears where both gears have rigid axle centres. This has been defined by Welbourn (Welbourn 1972; Welbourn 1979) as *the difference between the actual position of the output gear and the position it would occupy if the gear drive were perfectly conjugate.* The equation for gear transmission error may be expressed as below,

$$TE = \theta_g - (Z)\theta_p, \quad \text{rad}, \tag{1.1}$$

where Z is the gear ratio and $\theta_{g,p}$ denotes the angular rotation of the input and output gear in radians respectively. However, gears are sometimes assumed to vibrate only torsionally but this assumption is incorrect, as any model of gears must allow for lateral movement perpendicular to the gear axis, Smith 1999. As the shafts cannot be ignored in the T.E. definitions, Smith (Smith 1983) has defined the total Transmission Error as *the difference between the position that the output shaft of a gear drive would have if the gearbox were perfect, without errors or deflections, and the actual position of the output shaft.* It can be applied for the case of statical or dynamic, loaded or unloaded gears. The related measurement of the transmission error is given,

5

$$TE = \overset{g}{\dot{\theta}}_{g} - (Z)\overset{g}{\dot{\theta}}_{p}, \quad \text{rad / s}, \tag{1.2}$$

where Z is the gear ratio and $\overset{g}{\dot{\theta}}_{g,p}$ denotes the angular speed of the input and output shaft that is measured semi-statically. Equations (1.1) and (1.2) both have similar form, but the use of one or other of the equations for the research may result in significant differences in the resulting gear fundamental properties. The proposed research here is based on the use of equation (1.1).

1.7   Layout of the current study

The objectives of this research were the use of numerical approaches to develop theoretical models of the behaviour of spur gears in mesh.

This thesis consists of 8 chapters and the outline of each chapter is given below:

Chapter 1   This chapter presents a general introduction and describes the significance of the research work.   The concept of the combined torsional mesh stiffness and its development from previous research (Sirichai 1999) is presented.   The definitions of total transmission error and gear transmission error along with the major differences are discussed.   The components of total transmission error were re-classified with this research. Finally, the objectives to be achieved and the layout of the study is described.

Chapter 2   Presents a historical review of the study of the literature related to the research. It contains a significant presentation of relevant and pertinent publications on the subject of analysis and documents the vast amount of literature on gear mathematical models and measurements for vibration analysis and noise control.

Chapter 3   Presents some of the basic considerations required for applying finite element methods to gear modelling.   The brief history, development and theory of finite element analysis are also presented.   In particular, the non-linear problems that relate to the solution convergence and the application of adaptive re-meshing with the contact(s) using quad or brick elements are discussed.

Chapter 4   Introduces the involute and fillet tooth profile equations. The equations were used to generate the profile of the teeth by an APDL (*ANSYS Parametric Design Language*) program, so that the CAD/FEA method can be applied to avoid possible geometry data loss.   The stiffness of parts of the basic transmission unit (except the bearings) were studied. In particular, the variations of the distortion field in a meshing gear pair were analysed with various boundary conditions. The ratio of local deformation was defined.   The characteristics of local contact deformation with reference to the global deformation and the transmission error are also outlined.

Chapter 5   A wide range of FEA problems are often solved with 2D assumptions, and one of the reasons is the computational efficiency and cost. However, when the numerical analysis involves non-linear factors such as contact, fracture or other extreme load cases, the 2D assumptions can be restricted in a very narrowed range. A large amount of FEA calculations were made in this chapter.   The comparisons were concentrated on the torsional stiffness, first maximum principal stress and stress intensity factors that are obtained under assumptions of plane stress, plane strain and 3D analysis. All models were considered with thickness variations from 5mm to 300mm.   With the conclusion of this research, errors were found in the literature of previous research studies, especially when 2D assumptions were used with solid gears.

Chapter 6   The combined torsional mesh stiffness was generated with three major different considerations. First, the individual torsional stiffness was generated with the models of single and multiple tooth gears mating with the rigid line. Using the later model, the stiffness can be obtained over a complete mesh cycle, and it can also be derived from the results of the first model.   The individual torsional stiffness can further be used to generate the combined torsional mesh stiffness. Single tooth gear models with flexible contact were then analysed, and the results used to generate the combined torsional mesh stiffness. It has been noted that similar models were used by previous researchers (Kuang 1992; Arafa 1999; Wang 2000) to generate the combined torsional mesh stiffness over a complete mesh cycle. However, errors were found in the previous methods and a better solution has been proposed and used in this research. Finally, the FEA of multiple tooth

gear models with flexible contact was carried out, involving the use of adaptive mesh with contact (both 2D and 3D). Solution of the combined torsional mesh stiffness for involute gears in mesh was given, along with the definition of the handover region and its characteristics.

Chapter 7   Detailed analysis of static T.E. of spur gears in mesh including tooth profile modification is presented as the major part of this chapter.

Firstly, the detailed hand over process of involute gears in mesh is analysed over a complete mesh cycle. Results of most mechanical properties are given. Except for the static T.E., the results include the combined torsional mesh stiffness, ratio of local deformation and load sharing ratio, so that more precise details about the hand over region of recess and approach cases can be obtained.

Secondly, the detailed analysis with tooth profile modifications is given, in which the history of the research on the topic, current recommendations (standards) and the popular forms of the modification curves are introduced. The development of loaded TE o.p.c. is presented and its relationship with the amount of (tip) relief C_a is given by an approximate formula. Furthermore, the proposed tooth modification curve used in this research is introduced, and then analysis carried out on the short and the long tooth profile modifications. Some important results such as the relief starting point S_1 and S_2 are given. The characteristics of the static T.E. with centre distance variations and with a tooth root crack are also presented.

Finally, the results of the gears with a new tooth profile are presented.

Chapter 8   Presents the non-linear FE modelling of the standard involute spur gears in mesh, in which the polyamide (PA 6) material behaviours are simulated with ANSYS MELAS option, so that the analyses results of T.E., combined torsional mesh stiffness and load sharing ratio are expressed as the function of the input load at each temperature as well as a function of temperature when the input load remains stationary. Meanwhile, the detailed variations of the contact ratio and the handover regions are also presented. A

detailed analysis concerning the load-sharing ratio is presented and a difficulty with the standard theoretical solution is outlined. It also briefly introduced the analysis of optimal tipping on non-metallic gears, and the tipping analysis was also involved with the test gears.

Detailed experimental work is an important aspect of this chapter. The tooth profile inspections and the load – deflection measurements on a static gear test rig are presented. The experimental results are not only for the nylon gears but previous tests on the aluminium gears are also discussed.

Finally, the related error analysis is given which indicates several possibilities for improving the accuracy of both numerical and experimental results.

Appendix   Various analysis of metallic HCRG (High Contact Ratio Gears) and the 30° pressure angle nylon gears are discussed for future reference. Some customised ANSYS APDL programs are also presented.

CHAPTER 2

LITERATURE REVIEW

2.1　Overview

Gears are one of the most critical components in industrial rotating machinery. There is a vast amount of literature on gear modelling. The objectives in dynamic modelling of gears has varied from vibration analysis and noise control, to transmission errors and stability analysis over at least the past five decades. The ultimate goals in gear modelling may be summarised as the study of the following,

Stress analysis such as bending and contact stresses,

Reduction of surface pitting and scoring,

Transmission efficiency,

Radiated noise,

Loads on the other machine elements of the system especially on bearings and their stability regions,

Natural frequencies of the system,

Vibratory motion of the system,

Whirling of rotors,

Reliability, and fatigue life.

The models proposed by several investigators show considerable variations not only in the effects included, but also in the basic assumptions made. Although it is quite difficult to group the mathematical models developed in gear dynamics, Ozguven and Houser (Ozguven 1988; Ozguven 1988) have presented a thorough classification of gear dynamic mathematical models. In 1990, Houser (Houser 1990) and Zakrajsek et al. (Zakrajsek 1990) outlined the past and current research projects of gear dynamics and gear noise at Ohio State University's Research Laboratory and NASA Lewis Research Centre respectively. Du (Du 1997) also classified various gear dynamic models into groups.

The current literature review also attempts to classify gear dynamic models into groupings with particular relevance to the research presented in this thesis. It is possible for some models to be considered in more than one grouping, and so the following classification seems appropriate.

- Models with Tooth Compliance. There are a very large number of studies that include the tooth stiffness as the only potential energy storing element in the system. This group includes single tooth models and tooth pair models. For single tooth models, the objectives usually are tooth stress analysis. For the models with a pair of teeth, the focuses mostly are contact stress and mesh stiffness analysis. That is, the flexibility (torsional and/or transverse) of the shafts, bearings, etc., is all neglected. In such studies the system is usually modelled as a single degree of freedom spring-mass system. Some of the models have also been analysed using the Finite Element Method.

- Models for Gear Dynamics. Such models include the flexibility of the other elements as well as the tooth compliance. Of particular interest has been the torsional flexibility of shafts and the lateral flexibility of the bearings and shafts along the line of action. In some studies, the transverse vibrations of a gear-carrying shaft are considered in two mutually perpendicular directions, thus

allowing the shaft to whirl. In such models, the torsional vibration of the system is usually considered.

- Models With A Whole Gearbox. The studies in this group may be viewed as current and advanced studies and all elements in the system including the gear casing, are considered in the models. The gearbox may be single stage or multi-stage.

In the solution of the system equations, numerical techniques have usually been employed. Although most of the models for which numerical techniques are used are lumped parameter models, some investigators have introduced continuous system or finite element models. While closed form solutions are given for some simple mathematical models, numerical computer solutions have sometimes been preferred for non-linear and more complicated models, particularly in the earlier studies.

In some studies the main objective has been to find the system natural frequencies and mode shapes and, therefore, only free vibration analyses are made. However, usually the dynamic response of the system is analysed for a defined excitation. In most of the studies the response of the system to forcing due to gear errors and to parametric excitation due to tooth stiffness variation during the tooth contact cycle is determined. The models constructed to study the excitations due to gear errors and/or tooth stiffness variation provide either a transient vibration analysis or a harmonic vibration analysis by first determining the Fourier series coefficients of the excitation. Some studies also include the non-linear effect caused by loss of tooth contact or by the friction between meshing teeth. The excitation is then taken as an impact load and a transient vibration analysis is made.

2.2   Gear Modelling

Numerous mathematical models of gears have been developed for different purposes, the basic characteristics of each class of dynamic models along with the objectives and different parameters considered in modelling have been discussed in section 2.1. This

section presents a review of papers published in the areas outlined above, including brief information about the models and the approximations and assumptions made.

2.2.1   Models with Tooth Compliance

The basic characteristic of the models in this group is that the only compliance considered is due to the gear tooth and that all other elements have been assumed to be perfectly rigid. The model is either a single tooth model or a tooth pair model. For single tooth models, the objectives usually are tooth stress analysis. For models with a pair of teeth, the focus is mostly contact stress and meshing stiffness analysis. The resulting models are either translation or torsional. With torsional models one can study the torsional vibrations of gears in mesh, whereas with translation models the tooth of a gear is considered as a cantilever beam and one can study the forced vibrations of the teeth. In either of these models, the transmission error excitation is simulated by a displacement excitation at the gear mesh.

In 1956, Nakada and Utagawa (Nakada 1956) considered varying elasticity of the mating teeth in their vibratory model. Introducing an equivalent translation vibratory system simulated the torsional vibrations of two mating gears. The time variation of stiffness was approximated as a rectangular wave and closed form solutions of piecewise linear equations were obtained for different damping cases for accurately manufactured gear tooth profiles. Another mass and equivalent spring model was introduced in 1957 by Zeman (Zeman 1957). He neglected the variation of stiffness and analysed the transient effects of periodic profile errors. Harris's work (Harris 1958) was an important contribution in which the importance of transmission error in gear trains was discussed and photo-elastic gear models were used. In his single degree of freedom model, he considered three internal sources of vibration: manufacturing errors, variation in the tooth stiffness and non-linearity in tooth stiffness due to the loss of contact. He treated the excitation as periodic and employed a graphical phase-plane technique for the solution. Harris seems to have been the first to point out the importance of transmission error by showing that the behaviour of spur gears at low speeds can be summarised in a set of static transmission error curves. He

also appears to have been the first to predict the dynamic instability due to parametric excitation of the gear mesh.

In 1963, Gregory, et al. (Gregory 1963; Gregory 1963) extended the theoretical analysis of Harris (Harris 1958) and made comparisons with experimental observations. The torsional vibratory model of Gregory, et al., included a sinusoidal-type stiffness variation as an approximation. They treated the excitation as periodic, and solved the equations of motion analytically for zero damping and on an analogue computer for non-zero damping. The experimental data (Gregory 1963) and the computational results (Gregory 1963) generally confirmed Harris's contention that non-linear effects are insignificant when damping is more than about 0.07 of critical. It was claimed that when damping is heavy the simple theory of damped linear motion could be used. Aida, et al. (Aida 1967; Aida 1968; Aida 1969) presented examples of other studies in this area. He modelled the vibration characteristics of gears by considering the excitation terms due to tooth profile errors and pitch errors, and by including the variation of teeth mesh stiffness. In the model of Aida, et al., time varying mesh stiffness and periodic tooth errors were considered, and the model was used for determining stability regions and steady state gear vibrations. A comparison with experimental measurements was also made.

Rollinger and Harker (Rollinger 1967) investigated the dynamic instability that may arise due to varying mesh stiffness. They used a simple single degree of freedom model with an equivalent mass representing the inertia of the gear and pinion. Mesh stiffness variation was assumed to be harmonic. The solution of the resulting equation of motion was obtained by using an analogue computer, and it was shown that the dynamic load may be reduced by increasing the damping between the gear teeth or by reducing the amount of stiffness variation.

In 1967, Tordion and Geraldin (Tordian 1967) used an equivalent single degree of freedom dynamic model to determine the transmission error from experimental measurements of angular vibrations. They first constructed a torsional multi-degree of freedom model for a general rotational system with a gear mesh. Then, only the equations of the gears were considered for obtaining an equivalent single degree of freedom model with constant mesh

stiffness and a displacement excitation representing the transmission error. An analogue computer solution was used to obtain the transmission error from the measured angular accelerations. The transmission error was proposed to be used as a new concept for determining the gear quality, rather than individual errors.

In 1973, Wallace and Seireg (Wallace 1973) used a finite element model of a single tooth to analyse the stress, deformation and fracture in gear teeth when subjected to dynamic loading. Impulsive loads applied at different points on the tooth surface and moving loads normal to the tooth profile were studied. In the same year, Wilcox and Coleman (Wilcox 1973) also analysed gear tooth stresses. They developed a new accurate stress formula for gear teeth based entirely on the finite element method and presented a comparison between the new formula and the previous one.

In 1978, Remmers (Remmers 1978) presented a damped vibratory model in which the transmission error of a spur gear was expressed as a Fourier series. He used viscous damping and constant tooth pair stiffness, and considered the effects of spacing errors, load, and design contact ratio and profile modifications.

Rebbechi and Crisp (Rebbechi 1981; Rebbechi 1983) considered the material damping of the gear-wheel shafts, while the compliance of the shafts was neglected. The three-degree of freedom model was reduced to a two degree of freedom model for the study of the torsional vibrations of a gear pair, and an uncoupled equation, which gave the tooth deflection. The other effects included in the model were material damping inherent to the tooth, perturbations of input and output torque, arbitrary tooth profile errors, time variation of that error due to deformation, and perturbations of the base circle due to profile errors. The effects of kinetic sliding friction at the contact point and the sliding velocity on the dynamics of continuous meshing were also studied (Rebbechi 1983) and in 1996, Rebbechi, et al. (Rebbechi 1996), obtained measurements of the gear tooth dynamic friction under various speed and load situations.

In 1985, Wang (Wang 1985) studied the effect of torsional vibration in his model. The research was focused on the analytical evaluation of gear dynamic factors based on rigid

body dynamics and discussed different cases in which the transmission errors have different effects on the dynamic load. He commented that the transmission errors have a system wide effect and could be used to analyse rigid-body vibrating gear systems in which the gear deflection is not considered.

In the late 1980s, Ramamurti and Rao (Ramamurti 1988) presented a new approach to the stress analysis of spur gear teeth using FEM. Their new approach, with a cyclic system of gear teeth and with asymmetry of the load on the teeth, allowed computation of the stress distribution in the adjacent teeth from the analysis of one tooth only.   The boundary conditions imposed between the two adjacent teeth in the conventional FEM were avoided in their approach.

In 1988, Vijayakar, Busby, and Houser (Vijayakar 1988) used a simplex type algorithm to impose frictional contact conditions on finite element models. They established the contact equations with the frictional factor and solved them for known output moment load on the output gear. In their finite element model, they analysed their problem in two dimensions and in order to model the involute profile as closely as possible, a special five node linear transition element was used.   In the same year, Ozguven and Houser (Ozguven 1988) presented a non-linear model of a single degree of freedom system for the dynamic analysis of a gear pair.   In their studies, they developed two methods for calculating the dynamic mesh and tooth forces, dynamic factors based on stresses, and dynamic transmission error from measured or calculated loaded static transmission errors.   The first method was an accurate method, which included the time variations of both mesh stiffness and damping. The second approach was a more approximate method in which the time average of the mesh stiffness was used.

In 1990, Sundarajan and Young (Sundarajan 1990) developed a three dimensional finite element substructure method to improve the accuracy of calculation of the gear tooth contact and fillet stress in large spur and helical gear systems. The finite element analysis and pre-processing software they developed simplified the data input and reduced the manual effort involved in the analysis. When some parameters (misalignment for example) were changed, most of the stiffness matrices were not recalculated. They considered the

contact problem by using contact boundary conditions, which meant that the contact or area was defined in the analysis. One year later, Sundarajan and Amin (Sundarajan 1991) investigated the finite element analysis of a ring gear and the casing and presented another finite element computer program to solve this problem.

The contact conditions of gear teeth are very sensitive to the geometry of the contacting surfaces, which means that the finite element mesh near the contact zone needs to be very highly refined. However it is not recommended to have a fine mesh everywhere in the model, in order to reduce the computational requirements. Vijayakar and Houser (Vijayakar 1993) studied the contact analysis of gears using a combined finite element and surface integral method. They developed a Contact Analysis Program Package which supports stress contours, transmission errors, contact pressure distribution and load distribution calculation. Their approach was based on the assumption that beyond a certain distance from the contact zone, the finite element method accurately predicted deformations and the elastic half space method was accurate in predicting relative displacements of points near the contact zone. Under these assumptions, it was possible to make predictions of surface displacements that make use of the advantages of both the finite element method as well as the surface integral approach.

In 1994, a review of the current contact stress and deformation formulations compared to finite element analysis was given by Gosselin, et al. (Gosselin 1994). They presented an original approach to meshing line contact for spur gears and point contact for spiral bevel gear pairs using finite element analysis with contact elements and they then compared the contact deformation results with recognised analytical formulations. Their results showed that the contact deformations differ from 20% to 150% between the analytical approaches and FEM. In the same year, Chen, Litvin, and Shabana (Chen 1994) proposed an approach for the computerised simulation of mesh and contact of loaded gear drives that enables determination of the instantaneous contact ellipse, the contact force distributed over the contact ellipse and the real contact ratio. They also established a finite element model for the maximum bending stress calculation on a tooth. The friction forces between gear teeth, the elastic deflection of the body of the gear, the shaft and the bearings were neglected in their approach and their model.

2.2.2 Models for Gear Dynamics

Some of the early mathematical models, in which the stiffness and mass contribution of the shafts carrying the gears in mesh were ignored, showed good agreement with the experimental measurements. However, it was realized in the late 1960s and early 1970s that dynamic models in which the shaft and bearing flexibility were considered would be necessary for more general models. Unless the stiffness of these elements were relatively high or low compared to the effective mesh stiffness, the vibration coupling of different elements cannot be neglected. In general, a high degree of correlation was obtained between the experimental results and the predictions provided by many of the early single degree of freedom models. This can be explained by the fact that the experimental rigs used in such studies satisfied most of the basic assumptions made in the mathematical model. For example, a very short shaft might be assumed to be rigidly mounted in the transverse direction. In practical applications however, these assumptions may not always be satisfied and so one then needs more general models in which the flexibility and mass of the other elements are considered as well.

The models that could be considered in this group are either torsional models, in which only the torsional stiffness of the gear-carrying shafts is included, or torsional and translation models, in which both the torsional and transverse flexibility of the gear-carrying shafts are considered.

In the early 1960s, Johnson (Johnson 1962) used a receptance coupling technique to calculate the natural frequencies from the receptance equation obtained by first separately finding the receptances at the meshing point of each of a pair of general shafts. In the model, the varying mesh stiffness was replaced by a constant stiffness equal to the mean value of the varying stiffness and thus a linear system was obtained. His work was one of the first attempts to use mesh stiffness in coupling the torsional vibration of gear shafts. Mahalingam (Mahalingam 1968) presented a similar model in 1968, where the formulae for support receptance at a gear-wheel bearing was developed and then used to study the effects of gearbox and frame flexibility on the torsional vibration.

An important contribution in this area came in 1970 from Kobler, Pratt and Thomson (Kobler 1970) who concluded from their experimental results that dynamic loads and noise result primarily from the steady state vibration of the gear system when forced by transmission errors. They developed a six-degree of freedom dynamic model with four torsional degrees of freedom and one lateral degree of freedom in the direction of the tooth force on each shaft. They assumed the tooth mesh stiffness to be constant in their model and the spectrum analysis of the static transmission error for the single-stage reduction gear unit used was also given. In 1971, Kasuba (Kasuba 1971) used one and two degree of freedom models based on his previous work (Kasuba 1961), to determine dynamic load factors for gears that were heavily loaded. He used a torsional vibratory model, which considered the torsional stiffness of the shaft. He also argued that the rigidity of the connection shafts was much lower than the rigidity of the gear teeth in meshing, and then decoupled the meshing system. The tooth error in mesh was represented by a pure sine function having the frequency of tooth meshing. In his model the tooth meshing stiffness was time varying.

In 1972, Wang and Morse (Wang 1972) constructed a torsional model including shaft and gear web stiffness as well as a constant mesh stiffness. The model was represented by a spring mass system having many degrees of freedom. The transfer matrix technique was applied to give the static and dynamic torsional response of a general gear train system. It was found that the torsional natural frequencies and mode shapes determined from a free vibration analysis correlated with experimental results at low frequencies. Later, Wang (Wang 1974) extended this work to the linear and non-linear transient analysis of complex torsional gear train systems. In this later model he considered the variation of tooth stiffness, and included gear tooth backlash, linear and non-linear damping elements and multi-shock loading. Three different numerical methods that can be used in the solution of non-linear systems that cannot be approximated piecewise linearly were also briefly discussed in his work.

In the 1980s more and more complicated models were developed in order to include several other effects and to obtain more accurate predictions, while some simple models were still developed for the purpose of simplifying dynamic load prediction for gear

standards. In 1980, Iida, et al. (Iida 1980) investigated the coupled torsional-flexural vibration of a shaft in spur geared systems in which they assumed that the output shaft was flexible in bending and the input shaft was rigid in bending. They derived equations of motion for a 6-degree-of-freedom (DOF) system where the driving gear had a torsional DOF while the driven gear had x, y and torsional DOF due to mass imbalance and geometrical eccentricity. They assumed that the tooth contact was maintained during the rotation and that the mesh was rigid. Four years later, Iida and Tamura (Iida 1984) continued to study coupled torsional flexural vibration of geared shaft systems. In that study, their model consists of three shafts, rather than two shafts, one of them being a counter shaft.

Neriya, et al. in 1985 (Neriya 1985) also investigated the coupled torsional flexural vibration of a geared shaft system due to imbalance and geometrical eccentricity. The difference in the work with respect to Iida, et al. (Iida 1980) was that they used the finite element method to solve their problem. In their model, there were 6 beam elements for each of the driving and driven shafts that were coupled at the contact to account for the tooth flexibility. Their model had 41 degrees of freedom. They solved the free vibration problem to obtain the natural frequencies and mode shapes. The normal mode analysis was then employed to obtain the dynamic response of the system under the excitations arising from the mass imbalance and geometrical eccentricity in gears.

In early studies, the mesh stiffness of teeth was considered to be constant. Iwatsubo and Kawai (Iwatsubo 1984) studied the coupled lateral and torsional vibrations of geared rotors, considering mainly the effect of the periodic variation of mesh stiffness and a tooth profile correction. Their model had two simply supported rotors with a spur gear at the centre of each rotor. The stability condition of the system was analysed in their study. In the same year, Iwatsubo, Arii and Kawai (Iwatsubo 1984) analysed the coupled lateral and torsional vibration of the geared system constructed from a pair of spur gears using the transfer matrix method. In their research, they considered three cases in the analysis of the free vibration of the system: 1. The mesh force acting on the contact line was a function of the rotation of each gear, 2. The mesh force acting on the contact line was a function of the

rotation and flexure at each gear, and 3. The system was not coupled by the gears. The forced vibration caused by the mass imbalance of the gears was also calculated.

A new topic, the computer simulation of the torsional and flexural vibration in drive systems, was studied by Laschet and Troeder (Laschet 1984). They developed computer programs and applied simulation techniques to predict and analyse the performance of gears trains. The distinctive feature of their research was that the backlash of the gears was considered in their programs and CAD data of the gear geometry could be used in their programs.

In 1985, Wang (Wang 1985) developed a torsional only vibration model. He focused on an analytical evaluation of gear dynamic factors based on rigid body dynamics and discussed different cases in which the transmission errors have different effects upon the dynamic load. He commented that the transmission error had a system wide effect and could be used to analyse rigid-body vibrating gear systems in which the gear deflection was not considered.

Tavares and Prodonoff (Tavares 1986) proposed a new approach for torsional vibration analysis of gear-branched propulsion systems in 1986. Idle gears in a gear-branched system were modelled as part of the inertia of the master gear and the finite element method was used in their approach. In the same year, Umezawa, et al. (Umezawa 1986) set up a test gearing unit which consisted of an input shaft, countershaft and output shaft. The gears were placed at arbitrary positions on the shafts in their unit so that the effect of the countershaft on the bending vibration and on the sound radiation became clear. At almost the same time, Iida, et al. (Iida 1986) studied a three axis gear system but with some differences from Umezawa, et al., firstly, because the countershaft was on soft supports and secondly, the model was a coupled torsional-lateral vibration analytical model.

In 1992, a finite element model of a geared rotor system on flexible bearings was developed by Kahraman, et al. (Kahraman 1992). The coupling between the torsional and transverse vibrations of the gears was considered in the model. They applied the transmission error as excitation at the mesh point to simulate the variable mesh stiffness.

They presented three different geared systems as numerical examples and discussed the effect of bearing compliance on gear dynamics. The assumptions they used were that the gear mesh was modelled by a pair of rigid disks connected by a spring and a damper with constant value which represented the average mesh values and tooth separation was not considered.

Another model presented by Kahraman (Kahraman 1993) was a linear dynamic model of a helical gear pair. The model considered the shaft and bearing flexibility and the dynamic coupling among the transverse, torsional, axial, and rocking motions due to the gear mesh. The natural frequencies and mode shapes were predicted and the forced response due to the static transmission error was predicted. After the parametric study of the effect of the helix angle on the free and forced vibration characteristics of a gear pair, the conclusion was reached that the axial vibrations of a helical gear system could be neglected in predicting the natural frequencies and the dynamic mesh forces. The assumption for their model was that the gears were modelled as rigid disks, the clearances and stiffness changes of the bearings were neglected, and the system was assumed to be symmetrical about the transverse plane of the gears.

2.2.3   Models with a Whole Gearbox

The research models reviewed in this section are seen as being advanced because traditional analysis approaches mentioned previously in the gear dynamic area have concentrated on the internal rotating system and have excluded dynamic effects of the casing and flexible mounts. The focus of this group is on the dynamic analysis of the geared rotor system, which includes the gear pair, shafts, rolling element bearings, a motor, a load, a casing and flexible or rigid mounts.

In 1991, Lim and Singh (Lim 1991) presented a detailed study of the vibration analysis of complete gearboxes. Their research was based on previous studies including the bearing stiffness formulation (Lim 1990) and system studies (Lim 1990). They developed linear time-invariant, discrete dynamic models of an overall box by using lumped parameter and dynamic finite element techniques. They studied three example cases: case I, a single-stage

rotor system with rigid casing and flexible mounts; case II, a spur gear drive system with rigid casing and flexible mounts; and case III, a high-precision spur gear drive system with flexible casing and rigid mounts. They used the gear mesh coupling stiffness matrix to couple the two gears and used the bearing stiffness matrix to link the shafts and casing. In their finite element model, the gear, pinion, motor and load were simulated as generalised mass and inertia elements and the gear mesh stiffness matrix and bearing stiffness matrix were modelled as six-dimensional generalised stiffness matrices. They used the FEM software ANSYS to analyse their models. They made a parametric study of the effect of casing mass and mount stiffness on the system natural frequencies. A comparison of the casing flexural vibrations between the simulation and the experiment was presented.

Choy, et al. (Choy 1991) presented a vibration analysis with the effect of casing motion and mass imbalance for a multi-stage gear transmission in 1991. In order to investigate the effect of the casing motion and mass imbalance, four major cases of external excitations were examined in their study. They employed the modal method to transform the equations of motion into modal coordinates to solve the uncoupled system. They concluded that the influence of the casing motion on system vibration was more pronounced in a stiffer rotor system. In the same year, El-Saeidy Fawzi (El-Saeidy Fawzi 1991) presented an analytical model for simulating the effect of tooth backlash and ball bearing dead band clearance on the vibration spectrum in a spur gearbox. The contact between meshing teeth using the time-varying mesh stiffness and mesh-damping factor was discussed. From their study, they concluded that the backlash and bearing dead band clearance had a pronounced effect on the vibration spectrum of a gearbox. In this model, the gearbox casing was assumed to be rigid, therefore, both ends of each shaft had the same displacements. There was no experimental result to verify the analytical result of this research.

One year later, Choy, et al. (Choy 1992) continued their study on the multi-stage gear system. The work presented in that study was the development and application of a combined approach of using the modal synthesis and finite element methods in analysing the dynamics of multi-stage gear systems coupled with the gearbox structure or casing. In their solution procedure, modal equations of motion were developed for each rotor-bearing-

gear stage using the transfer matrix method to evaluate the modal parameters, and the modal characteristics of the gearbox structure were evaluated using a finite element model in NASTRAN. The modal equations for each rotor stage and the gearbox structure were coupled through the bearing supports and gear mesh.

After this study, they used their analytical model to predict the dynamic characteristics of a gear noise rig at the NASA Lewis Research Centre and then used experimental results from the test rig to verify the analytical model (Choy 1993). Their conclusions were that the dynamics of the casing can be accurately modelled with a limited amount of analytically predicted vibration modes, and that the characteristics and trends of the casing vibration spectra predicted by the analytical model were very similar to those found in the experimental data.

In 1992, Ong (Ong 1992) described the application of the eigenvalue economisation method coupled with the frontal solution technique to a vehicle transmission system comprising an integral bell-housing gearbox, extension housing, drive shaft and rear-axle assembly. In this study, super-elements were applied using the structural dynamic sub structuring technique for the finite element analysis. The pinion shafts were represented by beam elements and the gears and bearings were represented by lumped mass elements in the analytical model. Finally, a comparison was made between experimental results and the finite element method, which showed good agreement.

Most analyses of gearboxes appear to be concerned with the dynamic response and vibration characteristics. In 1994, Sabot and Peret-Liaudet (Sabot 1994) presented another phase of study, noise analysis of gearboxes. They pointed out that a troublesome part of the noise within the car or truck cab could be attributed to the gearbox and that this noise was associated with the vibrations induced by the transmission error which gives rise to dynamic loads on the teeth, shafts, bearings and casing. They computed the noise radiated by the gearbox casing using the Rayleigh Integral Formulation in which the acceleration response of the casing associated with the finite element method calculation was considered. Their results showed that although the test model was a simplified gearbox,

their numerical analysis provided a better understanding of the sound radiation characteristics of geared transmission systems.

At the same time, Kato, et al. (Kato 1994) developed a simulation method by integrating finite element vibration analysis and boundary element acoustic analysis for the purpose of evaluating the sound power radiated from the gearbox and achieved good agreement with the experimental results. In their model, each shaft was modelled using beam elements and the mass and rotating inertia of the gear was modelled as lumped masses and added to the shaft. Each of the rolling element bearings was represented as a spring and damper and the casing of the gearbox was modelled by a thin shell element in the finite element package program ISAP-6. Their acoustic analysis in the frequency domain showed that the sound power at the mesh frequency was greater than the sound power at other frequencies.

There have also been various studies aimed at modelling a single mechanical element, a complex system containing several gears as well as other mechanical or electrical elements and other special topics, as indicated by the following grouping;

Load Sharing Ratio (Chabert 1974; Remmers 1978; Drago 1979; Walford 1980; Bahgat 1983; Ozguven 1988; Kuang 1992; Liou 1992; Liou 1996; Litvin 1996; Zhang 1998).

Mesh Stiffness (Gargiulo 1980; Kahraman 1991; Kuang 1992; Brousseau 1994; Daniewicz 1994; Sirichai 1996; Velinsky 1996; Du 1998; Elkholdy 1998; Gosselin 1998; Nadolski 1998).

Bearing Stiffness (Childs 1980; Gargiulo 1980; Bahgat 1981; Smith 1987; Lim 1990; Lim 1990; Kahraman 1991; Lim 1991; Lim 1992).

Shaft In A Gear System (Johnson 1962; Iida 1980; Iida 1984; Neriya 1985; Iida 1986; Lin 1988; Prasad 1992; Zhong-Sheng 1993; Okamoto 1994).

Casing Analysis Of A Gearbox (Drago 1979; Randall 1980; Randall 1984; Mcfadden 1985; Tavares 1986; Houser 1990; Randall 1990; Zakrajsek 1990; Sundarajan 1991; Choy 1992; Inoue 1992; Maruyama 1992; Oswald 1992; Oswald 1992; Perret-Liaudet 1992; Kato 1994; Kissling 1994; Oswald 1994; Sabot 1994; Zhang 1994; Zhang 1994; Du 1997).

Gear Transmission Error Measurement (Gregory 1963; Tordian 1967; Hayashi 1981; Houser 1989; Rebbechi 1992; Vinayak 1992; Bard 1994; Barnett 1994; Munro 1994; Velex 1995; Houser 1996; Sweeney 1996).

Transmission System (Drago 1979; Ong 1992; Choy 1995; Choy 1996; Choy 1996; Forrester 1996; Regalado 1998).

Computerized Design And Generation Of Gears (Litvin 1993; Litvin 1993; Blazakis 1994; Zhang 1994; Litvin 1995; Litvin 1995; Litvin 1996; Litvin 1996; Seol 1996; Seol 1996; Litvin 1997; Litvin 1998; Litvin 1998; Litvin 1998).

Gear Geometry (Chen 1992; Fujio 1992; Kin 1992; Kubo 1992; Tsai 1992; Donno 1998; Dooner 1998; Feng 1998; Su 1998).

Gear Noise Design (Aida 1967; Aida 1968; Aida 1969; Kobler 1970; Daly 1979; Drago 1979; Welbourn 1979; Smith 1987; Baron 1988; Houser 1990; Randall 1990; Randall 1990; Zakrajsek 1990; Mark 1992; Maruyama 1992; Oswald 1992; Oswald 1992; Alattass 1994; Lewicki 1994; Oswald 1994; Sabot 1994; Tuma 1994; Zhang 1994; Zhang 1994; Litvin 1995; Roosmalen 1995; Wang 1996; Cheng 1998; Stadtfeld 1998).

Stress Analysis (Arikan 1989; Arikan 1991; Arikan 1992; Moriwaki 1993; Rao 1993; Baret 1994; Daniewicz 1994; Vijayarangan 1994; Lu 1995; Refaat 1995; Litvin 1996; Kalluri 1998; Kim 1998; Richard 1998).

Modification of Gear Geometry (Walker 1938; Harris 1958; Niemann 1970; Tobe 1976; Wang 1978; Kishor 1979; Cornell 1981; Kiyono 1981; Terauchi 1981; Lin 1989a; Rosinski 1992; Li 1994; Munro 1994; Palmer 1995; Walton 1995; Walton 1998).

Non-Metallic Gears (Yelle 1981; Terashima 1986; Tsukamoto 1986; Janover 1989; Walton 1989; Enzmann 1990; Tsukamoto 1990; Breeds 1991; Kral 1991; Baumgart 1992; Kudinov 1992; Walton 1992; Zhang 1992; Mao 1993; Nabi 1993; Solaro 1993; Tessema 1993; Tessema 1994; Walton 1994; Koffi 1995; Tessema 1995; Walton 1995; Williams 1995; Du 1997; Nitu 1997; Smith 1997; White 1997; Kleiss 2000; Kurokawa 2000; Luscher 2000; Panhuizen 2000; Bushimata 2001; Wright 2001; Alagoz 2002; Andrei 2002).

High Contact Ratio Gears (Cornell 1978; Townsend 1979; Rosen 1982; Elkholdy 1985; Barnett 1988; Lee 1991; Lin 1993; Yildirim 1994; Yildirim 1999; Yildirim 1999)

CHAPTER 3

GUIDE LINES FOR FEA GEAR MODELING

3.1   INTRODUCTION

3.1.1   Chapter Overview

This chapter presents some of the basic considerations required for applying finite element methods to gear modelling in this research. Some features may exceed the capability of the currently available software resources but the author believes the considerations are necessary for the research to be continued in the future.

3.1.2   Brief History of Finite Element Analysis

Structural mechanics has been applied in the building industry for the past one hundred years (Hoff 1956). During that time, the stiffness matrix of bar and beam elements were derived from the theory of elementary strength of materials. With the development of the direct stiffness method, the global matrix associated with load and boundary condition was

formed. Courant (Courant 1943) in 1943 used an assemblage of triangular elements and the principle of minimum potential energy to study the St. Venant torsion problem in which he suggested piecewise polynomial interpolation over triangular sub regions as a way to obtain approximate numerical solutions. He recognized this approach as a Rayleigh-Ritz solution of a variation problem. This was the basis of the finite element method, as we know it today.

With the availability of the digital computer in 1953, stiffness equations in matrix notation could be solved (Levy 1953). In 1960, the name *finite element method* was introduced by Clough (Clough 1960). Soon after that, the method was recognized as a general method of solution for partial differential equations with its efficacy.

In 1965, Zienkiewicz and Cheung (Cheung 1965) reported that the finite element method was applicable to all field problems that can be cast into variation form so that the method received an even broader interpretation. After development for two decades, the acceptance of the method was worldwide.

Today there are more software options. More recently, finite element packages have been extended to include non-linear static stress, dynamic stress (vibration), fluid flow, heat transfer, electrostatics, and FEA based stress and motion analysis capabilities. These capabilities are frequently combined to perform analyses that consider multiple physical phenomena, tightly integrated within a CAD interface.

3.2   Energy and Displacement

3.2.1   The Fundamental Equation

In most cases, the finite element method uses the total potential energy of the system instead of a differential equation to solve engineering analysis problems. The approach uses the stationary principle of total potential energy which states that among all the permissible configurations, the actual configuration (u) will make the total potential energy V(u) stationary, or, mathematically,

$$\delta\, V(u) = 0. \tag{3.1}$$

In a static analysis,

$$V(u) = U(u) - W(u), \tag{3.2}$$

where U is the internal energy which is equal to the strain energy, given by,

$$U = \tfrac{1}{2}\int \varepsilon^{T} \cdot C \cdot \varepsilon \; d\Omega, \tag{3.3}$$

and the external energy W is equal to the work done by an external load q,

$$W = \int qu \, d\Omega. \tag{3.4}$$

Here, ε is the strain vector, C is the constitutive matrix and $d\Omega$ is the infinitesimal volume. If the system is discretized into elements, then we can write,

$$U = \sum_{e} U_{e} \quad \text{and} \quad W = \sum_{e} W_{e}, \tag{3.5}$$

where,
$$U_{e} = \tfrac{1}{2}\int \varepsilon_{e}^{T} \cdot C_{e} \cdot \varepsilon_{e}\, d\Omega_{e} \quad \text{and} \quad W_{e} = \int q_{e} u_{e}\, d\Omega_{e}. \tag{3.6}$$

The nodal displacement vector, u_{e} can also be written as,

$$u_{e} = H \cdot \mathbf{u}_{e}, \tag{3.7}$$

where H is the shape function (or interpolation function). The strain vector can then be obtained by direct differentiation to be,

$$\varepsilon_{e} = \partial u_{e} = (\partial H) \cdot \mathbf{u}_{e} = \mathbf{B} \cdot \mathbf{u}_{e}, \tag{3.8}$$

where ∂ is an appropriate differential operator and $\mathbf{B}$ is the strain-displacement matrix. Hence, we can write,

$$U_{e} = \tfrac{1}{2}\mathbf{u}_{e}^{T} \cdot \left(\int \mathbf{B}^{T} \cdot C \cdot \mathbf{B}\, d\Omega_{e} \right) \cdot \mathbf{u}_{e} = \tfrac{1}{2}\mathbf{u}_{e}^{T} \cdot \mathbf{K}_{e} \cdot \mathbf{u}_{e}, \tag{3.8}$$

and
$$W_{e} = \int q_{e} H \cdot \mathbf{u}_{e}\, d\Omega_{e} = \mathbf{f}_{e} \cdot \mathbf{u}_{e}, \tag{3.9}$$

where $\mathbf{K}_{e}$ is the element stiffness matrix, and $\mathbf{f}_{e}$ is the element equivalent force. They become,

$$\mathbf{K}_{e} = \int \mathbf{B}^{T} \cdot C \cdot \mathbf{B}\, d\Omega_{e},$$

and
$$\mathbf{f}_{e} = \int q_{e} H\, d\Omega_{e}. \tag{3.10}$$

If it is supposed that the element displacement vector $\mathbf{u}_{e}$ is related to the system nodal displacement vector $\mathbf{u}$ through the transformation $\mathbf{T}_{e}$, then

$$\mathbf{u}_e = \mathbf{T}_e \cdot \mathbf{u} \,. \tag{3.11}$$

Equations 3.2, 3.5, 3.8 and 3.9 then give,

$$V(u) = \sum_e \left(U_e - W_e \right),$$

$$= \sum_e \tfrac{1}{2}\mathbf{u}_e^T \cdot \mathbf{K}_e \cdot \mathbf{u}_e - \sum_e \mathbf{f} \cdot \mathbf{u}_e,$$

So that we have

$$V(u) = \tfrac{1}{2}\mathbf{u} \cdot \left(\sum_e \mathbf{T}_e^T \mathbf{K}_e \mathbf{T}_e \right) \cdot \mathbf{u} - \left(\sum_e \mathbf{f}_e \cdot \mathbf{T}_e \right) \cdot \mathbf{u} \,.$$

The variation principle (3.1) gives,

$$\delta\, V(u) = \delta\, \mathbf{u}^T \cdot \left[\left(\sum_e \mathbf{T}_e^T \mathbf{K}_e \mathbf{T}_e \right) \cdot \mathbf{u} - \left(\sum_e \mathbf{f}_e \cdot \mathbf{T}_e \right) \cdot \mathbf{u} \right] = 0,$$

or, written in standard form,

$$\mathbf{K} \cdot \mathbf{u} = \mathbf{f}, \tag{3.12}$$

where

$$\mathbf{K} = \sum_e \mathbf{T}_e^T \mathbf{K}_e \mathbf{T}_e \quad \text{and} \quad \mathbf{f} = \sum_e \mathbf{f}_e \cdot \mathbf{T}_e,$$

are the system stiffness and the force vector respectively. Equation 3.12 cannot be solved for system nodal displacement vector $\mathbf{u}$ for given load vector $\mathbf{f}$ until it has been modified to account for the boundary conditions. In general elasticity problems, the displacement field or the set of nodal displacements cannot be found unless enough nodal displacements are fixed to prevent the structure from moving as a rigid body when external loads are applied.

3.2.2   The Major Limitation On Gear Transmission Error Study

For a gear set, the major components of total transmission error are the tooth geometry error, imperfect mounting and elastic deformation of the meshing gear pair. In most cases, for a precision gear set, the elastic deformation is the main component of the transmission error and the determination of this component is one of the main tasks in the proposed research. However, other components in some situations can also be significant for the total transmission error. One of the examples is a meshing gear pair with tip-relieved teeth. When the applied load is relatively small, the "rigid body motion" (rotation) will be the main component of the total transmission error. In such a case, trying to use the FEA program to determine the total displacement (total angular rotation, which includes the initial rigid body motion and the final elastic deformation) will be very difficult. Contact

analysis with initial un-connected bodies is a very difficult problem as the stiffness matrix **K** in the fundamental equation 3.12 becomes singular and unsolvable. As mentioned in the last section, finite elements require at least some stiffness connecting all the elements together along with sufficient displacement constraints to prevent rigid-body motion.

In ANSYS®, with this case, the program will issue *pivot ratio* warnings. The program will continue to try to solve the problem, but it is likely to get either a *negative main diagonal* message or a *DOF limit exceeded* message.

ANSYS® offers the following options to overcome the difficulty in convergence.

1. *Build the models in the just-touching position*. This option seems the easiest solution, but it requires the user to know what the position is. If the surfaces on both bodies are curved or irregular (caused by surface damage, plasticity), this certainly is difficult.

2. *Use imposed displacements to move it into position*. Again, the "free" body is moved into its starting position using a specified displacement value. If the actual initial contacting positions are not previously determined in advance, this also causes difficulty.

3. *Use weak springs to connect the bodies*. This is a interesting option, and is worth a try in some cases. In this technique, the user would add springs to connect the two bodies. The suggested spring stiffness would typically be 6 to 8 orders of magnitude weaker than the contact stiffness. However, care must be taken when very flexible elements are connected to very rigid elements, as the finite element solution can render poor solutions for displacement due to round off error, or matrix ill-conditioning. Ill-conditioning errors typically manifest themselves during the solution phase of an analysis. A detailed example of this has been given by Lepi (Lepi 1998).

4. *Solve the problem dynamically*. In a mesh cycle of a meshing gear pair, if part of the solution is obtained by static (no gap for contact) analysis and the other part by dynamic analysis, then the overall solution wouldn't be so good for the study of gear transmission error.

The state above is not peculiar to the application of the ANSYS® software. This capability is missing from many standard FEA programs (Dvorak 1999), and currently is the major

limitation for gear transmission error study using finite element analysis, especially with limited software resources.

A recently developed analysis method that is likely to be one of the keys for solving this problem is called *The Precise Solid Method (PSM)* from Precision Analysis Int., and it promises to improve the relationship between CAD and analysis technologies. The feature of mesh-less analysis and highly accurate solutions on solids was introduced in the paper by Kurowski (Kurowski 2000). Some other interesting features were presented by Dvorak (Dvorak 1999), where he explained that the new method tolerates point boundary conditions that do not produce stress at the point. Such "dummy" constraints only restrain motion. The software is also able to display rigid body motion at the beginning of the solution. However, contact and non-linear analysis is expected in the future. PSM theoretically can simulate any kind of phenomena that is described with differential equations as boundary value problems (Kurowski 2000).

3.3   Methods for Accurate FEA Solution

3.3.1   h- and p- Method

The h- method for FEA entered the engineering world in the 1970s, and is a common approach for solving analysis problems. This method involves the use of lower order displacement assumptions (linear or quadratic) and increases the number of elements in areas where the displacement is expected to be a non-linear function. The error between the exact displacement and the finite element solution decreases with an increasing number of smaller elements in the chosen areas. Theoretically, when the number of elements used in a finite element model approaches infinity, the error between the finite element solution for displacement and the exact displacement is expected to approach zero. (The error between predicted and exact energy is also expected to approach zero.)

The p-method dealt with the more complete design and was introduced in the early 1990s. To calculate displacements, the p-method manipulates the polynomial level (p-level) of the finite element shape functions, which are used to approximate the real solution so that the

results obtained are to a user-specified degree of accuracy. The p-method can improve the results for any mesh automatically. Usually, the elements are mid-noded. In ANSYS® the range within which the p-level may vary can be controlled locally through the p-element KEYOPT settings (KEYOPT(1) and KEYOPT(2)) or globally across the entire model with the command PPRANGE. By default, the p-level range is from 2 to 8. More detailed discussion about the p-method can be found in Strang (Strang 1973), Babuska (Babuska 1988), and SzabO (SzabÒ 1991).

The p-method solution option offers many benefits over the traditional h-method. The most convenient benefit is in the ability to obtain good results to a desired level of accuracy without rigorous user-defined meshing controls. In addition, the p-method adaptive refinement procedure offers error estimates that are more precise than those of the h-method, and can be calculated locally as well as globally (stress at a point rather than strain energy). For example, if a high accuracy solution at a point is needed, such as for fracture or fatigue assessments, the p-method offers an excellent means for obtaining these results to the required accuracy.

Modern FEA software can combine the h- and p-adaptive approaches in a third method called the hp-method or the hp-adaptive solution. Mixing the two technologies into a single model lets users construct most structures with h-elements to obtain global responses while areas of particular interest can be modelled with p-elements to improve solution accuracy. The p-elements tolerate distortions and shapes that render standard or h-elements unreliable.

3.3.2   Methods for Non-linear Contact Analysis

Finite element analysis of meshing gear pairs will be subject to non-linear contact analysis. In this situation, the contact is highly non-linear because one or both of the following are unknown:

- The actual regions of contact are unknown until the problem has been solved. Depending on the load, material, boundary conditions and other

factors, and surfaces can come into and go out of contact with each other in a largely unpredictable and abrupt manner.

- Most contact problems need to account for friction. There are several friction laws and models to choose from, and all are non-linear. Frictional response can be chaotic, making solution convergence difficult.

From a mathematical point of view, both the system stiffness matrix **K** and load vector **f** in equation 3.12 may be functions of nodal displacement. This requires significant computer resources to solve. For example, when the (traditional) Newton-Raphson method is employed to solve such non-linear equations, the analysis involves using a series of linear approximations with corrections. Each linear approximation requires a separate pass, or iteration, through the program's linear equation solver. Each new iteration is about as expensive as a single linear-analysis solution. (In ANSYS®, the iteration shows up as equilibrium iteration.)

There are many papers on the application of the h-method to the solution of contact problems. A comprehensive review can be found by Zhong (Zhong 1992) including many references. When the h-method is used in contact problems for stress analysis, in most cases, the mesh is not sufficiently refined to indicate the presence of singularities in the boundary points of the contact zone (Paczelt 1999). The use of the p-method for the solution of contact is relatively recent (Lee 1993; Gabbert 1994). In this case, the analysis is typically high enough (shape function orders) for the singularities to indicate oscillations in the numerical solutions. In the paper of Lee and Oden (Lee 1993), the hp-method was used which produced a fine mesh at the contact zone with p=2. In the paper of Gabbert (Gabbert 1994), special "pNh elements" were used in the contact zone. These elements incorporate piecewise linear approximations on the contact edges or surfaces which are blended with the standard basis functions of the p-version elements. However, in both cases, there are stress discontinuities between the h- and p- elements or in the hNp-elements. In the paper by Paczelt (Paczelt 1999), a special form of the hp-method was used that combines the p-extension with a minor iterative modification of the mesh. A very high accuracy solution was achieved, but the relative model didn't account for friction.

As presented above, for the stress analysis, the p- or hp-method is desired. The h-method, however, is relatively easy to use and all standard FEA programs support the method. On the other hand for example, ANSYS®, does not by default support the p- or hp-method in contact analysis. In choosing the analysis method one also has to consider the type of gradient output that is desired. If one is analysing a structure for maximum displacement, a somewhat coarse mesh by h-method might be sufficient. More details of this will be discussed in the next section.

3.4   Rate of Convergence

3.4.1   The Rate of Displacement and Stress

The displacement based FEA approach is currently the most common, and the term *finite element method* is typically used without the modifier *displacement based.* (There are other means of developing a finite element solution like the hybrid method that uses both an assumed displacement field and an assumed stress field. Only the displacement based FEA is used in this research). The primary unknown in the finite element method is the nodal displacement. The finite element method generates an approximate solution for displacement, and then typically uses the displacement to calculate approximate values of stress and strain that may be called derivative values as secondary unknowns. At any given point in a structure, an FEA predicted value of displacement could be either too large or too small, highlighting one of the difficulties in evaluation of convergence. In light of this, proofs of h-convergence are often stated in terms of *norms*. Using the norm, a formal proof of convergence shows that the total potential energy computed by FEA converges to the exact value as the size of the largest element dimension approaches zero. Convergence in displacement is anticipated with convergence in energy, but the convergence rates of these two matrices are not normally the same.

The convergence of displacement (Lepi 1998) can be expressed as,

$$\text{displacement convergence} \equiv \frac{e_2}{e_1} = O\left(\frac{h_2}{h_1}\right)^{p+1} \qquad , \qquad\qquad (3.13)$$

The equation (3.13) states that convergence is defined in terms of the error associated with the two solutions, e_1 and e_2. The relative error is a function of the largest element size h_1

35

and h_2 in each of the models, and the order of the interpolation function p. O denotes "of the order". Stress convergence may be computed using a similar equation,

$$\text{stress convergence} = O\left(\tfrac{h_2}{h_1}\right)^{p+1-r} , \qquad (3.14)$$

where $r \equiv$ order of derivative,

and the convergence of stress is controlled by both the order of the interpolation polynomial and the highest order of the derivative(s) used to define the strain. It should be noted that the stress is not expected to converge as quickly as the displacement for a given degree of interpolation. The practical application is that if one is analysing a structure for maximum displacement, a somewhat coarse mesh might be sufficient, whereas a more refined mesh would be required for accurate stress analysis (Lepi 1998).

3.4.2   Comparison

The typical component of the basic transmission unit is a pair of meshing gears. A series of FEM (2D) calculations on a pair of meshing gears is presented here. The results were used to examine the actual convergence rate of the displacement (angular rotation) and the stresses (SMX, $\sigma_{1\max}$). Figure 3.4.1 shows a pair of standard involute spur gears in contact at the pitch point (material: T6 aluminium). While one of the gears is restrained at the hub, the torque load T is applied on the other gear's hub. The displacement θ on the pinion hub has a unique value because a coupled equation was used to enable the hub to be rigid in rotation.
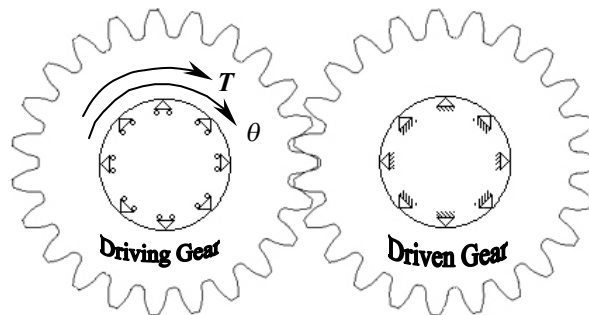
Figure 3.4. 1   A pair of meshing gears.

Two critical stresses (SMX, $\sigma_{1\max}$) were chosen to be calculated, as follows,

- SMX --- the maximum von Mises stress should occur at the contact point. The von Mises criterion is best applied (and best understood) when used to predict the onset of yielding in a structure where the material behaves in a ductile fashion.

- $\sigma_{1\max}(S_{1\max})$ --- the maximum (principal) tensile stress that is near the root of the teeth. The maximum principal stress theory suggests that the largest principal tensile stress is responsible for cleavage associated with (brittle) fracture.

Table 3.1 shows the results from an initial coarse mesh which has only 1802 nodes, with the refinement gradually increasing the mesh density until the final model (Model 18) has reached 17466 nodes. The displacement and stress values with their positions for each refinement are also listed.

Free mesh refine at contact tooth	Nodes No.	UY(θ *R) mm$\times 10^{-3}$	SMX at Contact (M Pa)	$\sigma_{1\max}$ (M Pa)	$\sigma_{1\max}$ Position
Model1	1802	5.760	51.892	25.767	near root
Model2	2315	5.810	74.592	28.473	near root
Model3	2779	5.954	99.238	30.108	near root
Model4	3392	6.028	143.028	43.667	near contact
Model5	4021	6.106	147.477	34.046	near contact
Model6	4691	6.115	178.136	47.681	near contact
Model7	4986	6.152	177.194	39.344	near contact
Model8	5393	6.207	221.486	51.052	near contact
Model9	6049	6.157	195.002	46.008	near contact
Model10	6385	6.193	207.859	44.708	near contact
Model11	7035	6.240	240.872	55.034	near contact
Model12	7604	6.190	219.308	37.915	near contact
Model13	8241	6.159	231.132	49.985	near contact
Model14	8710	6.194	256.647	34.392	near root
Model15	9417	6.190	236.885	38.184	near contact
Model16	10115	6.170	219.744	37.066	near contact
Model17	12755	6.171	220.416	37.461	near contact
Model18	17466	6.177	250.729	34.763	near root

Table 3.1.   FEA calculation results.

Figure 3.4.2 and 3.4.3 clearly show that when the mesh density is just over 5000 nodes, the displacement has almost certainly converged. The stress at the contact (maximum Van Mises stress) does not appear to have converged even when the mesh density has reached 8000 nodes.
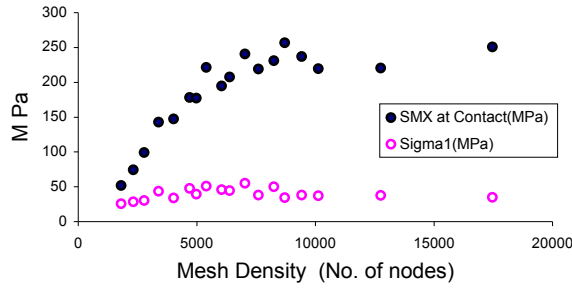
Figure 3.4. 2   The stress convergence
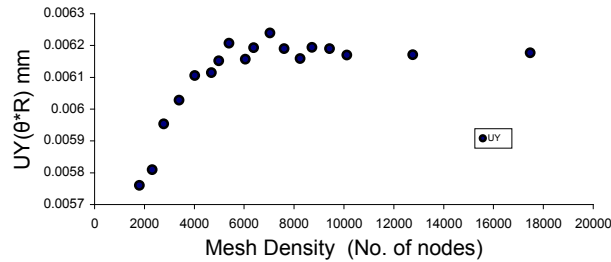
Figure 3.4. 3   The displacement convergence

Note that $\sigma_{1\max}$ reaches its highest value close to the largest displacement value, however, $\sigma_{1\max}$ jumps to the position near the contact area with increasing mesh density at the contact tooth, except when some extra refinement was applied to the tooth root on Model14 and Model 18.   Further calculations were carried out with Model 6, with the refinements applied to the area of the tooth root and the hub.   There were two reasons for the further calculations:

- To verify the position of $\sigma_{1\max}$.

- To check the other influences (other than contact) on the displacement convergence.

The results in Table 3.2 show that a refinement on the tooth root (the main part) and the hub is necessary for determination of the convergence of $\sigma_{1\max}$, but that the relative influence on the displacement convergence is minor.

Refine at roots and hub	Nodes No.	UY(θ *R) mm (R-hub radia)	SMX at Contact (M Pa)	$\sigma_{1\max}$ (M Pa)	$\sigma_{1\max}$ Position
Model6	4691	0.006115	178.136	47.681	Near contact
Model6-1	6049	0.006157	195.771	46.36	Near root
Model6-2	6408	0.006157	195.96	46.569	Near root
Model6-3	6563	0.006156	195.871	46.352	Near root

Table 3.2.   FEA results of further refinement for specify $\sigma_{1\max}$ position.

The primary requirement for building FEA models of meshing gear pairs has been obtained from these results. The model below is one of the examples used in the research for obtaining reliable converged displacement values.
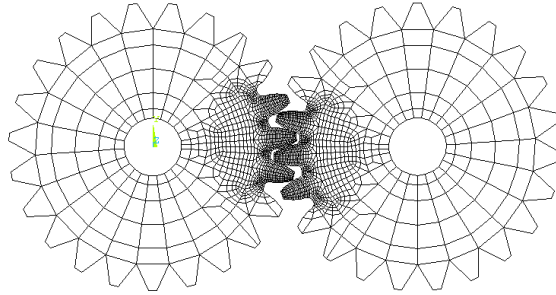
Figure 3.4. 4   Finite element model of a meshing gear pair

Mapped Mesh	Nodes No.	UY (θ *R) mm	SMX at Contact(M Pa)	$\sigma_{1\,max}$ at tooth root(M Pa)
2D-183PlaneStress	7600	0.006216	134.86	34.581

Table 3.3. Data for mapped mesh (Figure 3.4.4)

3.5   Modelling

The most time consuming step of finite element analysis is creating the finite element model. After determining the type of analysis required and the characteristics of the operating environment, a finite element model must be produced with appropriate analysis parameters, such as loads, constraints, element choice and a suitable mesh.

3.5.1   CAD vs. FEA

First of all, the CAD/FEA interoperability has to be considered. Generally, there are three methods:

> 1) The CAD universal file format method.
>
> 2) The "one window away" CAD/FEA method.
>
> 3) The "one window" CAD/FEA method.

The first method has been widely used. It requires the CAD solid model to be exported with a neutral file format, such as IGES, ACIS or Parasolid. The neutral file is then imported into the FEA system for set up and analysis. The major draw back with this method is the loss of CAD geometry data that can happen during the translation of the

model. The second method is used in multi-processor FEA analysis or in the case when a single interface is used for multiple CAD packages.

Nowadays, many FEA vendors build analysis capabilities into the CAD solid modeller. The files no longer need to be translated so that geometry data isn't lost. However, this "one window" CAD/FEA method often encounters operating difficulties that are time consuming to fix or impossible to use for building complex models because the FEA providers often simplify their one-window versions due to space and interface limitations. If the file translator schemes worked, it would be an ideal method for quickly building geometry required for this research. For a reasonably effective analysis, no matter which method above is used, the geometry must be simplified by deleting features (such as keyways away from the area of interest) that will not significantly affect the desired results. This "disfeaturing" process should result in a geometry entity that will define a relatively easy-to solve mathematical model (when subjected to the loading and boundary conditions).

3.5.2   Mesh with high order elements

Once the geometrical model is available, the next step in the analysis process is to create the mesh. The use of an adequate finite element mesh is crucial. An adequate mesh consists in using proper types of elements and applying a quality mesh (no excessive distortion).

Both quadrilateral (2D) and hexahedral (3D) elements are better suited for solid elasticity modelling. They are the most commonly used elements for non-linear analysis. For a given mesh density with high order, the elements create edges that adapt more closely to curved surfaces than similarly sized linear elements.   They also produce better mathematical formulations that result in the element being less sensitive to distortion and poor orientation in the model due to complicated geometry.

However, in the past when contact boundary conditions were present, high-order elements have been avoided for the reason that the mid-side nodes do not behave the same as the

corner nodes. The new 18X series second order elements in ANSYS[®] (since version 5.6), provide even higher accuracy for meshes and are particularly suitable for modelling curved boundaries in contact. They were successfully used in this research. On the down side, high order elements require much greater computational resources because many of the nodal DOF's are wasted, and the problem takes more time to solve. One technique which could be considered to deal with this involves using some linear elements, with far fewer nodal DOF's, in areas of constant stress, then applying the constraint equation on each edge between the high order element and the linear element as shown in Figure 3.5.1.
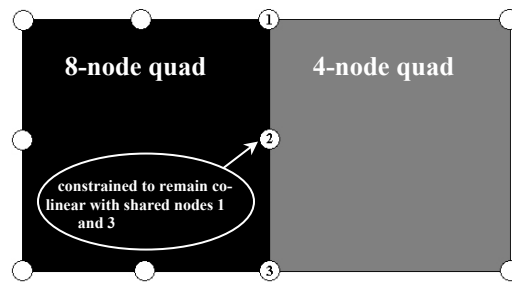
Figure 3.5. 1   Joining an 8-node quadrilateral element to a 4-node element.

In MSC/MARC[®], the "glue" option can be used to automatically apply this type of constraint connection. However, the option of automatic constraint is not available for all FEA packages, especially if the model is to be re-meshed several times. With many thousands of elements, the specification of the constraint equations for each element pair may prove tedious, while at the same time introducing another potential source of error.

For 3D modelling, eighteen strain states are needed to completely define linearly varying strains when polynomial displacement assumptions are used. A 20-node hexahedron can represent all 18 linear strain states, and in addition, 21 quadratic strain states. However, due to the limitations of automatic mesh generation with hexahedron elements in ANSYS[®], especially when the geometry is complex, a high order tetrahedron element with 10 nodes was considered. Despite some disadvantages commonly associated with the 10-node tetrahedral element (Lepi 1998), it at least represents all the 18 strain states, and produces results at least as good as the 8-node hexahedron.

It's important to note that with the p-method, the 10-node tetrahedron forms system matrices with smaller bandwidth than the 20-node hexahedron. This means that with the p-

method, the 10-node tetrahedron provides accuracy comparable to that of the 20-node hexahedron with a faster solution (Niazy 1997).

A good mesh pattern is one that is as coarse as possible on uninteresting areas, yet as fine as necessary for accurate results where it encounters contact or high stresses, (Thilo Trantwein, managing director of ACES Ing GmbH in Stuttgart, Germany, (www.acesgmbh.de)). There are three areas in a gear that have to be meshed with finer elements. The first is near the region of contact where the mesh density in the area should be the highest in the model as has been discussed in 3.4.2. The second area is near the root of the tooth in contact, where the requirement on the mesh density here is at least fine enough to show the correct $\sigma_{1\max}$ in the area. The third area is around the hub where only a minor refined mesh is required. Over a mesh cycle, the contact from one pair of teeth changes to two pairs (or vice-versa), which causes a constraint condition change on the hub. Also, an adequate mesh density is required in the gear body underneath the teeth in contact.

However, to produce an accurate result one also has to consider mesh quality. Using quad mesh well-shaped elements, (no excessive distortion), is essential in mapped mesh situations. Care must be taken when using mesh grading or transition mesh to prevent numerical problems due to placing very stiff elements directly adjacent to very flexible larger ones. The stiffness of an element $\underline{\underline{K}}$ can be expressed as,

$$\underline{\underline{K}} \propto \frac{E}{V}. \tag{3.15}$$

Hence, the stiffness of an element is directly proportional to the elastic modulus and inversely proportional to size. As recommended by Cook (Cook 1989), the element stiffness $\underline{\underline{K}}$ should not change by more than a factor of three across adjacent elements. Under this guideline, the model in Figure 3.5.2 would be considered poor.
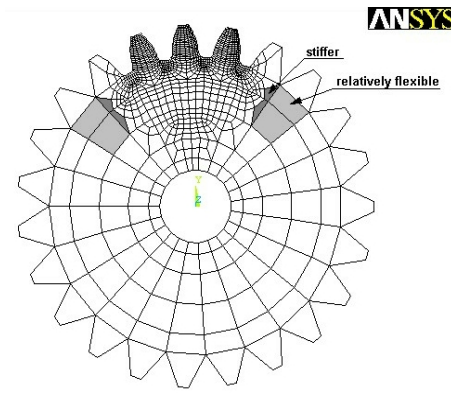
Figure 3.5. 2   Example of poor mesh transition

Furthermore, considering the particular features of this research involving calculations on more than 100 different contact points in a mesh cycle, creating a *well-shaped boundary-aligned* mesh (on the tooth flank face) is vitally important for obtaining quality results. One method for obtaining even higher accuracy results without considering manually created *well-shaped boundary-aligned* mesh is to use the ANSYS[®] built in *smart mesh* capability in contact areas. This can be used to obtain automatic adaptation re-mesh with contact at every point in the mesh cycle, as illustrated in Figure 3.5.3.

3.5.3   Element Distortion

Finite element modelling of gears and gears in mesh with 2D assumptions of plane stress or plane strain is relatively easy. With a few efforts, the requirement for producing all quads well shaped elements with no excess distortion and well shaped-aligned boundary elements in mesh can also be met. Combined with mapped meshing, automatic adaptation re-mesh with contact can produce higher accuracy results for 2D modelling. Figure 3.5.4 displays four of the 2D models used in this research. For transmission error study throughout the mesh cycle, all models can produce acceptable results. For stress analysis specially for finding local detail of the maximum stress in the critical areas, further refinements are required.

The requirement for 3D modelling of meshing gear pairs involves the use of (high order) brick elements in this research. Automatic mesh volumes such as gears in mesh with brick elements are not available currently.   With the available technique, the modelling procedure produces a 2D model then extrudes it into 3D or produces the volume of the gear, then sweeps it with 2D elements. For controlling the 3D mesh pattern, the mapped

43

mesh for the 2D model of the source area of the gear volume can be used. The other controlling factor is in deciding how many divisions for the extrusion or the sweeping. Due to the difficulty in applying different divisions in different areas, the distorted elements can hardly be avoided. Even when building a huge model, there usually are large numbers of distorted elements in the low stress area. So 3D mesh using brick elements is limited with finer mesh. Figure 3.5.5 is an example of mesh adaptation for contact with brick elements.
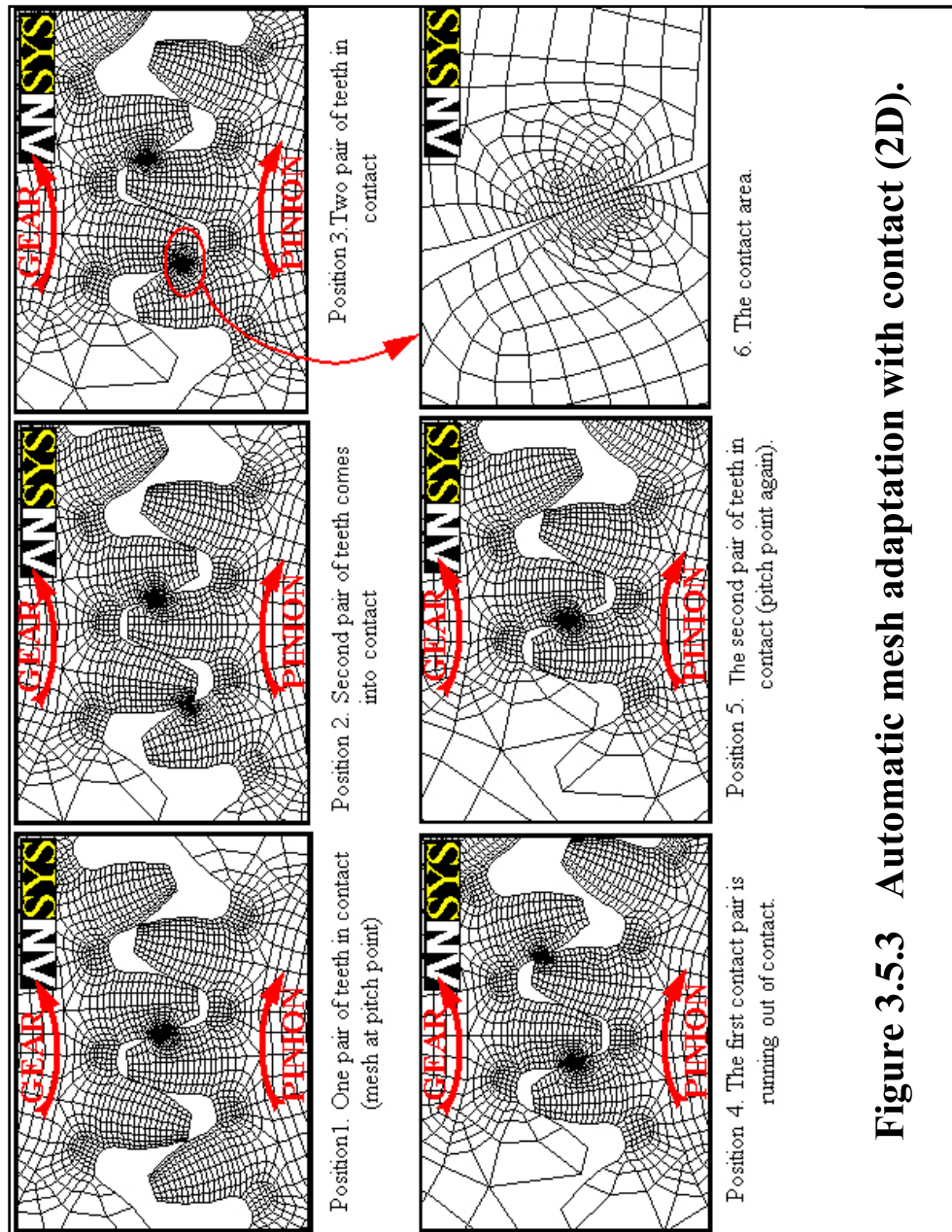
Figure 3.5.3   Automatic mesh adaptation with contact (2D).
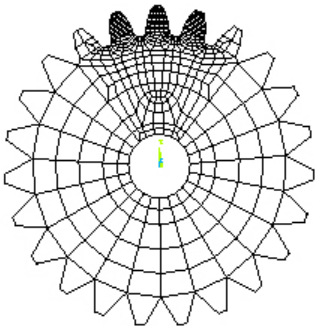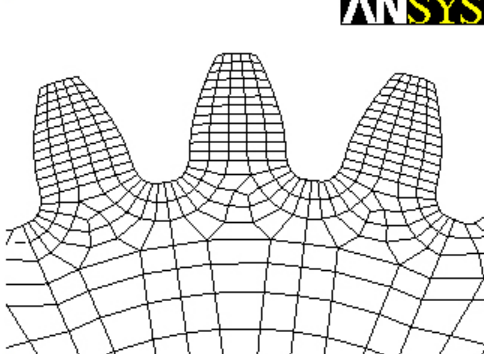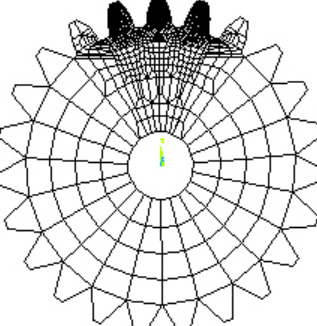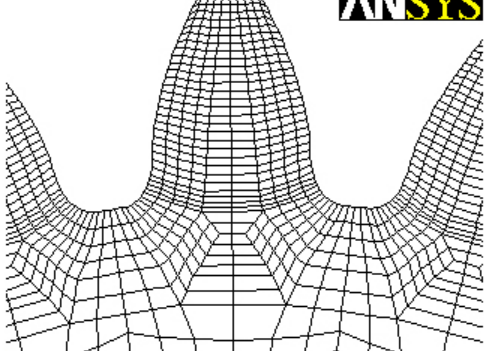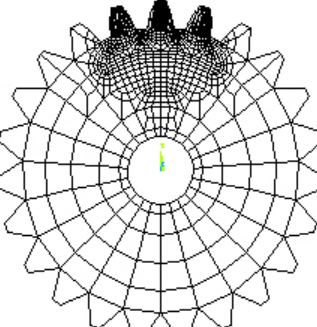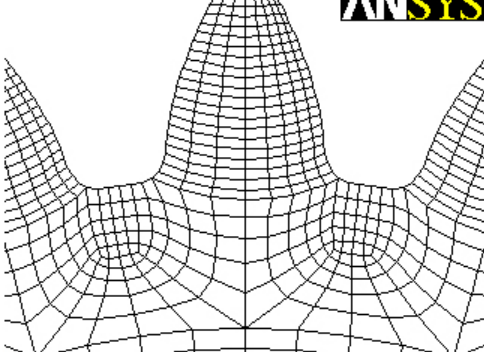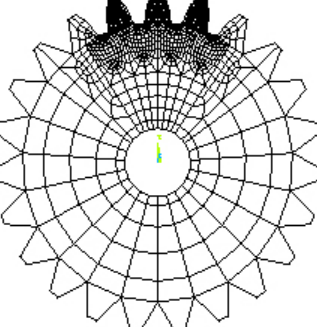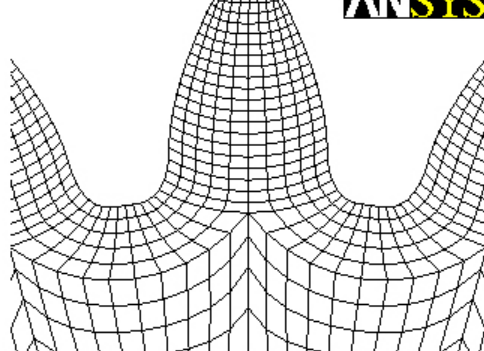
No. of nodes	Models	Details
669		
4850		
3800		
4216		

Figure 3.5. 4 2D mesh patterns

45
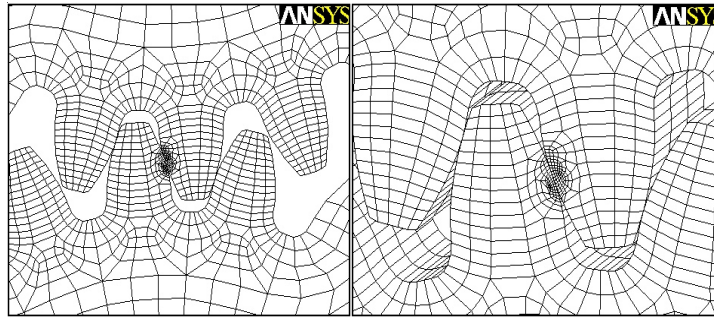
Figure 3.5. 5   Mesh adaptation with contact using brick elements produced by the 2D model extrusion or sweeping the 2D pattern through the volume

The critical stage for building the 3D model above is to decide how many divisions are required for extrusion or sweeping. If not enough divisions are used, distorted elements with large aspect ratios will be present due to the previous 2D mesh adaptation with contact that has produced many small elements in the region near the point of contact. Figure 3.5.6 shows the distorted elements by issuing an element check option in ANSYS[®] when the division is three.
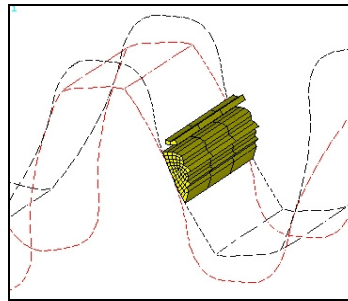
Figure 3.5. 6   Distorted elements on one of the gears.

In this case, the element check option also provides a shape-testing summary as shown in Table 3.4,

<<<<<< SHAPE TESTING SUMMARY >>>>>>				
Element count 4323 SOLID186				
Test	Number tested	Warning count	Error count	Warn+Err %
Aspect Ratio	4323	309	0	7.15%
Parallel Deviation	4323	3	0	0.07%
Maximum Angle	4323	0	0	0.00%
Jacobian Ratio	4323	0	0	0.00%
Warping Factor	4323	0	0	0.00%
Any	4323	309	0	7.15%

Table 3.4.   Elements shape testing summary.

It can be seen that 309 of a total of 4324 elements have exceeded the aspect ratio warning limit and they are all located in the high stress area. The other type of distortion, such as parallel deviation, only occurred in 3 elements and its influence on the accuracy of the FEA solution is considered minor compared with the one of large aspect ratio. The large aspect

ratio can be limited in the high stress area if more divisions are to be used to extrude the 2D into a 3D model, but a very large model may result with lots of distorted elements in the low stress area. Figure 3.5.7 shows the extruded 3D model with 13 divisions.
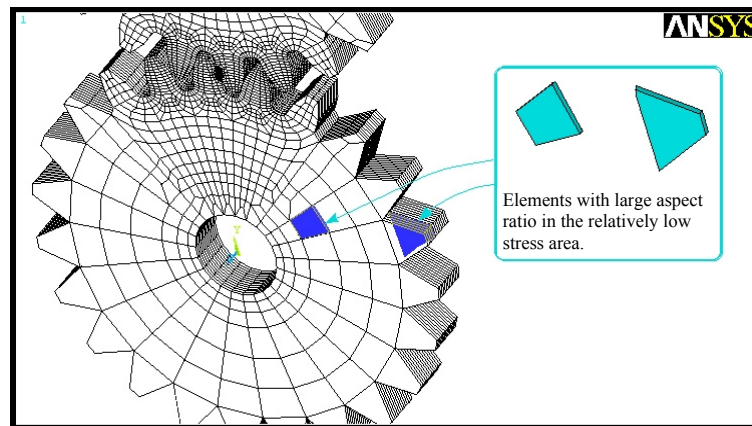
Figure 3.5. 7   Thirteen division model containing 89095 nodes, showing distorted elements in the low stress area.

The model in Figure 3.5.7 is a very large model for FE analysis using existing PC hardware. To solve the model in 10 sub steps with a PC PIII − 800 MHz with 1GB Ram memory, the total run time could be 100 hr+. An alternative way to build the 3D model is to apply different divisions in different areas as shown in Figure 3.5.8.
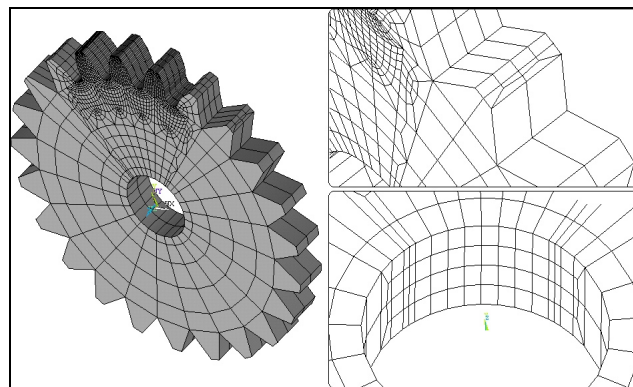
Figure 3.5. 8   Illustration of transition of the divisions.

The figure illustrates the number of divisions changing from 2 to 4. The result is a reduced element distortion in both low and high stress areas, and a reduced model size. Applying the transition of the division involves combining the extrusion and the swept volume. The model seems to produce acceptable solutions for displacements. However, when checking elements, it some times gave messages such as,

*** WARNING ***   CP= 17.806   TIME= 00:42:26
ELEMENT 1079071637 DOES NOT EXIST.

The warning means that somewhere in the model, "ghost" elements exist, containing something unpredictable. Further debugging efforts are then needed.

3D modelling of gears or gears in mesh using brick elements has been discussed as above, where its required to eliminate the distorted elements in high stress areas so that reliable finite element analysis data can be obtained from the model. Meanwhile one should beware not to produce a very large model that requires enormous computer time for solution. Full 3D modelling of gears or gears in mesh is required in most general cases such as when shafts and bearings are included in the model, also in the cases of crowned flank face gears and non-through cracked teeth and many other situations that have to be modelled in 3D.

In a special case, such as in the modelling of two standard involute gears in mesh, when ignoring the hub centre movement of each gears, the 3D modelling can be applied on one half of the volumes that are separated by the symmetry plane, as shown in Figure 3.5.9.
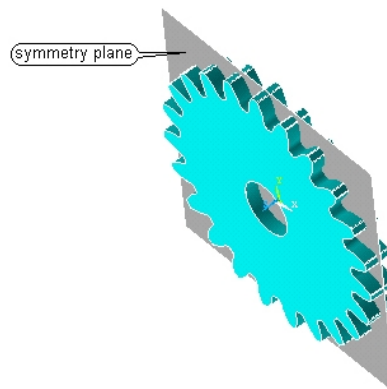
Figure 3.5. 9   The symmetry plane of a gear.

3.6   Verifying Results

As a general rule, post analysis checks, such as reasonable displacements, animation and reaction forces summing to give the applied load, and evidence supports such as closed-form calculation and experimental testing should always be used to judge if the FEA results correlate with the response of the physical structure.

A closed-form calculation (Jia 2001) has shown that it is particularly useful for verifying the results in this research, and experimental testing will be presented in a later chapter.

CHAPTER 4

INVESTIGATION INTO THE STIFFNESS PROPERTY

4.1   INTRODUCTION

This chapter introduces the involute and fillet tooth profile equations that are used to generate the profile of the teeth by an APDL (*ANSYS Parametric Design Language*) program, so that the "one window" CAD/FEA method could be applied to avoid the possible geometry data loss.   The stiffness of the basic transmission unit (except the bearings) was then studied where, in particular, the variations of the distortion field in a meshing gear pair were analysed with various boundary conditions.   The ratio of local deformation was also defined and the characteristics of the local contact deformation on the global deformation, related to the transmission error.

4.2   The Use of a Specified Coordinate System

When the need arises for imposing loads or displacement boundary conditions in a direction that is not aligned with the global coordinate system, a specified coordinate system, local coordinate system or working plane, may be defined at a desired location. The nodal coordinate system, which by default is parallel to the global Cartesian coordinate system in ANSYS®, of selected node(s) can be rotated into the specified coordinate system. The other way to rotate the nodal coordinate system may be by using known rotation angles or direction cosine components.   Input data that may be interpreted in the rotated nodal coordinate system includes component values of the following,

- Degree of freedom constraints,
- Forces,
- Master DOF,
- Coupled nodes,

and
- Constraint equations.

As shown in Figure 4.2.1, the nodal coordinate system of the nodes on the hub were rotated into the working plane, defined as cylindrical, which has been moved to the centre of the hub. The applied boundary conditions (WX_i=0 or r_i=0) constrain the gear hub radially, allowing only free rotation. The restrained nodes also couple with the master node, which means that any constrained nodes would have the same value on WY (or θ) if there were deformation or rigid body motion of the gear. Input torque can be expressed as the sum of the applied nodal forces at radius r, where T is the input torque load, n is the total number of constrained nodes, f_i is the tangential nodal force (usually f_i = f, f is constant value) and r is the hub radius.

$$T = \sum_{i=1}^{n} f_i \cdot r,\qquad\qquad (4.1)$$
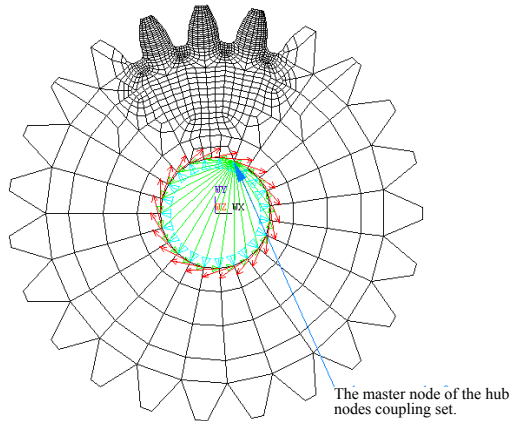
Figure 4.2. 1   Load, boundary conditions and coupled set nodes on the gear hub.

For clarity of the loads and boundary conditions in Figure 4.2.1, only the corner nodes are selected and they are symmetrical to the hub. In the case of problems related to coupled field analysis, for example heat transfer, loads should not be applied on mid-side nodes. However, in the proposed research, for computing global displacements, particularly with non-linear contact, loads are applied on as many hub nodes as possible, including mid-side nodes while they are necessarily kept symmetrical to the hub. Otherwise, a small point

load could cause a very localised deformation that would not correlate with global measurements. Figure 4.2.2 shows an example of a poorly loaded case.
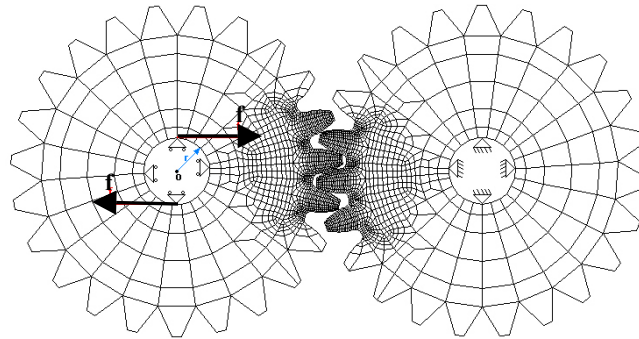
Figure 4.2. 2   Poorly loaded model.

4.3   Tooth Profile Generation

The finite element model of spur gears in mesh developed in this thesis was initially based upon test gears that have been used since an experimental investigation by Sirichai (Sirichai 1996), and the test gear parameters are shown in Table 4.1. The test gears have a ratio of 1:1. The involute and fillet tooth profile equations used in the finite element model have been introduced by references (Litvin 1989; Townsend 1991; Kuang 1992). For most of the other gears, profile equations can be found in references (Litvin 1993; Litvin 1993; Zhang 1994; Litvin 1995; Litvin 1995; Litvin 1996; Litvin 1996; Seol 1996; Seol 1996; Litvin 1997; Donno 1998; Feng 1998; Litvin 1998; Litvin 1998; Litvin 1998). This section shows some of the basic equations used for calculating gear tooth involute profile coordinates and gear tooth fillet coordinates. Alternative ways (programs) for generating the involute and fillet tooth profile are also given.

Gear type -------------------------------- Standard involute, full-depth teeth
Material---Aluminum
Modulus of elasticity, E--69
Poisson's ratio, ν-- 0
Friction coefficient-- 0
Number of teeth N --- 23
Pressure angle --20
Module Mn -- 6
Pressure angle, deg ---20
Addendum, a (mm) ---Mn
Dedendum, b (mm) --- 1
Face width, mm (in.) ---15
Theoretical contact ratio --- 1
Theoretical angle of meshing cycle---24

Table 4.1.   Test Gear Parameters

51

The following algorithm calculates the coordinates of an involute and fillet tooth profile based on the tooth profile generating method introduced by (Litvin 1989; Kuang 1992). The following equations for the generated involute curve AB and fillet curve BC tooth profile as shown in Figure 4.3.1 are valid for gears conjugate to the counterpart basic rack where,

- M_n is metric normal module, mm (for spur gear expressed M)
- N is number of teeth
- Addendum, $a = \alpha M_n$ (usually $\alpha = 1.0$)
- Dedendum, $b = \beta M_n$ (usually $\beta = 1.25$)
- Tip radius, $r_c = \gamma M_n$ (usually $\gamma = 0.25$)
- ϕ is pressure angle
- Addendum modification coefficient $X = e/M_n$
- e is cutter offset
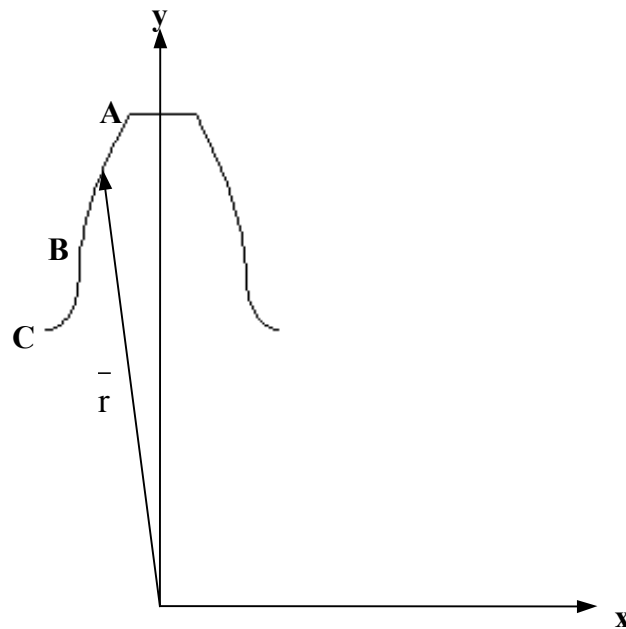
Figure 4.3. 1   Coordinate system for generating involute and fillet tooth profiles.

The parametric representation coordinates of the involute profile (curve AB) is,

$$\bar{r}(\theta) = \begin{Bmatrix} x(\theta) \\ y(\theta) \end{Bmatrix},$$ (4.1)

52

where coordinates of the involute curve are given by equation (4.2) and (4.3),

$$x(\theta) = \frac{N \cdot Mn}{2} \left\{ \sin(\theta) - \left[\left(\theta + \frac{\pi}{2N} \right) \cos\phi + \frac{2X}{N} \sin\phi \right] \cos(\theta + \phi) \right\}, \tag{4.2}$$

and

$$y(\theta) = \frac{N \cdot Mn}{2} \left\{ \cos(\theta) + \left[\left(\theta + \frac{\pi}{2N} \right) \cos\phi + \frac{2X}{N} \sin\phi \right] \sin(\theta + \phi) \right\}. \tag{4.3}$$

The parameter θ, in radians, of the involute curve is limited to the following range,

$$\theta_{min} \le \theta \le \theta_{max} \tag{4.4}$$

where the parameters θ_{min} and θ_{max} of the involute curve are given by equation (4.5) and (4.6),

$$\theta_{min} = \frac{2}{N} \left[U + (V + X) \cot\phi \right], \tag{4.5}$$

and

$$\theta_{max} = \frac{1}{N \cos\phi} \sqrt{(2 + N + 2X)^2 - (N \cos\phi)^2} - \left(1 + \frac{2X}{N} \right) \tan\phi - \frac{\pi}{2N}. \tag{4.6}$$

The parameters U and V of the involute curve are given by,

$$U = -\left[\frac{\pi}{4} + (\alpha - \gamma) \tan\phi + \frac{\gamma}{\cos\phi} \right], \tag{4.7}$$

and

$$V = \gamma - \alpha. \tag{4.8}$$

The parametric representation coordinates of the fillet profile (curve BC) is given by

$$\bar{r}(\theta) = \begin{Bmatrix} x(\theta) \\ y(\theta) \end{Bmatrix}, \tag{4.9}$$

where coordinates of the fillet curve are given by equation (4.10) and (4.11),

$$x(\theta) = Mn \cdot (P\cos\theta + Q\sin\theta), \tag{4.10}$$

and

$$y(\theta) = Mn \cdot (-P\sin\theta + Q\cos\theta). \tag{4.11}$$

The parameter θ of the fillet curve is limited to the following range,

$$\theta_{min} \le \theta \le \theta_{max}, \tag{4.12}$$

where the parameters θ_{min} and θ_{max} of the fillet curve are given by equation (4.13) and (4.14),

$$\theta_{min} = \frac{2}{N}[U + (V + X)\cot\phi], \tag{4.13}$$

and

$$\theta_{max} = \frac{2U}{N}. \tag{4.14}$$

The parameters P, Q, and L of the fillet curve are given by,

$$P = \frac{\gamma}{L} + \left(U - \frac{N\theta}{2}\right), \tag{4.15}$$

$$Q = \frac{2\gamma}{L} \cdot \left(\frac{V + X}{2U - N\theta}\right) + V + \frac{N}{2} + X, \tag{4.16}$$

and

$$L = \sqrt{1 + 4\left(\frac{V + X}{2U - N\theta}\right)^2}. \tag{4.17}$$

As a general method, an AutoLisp, (AUTODESK. 1997), AutoCAD programming language for generating the points of an involute and fillet tooth profile is given in Appendix A. It can be copied as plain text then read by AutoCAD to create a series of points of the curve. Once the profile or entire geometry is created then it can be transferred to a FEA program.

The ideal method for this research is the "one window" CAD/FEA method. A program writen with APDL (*ANSYS Parametric Design Language*) for generating the points of the curve directly in ANSYS® is rather simple. In this research the program is developed to

```
/GST,ON
/PREP7
pi=3.1415926                                              !start input data
x1=0
fi=pi/9
g1=0.25
a1=1
n=23
m=6
nu=200                                                    !200 points in curve AB
nu2=120                                                   !120 points in curve BC
u=-(pi/4+(a1-g1)*tan(fi)+g1/cos(fi))                      !user can decide any number in each curve
v=g1-a1                                                   !u, v are parameter
thmin=(u+(v+x1)/tan(fi))*2/n
thmax=((2+n+2*x1)**2-(n*cos(fi))**2)**0.5/(n*cos(fi))-(1+2*x1/n)*tan(fi)-
pi/(2*n)                                                  !th stand for theta- θ
inc=(thmax-thmin)/nu
*do,i,1,(nu+1)                                            !inc-the angel increment
th=thmin+inc*(i-1)                                        !start a loop to produce points for AB
x=(n*m/2)*(sin(th)-((th+pi/(2*n))*cos(fi)+(2*x1*sin(fi))/n)*cos(th+fi))
y=(n*m/2)*(cos(th)+((th+pi/(2*n))*cos(fi)+(2*x1*sin(fi))/n)*sin(th+fi))
k, ,x,y,,
*enddo
thmax2=2*u/n
inc=abs(thmax2-thmin)/nu2                                 !thmin2=thmin
*do,i,1,(nu2+1)
th=thmin+inc*(i-1)                                        !start loop to produce points for BC
labc=(1+4*(((v+x1)/(2*u-n*th))**2))**0.5
pq=(g1/labc)+(u-n*th/2)                                   !labc, pq and qp are parameter L, P and Q
qp=2*(g1/labc)*(v+x1)/(2*u-n*th)+v+(n/2)+x1
x=m*(pq*cos(th)+qp*sin(th))
y=m*(-pq*sin(th)+qp*cos(th))
k, ,x,y,,
*enddo
finish
```

produce splines through the points to create the geometry area as a 2D solid, as shown in
Table 4.2.

<div align="center">Table 4.2.   APDL program for producing involute coordinates.</div>

4.4   Gear Body

Most of the previously published finite element work with gear models has involved only
partial tooth models. In an investigation of gear transmission errors using factors such as
variation combined torsional mash stiffness, the whole body of the gear in mesh must be
modelled. Sirichai (Sirichai 1999) developed the concept from the performance of the
contact element point of view. However, regardless of the local deformation, the effect that
gear body flexibility has on the torsional stiffness has to be studied. The results in this
section will show that the torsional stiffness varies with the gear body due to different
constraints on the dedendum circle. The influences of the gear body on the total torsional
stiffness were normally ignored by partial tooth models. The gear body is taken from the
dedendum circle of the gear, as shown in figure 4.4.1.
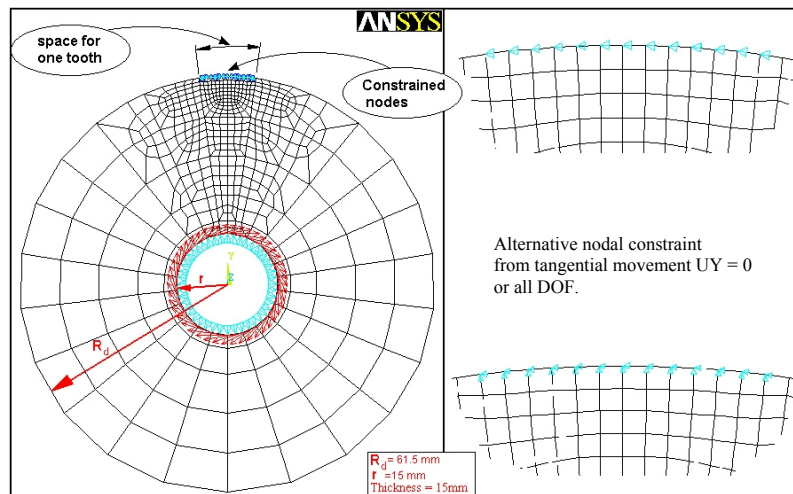
Figure 4.4. 1   The model of the gear body with its load and boundary conditions.

As shown, the nodes on the hub were constrained from radial movements. The model used a coupled set of nodes and equivalent nodal forces were applied.   The constrained nodes on the outer circle are shown in Figure 4.4.1, where they are alternatively constrained from tangential movement only (UY=0, when the coordinate system is cylindrical), or all DOF. The FEA results for the stiffness under the application of a torque load are given as shown in Figure 4.4.2.
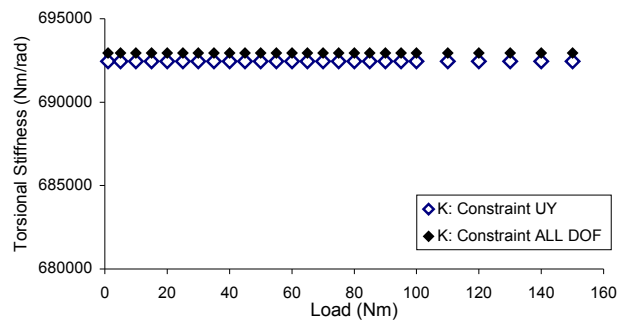
Figure 4.4. 2   The variation of the stiffness caused by type of constraint.

The results show a difference in the torsional stiffness with changing constraint from all DOF to only UY, where the stiffness decreased from 692946.03 Nm/rad to 692452 Nm/rad, an amount of 494.08 Nm/rad. This difference can be ignored considering the percentage difference is only 0.07%.   Further investigation of the model involved extending the constraint on the outer circle from one tooth space to two teeth space considering nodes constrained from tangential movement that would be allowed to rotate about the tooth root if the tooth was present. The model has been re-meshed and the details are given in the following figure.

56
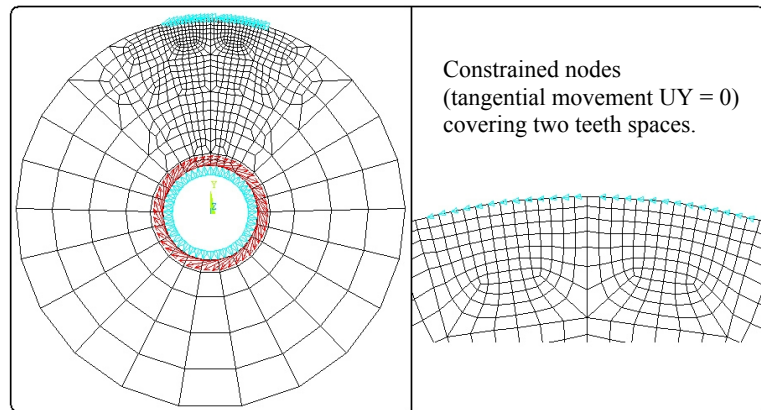
Figure 4.4. 3   The re-meshed model showing constraints over two teeth space.

The torsional stiffness, as shown from the previous calculation, can be obtained with a series of input torque loads. The results can be compared as shown in Figure 4.4.4.
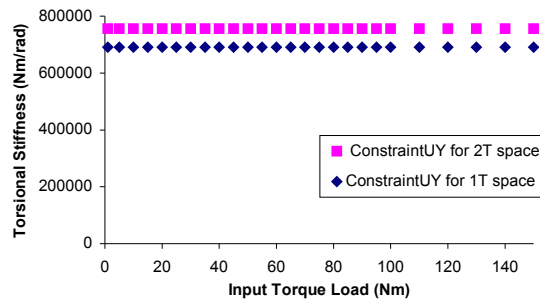
Figure 4.4. 4   The variation of the stiffness caused by increasing the constraint space.

The torsional stiffness was calculated to reach 755709.74 Nm/rad with the two teeth space constraint, which is 63257.74 Nm/rad higher than the stiffness obtained with one tooth space constraint. The torsional stiffness has thus increased by 8.6%. Such a difference for partial tooth models is very large and cannot be ignored. To ensure the correct modelling, this shows that the whole body of the gears in mesh must be modelled.

4.5   The Variations of Distortion Field in the Meshing Gears

For a constant input load, the distortion field in the gear was found to change with meshing position. The significant change occurs when the meshing of the teeth changes from the single pair to double pair in contact and vice-versa if the gears are perfect. From FEA results, the von Mises stress in the gear can be plotted, which reveals the distortion field as

the von Mises stress computes the magnitude of stress that tends to distort a body, as given below,

$$\sigma_{mises} = \sqrt{\frac{1}{2}\left[\left(\sigma_{xx} - \sigma_{yy}\right)^2 + \left(\sigma_{yy} - \sigma_{zz}\right)^2 + \left(\sigma_{zz} - \sigma_{xx}\right)^2\right] + 3\left(\sigma_{xy}^2 + \sigma_{yz}^2 + \sigma_{zx}^2\right)}. \qquad (4.18)$$

It should be noted that the von Mises stress is always positive, since distortion is considered neither positive nor negative. The following Figure 4.5.1 and 4.5.2 were obtained from the FEA results of a 2D plane stress model and a 3D model. It can be seen that the von Mises stress field in 2D and 3D models are different in extent in both figures. The 3D element model can represent all 18 linear strain states, which meets the requirement for completely defining the linear strain variations when polynomial displacement assumptions are used. So, when predicting the von Mises stress field, a better global response was obtained with the 3D model.
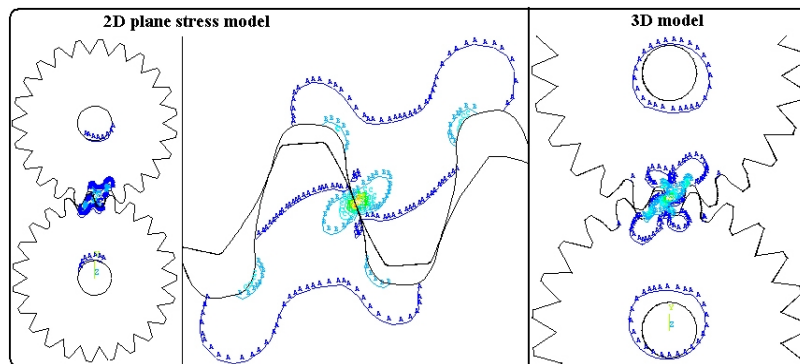
Figure 4.5. 1   The von Mises stress field for single pair of teeth in contact at the pitch point.
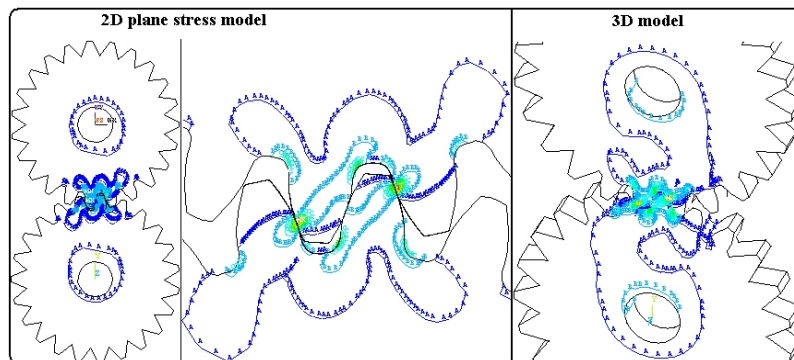
Figure 4.5. 2   The von Mises stress field for double pair of teeth in contact (midpoint).

It has been noted, in both 2D and 3D models, that one of the major differences between the case of Figure 4.5.1 and Figure 4.5.2 is that the von Mises stress field changes dramatically in the area around the hub. These changes can be further confirmed by the plots of the load-reaction forces of the models from the FEA solutions, as shown in the Figure 4.5.3,

58
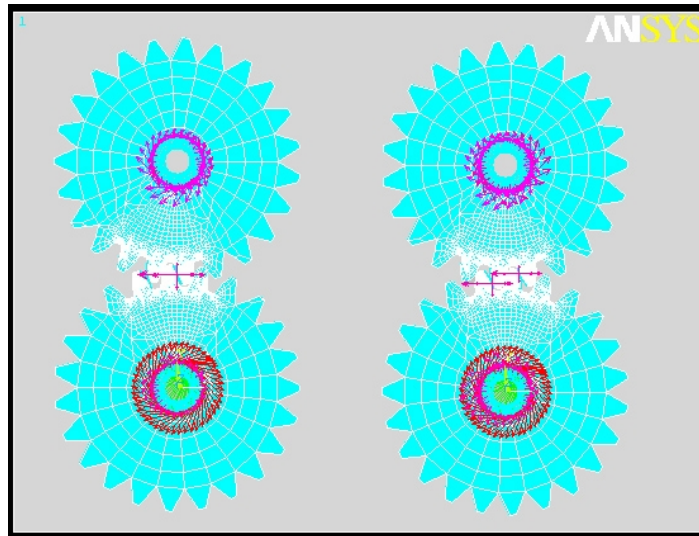
Figure 4.5. 3   The load reaction forces for one tooth and two teeth in contact.

The reaction forces around the hub tend to be even when two pairs of teeth are in contact, and the even loads and boundary conditions around the hubs are believed to be the main reason. In application, a single keyway is often used to transfer the torque, as shown in Figure 4.5.4,
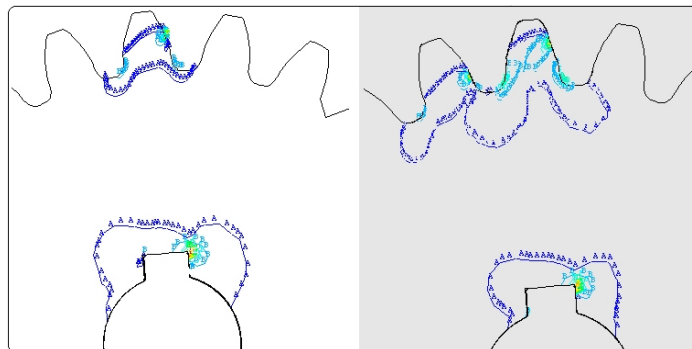
Figure 4.5. 4   The distortion field for one tooth and two teeth in contact.

In this case, the von Mises stress field around the hub has only minor changes when the contact teeth change from one pair to two pairs in mesh.

4.6   Shaft

The shaft is an important component in the gear transmission system. In most cases, the torsional stiffness of the shaft is lower than the stiffness of the gears. In the case of uneven input torque load, the shaft could contribute the major part of the system transmission error

(or total TE). This research has concentrated on the study of the shaft under the steady input torque load. The study is trying to find out the properties of the components such as stresses and strains with varying boundary conditions. The basic FEA model of a shaft is shown as in Figure 4.6.1.
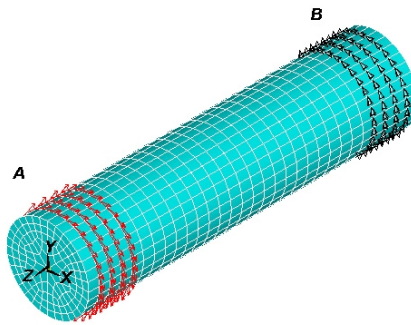
Figure 4.6. 1   The basic FEA model of a shaft.

The considered boundary conditions are:

- Coupling those nodes in rotation at input end A while applying the equivalent tangential nodal forces or without the nodes coupling.

- Tangential constraints at output end B can be applied on those nodes that form a full circle as shown in the Figure 4.6.1, or applied on part of those nodes as shown in Figure 4.6.2,
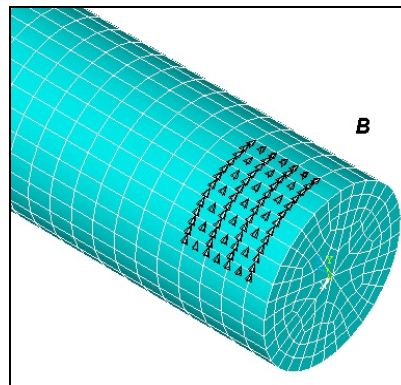
Figure 4.6. 2   The partial constraints at output end B.

According to the boundary conditions, the FEA model of the shaft was calculated with four cases as shown in Figure 4.6.3. So far, it has been found that a minor elastic strain on the surface of the shaft changes with the varying boundary conditions at output end B. This indicates that the gear mesh conditions could be monitored by the measurement from a high order property such as strain from the shaft. A related example will be discussed in more detail in a later chapter.
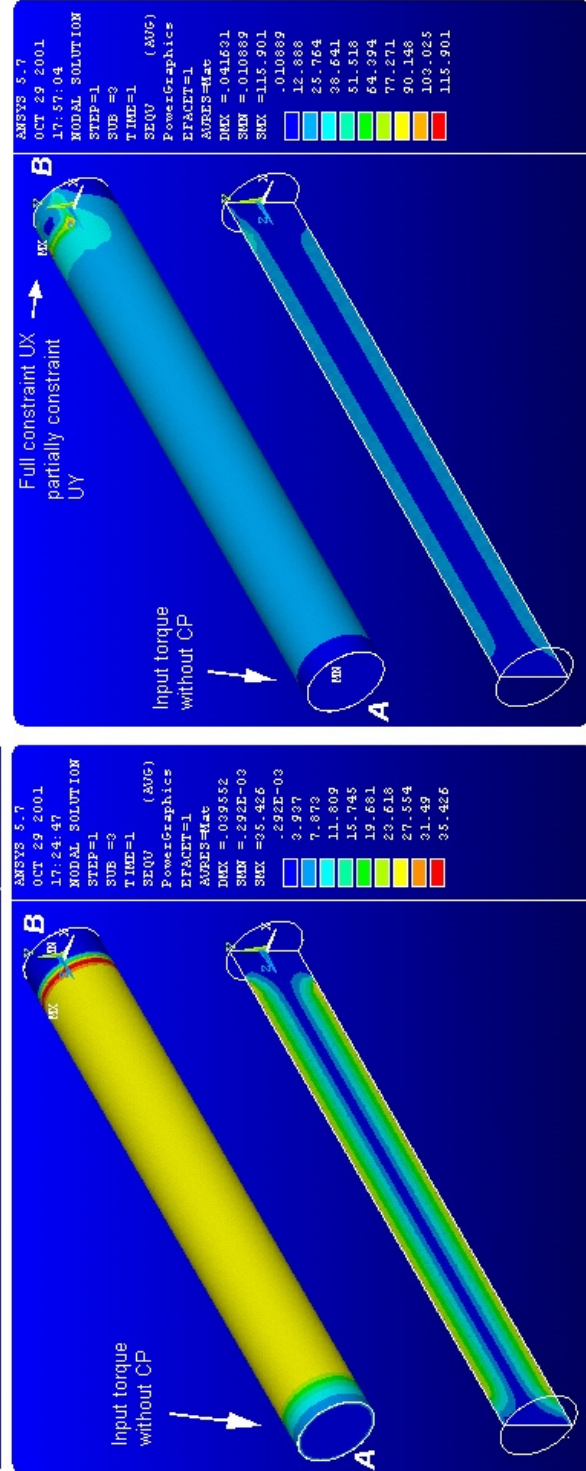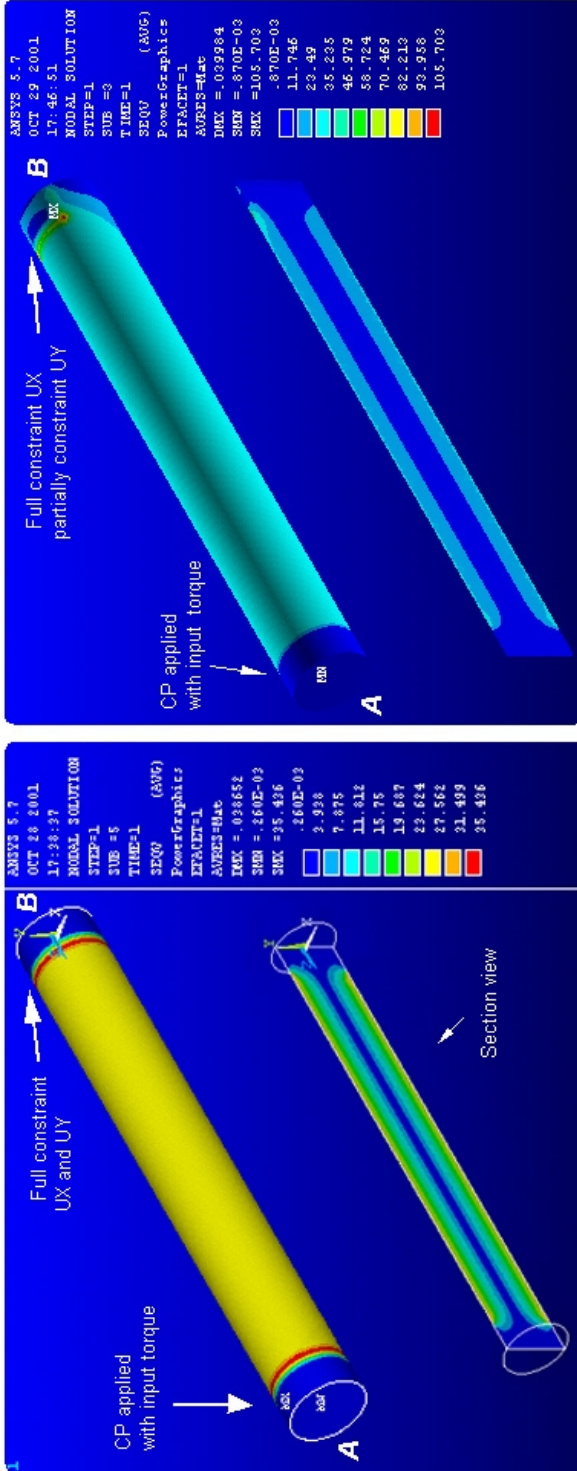
Figure 4.6.3

The von Mises stress field in the shaft under 4 types of boundary conditions.

*The coordinate system is cylindrical.

61

4.7   Ratio of Local Deformation

The ratio of local deformation can be defined as,

$$R_{T,ANG} = \theta_c / \theta .$$ (4.19)

where θ is the total angular rotation of the input gear hub while the output gear has been fully constrained at its hub where both input and output gears are flexible. θ_c represents the angular rotation of the input gear hub which is only due to the local contact deformation and sliding from the contact tooth. The subscripts T and ANG denote the input torque and mesh position respectively. For example, with the test gear in this research (Table 4.1), ANG = $0°$ is the meshing gear pair in the position where the contact involves one pair of teeth and the contact point is at the pitch point. When the mesh position is in the middle of the zone with two pair of teeth in contact, ANG = $7.83°$. Figure 4.5.3 has shown the mesh positions and the model used for the determination of the value of θ. To determine the value of θ_c at the position ANG = $0°$, the FEA model as shown in Figure 4.7.1 has been used.
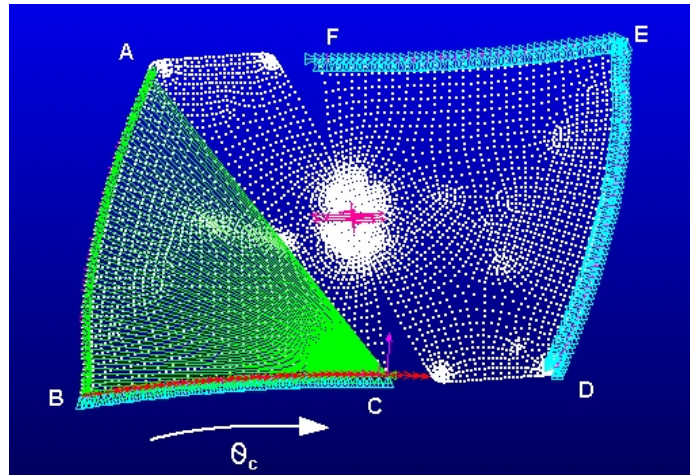
Figure 4.7. 1   The FE model for evaluation of the effect of the local deformation.

As shown in Figure 4.7.1, the nodes attached to the edge DEF were constrained in all DOF, while the nodes attached to the edge BC were constrained radially so that the tooth is able to rotate about the hub centre. Equivalent tangential nodal forces have been applied on those nodes that attach to the edge BC, while those nodes attached to the edge ABC were coupled together in rotation about the hub centre as the tooth's shear and bending displacements have to be limited. At the mesh position ANG = $7.83°$ the model for evaluation of θ_c was extending to two pair of teeth in contact, as shown in Figure 4.7.2,
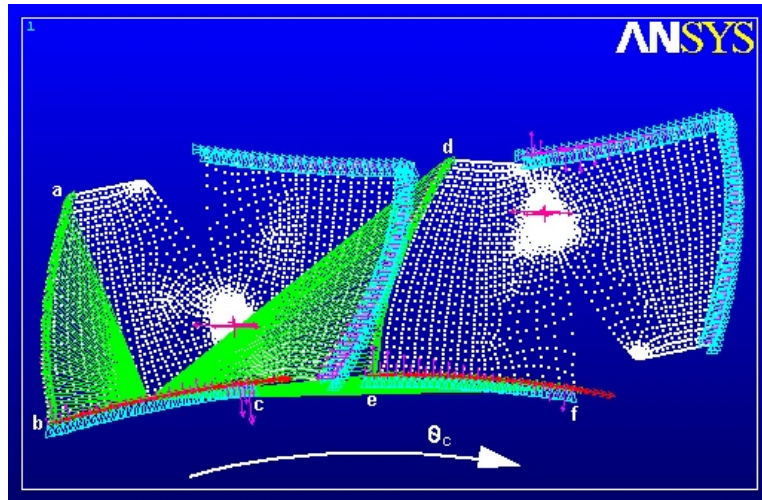
Figure 4.7. 2   The extended FE model for evaluation of the effect of the local deformation.

The procedures for building this model are basically the same as for the previous one. It can be seen that the nodes attached to the edge of **abc** and **def** remain as one node coupling set. So, for the input load T = 76.2 Nm, the FEA results can be given as below,

$$R_{76.2,0^\circ} = 25\% \text{ and } R_{76.2,7.83^\circ} = 16.7\%.$$

The results have shown that the effects of the local deformation to the total angular rotation θ are significantly different for the single pair and double pair of teeth in contact.

In the position ANG = 0°, because the contact is at the pitch point, theoretically there is no sliding between the contact teeth, therefore θ_c and θ can be considered as pure elastic deformations. $R_{76.2,0^\circ}$ is very close to the particular value of 25% which Coy and Chao (Coy 1982) obtained from a partial tooth model as the ratio of total pure elastic deformation. However, when the contact is not at the pitch point, both θ_c and θ contain elastic deformation and rigid body motion. From another point of view, once the sliding in the contact cannot be ignored, both θ_c and θ will not be considered as pure elastic deformation. So, the effects of local deformation as the ratio $R_{T,ANG}$ has to be studied in the entire mesh cycle, the details of which will be discussed in Chapter 6.

In a mesh position, the ratio $R_{T,ANG}$ also changes with the changing of the input torque load, because the contact area varies with any variation of the input torque load. A series

of calculations were taken with the model as shown in Figure 4.7.1 for various input torque loads from 5Nm to 150Nm, with the major load increment of 15Nm. With the contact area increasing as shown in Figure 4.7.3, the ratio $R_{T,ANG}$ decreases from 27.2% to 24.3% as shown in Figure 4.7.4.

Input torque 5Nm   Input torque 150Nm
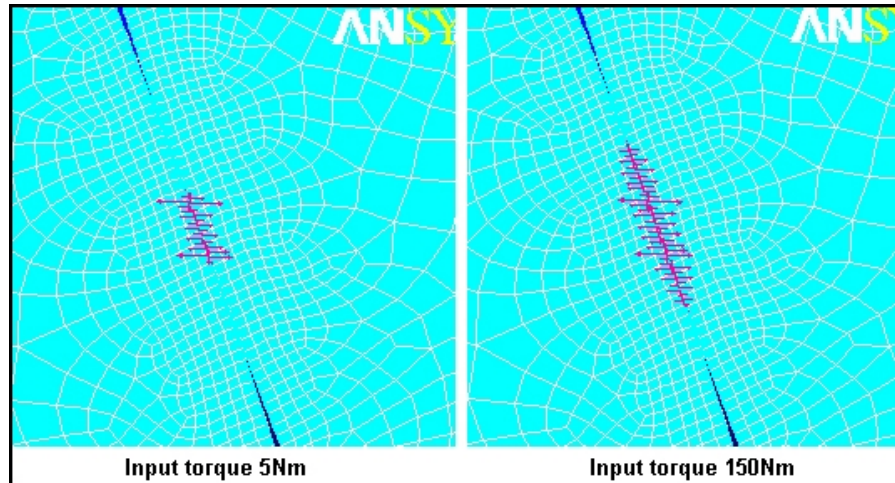
Figure 4.7. 3   The contact areas shown by the reaction forces.
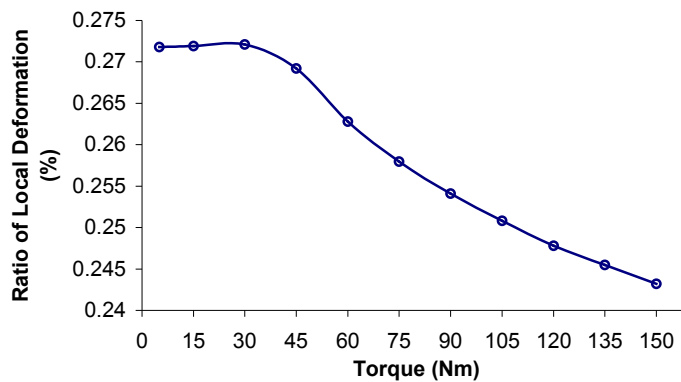
Figure 4.7. 4 $R_{T,ANG}$ as a function of input torque at the pitch point.

The difference of $R_{T,ANG}$ inside the input torque loads was 2.9% with the mesh position in the pitch point. This difference would be smaller if the mesh position were inside the double pair zone.

Finally, it has to be mentioned that the FE models for evaluation of the ratio $R_{T,ANG}$ appear to be suitable for the test gears in this research, and that the ratio should also depend on the thickness of the gear (or the back up ratio) as well as the material of the gear.

CHAPTER 5

PLANE STRESS VERSUS PLANE STRAIN

5.1   INTRODUCTION

In general, when a gear is subject to a transmitted load, the stress conditions near the areas of contact and the tooth root, are neither plane stress nor plane strain, but are three-dimensional. However, most previous FEA models on standard involute gears reduce the problems to two dimensions and many of them provide acceptable approximations. In two-dimensional models, at least one of the principal stresses or strains is assumed to be zero, and the model is either plane stress or plane strain respectively. Examples of models based on plane stress assumptions include (Muthukumar 1987; Lewicki 1997; Arafa 1999), and some based on plane strain elements include (Kuang 1992; Filiz 1995; Sirichai 1997; Sirichai 1999). It should be noted that most of the models didn't have significant differences in geometry. So the question remains as to why one would use a plane stress or a plane strain assumption. There appear to be no obvious criteria for choosing either approach for 2D gear modelling. On the other hand, as a general guide which is based on elasticity theory (Arthur 1987; Richards 2001), for FE modelling of a thin plate with in-plane loads and boundary conditions, the plane stress assumption should be used regardless of whether the solutions are for displacements or for stress. Once again questions are raised as to what extent the special structure (a thin gear) will produce results with similar

errors to that of the thin plate when plane stress assumptions are used. For gears subject to contact, fracture and other situations, it is not known if the plane stress or the plane strain assumption is the most appropriate.

The understanding of these issues is vitally important for ongoing gear transmission error studies and other gear studies too, so they are the major research objectives discussed in this chapter.

5.2   Stiffness

One of the aims of this research was to try to find out the effect of changing geometry (thickness) on the variations of the stiffness in different models (three cases). The first model was a simple disk as shown in Figure 4.4.1. Twelve different thicknesses varying from 5mm to 300mm were considered. For each disk thickness, the various loads including 10, 30, 50, 70, 90, 110 and 130 Nm were applied and for each load, the result of torsional stiffness as K1, K2 and K3 (K1 – plane stress, K2 – plane strain, K3 – 3D) were calculated under assumptions of plane stress, plane strain and 3D models respectively. Figure 5.2.1 shows the variations of these stiffnesses, where it can be observed that K3 varies mainly between K1 and K2. Figure 5.2.2 gives the comparisons of the three curves by showing the difference between K1, K3 and K2, K3.

As Figure 5.2.3 shows, when the disk has thickness of 10mm and 15mm, the relative error has a minimum value if the disk is modelled with the plane stress assumption, whereas there will be a maximum error value if the plane strain assumption was used. When the thickness is 160mm, the result shows a cross over point, where both 2D assumptions have the same value of the error. With further increasing disk thickness, the error from the plane strain assumption decreases and that of plane stress increases. This is in agreement with the conventional solid elasticity theories.

The second model was based on a pair of meshing gears, each of them simplified with one tooth only. One of the gears was further simplified as a rigid involute surface as shown in Figure 5.2.4.
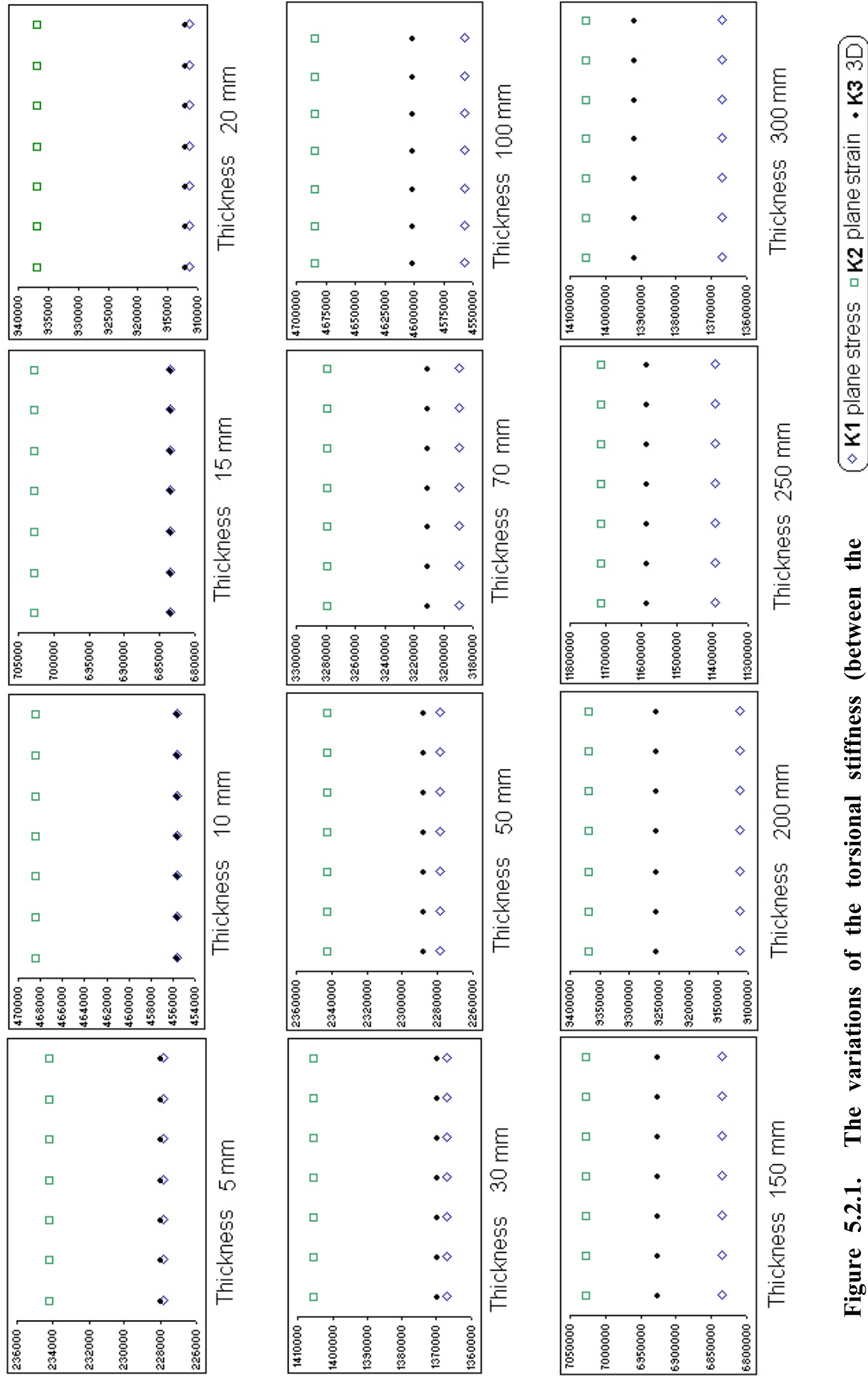
Figure 5.2.1. The variations of the torsional stiffness (between the different assumptions) as functions of the thickness.

67
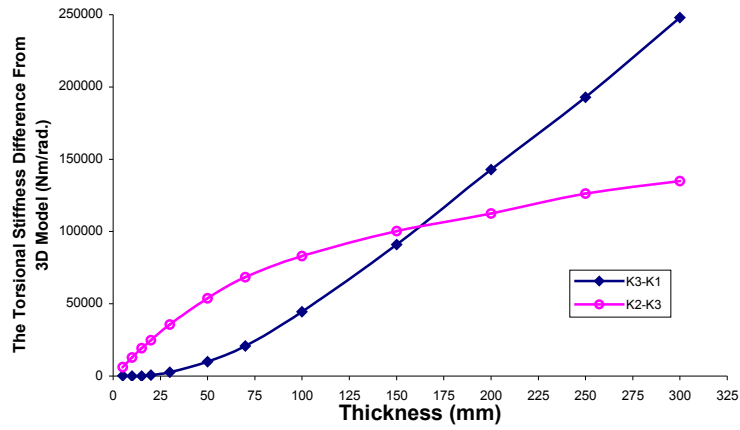
Figure 5.2. 2   The absolute errors of model 1.
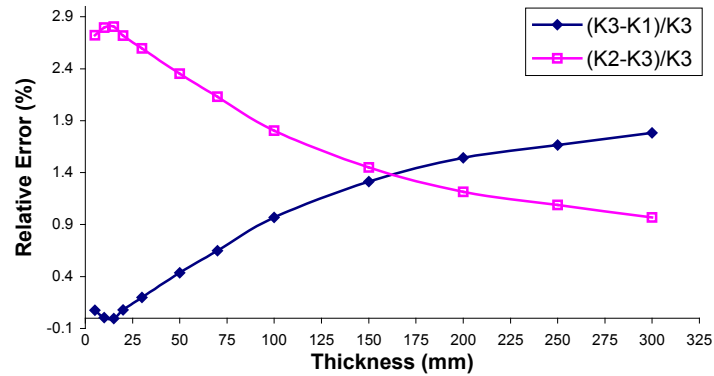
Figure 5.2. 3   Relative errors of model 1.
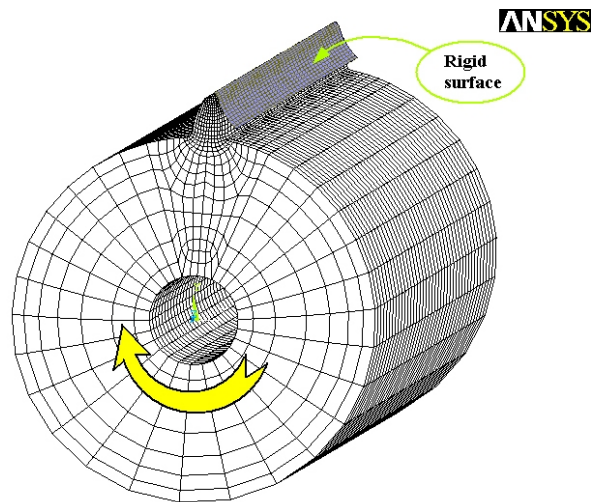
Figure 5.2. 4   Second gear model.

The calculation procedures for the second gear model were identical to those used with the first model. The results have shown the difference in absolute errors compared with the first model as shown in figure 5.2.5.
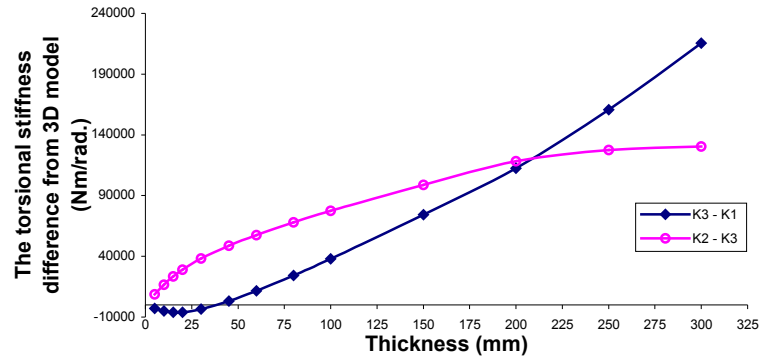
Figure 5.2. 5   The absolute errors from the second model.

It can be seen that the errors have reduced when the plane stress assumption was used for the thinner model and the crossover point of the curves was extended from the thickness at 160mm to 210mm.   This shows that the absolute errors varying with the thickness are slower than that of the first model.   Similarly, the relative errors can be produced as shown in Figure 5.2.6.
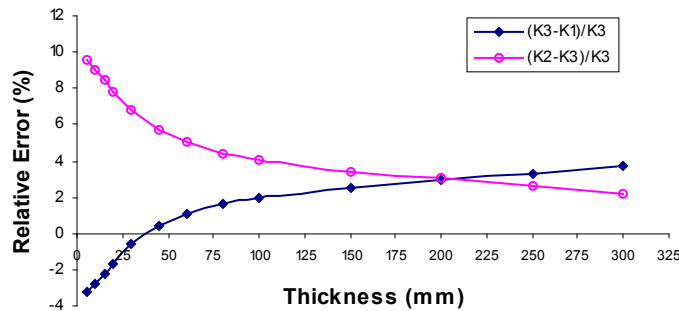
Figure 5.2. 6   Relative errors from the second model.

Figure 5.2.6 has shown the significant difference between the first model and the second model.   Using the plane strain assumption to model a disk the relative errors are less than 3%, but to model a gear with 200mm thickness, the errors are greater than 3% when compared with the 3D model.   Under the plane stress assumption, within the thickness range from 10mm to 200mm, the relative errors of the gear model are less than 3%. However, the errors are quite different when the thickness is less than 20mm.   These results are important for gear transmission error (displacement) studies.   As an example of the test gear model (15mm thickness), there are basically 2% errors in solutions of displacements when the plane stress assumption was used, whereas about 8.3% error will be present if using the plane strain assumption.   In the displacement field, it has been shown that the gear is different from that of a simple disk.

69

The third model is similar to the previous one, but now a 4mm crack is located in the root area as shown in Figure 5.2.7.
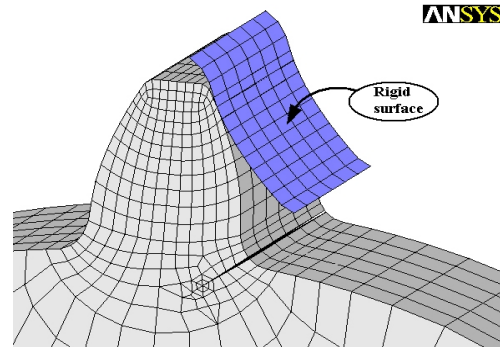
Figure 5.2. 7   The third model with a tooth crack.

One of the major differences from all previous models is that the crossover point of the error curves is now located inside the 50mm thickness, as shown in Figure 5.2.8.
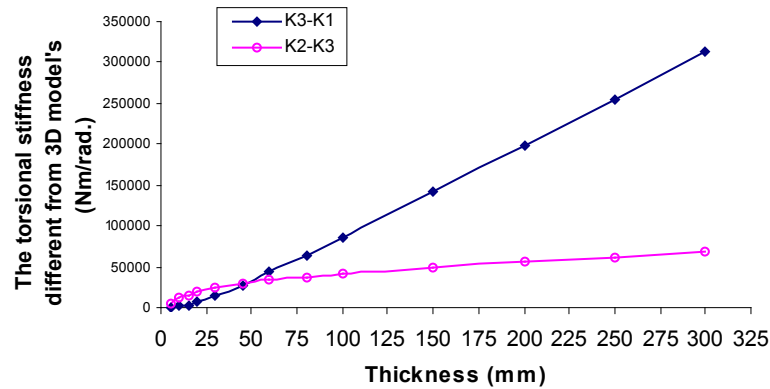
Figure 5.2. 8   The absolute errors of the third model.

Consequently, using the different assumptions can significantly alter the relative errors in the solutions for displacement, depending up on the thickness, as can be seen in Figure 5.2.9.
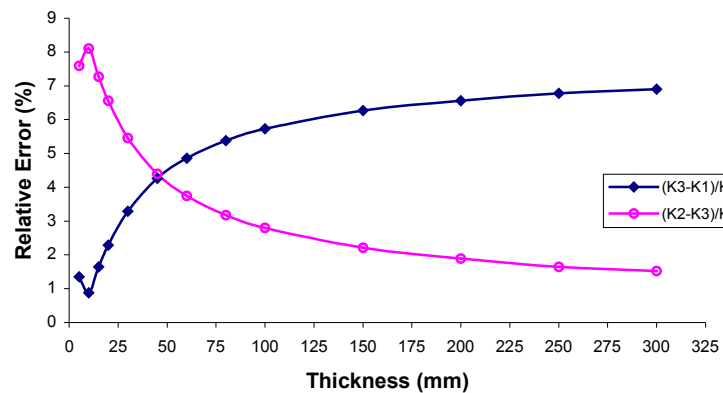
Figure 5.2. 9   Relative errors of the third model.

Figure 5.2.9 shows that the plane stress assumption can only be used in a very narrow range if the relative error is not allowed to be greater than 3%. When the thickness is inside the range from 25mm to 90mm, both 2D assumptions cannot avoid the errors that are greater than 3%. Meanwhile, the range for the plane strain assumption with lower errors has increased since the error is less than 3% when the thickness is greater than 90mm. If the torsional stiffness in model 1 is assigned to be K(11) for plane stress, K(12) for plane strain and K(13) for the 3D model, then the model 2 results will be given by K(21), K(22) and K(23), and the model 3 results will be K(31), K(32) and K(33) for the relative stiffness. Further comparison between the model results can then be made as shown in Figure 5.2.10.
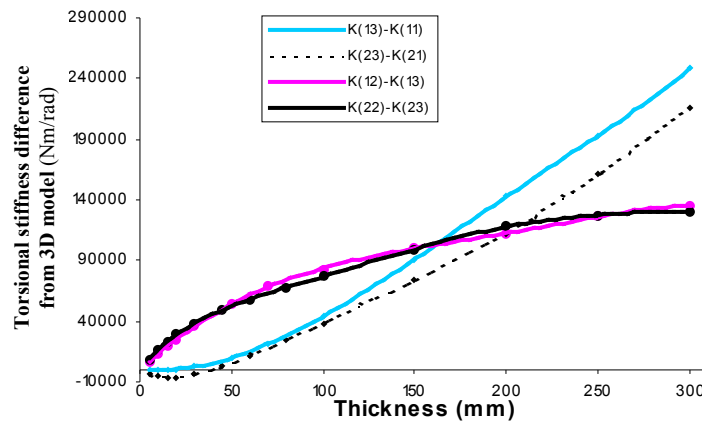
Figure 5.2. 10   Comparison of absolute stiffness errors from model 1 and model 2.
(absolute error here is referred to the absolute value of the difference between the amplitudes.)

It can be seen in Figure 5.2.10 that the absolute errors from model 1 and model 2 are of similar magnitude. Under the plane strain assumption, the absolute errors from both models show the same trends even though there is a significant difference in the relative errors. When the tooth thickness is less than 50 mm (about 1/3 of maximum in plane dimension), the plane stress assumption shows less error in comparison to the 3D model result. When the thickness is between 5mm and 300mm (which is about the maximum in plane dimension of the gear), the plane stress result shows less error than the plane strain result. When the thickness becomes the major dimension of the model, the plane strain assumption should therefore be chosen if the study is to be based on a 2D assumption.

Similar comparison between model 2 and model 3 is shown in Figure 5.2.11, where a significant difference in absolute errors is easy to see.
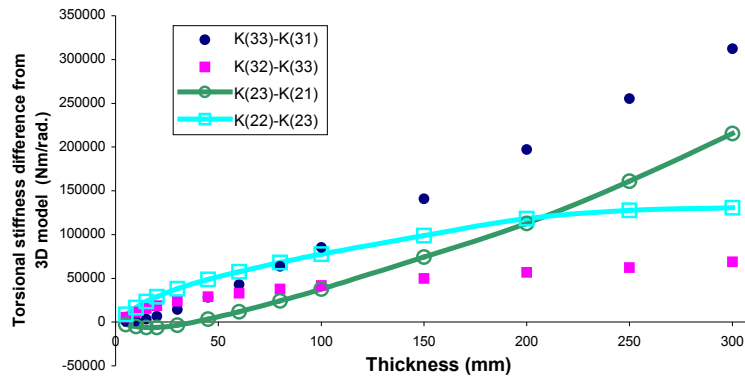
Figure 5.2. 11   Comparison of absolute stiffness errors from model 2 and model 3.

As mentioned before, due to the through crack in the tooth root, the thickness that is suitable for plane stress assumption has reduced to about 20mm.   Within the thickness, which is about 1/3 of the major dimension, this shows that the plane stress is still a better assumption than plane strain.   The comparison of the relative errors from all the models has been made as shown in Figure 5.2.12.
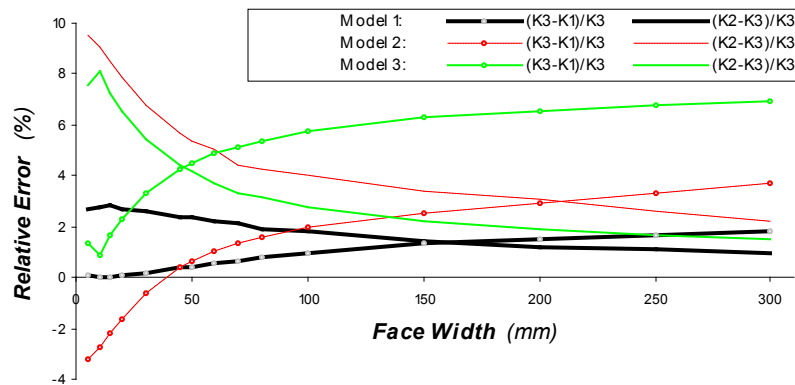
Figure 5.2. 12   Comparison of the relative errors of the torsional stiffness.

It has clearly been shown that when using 2D assumptions to model gears for solutions of the displacements it is hard to avoid errors associated with the plane stress and plane strain assumptions.

5.3   Stress

Though the results obtained from the stiffness analysis presented above are sufficient for guiding the following gear transmission error study, theoretically, stresses (the higher order products yielded from FEA analysis) will verify the important difference between the

models and many experts indicate that stress analysis should always be used to give the most reliable results.

The stress analysis developed here will concentrate on a one-tooth gear model (Figure 5.2.4) and a one-tooth gear model with a crack at the tooth root (Figure 5.2.7). The analysis procedures are similar to those used for the stiffness analysis, with each model varying with different thickness from 5mm to 300mm, and all calculations achieved with an input torque load of 76.2Nm. For T6 aluminium, there is a wide range of input torque loads that can be applied on the models in the elastic range (Sirichai 1999). 76.2Nm is in the middle range of the loads for the thinnest gear model (5mm thickness) and with this load, the comparison with previous research (Sirichai 1999) is relatively easy. The FEA results for the one tooth gear model are given in Table 5.1.

thickness (mm)	Plane Stress		Plane Strain		3D		Stress difference from 3D		SINT difference from 3D	
	S1max(Mpa)	SINT	S1max(Mpa)	SINT	S1max(Mpa)	SINT	31	32	31	32
5	136.771	202.730	111.890	186.960	141.130	241.830	4.359	29.240	39.100	54.870
10	68.410	101.320	55.967	93.442	73.101	121.540	4.691	17.134	20.220	28.098
15	45.612	67.533	37.317	62.286	49.753	84.045	4.141	12.436	16.512	21.759
20	34.211	50.646	27.990	46.711	36.125	65.892	1.914	8.135	15.246	19.181
30	22.809	33.761	18.661	31.139	23.813	45.081	1.004	5.152	11.320	13.942
45	15.206	22.506	12.441	20.758	15.396	30.097	0.190	2.955	7.591	9.339
60	11.405	16.879	9.331	15.568	11.436	22.489	0.031	2.105	5.610	6.921
80	8.554	12.659	6.999	11.676	8.525	16.818	-0.029	1.526	4.159	5.142
100	6.843	10.127	5.599	9.341	6.803	13.421	-0.040	1.204	3.294	4.080
150	4.562	6.751	3.733	6.227	4.519	8.935	-0.043	0.787	2.184	2.708
200	3.422	5.064	2.800	4.670	3.383	6.697	-0.039	0.583	1.633	2.026
250	2.737	4.051	2.240	3.736	2.702	6.287	-0.035	0.462	2.236	2.551
300	2.281	3.376	1.867	3.114	2.249	5.238	-0.032	0.382	1.862	2.125

Load is constant at 76.2Nm.

Table 5.1. FEA results for one tooth model.

$S1_{max}$ refers to the maximum first principal stress, and SINT refers to the stress intensity factor. The stress difference between the 3D model and the plane stress model is denoted by 31 and 32 represents the difference between the 3D model and the plane strain model. Here we are concerned with the relative errors, and the 3D model has been taken as the reference. The following table gives the relative errors.

thickness (mm)	Relative Stress Errors (%)		Relative SINT Errors (%)	
	for Plane Stress	for Plane Strain	for Plane Stress	for Plane Strain
5	3.09	20.72	16.17	22.69
10	6.42	23.44	16.64	23.12
15	8.32	25.00	19.65	25.89
20	5.30	22.52	23.14	29.11
30	4.22	21.64	25.11	30.93
45	1.23	19.19	25.22	31.03
60	0.27	18.41	24.95	30.78
80	0.34	17.90	24.73	30.57
100	0.59	17.70	24.54	30.40
150	0.95	17.40	24.44	30.31
200	1.15	17.24	24.38	30.26
250	1.31	17.11	35.57	40.58
300	1.44	17.01	35.56	40.56

Table 5.2. The calculated relative errors.
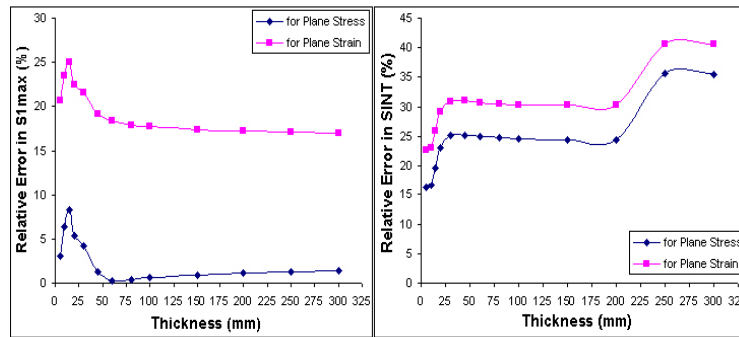
Figure 5.3. 1   The relative errors of one tooth model.

Figure 5.3.1. shows that using the plane strain assumption to predict maximum first principal stress in a gear has far more error than using the plane stress assumption. However, when the gear thickness is 15mm, both assumptions have a maximum error given by 8.3% for the plane stress assumption, and 25% error for the plane strain assumption. With increasing thickness, the error from the plane strain assumption decreases slowly, almost linearly, whereas the error from the plane stress assumption increases linearly. In this case the plane stress assumption shows a lower error for predicting the maximum first principal stress over a wide range of thickness values of the gear. Figure 5.3.1 also shows that the 2D assumption is not accurate for predicting the maximum stress intensity factor because the minimum error for the plane stress assumption is 16.2% and that for the plane strain assumption is 22.7%. Overall the plane strain assumption gives higher error values compared with the 3D model. Under both 2D assumptions, $SINT_{max}$ and $S1_{max}$ occur at the same physical location in the FE model, and the positions do not change with varying thickness. The locations for $SINT_{max}$ and $S1_{max}$ are shown in Figure 5.3.2.
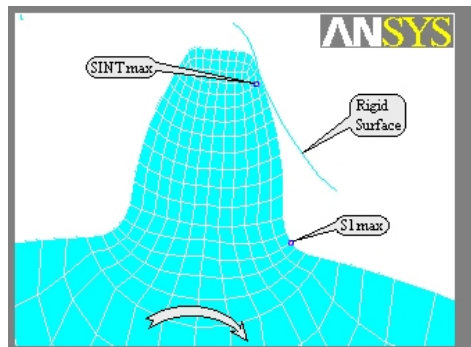
Figure 5.3. 2   The position of $SINT_{max}$ and $S1_{max}$ under 2D assumptions.

It has been found that in the 3D case, the position of $S1_{max}$ always changes with varying thickness, and both $SINT_{max}$ and S1max always occur on the surface. Figure 5.3.3 shows the change of $SINT_{max}$ and $S1_{max}$ positions with the varying thickness.

74
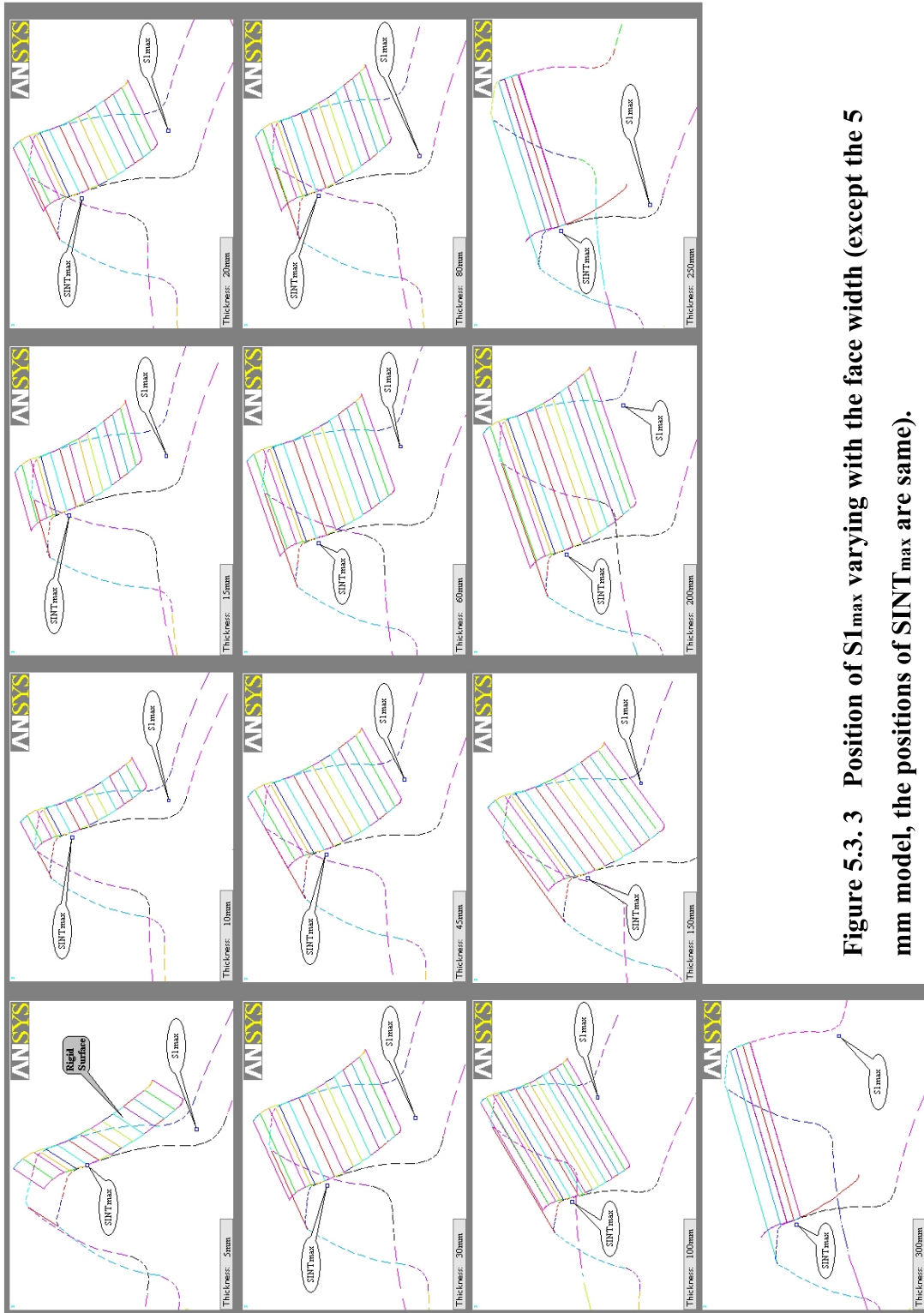
Figure 5.3.3 Position of S1$_{max}$ varying with the face width (except the 5 mm model, the positions of SINT$_{max}$ are same).

In the model with the 4mm crack at the tooth root (Figure 5.2.7) using the same analysis, the relative errors of S1$_{max}$ are obtained as shown in Table 5.3, and they were all found to be located at the crack tip.

75

thickness (mm)	S1$_{max}$ (Mpa)			Relative Errors (%)	
	Plane Stress	Plane Strain	3D	for Plane Stress	for Plane Strain
5	471.330	496.000	566.650	16.82	12.47
10	235.950	248.100	285.350	17.31	13.05
15	157.360	165.410	185.360	15.11	10.76
20	118.050	124.420	136.220	13.34	8.66
30	78.713	82.961	90.938	13.44	8.77
45	52.482	55.314	59.991	12.52	7.80
60	39.364	41.488	44.237	11.02	6.21
80	29.525	31.117	32.910	10.29	5.45
100	23.620	24.895	26.258	10.05	5.19
150	15.748	16.597	17.438	9.69	4.82
200	11.811	12.448	13.050	9.49	4.61
250	9.449	9.959	10.418	9.30	4.41
300	7.874	8.299	8.676	9.24	4.34

Table 5.3. FEA results of one tooth cracked model.

The comparison of the relative errors can be shown in Figure 5.3.4.
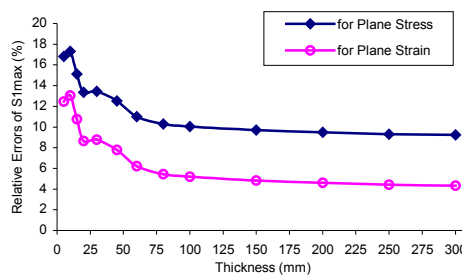
Figure 5.3. 4   The relative errors of S1max.

Compared with Figure 5.3.1, this result shows the opposite conclusions than for the model without the tooth crack. It was found that the results obtained using the plane strain assumption to predict S1$_{max}$ in a gear with the root crack are better than the results obtained from using the plane stress assumption. However, when the gear is thinner than 25mm, the errors from using the 2D assumptions can be significant. For global SINT$_{max}$, in the 3D case, not all SINT$_{max}$ positions were located at the crack front. When the thickness varies from 30mm to 60mm, the global SINT$_{max}$ values were located near the contact point on the surface. However, the maximum SINT of the crack front, SINT$_c$ was still located in the position of S1$_{max}$, and the global SINT$_{max}$ and local SINT$_c$ are close given by 51.842 and 51.728 respectively for the 30mm model, and 25.857 and 25.723 respectively for the 60mm model. Figure 5.3.7 shows the locations of S1$_{max}$, SINT$_{max}$ and SINT$_c$ (SINT$_c$ is in the crack tip or the maximum value in the crack front) in all models. For the 2D case, SINT$_{max}$ was located at the crack tip for plane stress models. However, when using plane strain assumptions, they are not located at the crack tip but near the contact point. In this case, the relative error for SINT$_{max}$ (compared with 3D) was low when the gear is thicker than

25mm, but the comparison was not made in the same location. In the same location (crack tip and crack front), the relative errors are much higher as shown in Figure 5.3.5.
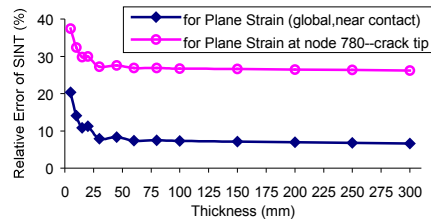
Figure 5.3. 5   The relative errors of $SINT_{max}$ and $SINT_c$.

For the comparison, $SINT_c$ was calculated so that the comparison was made for all models SINT at the crack tip or at the crack front. The results are shown in Table 5.4.

thickness (mm)	SINTc			Relative Errors (%)	
	for Plane Stress	for Plane Strain	3D	for Plane Stress	for Plane Strain
5	471.330	224.948	359.280	31.19	37.39
10	235.950	112.525	166.460	41.75	32.40
15	157.360	75.019	106.900	47.20	29.82
20	118.050	56.439	80.555	46.55	29.94
30	78.713	37.633	51.728	52.17	27.25
45	52.482	25.092	34.652	51.46	27.59
60	39.364	18.820	25.723	53.03	26.84
80	29.525	14.116	19.299	52.99	26.86
100	23.620	11.293	15.410	53.28	26.72
150	15.748	7.529	10.259	53.50	26.61
200	11.811	5.647	7.677	53.85	26.45
250	9.449	4.517	6.131	54.11	26.33
300	7.874	3.765	5.102	54.34	26.20

Table 5.4.   The calculated relative errors of SINT at the crack tip.

Figure 5.3.6 clearly shows that the calculation of SINT at the crack tip using the plane strain assumption contains less errors than that obtained using the plane stress assumption, except for the case where the thickness is very thin (eg. 5mm). Because the comparison is made at the crack tip or the crack front for these models, these results are in agreement with common fracture mechanics theories. Except for the analysis of thin plates, the asymptotic or near-crack-tip behaviour of stress is usually thought to be that of plane strain (ANSYS 2000).
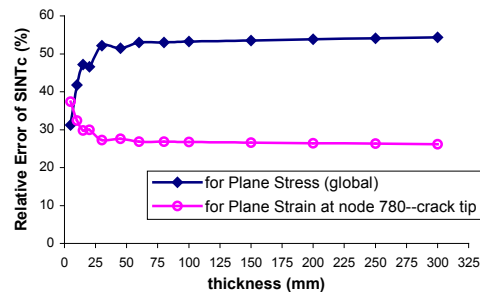
Figure 5.3. 6   The relative errors of SINT at the crack tip.
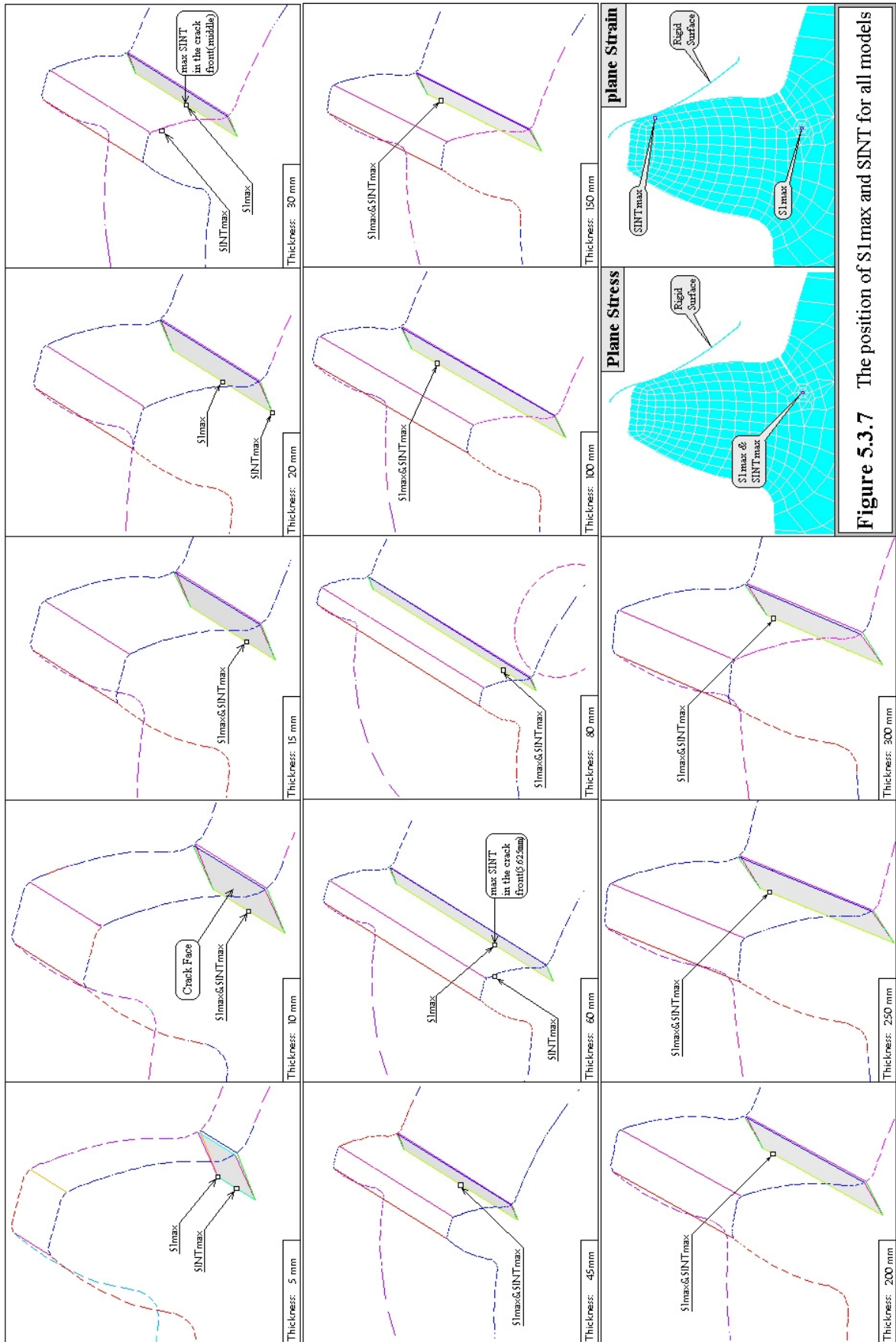
Figure 5.3.7 The position of S1max and SINT for all models

78

From a general case, Anderson (Anderson 1995) has analysed the state of stress and strain variations near the crack front (r<<B) through a certain thickness as illustrated in Figure 5.3.8.
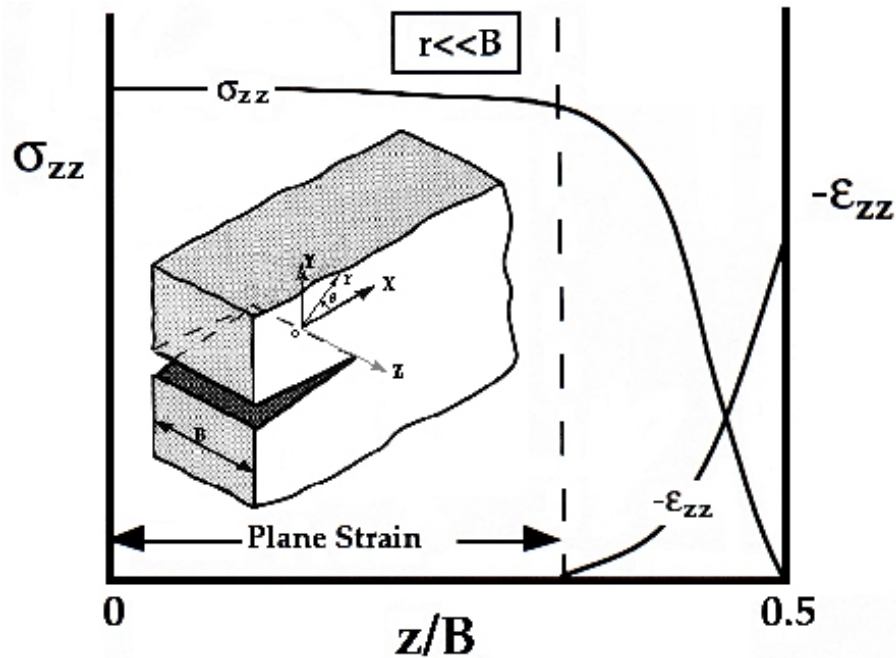
Figure 5.3. 8   Schematic variation of transverse stress and strain through the thickness at a point near the crack tip(Anderson 1995).

At the mid-plane (Z = 0), plane strain conditions exist and $\sigma_{zz} = \upsilon(\sigma_{xx} + \sigma_{yy})$. For the material on the plate surface (Z = ±B), a state of plane stress exists (because there are no stresses normal to the free surface). There is a region near the plate surface where the stress state is neither plane stress nor plane strain and this is the region where most of the S1max results were found in this research.

Figure 5.3.9 is a plot of σ_{zz} as a function of z/B and r/B. These results were obtained from a 3D elastic-plastic finite element analysis performed by Narasimhan and Rosakis (Narasimhan 1988). Note the transition from plane strain (z = 0) to plane stress as r increases relative to thickness.

Both cases above illustrate the variations of 2D-closed state in a 3D situation. They show that when the structure is analysed with fracture mechanics theory, for a certain thickness, there are differences in the result if 2D analysis is needed, compared with 3D analysis.
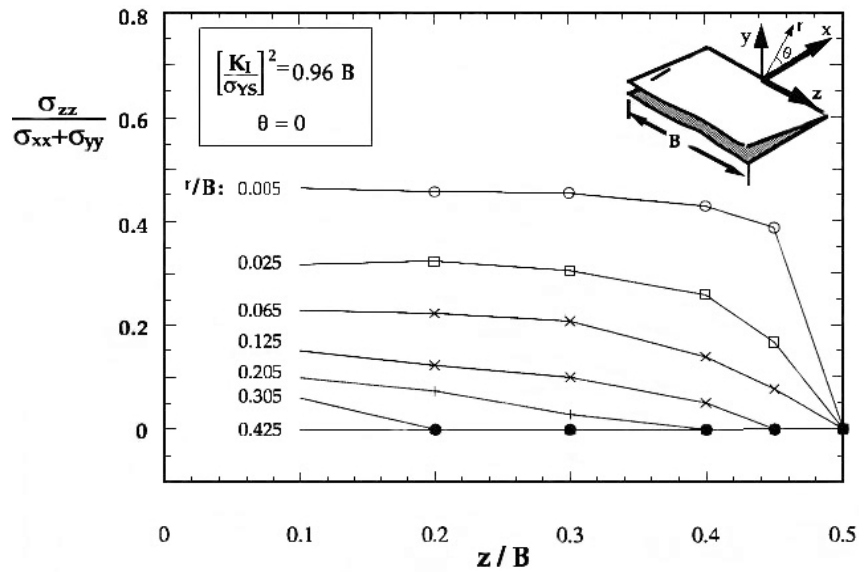
Figure 5.3. 9   Transverse stress through the thickness as a function of distance from the
crack tip (Narasimhan 1988).

For the varying thickness, the variations through the thickness of stress S1 and SINT in the critical point should be produced as an important proof for this research. The following figure (Figure 5.3.10) gives the results for the one tooth model and Figure 5.3.11 shows the results for the model with a root crack.

It should be noted that the maximum SINT at the crack tip or in the crack front, in the sense of fracture mechanics, is given by $K_{(total)}$ and $K_{(total)} \neq K_I + K_{II} + K_{III}$. As the current research is concentrating on the comparison of the global response of the structure, details of fracture parameters such as K_I, K_{II}, K_{III} and others have not been calculated.

5.4   Conclusion

Overall, the plane stress assumption can produce well-matched results with 3D models. However, care must be taken not only for the model's geometry, if the model is subject to fracture. In this instance the assumption might only be valid in a very limited range. Failure to understand these results may lead to large errors in the analysis results.
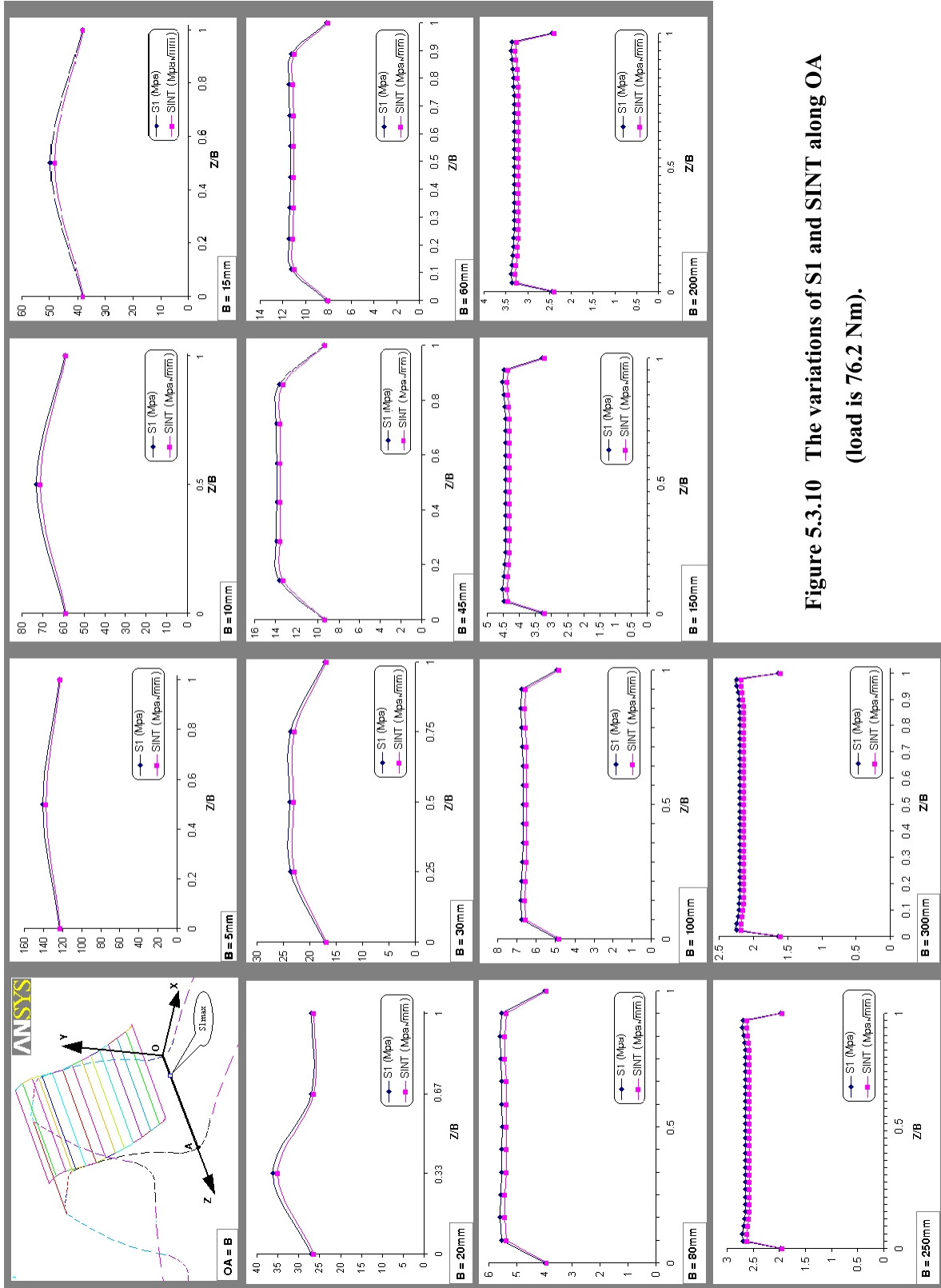
Figure 5.3.10   The variations of S1 and SINT along OA (load is 76.2 Nm).
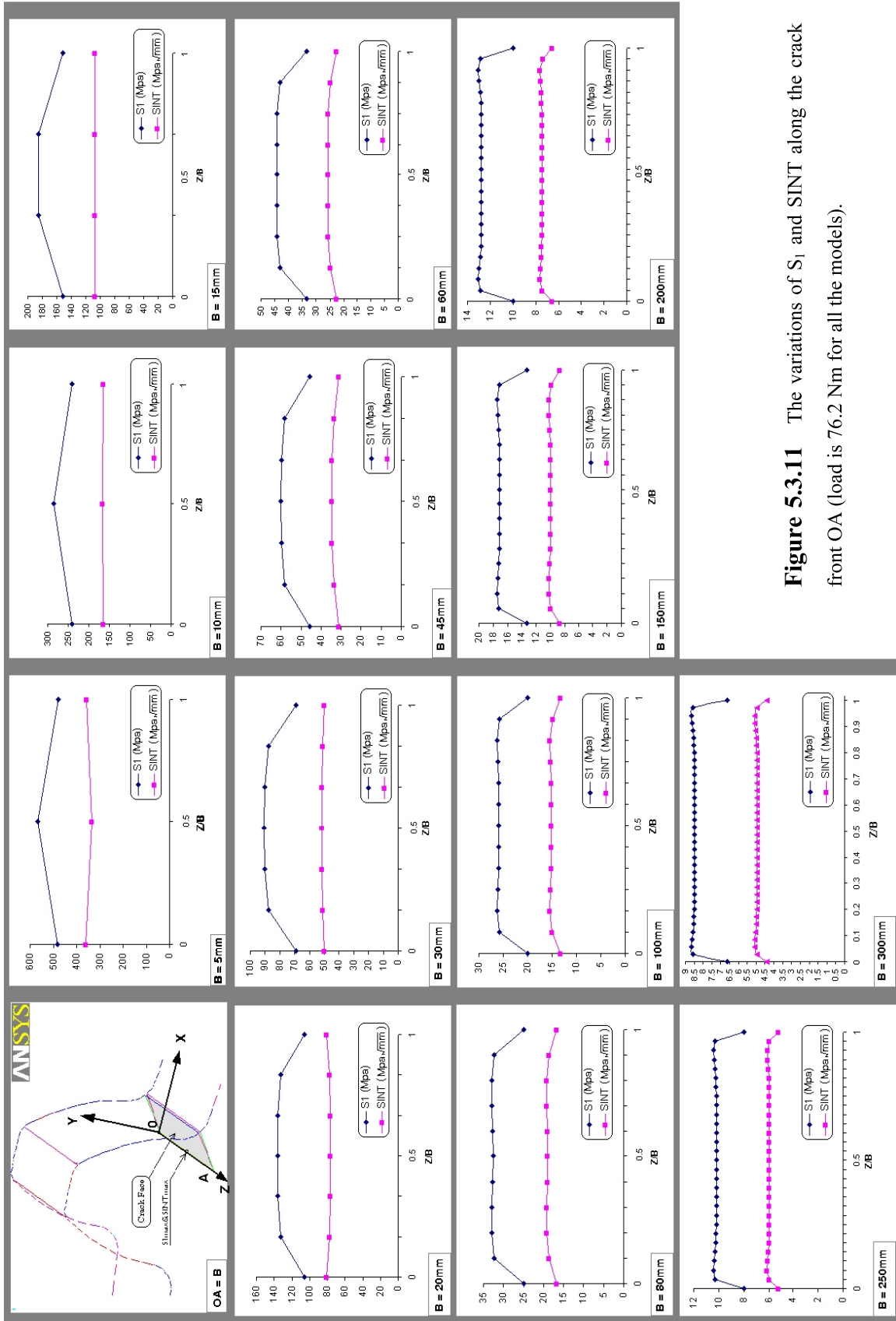
Figure 5.3.11 The variations of S_1 and SINT along the crack front OA (load is 76.2 Nm for all the models).

CHAPTER 6

THE COMBINED TORSIONAL MESH STIFFNESS

6.1   INTRODUCTION

In recent years, many different procedures have been developed to model the behaviors of gears in mesh. Examples of this can be seen in references (Tordian 1967; Remmers 1978; Drago 1979; Gargiulo 1980; Walford 1980; Hayashi 1981; Bahgat 1983; Ozguven 1988; Kahraman 1991; Kuang 1992; Liou 1992; Rebbechi 1992; Vinayak 1992; Bard 1994; Brousseau 1994; Daniewicz 1994; Kowalczyk 1994; Munro 1994; Refaat 1994a; Refaat 1995; Velex 1995; Liou 1996; Litvin 1996; Sirichai 1996; Sweeney 1996; Velinsky 1996; Sirichai 1997; Underhill 1997; Elkholdy 1998; Gosselin 1998; Nadolski 1998; Zhang 1998; Arafa 1999; Sirichai 1999; Wang 2000). One of the many factors, which can be investigated, is the torsional mesh stiffness variation as the gear teeth rotate through the mesh cycle. For prediction of the torsional mesh stiffness, FEA modelling in particular can encompass three major stages: analysis with partial tooth models, analysis with single tooth gear models and analysis of multi-teeth gears in a complete mesh cycle. With continuing software and hardware developments, it is expected that advances with gearing analysis will involve FEA 4D models associated with coupled field problems and non-linear materials etc., over the next few years.

With the current modelling capability, it is possible to predict the combined torsional mesh stiffness of two spur gears (multi-teeth) in mesh, where one of the gear hubs is restrained from rotating, with the other gear hub having a torque input load. The combined torsional mesh stiffness of two gears in mesh is calculated at each selected position in the mesh cycle, and the overall FEA solution shows that the combined torsional mesh stiffness varies with the meshing position as the teeth rotate within the mesh cycle. In particular, the combined torsional mesh stiffness decreases and increases dramatically as the meshing of the teeth changes from the double pair of teeth in contact, to the single pair of teeth in contact and vice-versa (Sirichai 1999).

6.2   The Individual Torsional Stiffness

In order to understand the combined torsional mesh stiffness, the variations of the individual torsional stiffness for each of the gears in the mesh cycle have to be studied. However, to predict the individual torsional stiffness for one of the gears in mesh is a rather complex procedure, due to the non-linear contact. The actual position of the contact(s) is usually unknown until the solution for both gears in mesh is completed.

A simple strategy for overcoming the difficulties can be developed, with a small torque input load, where one of the meshing gears can be modelled with rigid elements. In this case, the solutions for the combined mesh stiffness in the mesh cycle are those given by the individual torsional mesh stiffness. When the input load is large, there certainly are errors in this strategy, and the relative error has to be estimated.

6.2.1   The Use of Rigid Elements

The use of rigid elements involves the use of MPC (multipoint nodal constraints) without the analyst having to write out the constraint equations. This capability is available in ANSYS® and in many other codes. It's important to note that the term "rigid element" may be somewhat misleading. Recent publications have used very stiff elements instead of using MPC based rigid elements in gear stiffness studies, where the elements are essentially rigid relative to other elements in the mesh. However, as stated in section 3.2.2,

the connection of a very stiff element with a very flexible one is not recommended, due to the associated numerical problems.

The advantages of using "rigid elements" are that they allow the imposition of common multipoint constraints without having to actually write out the constraint equations. Since they are essentially MPC's, they avoid numerical errors associated with matrix ill conditioning that very stiff elements would cause (Lepi 1998).

6.2.2   The Individual Torsional Stiffness of a Single Tooth Gear Model

If one of the mating gears is rigid, and the input torque is small, the elastic gear will produce a combined torsional mesh stiffness that is at least close to the real individual torsional stiffness with the same input load (note: the combined torsional mesh stiffness is not constant with input load, as discussed in a later section).

In the 2D case, modelling one of the mating gears as rigid (as for the driven gear in Figure 6.2.1) is as simple as modelling a line segment AB with rigid contact elements with compatible mesh density. Table 4.1 has given the parameters for the gears in this model.
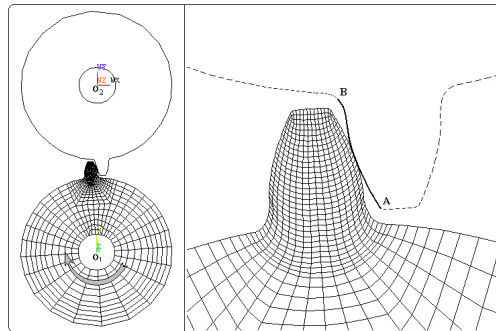
Figure 6.2. 1   The model for prediction of individual torsional stiffness
(The driven gear is simplified as a rigid line AB).

As shown in section 4.2, the input torque load, boundary conditions and nodal couplings are applied on the drive gear (pinion) hub. In order not to over constrain the model, line AB should be left "free" after meshing with rigid line elements. The first solution is calculated at the mesh position of the pitch point (0 degrees, as shown in Figure 6.2.1), then the pinion is rotated with an angle increment and the line AB is rotated about O_2 for the next solution. There were 107 angular increments used here to cover the mesh cycle.

Calculations were carried out by using a looping program written with APDL (*ANSYS Parametric Design Language*). In ANSYS®, the solution for angular displacement is given by tangential displacement values under the defined polar coordinate system. Because the nodes on the drive gear hub were coupled with the master node in rotation, they will all have the same tangential displacement value UY as the master node. The program automatically saves each solution (UY) in the file such as PRNSOL.lis. When the looping is finished, the solution data will be input to Microsoft Excel so that a further calculation for the stiffness can be done as well as graphical representation of the numerical solutions produced.

As given, the hub radius was $r = 15mm$. If $\Delta\theta$ denotes the elastic angular rotation of the pinion hub, then

$$UY = r * \Delta\theta \quad , \tag{6.1}$$

so, the stiffness can be calculated by,

$$K = M / \Delta\theta = M * r / UY , \tag{6.2}$$

where M is input torque load.

Figure 6.2.2 and Figure 6.2.3 give the results for this single tooth model.
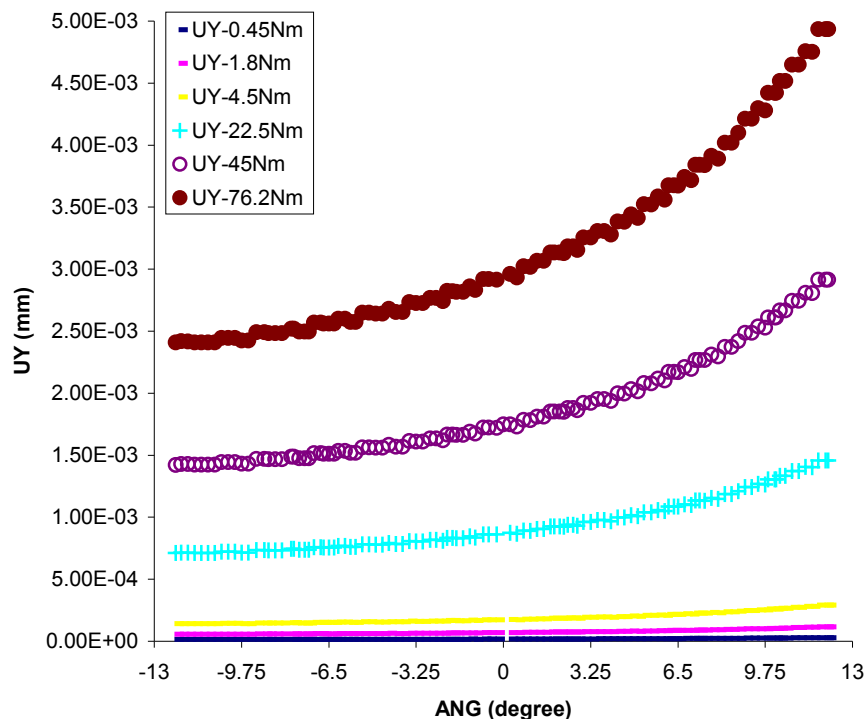
Figure 6.2. 2   FEA solution data for displacements under varying load.
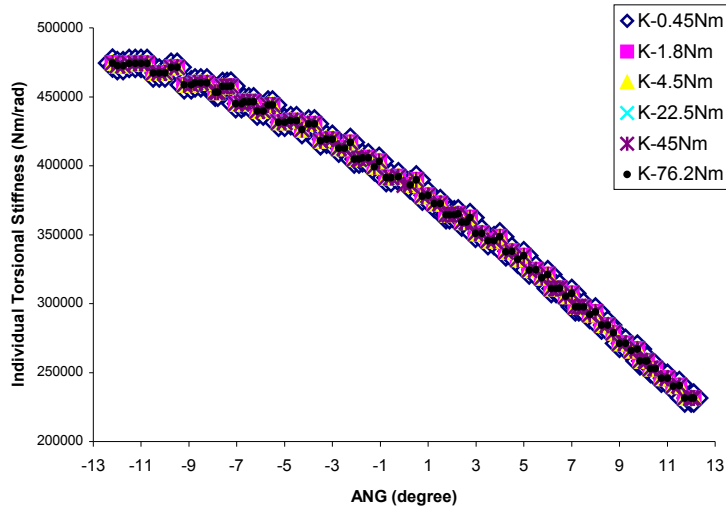
Figure 6.2. 3   The individual torsional stiffness

From Figure 6.2.3 it is hard to tell there are six series of stiffness data that have been produced by the series load. Taking the series produced by the minimum load as a basis for comparison with the one produced by the maximum load, the relative errors can be calculated as shown in Figure 6.2.4. The maximum error is only 0.0012%. This doesn't mean that with increasing input load the model can still produce accurate results, as previous research (Sirichai 1999) has shown that load vs. stiffness results at positions in the mesh cycle are slightly non-linear.   Using rigid elements may reduce the system nonlinearity.
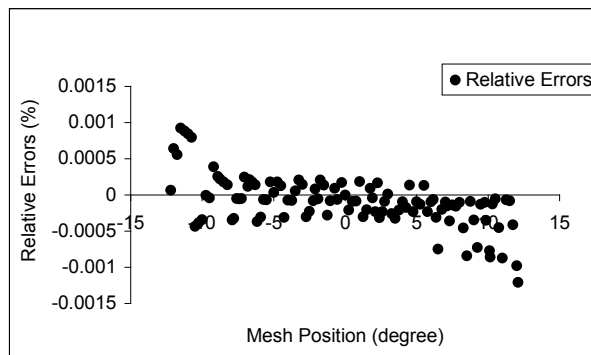
Figure 6.2. 4   Relative errors of the torsional stiffness between the
case of minimum and maximum load.

The results in Figure 6.2.4 have shown that within a wide range of input load, the model can produce results for individual torsional stiffness as accurate as that of the minimum loads.

6.2.3 The Individual Torsional Stiffness of a Multi-Tooth Gear Model

In order to obtain the individual torsional stiffness covering a complete mesh cycle, the rigid line on the driven gear can be extended onto the next two teeth (the minimum can be just one if there is no damage on the gear teeth). The meshed model is as shown in Figure 6.2.5. The driven gear in the meshed model is presented as three segments of rigid line elements. Each segment is meshed with a compatible mesh density. The overall mesh density was obtained with 4790 nodes.
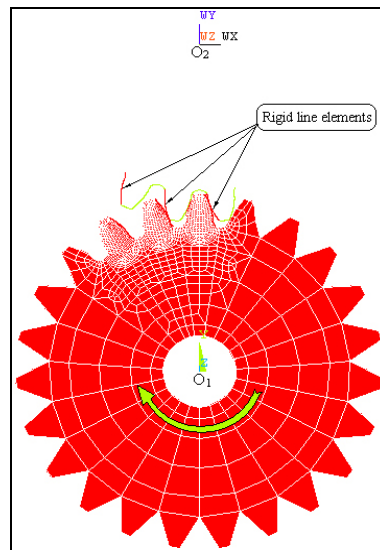
Figure 6.2. 5   The model of meshing with multi-rigid lines.

FEA calculation procedures were the same as those used in previous models. The results are given in Figure 6.2.6 and 6.2.7.
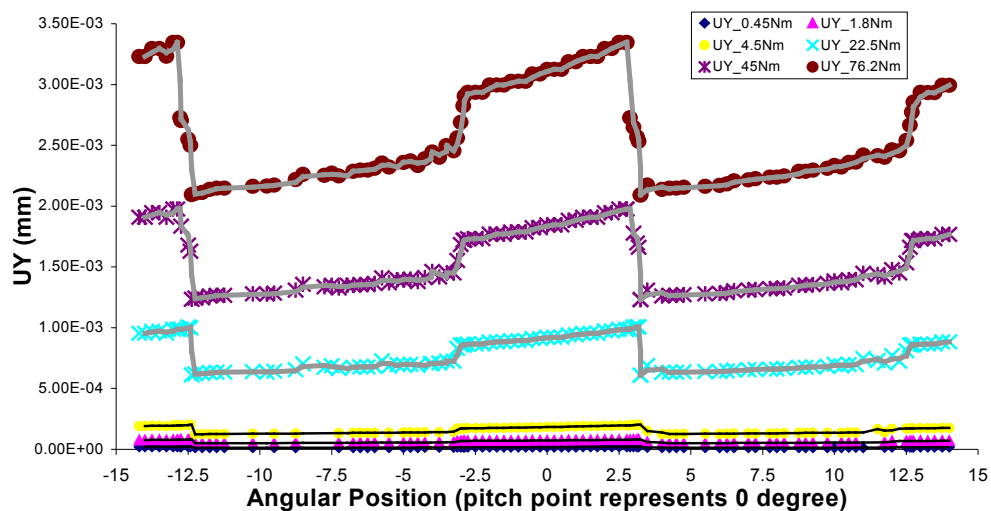
Figure 6.2. 6   FEA solution data for tangential displacements on pinion hub under various load.
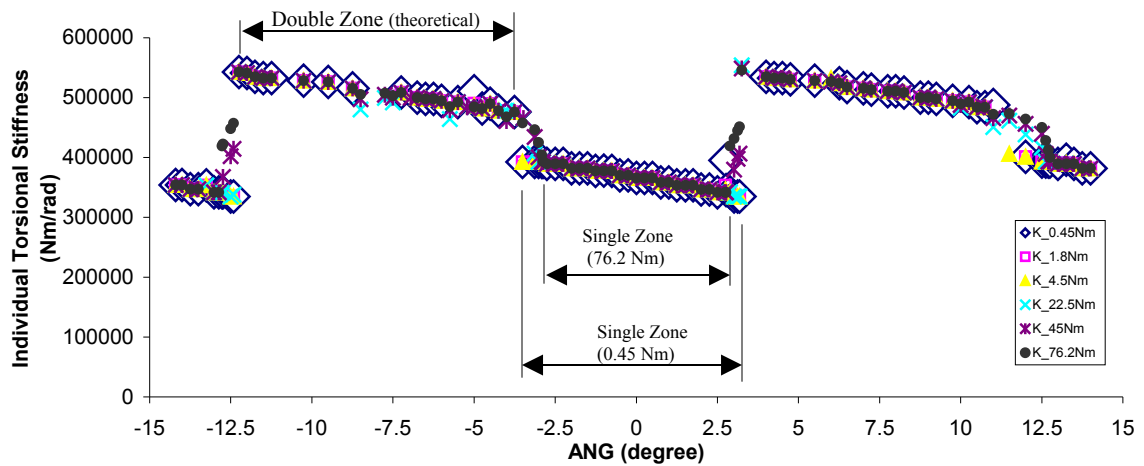
Figure 6.2. 7   The individual torsional stiffness produced by various loads.

The major trend for the individual torsional stiffness over a complete mesh cycle is shown in Figure 6.2.7. It can be seen that the hand over points from single to double teeth contact move slightly with increasing load, so that the single zone reduces when the input load increases, while, the double zone is relatively stable. As expected, due to the unmodified involute profile of the teeth (without tip-relief), the solutions for the hand over points are difficult particularly for small load. With increasing load, the solutions tend to smooth out at the hand over points, because for sliding contact the FEA solver handles pressured sliding (surface to surface contact) better than a tip touching one (point to surface contact), specially when the load option for the FEA solver was the default "ramped load". For example, if the model at the hand over mesh position was solved in eight sub-steps, the first solution was solved with 1/8 input torque load. For this solution, the point to surface contact may occur with large sliding, which may lead to a non-converging solution. This may indicate that when the input torque is small, the choice for "step load" option (one take all) may be a better option. However, if the solution converged, using the "ramped load" option, the solutions were usually found to be more accurate.

6.3   The Combined Torsional Mesh Stiffness

6.3.1   Derived From The Individual Torsional Mesh Stiffness

Instead of rigid line elements, now consider there is a single tooth elastic driven gear pair (ratio 1:1) and its individual torsional stiffness variation in the mesh cycle has a similar

curve to the previous results but with reverse variation. The cross over point for the curves should be the pitch point, as shown in Figure 6.3.1.
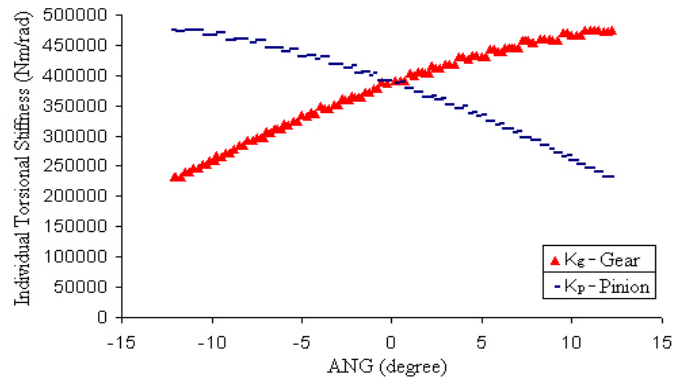
Figure 6.3. 1   The torsional stiffness of gear and pinion

At any position in the mesh cycle, gears can be modelled as two torsional springs connected in series. The system stiffness against input torque, so called the combined torsional mesh stiffness at each position, can be calculated by the following equation,

$$K_m = \frac{K_p \cdot K_g}{K_p + K_g} \ ,$$

(6.3)

where K_p is the individual torsional stiffness of the pinion and K_g is the individual torsional stiffness of the gear. K_m denotes the combined torsional mesh stiffness and the result is plotted in Figure 6.3.2.
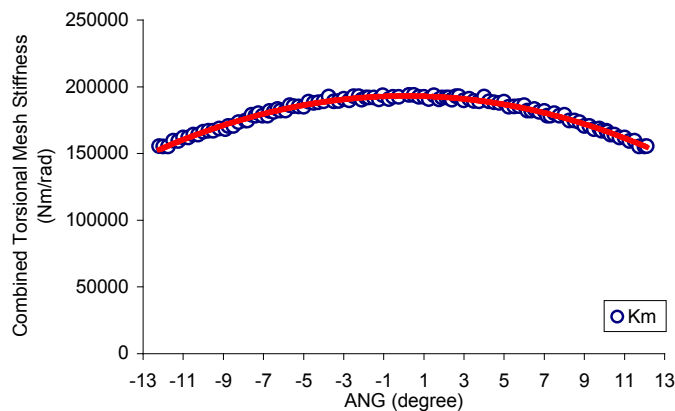
Figure 6.3. 2   The combined torsional mesh stiffness for single pair of teeth in contact.

Similarly, once the individual torsional stiffness of a multi – tooth pinion over a complete mesh cycle is obtained, the stiffness for the gear can be produced as shown in Figure 6.3.3, as long as the mating gears are the same.

90
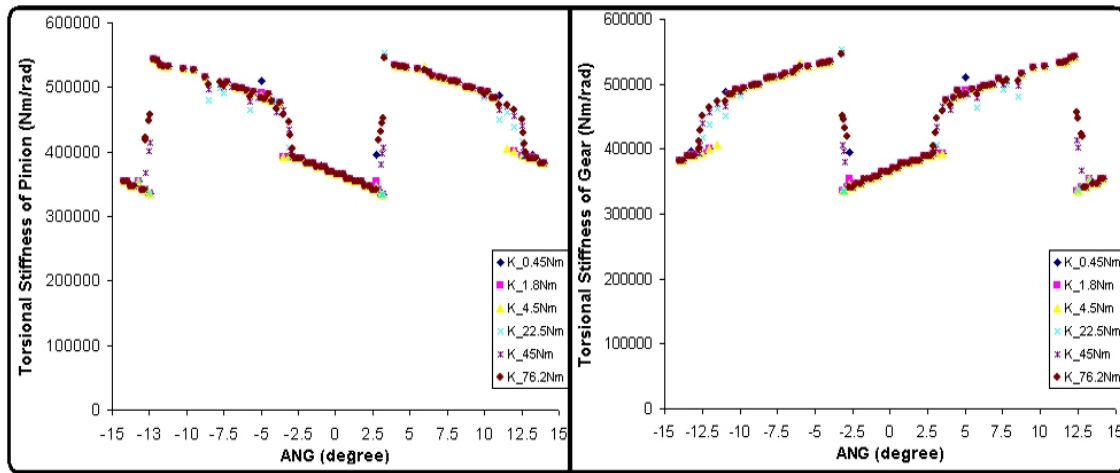
Figure 6.3. 3   The individual torsional stiffness of pinion and gear in a complete mesh cycle.

Equation (6.3) can be used to calculate the results for the combined torsional mesh stiffness for different torque loads. Figure 6.3.4 shows the combined torsional mesh stiffness results for a minimum and a maximum input load.
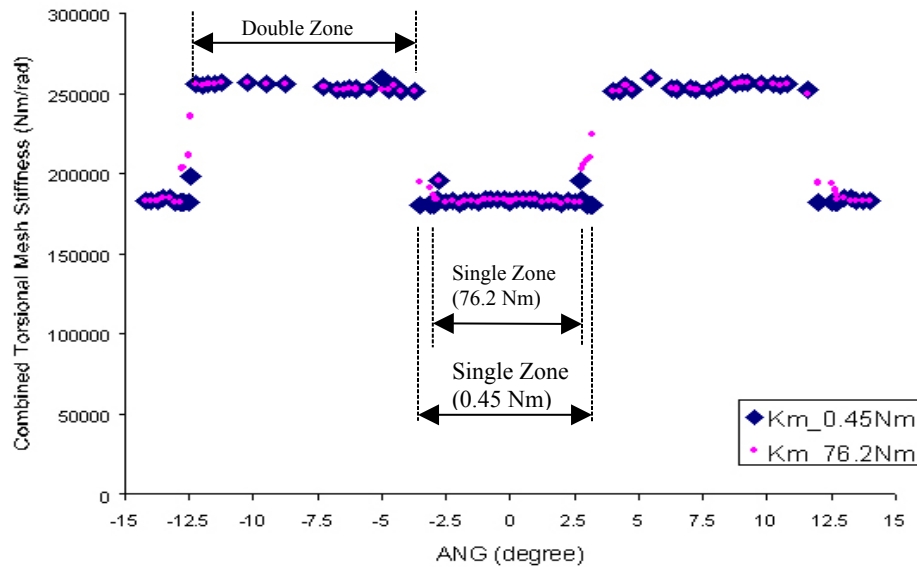
Figure 6.3. 4   The comparison of combined torsional mesh stiffness results produced by the minimum load and maximum load.

From the results shown in Figure 6.3.4, the mesh position ANG varies over the complete mesh cycle. The dramatic change of the combined torsional mesh stiffness can be seen to occur near the hand over points from single to double teeth in mesh and vice versa. The results tend to be flat over the zone when the single pair of teeth is in contact, which is identical to the single tooth gear model results shown in Figure 6.3.2. Near the hand over points, a difference occurs between the stiffness results produced by the different loads.

91

This result has also been shown in the individual torsional stiffness curves shown in Figure 6.2.7. The curves also tend to be symmetrical about the pitch point, with improvement of the model and its solution.

6.3.2   Models With Flexible Contact

The 2D model in Figure 6.3.5 has been used to calculate the combined torsional mesh stiffness. After applying the adaptive re-mesh with the mating position (similar to that shown in Figure 3.4.4), the contact line elements were created in the possible contact areas with the Real Constants of the materials.
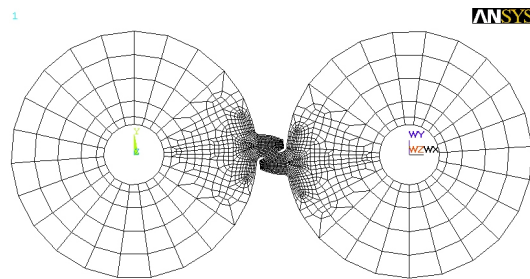
Figure 6.3. 5   The single tooth mating gears.

The mapped mesh associated with the adaptive re-mesh near the contact areas was the main strategy for obtaining accurate results in this research. One of the major requirements for the use of mapped mesh was that the model solution convergence could be easily examined. When using mapped mesh it is essential that a monotonic convergence curve be obtained. For the comparison, the results obtained with the free mesh model are also presented. The free mesh results were only calculated with an input load of 76.2 Nm. Results are given in Figure 6.3.6 and Figure 6.3.7.
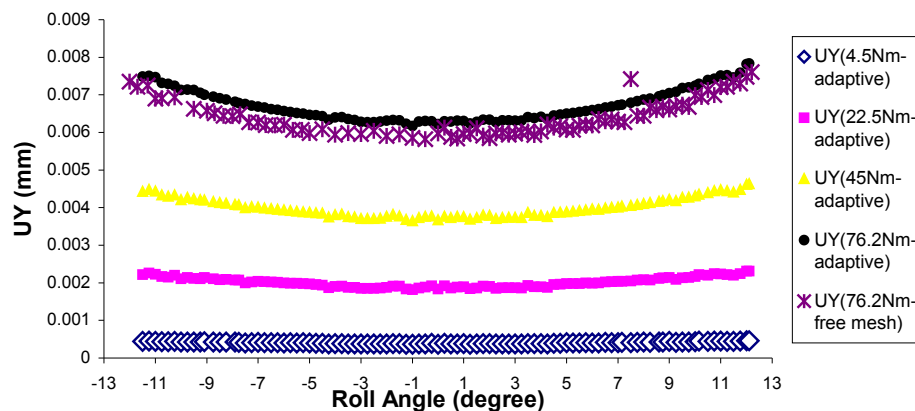
Figure 6.3. 6   The (tangential) displacement of pinion hub under various loads.
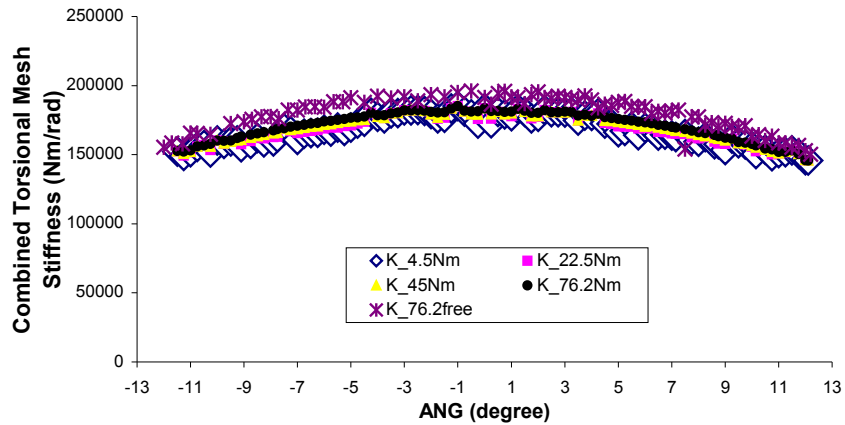
Figure 6.3. 7   The combined torsional mesh stiffness results.

Figure 6.3.7 has shown that the combined torsional mesh stiffness increases slightly with the increase of the load, mainly due to the increasing amount of area in the contact region. At the pitch point the stiffness was predicted to increase by 0.02% from the minimum input load to the load of 76.2 Nm. It would be expected that this would further increase if the input load continued rising in the elastic range of the structure. On the other hand with free mesh (Wang 2000), it was hard to produce solutions with such small variations and the solution error of 0.07% was found at the pitch point compared with the adaptive mesh. Further comparison, taking into account the stiffness derived from the individual torsional stiffness of the single tooth gear model (contact with rigid line), is shown in Figure 6.3.8.
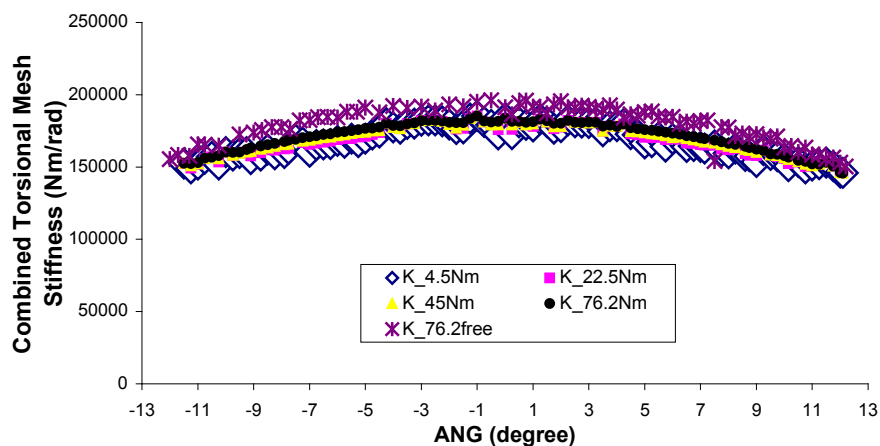
Figure 6.3. 8   Comparisons of the stiffness with the calculated stiffness.

It can be seen that the calculated stiffness results are significantly different from the adaptive mesh results, but they are at least as accurate as the free mesh results.

6.3.3   The Problems with Single Tooth Gear Models

A number of problems occur when using single tooth models for producing the combined torsional mesh stiffness over a complete mesh cycle.   Three examples of single tooth models used in previous research by Kuang (Kuang 1992), Arafa (Arafa 1999) and Wang (Wang 2000) are presented in Figure 6.3.9, 6.3.10 and 6.3.11.
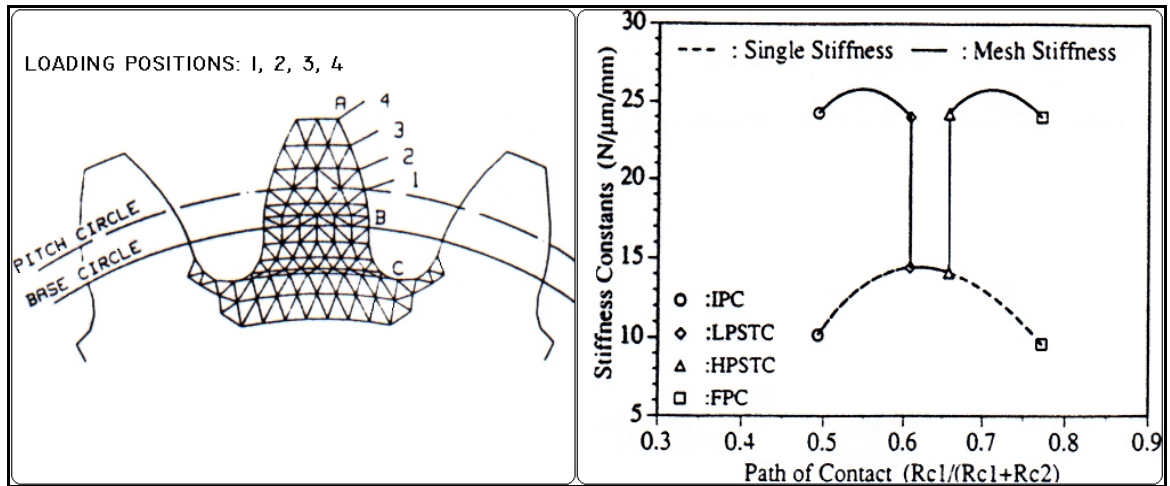
Figure 6.3. 9   Kuang's model and result (Kuang 1992).
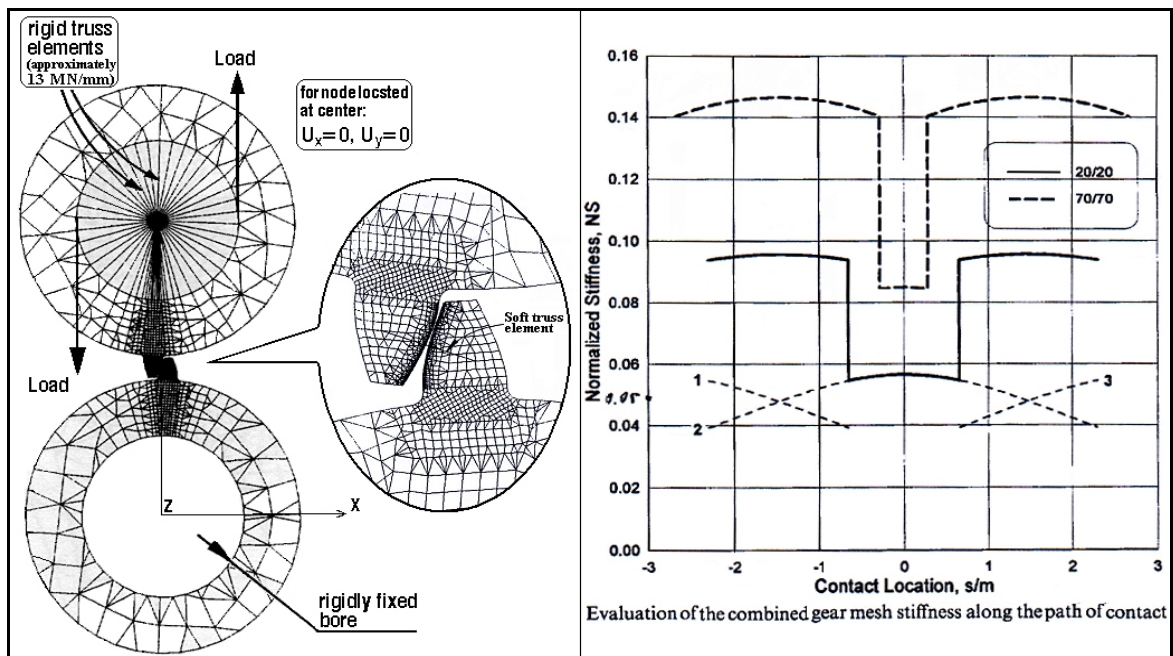
Figure 6.3. 10   Arafa's model and results (Arafa 1999).
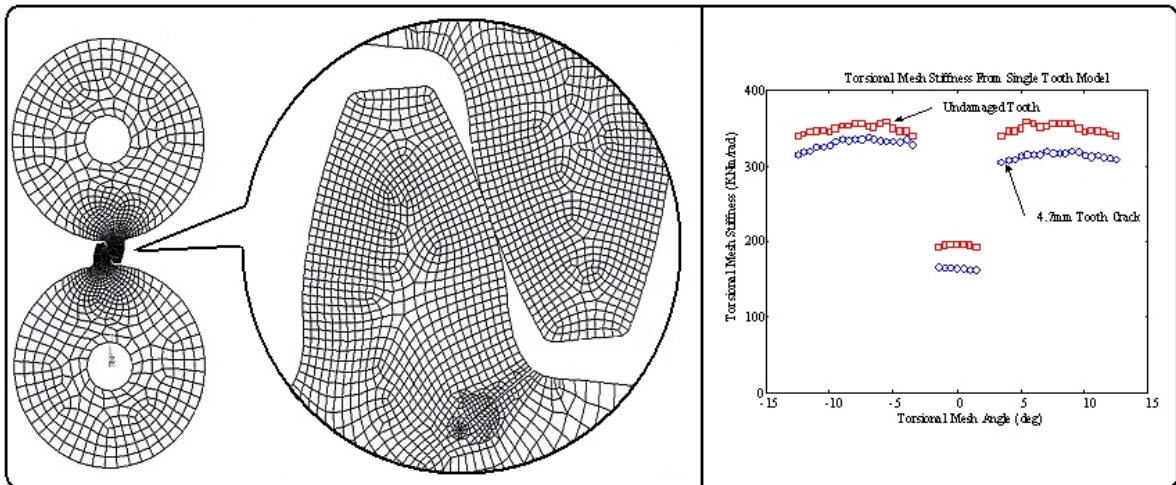
Figure 6.3. 11 Previous model of this research and its results, Wang's model (Wang 2000).

The common error in the above examples is that they incorrectly predict the combined torsional mesh stiffness in the zone of double pair of teeth in contact, because the stiffness of the mesh is far too high. Such high stiffness was developed by parallel superposition of the corresponding single tooth stiffness of the tooth pairs in contact. It was expressed as,

$$K_m = K_s^A + K_s^B. \tag{6.4}$$

The equation above can be illustrated as shown in Figure 6.3.12,
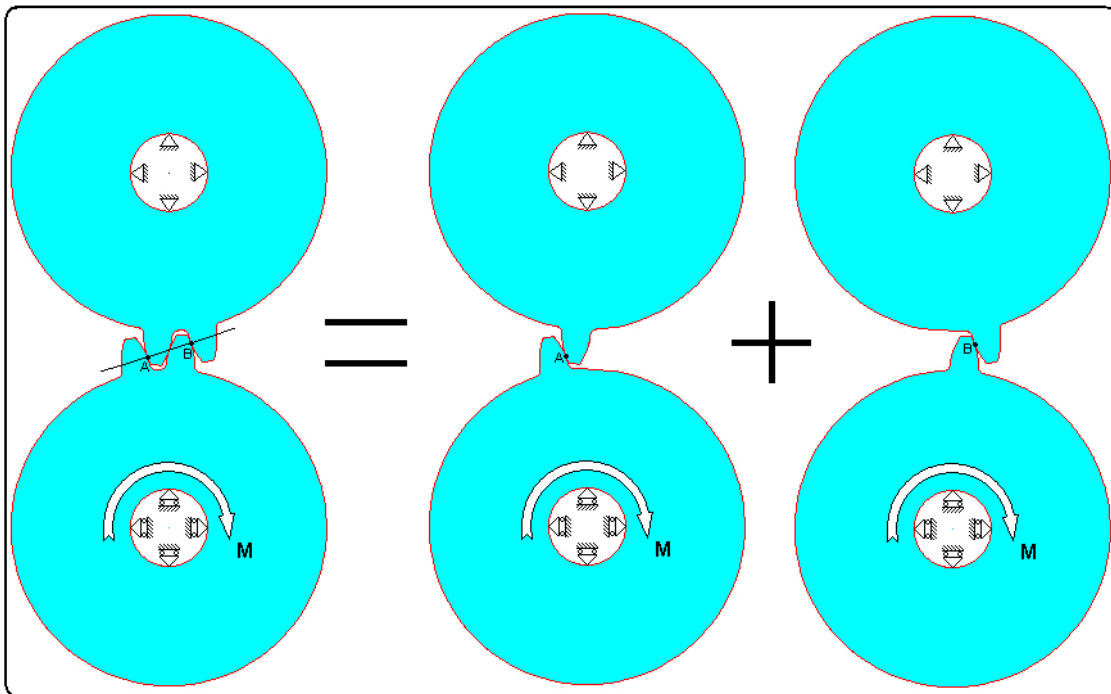
Figure 6.3. 12   The illustration of equation (6.4).

where K_s^A, K_s^B stand for the combined torsional mesh stiffness of the single tooth gear model at mesh position A and B respectively. It can be seen that the error results from each

of the two teeth sharing the one gear body, resulting in the high stiffness by parallel calculation.

Another type of prediction for the combined torsional mesh stiffness when the double tooth pair are in contact, is calculated by combining the individual torsional mesh stiffness of the double tooth pair $K_p^{A,B}$ (for pinion) and $K_g^{A,B}$ (for gear) as springs connected in series, where the superscript ^{A,B} denotes the contact point of each tooth pair along the path of contact of the double tooth pair contact zone. This is illustrated as shown in Figure 6.3.13.

$$K_m^{A,B} = \frac{K_p^{A,B} \times K_g^{A,B}}{K_p^{A,B} + K_g^{A,B}}$$
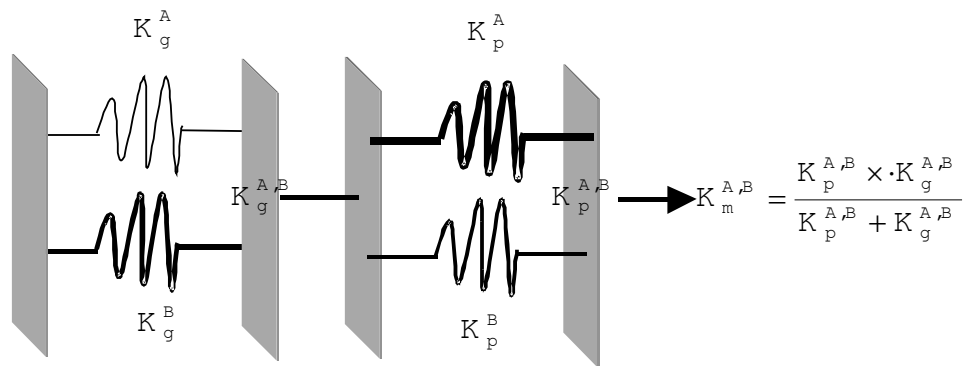
Figure 6.3. 13   A parallel spring connected in series (Sirichai 1999).

Once again, the parallel calculation was used for $K_p^{A,B}$ and $K_g^{A,B}$ which will result in much higher stiffness. If $K_p^{A,B}$ and $K_g^{A,B}$ are calculated as results that have been shown in Fig. 6.3.3, there wouldn't be a large error except at the hand over points. However, in this section, it is interesting to use the previous results to generate a closed form calculation to predict the combined torsional mesh stiffness in the double pair zone.

In most cases, gear body stiffness is a significant component of the total torsional stiffness of a gear. According to the analysis here, the gear body stiffness is 2-4 times higher in magnitude than a single tooth on its own. In general, the gear body stiffness will not be a constant value in the single zone or in the double zone and between these two zones there would be a maximum change in the stiffness. Recall from chapter 4, that the constraint on the gear body from rotation within one tooth space to two teeth space resulted in the torsional stiffness increasing by 8.6%. This shows that the torsional stiffness variations of the gear body in the double zone (or in the single zone) is believed to be smaller than 8.6%.

Now, an assumption can be made by assuming the torsional stiffness of the gear body has a constant value in the double zone of $K_B = 755709.74$ Nm/rad (See section 4.4). The nominal tooth stiffness can then be calculated in the single tooth pair mesh cycle. The nominal tooth stiffness can be defined as a partial tooth stiffness, which is connected with the gear body stiffness in the manner of a series spring in the single tooth mesh zone. The individual nominal tooth stiffness can then be calculated with the results in Figure 6.2.3. It also can be calculated as combined nominal tooth stiffness with the results in Figure 6.3.8. The procedure will be simplified if we choose to calculate the combined nominal tooth stiffness, where the combined nominal tooth stiffness as expressed below,

$$\underline{K}_m = \frac{K_B \times K_{m,s}}{K_B - 2K_{m,s}}, \tag{6.5}$$

where $K_{m,s}$ represents the combined torsional mesh stiffness of the single tooth gear model, in a single tooth pair mesh cycle, and K_B represents the stiffness of the gear body. $K_{m,s}$ can be the stiffness derived from the model of the single tooth gear in contact with the rigid line as shown in Figure 6.3.8. The results are given in Figure 6.3.14.
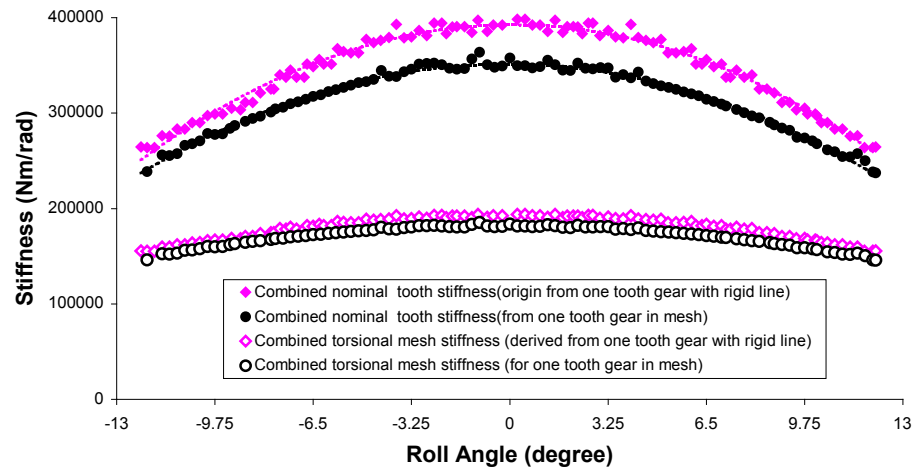
Figure 6.3. 14   Combined nominal tooth mesh stiffness.

Here, the combined torsional mesh stiffness of the gears (as shown in Figure 6.3.12, in the double zone) has been separated as three portions, body-teeth-body, as illustrated in Figure 6.3.15.
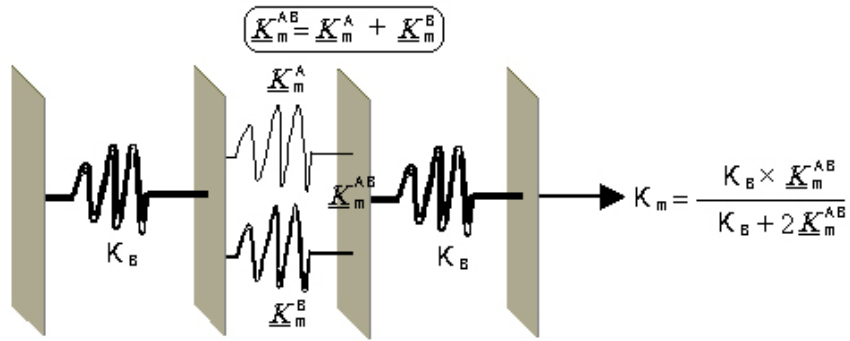
Figure 6.3. 15   A parallel spring connected for meshing teeth and in series with both gear bodies.

As shown above, the combined torsional mesh stiffness for the double pair of teeth in mesh can then be calculated as,

$$K_m = \frac{K_B \times \underline{K}_m^{A,B}}{K_B + 2\underline{K}_m^{A,B}} ,$$
(6.6)

where $\underline{K}_m^{A,B}$ is calculated as a parallel spring, and $\underline{K}_m^A$ and $\underline{K}_m^B$ are calculated in the mesh positions A and B respectively. The combined mesh stiffness K_m is plotted as shown in Figure 6.3.16.
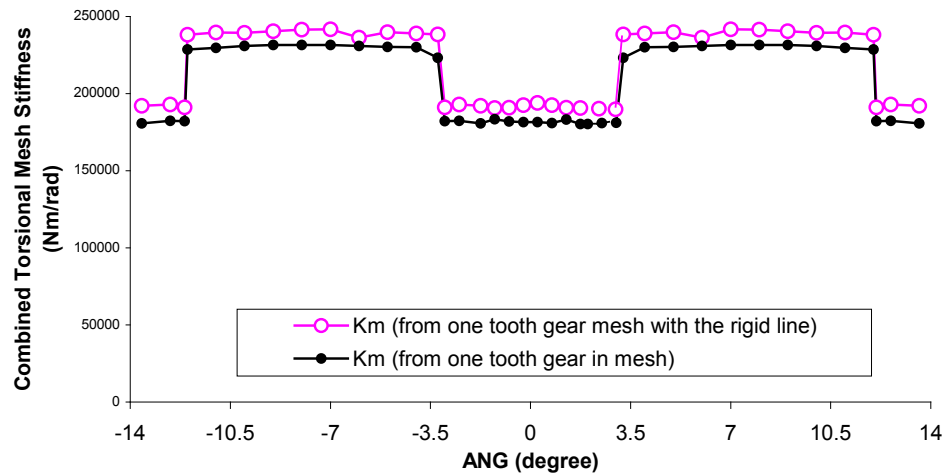
Figure 6.3. 16   The combined torsional mesh stiffness.

In Figure 6.3.16, the single zone data was taken from Fig. 6.3.8 so that the combined torsional mesh stiffness in a complete mesh cycle has been produced. Due to the use of two different data sources, the combined torsional mesh stiffness has an overall 4.5% difference.   With the data sources from the elastic meshing teeth, the result of this

98

calculation is at least as accurate as the one derived from the individual torsional stiffness that has been shown in Figure 6.3.4, but the calculations here are much easier. The basic stiffness sharing inside the meshing gear pair as that given in Figure 6.3.15 has been proven and it can be considered as one of the quick methods to evaluate the basic gear stiffness property.

6.4   The Complete FE Gear Model with Flexible Contact

The complete FE model of a meshing gear pair with flexible contact is more realistic than the previous models in simulation of the combined torsional mesh stiffness for gears in mesh. For undamaged gears in mesh, FEA calculations for the displacements are carried out over half of a complete mesh cycle. A complete mesh cycle for the test gears is 24.912 degrees. If the FE model contains a tooth crack, FEA calculations will be carried out over a complete mesh cycle, which must cover the entire damaged tooth.

6.4.1   2D Modelling

Here, the plane stress assumption was used in the 2D FE modelling gears in mesh with flexible contact as shown in Figure 6.4.1.
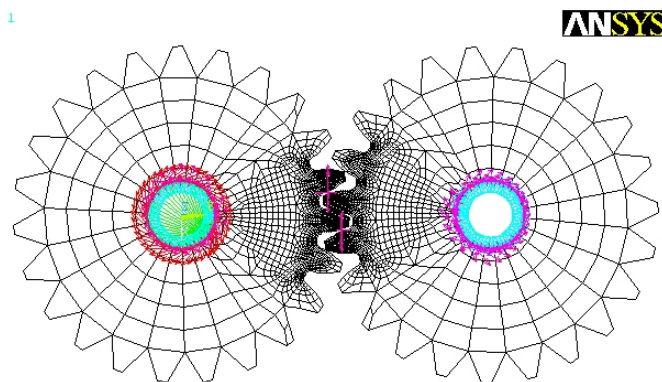
Figure 6.4. 1   The loads, boundary conditions, coupling and reaction forces of
the 2D plane stress model.

The ANSYS$^{®}$ eight node quad 183 series elements were chosen to produce a primary mapped mesh. Within a looping program, adaptive re-mesh with contact was used at each mesh position. The results were automatically saved to the computer network disk. At the end of the loop, the program searched for the input load increments for the starting of the

next loop. The solutions for the displacements under an input load of 5Nm to150Nm (5Nm increment) were repeated over the complete mesh cycle, as shown in Figure 6.4.2.
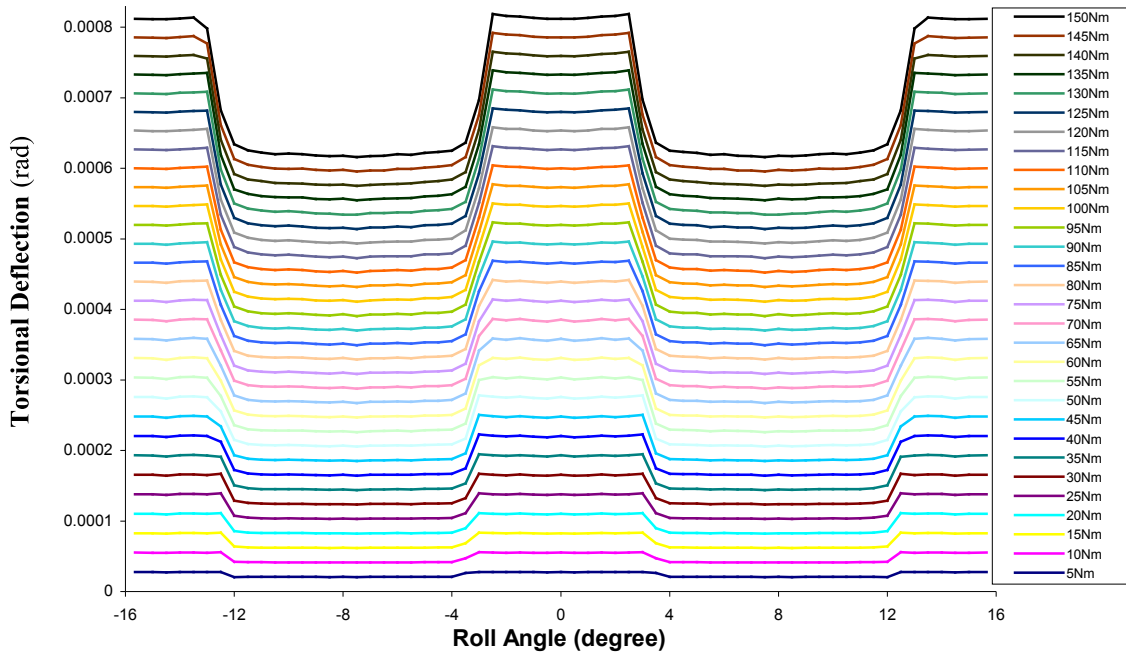
Figure 6.4. 2   The angular rotations of the input gear hub in a complete mesh cycle under various input loads.

The FEA solution was for θ, the angular rotation of the input gear hub in the mesh cycle under the input load series. It can be seen, from Figure 6.4.2 that the angular rotation appears to increase linearly in the single zone and double zone with the increase of the input load. With the results of the displacements from Figure 6.4.2, the combined torsional mesh stiffness over the complete mesh cycle can be produced for the various input torque loads, as shown in Figure 6.4.3.
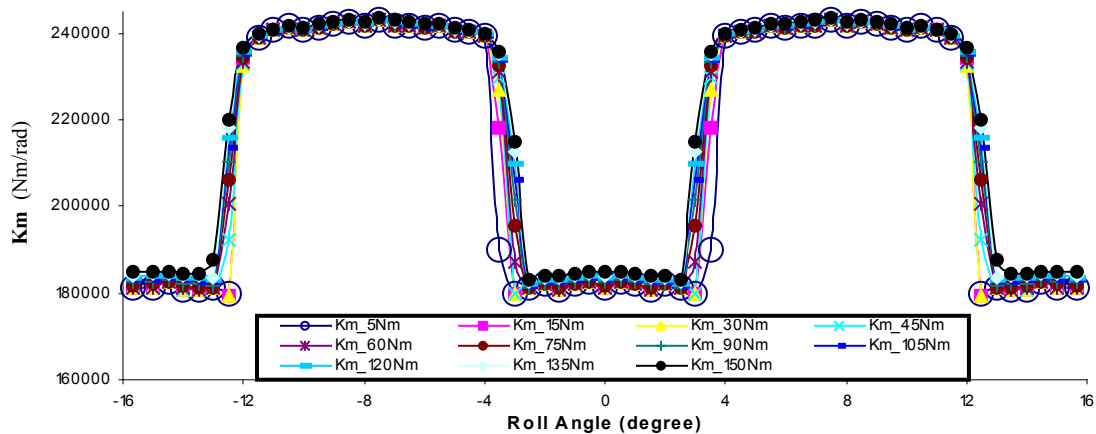
Figure 6.4. 3   The combined torsional mesh stiffness over a complete mesh cycle produced by various input torque loads.

In previous research, the combined torsional mesh stiffness has been assumed to be constant at each mesh position, so that the combined torsional mesh stiffness was independent of the input torque load (Du 1997; Sirichai 1997; Sirichai 1999; Svicarevich 1999; Jia 2000). Using the adaptive re-mesh with contact, accurate results have been obtained as shown in Figure 6.4.3, where it has been shown that the stiffness curve varies with the input torque load. In these solutions, except for the hand over points, the maximum stiffness difference in the (common) single and double zone is only about 0.01%. So, for most metallic gears in mesh, this difference might be ignored. It should be noted however, that the hand over points of the stiffness curve change their positions with various input torque loads. For the input torque variation from 5Nm to 150Nm, as given in Figure 6.4.3, the results show nearly one degree of difference.

6.4.2   3D Modelling

Due to the difficulty in solution convergence at the hand over points, the 2D FE model hasn't produced enough converged solutions of the stiffness in the hand over points, as seen in Figure 6.4.3. For more detailed analysis, 3D modelling using brick elements and adaptive re-mesh with contact was carried out as shown in Figure 6.4.4. where it was found to be particularly useful for overcoming the difficulty in solution convergence.
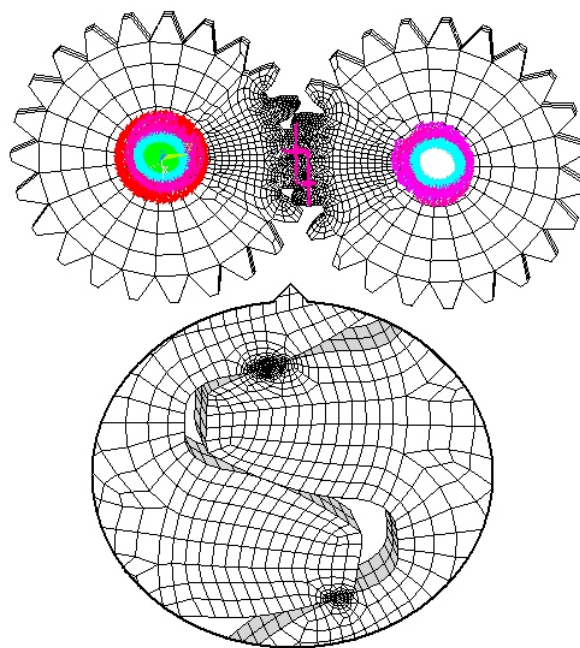
Figure 6.4. 4 The details of the 3D model.

The elastic angular rotations of the input gear hub θ were calculated under a series of input torque loads. The solutions were for a complete mesh cycle with concentration on the angular ranges near the hand over points. The results also compared with the previous solutions (Wang 2000) that were produced by 3D mapped mesh as shown in Figure 6.4.5.
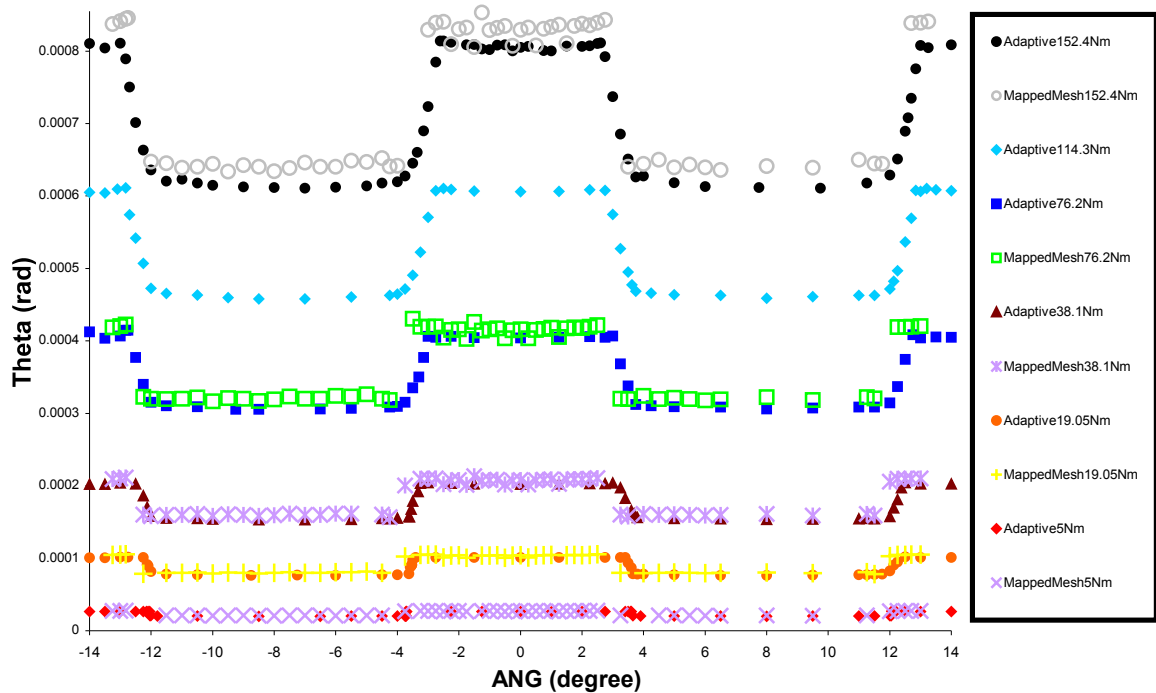
Figure 6.4. 5   The solutions for displacement produced by 3D models.

It can be seen that the 3D adaptive re-mesh with contact, using brick elements, produced results much better than that of 3D mapped mesh, especially for high input load and near the hand over points. It has been found that the hand over from the single zone to the double zone or vice-versa gradually changes in a narrow region, the hand over region, covering 0.02 degrees when the input load is 5Nm. The hand over region increases with the increase of the input load, to cover 1.1 degrees for the input load of 150Nm. The data produced by the displacement curves in those regions also show a change from convex to concave curves between the input load of 38.1Nm or less and 76.2Nm or greater.

The combined torsional mesh stiffness then can be given as the raw data shown in Figure 6.4.6 and the simplified stiffness curves under various input loads were produced as shown in Figure 6.4.7.
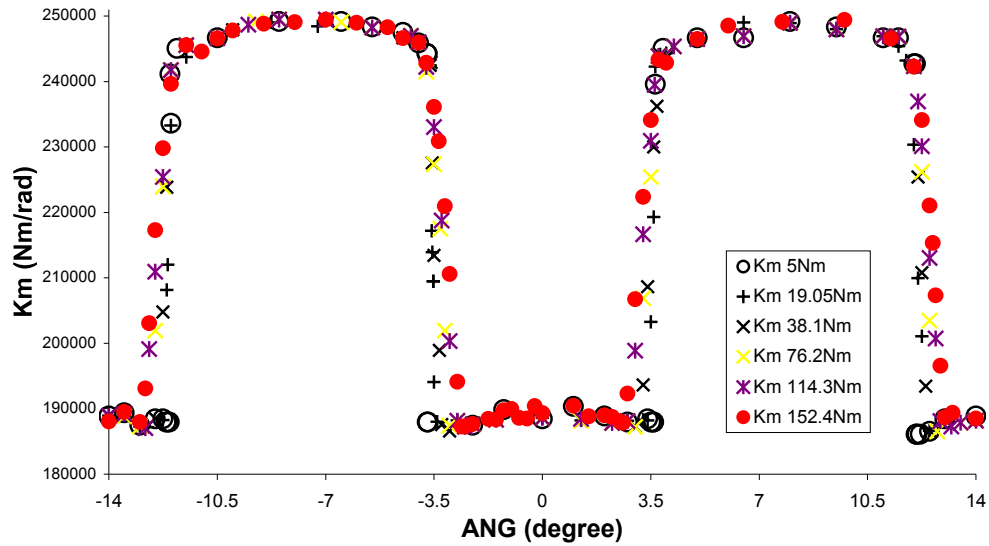
Figure 6.4. 6   The torsional mesh stiffness as a function of load.
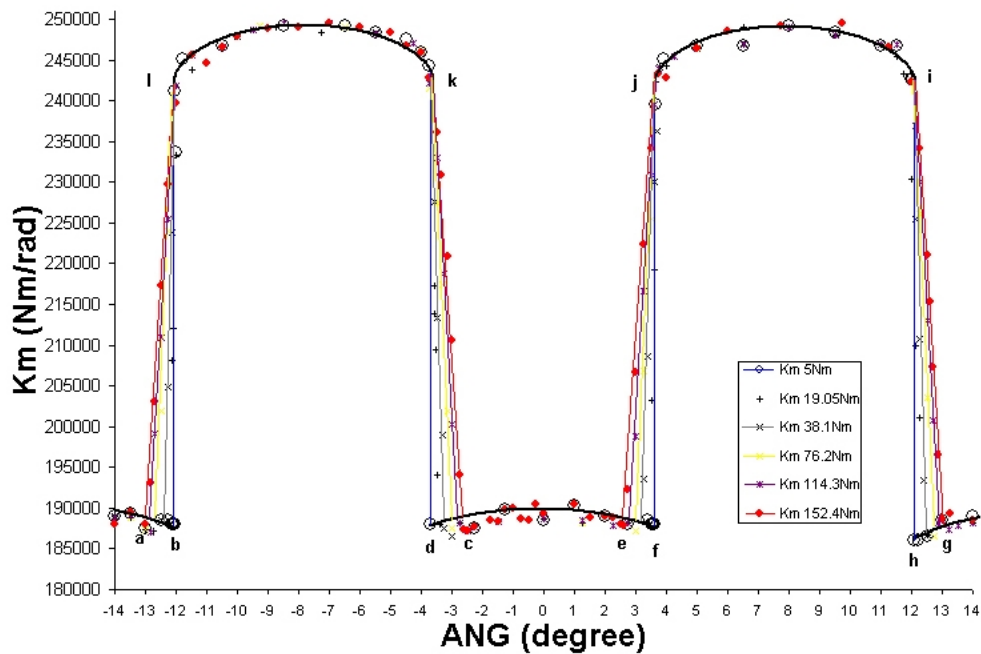
Figure 6.4. 7   The simplified curves of the combined torsional mesh stiffness.

For the study of the major characteristics of the combined torsional mesh stiffness, it is necessary to produce the simplified stiffness curve as shown in Figure 6.4.7.   The simplifications include the following aspects,

• The stiffness difference due to the different input load, in the single zone and double zone, were ignored, because for metallic gears in mesh the differences were less than

0.02% (section 6.3.2, 6.4.1). So common curves such as lk, df and ji, can be developed as shown in Figure 6.4.7.

- In Figure 6.4.5 the displacements in the hand over regions for the larger loads have been shown to be concave, so the stiffnesses in these regions are truly non-linear. However, for metallic gears, a linear approximation is close enough, as can be seen in Figure 6.4.7.
- With increasing input load, the hand over region changes only by the movement of the bottom hand over point, such as position b moving along the common curve towards a. The movement distances for the bottom hand over points as a function of input load can be given as shown in Figure 6.4.8.
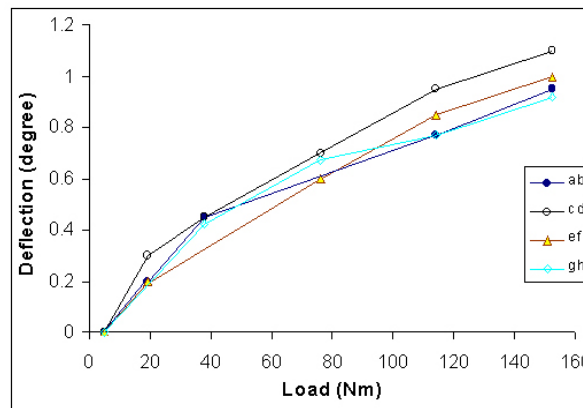
Figure 6.4. 8   The hand over regions versus input load.

Theoretically, point b as in Figure 6.4.7 will have the same angular mesh position as the point l, if the input load is 0 rather than 5Nm. Points i, j, k and l are truly the theoretical hand over points. While the actual hand over points always fall in the bottom of the common curve (single zone), they represent when the second pair of teeth come into contact and start to share the load. Now, for perfect involute gears in mesh, the hand over region can be defined as *the region of the mesh position that is between the actual and theoretical hand over points.*

For a certain load condition, the (variation of) hand over region will be highly reliant on the material property. It could be very narrow for steel gears in mesh, while for non-metallic gears in mesh, for example nylon gears under a certain temperature; their hand over regions can reach or cross each other so that the single zone of the stiffness curve can be significantly reduced, as discussed further in chapter 8.

CHAPTER 7

THE STATIC TRANSMISSION ERROR

7.1   INTRODUCTION

The term transmission error is used to describe the difference between the theoretical and actual input and output angular motion of gears in mesh, as shown in Figure 7.1.1. At low speed, the angular motions can be represented as angular positions of the input and output ends, so that the transmission error can be expressed in angular units as shown in equations (1.1).
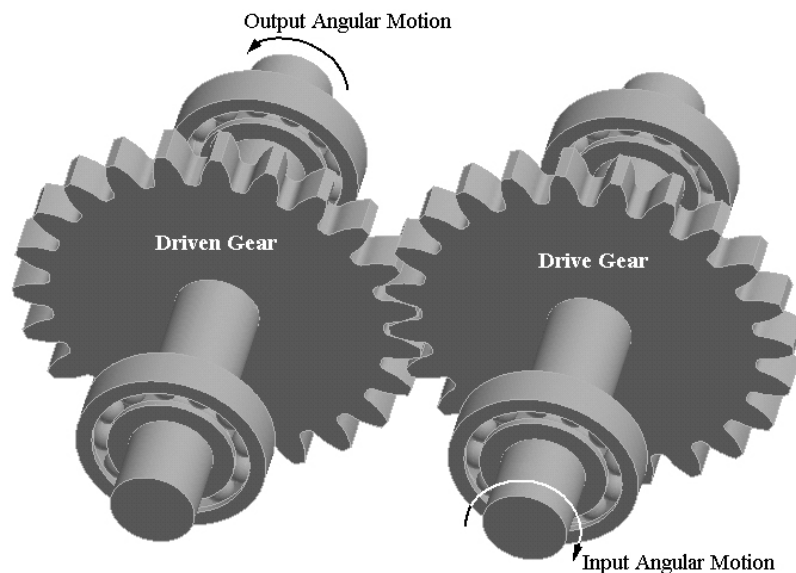
Figure 7.1. 1   Illustration of gears in mesh.

Transmission error is considered to be one of the main important causes of gear noise and vibration. Numerous works have been published on gear transmission error measurement (Gregory 1963; Hayashi 1979; Hayashi 1981; Vinayak 1992; Daniewicz 1994; Munro 1994; Yau 1994; Velex 1995; Munro 1997). Experimentally, rolling gears together with backlash operating at their proper centre distance have been used for transmission error testing. The input and output angular motion characteristics of the gears are normally measured by encoders and associated electronics. The data can be presented in graphical analogue form or can be further processed by Fast Fourier Transform (FFT) techniques to aid in pinpointing the source of excitation.

However, the measurement of transmission errors from test rigs has traditionally not shown a great amount of detail within each meshing cycle. Secondly, the manufacturing geometrical errors such as spacing errors and run out error can be much greater than the loaded transmission error. Therefore the results of gear transmission error measurement from the test rig is greatly influenced by manufacturing irregularities, as noted in previous test rig results (Gregory 1963; Tordian 1967; Hayashi 1981; Houser 1989; Rebbechi 1992; Vinayak 1992; Bard 1994; Barnett 1994; Munro 1994; Velex 1995; Houser 1996; Sweeney 1996).

Two types of transmission error are commonly referred to in the literature. The first is the manufactured transmission error, which can be obtained for unloaded gear sets when they rotate in single flank contact. The manufactured transmission error is affected most by profile inaccuracies, spacing errors, and gear tooth run out. Gears that are rigid and that have perfect involute profiles and no spacing or run out errors should produce a perfectly straight transmission error trace, which would result in a spectrum with no peaks at discrete frequencies. It has also been shown that there is a direct relation between the manufactured transmission error and noise, (Welbourn 1972; Welbourn 1979; Smith 1983; Smith 1987; Smith 1987; Baron 1988).

The second is the loaded transmission error, which is similar in principle to the manufacturing transmission error but takes into account tooth bending deflection, shearing

displacement and contact deformation due to load. When gears operating at low speed are loaded, two additional factors contribute to the transmission error (Townsend 1991),

- A constant component due to the mean tooth compliance. This component is of major significance in choosing appropriate profile modifications, but of much less significance with regard to its contribution to mesh frequency noise,

and

- A time-varying component that is a function of gear tooth geometry and torsional mesh stiffness variation, as well as the manufactured transmission error. This component contributes heavily to mesh frequency noise.

As gears are run at higher speeds, a dynamic component that is a function of the system dynamics, (Ozguven 1988), must be included with the low speed effects aforementioned.

From previous experimental results, the time varying component of transmission error, which is periodic at the tooth mesh frequency, has been shown to relate to gear noise amplitude (Smith 1983; Smith 1987). In fact, it has been shown that the transmission error of spur gears, which have large changes in torsional mesh stiffness, can be reduced significantly by applying appropriate profile modifications (Gregory 1963; Welbourn 1979; Baron 1988; Alattass 1994; Oswald 1994; Litvin 1995; Wang 1996).

The primary purpose of this chapter is to develop the detailed static transmission error over one completed cycle of mesh, in which the effect of the tooth profile modifications is included. The method developed for FEA solution of the detailed static transmission error with tooth profile modifications has general applicability for solutions relating to the components like profile, spacing and run out errors, and it can also be used for creation of gears with new tooth profiles. It has been noted that the related components above are all in the first order, in contrast to the elastic deformations that are higher order components.

For the ongoing research, it is necessary to re-classify the components that contribute to the total (static) transmission error,

1. First order components: including profile, spacing and run out errors from the manufacturing process.   Geometric errors in alignment and tooth profile modifications are also classified here and they typically add "rigid body motion" into the total transmission error.

2. Higher order components: including the elastic deformation of the local tooth contact, tooth bending, shearing, some rotation about the tooth root and the deflection of the gear body due to the transmitted load through and transverse to the gear rotational axis.

3. Higher order dependent components: the relative sliding at the contact(s) is a first order component, however, this component is dependent on the variation of the higher order components. This special component can also be classified into the *loaded transmission error,* in contrast with the other first order components that can be counted as *unloaded transmission error.*   These components also include geometric errors that may be introduced by static and dynamic elastic deflections in the supporting bearings and shafts.

The higher order components store strain energy and some of the first order components are likely to initiate the energy release with considerable speed with the potential to cause system vibration. From the elastic strain energy point of view, the variations of higher order components can transmit their influence to the whole system easily or cause global effects, such as to the shafts, within various rotation speed ranges.   The first order components, especially when the load is light, tend to cause a more local effect and produce noise.   It has been shown that there is a direct relationship between noise and most of the first order components, (Welbourn 1972; Welbourn 1979; Smith 1983; Smith 1987; Smith 1987; Baron 1988).

7.2   Static Transmission Error for Perfect Involute Gears in Mesh

When gears are unloaded, a pinion and gear with involute profiles should theoretically run with zero transmission error. However, when gears with involute profiles are loaded, the combined torsional mesh stiffness of the gears change, as shown in chapter 6, causing variations in angular rotation at the output gear hub or the shaft. At each particular meshing position, the angular rotation of the loaded drive gear due to tooth bending, shearing and contact displacement is calculated in the gear reference frame by restraining

the driven gear from rotating. In relation to the drive gear reference frame, it is restrained from further rotating, while the torque input load and the resulting angular rotation of the gear is computed. The angular rotation is the static transmission error of gears under load at low speed, which can be expressed in angular units as shown in equation (1.1). The procedures above can be illustrated as in Figure 7.2.1, in which the bearings are assumed to be rigid and shaft bending is negligible.
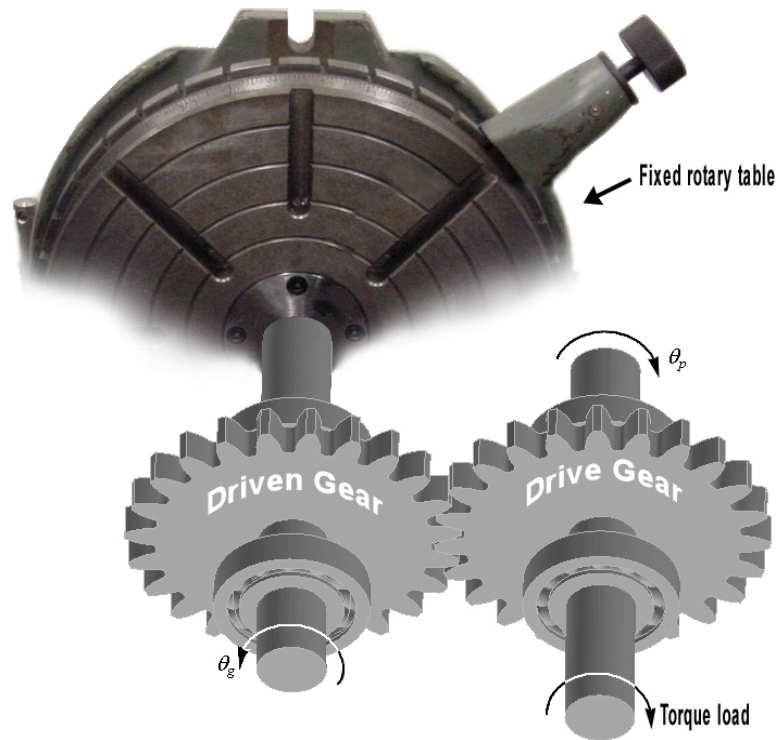
Figure 7.2. 1   With the gear ratio 1:1, static T.E. is shown as $\theta_p - \theta_g$.

For perfect involute gears in mesh, with rigid mounting and linear elastic material properties, the relationship between the input torque T and the angular rotation of the gear hubs θ exists throughout every position of a mesh cycle as shown in equation (7.1),

$$T = K_m \cdot \theta ,$$
(7.1)

where K_m represents the combined torsional mesh stiffness. θ represents the relative angular position difference between the hubs of the mating gears in mesh which is due to the pure elastic deformation. θ remains zero only if the mating gears are perfectly rigid. So, in a mesh cycle, θ will denote the transmission error of the mating gears. In the 2D modelling example shown in Figure 6.4.1, the transmission error will be the same as in Figure 6.4.2 and is represented here as a function of torque input loading as shown in Figure 7.2.2.

109
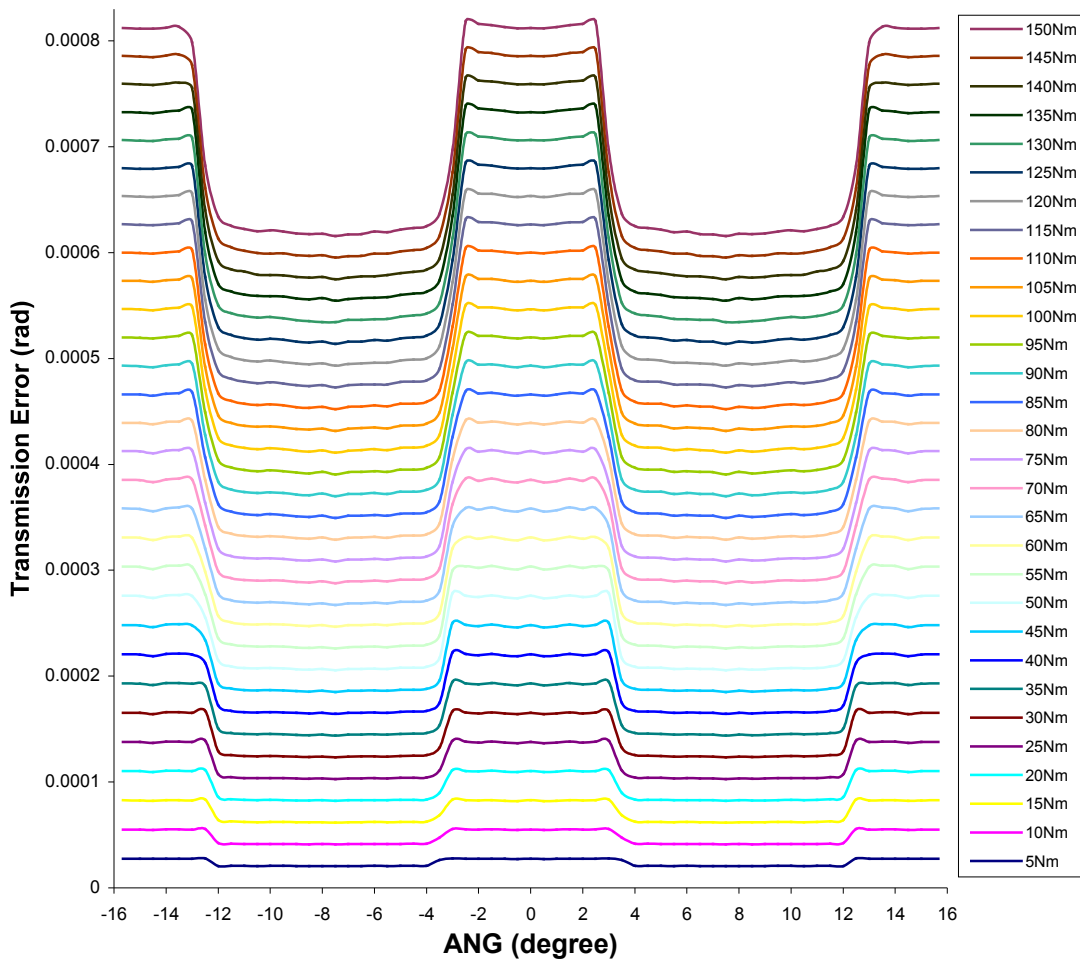
Figure 7.2. 2   The transmission error of mating gears over a complete mesh
cycle under various input loads

Further investigations of the transmission error were accomplished using 3D modelling of the mating gears. Due to the time consuming nature of solving 3D models, the input loads of 5Nm, 19.05Nm, 38.1Nm, 76.2Nm, 114.3Nm and 152.4Nm were considered. As shown in Figure 3.13, the 3D modelling was based on half of the volume as separated by symmetry. The 3D model was mapped meshed with 20 node brick elements containing 35456 nodes. Automatic mesh adaptation with contact was also used to increase the solution accuracy and the computational efficiency. The adaptive meshed model contained about 27000 nodes for one pair of teeth in contact and about 28000 nodes for two pairs of teeth in contact. The 3D results of the transmission error were obtained, as shown in Figure 7.2.3.
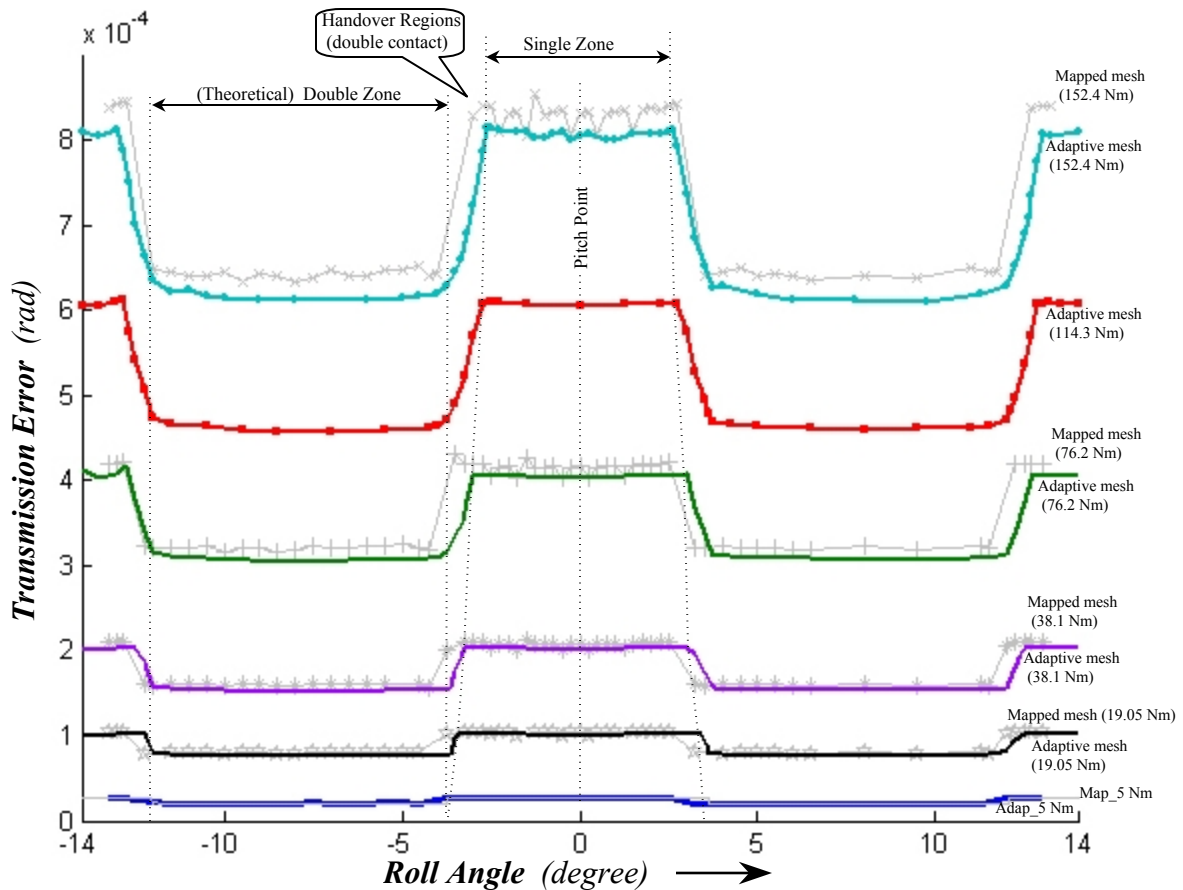
Figure 7.2. 3   Static T.E. of 3D modelling with adaptive and mapped mesh.

It can be seen in Figure 7.2.3, that the major difference between the two methods is the results in the hand over region (details about the hand over region can be referred to in section 6.4.2). The mapped mesh results were observed to be unsymmetrical about the pitch point (0 degrees), by up to 0.5 degrees and abrupt changes from the single zone to the double zone and vice-versa were also obtained. The adaptive mesh results produced much smoother symmetrical curves and more gradual changes in the hand over regions. With the input loads increasing from 5Nm gradually to 152.4Nm, the following conclusions were obtained from the adaptive mesh results:

1. The convex nature of the curve in the hand over region gradually changes from positive to negative convexity.

2. The changes from the double zone to the hand over region (or vice-versa) become smoother, while the changes from the single zone to the hand over region (or vice-versa) get sharper as the load increases.

3. It was observed from the results that the length of the single zones were decreased as the load increased by an amount up to 2 degrees, while the double zones were relatively stable in their size. The hand over regions were observed to extend into the single zone region.

The comparisons can also be made between the 2D and 3D modelling results using adaptive mesh as shown in Figure 7.2.4. The 2D results show similar features as shown for the 3D results; however, the 2D modelling produced fewer details in the hand over region. In comparison with the results from 3D modelling with the mapped mesh, the 2D adaptive mesh results can be seen to be more reasonable. The difference between the 2D and 3D modelling becomes obvious when the input load is large, with a 4.31% relative error in the magnitude of the transmission error being found in the single zone with the input load of 152.4 Nm.
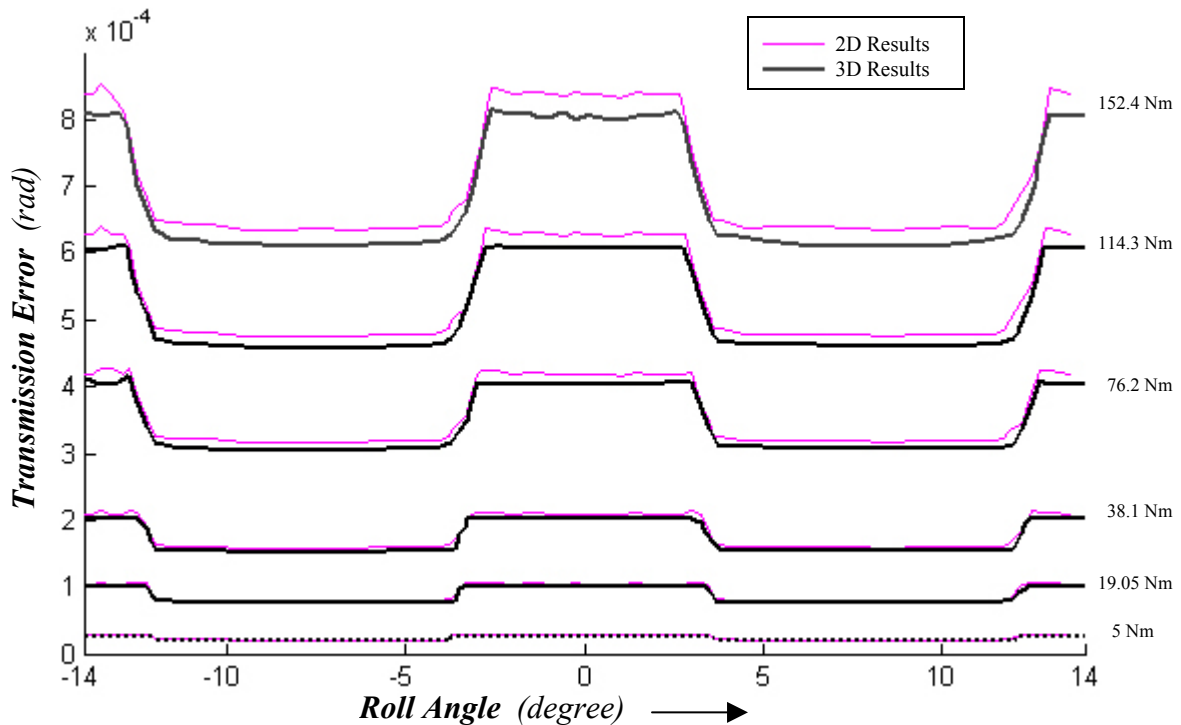
Figure 7.2. 4   T.E. results comparison between 2D and 3D modelling
(adaptive meshes applied on both models).

It should be noted from this analysis that 2D modelling with adaptive mesh is able to produce acceptable results for transmission error studies when compared with 3D modelling. It can be achieved with greatly reduced computational time when using 2D analysis.

7.3   Detailed Hand Over Process of Involute Gears in Mesh

The analysis has shown that the use of adaptive meshing is able to reveal more details about the change over between the single zone and the double zone, defined as the hand over region. However, previous research on gear dynamic models has ignored the effect of gear flexibility (hand over regions) (Cornell 1978; Kubo 1980; Terauchi 1981; Yang 1985; Velex 1989; Lin 1989a; Du 1997; Svicarevich 1999; Jia 2000; Howard 2001; Jia 2001) This means the zone of tooth contact and average tooth mesh stiffness are underestimated, and the individual tooth load is overstated. The analysis by Lin et al. (Lin 1994) shows that neglecting this flexibility (hand over regions) results in underestimating resonant speed and overestimating the maximum dynamic load, the errors are considerable within moderate gear contact ratio (about 1.6) and will be significant with higher gear contact ratio.

The hand over region was also described by Lin (Lin 1994) as the extended tooth contact region, as shown in Figure 7.3.1. Lin used the concept of T.E. separation to generate the separation curves BS_r and CS_a for the case of recess and approach respectively as shown in (a), then combined with the double zone T.E. and the reduced single zone T.E. to produce the final T.E. curve as shown in (b). This work was a considerable progress in the research field, especially for material with higher modulus under light load conditions. However, there is a major limitation in use of the separation curves in this case due to the incompatibility between the separation and the T.E. curves:

- TE separation, also known as the *transmission error outside the normal path of contact*, $TE_{o.p.c.}$ (Munro 1999), has been calculated geometrically without consideration of the elastic deformations. It has been found to be well suited for the evaluation of the effects on T.E. caused by manufacturing errors, wear and other geometric errors.
- The T.E. (curve) presented here (Figure 7.3.1) is the load T.E. of the perfect involute spur gears, and is only depending on the load, boundary conditions and the material flexibility.

So, the use of the T.E. separation is actually not suitable for describing the loaded T.E. behaviours.

(a) Theoretical Static Transmission Error and Separation Distance

The gap between the T.E. curve and the separation curve is observed. [The gap should be load dependant in this case.]

(b) Comparison of Static Transmission Error with Effect of Extended Tooth Contact Both Included and Ignored
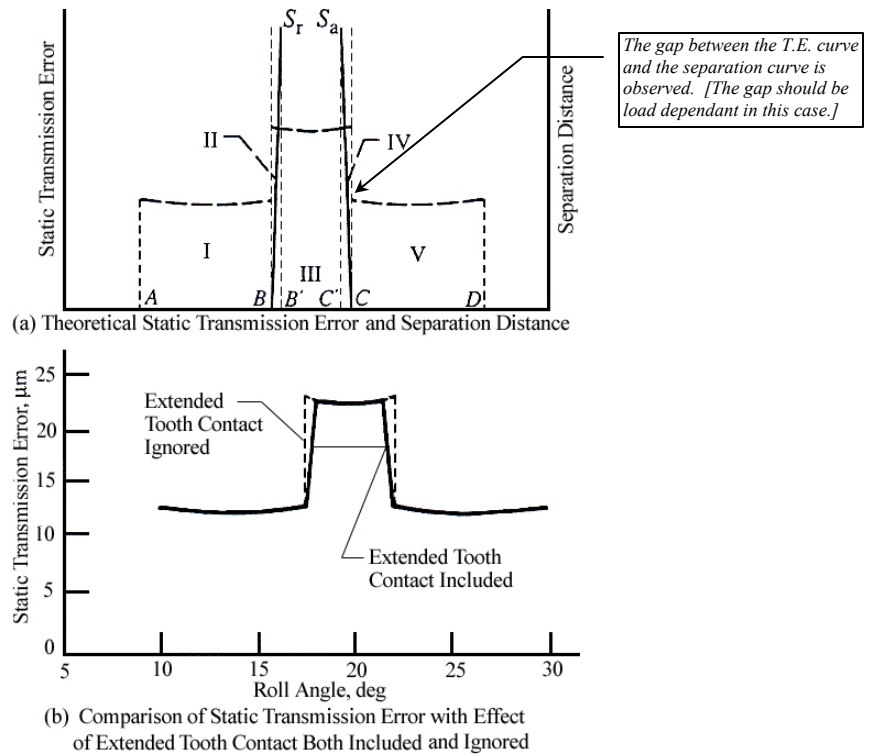
Figure 7.3. 1   Static transmission error and separation distance for gears with contact ratio = 1.64 (Lin 1994).

The handover region defined in this research is valid only when gears are loaded, and evaluations can only be carried out with numerical methods such as FEA. The following sections will give detailed features of the handover region.

7.3.1   Ratio of Local Deformation Over a Complete Mesh Cycle

The local deformation of the contact tooth is one of the most complex components of the meshing gears. The ratio of local deformation represents the influence to the deflection of the global gear system (total T.E.) by local contact(s). It also represents the character of the meshing gears in different mesh positions.

In chapter 4 section 7, the ratio of local deformations in two particular mesh positions has been defined. However, it is necessary to produce a curve for the ratio of local deformation over a complete mesh cycle to enable us to further explore the mechanism of gears in mesh. Local deformation θ_c is represented as shown in Figure 7.3.2, where some details can be referred to chapter 4.

114
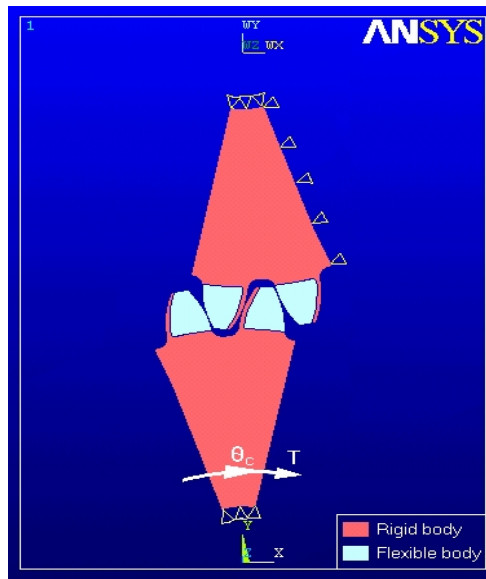
Figure 7.3. 2   Illustration of the local deformation θ_c under input torque load T.

Generally, the components of the local deformation θ_c are elastic contact deformation and the sliding at the contact points, the latter component caused by rigid body motion. When the contact is at the pitch point, the amount of sliding can be ignored, and θ_c may be considered as pure elastic deformation.

The FEA solutions of the local deformation over a complete mesh cycle were obtained from 78 points covering a complete mesh cycle with several points occurring in the hand over region. The local deformation θ_c was also compared with θ, the solutions of the complete elastic gears in mesh, as shown in Figure 7.3.3 when the input load was 76.2Nm.
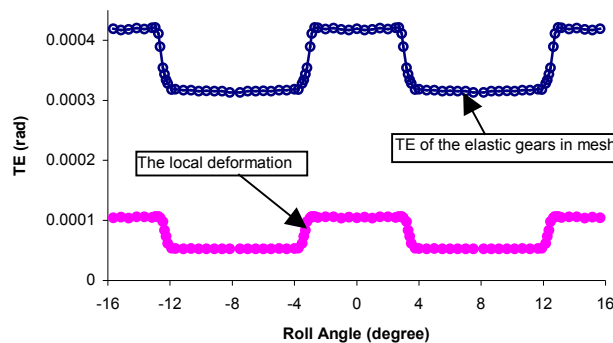
Figure 7.3. 3   The local deformation over a complete mesh cycle.

The curve of the local deformation is noted as being similar to that of the transmission error of the elastic gears in mesh, and both 2D adaptive mesh results were found to be about

115

4.31% above the corresponding results obtained from the 3D models. As the investigation here concerns the *ratio of local deformation* θ_c / θ (see function 4.19), the difference from the results obtained with 3D models would be minimized. The ratio of local deformation for the input load 76.2Nm is given as shown in Figure 7.3.4.
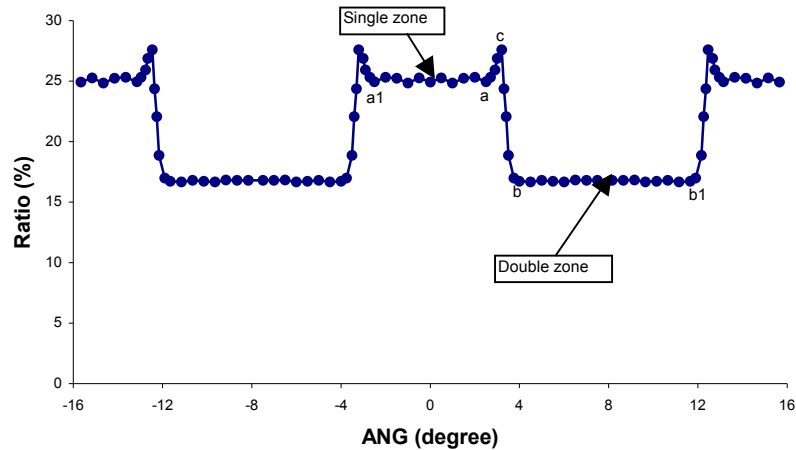
Figure 7.3. 4 The *ratio of local deformation* for the input load 76.2Nm.

It can be seen from the results that the ratio in the single zone aa_1 averages close to 25% while in the double zone bb_1 the ratio averages approximately 16.7%. The hand over region ab here is estimated to cover the range from 2.7^0 to 3.75^0. The maximum value of the ratio is 27.6% at c which is located at 3.2^0, close to the middle of the hand over region. The corresponding results for the increased input loads of 114.3Nm and 152.4Nm are given in Figures 7.3.5 and 7.3.6 respectively. The ratio in the single zone was found to have decreased to 24.5% and 24% respectively, approximately 1% lower than before the higher load is used. The hand over region was found to have increased by 0.2^0 with position a shifting from 2.7^0 to 2.5^0 as the load increased.
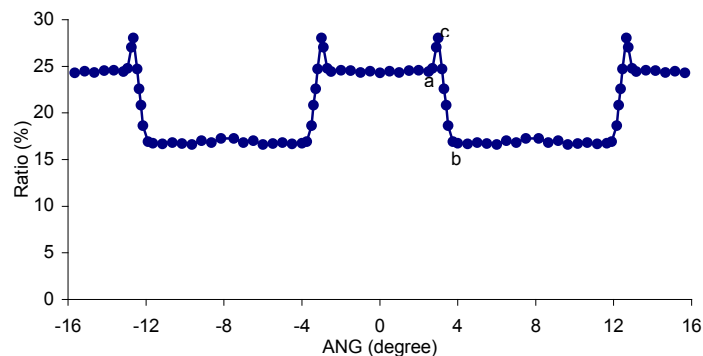
Figure 7.3. 5 The *ratio of local deformation* for the input load 114.3Nm.

116
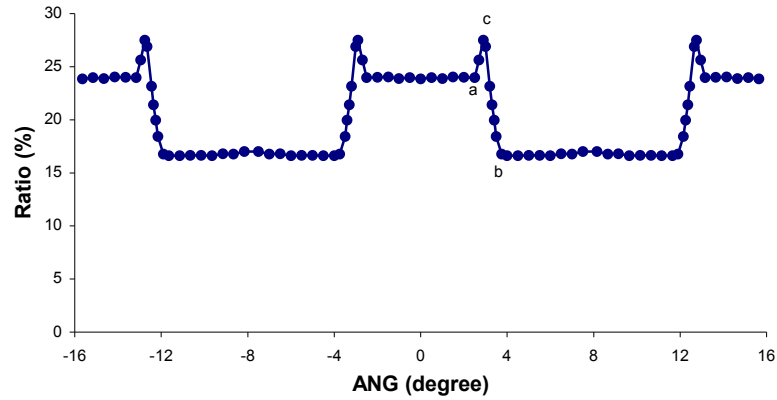
Figure 7.3. 6   The *ratio of local deformation* for the input load 152.4Nm.

An analysis of smaller loads was also conducted with a series of input loads varying from 38.1Nm to 1Nm. The input loads were unevenly spaced here, because the ratio of local deformation in the hand over region was found to dramatically change within this range of input load, especially when the input load was about 8Nm. The series of input loads used here were 38.1Nm, 30Nm, 25Nm, 19.05Nm, 15Nm, 10Nm, 8Nm, 5Nm and 1Nm. The ratio of local deformation is given for each input load, as shown from Figures 7.3.7 to 7.3.15 respectively, and combined as shown in Figure 7.3.16.
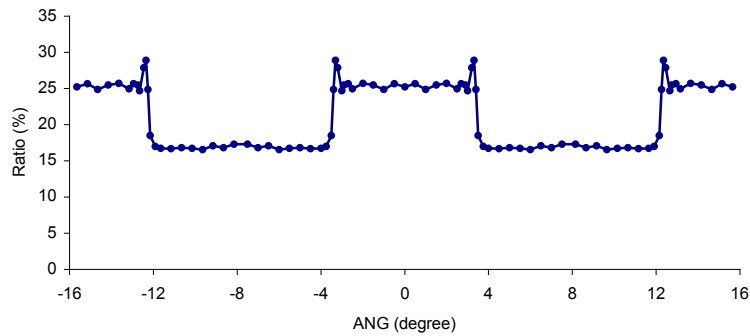
Figure 7.3. 7   The *ratio of local deformation* (load 38.1Nm).
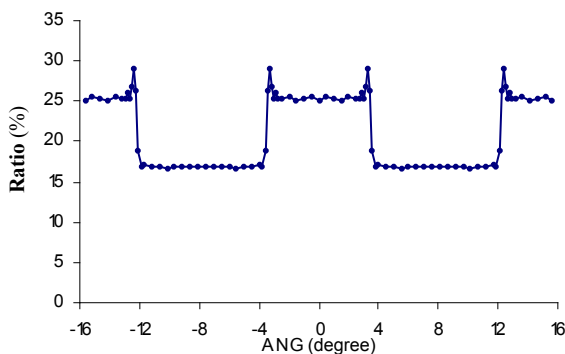
Figure 7.3. 8 The *ratio of local deformation* (load 30Nm).
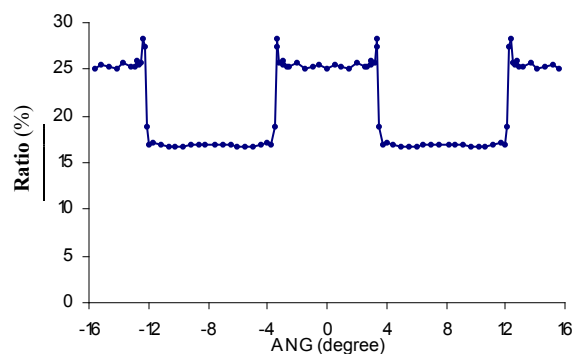
Figure 7.3. 9 The *ratio of local deformation* (load 25Nm).

117
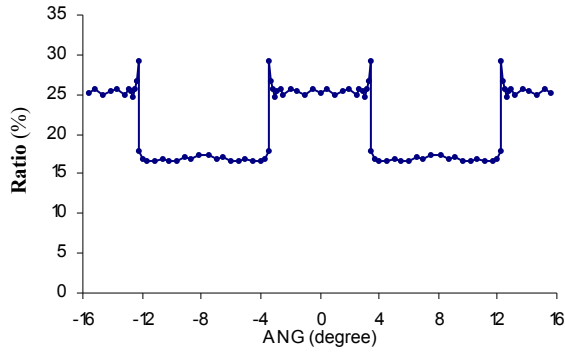
Figure 7.3. 10 The *ratio of local deformation* (load 19.05Nm).
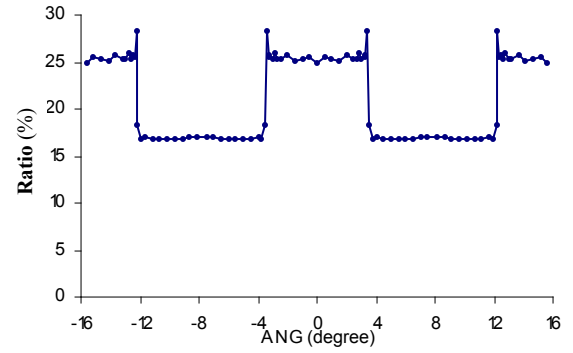
Figure 7.3. 11 The *ratio of local deformation* (load 15Nm).
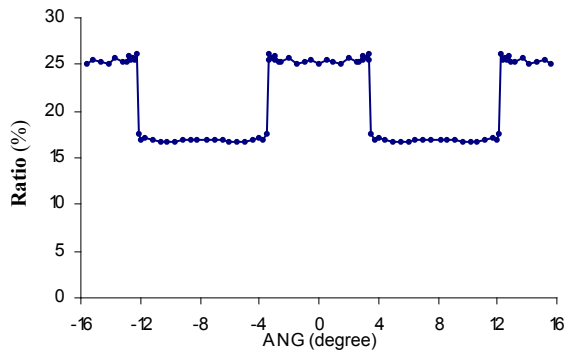
Figure 7.3. 12 The *ratio of local deformation* (load 10Nm).
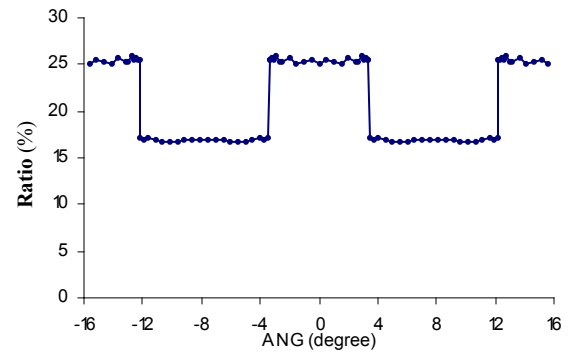
Figure 7.3. 13 The *ratio of local deformation* (load 8Nm).
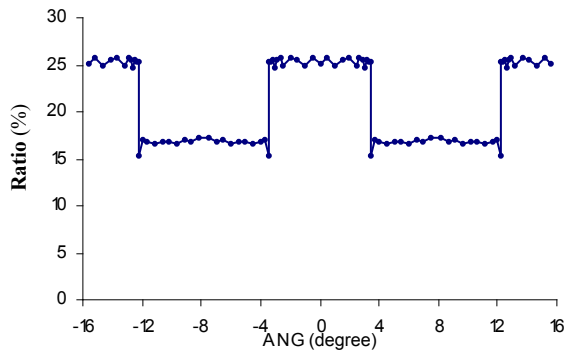
Figure 7.3. 14 The *ratio of local deformation* (load 5Nm).
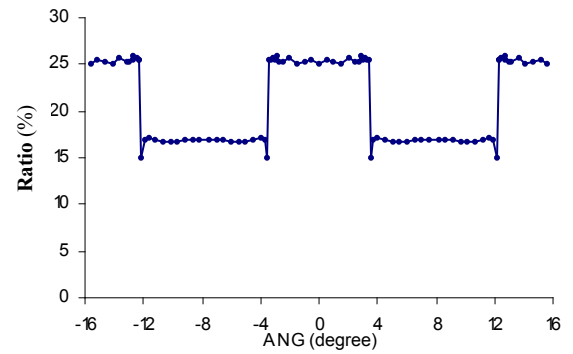
Figure 7.3. 15 The *ratio of local deformation* (load 1Nm).

Throughout the results above, the maximum ratio of local deformation of 29% was found in the hand over region when the input loads were in the region between 38.1Nm and 19.05Nm. While the hand over region decreased with the decrease of the input load, the hand over region was reduced to 0.5^0 which was about half of the maximum size of the hand over region when the input load was 30Nm. Further decreases in the input load from 15Nm to 10Nm, resulted in the maximum ratio of local deformation being reduced from 28% to 26% respectively and the positions remained in the hand over region. When the

input load was 8Nm, no significant abrupt changes to the ratio of local deformation were observed in the hand over region. Finally, when the input load was dropped to 5Nm and 1Nm, the minimum ratio of local deformation of 15.4% and 14.9% were found respectively. The minimum ratio was found to be located at the same position of 3.5^0 which was still inside the hand over region. Ignoring the hand over region, the ratio of local deformation in the single and double zones were relatively steady for the input load of 38.1Nm and less, with average values of 25% for the single zone and 17% for the double zone.

The overall configuration of the ratio of local deformation with the input loads from 1Nm to 152.4Nm is given, as shown in Figure 7.20. It has been shown that the abrupt changes to the deformation ratio as a function of mesh angle mainly occurred in the hand over region. The variations of the ratio of local deformation were in agreement with the previous research on the variations of the hand over region as discussed in section 7.2.1.

The large ratio of local deformation indicates that contacts at (or near) the tooth tips consist of large elastic (or plastic) deformation as well as large sliding. This result may be useful for further research into the failure analysis of gear flank face conditions. Further study into the ratio of local deformation may also help to design a suitable tooth tip relief so as to modify the shape of the gear transmission error.

7.3.2 Detailed Analysis – T.E. and Load Sharing Ratio

Section 7.2 has proven the existence of changes within the hand over regions by using adaptive meshing and desired results can be achieved with finer level of 3D adaptive meshing as long as the computational time is not excessive. 2D adaptive mesh models can produce similar results to that of 3D modelling, but less detail will be observed in the hand over regions, unless a finer level adaptive mesh is carried out. A finer 2D adaptive mesh model was conducted here with a mesh density of up to 21000 nodes with the element dimension near the contact(s) of about 0.033 mm. More realistic stress fields near the contact(s) should be observed with such a fine mesh, as shown in Figure 7.3.17.
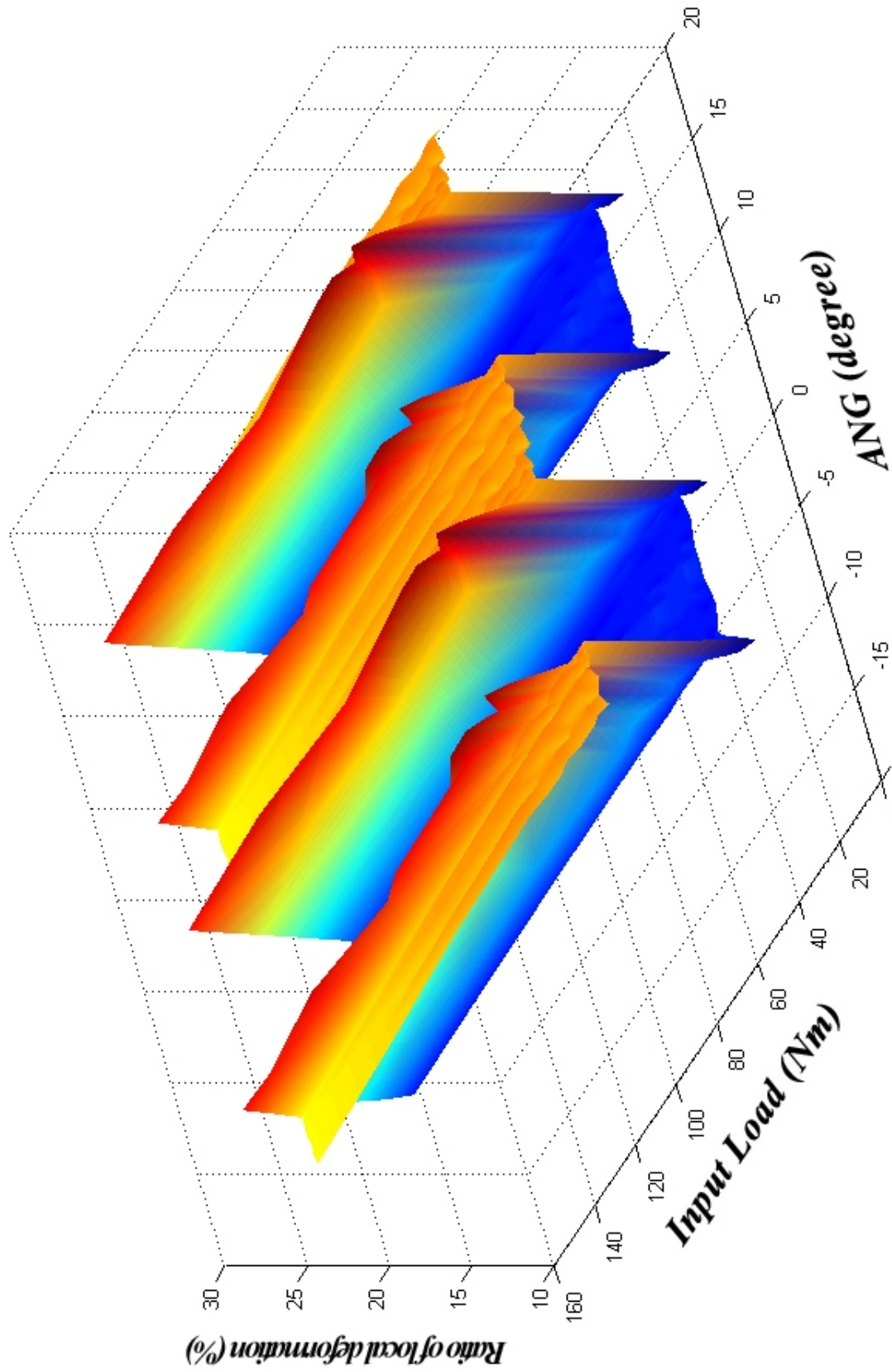
Figure 7.3.16   The overall configuration of the ratio of local deformation.
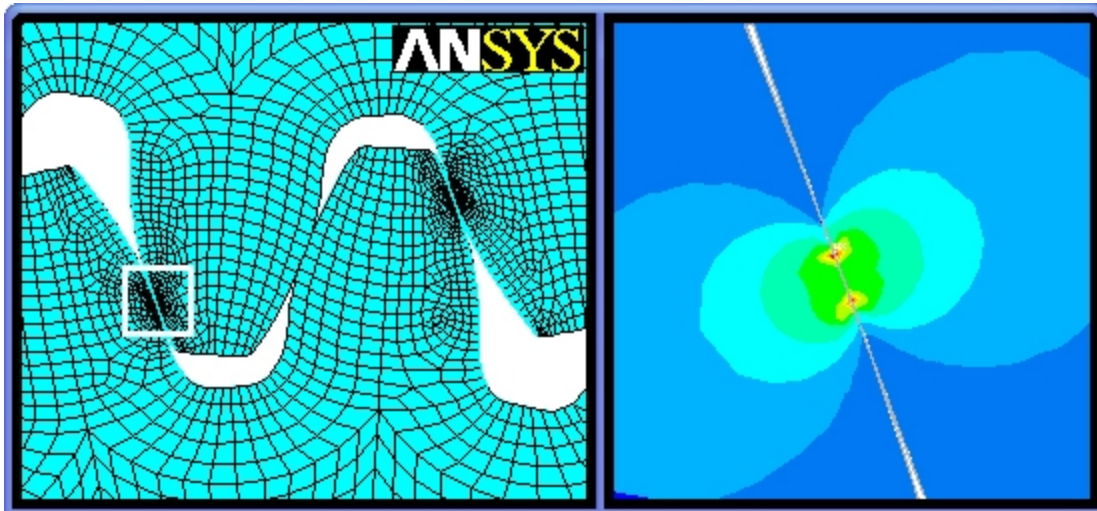
Figure 7.3. 17   More realistic stress fields near the contact(s) with a finer adaptive mesh.

The precision FEA results of T.E. (as shown in Figure 7.3.18) are able to provide detailed variations of the critical points that are positioned at the edge of the single zone for various input loads. Those critical points include both the recess case (start of the single zone) and the approach case (end of the single zone). The results listed in Table 7.3.1 have shown that the recess case is slightly different from that of the approach case as discussed further here; i) *Minor difference between the T.E. values.* When the input load is 5 Nm or greater, the T.E. results for the recess case are slightly larger than for the approach case. When the input load is 1 Nm, the greater value of T.E. is found at the approach case.

Single zone edge points / Input load	Recess		Approach	
	Position (degree)	T.E. (rad)	Position (degree)	T.E. (rad)
152.4 Nm	-2.55	8.6856E-04	2.64	8.6505E-04
114.3 Nm	-2.75	6.5625E-04	2.8	6.5200E-04
76.2 Nm	-2.9	4.4283E-04	2.93	4.4142E-04
38.1 Nm	-3.15	2.2461E-04	3.15	2.2435E-04
19.05 Nm	-3.3	1.1312E-04	3.3	1.1283E-04
5 Nm	-3.5	2.9675E-05	3.5	2.9546E-05
1 Nm	-3.635	5.9157E-06	3.63	5.9473E-06
* Position is counted as the rolling distance away from the pitch point.				

Table 7.3.1.   Details of the single zone edge points under various input loads.

However, the differences between the T.E. of recess and approach for each input load are very small, as the maximum (relative) difference of 0.7% occurs when the input load is 114.3 Nm. ii) *Difference between their sizes.* When the input load is 1 Nm, the hand over region is very small.
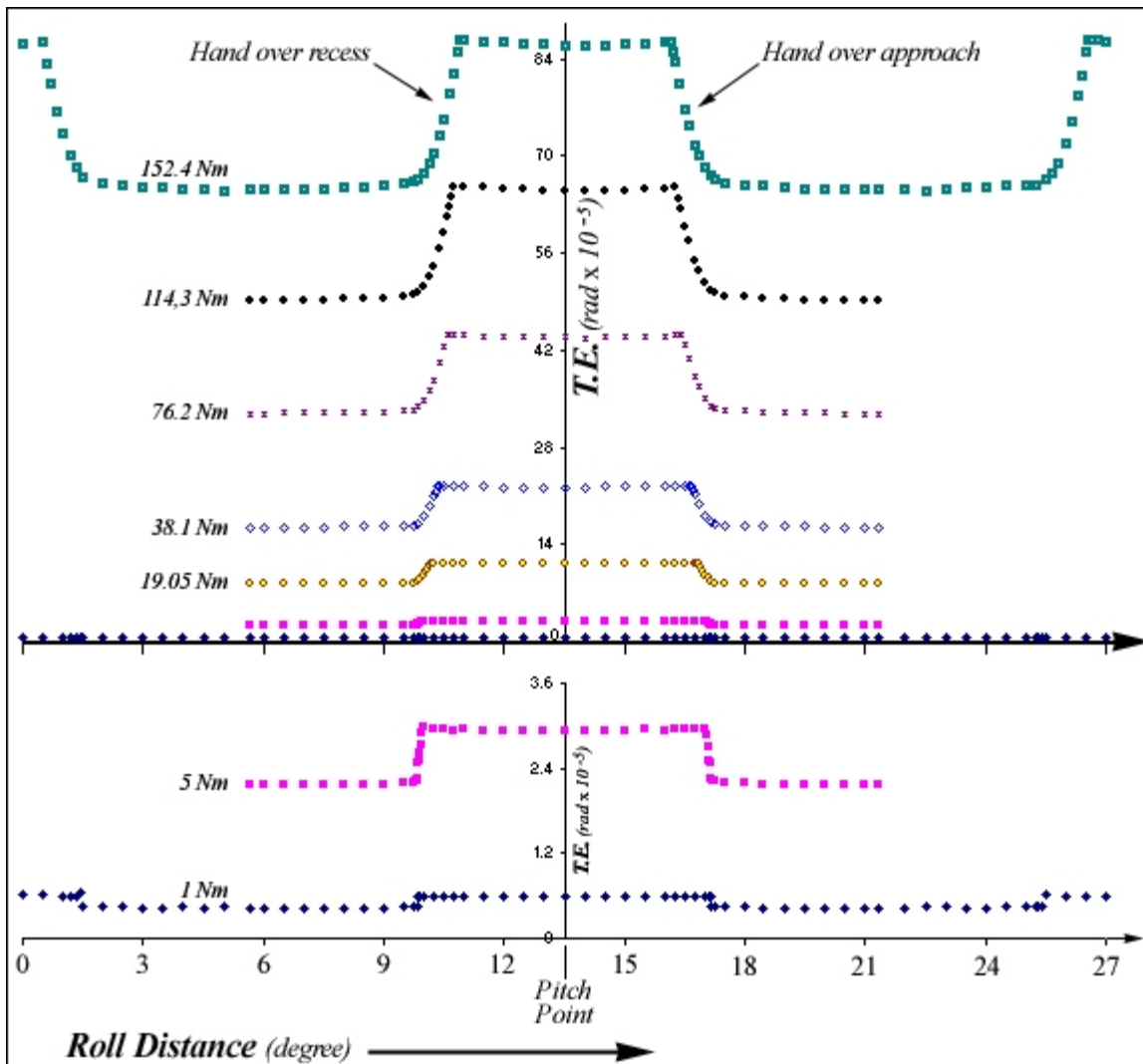
Figure 7.3. 18   The precision analysis results of T.E. under various loads.

In the recess case, the hand over region is in between −3.64 to −3.635 degrees as counted from the pitch point (the pitch point is at 0 degree). While for the approach case it is between 3.63 to 3.635 degrees. When the input load is 76.2 Nm or greater, the results show different expansion rates of the hand over regions. When the input load is 152.4 Nm, there is 0.99 degree in difference between the single zone edge points that makes the T.E. asymmetrical to the pitch point, and the width of the hand over regions are 1.085 and 0.99 degrees for the recess and the approach case respectively. It should be noted that the width of the recess hand over region is always wider than that of the approach. Those features above can be illustrated in Figure 7.3.19, however the T.E. differences cannot be visually observed.
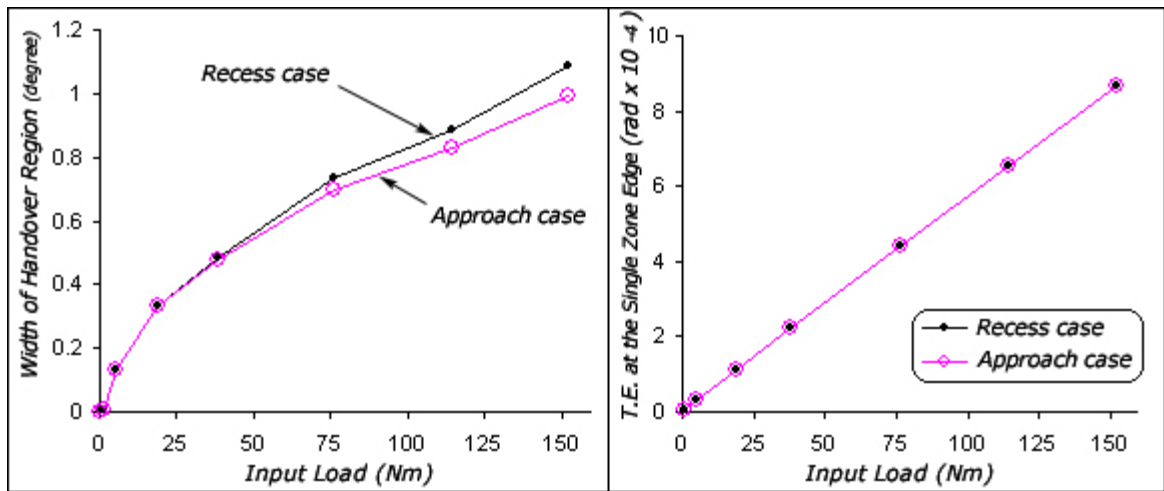
Figure 7.3. 19 Diagram illustrates Table 7.3.1.

The same FEA calculations can also produce results for the load-sharing ratio, as shown in Figure 7.3.20.
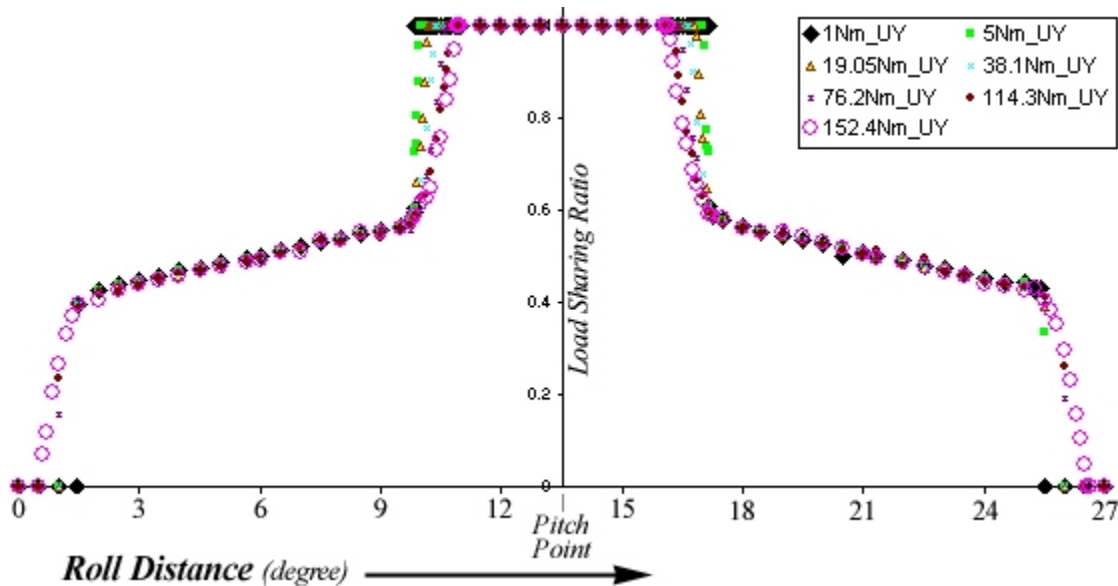
Figure 7.3. 20   Load sharing ratio under various input loads.

The variation of the load-sharing ratio can be noted in the change over between the single and the double zone. Over a complete mesh cycle, four domains I, II, III and IV will be produced by the load sharing curve sweeping with the input load from the minimum (1 Nm) to the maximum (152.4 Nm) load, as shown in Figure 7.3.21.
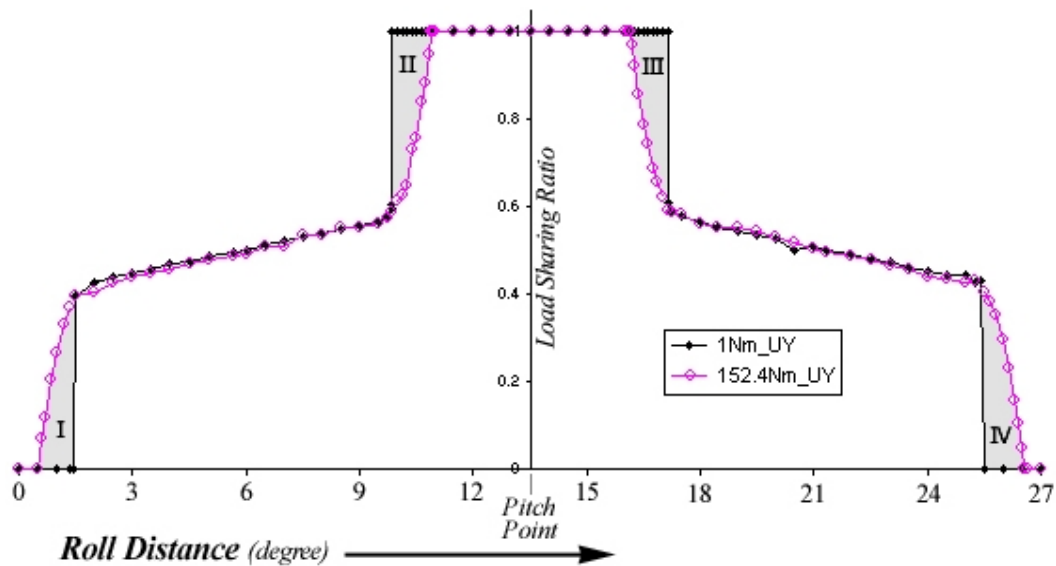
Figure 7.3. 21 Domains of load sharing ratio under certain range input loads.

Theoretically, domain I = domain III for the approach cases and domain II = domain IV for the recesses. The double zones remain relatively stable with load, whereas the single zone results obviously change with load.

7.3.3   Conclusion

The existence of the hand over region is due to the flexibilities of the mating gears, so it has a general application in geared transmission systems.   In the hand over region, the mechanism properties of the mating gears such as combined torsional mesh stiffness, ratio of local deformation, load sharing ratio and the T.E. are changing rapidly as shown in Figure 7.3.22.   For metallic gears in mesh, these changes occur in a relatively narrow range.   However, some of the properties are difficult to predict, especially when the material modulus is high. Approximate expression (T.E.) can be obtained (Lin 1994) as long as the width of the hand over region is estimated correctly (in such a case, the difference between the recess and the approach may be ignored).   When the material modulus is low, approximate curves may not be practicable. However, for wider handover regions, the values of the properties are relatively easier to be predicted by numerical methods. In general, it's not desirable to have rapid changes of the mechanism properties. Modifications to tooth profiles, including tip relief will be more important for material with higher modulus values.

There are some points to note about Figure 7.3.22;

1. The combined torsional mesh stiffness is no longer showing the "common" path (such as in Figure 6.30) due to the finer meshed FEA model.

2. The ratio of local deformation was produced by a different FEA model (coarse meshed) so that the hand over regions are slightly different.

7.4   Tooth Profile Modifications (Tip Relief)

It has been discussed in 7.2.1 that the transmission error of the (pure involute) gears changes rather dramatically in the hand over region with increased input load, where the tooth tip runs into the mating tooth flank surface with large sliding (called edge or corner contact). This dramatic change in transmission error is a major factor in subsequent tooth flank surface spalls and system vibration and noise. For most metallic gears, such as steel gears, the hand over region would be much narrower than the one shown here for the aluminium gears. For steel gears the large ratio of local deformation and the abrupt nature of the changes in the narrower region on the harder surface would give rise to high stress and rapid failure (spall, crack).

Manufacturing errors can add to these effects so that it is necessary to relieve the tooth tip. There are different types of tip relief according to various applications and requirements, but they would have the same effects on the meshing gears:

- Altering the components of the *ratio of local deformation* by reducing the local elastic deformation that causes high stresses, and avoiding corner contact.

- In extending the range of the sliding contact, an extra margin of the angular rotation (of the input gear hub) is gained (specially) in the double zone. In other words, rigid body motion is added in the double zone. That means it is possible to gain a smoother curve of the gear transmission error with a certain input load.

If the first point were considered of more importance in the application, then a short tip relief design would be chosen. If the second point or both were considered of primary importance then one must choose a long tip relief design. Long and short tip relief will be discussed in this section.
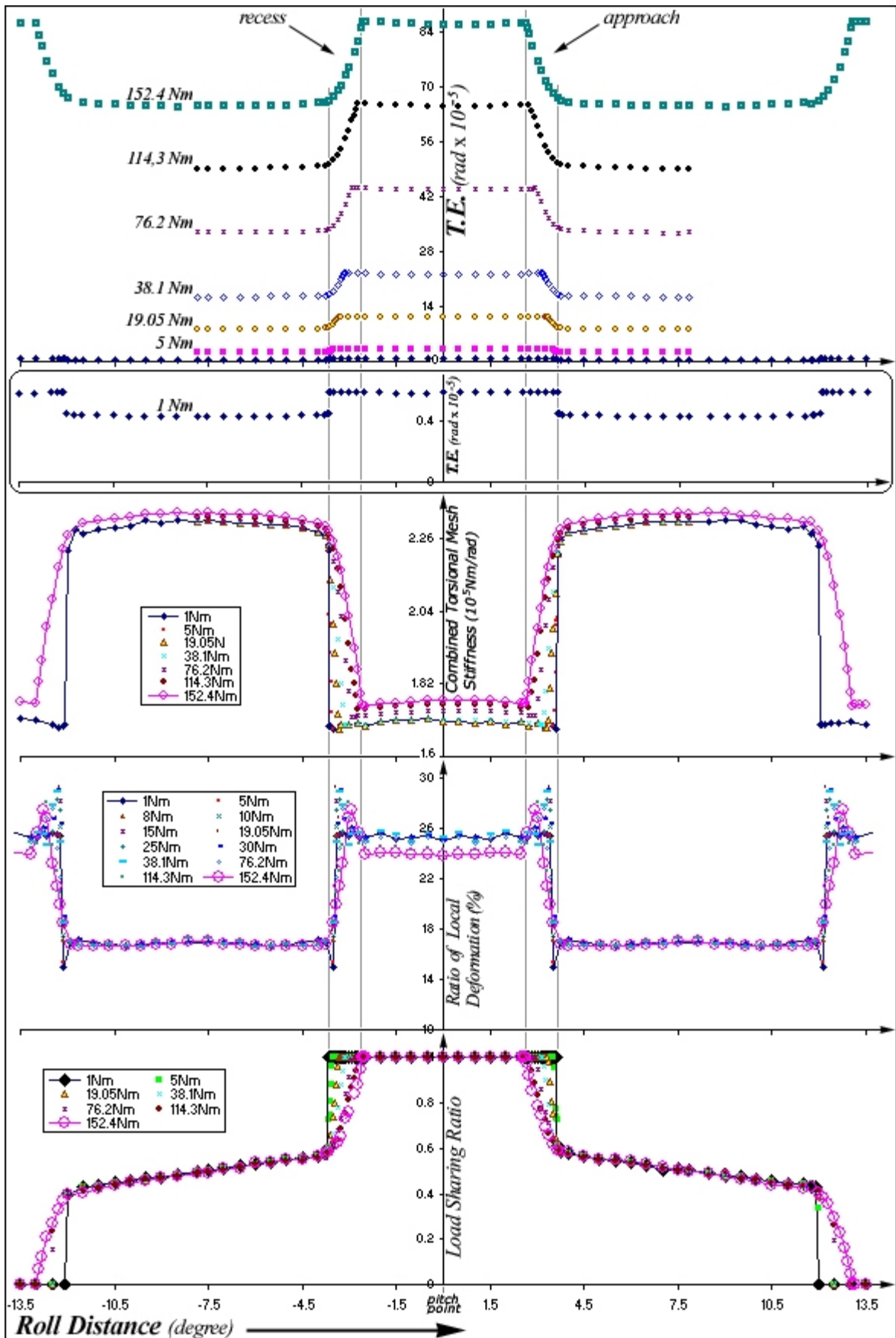
Figure 7.3. 22   The hand over process of involute gears (ratio 1:1) in mesh.

7.4.1 The History and Some Questions

Tooth profile modification of (involute) gears has been an accepted practice in gear design since the late 1930s when the theory behind this was proposed by Walker (Walker 1938). Figure 7.4.1 has shown his results on a short and a long profile modification.
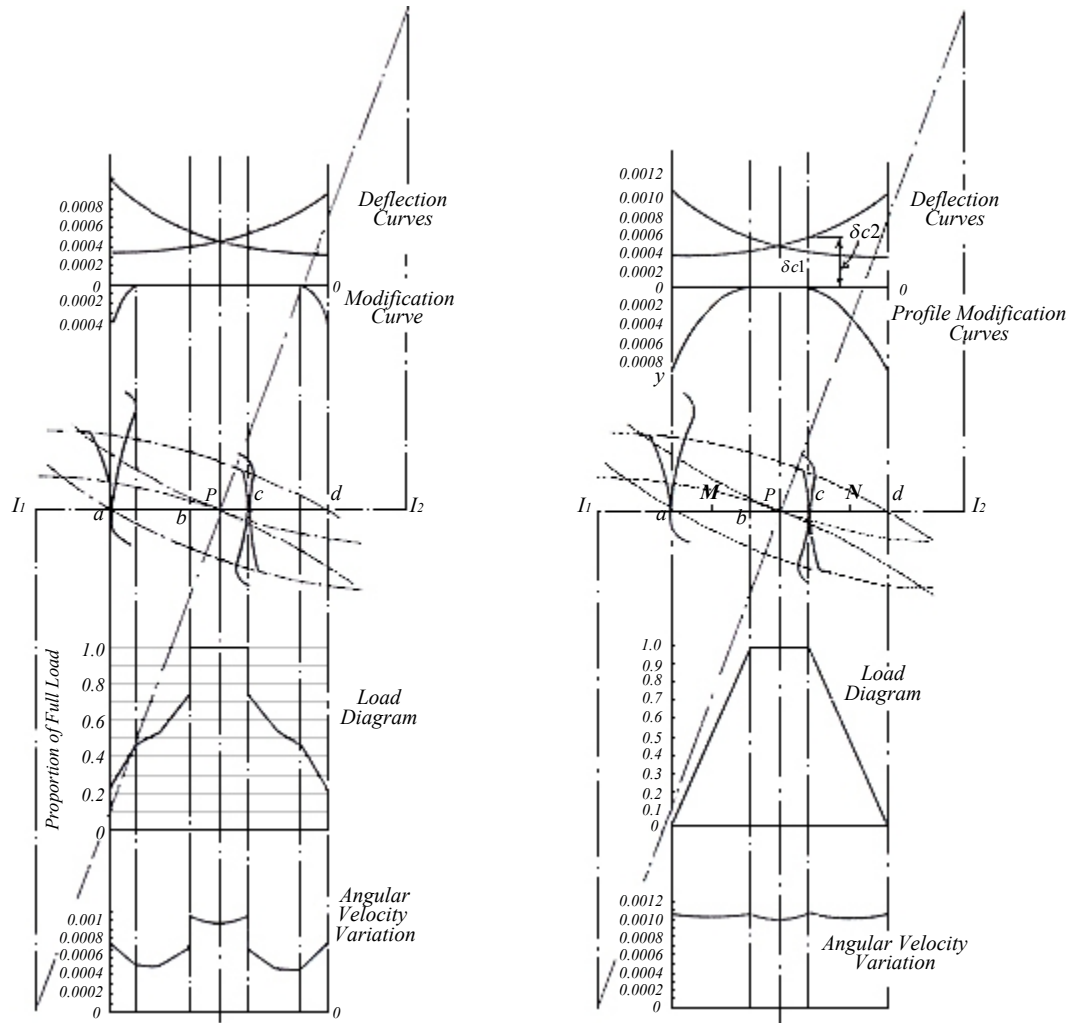
Figure 7.4. 1   Walker proposed results on a short and a long profile modification(Walker 1938).

The most significant step forward in the understanding of gear kinematics was made in the late 1950s by Harris (Harris 1958), who proposed the relationship between the T.E. of tip-relieved gears and different input loads under quasi-static conditions, which was presented as a series of plots against the gear rotation. The plots are now known as Harris maps and have become a very powerful tool for clear understanding of gear kinematics and can help to predict their dynamic behaviour. In the 1960s, Munro and Gregory (Munro 1962; Gregory 1963) continued work on a back-to-back test rig for measurement of the

127

transmission error by means of optical gratings and considerable progress was made in understanding spur gear dynamics. Subsequent research has put the design of profile relief on a proper scientific basis (Niemann 1970; Munro 1990; Munro 1994; Rosinski 1994; Yildirim 1994; Palmer 1995).

One recent considerable step forward was made by Lin et al. (Lin 1994; Lin 1994), who came up with an analytical formula for calculation of T.E. and load sharing ratio as shown in Figure 7.4.2 and presented a thorough analysis of its effects on spur gear transmission.

The profile modification made by Lin was anticipated with Walker's long profile modification which starts from the tooth top land and extends to the HPSTC (Highest Point of Single-Tooth Contact). One of the questions is whether the HPSTC (including the LPSTC - Lowest Point of Single-Tooth Contact) should be as, conventionally, the fixed position of the tooth profile that consequently results in the contact ratio independent of the input load. However, the results achieved with adaptive mesh (see section 7.2.1) have shown the existence of the hand over region between the single and double zone where the single zone will be reduced by the extension of the hand over regions with the input load increasing, so that both the HPSTC and LPSTC will move toward the pitch point resulting in the increase of the contact ratio.

Lin's result does show that the single zone changes with the amount of normalized modification $\Delta = 1.25$ as shown in Figure 7.4.2. However, the amount of change of the single zone, according to this research, is load dependent and contributes to the double zone variations. So that, according to Lin's calculations, the drop in contact ratio may not be correct.
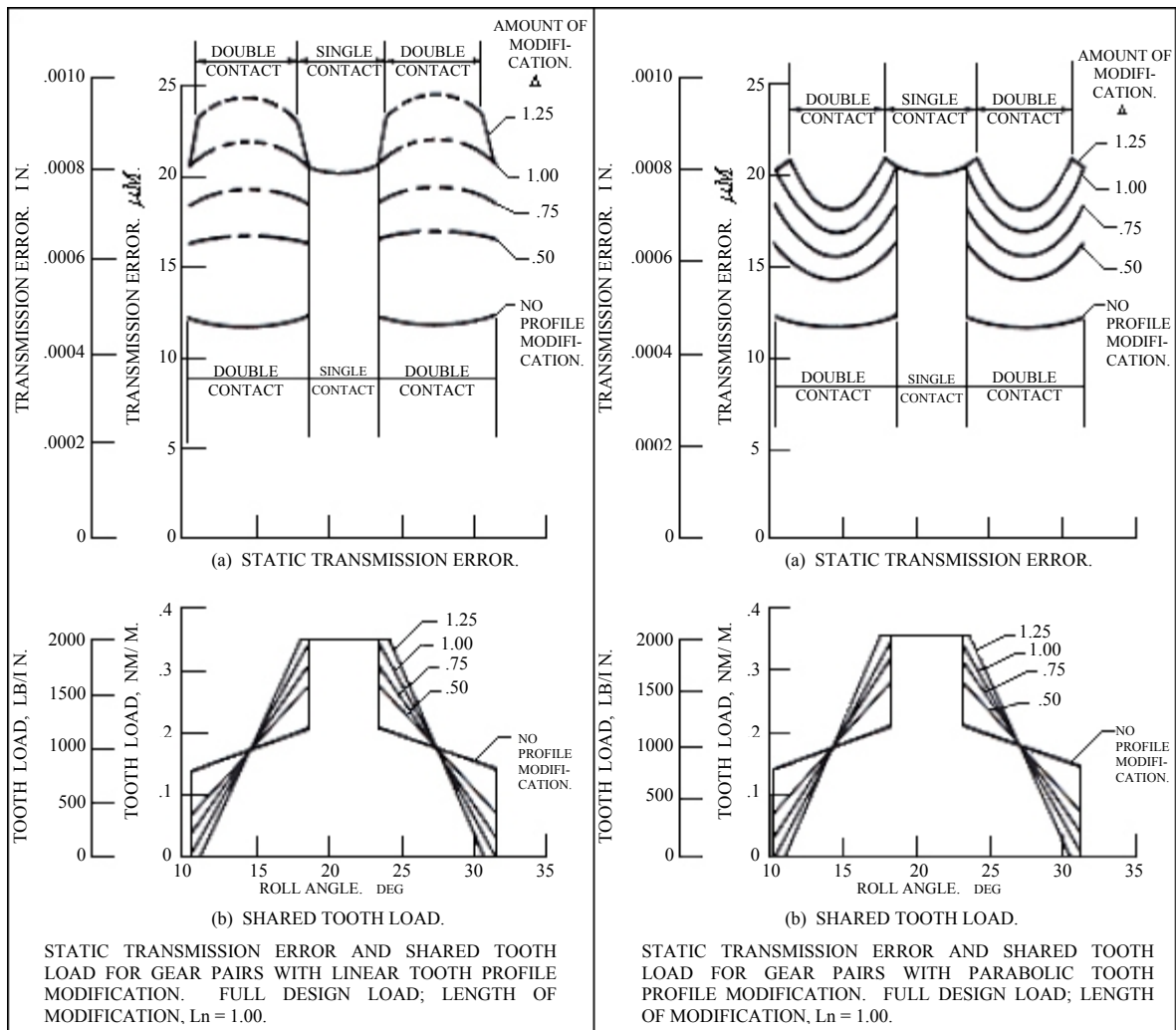
Figure 7.4. 2   Lin's results of linear and parabolic profile relief (Lin 1994).

7.4.2   The Current Recommended Tip Relief Allowances

It is noted that excessive thinning of the tooth profile could result in a significant reduction in load carrying capacity, and will result in a reduction in load sharing and this in turn can lead to a decrease in bending fatigue strength (Walton 1995). The existing standards of metallic gears such as British Standard (BS 1970), ISO (ISO/DIS 1983) and DIN Standard (DIN 1986) (Figure 7.4.3) give the maximum amount of tip and flank modifications to prevent the possible over – tipping. However, there are no precise recommendations for applying the modifications in all these standards. Below these limits the designer is free to choose the amount of relief and the form combinations.

(a) BS 436: Part 2: 1970 (8).

(b) ISO standard (9).

(c) DIN 876 (FEB 86).

Normal Module	Mn	-	25.4/DP
Pressure angle	α	-	20º
Fillet radius	Pf	-	0.38 Mn
Tooth depth	hp	-	2.25 Mn
Gear addendum	hap	-	Mn
Gear dedendum	hfp	-	1.25 Mn
Pitch	P	-	π Mn
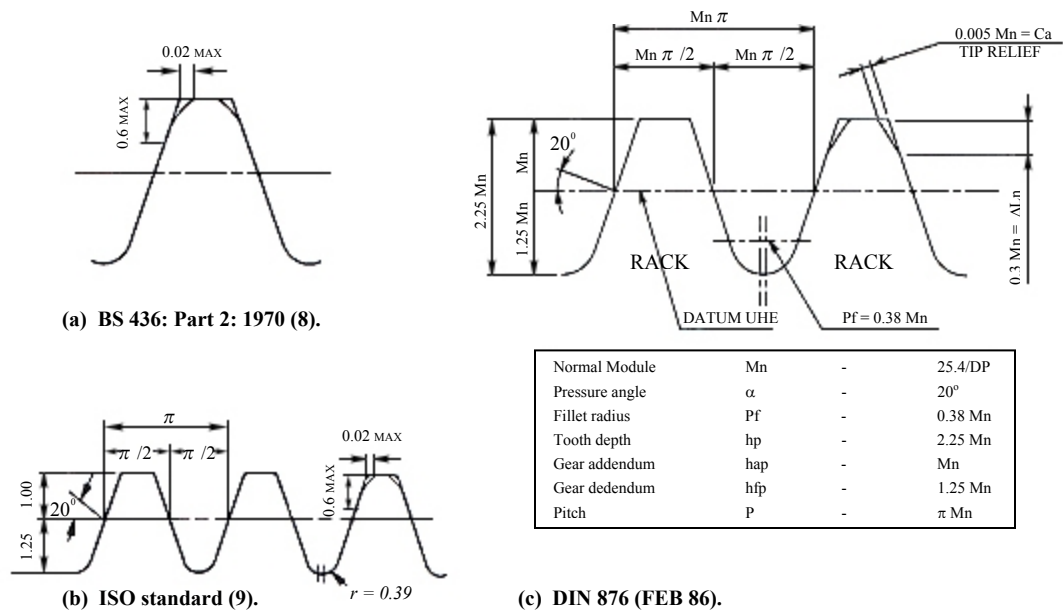
Figure 7.4. 3   Tip relief for a metric module of 1 mm on the basic rack.

Figure 7.4.3 has shown that the British Standard (a) and the ISO standard (b) give the same recommendations for the maximum relief on a basic rack of metric module 1 mm and all the dimensions are a function of the actual module m as shown in (c) where M_n = m. However, the DIN standard has been shown to be more restrictive on tip relief.

7.4.3   The Form of the Tooth Profile Modification

There are various types of curves that could be used for the shape of the modification of the gear tooth profile. Linear and parabolic curves are common for tooth profile modifications, as shown in Figure 7.4.4.

It should be noted that the linear and straight-line relief are not the same as the line OT (Figure 7.4.4 (b)) represents the pure involute curve. In application, gear companies often supply gears (of manufacturing standard) with straight-line tip relief due to the small amount of tip relief modification that is easy to manufacture.   The shape of the modification on the tooth profile can also be an involute curve with a limited minimum radius under British Standard (revised standard No. 436 – 1940) as shown in Figure 7.4.5.
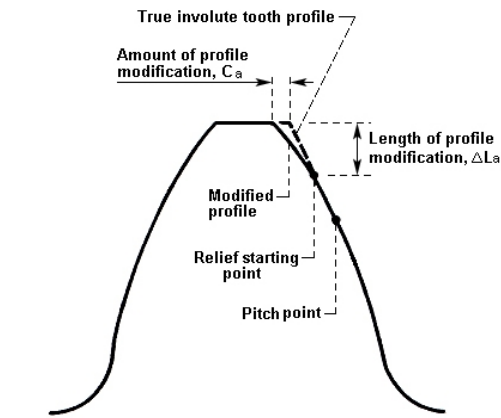
(a) Gear tooth with modified tooth profile.
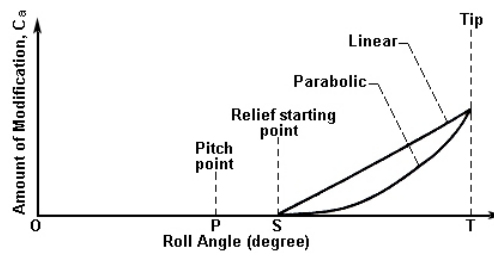
(b) Linear and parabolic form of the modified tooth profile.

Figure 7.4. 4   Example of linear and parabolic tooth modification.
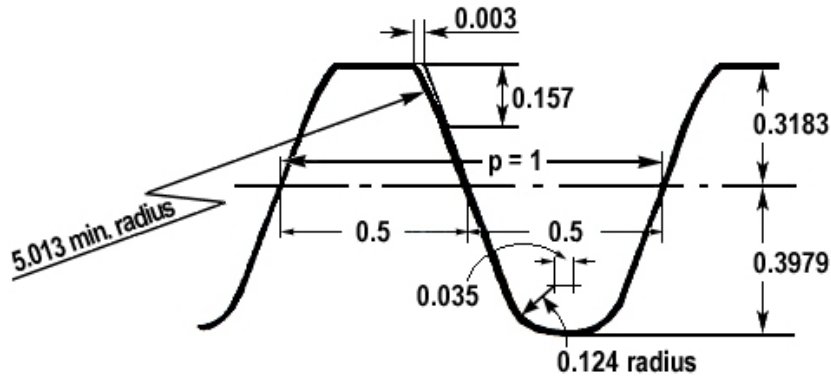
Figure 7.4. 5   The basic rack of circular pitch 1 and the involute tip relief (p is the circular pitch).

Each different form of the curve used for tooth profile modification can cause a significant difference in the gear mesh characteristics, especially when the modification is applied on a significant part of the original involute profile, such as the example of the transmission errors shown in Figure 7.4.2. An extreme case given by Smith (Smith 1999) involved the use of tip and root relief, as indicated in Figure 7.4.6, where the two meet roughly at the pitch point. Regardless of whether the tip relief form used is linear or parabolic, the gear (in concept) is no longer an involute one, and some basic properties of the gears in mesh

131

can vary in a complex manner, such as the pressure angle. So, special considerations may be needed when considering applying a long modification.
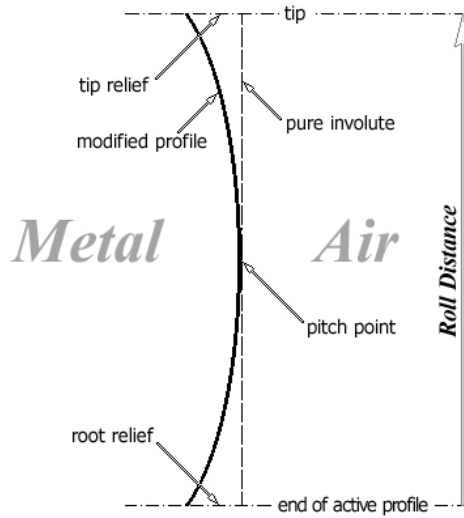
Figure 7.4. 6   Tip and root relief applied on a gear (Smith 1999).

In this research, choosing the form of the modified tooth profile is based on the following considerations.

- *Simple and less variation.*   The form of the modified profile will have little or no change from the original involute curve. This could also be easier to manufacture.

- *Fits the global deformed shape.*   In previous research, the forms were generated with detailed consideration of the local tooth deformed shape. The parabolic form may provide a more suitable deformed shape for the local tooth bending (such as when the module Mn is large).

FEA of gears in mesh at or near the corner contact was carried out for the study of the actual tooth deformation characteristics. Figure 7.4.7 shows part of the von Mises stress of the meshing gear pair, where the material is nylon (PA 6), the input load is 30 Nm and the temperature is at 23 C^0 (more detailed analysis of nylon gears in mesh can be referred to in the next chapter).

The global deformations of the tooth are observed, consisting of the tooth rotation about its root and the tooth movement near the tangential direction of the base circle. In order to find the local tooth deformation, the original tooth profile (edge before the load) was rotated and moved to match the deformed tooth. The best match was made in which the rotation was 1.3 degree at the screen (Figure 7.4.7) geometric centre, as shown in Figure 7.4.8.
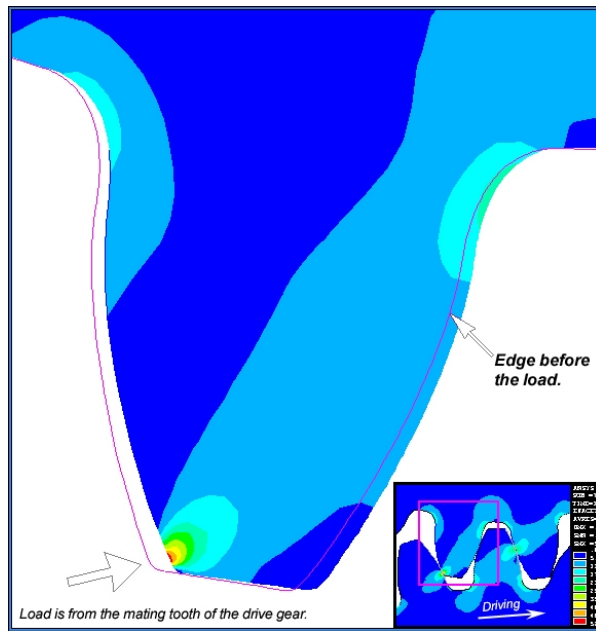
Figure 7.4. 7   The von Mises stress of the mating tooth and its edge before the load.
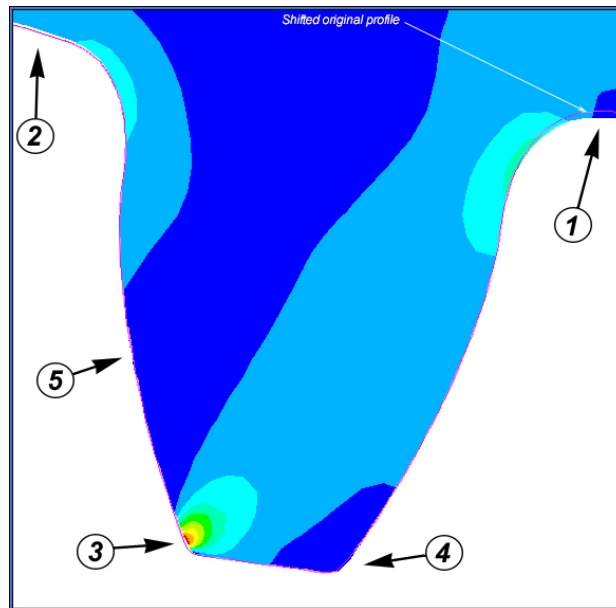
Figure 7.4. 8   Illustration of the major local tooth deformations.

It can be seen that the tooth root deformations (at locations 1 and 2), specially that in compression, are the major components that cause the tooth (global) rotation. The tooth local deformations are observed at location 3, 4 and 5, where they are much less than the global deformations, particularly the tooth bending (shown at location 5) which was small. Except for the deformation at the contact, the shearing deformation near the tooth top land is also one of the significant tooth local deformations when corner contact is present.

133

In conclusion, the tooth rotation of the global deformation is the most significant component when the corner contact is present. It may be worth investigating the use of a rotated original tooth profile as the form of the modified profile curve, which is simpler than the linear and parabolic profile relief and so may be easier to manufacture. Such an involute tooth profile modification will be used in this research, the details of which are illustrated in Figure 7.4.9.
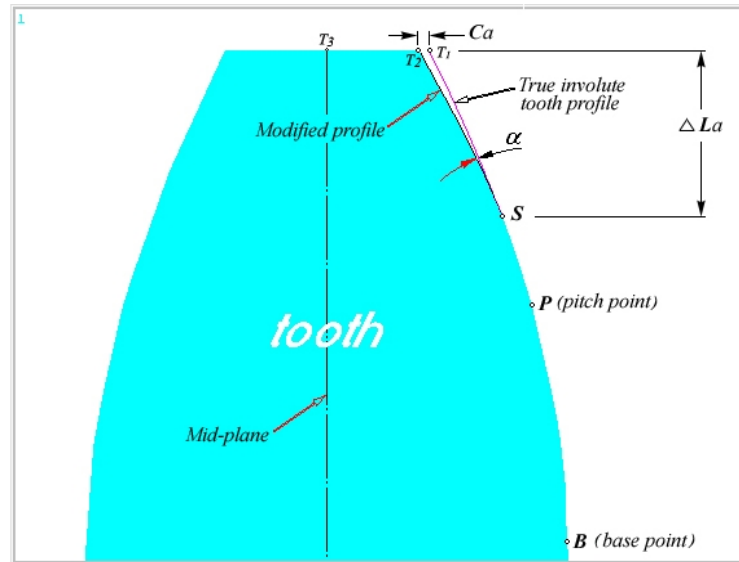
Figure 7.4. 9   Illustrations of an involute tooth profile modification.

The amount of the modification Ca can be achieved by rolling the section of the original involute curve ST_1 at the relief start point S with an angle α, so that the gears are always mating with involute profiles. There can also be a round off with a radius of 0.3 to 0.5 mm at the tooth tip T_2 in order to assist the FEA solution convergence if corner contact occurs.

7.4.4   TE$_{o.\,p.\,c.}$ and C$_a$ Due To Elastic Deformation

The first attempt to understand the geometry of corner contact in detail was made by Richardson (Richardson 1958) before Harris suggested the concept of TE. He calculated the value of what would now be termed the *transmission error outside the normal path of contact*, TE$_{o.\,p.\,c.}$ (i.e. when the contact occurs at the tooth corner) (Munro 1999). In 1962, Munro (Munro 1962) proposed a different approach for calculation of TE$_{o.\,p.\,c.}$. It involved

134

the use of some approximations that lead to a conveniently simple formulae. In 1975 Seager (Seager 1975) produced some work on analysis of Munro's (Munro 1962) developments. More recently, a considerable step forward was made by Lin et al. (Lin 1994) (approach case) and Munro (Munro 1999) (recess case). The paper of Munro's presented more results on corner contact theory, bringing all hitherto acquired knowledge on this subject into systematic order.

$TE_{o.p.c.}$ is geometrically defined as the distance AK (approach case) and DF (recess case) along the path of contact as shown in Figure 7.4.10.
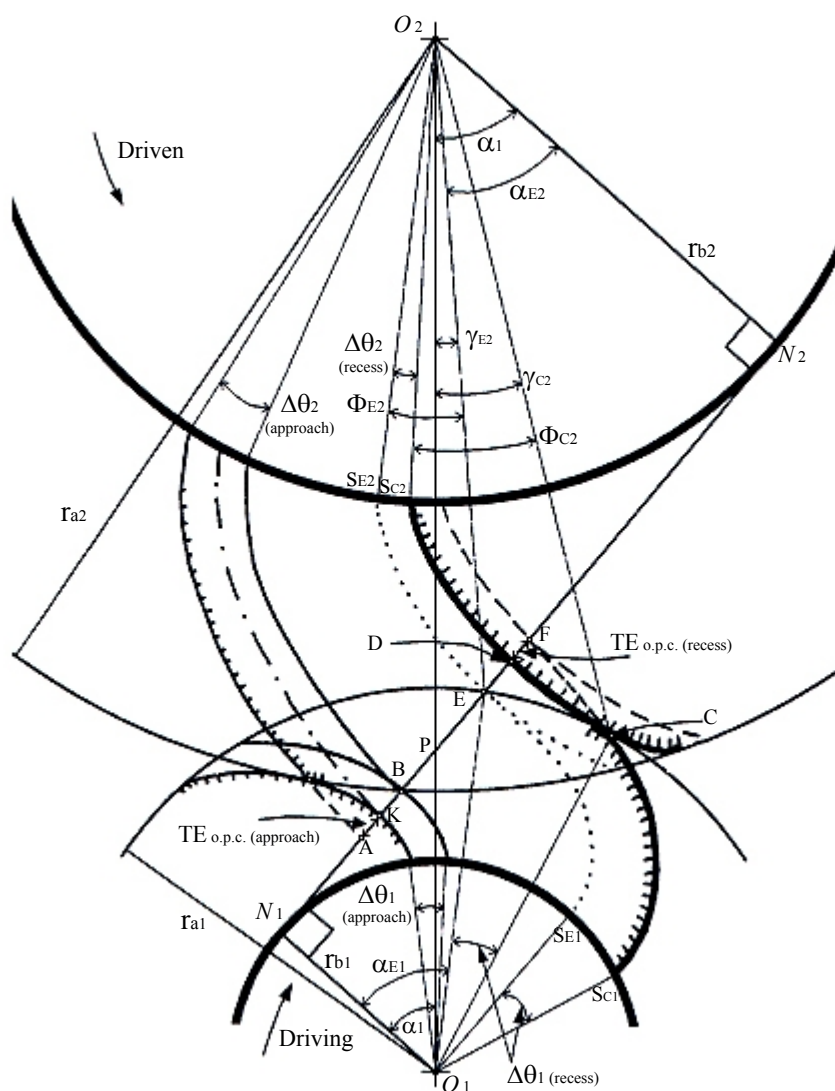
Figure 7.4. 10   Tooth pairs of spur gears in mesh at the beginning (B), end (E) and beyond the normal path of contact and the definition of the transmission error outside the normal path of contact, $TE_{o.p.c.}$, in recess and approach (Munro 1999).

TE$_{o.p.c.}$ definitions and the calculation formulas (Lin 1994; Munro 1999) are very important for the study of various cases such as how the profile, wear and alignment errors lead to the corner contact. It should be noted that the validation of the formulas are limited within gears containing only first order (imperfect) components that cause rigid body motions. When gears are loaded, they are elastically deformed, contain higher order and the *higher order dependent components*. Loaded TE$_{o.p.c.}$ are no longer calculated with any existing formulas, as FEA evaluation of loaded TE$_{o.p.c.}$ is now readily possible.

Thus TE$_{o.p.c.}$ can be classified as the unloaded or loaded type, where unlike the unloaded, the loaded TE$_{o.p.c.}$ is load dependent. A sample analysis of loaded TE$_{o.p.c.}$ is shown in Figure 7.4.11.
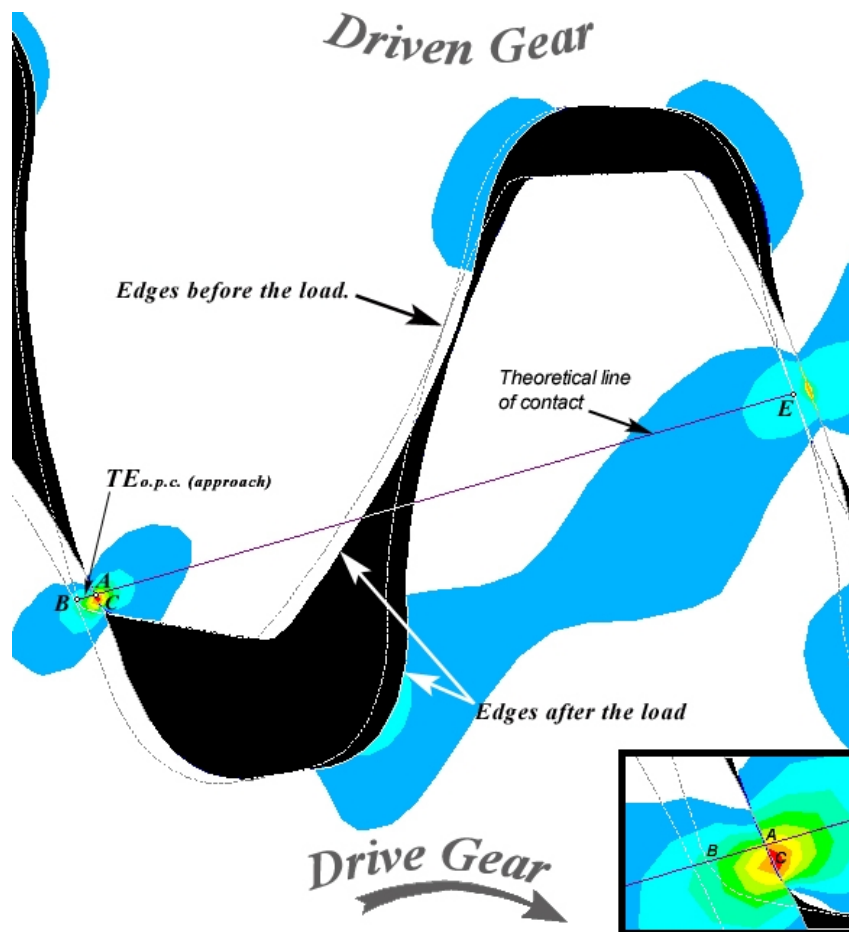
Figure 7.4. 11 Loaded TE$_{o.p.c.}$ in approach case (pure involute gears in mesh, ratio= 1:1, round off radius at the tips is 0.4 mm).

136

The loaded $TE_{o.p.c.}$ is the distance AB along the theoretical line of contact between the drive gear tooth profile and the theoretical driven gear tooth profile. Loaded $TE_{o.p.c.}$ occurs mainly due to the non-unique global torsional deflections between the drive and driven gear, as explained with Figure 7.4.12.
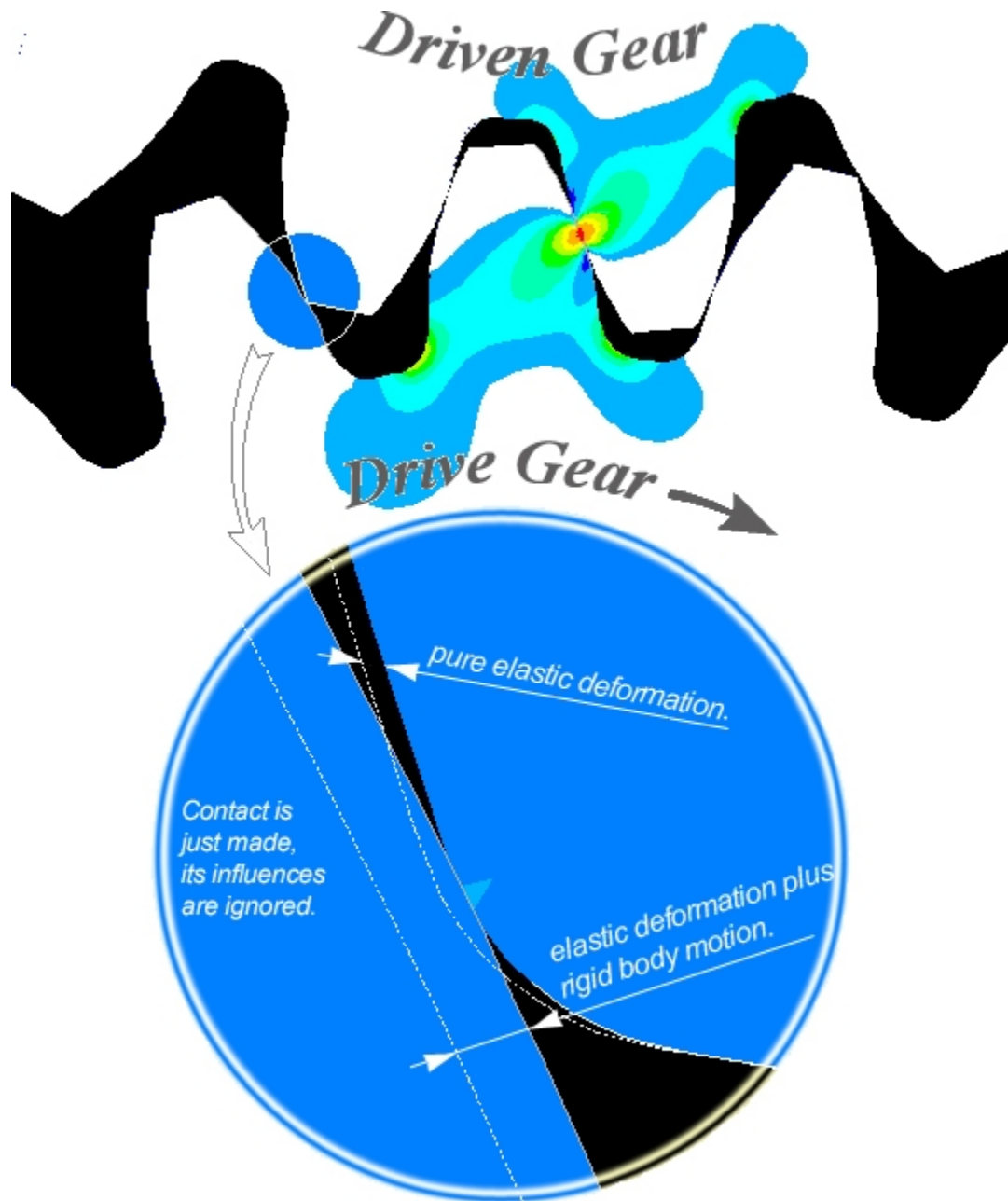
Figure 7.4. 12   Detailed deflections of the drive and driven gear where
the corner contact (approach) is about to take place.

Except for the elastic deformation of the drive gear, the deflected driven gear also leads the drive gear hub motion, so called the rigid body motion and the *higher order dependent component*. Moreover, the pure elastic deformation of each gear is also varying simultaneously with the mesh position changes, as the individual torsional stiffness (see chapter 6.2) of each gear is varying asymmetrically. These complex deflection relations will result in a slight difference between $TE_{o.\,p.\,c.\,(approach)}$ and $TE_{o.\,p.\,c.\,(recess)}$, as well as a slight asymmetry in the T.E. curve (as seen in Figure 7.4.13), if gears were kept rolling in the same direction.
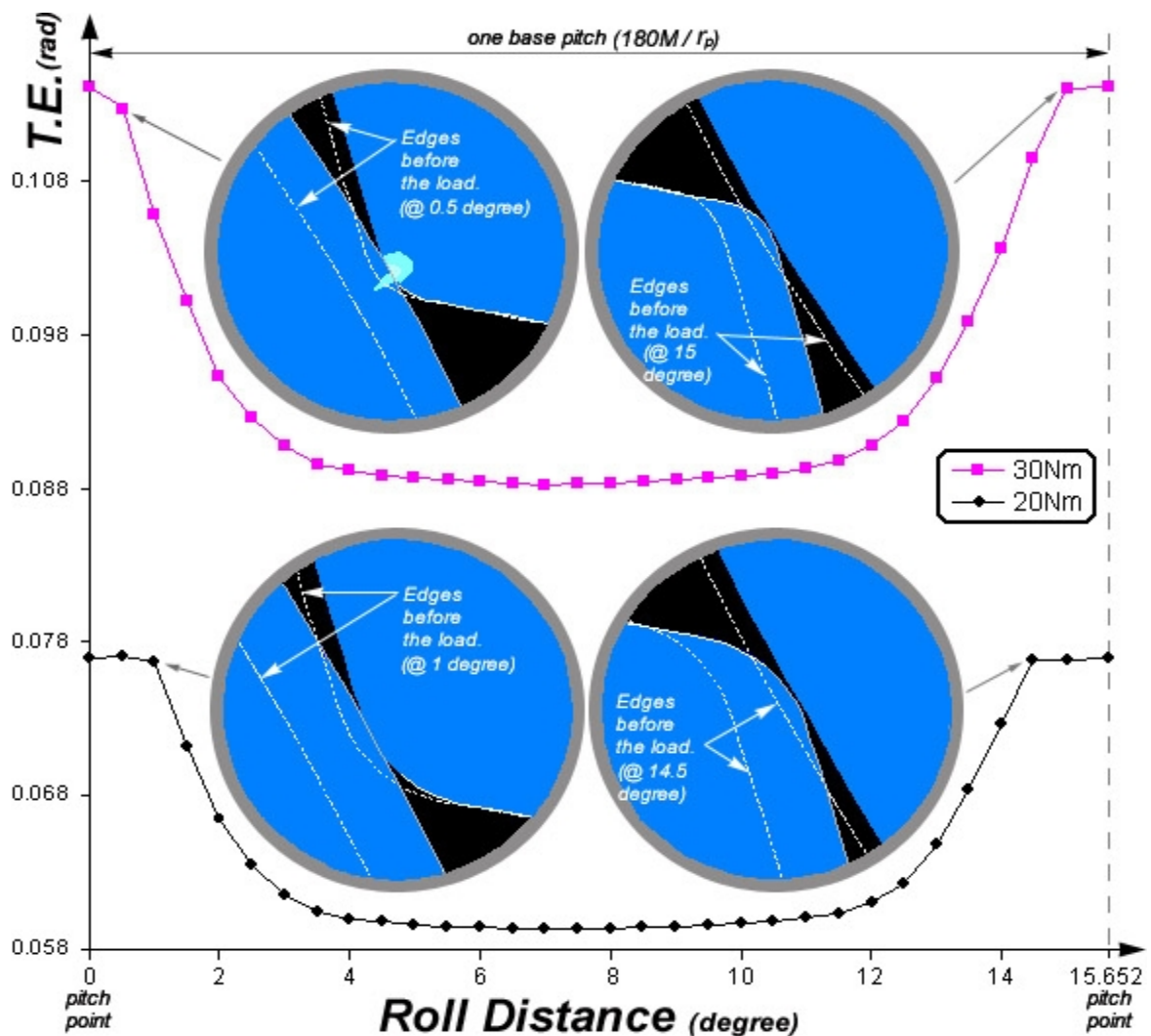
Figure 7.4. 13 Illustrations of the slight asymmetry in the T.E. curve of nylon gears in mesh (note: the roll angle increment is 0.5^0 except the last one that is 0.652^0).

It can be clearly seen that the positions when the (corner) contact take place, (approach case) and when it finishes (recess case), are asymmetric to the centre of the base pitch which will become more obvious with heavier load. When the load is very light, the T.E. curve tends to be symmetric and for zero load, there are no deflections, which should produce a symmetric T.E. curve – including the case of contact ratio smaller than 1. Without the concept of loaded $TE_{o.\,p.\,c.}$ some confusions could be made in the analysis, as shown in Figure 7.4.14.
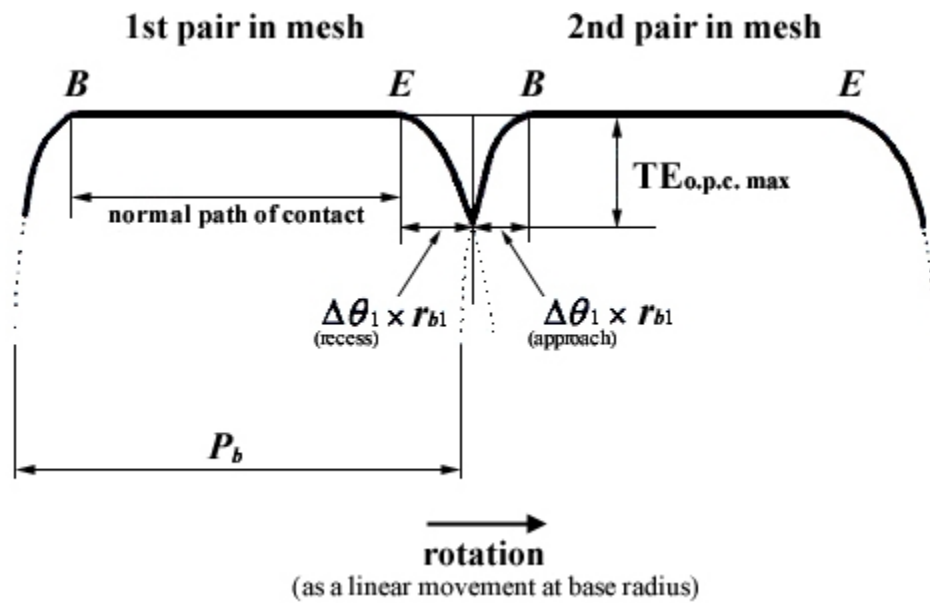
Figure 7.4. 14   Theoretical transmission error curve with corner contact taking place (no profile relief, no manufacturing errors, zero load applied, contact ratio smaller than 1) (Munro 1999).

As mentioned before, loaded $TE_{o.\,p.\,c.\,(approach)}$ and $TE_{o.\,p.\,c.\,(recess)}$ are also slightly different, but the amount of difference is very small as found in most cases of this research (including gear ratio 1:1 to 1:2) and technically difficult to be observed. However, the research is more interested in their maximum values, where the difference between their maximum values can be represented by their different T.E. values, as shown in Figure 7.4.15, which is the part of the analysis results in Figure 7.2.3. At this situation, the $TE_{o.\,p.\,c.}$ and T.E. provide different measurements for the same deflections. Figure 7.4.16 illustrates the FEA result evaluated at the $TE_{o.\,p.\,c.\,(approach).\,max.}$ while the contact is just about to be made at C.
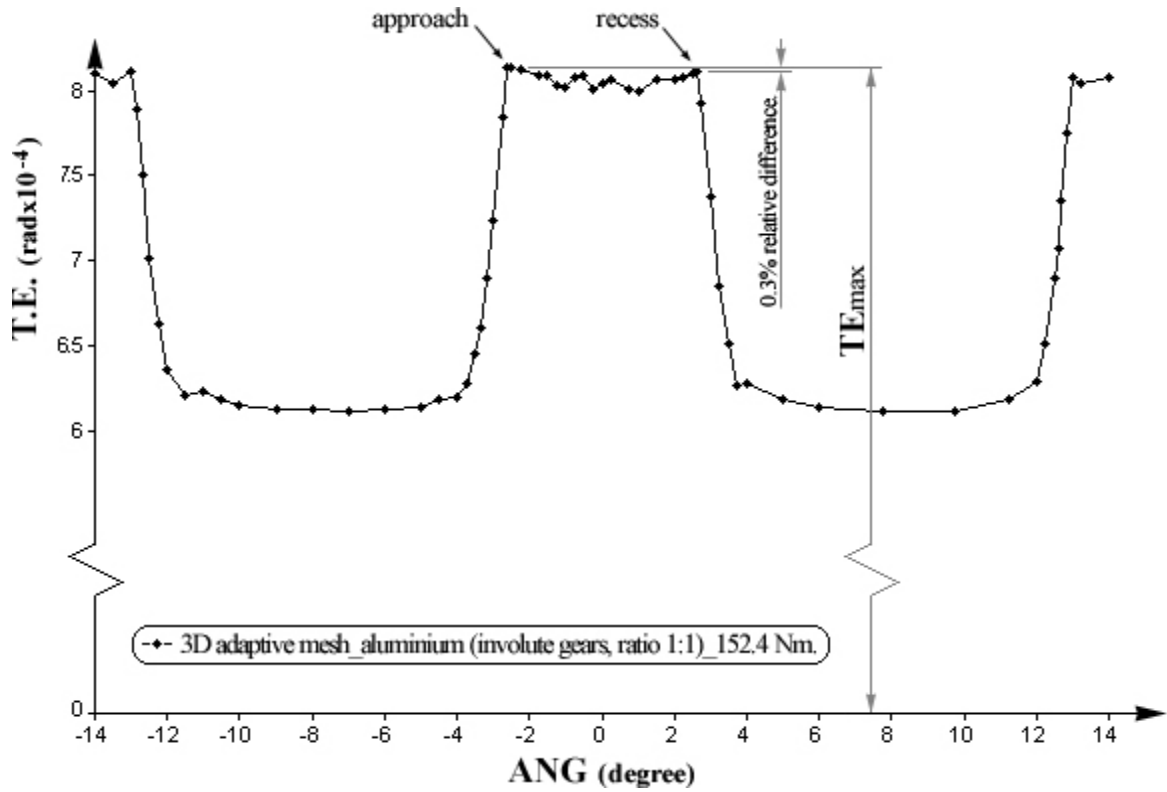
Figure 7.4. 15   Illustration of the T.E. peak values.

In order to eliminate the corner contact that occurs due to the deflections of gears under load, the amount of tip relief C_a has to be evaluated (geometrically) by the loaded $TE_{o.\,p.\,c.\,(approach).\,max.}$, and technically C_a can be expressed by TE_{max}. An approximate formula for the minimum amount of tip relief can be given by,

$$C_a\big|_{min} \, B \, r_b \cdot TE_{max} \cdot \left| \frac{\cos(20^0 + \dfrac{270^0}{N})}{\cos(20^0 - \dfrac{360^0}{N} + \dfrac{\sqrt{r_p^2 - r_b^2}}{r_b} - \arccos\dfrac{r_b}{r_p})} \right| . \tag{7.2}$$

140

Theoretical position of the begining double contact pair.

E

Edges after the load.
(the actual position for the begining of the next pair).

Edges before the load.

B

C

$TE_{o.p.c.\ (approach)\ max.}$

Driving
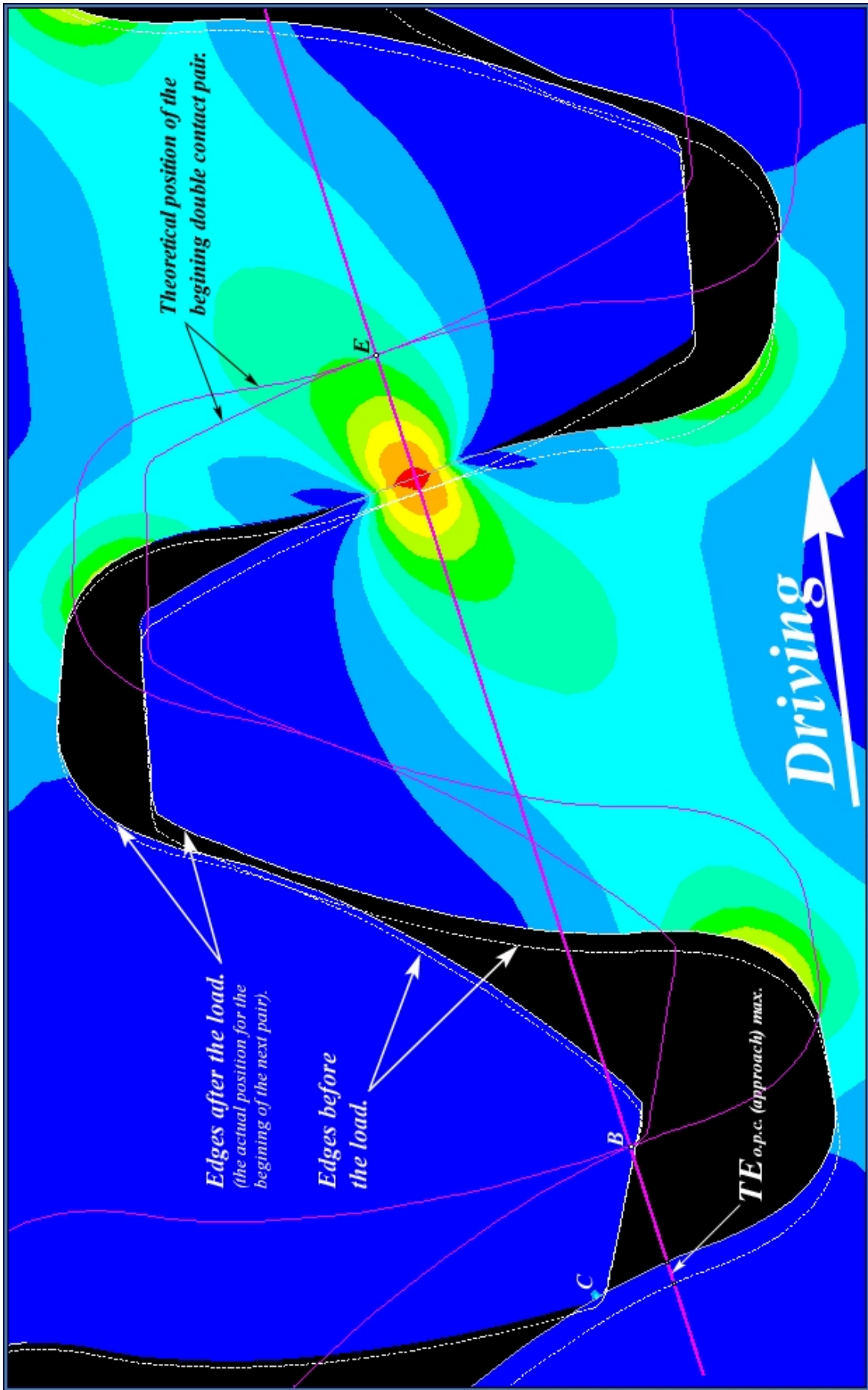
Figure 7.4.16 FEA evaluation of TE$_{o.p.c.}$ (approach). max..

141

where r_b and r_p are the base and the pitch circle radius respectively, N is the number of teeth, the formula is only for gear ratio 1:1. For gears with large ratio, especially when the pinion (the smaller one, usually the drive gear) has fewer teeth, there should be some variations between loaded $TE_{o.\,p.\,c.\,(approach)}$ and $TE_{o.\,p.\,c.\,(recess)}$, consequently the relief C_a on the driven gear teeth (approach case) and pinion teeth (recess case) will be different. Further development of the formula (7.2) for general cases would require large FEA calculations.

For the special case (gear ratio 1:1) and this research, formula (7.2) is convenient and its calculations can be further simplified by ignoring the T.E. variations within the single contact zone. The value of TE_{max} can be calculated with the single tooth gear model or even the model of the single tooth gear contact with a rigid line (chapter 6).

This section has discussed the FEA evaluation of $TE_{o.\,p.\,c.}$ which is due to deflections, so called the loaded $TE_{o.\,p.\,c.}$ compared to that of the traditional $TE_{o.\,p.\,c.}$ which was for the unloaded case, and calculated with geometrical formulas. Once the loaded $TE_{o.\,p.\,c.\,max.}$ is known, the required tip relief C_a can be evaluated geometrically (with some approximations) for preventing corner contact. In general cases, C_a can be calculated from both loaded and unloaded $TE_{o.\,p.\,c.\,max.}$. The formulas for calculation of unloaded $TE_{o.\,p.\,c.}$ have been given by Munro (Munro 1999).

7.4.5   Additional Consideration On Tooth Modification

If the gear face width is significant (such as pinion) or the material of the gear(s) has a low Young's modulus (such as Nylon), a longitudinal modification may be required, as shown in Figure 7.4.17. The modification is expected to achieve a unique load w' (the reaction force) along the tooth face width. However, the modification due to heavy load could lead the gear to be a non-standard form and as a result, the line of action will vary along the shaft. Investigations on the combination effects of T.E., load sharing, contact ratio and so on have not been found.
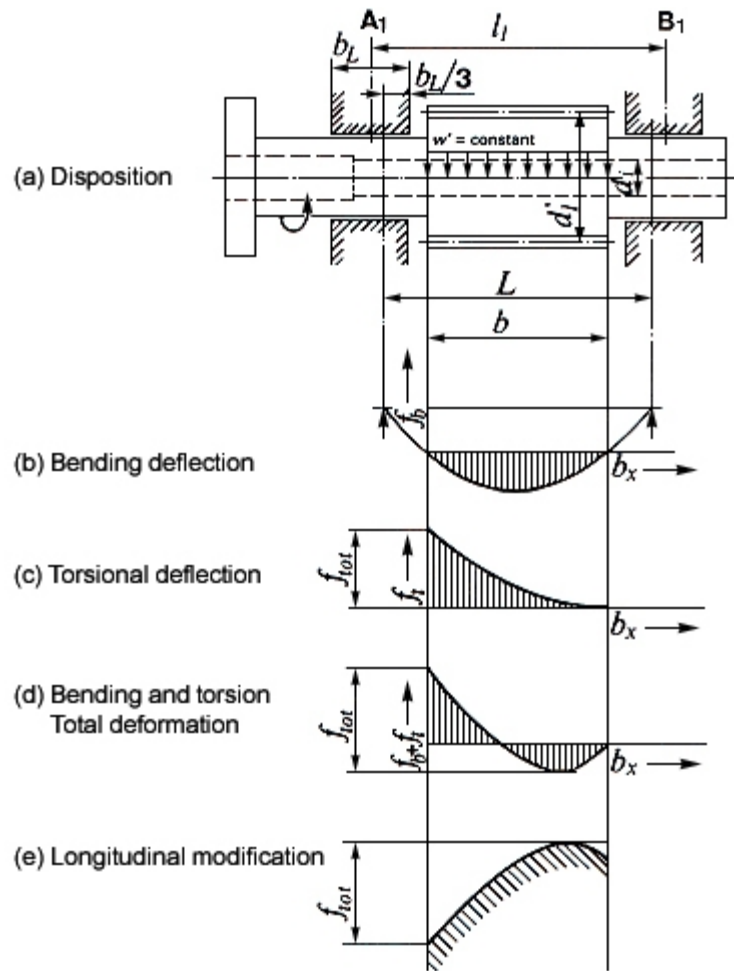
Figure 7.4. 17 Elastic deformation of the pinion and longitudinal modification (MAAG 1990).

7.4.6   Harris Mapping - Long and Short Tip Relief

The term "Harris Maps" refers to the diagram that describes the handover process of a meshing gear pair with the measured and predicted transmission error curves at different torque levels, as developed by Harris (Harris 1958). At the time, gears were tested under quasi – static conditions, and the results are shown in Figure 7.4.18.

Harris maps clearly show that for a gear pair having a particular (long) tip relief, there exists a design load where the transmission error is minimised. Other investigators such as Gregory et al. (Gregory 1963), Lin et al. (Lin 1994), Munro and Yildirim (Munro 1994), Kahraman and Blackenship (Kahraman 1999) have shown that the design load concept is valid under dynamic conditions as well using straight line, linear and other more complex modifications.

143

(a) Load – Displacement – Rotation for Uncorrected Involute Teeth, 20 – deg Pressure Angle, Both Gears 48 Teeth.

(b) Load – Displacement – Rotation for Gears with Involute Teeth and Heavy Profile Correction to Give a Short Period of Transfer of Load from One Pair of Teeth to the Next.

(c) Loads and Profile Correction for Constant Angular Velocity at 4000 lb/in. face.
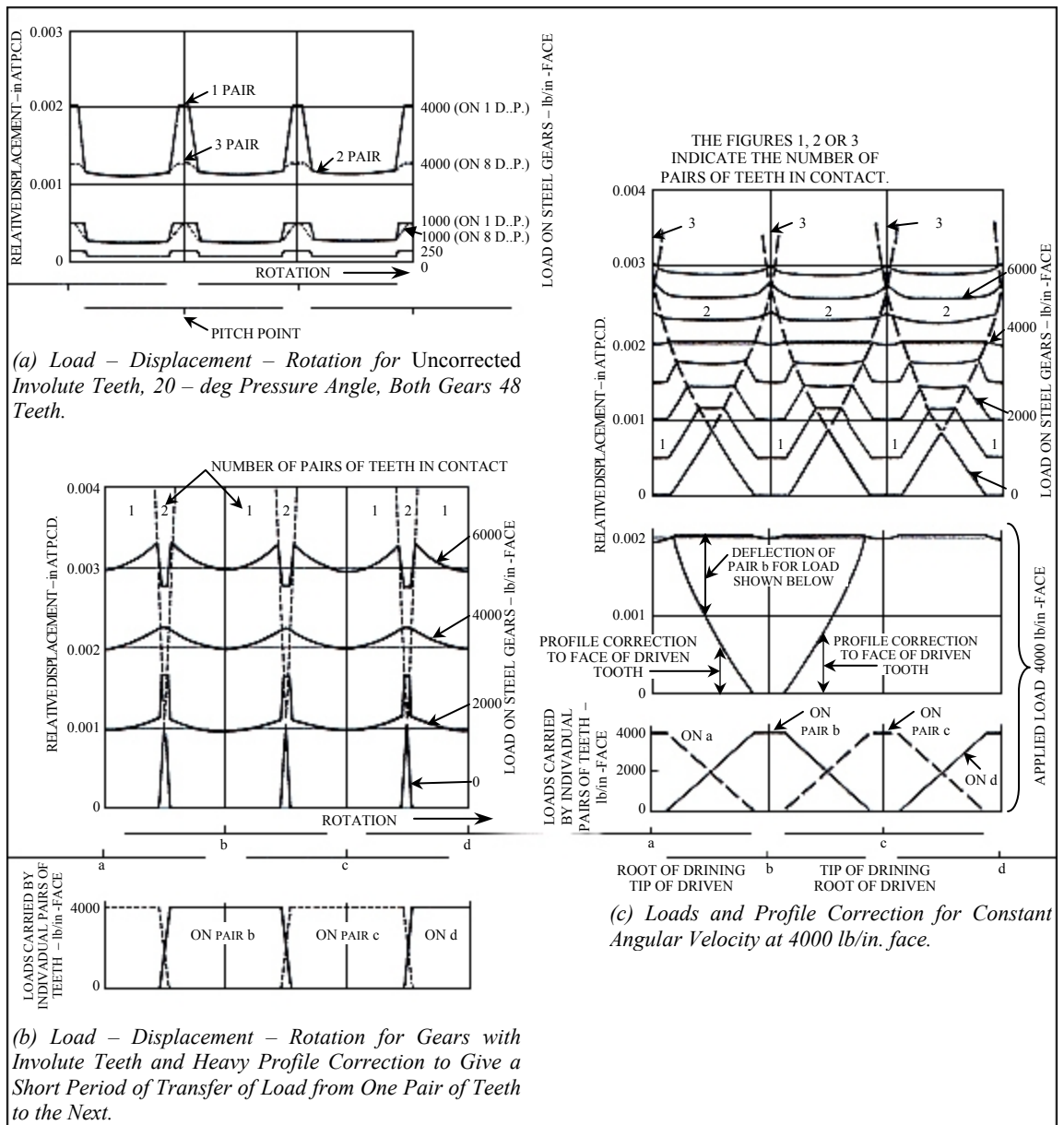
Figure 7.4. 18   The static transmission errors produced by Harris (Harris 1958).

However, the original works made by Harris (as shown in Figure 7.4.18 **b** and **c**) didn't show correct T.E. curves above the design load, as the variations with the load have shown little possibilities for the occurrence of corner contact (or the protrusion of the single zone T.E.). Five years later, Gregory, Harris and Munro presented their works (Gregory 1963) in which the diagram of T.E. vs. loads is shown as in Figure 7.4.19.

The developed Harris maps (Figure 7.4.19) were based on Weber's (Weber 1949) data on tooth deflection under load.
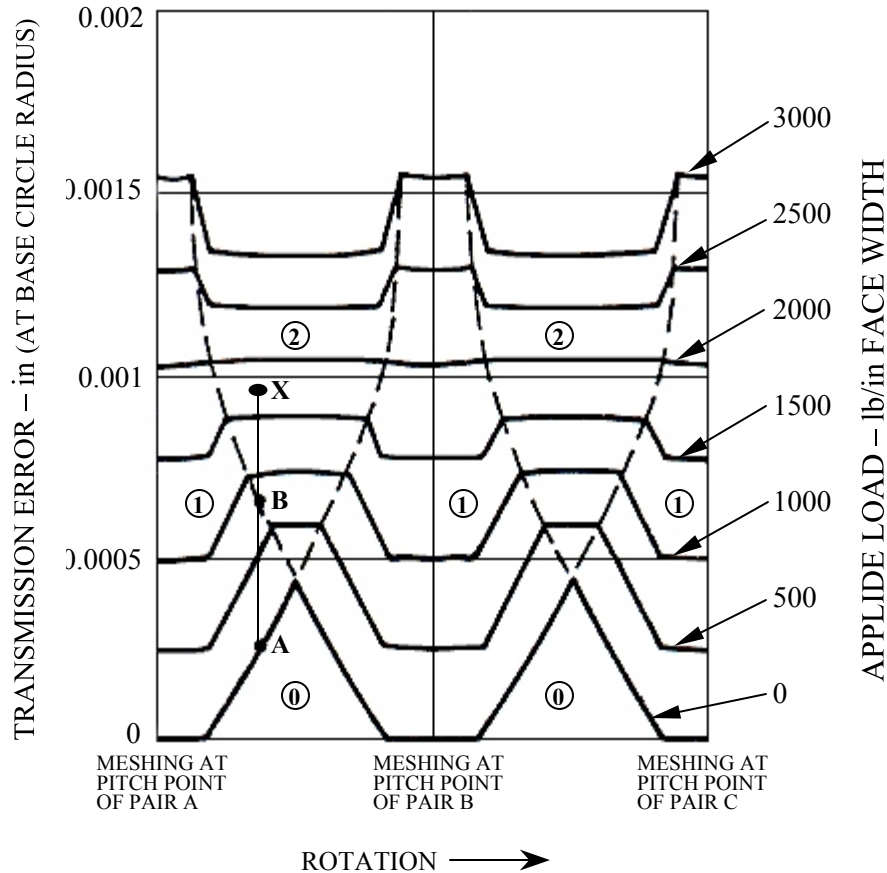
Figure 7.4. 19 Designed static transmission error curves (Gregory 1963).

In 1970, the ideas of long and short tip relief designs were introduced and developed by Neimann (Niemann 1970) and Munro respectively. Those designs were for the two extreme load cases. The explanations will refer to the "modern" Harris maps as shown in Figure 7.4.20 and 7.4.21 as revised by Smith (Smith 1999). Figure 7.4.20 shows the variations of transmission error with various input load for a long linear tip relief design, which is aimed at producing minimum noise at the "design load".

It can be seen that curve **n** represents the transmission error with zero input load, and the deflections are rigid body motions in the regions centered at **C** – the middle of the double contact zone. When gears are loaded, elastic deflections take place with large amplitudes in the single zone. For the particular input load, curve **d**, the elastic deflection of the single zone catches up to the combined deflections of the double zone. Hence, the overall transmission error is balanced, but is not zero (the T.E. concept is based on function 1.1, otherwise, based on function 1.2 the design load T.E. will be zero). As the curve of the

145

transmission error is perfectly straight, it shouldn't cause vibrations outside the system throughout the shafts. Curve **o** is the transmission error when the input load exceeds the design load, and the deflection in the single zone exceeds that of the double zone. Input loads in a range near the design load would produce transmission error, such as curve **o**, but the transmission error is still smoother than that of pure involute gears with the same input load. So, (long) tip relief design is not only for obtaining a smooth transmission error in the design load, but it also has benefits for other input loads that are in a range near the design load.
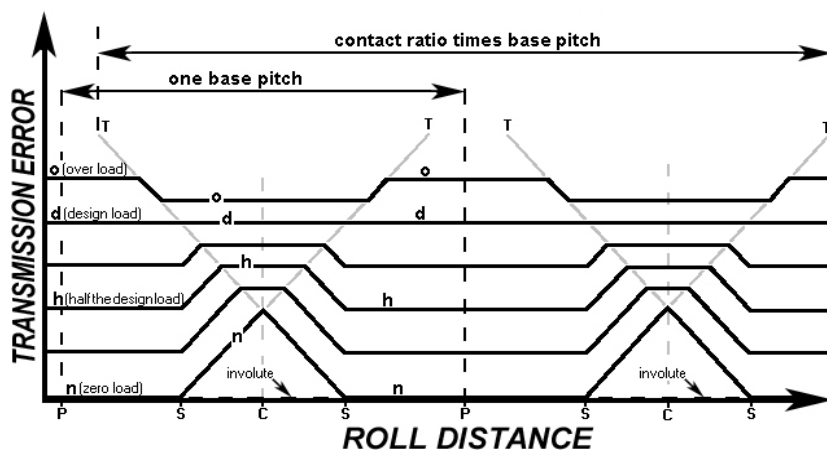
Figure 7.4. 20 Harris maps of deflections and long tip relief (Smith 1999).

To have a quiet running gear design at very light load is often a requirement since machinery often operates under light or cruise condition. This is the requirement for short tip relief design. In practice, it's usual to have the relief varying linearly, starting well above the pitch point so that there is a significant part of the meshing cycle where two "correct" involutes are in mesh. A short tip relief design gives transmission error with various input loads as shown in Figure 7.4.21. Again, the hand over regions have been ignored.
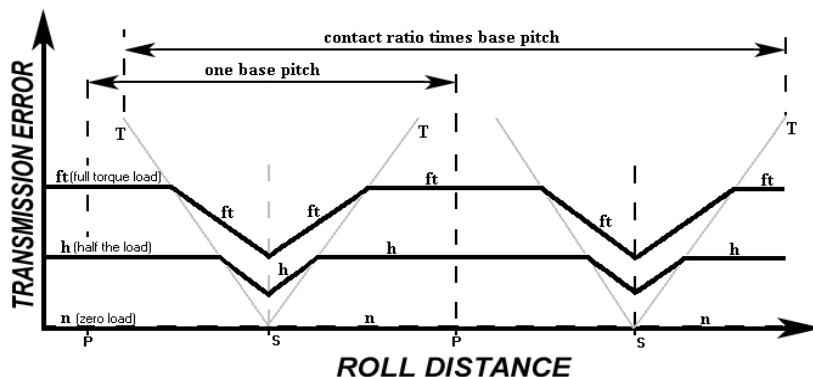
Figure 7.4. 21 Harris map of deflections with short tip relief

146

It can be seen that the pure involute extends for the whole of a base pitch so there is no tip relief encountered for light loads as for curve **n**. However, the tip relief still allows for all deflections (and errors). Palmer and Munro (Palmer 1995) have succeeded in obtaining good agreement between the predicted and measured transmission error with various input loads in a test rig.

However, numerical simulations such as FEA modelling of tip relieved gears in mesh have not been used extensively due to the difficulties in solution convergence when encountering contact problems, and the limitations in solving unconstrained bodies. Development of the numerical simulations will add further capability in tip relief design, opening the door to the creation of new types of gears. In the following section, a new technique for FEA simulations of tip relieved gears in mesh will be discussed which to some extent has succeeded in overcoming these problems.

Section notes:
1. *The design load of the long tip relief design is referring to the condition where vibration and noise has to be minimized. It is different from the maximum design load the drive can take.*
2. *Both the over load and the full torque load of the long and the short tip relief designs will not encounter corner contact.*

7.4.7 Solving Unconstrained Structures

As a preliminary step in this topic, it is straightforward to add a link element between the drive and driven gear or to add link elements on the drive gear when the driven gear is fully constrained at its hub. Once the input torque is loaded, the elastic deformation of the link element(s) will take place, until the drive gear has touched the driven gear. This will assist the modelling of the meshing gears when they are running with a tip-relieved section. The application of the link element is illustrated as in Figure 7.4.22.

It seems that the unconstrained rigid body motion problem has been solved when a solution check shows that the effect of the link element on whole system stiffness is very small. However, the overall solution (for a short tip relief) does not satisfy the Harris map at all, as seen in Figure 7.4.23.
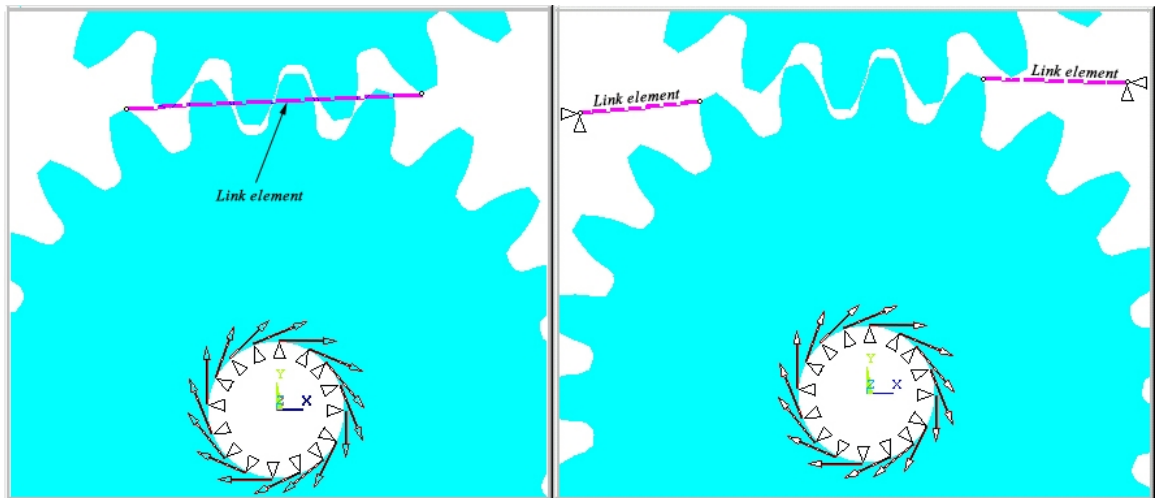
Figure 7.4. 22   Preliminary models of the link element.
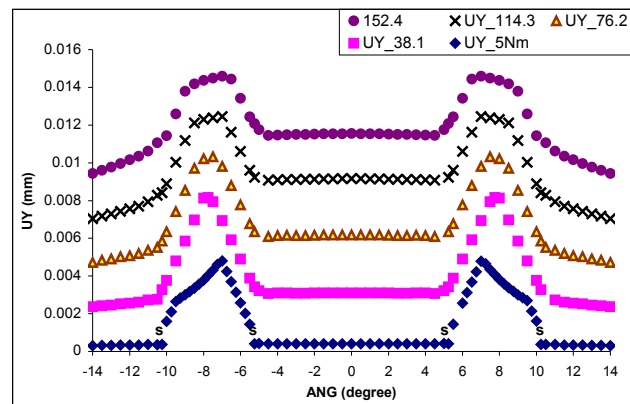
Figure 7.4. 23   Failed solutions for short tip relieved gears in mesh.

According to this type of analysis, extra care must be taken, for any change to the final tooth deflections can result in a totally different transmission error result. It should be noted firstly that for this type of connection between the gear body and the link element, the potential exists for numerical errors of the system matrix. The lower the stiffness of the link element, the longer the computer time for solution and the harder it will be to obtained solution convergence. Secondly, a 0.005mm error in the profile at the tooth tip will cause a significant difference in the shape of the transmission error. So, considering the fact that the stiffness of the link element cannot be too low, it will always tend to push the mating teeth away. It can be seen in Figure 7.4.23 that the relief starting point **s** is located where it shouldn't be; it looks rather like a long tip relief. The numerical method approach for solving such a problem involves the elimination of the numerical error in the system matrix, which is due to the soft element directly connecting to stiffer elements. One of the goals to be achieved involves the removal of the link element from the system. As Figure

148

7.4.24 illustrates, the link element can be connected to the master node of the input gear hub, which means the nodes of the input gear hub have to be coupled in rotation about the global coordinate system so that the numerical error can be limited within a wide range of stiffness of the link element. In order to minimise some arbitrary effects, in each position of the mesh cycle, the length and the orientation of the link element have to remain constant and tangent to the input gear hub. Because the adaptive re-mesh doesn't affect where the master node is located on the gear hub in the mesh cycle, once the length of the link element is defined, the coordinates of the other end of the link element can be obtained by,

$$x_1 = \overline{OD} \cdot \cos[90^0 - \theta - (\alpha + ANG)], \qquad (7.3)$$

$$y_1 = -\overline{OD} \cdot \sin[90^0 - \theta - (\alpha + ANG)], \qquad (7.4)$$

as illustrated in Figure 7.4.25.
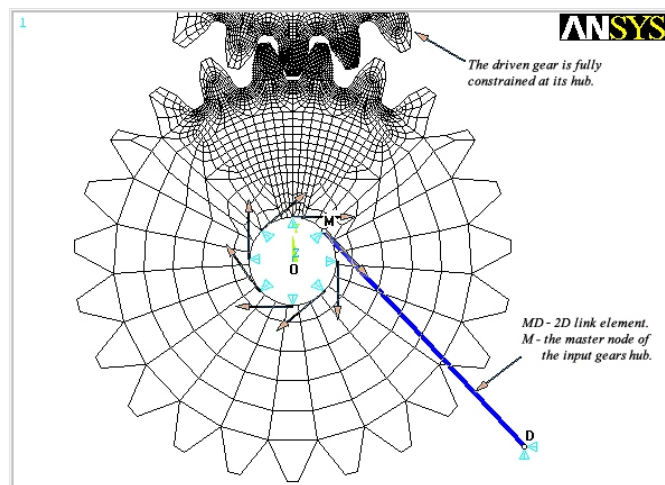
Figure 7.4. 24   The model for solving tip relieved gears in mesh.
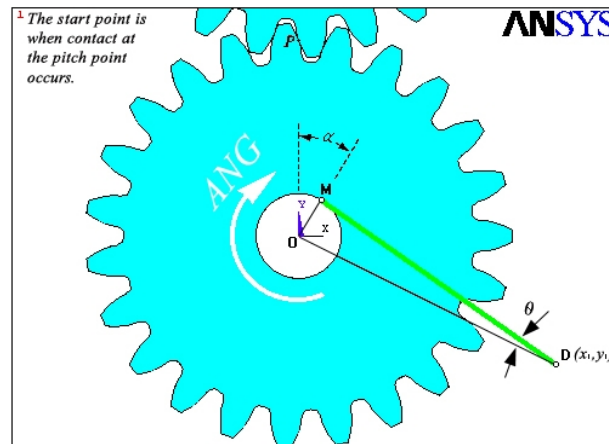
Figure 7.4. 25   The coordinates of the link element.

149

As part of the looping program, the generation of the required link element will involve commands such as those shown in Table 7.1.

CSYS,0 !* OD=101.1187420807834218975649377962 !* *afun,deg ALPHA=atan(12.255/8.6502) THETA=atan(15/100) FAI=90-THETA-(ALPHA+ANG(%FNAM%)) X1=OD*cos(FAI) Y1=-OD*sin(FAI) !* !* K, ,X1,Y1,, NKPT,0, 240 !* TYPE, 2 MAT, 2 REAL, 1 ESYS, 0 SECNUM, TSHAP,LINE !* FLST,2,2,1 FITEM,2,8977 FITEM,2,2069 E,P51X	! Activate the global cartesian coordinate system. ! The length of the link element has been defined as 100 mm. ! Angle expressed in degrees. ! ANG ( ) is an array parameter and its dimensions of meshing position. FNAM is the name of the scalar parameter to be used as the loop index. ! Create a key point at D (x_1 , y_1) . ! Generator node at the key point. ! Generator link element MD with type 2 material properties.

Table 7.1. The program for generating the link element in the mesh cycle.

The link element death option, alternatively, can be achieved if the stiffness of the link element has been carefully chosen to be related to the input load and issuing a sufficient number of iterations in the first load step. When the solution is obtained, it has to be checked to ensure the link element was "killed". One of the checks is querying the Von Mises stress of the link element in the postprocessor, as shown in Figure 7.4.26.
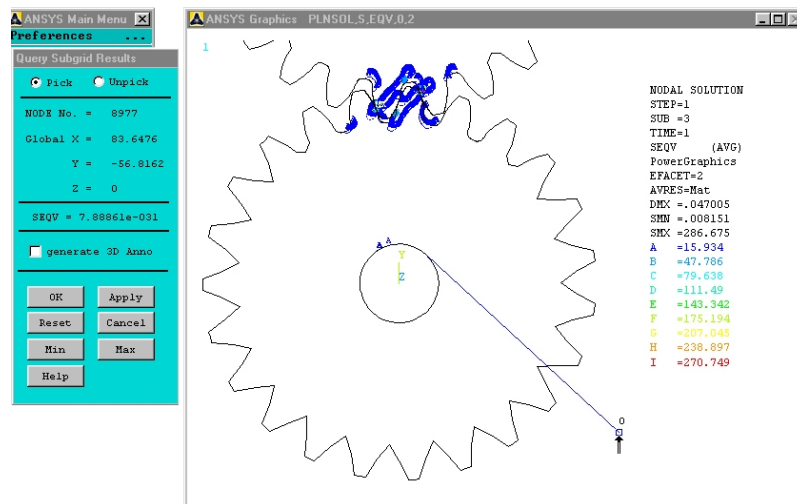
Figure 7.4. 26 Query the result of Von Mises stress to ensure the element death.

7.4.8 The Analysis of Short Tip Relieved Gears in Mesh

A short tip relief involves the relief starting point well above the pitch point, but close enough to the actual change over point (or the hand over region) so that a smooth transmission error in the mesh cycle is obtained when the input load is very light. According to the amount of the relief, high contact stresses can be avoided when the teeth change over. In this research, the short tip relief starts at point **s**, as seen in Figure 7.4.27, where the pure involute profile section ST_1 takes 1/3 of the entire involute curve above the pitch point. If the pure involute profile section ST_1 is rotated by a small angle α then it has to have a minor extension in order to reach the tooth tip at T_2. The amount of tip relief C_a is T_1T_2 which is achieved by removing the metal from area ST_1T_2. Finally, the new tip is rounded off with a 0.5mm radius.
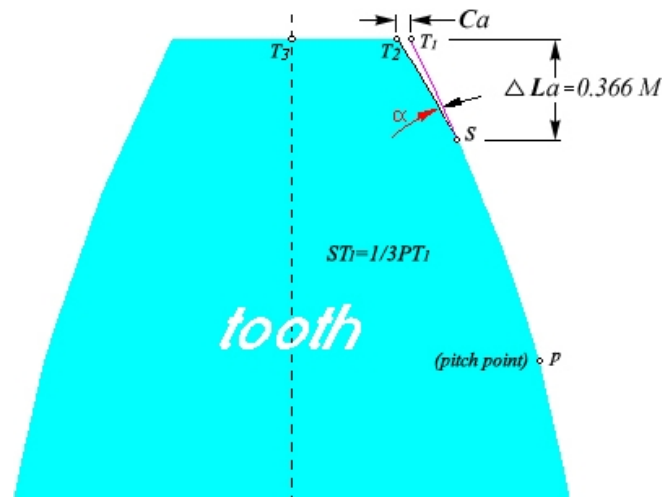
Figure 7.4. 27 The typical short tip relief.

Seven FE models were established for the study of short tip relieved gears in mesh, each of the models with its own relief angle α. The parameters of each model are listed, as shown in Table 7.2.

parameters / Model name	C_a		Length of Modification		Segment ST1 rotation angle
	Absolute value (mm)	Normalized value	Absolute value ΔLa (mm)	Normalized value Ln	α (degree)
R1thd01	0.005	0.042	2.2	0.61	0.005
R1thd02	0.009	0.075	2.2	0.61	0.009
R1thd03	0.014	0.12	2.2	0.61	0.014
R1thd05	0.023	0.192	2.2	0.61	0.023
R1thd09	0.042	0.35	2.2	0.61	0.042
R1thd16	0.075	0.625	2.2	0.61	0.075
R1thd24	0.114	0.95	2.2	0.61	0.114

Table 7.2. The parameters of the short tip relieved models.

151

It can be seen, the normalised parameters for each model are also given. The normalisations are referred to the maximum allowance of current standards, such as **BS 436: Part2: 1970 (8)**, for example the normalised relief length L_n can be expressed as,

$$L_n = \frac{the\ \ actual\ \ relief\ \ length : \Delta L_a}{the\ \max.\ \ allowable : 0.6 * M}, \tag{7.5}$$

so, the normalised parameters are non-dimensional. Using the normalised parameters can also be used to check whether current standards are still suitable for some special cases (such as non-metallic gears).

Over a complete mesh cycle, FEA simulations for each model under various input loads were carried out with looping programs. The input loads used included 5Nm, 38.1Nm, 76.2Nm, 114.3Nm and 152.4Nm. The results for each model are given in the following figures from Figure 7.4.28 to 7.4.34 respectively.
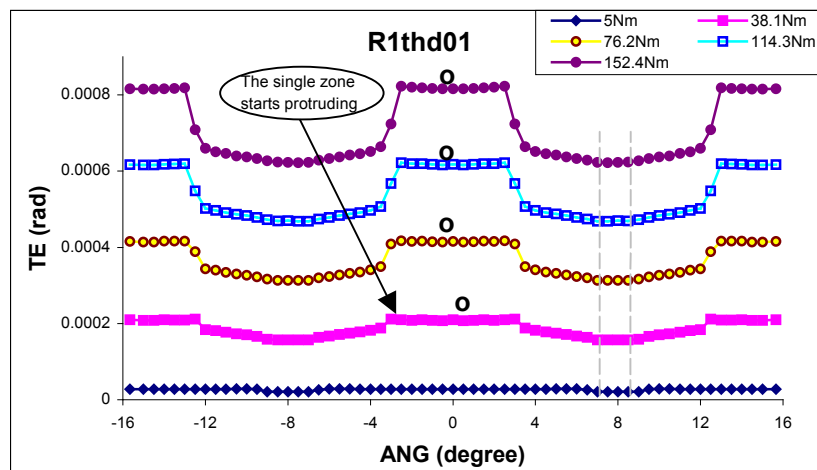
Figure 7.4. 28   The transmission error of the model R1thd01, $\alpha = 0.1^0$.
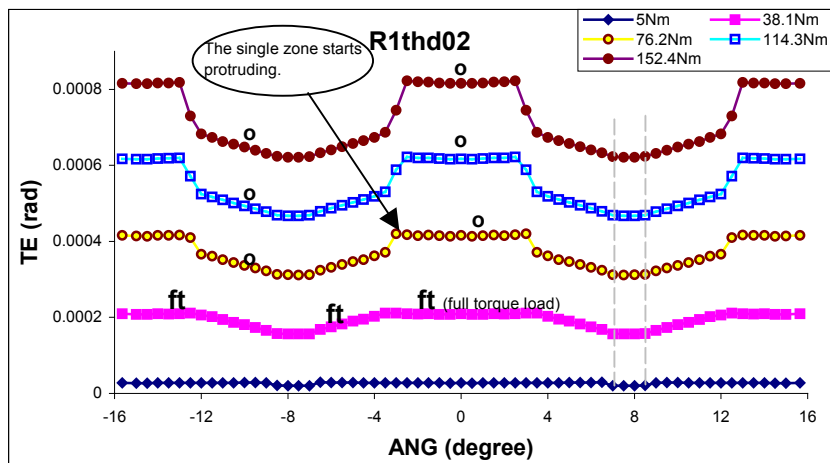
Figure 7.4. 29   The transmission error of the model R1thd02, $\alpha = 0.2^0$.

152
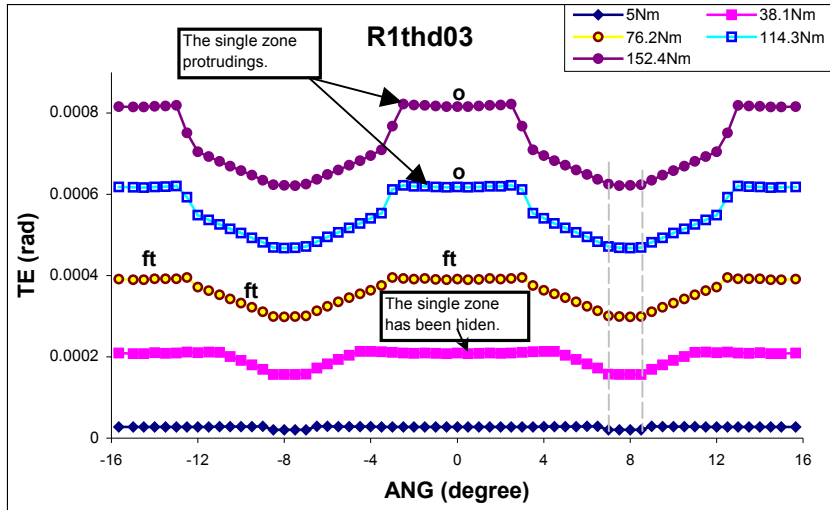
Figure 7.4. 30   The transmission error of the model R1thd03, $\alpha = 0.3^0$.
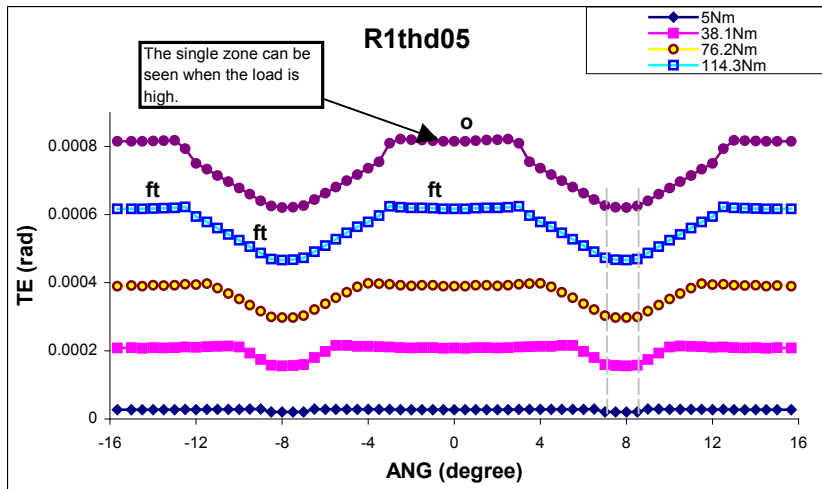
Figure 7.4. 31   The transmission error of the model R1thd05, $\alpha = 0.5^0$.
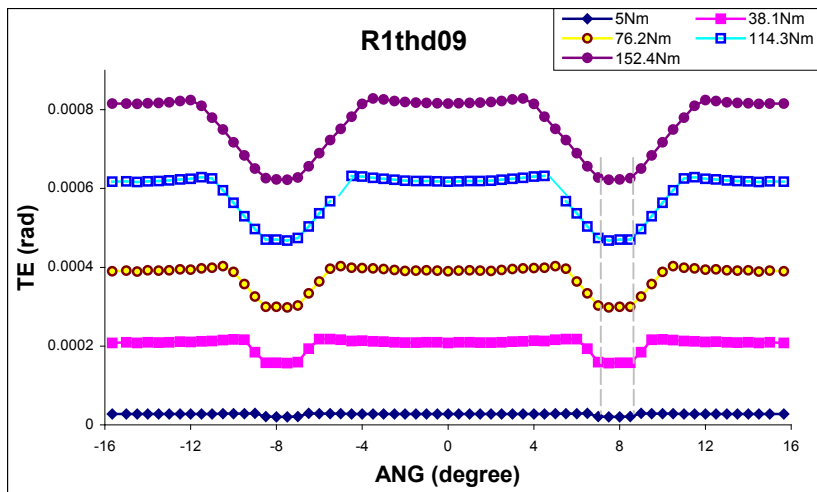
Figure 7.4. 32   The transmission error of the model R1thd09, $\alpha = 0.9^0$.
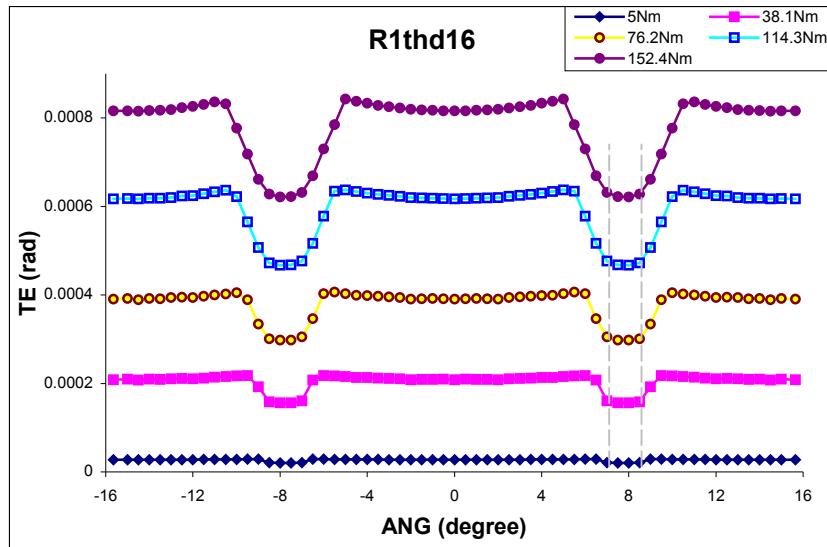
Figure 7.4. 33   The transmission error of the model R1thd16, $\alpha = 1.6^{0}$.
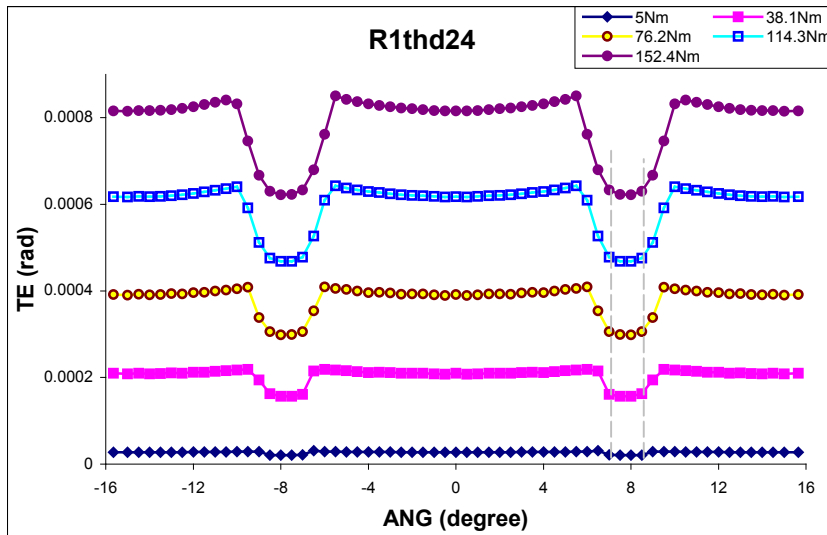
Figure 7.4. 34   The transmission error of the model R1thd24, $\alpha = 2.4^{0}$.

The results above have shown,

- The double zone retains its TE value unaffected by the tip relief within a small preserved region located in the middle of the double zone. This is for all the cases and the input loads. Values outside the small region almost linearly increase towards the single zone. The increasing ratio is dependent on the amount of the relief α or C_a, and is independent of the input loads.

- The transmission error of the single zone retains its value, unaffected by the tip relief (ignoring the handover regions).

154

- The double zone T.E. value can not exceed that of the single zone; or the maximum values of the double zone T.E. will fall into the trend of the single zone data, so that is looks like the single zone has been extended when the load is increased. However, the single zone has been hidden by the double zone data.

- Within the range of the input loads, the protruding nature of the single zone can be clearly seen when the relief angle α is 0.5^0 or less, in such cases the "protection" of tip relief does not exist. The full torque design load with short tip relief may be defined as the input load which prevents the single zone from protruding.

- When the input load is very light, the transmission errors of all the models should have the same path, as they are only relying on the relief start point **s**. A comparison has been made between all the tip relieved models as well as a model with unmodified teeth (pure involute gears in mesh), for an input load of 5Nm for each model, the result of which can be seen in Figure 7.4.35.
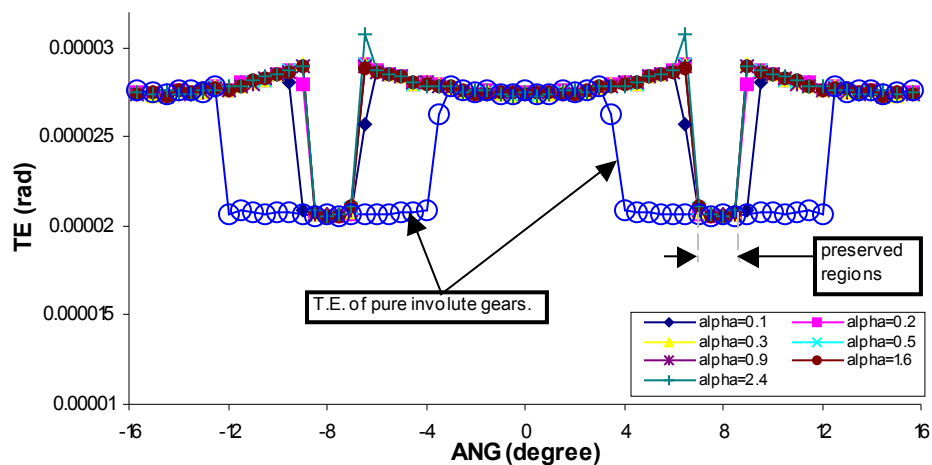
Figure 7.4. 35 Comparisons between all the models with an input load of 5Nm.

There are two small differences in the two extreme cases of α equal to 0.1^0 and 2.4^0, that could be due to numerical errors. The rest of the tip-relieved models appear to remain the same. The existence of the preserved region suggests this type of tip-relief design may not be suitable for light load or cruise conditions because the change over appears to be similar to that of pure involute gears and may cause surface spalls with the machine constantly running.

- A small preserved region in the middle of the double zone was found in all cases. All the preserved regions are nearly the same, within a 1.5^0 width. This is the

155

major difference in comparison with the Harris mapping result. Such a difference is due to the relief being too short. Further calculations and investigations have been made on this difference and will be presented in the following section.

7.4.9   Investigation of the Short and Long Tip-relief

If the relief starting point s is in the middle of the involute curve above the pitch point as seen in Figure 7.4.36, the relief is recognized as part way between the short and long relief.
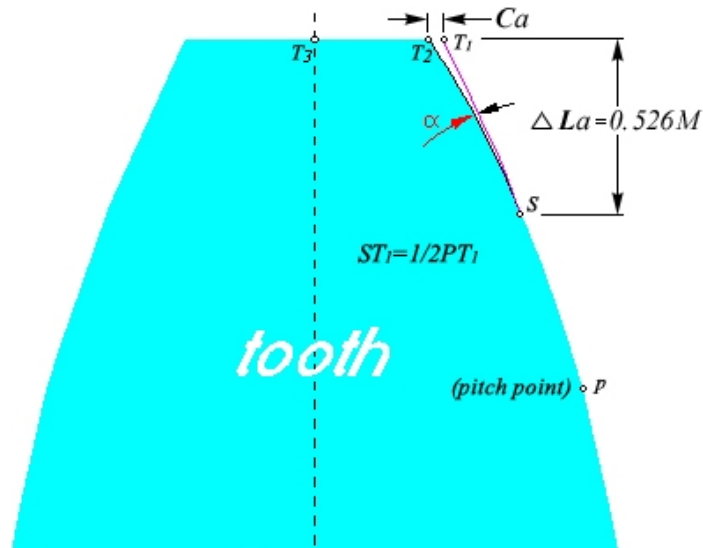
Figure 7.4. 36   The tip – relieved tooth.

Two FE models have been established for the study of the various types of relief. The parameters of each model are listed, as shown in Table 7.3.

Parameters	C_a		Length of Modification		Segment ST1 rotation angle
Model name	Absolute value (mm)	Normalized value	Absolute value ΔLa (mm)	Normalized value Ln	α (degree)
Rhalf03	0.020	0.167	3.156	0.877	0.3
Rhalf05	0.034	0.28	3.156	0.877	0.5

Table 7.3.   The tooth parameters.

FEA solutions for the transmission error of each model are shown in Figure 7.4.37 and Figure 7.4.38.
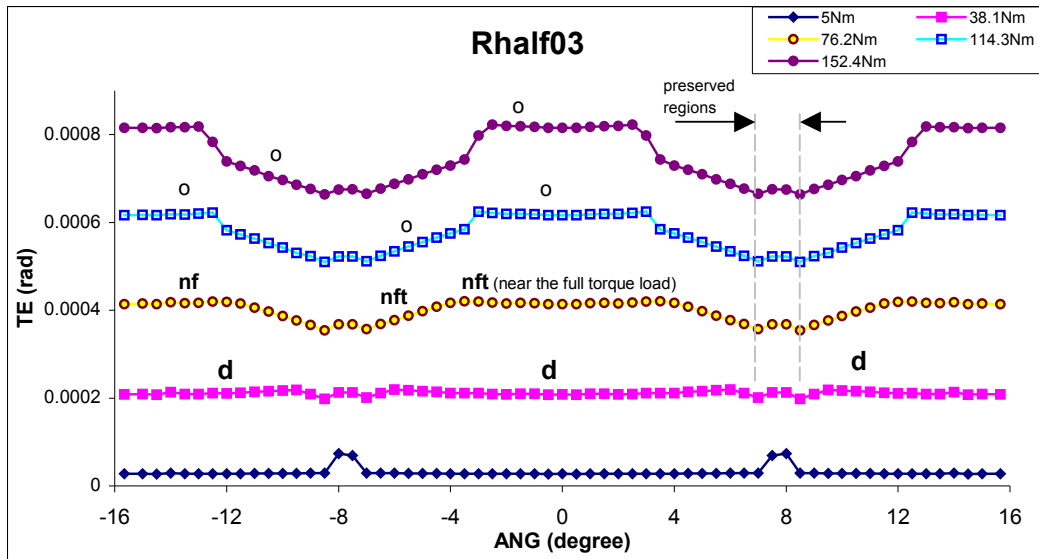
Figure 7.4. 37   The transmission errors of model Rhalf03, $\alpha = 0.3^{0}$.
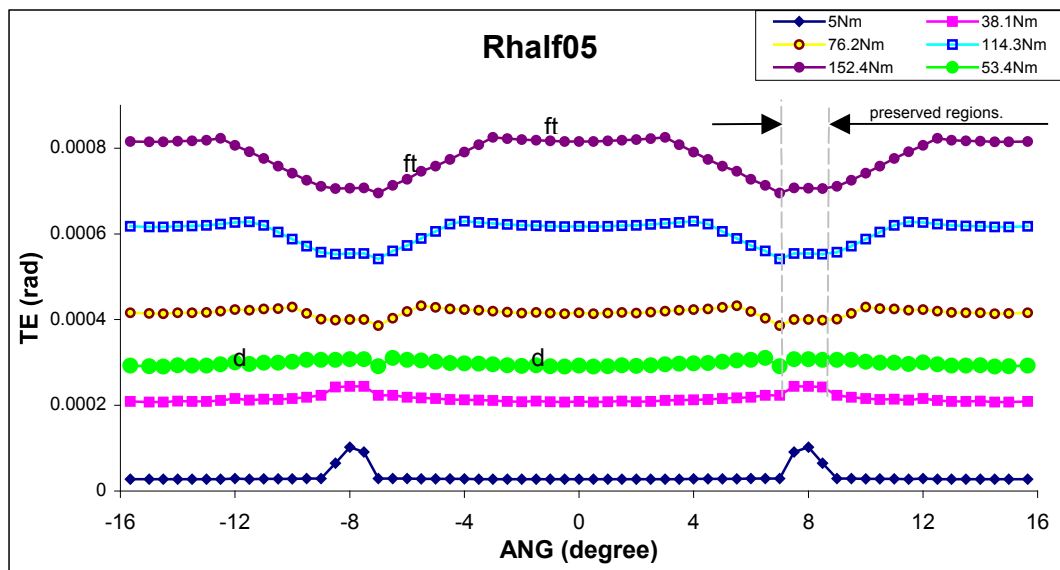
Figure 7.4. 38   The transmission errors of model Rhalf05, $\alpha = 0.5^{0}$.

The results have shown long tip relief characteristics similar to that of Harris maps, except near the preserved region in the middle of the double zone with its "fixed" size 1.5^{0}, which is similar to the behaviour of short tip relief. Figure 7.4.39 and 7.4.40 compare the results with that of pure involute gears in mesh and the differences in the preserved region are almost the same in most cases. The over load curve **o** in Figure 7.4.37 has shown its difference with that of Harris map, in this case the "protection" of the tooth tip relief does not exist due to the appearance of the protruding single zone TE. It has been found from

the results of both models that the design load (curve **d**) rises from 38.1Nm to 53.4Nm with the increasing amount of 0.2^0 in the relief angle, meanwhile the full torque curve was increased from 76.2 Nm to 152.4 Nm.

It has been recognized that the real starting point between the short and the long tip relief should exist with characteristics such that the preserved regions remain as their minimum width which may be just a point (zero width). The value in the region should still be the same as that value in the middle of the double zone of standard involute gears in mesh. If S_1 is used to denote this particular relief starting point, when a tip relief starts beyond the point S_1 ($ST_1 > S_1T_1$), the preserved region will start to move away from that of the standard involute gears with the input loads. The further the tip relief starts away from S_1, the wider the preserved region will be. On the other hand, the shorter the ST_1 length, the wider the preserved regions will be, but in this case the preserved regions will always keep the same value as that of standard involute gears. S_1 can be defined as such a *floating point*. In order to find out the *floating point*, a few models have been built and looping programs generated for each of them. FEA solutions for each model have been examined, and the results for one particular model with the tip relief starting position $ST_1 = \frac{5}{12}PT_1$, and the tooth parameters listed in Table 7.4 will be presented.
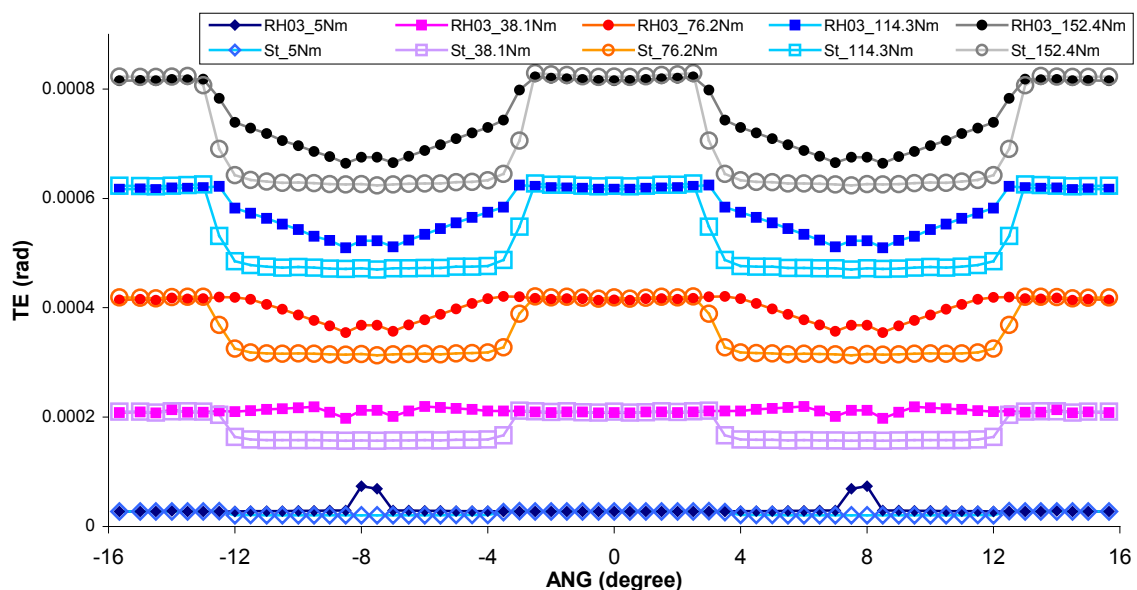
Figure 7.4. 39 Comparison TE between standard involute gear model and the model Rhalf03, $\alpha = 0.3^0$.
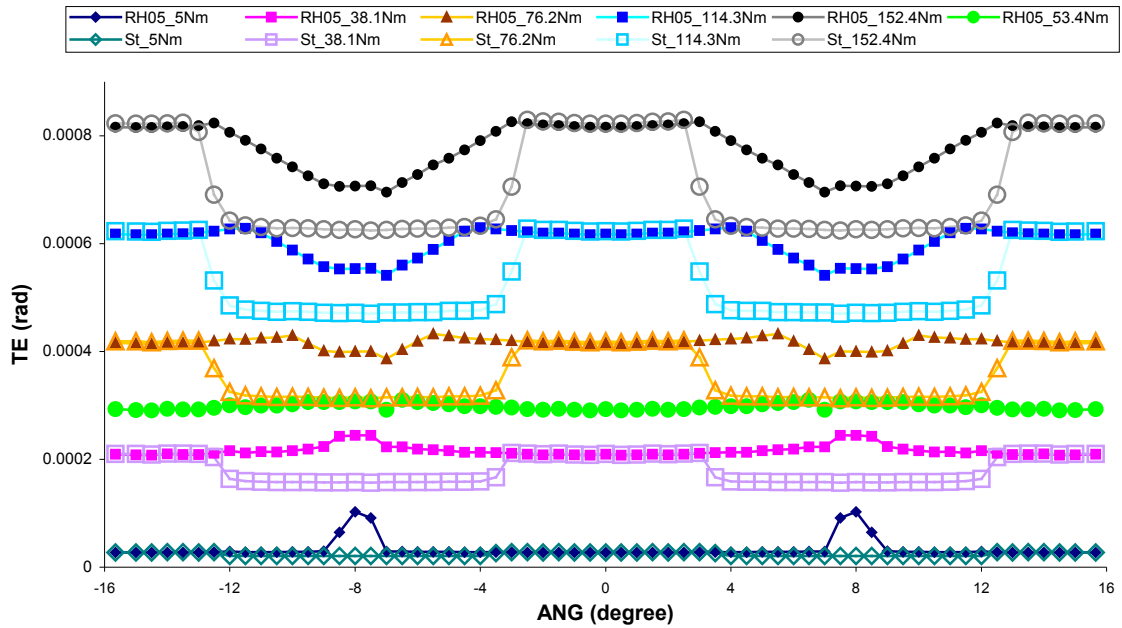
Figure 7.4. 40 Comparison TE between standard involute gear model and the model Rhalf05, $\alpha = 0.5^{0}$.

Parameters	C_a		Length of Modification		Segment ST1 rotation angle
Model name	Absolute value (mm)	Normalized value	Absolute value ΔLa (mm)	Normalized value Ln	α (degree)
R5out12_03	0.016	0.13	2.676	0.743	0.3
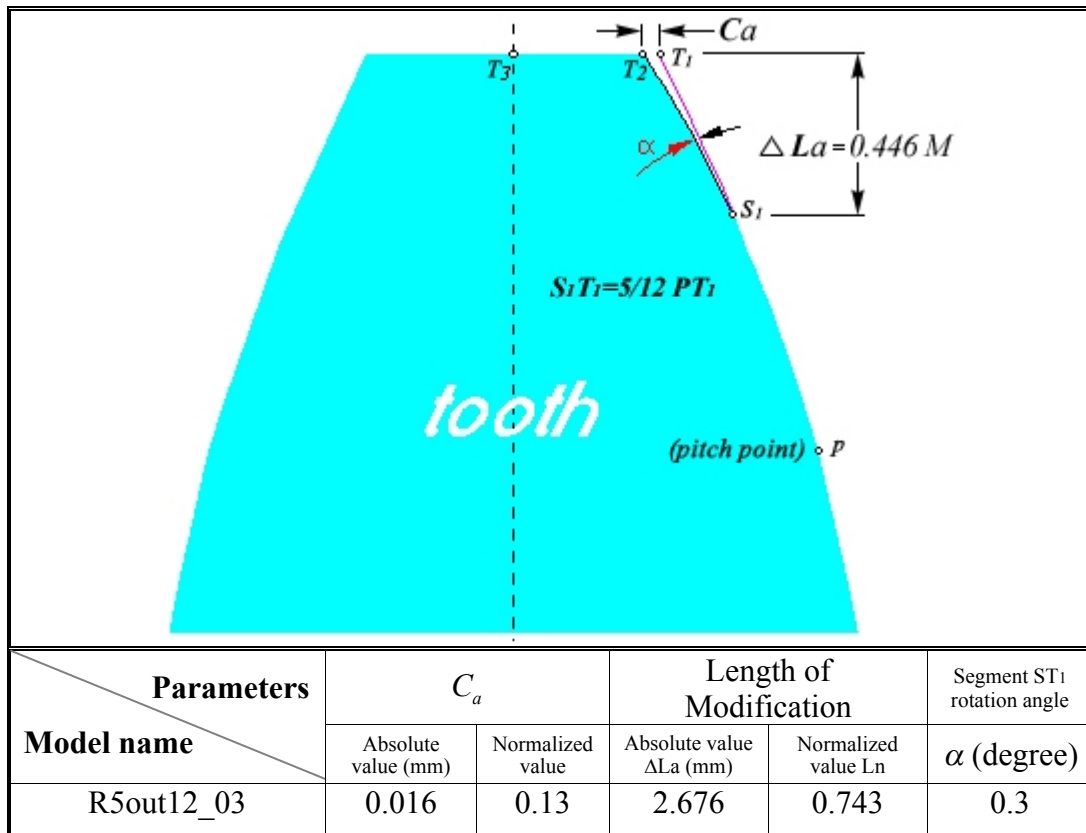
Table 7.4. The tooth parameters.

The FEA solutions for the transmission error compared with that of a standard involute gear are shown in Figure 7.4.41.

159
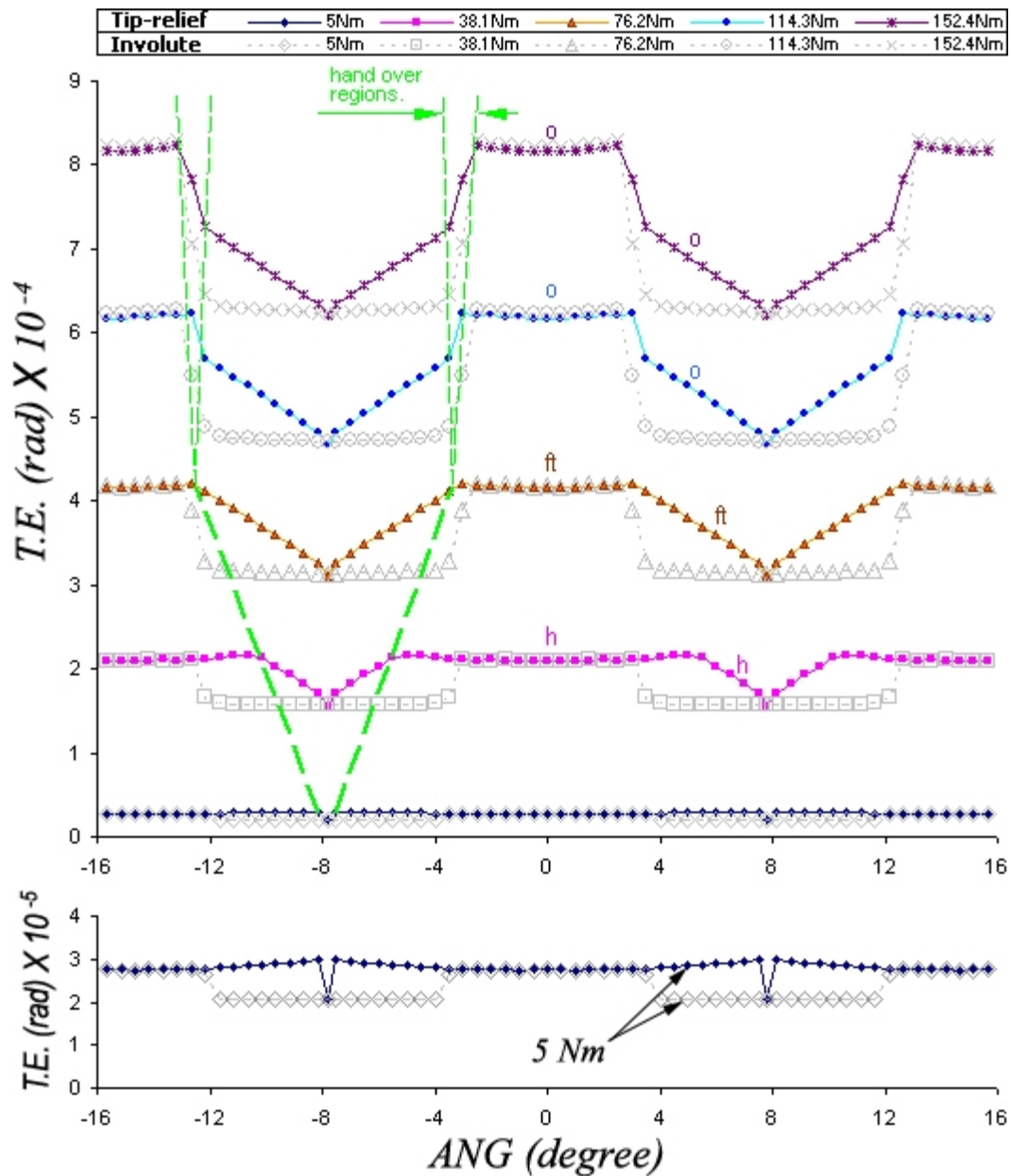
Figure 7.4. 41 Transmission errors of model R5out12_03, $\alpha = 0.3^{0}$.

The results clearly show that the short tip relief design has reached its limit and this represents the longest relief that will meet the requirements of the short tip relief design. For this particular gear, the *floating point* is located at S_1 where $S_1 T_1 = \dfrac{5}{12} PT_1$. Especially, within the full torque load, the transmission error variations are very close to Harris predictions for the short tip relief design. Over load curves are above the curve of the full torque load, where the protruding single zone transmission error can be seen. The variations of the hand over regions in the over load curves are also observed. When the

160

input load is very light, such as 5 Nm, a much smoother T.E. is achieved compare to Figure 7.4.35. Moreover, there is no edge contact observed with light load which means short tip-relieved gears will avoid early spalling, especially for gears constantly running with light load.

7.4.10 The Analysis of Long Tip Relieved Gears in Mesh

Further extension of the relief starting point **s** from the tooth tip is expected to gain smoother TE at the design load. The first long tooth relieved gear model was built with the relief having 2/3 of the involute curve above the pitch point. The tooth details are shown in Figure 7.4.42 and the parameters are listed in Table 7.5.
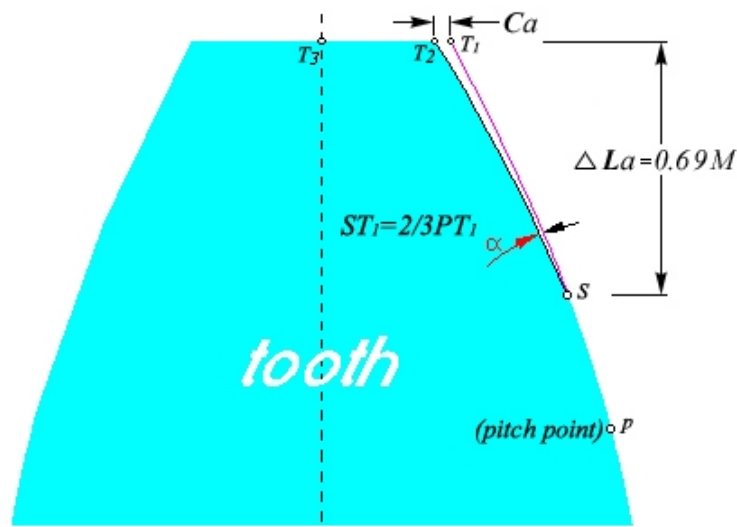
Figure 7.4. 42 Long tip relief.

Parameters	C_a		Length of Modification		Segment ST_1 rotation angle
Model name	Absolute value (mm)	Normalized value	Absolute value ΔLa (mm)	Normalized value Ln	α (degree)
R2thd025	0.022	0.183	4.14	1.15	0.25

Table 7.5. Tooth parameters of model R2thd025, $\alpha = 0.25^0$.

The FEA results with their details are illustrated in Figure 7.4.43.

The results show similar improvements of the TE at the design load when compared with the results that have been obtained in Figure 7.4.37 and 7.4.38. For the design load curve, the slight downward changes at the edge of the preserved regions can be seen. The wider

preserved regions are also observed due to the longer relief length compared to that of the model Rhalf03 and Rhalf05 (Figure 7.4.37 and 7.4.38). The comparison of results between the long tip relief and the standard involute gears in mesh is shown in Figure 7.4.44.
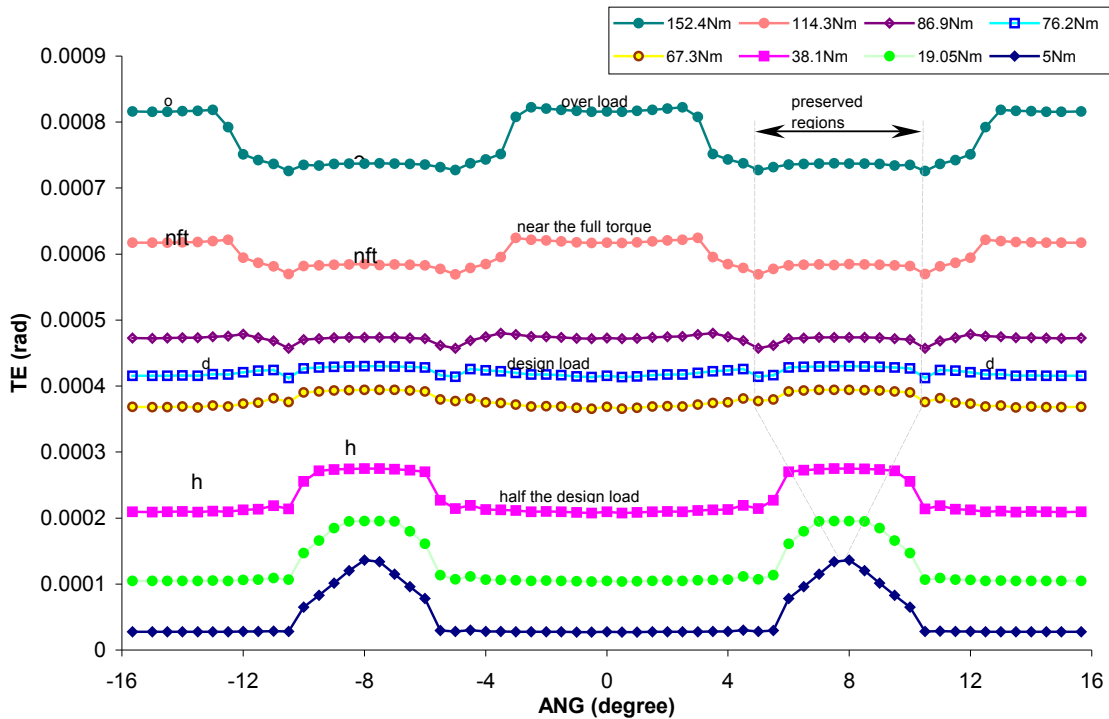
Figure 7.4. 43 Transmission errors of model R2thd025, $\alpha = 0.25^{0}$.
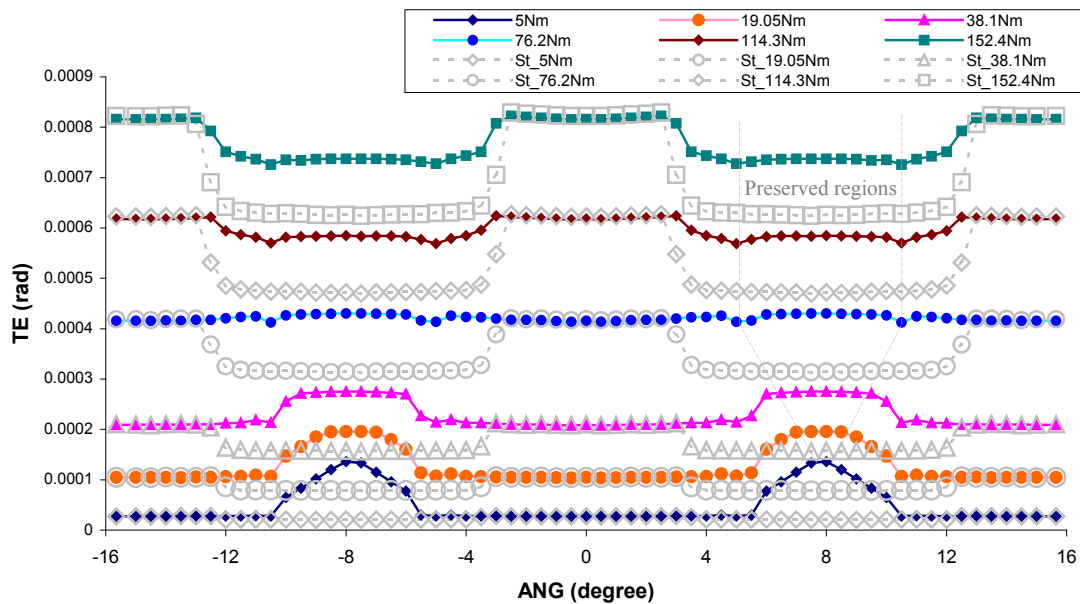
Figure 7.4. 44 The comparison of the TE of standard involute gears and the long tip - relief gears in mesh.

The longest tip relief design extends the relief starting point **s** from the tip to the pitch point, which is the traditional long tip relief concept (Smith 1999), as shown in Figure 7.4.45. Two relevant models Rp01 and Rp02 have been established with their relief angles of α = 0.1 and 0.2 degrees respectively. The tooth parameters are listed in Table 7.6.
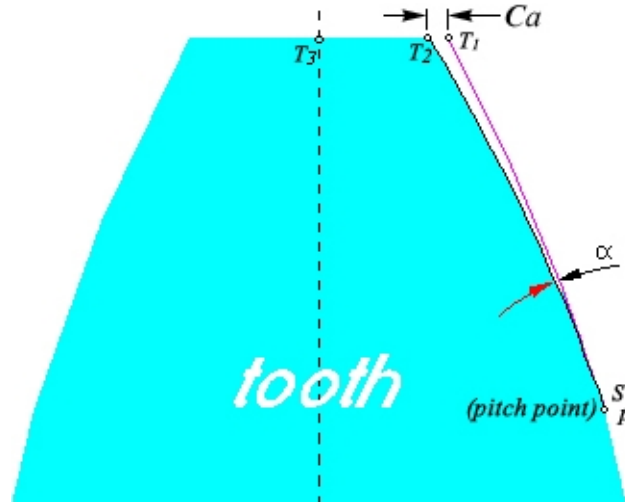
Figure 7.4. 45 The maximum length of the tip relief.

Parameters / Model name	C_a		Length of Modification		Segment ST1 rotation angle
	Absolute value (mm)	Normalized value	Absolute value ΔLa (mm)	Normalized value Ln	α (degree)
Rp01	0.013	0.11	6	1.67	0.1
Rp02	0.026	0.22	6	1.67	0.2

Table 7.6. The parameters of the tip relieved tooth.

The FEA solutions for the transmission error have been obtained, and the results for each model compared with that of standard involute gears in mesh, as shown in Figure 7.4.46 and 7.4.47 for $\alpha = 0.1^0$ and $\alpha = 0.2^0$ respectively.
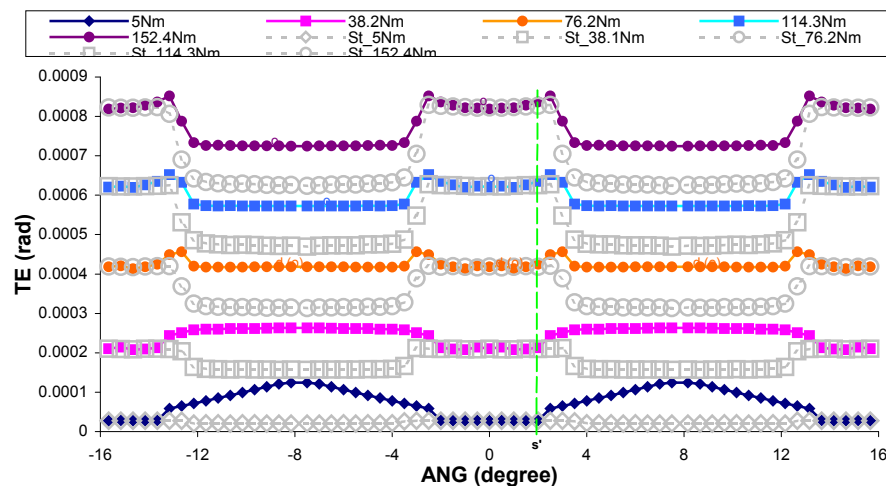
Figure 7.4. 46 Transmission errors of the model Rp01, $\alpha = 0.1^0$.

163
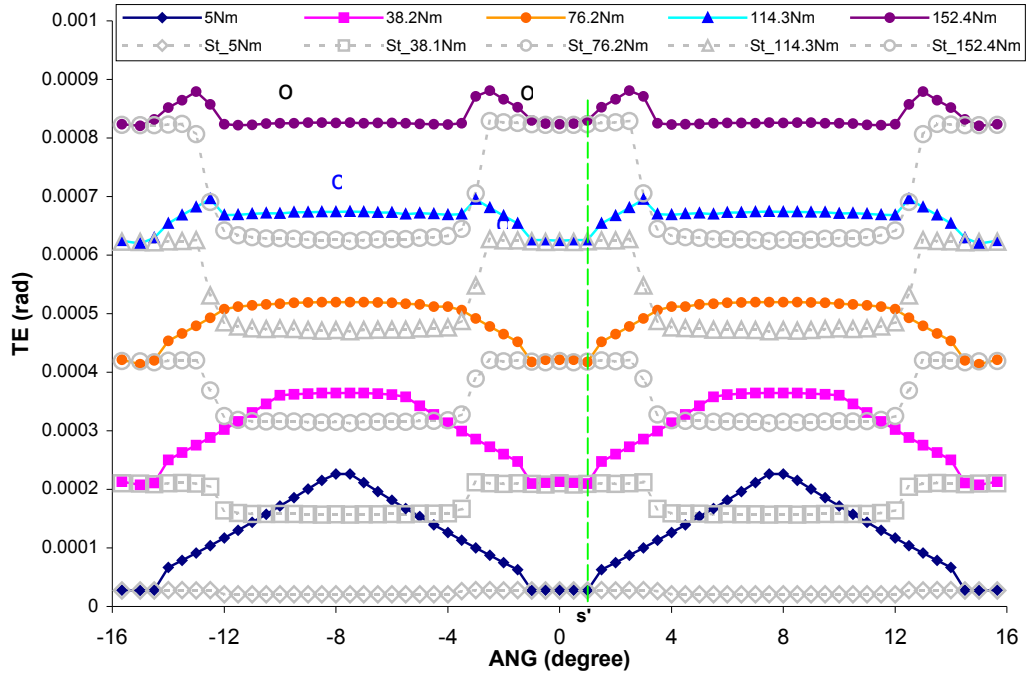
Figure 7.4. 47 Transmission errors of the model Rp02, $\alpha = 0.2^{0}$.

The results from both models show that neither can meet the requirements of a smooth T.E. at the design load while providing sufficient protections for the tooth flank face. The design load for Rp01 shows an over load condition in the single zone T.E. especially with the hand over region increasing. With the tooth tip relief increasing as shown in Figure 7.4.47, the single zone T.E. rises rapidly during the hand over region before the "design load" has been reached. It should be noted that the relief start point of the T.E. **s'** does not match the actual relief starting point which is at the pitch point. The location of **s**' is dependent on α, usually the larger α, the closer to the actual relief starting point will be observed. Those results, however, are valuable since they have shown the variations of the preserved region and reveal the important changes to the T.E. It might be expected that a critical tip relief starting point S_2 could be found, where the design load T.E. will be smooth. A relevant model has been built with its tooth relief as shown in Figure 7.4.48 and the tooth parameters are listed in Table 7.7.

Parameters	C_a		Length of Modification		Segment ST1 rotation angle
Model name	Absolute value (mm)	Normalized value	Absolute value ΔLa (mm)	Normalized value Ln	α (degree)
R5out6_025	0.026	0.217	5.124	1.423	0.25

Table 7.7.   The tooth relief parameters.

164
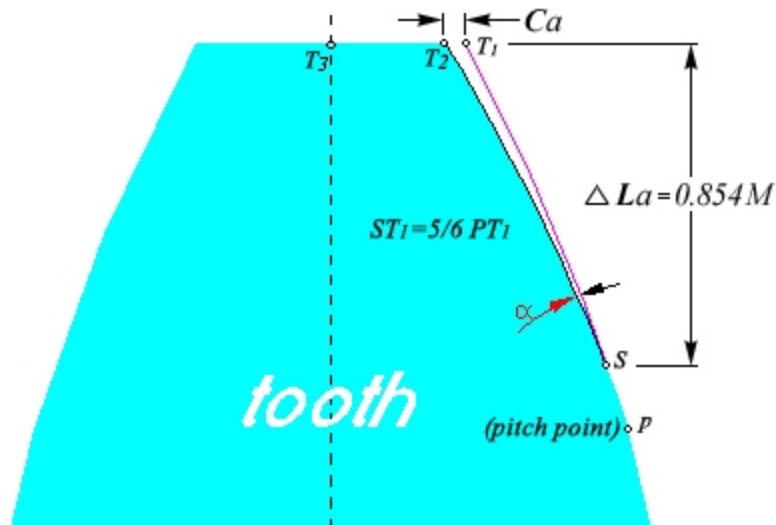
Figure 7.4. 48   Details of the tooth relief.

FEA solutions for the transmission errors have been obtained as shown in Figure 7.4.49. Two loops of the programs for the input loads 133.35Nm and 138.35Nm were used, and then the design load of 133.35Nm was found. As seen from the T.E. calculations, the T.E. now appears to be very smooth with only a minor ripple. The small ripple means that the critical relief starting point S_2 has not been precisely reached yet, but the starting point of the tip relief must be very close. With the design load curve getting smoother, it should be noted that the over load curve is coming down and is very close to the design load. If the preserved region extends to its maximum, which is in the double zone width, the protruding section of the T.E. in the single zone will be present for any input load greater than the design load. Here the single zone and the double zone refer back to that of the standard involute gears in mesh.

Tip relief designs have been discussed, in which it can be seen that the tooth modifications are small but the influence to the gear transmission error is significant. For the tooth tip-relief modifications, two critical relief-starting points S_1 and S_2 have been found which effect the variations of the double zone *preserved regions* that have been defined in this section. The concept of the full torque load and the over load torque have been clarified in the sense of tooth flank surface protection. Specially, the full torque load should be taken into account by gear designers to avoid early spall failure (pitting or crack) on the gear flank face.

165
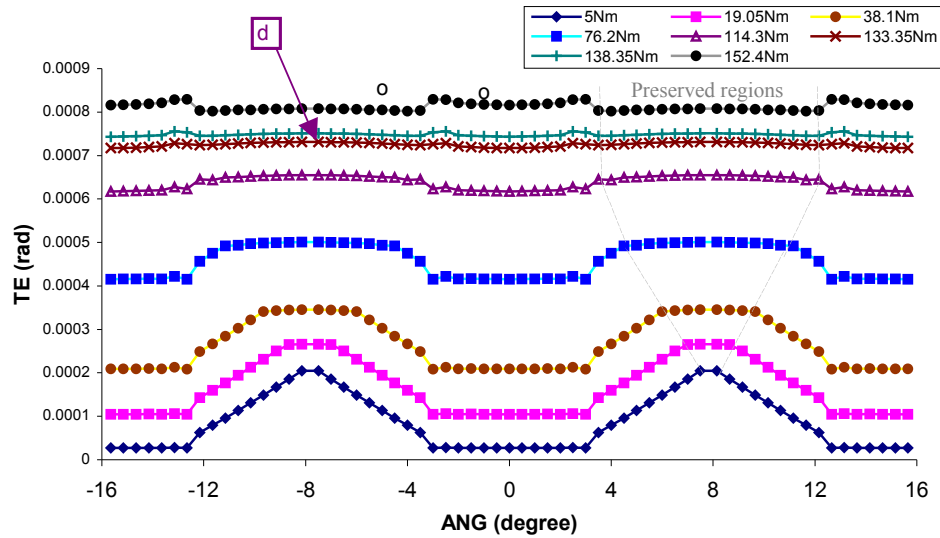
Figure 7.4. 49 Transmission errors of the model R5out6_025.

7.5 The Effect of Modifying the Centre Distance

The previous methods used in the analysis of tip-relieved gears in mesh can also be used to investigate the effect of modifying the centre distance of the gears in mesh. Firstly, a fixed increment of 0.2 mm along the line of original centre distance was considered, and the FEA solutions for the transmission errors under various input loads were obtained. The results over a complete mesh cycle are shown in Figure 7.5.1 as a function of input load.
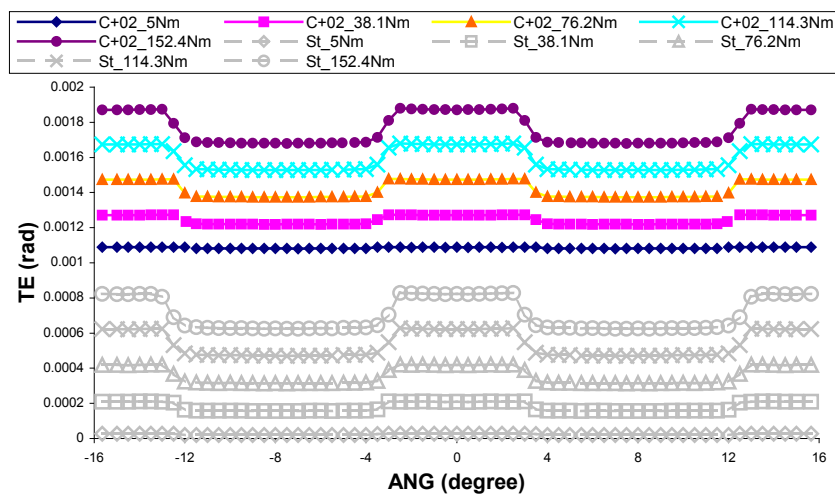
Figure 7.5. 1 The transmission errors with modified centre distance.

It should be noted there is a group of data in the bottom of the figure, which is for the meshing gears without any modifications. It can be noted that the shapes of the transmission error curves between the two groups are slightly changed in their hand over

166

regions, but the major difference between the two groups is in their absolute T.E. values. For the maximum input load, the difference (relative error) was 227.5% in the single zone and 269% in the double zone. When the input load was 5Nm, the difference (relative error) was up to 3947%. Concerning the relative errors it should be noted that if a specific geometry error (misalignment or eccentricity, etc.) were present, the relative transmission error would tend to an infinite value when the input load tends to zero. For an input load of 76.2Nm, considering 0.2mm as the maximum change of the centre distance, FEA solutions for the transmission error of the meshing gears with various increments decreasing to 0.005mm have been obtained, as shown in Figure 7.5.2.
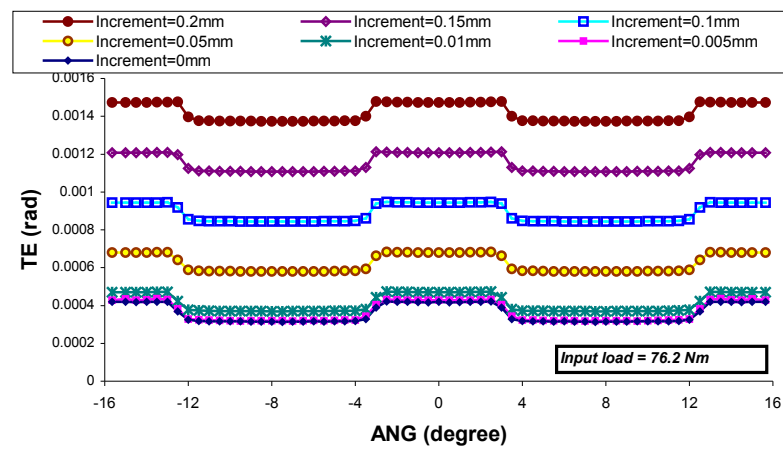
Figure 7.5. 2 T.E. of various centre distance modifications.

The relative errors can be found from,

$$(TE_{INC} - TE_{ST})/TE_{ST},\qquad(7.5)$$

where TE_{INC} is the transmission error with a certain increment of the centre distance and TE_{ST} is the transmission error of standard involute gears in mesh (without misalignment or tip-relief). The relative errors of each increment are given, as shown in Figure 7.5.3.

The results have shown an almost linear increase in the relative errors with the centre distance increment from 0.05mm to 0.2mm. For the small centre distance increment of 0.01mm, the relative errors were found to be 17.5% in the double zone and 12.2% in the single zone. For the minimum increment of 0.005mm, the relative errors were found to be 4.7% (maximum) in the single zone and 0.8% (minimum) in the double zone. Under normal operating conditions, the running gear pair can have such small variations in their centre distances. The centre distance variation will not be a fixed value so that considering

the combination of possible profile errors and other types of misalignments, the experimental measurement of gear transmission error becomes extremely difficult.
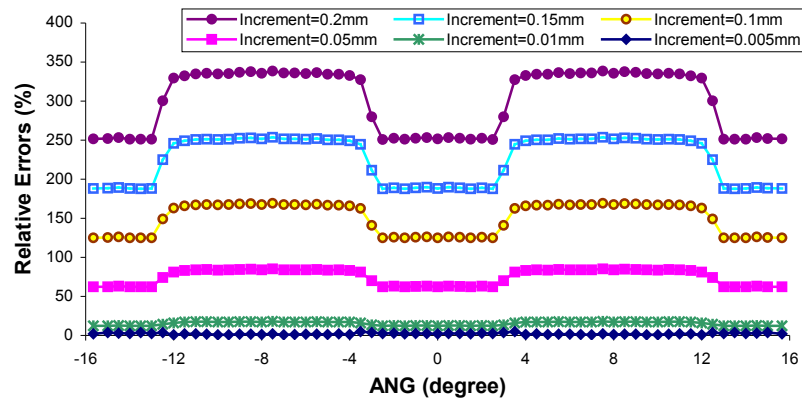
Figure 7.5. 3 The relative errors as a function of centre distance.

7.6   T.E. in the Presence of a Tooth Root Crack

In order to improve the vibration condition monitoring of gear systems, detailed knowledge of the vibration generation mechanisms for various types of failure are required (Du 1997). One of the recent modelling approaches (Howard 2001) involves the use of coupled torsional and transverse motions of the shafts, along with the changes to the tooth bending stiffness as the teeth go through the mesh point. The effect the single tooth crack has on the frequency spectrum and on the common diagnostic functions of the resulting gearbox component vibrations can be obtained, where the tooth stiffness is modelled using finite element analysis to ascertain the changes to the teeth stiffness as a function of gear rotation. The details of the finite element model near the root crack of 3.5 mm are shown in Figure 7.6.1.
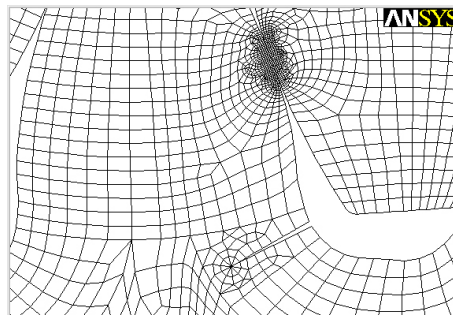
Figure 7.6. 1   The details of the tooth crack of 3.5 mm.

It should be noted that the all-quad element model is no longer possible due to the necessity of using the triangle elements to mesh the singularity in the region near the crack front. Right at the crack tip (2D), 10 special triangular elements were used with their mid-side

168

nodes located at ¼ of their adjacent edges from the crack tip (Anderson 1995). The LEFM (linear elastic fracture mechanics) assumption was used in the analysis. The solutions for the transmission error were obtained, as shown in Figure 7.6.2.
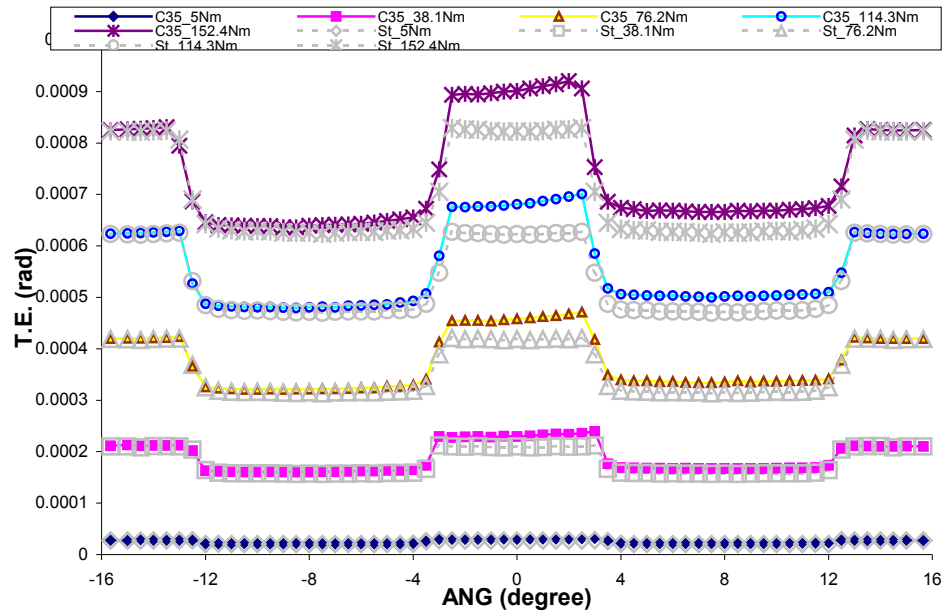
Figure 7.6. 2   T.E. of the involute gear in mesh with a localized tooth crack.

The LEFM assumption is valid only as long as the non-linear material deformation is confined to a small region surrounding the crack tip. In many materials, it is virtually impossible to characterise the fracture behaviour with LEFM (Anderson 1995), and an alternative gear model with a (single) root crack is required. An elastic-plastic fracture mechanics model of the cracked tooth behaviour under various load conditions should be carried out so that the crack tip opening displacement (CTOD) or the J contour integral can be evaluated. The associated parameters such as the component of plastic mouth opening displacement and the hinge point can be obtained and used to determine the modified tooth profile which is due to the plastic deformation at the crack tip. Once the modified tooth profile is known, the analysis for the transmission error can be carried out using the method that has been used for tip relieved gears in mesh. However, detailed analysis with elastic-plastic fracture mechanics applies to the cracked gear(s), and the analytical or experimental analysis are currently not included in this research. As a preliminary study on the topic, the evaluations of the transmission error with the crack tip plasticity will be investigated with assumptions, the details of which are shown in Figure 7.6.3.
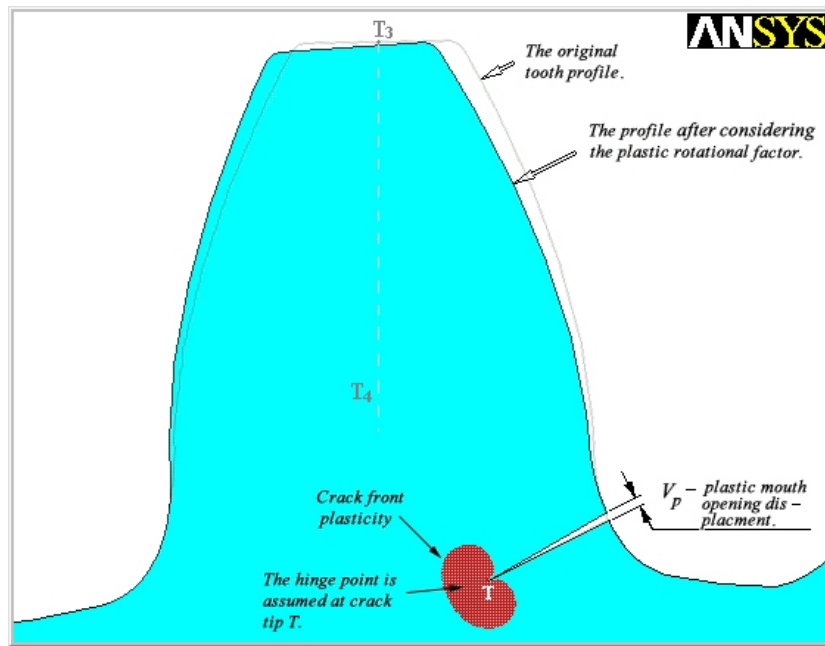
Figure 7.6. 3 The tooth profile modification due to the crack front plasticity.

It can be seen that the hinge point is assumed to occur at the crack tip. This is because compared with the structure dimension, the distance from the crack tip is very small. The major part of the tooth, especially the mating side profiles above the crack, rigidly rotate about the hinge point where the hinge model assumption is used (Anderson 1995). In what extent the hinge model is suitable for the cracked tooth is a critical task and it may be investigated in the future. V_p represents the plastic component of the mouth opening displacement which is illustrated in Figure 7.6.4.
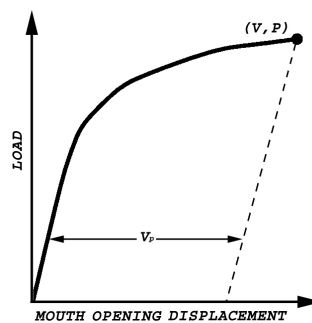
Figure 7.6. 4 The crack mouth opening displacement.

FEA solutions for the transmission error were carried out using the more realistic models of tip-relieved gears in mesh. Model Rhalf05 (see Figure 7.4.36 and Table 7.3) was used under the consideration of profile modification due to a 3.5mm root crack. The crack orientation angle was 67.4 degrees between the crack and the original tooth symmetry line

170

T_3T_4 (see Figure 7.6.3). According to Lewicki (Lewicki 1997) the angle greater than 45 degrees is realistic for this model. It has been assumed that the plastic component of the crack mouth opening displacement was 0.005mm, which results in the tooth rotation about the hinge point of 0.082 degrees. The transmission errors under various input loads are presented in Figure 7.6.5, and the results are also compared with that of the un-cracked gear model over a complete mesh cycle.
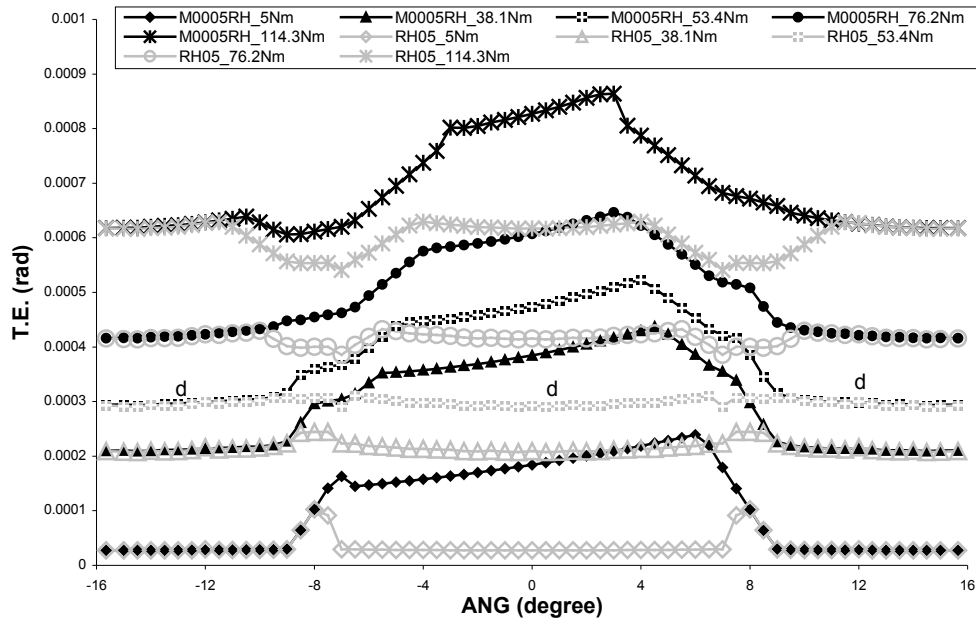
Figure 7.6. 5 T.E. of cracked gears in mesh with permanent tooth deformation.

The results have shown that the maximum change in T.E. of 2×10^{-4} (rad) can be found in each curve even at the design load. The abrupt starting and ending positions, however, in this case also rely on the relief starting point.

FEA solutions for the transmission error have produced results for the tip-relieved gears in mesh with the root crack under the assumption of LEFM (linear elastic fracture mechanics). The results can also be compared with those of the un-cracked gears in mesh over a complete mesh cycle as seen in Figure 7.6.6.

It should be noted that when the input load is smaller than the design load (53.4 Nm) the transmission error path is actually smoother than that of the un-cracked gears in mesh. So far, the transmission error behaviour of the meshing gear pair has been investigated under

171

three considerations with the same root crack, (i) the standard involute meshing gears analysed with the LEFM assumption, (ii) the analysis of tip relieved gears, and (iii) the tip relieved gears analysed with its permanent deformation due to the plasticity at the crack tip. Over a complete mesh cycle, the transmission error behaviours are significantly different to each other, as shown in Figure 7.6.7.

For the modelling of tip-relieved gears in mesh using the LEFM assumption, the results should be valid for light load conditions. An example can be used to highlight the diagnostic consequences, as shown in Figure 7.6.6. When the input load is less than the design load, the transmission error curves may be smoother than that of the un-cracked gears in mesh. In this case, gear diagnostic techniques using the gear case vibration may fail to detect the root crack. This may provide a clue for gear diagnosis. If the design load is light, so that the LEFM assumption is valid, the gear diagnosis through the gear case vibrations may fail to detect the root cracks due to the gears constantly running within their design load (cruise conditions). With the hinge model assumption, the effect of the 0.005 mm plastic mouth opening displacement on the transmission error becomes significant, but the question is to what extent the hinge model is suitable for the cracked tooth. The validation of the hinge model as applied to the cracked tooth should depend on the crack length, the orientation as well as the gear thickness (back up ratio) amongst other factors. For a certain plastic mouth opening displacement, it has been suspected that the tooth may rigidly rotate about the hinge point. In that case, the actual rotation angle may be less than what it was, due to the elasticity of the surrounding material outside the plastic zone. From another point of view, if the actual rotation angle is greater than what it was, the gear failure diagnostic task will be made easier. If the actual rotation angle, as suspected, is less than what it was, the actual transmission error curve under the certain input load will fall in between the curves produced by the LEFM assumption and the hinge model assumption. There will be a domain in the mesh cycle for each input load that is between the curves produced with the above two assumptions, as shown in Figure 7.6.8. The domain size to some extent represents the amount of maximum plastic deformation when the hinge model is used. It also contains rigid body motions, – the sliding component due to the rotated tooth profile. So, in this case the domain represents both possibilities.
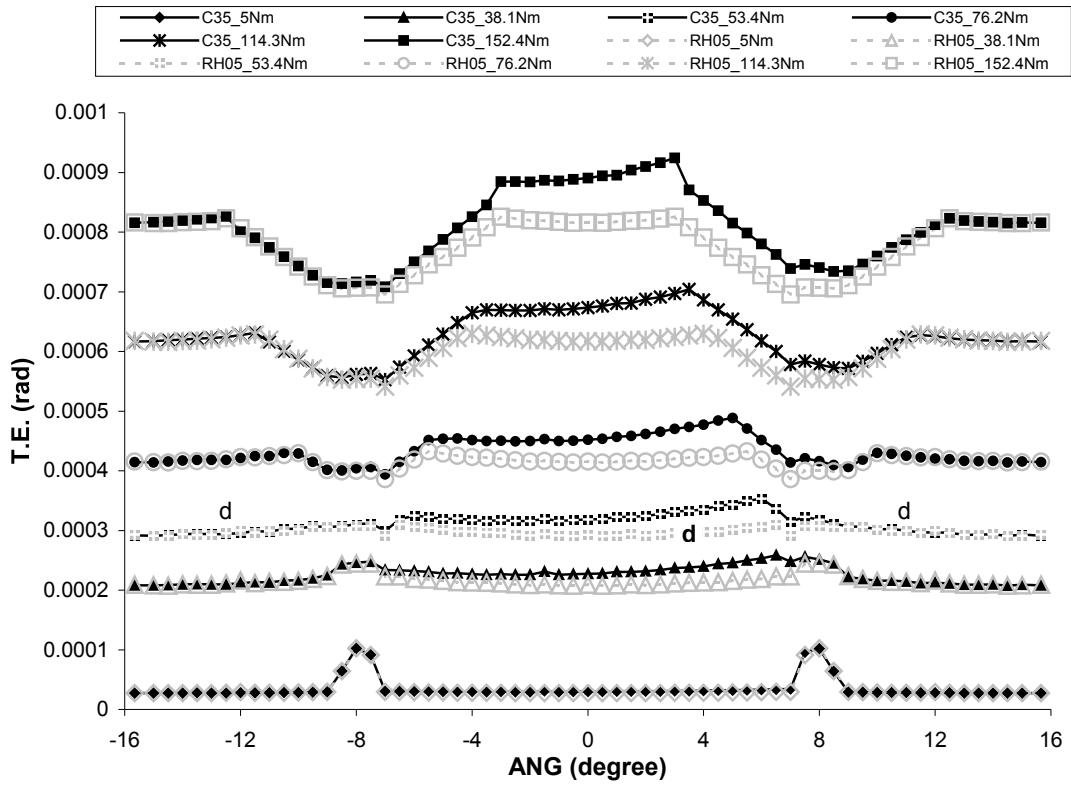
Figure 7.6. 6   T.E. of the tip-relieved gears in mesh with LEFM assumption.
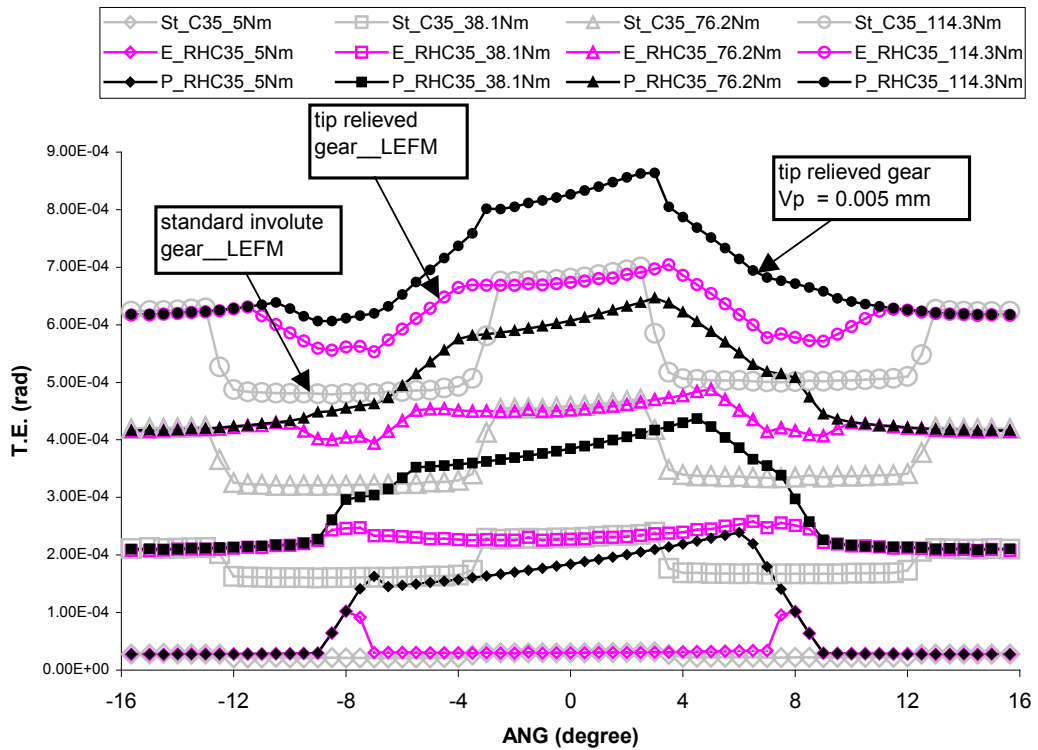
Figure 7.6. 7   T.E. of the cracked gears under different assumptions.

173
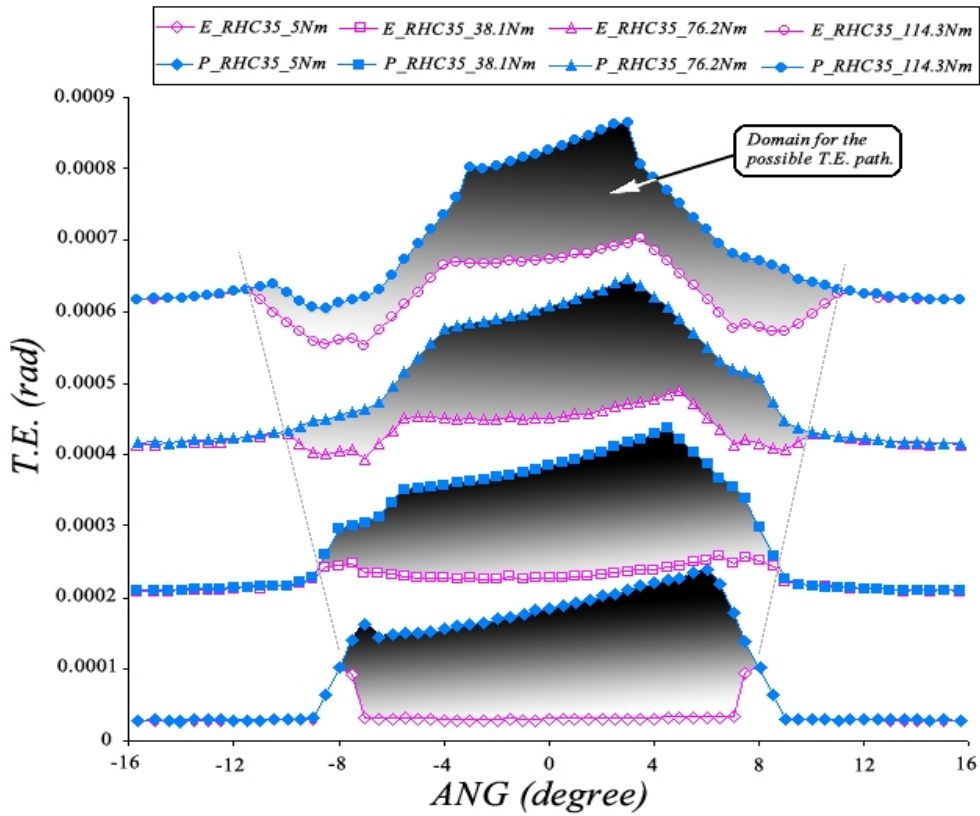
Figure 7.6. 8   The domains for the possible T.E. path.

The actual T.E. path can be estimated within the major trend of the variations, as shown in Figure 7.6.9.
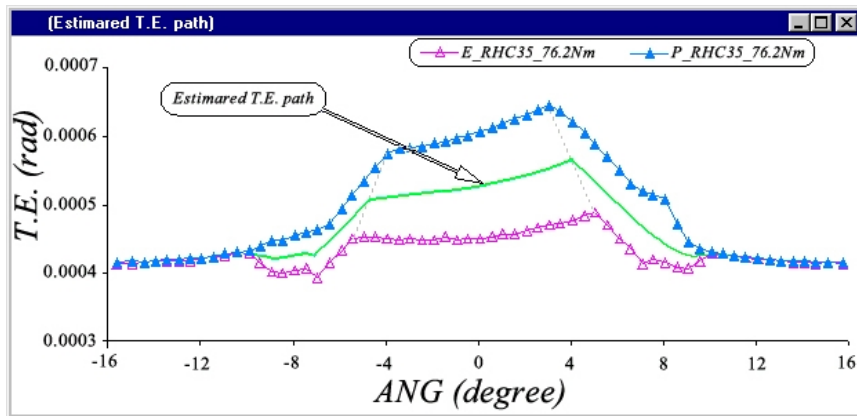
Figure 7.6. 9   Sample of an estimated T.E. path.

As shown, the estimated T.E. path was taken to be the mean of the two assumptions, for the input load of 76.2 Nm. The different curves could be used for gear failure (root crack) detection and diagnosis through gear case vibration and would give results with different reliabilities and also analysis with different difficulties.

7.7   New Tooth Profiles for Reducing Gear Vibration Below the Design Load

Based on the knowledge of existing gear transmission error studies, it may be possible to design gears with new tooth profiles having the following features:

- Usually at the design load, the transmission error has downward protrusions as shown in section 7.3. The new tooth profile will have no abrupt protrusions at the design load.

- When the input load is lighter than the design load, the curves of the transmission error should vary smoothly up and down in the mesh cycle, so that the vibration level is reduced.

A few models have been build with the new tooth profiles that were created by applying a combination of back lash and (original) curve rotation, model New_A01, New_A02 and New_A055 which were aimed at obtaining smoother T.E. curves at different levels of design load. FEA solutions for the transmission errors are shown in Figure 7.7.1, 7.7.2 and 7.7.3.
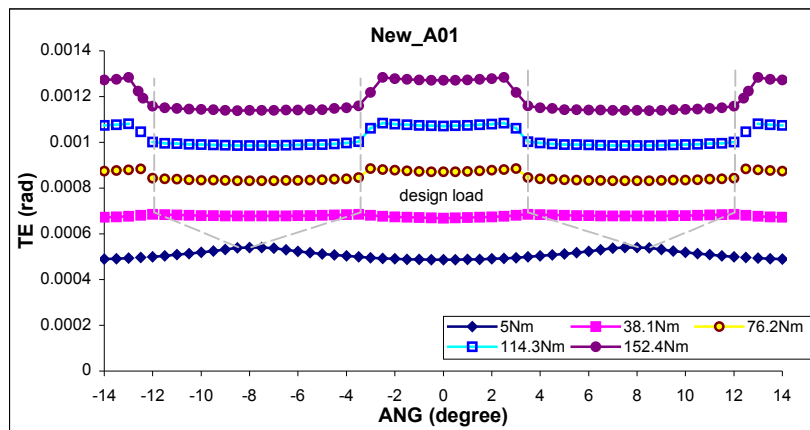
Figure 7.7. 1   Transmission errors of model New_A01.
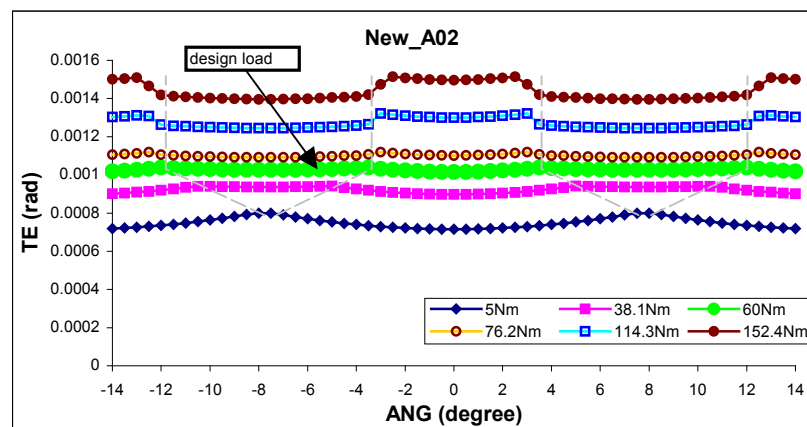
Figure 7.7. 2   Transmission errors of model New_A02.

175
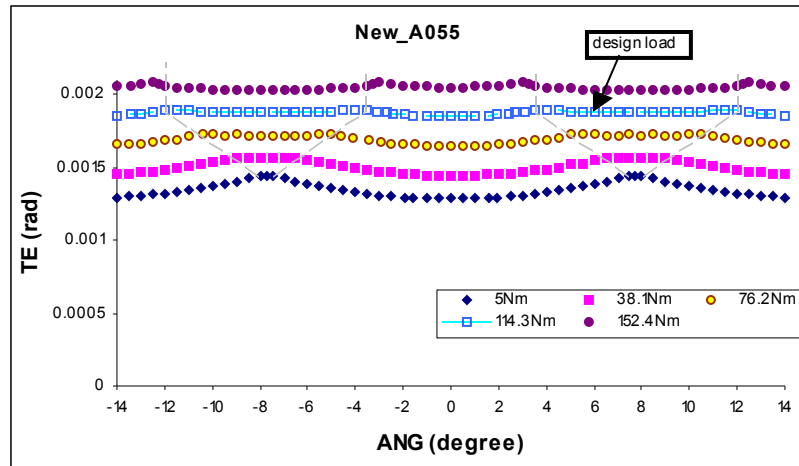
Figure 7.7. 3   Transmission errors of model New_A055.

It can be seen that the smoothness of the transmission error curves have been improved within different levels of the design load. With an input load lighter than the design loads, the transmission errors vary smoothly up and down in the mesh cycle as required. However, if the input load is greater than the design loads, the over load occurs quite easily.

For the purpose of the tooth flank surface protection while the input load is high, new tooth models New B01_01 and New B01_03 have been designed with smooth T.E. results gradually increasing up to the full torque load. The results of the transmission errors are shown in Figure 7.7.4 and 7.7.5. However, as seen from the results the higher the full torque load, the more T.E. variations appear at the design load.
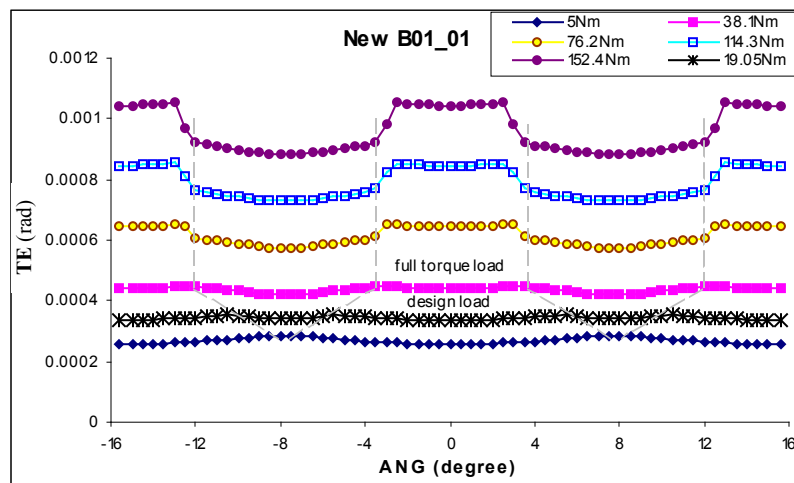
Figure 7.7. 4   Transmission errors of model New B01_01.
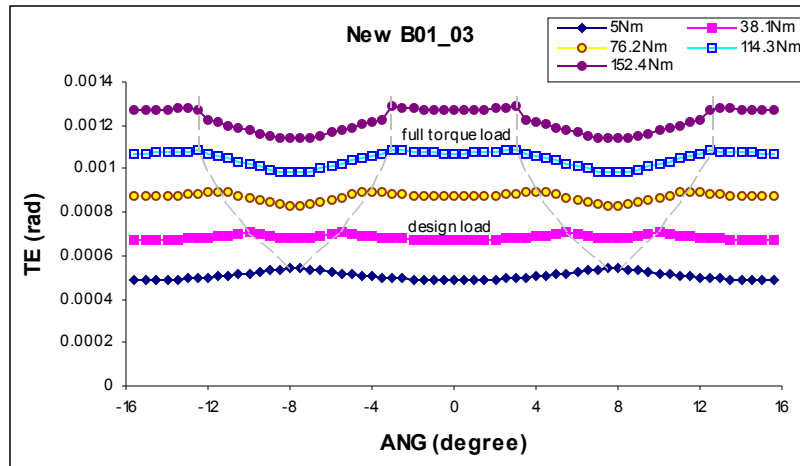
Figure 7.7. 5   Transmission errors of model New B01_03.

Model New C02_01 was designed to have the features midway between that of the previous two groups. The transmission errors are shown in Figure 7.7.6.
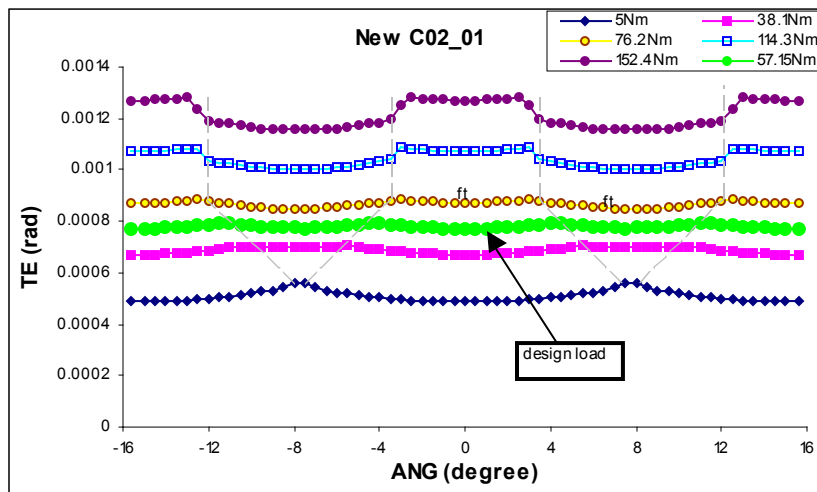
Figure 7.7. 6   Transmission errors of model New C02_01.

The meshing gears with the new tooth profiles are still under development. To further develop gears with the new tooth profiles, however, would require extensive experiments, which is beyond the scope of the current research.

The new gears may well be suitable for situations where the input load is within the design load. However, if a root crack is present these gears may not be desirable for gear diagnostic purposes as only a minimal change in the T.E. was observed. Examples can be seen in Figures 7.7.7 and 7.7.8 where 3.5 mm root cracks were present.
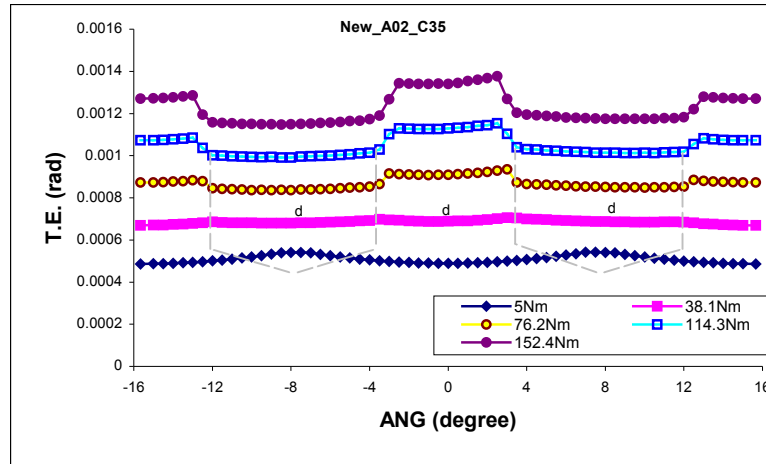
Figure 7.7. 7   T.E. of model New_A02 with a 3.5mm root crack.
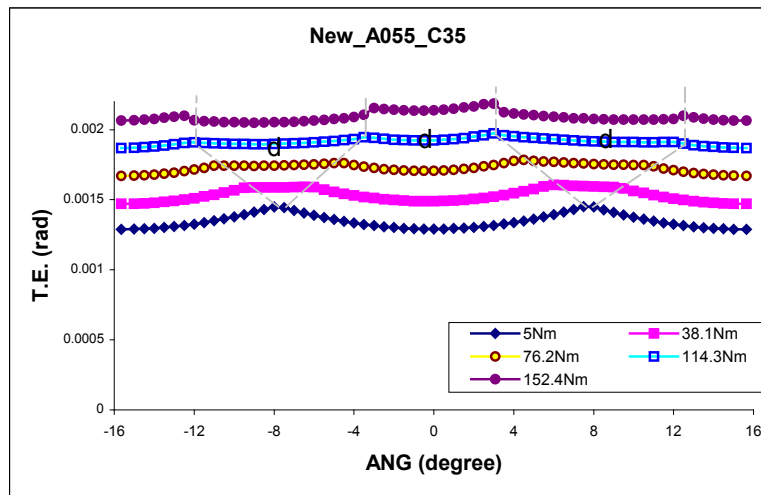
Figure 7.7. 8   T.E. of model New_A055 with a 3.5mm root crack.

7.8   Transmission Error Control

Transmission error is load dependent and has a major influence on the system vibrations. In some applications, a smooth transmission error within a wide range of input load is desired and sometimes it is vitally important. For example, the T.E. may be quiet when a submarine is in cruise condition, but it may be loud when sudden acceleration is required. Gears with certain load capacities (not including high contact ratio gears) are nearly impossible to design with smooth transmission error over the full range of input loads. However, to some extent, a smooth transmission error may be possible over a certain range of input loads.

There are two methods of treatment of the gear system. The first method is based on the studies of the meshing gears with the new tooth profile as in the previous section. These studies have found that the design loads can vary with minor changes of the centre distance. Examples can be seen in Figure 7.8.1 and Figure 7.8.2.
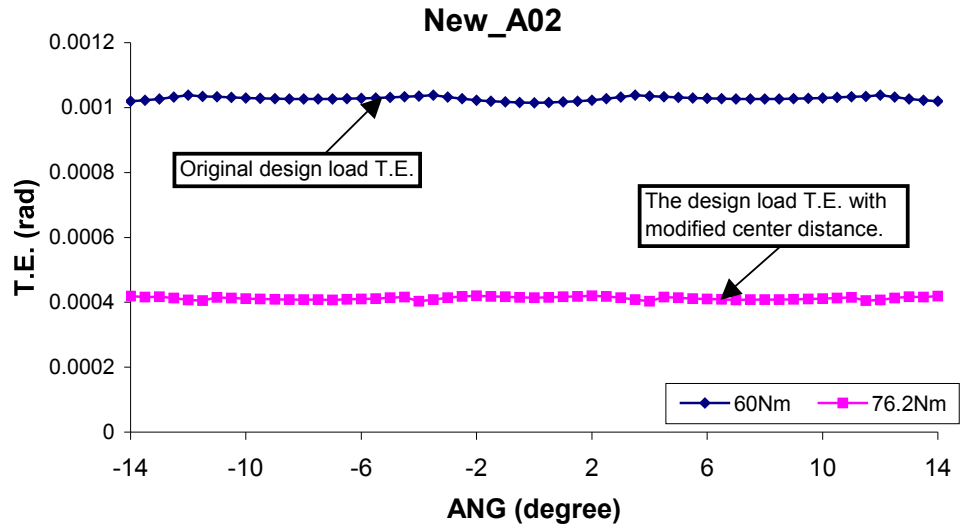
New_A02

Figure 7.8. 1   Design load T.E. of model New_A02.
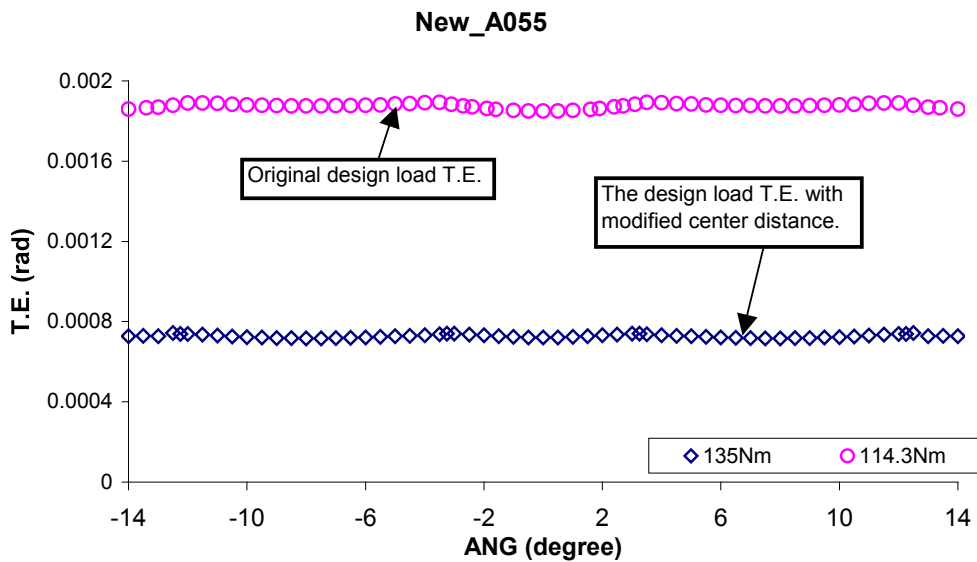
New_A055

Figure 7.8. 2   Design load T.E. of model New_A055.

With a 0.13 mm change in centre distance, the design load T.E. of model New_A02 was found to vary smoothly, and more significantly the input design load was found to change from 60 Nm to 76.2 Nm, an increase of 27% over the original design load. The case for model New_A055 with a 0.24 mm centre distance change resulted in an increase of 18% of the design load. Model New_A055 is designed for a higher input load.

It has been shown therefore that the design load T.E., to some extent, can be controlled by modifying the gear centre distance. However, it may not be easy to control such small movements in the gear centre distance. Reliable measurements would also be required for applying such control. The reliable signals, however, may not be vibration signals, but may be higher order components of the actual meshing gears such as stress or strain. This will be discussed further in the following section.

The second conceptual method for controlling T.E. involves the application of force(s) along the gear centre distance through the shafts in each mesh cycle, since the centre distance is sensitive to the transmission error (see 7.4). The control of the magnitude of the pulse(s) and the phase frequency modulations can be complicated, especially for high-speed applications.

7.9   FEA of High Order Components – Meshing Gears With Shaft

Rather than considering the use of vibration signals for gear fault detection, an analysis has attempted to concentrate on the use of high order components of the actual mating gears with their shafts. Elastic strains (same order of stress) of the mating gears and their shafts would provide a direct indication of the behaviour of the mating gears. The research on gear stiffness properties developed in Chapter 4 has found that the distortion field in the area near the hubs between the contacts varies depending on the number of teeth in contact. With two teeth in contact, it was found that the reaction forces in the hub tend to spread symmetrically about the gear body. With a single tooth contact, the symmetrical nature of the stress field becomes distorted. If a single keyway is used, it has been found that the variations of the distortion field in the area near the hub become difficult to observe.

In order to find the resulting elastic strain variations on the shaft, a series of 3D gear-shaft models were established. Figure 7.9.1 shows the basic 3D model that was developed in this research. A pair of standard involute gears with a 120mm×30mm shaft is shown along with the mapped mesh using 20 node brick elements.
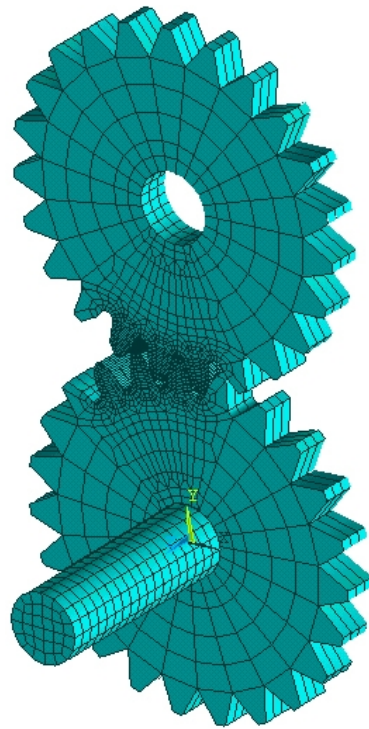
Figure 7.9. 1   The basic 3D model.

The model as shown contained 23673 nodes.   If the nodes in the contact area between the shaft and the gear hub were coupled in rotation, this would simulate a fine spline with an interference fit between the gear and the shaft. Models containing spline fits can easily be extended to very large models.   An example of an eight-spline shaft with gear hub interference fit would result in a 50,000-node model.   The whole model can be further extended to 70,000 nodes if a rotor is included, as seen in Figure 7.9.2.   The solution of such a model may require more than three days for one solution using a standard PC (PIII 800 Mhz, 1 GB SDRAM).
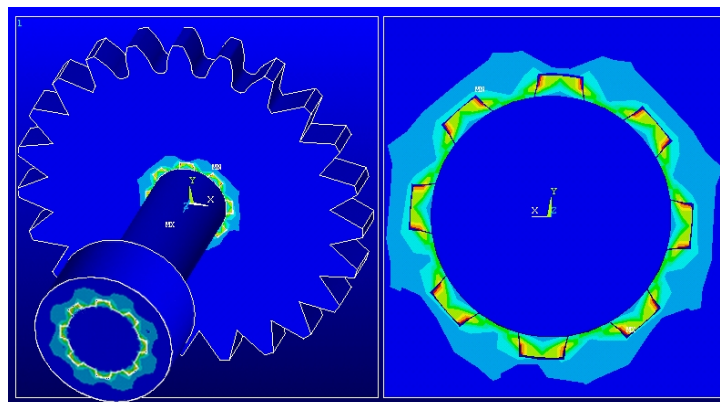
Figure 7.9. 2   Splines with interference fit.

181

In the actual FEA solution the model has to be simplified. As long as there is more than a single keyway between the shaft and the gear, the elastic strains on the shaft may vary throughout the mesh cycle. The particular measurements of interest are those in the section of the shaft that is near the gear hub. The section length of interest should cover the diameter of the shaft (Saint-Venant's Principle), and for this model the length of 30 mm was chosen. Figure 7.9.3 shows the locations where the elastic strains EPEL Y were measured within the global cylindrical coordinate system.
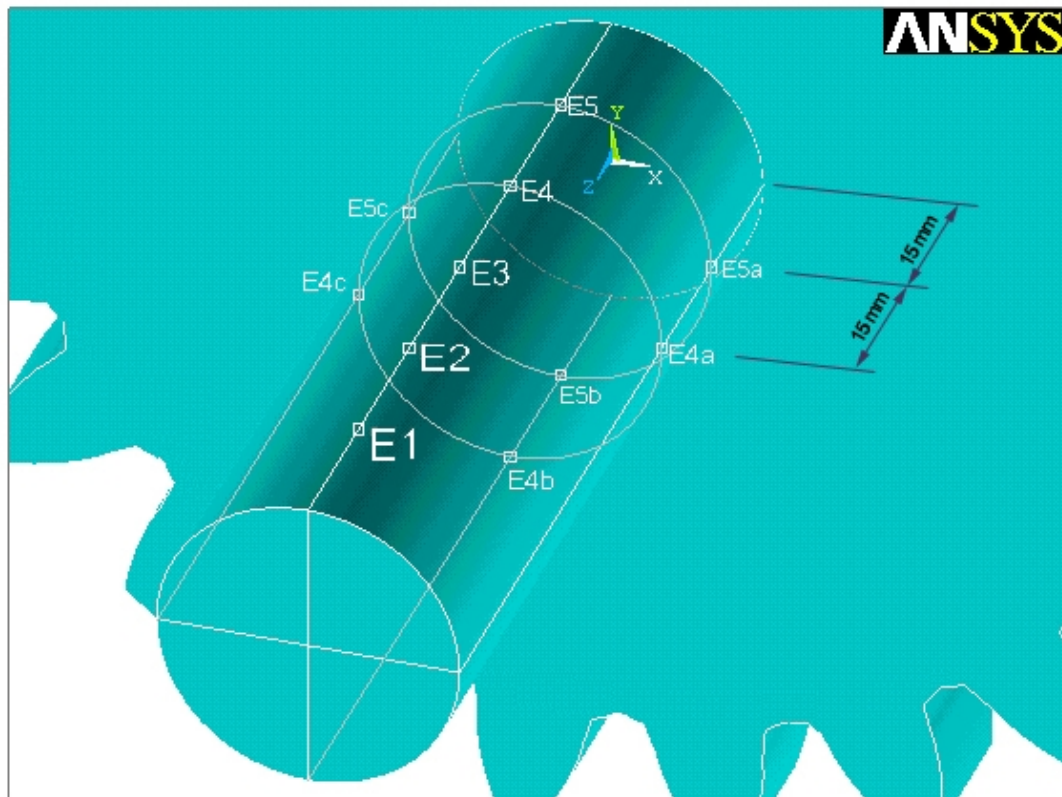
Figure 7.9. 3   The locations where the elastic strain was measured.

FEA solutions for the elastic strains at the specified locations along with the transmission error were calculated. Instead of using a spline fit, the nodes in the common area between the shaft and the gear were coupled in rotation. With the input load of 76.2 Nm, the FEA model was solved with 15 sub steps in each position of the mesh cycle, and the results are shown in Figure 7.9.4.
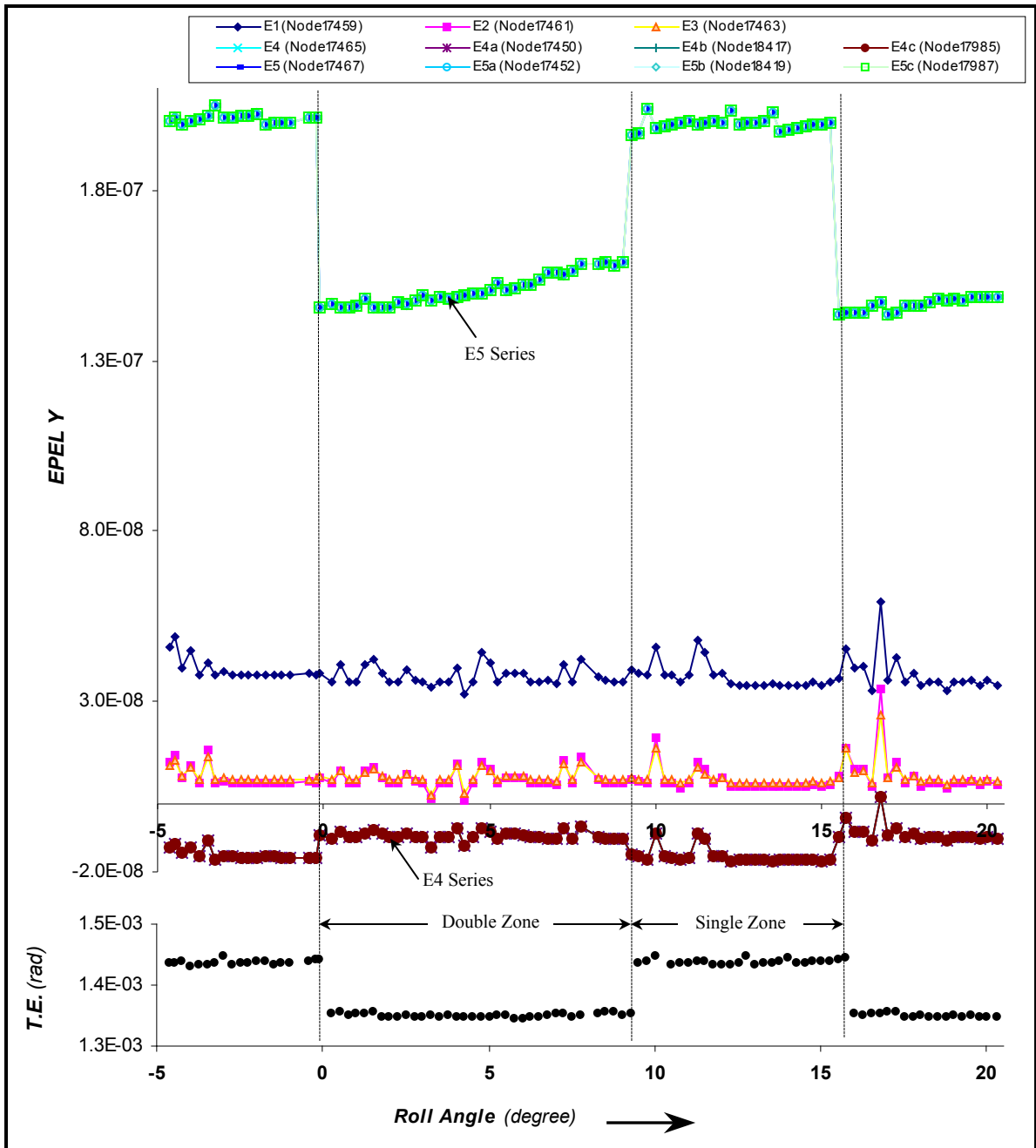
Figure 7.9. 4 Elastic strains over a complete mesh cycle.

It can be seen, over the mesh cycle, that the elastic strain variations at E1, E2 and E3 generally obey Saint-Venant's Principle. The abrupt protrusions may be due to the use of the mapped mesh (adaptive mesh may reduce the effect). The elastic strains at the E4 and E5 positions appear to vary with the transmission error as measured at the input end of the shaft. It was also noted that the strains were symmetrical to the axle of the shaft since the elastic strain EPEL Y in each location of the E4 series (E4, E4a, E4b and E4c) or the E5

series (E5, E5a, E5b and E5c) were exactly same. Figure 7.9.5 shows the FEA results of the elastic strain EPEL Y in the E4 and E5 locations with a 4.7 mm root crack.
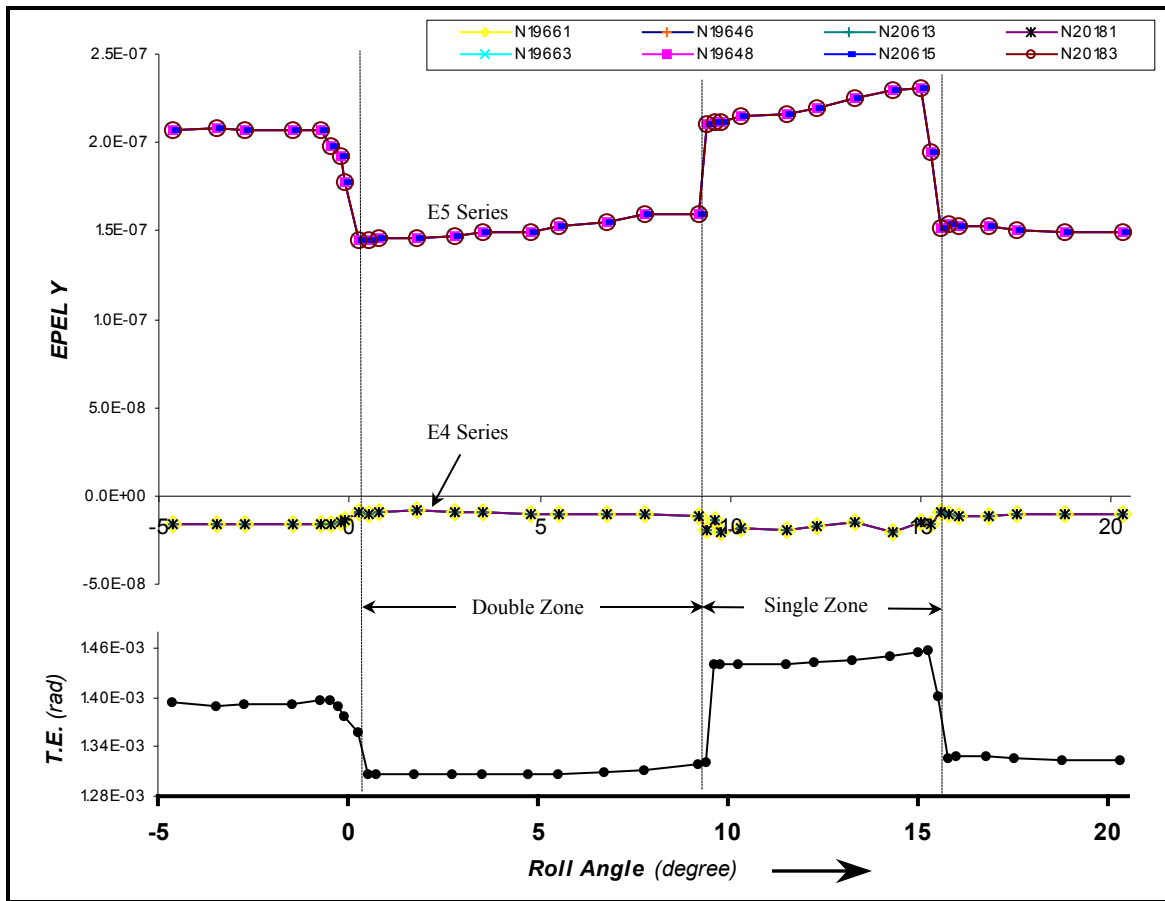
Figure 7.9. 5 Elastic strains of the model with a 4.7 mm root crack
(FEA solutions were in 20 sub steps).

It should be noted from the results that the root crack could also be found by the elastic strains, especially by the elastic strains of the E5 series. Once again, the elastic strains of the E4 series or E5 series are perfectly symmetrical to the axle of the shaft due to the boundary conditions between the shaft and the gear. If keyways or a splined shaft were used, combined with manufacturing or other errors, the stress or strain states of the shaft near the hub will become more complex. Further analysis was conducted with a refined mesh at the shaft near the hub, where a 4 spline shaft was used. The shaft splines and the gear were interference fitted.   The manufacturing and other geometrical errors were considered by making the boundary conditions between each of the splines slightly different. The numbers of the locations for the elastic strain measurements were increased in the region within 30 mm of the gear hub, as seen in Figure 7.9.6.

184
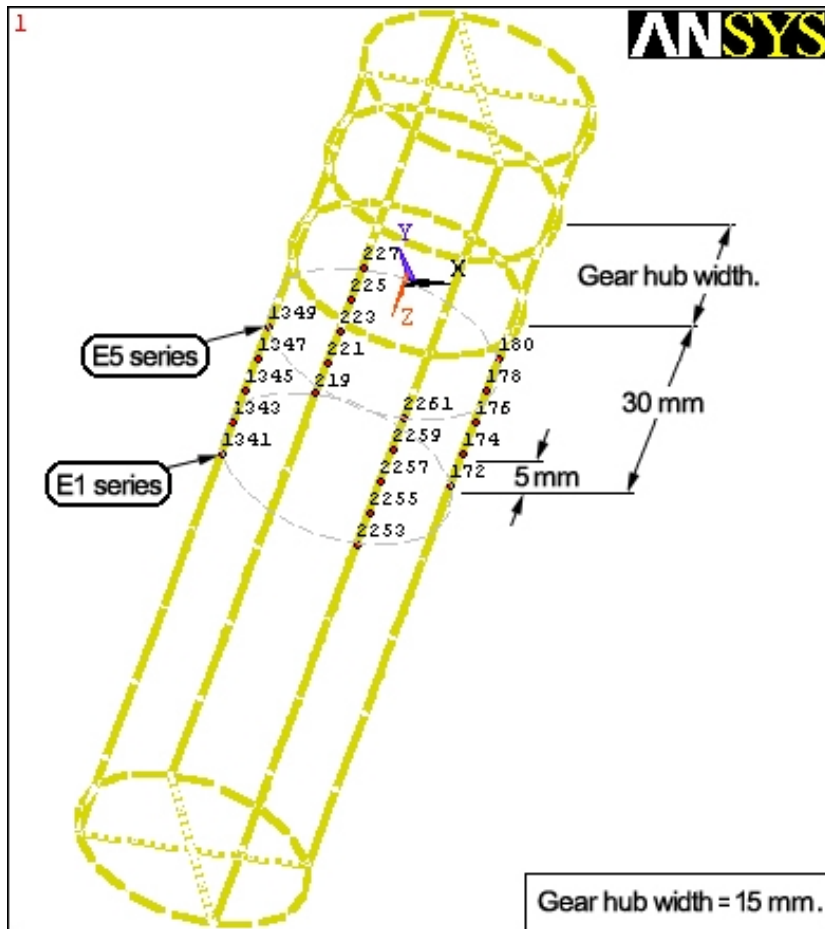
Figure 7.9. 6   The relocated series of measurements.

A series of locations were shifted from the E1 series to the E5 series positions, and each of them contained 4 locations coincident with the nodes in the circle of the section evenly arranged at 90^0 intervals. FEA solutions for the elastic strains at the specified locations along with the transmission error calculations have been carried out, and the results are shown in Figure 7.9.7.

It can be seen that the elastic strains in each location of the series are no longer symmetrical about the axis of the shaft, however, the amount of variations from the single zone to the double zone remain stable. This shows that the strain measurements should be concentrated on the relative changes of the elastic strain over the mesh cycle. Elastic strain measurements can also find a small root crack, such as 1.5 mm root crack in the same model, as shown in Figure 7.9.8.
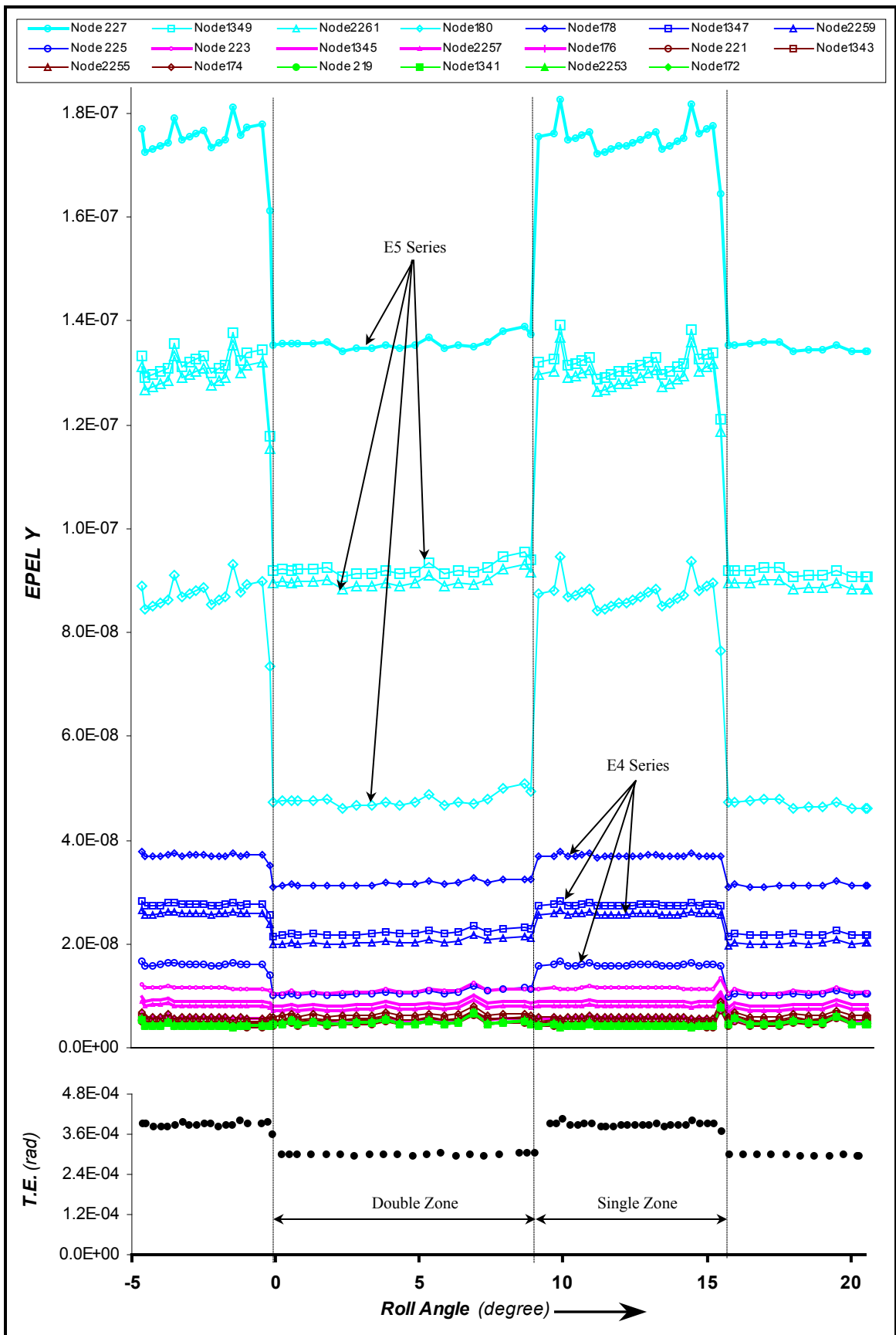
Figure 7.9. 7 Elastic strains over a complete mesh cycle (FEA solutions were in 8 sub steps).

186
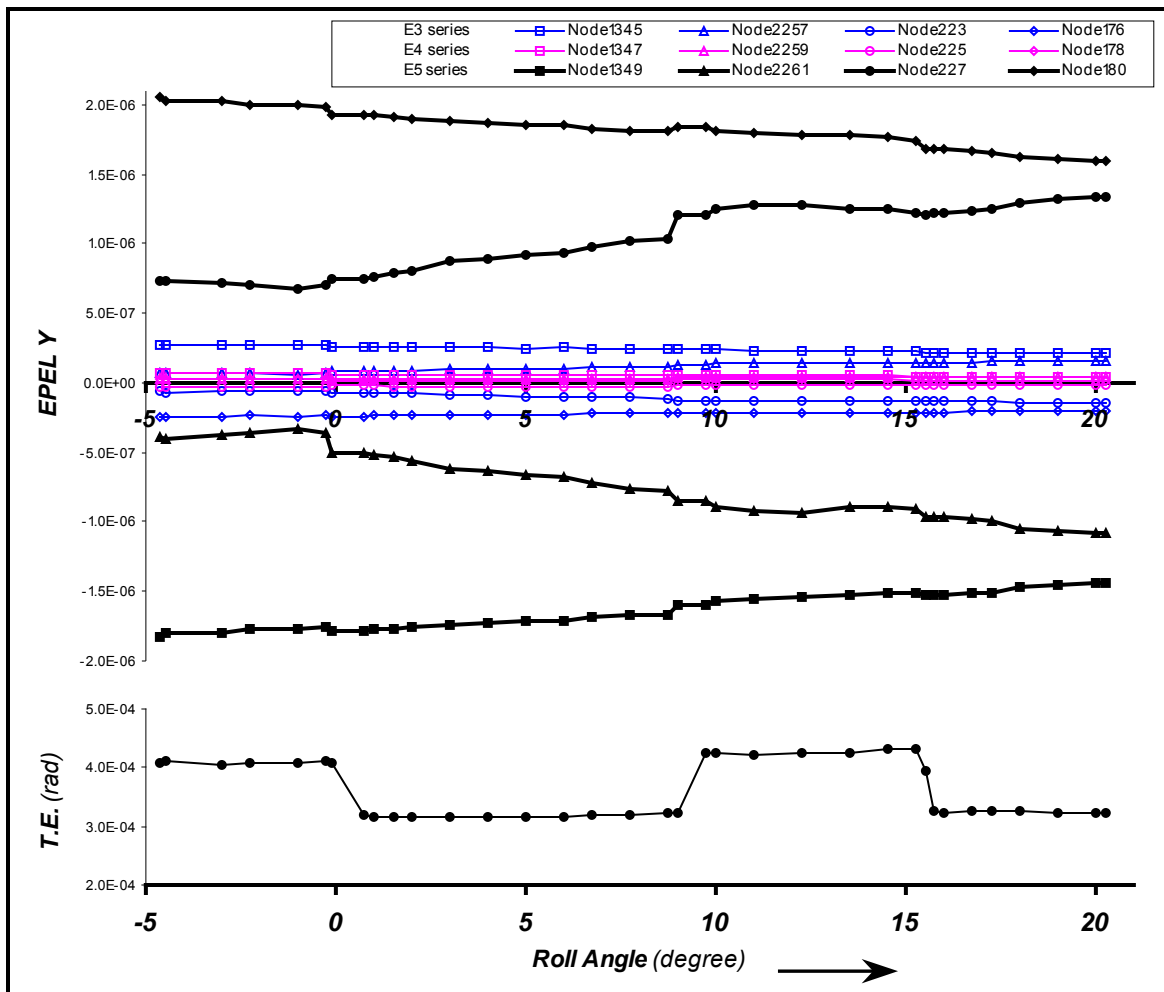
Figure 7.9. 8 Elastic strains of the model with a 1.5 mm root crack.

For such a case, it would be difficult to find the root crack through the transmission error or vibration measurements of the gear case.

Perfect involute gears in mesh along with an input shaft have been analysed. The elastic strains on the surface of the shaft near the gear hub have been found to vary in form with the transmission error over the mesh cycle. It has been recognized that the elastic strains have more capability to reveal the details of the gear-shaft system if the measurements were obtained from both input and output shafts. This investigation has shown that the presence of a root crack changes the strain measurements on the shaft. The changes in the shaft strain appear to be larger than the curves providing changes to the T.E. due to the presence of the crack. Further studies are expected to improve the capabilities of condition monitoring and controlling transmission system noise and vibrations.

187

CHAPTER 8

THE ANALYSIS OF NON-METALLIC GEARS

8.1   General Introduction

Applications for non-metallic gears are growing rapidly, specially within office equipment where the demand is for faster and quieter mechanisms. Non-metallic gears are also getting more involved with the power transmitted systems such as vehicle parts. In general, thermoplastic poly-condensates are used to manufacture plastics, industrially known as polyamides (PA). However, reinforced composites with fibers have also become more realistic in application where non-standard involute tooth forms are used to effectively reduce wear and extend the gears service life.

The advantages and useful features in using non – metallic gears comprise their

- Low weight,

- High wear resistance, good slip and dry – running properties,

- Good resistance to solvents, fuels and lubricants,

- Low noise and high resilience,

- Non – toxicity.

However, the limitations are also significant including the fact that standard polyamides have limited resistance to high temperature, have lower load carrying capacity than their metal counterparts, have high coefficients of thermal expansion and moisture content which impairs mechanical properties and affects the structure dimensions. They are much more complex materials than metals and are therefore, more difficult to analyse. As a result there has been less work done on polymer and composite engineering components and the engineer is often forced to experiment when developing new products (Walton 1995).

8.2   Previous Research

In recent years, a few different procedures have been developed to model the behavior of non – metallic gears including material composites. Examples of this can be seen in references (Yelle 1981; Terashima 1986; Tsukamoto 1986; Janover 1989; Walton 1989; Enzmann 1990; Tsukamoto 1990; Breeds 1991; Baumgart 1992; Kudinov 1992; Walton 1992; Zhang 1992; Mao 1993; Nabi 1993; Solaro 1993; Tessema 1993; Tessema 1994; Walton 1994; Koffi 1995; Tessema 1995; Walton 1995; Williams 1995; Du 1997; Nitu 1997; Smith 1997; White 1997; Kleiss 2000; Kurokawa 2000; Luscher 2000; Panhuizen 2000; Bushimata 2001; Wright 2001; Alagoz 2002; Andrei 2002). However, little has been published to date on the mechanism properties of non-metallic gears in mesh. One of the rare examples as shown in Figure 8.2.1 (Du 1997) presents results of the gear mesh stiffness obtained by FEA, where the results for both steel and nylon gears were provided over a complete mesh cycle.

Despite the lack of detail on the gear parameters (Du 1997), the results for Du's nylon gears can be improved either by Walton's analysis on the flexibility of non – metallic gears or by using the results on the hand over region in Chapter 6. This is due to the linear material assumption as used by Du. Tessema and Walton (Tessema 1994) have further

confirmed there should be tip-relief different from that used in metal gears. To obtain the correct transmission error of involute non-metallic gears in mesh is fundamentally important. The fundamental analysis will give indications for the further analysis including fiber reinforced materials and tooth profile modifications. The fundamental analysis including experiments will be presented in this chapter.
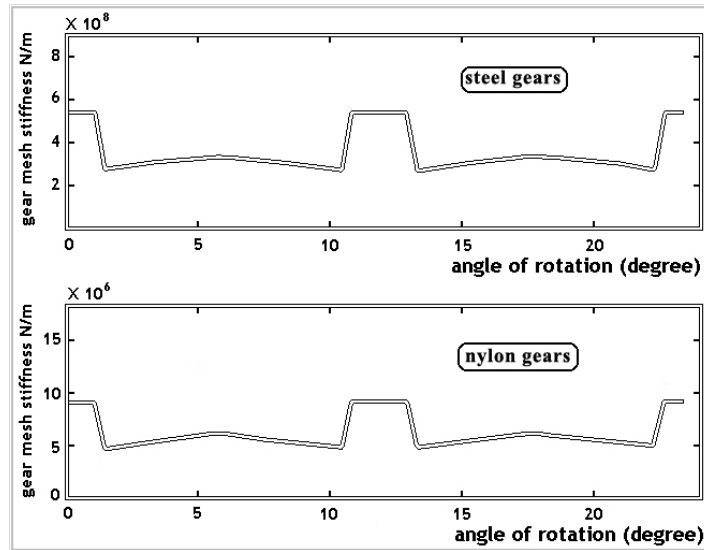
Figure 8.2. 1   Gear mesh stiffness (Du 1997).

8.3   Modelling Material Nonlinearities

A number of material-related factors can cause a structures stiffness to change during the course of an analysis. Non-linear stress-strain relationships of *plastic, multilinear elastic,* and *hyperelastic* materials will cause a structures stiffness to change at different load levels (and, typically, at different temperatures). *Creep, viscoplasticity,* and *viscoelasticity* will give rise to nonlinearities that can be time, rate, temperature, and stress-related. *Swelling* will induce strains that can be a function of temperature, time, neutron flux level (or some analogous quantity), and stress. Any of these kinds of material properties can be incorporated into FEA if appropriate element types are used.

The parameters of the gear (sets) that were used in the FE models and the simulation were shown in Table 4.1.   The non-metallic material used here was one of the standard polyamides – cast nylon PA 6 - G and the Young's modulus is given in Figure 8.3.1 by H. Domininghaus (Domininghaus 1993).   Poisson's ratio was 0.4 as given by the material

190

supplier. According to the data that can be obtained, the Multilinear Elastic (MELAS) material behaviour option was used in the analysis. The ANSYS MELAS material behaviour option describes a conservative (path-independent) response in which unloading follows the same stress-strain path as loading. Thus, relatively large load steps might be appropriate for models that incorporate this type of material nonlinearity. In case the material displays non-linear or rate-dependent stress-strain behaviour during the analysis, it must be defined in the non-linear material property relationships in terms of a data table, as seen in Figure 8.3.2.
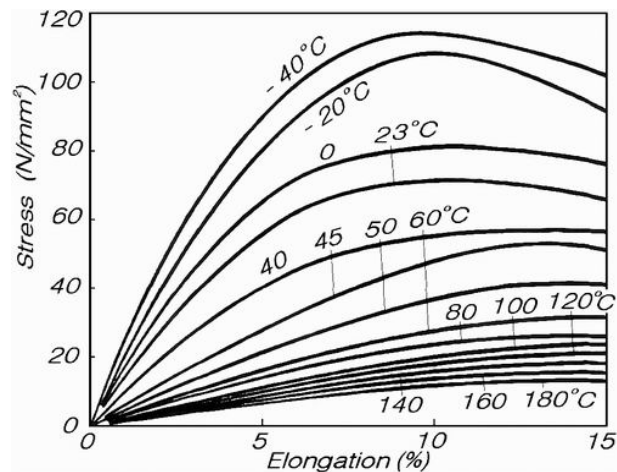
Figure 8.3. 1 Stress/strain diagram for PA6 (dry) at various temperature (Domininghaus 1993).
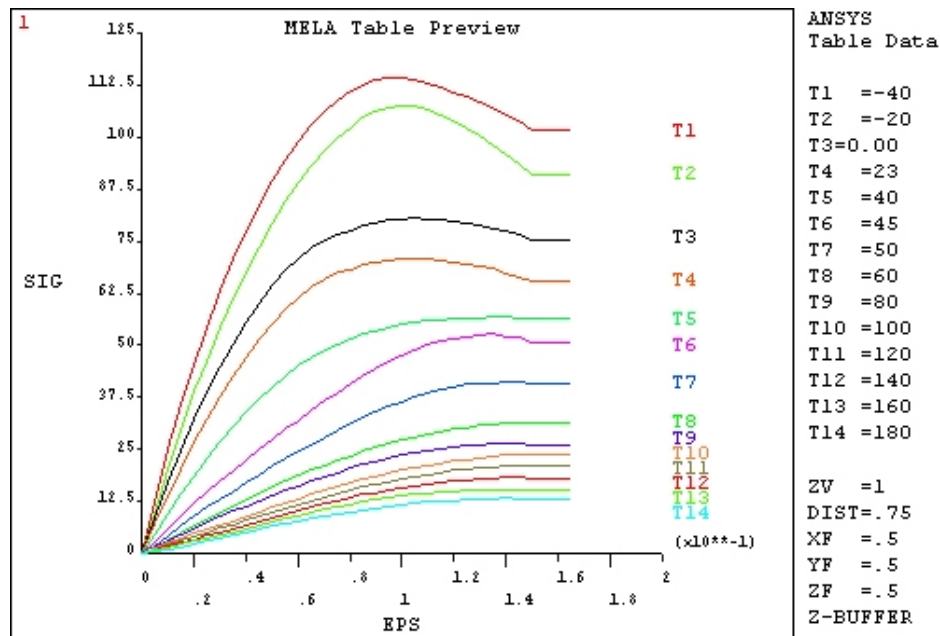
Figure 8.3. 2 MELA table preview.

191

It has to be stressed that the availability of the material properties is often one of the limitations that will restrict the analysis. The desired analysis option is **Anisotropic** (ANISO), which allows for different stress – strain behaviour in the material x, y and z directions and more importantly allows for different behaviour in tension and compression. The research in this current stage used the stress/strain diagram (Figure 8.3.1), which was produced by the accelerated tensile test (Domininghaus 1993). The analysis results will likely present some considerable overestimate of the T.E. (displacement) and an underestimate of the torsional mesh stiffness (polyamide is considered to be some what stiffer in compression than in tension).

The friction coefficient can also be an important factor in the modelling. Figure 8.3.3 shows that the friction coefficient is dependent on both load and running time (temperatures).

(a) Dependence of the coefficient of sliding friction on mean bearing pressure.
Roughness height for PA, polyamide
R_Z =1.5 to 3 μm/0.059 to 0.118 mil .

(b) Coefficient of sliding friction for PA 66 against various metals as a function of running time (axial) bearing test rig, dry, pv=0.015 N/mm^2 * m/s; 7.0 psi * ft/min
a   Cu/Zn alloy to DIN 17660
b   Al alloy to DIN 1725
c   GG 22 to DIN 1691
d   Steel 16 MnCr 5 to DIN 17210; 52 HRC

Figure 8.3.3   The friction behaviours of polyamide (Domininghaus 1993).

FE modelling of non-metallic gears in mesh including the variation of friction coefficient is important since, (for dry unlubricated gears in mesh) wear is dominant in the gear service life (Walton 1995). While, this will add more difficulties to the modelling task, the contact ratio can also change dramatically with load and temperature. One of the strategies is to model the meshing gears with a lower constant friction coefficient (e.g. 0.1). The friction coefficient of Figure 8.3.3 can then be inserted for each relative meshing tooth pair according to the contact stress at each mesh position over a mesh cycle, then the solution

re-evaluated. Such procedure can be repeated until the results are satisfactory. However, there is reluctance to do such tremendous FE calculations without considering the use of the realistic compression stress/strain diagram.

8.4   Element and Mesh

The available elements for the research using the ANSYS MELAS material behaviour option are plane 42 for 2D modelling and solid 45 for 3D modelling. Both quad and brick elements can be used without the mid-side nodes. The procedures for applying mesh adaptation with contact are no different with that of metallic gears. However, when using solid 45 to build the 3D model, the number of element divisions along the rotation axis will be limited as the low order element can only handle limited distortions, especially in the aspect ratio. As the adaptive mesh produced many small elements near the contact points, it required more divisions along the tooth width, consequently there will be a large number of distorted elements in the low stress area, as seen in Figure 8.4.1.
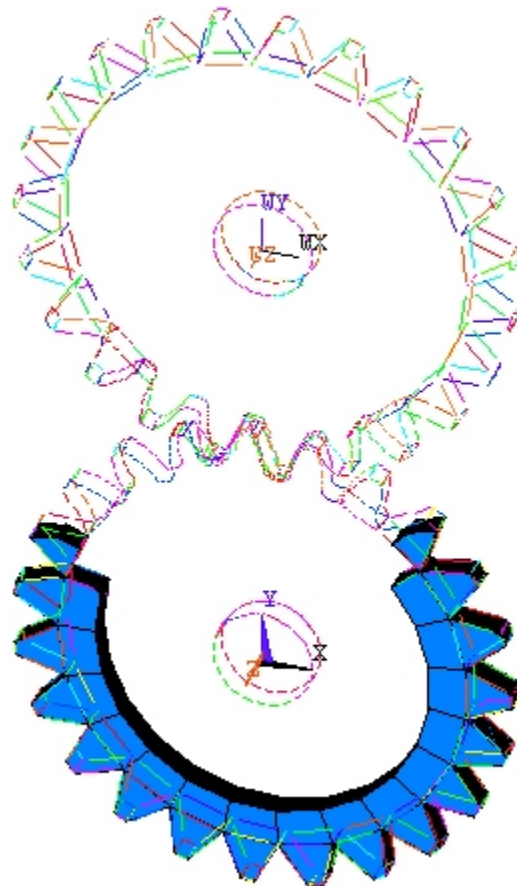
Figure 8.4. 1   The *element check* has shown the distorted elements.

The easiest way for applying adaptive mesh without distorted elements is to increase the element number in the low stress area, but the computational efficiency will be poor. Alternatively the transition of the division between low and high stress areas can be made, but that is extremely time consuming for building the model. For the current stage, 2D plane stress models were used. The model and its detailed adaptive mesh are shown as in Figure 8.4.2.
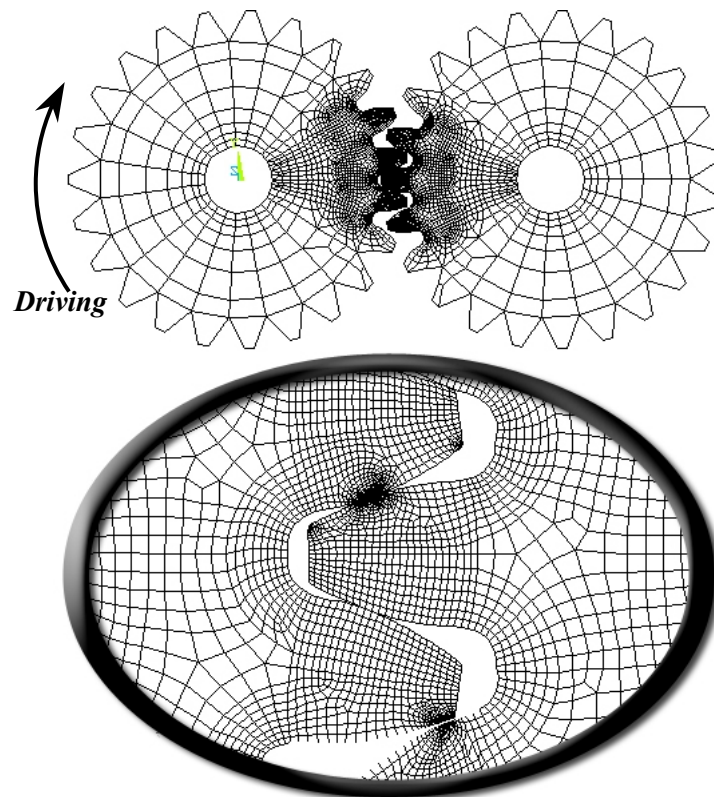
Figure 8.4. 2   The 2D model and the adaptive mesh.

8.5   Transmission Error

The application of polyamide material to sliding contact is highly non-linear. To obtain accurate solution results for the subsequent calculation of the transmission error, the choice of the proper number of sub steps is important. The analysis approach here chose 10 sub steps in an altering range of minimum 5 to maximum 50 sub steps for the solutions. It was noted that if the major sub steps were set greater than 15, better solutions were achieved. However, the computing time was greatly affected. For each temperature, the quantity of FEA calculations was equivalent to that of metallic gears.

194

8.5.1 T.E. as Function of Input Load at Each Temperature

The calculations at each temperature were initially calculated with an input load of 1 Nm. This load was then gradually increased until the triple contact zone was obvious. Unlike the nature of HCRG (high contact ratio gears), the triple contacts of LCRG (low contact ratio gears) always leads to premature contacts, as shown in Figure 8.5.1.
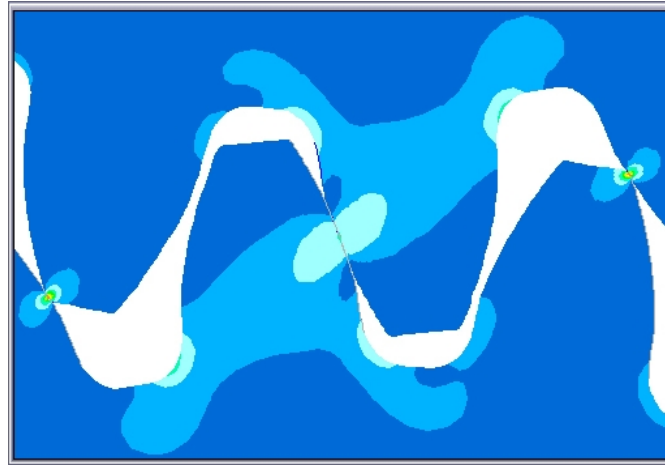
Figure 8.5. 1 The typical triple contacts of the nylon (PA6) gears.

The load and the temperature can easily increase the contact stress at the tooth tips, therefore high friction forces will be at the contacts where naturally the highest relative movement (rapid wear) occurs in such condition. The triple contact zones at each temperature are shown in Figure 8.5.2 to 8.5.15.
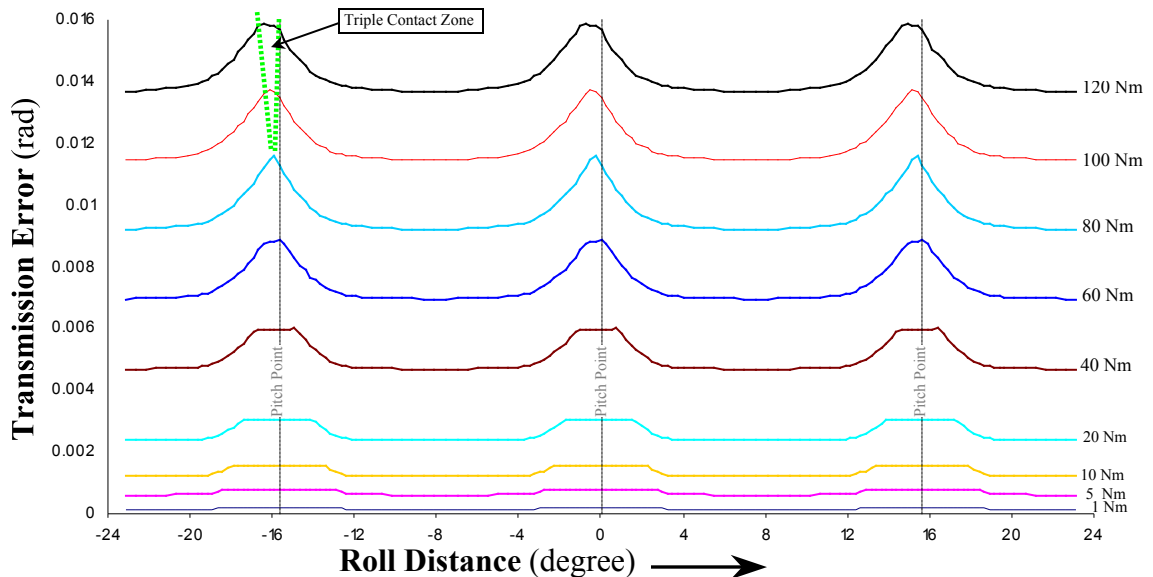
Figure 8.5. 2 T.E. under various input loads when the temperature is at $-40^{\circ}C$.

195
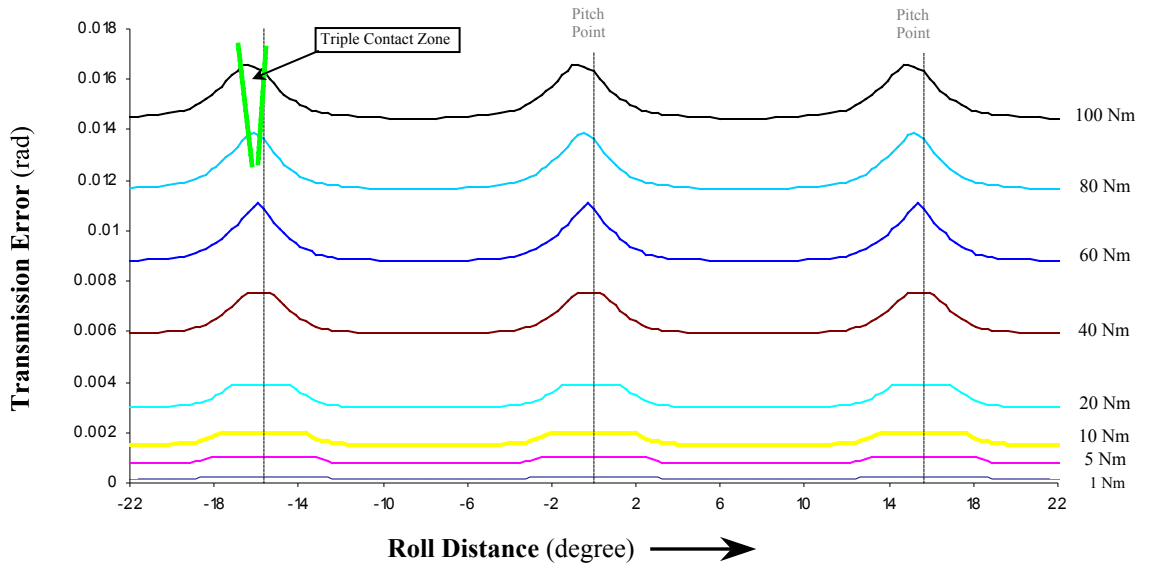
Figure 8.5. 3   T.E. under various input loads when the temperature is at $-20^{\circ}C$.
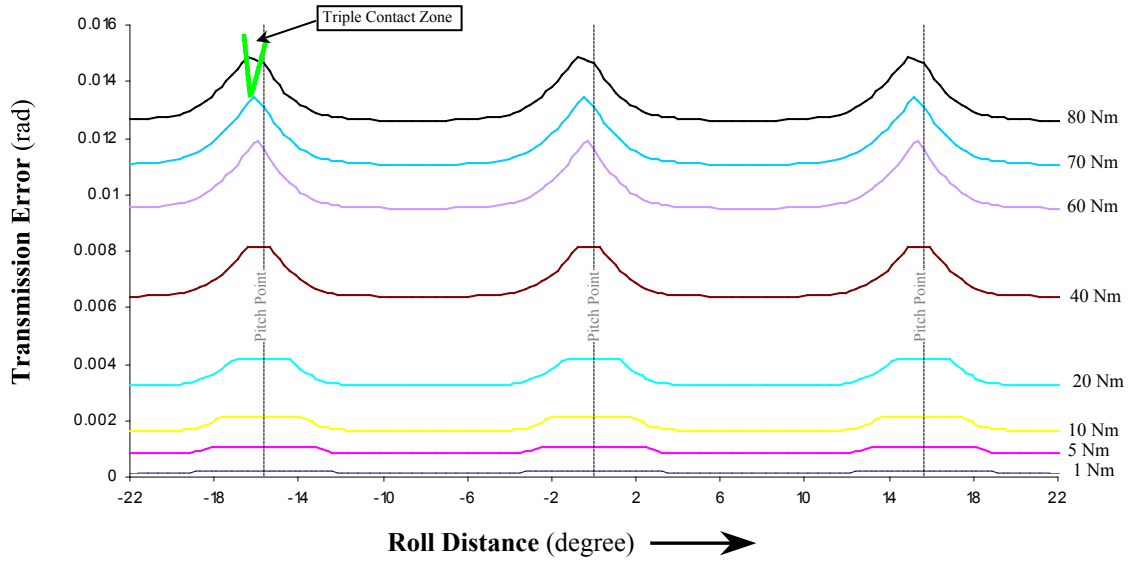
Figure 8.5. 4   T.E. under various input loads when the temperature is at $0^{\circ}C$.
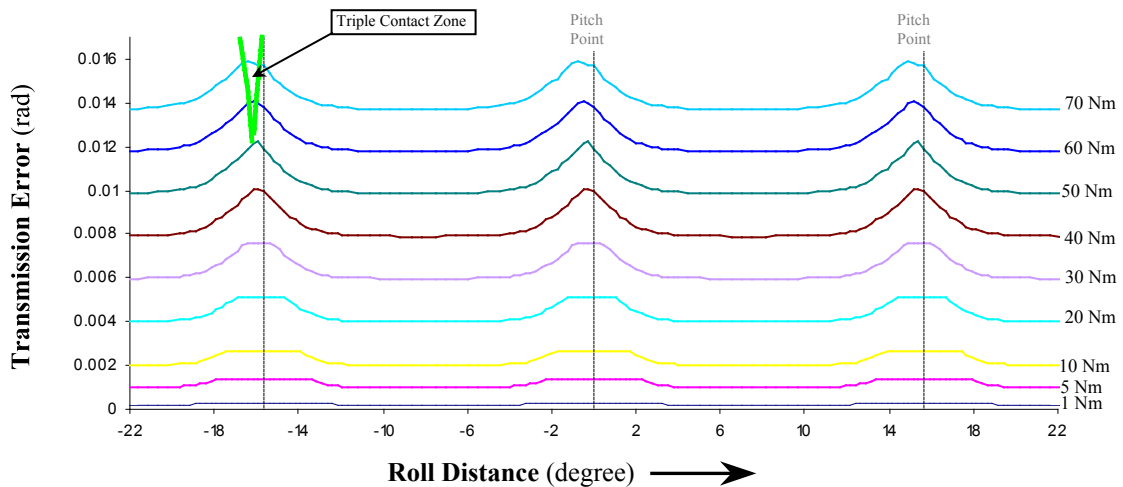
Figure 8.5. 5   T.E. under various input loads when the temperature is at $23^{\circ}C$.
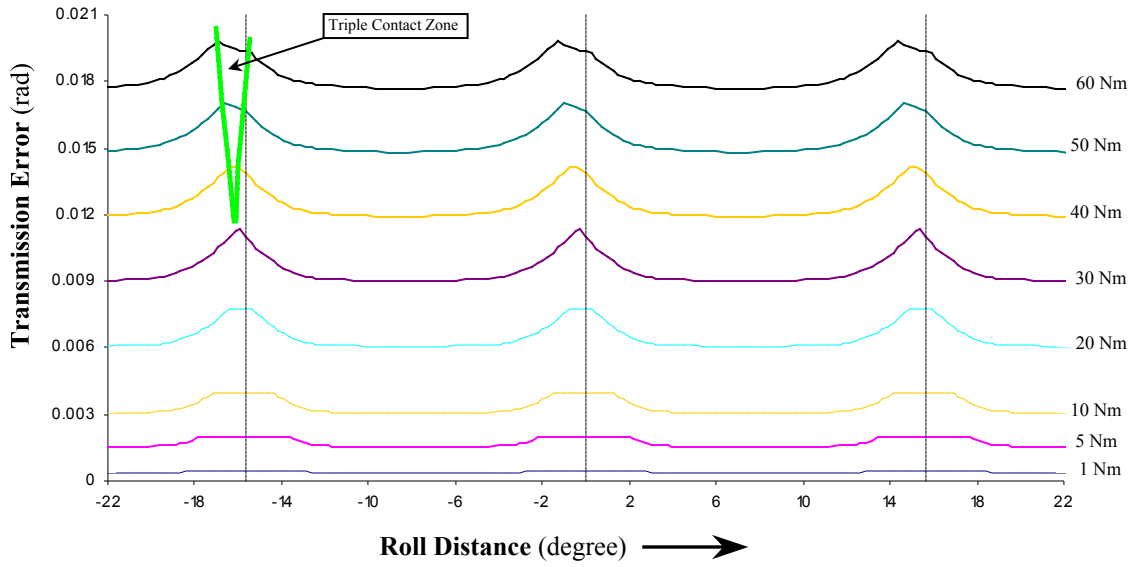
Figure 8.5. 6 T.E. under various input loads when the temperature is at $40^{o}C$.
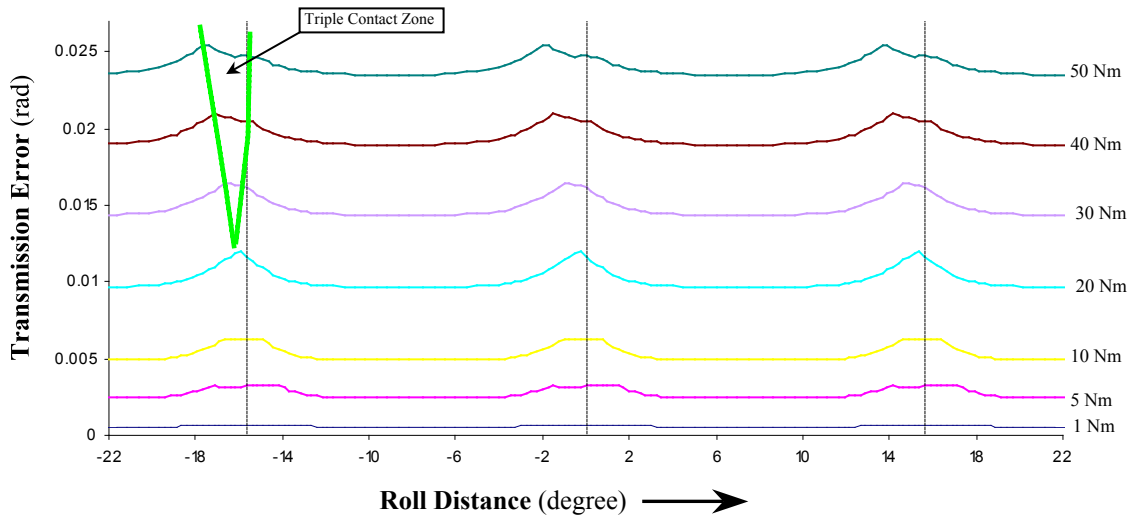
Figure 8.5. 7 T.E. under various input loads when the temperature is at $45^{o}C$.
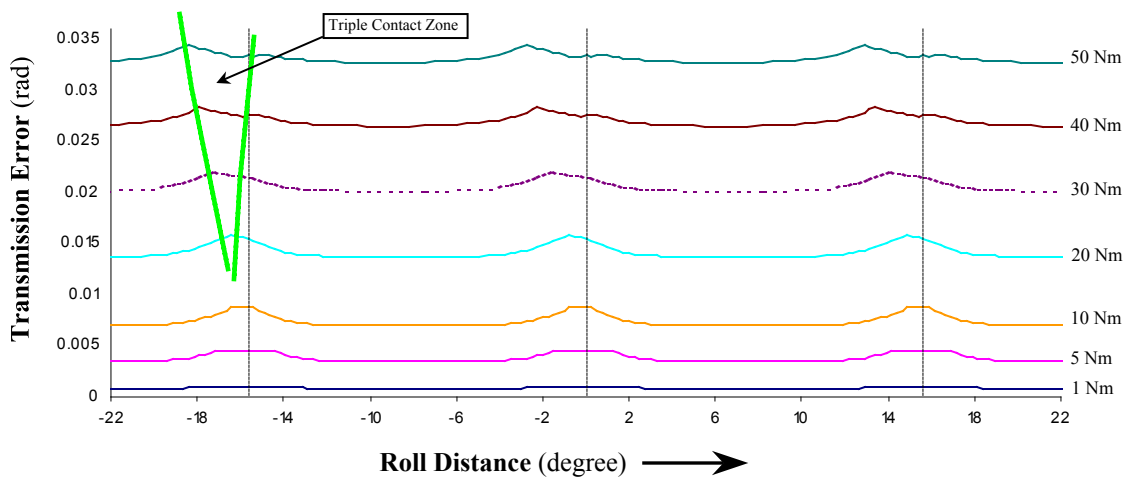
Figure 8.5. 8 T.E. under various input loads when the temperature is at $50^{o}C$.
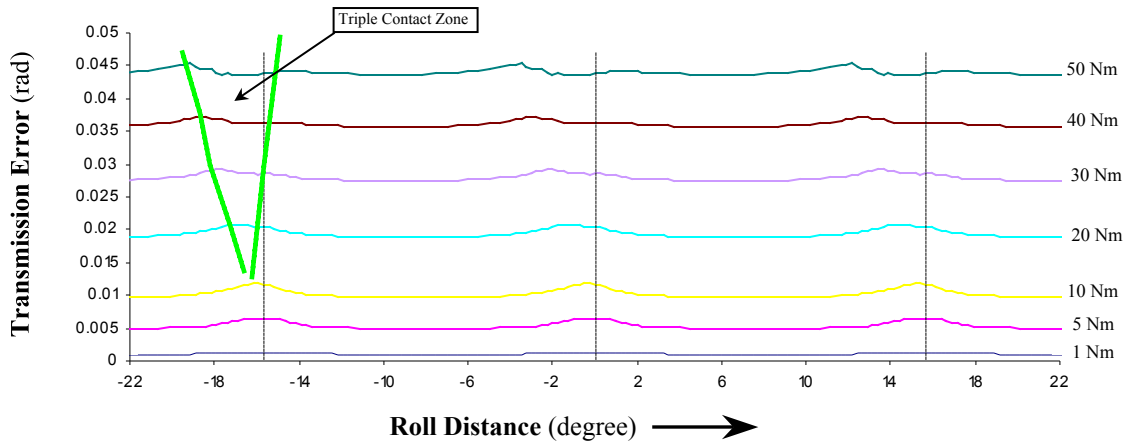
Figure 8.5. 9 T.E. under various input loads when the temperature is at $60^{o}C$.
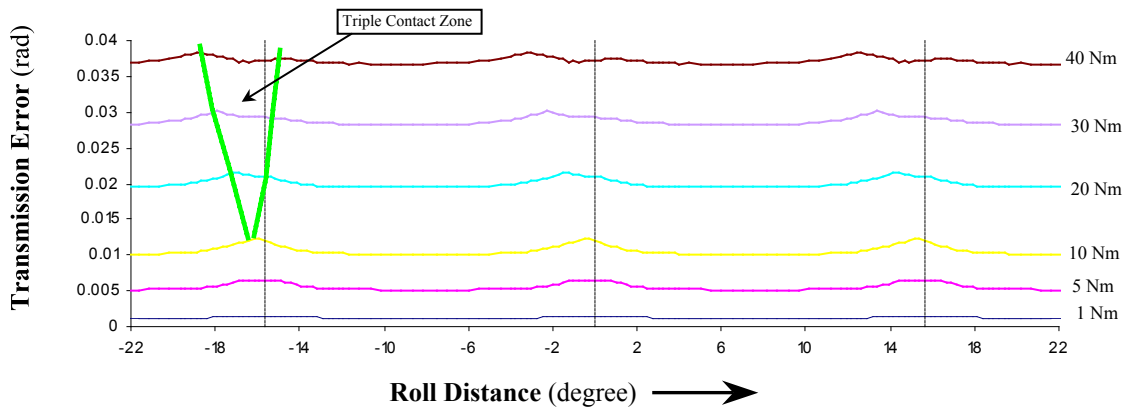
Figure 8.5. 10 T.E. under various input loads when the temperature is at $80^{o}C$.
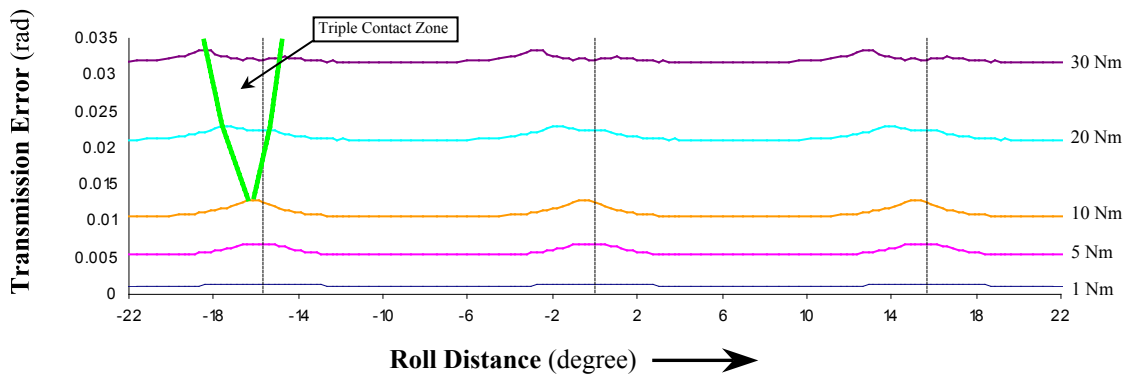
Figure 8.5. 11 T.E. under various input loads when the temperature is at $100^{o}C$.
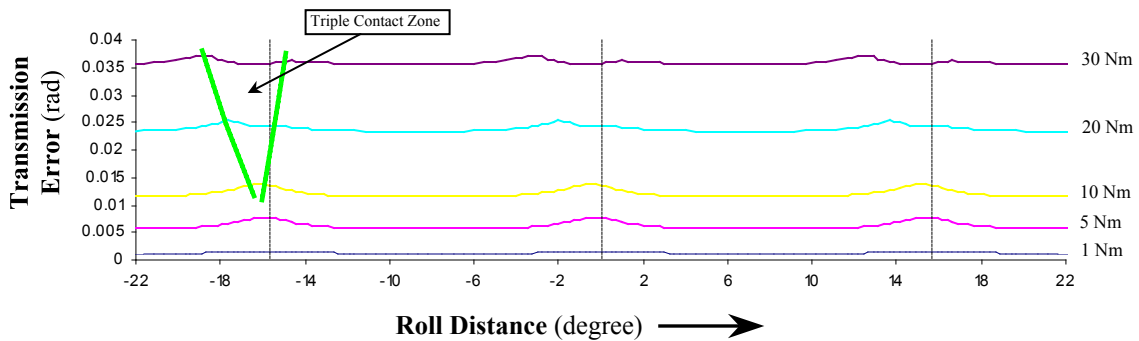
Figure 8.5. 12 T.E. under various input loads when the temperature is at $120^{o}C$.

198
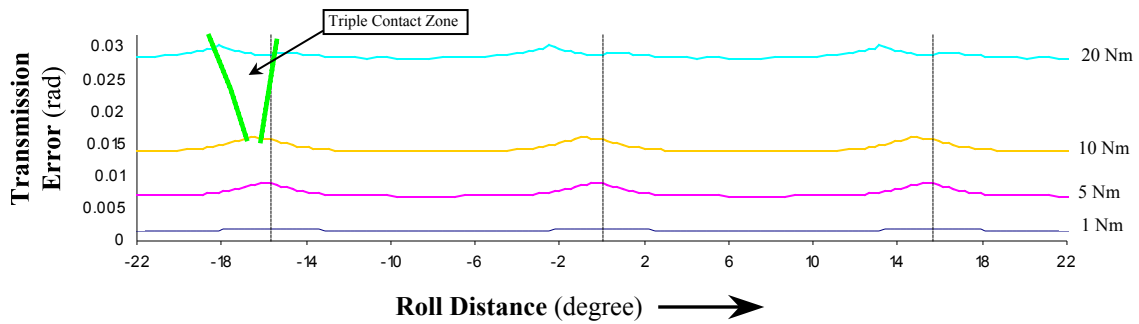
Figure 8.5. 13 T.E. under various input loads when the temperature is at $140^{o}C$.
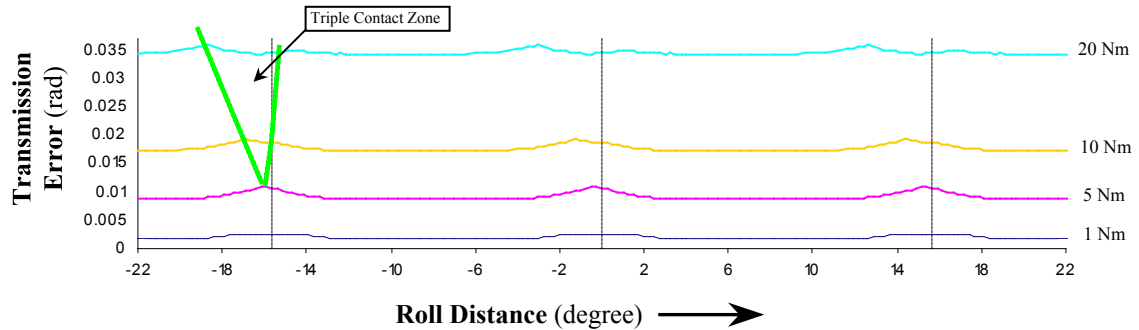
Figure 8.5. 14 T.E. under various input loads when the temperature is at $160^{o}C$.
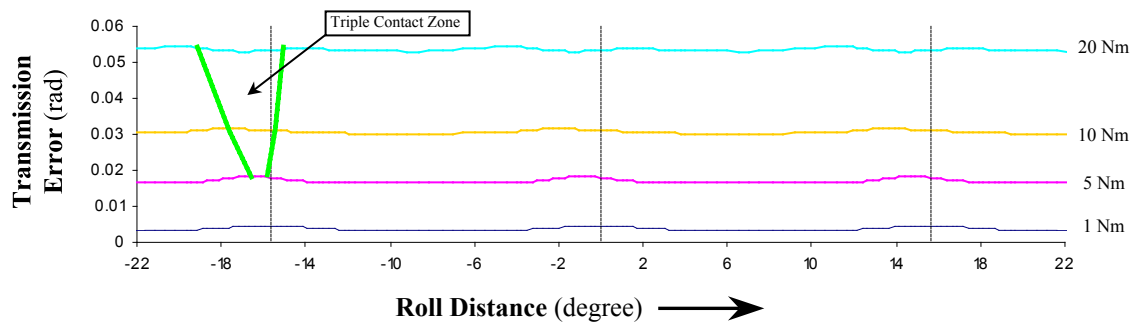
Figure 8.5. 15 T.E. under various input loads when the temperature is at $180^{o}C$.

Results above have shown the distinguishing characteristics of the T.E. (contrast to that of metallic gears) due to the flexibility of the material under load and temperature. It should be noted that,

1. Triple contact does occur, especially when the temperature is not too low. In most cases, T.E. of triple contact zones have shown higher values than that of the double contact zones. Such high contact ratio character is a significant difference compared to that of conventional high contact ratio (metallic) gears (see Appendix C)

2. The triple contact zones do not appear symmetrical over the tooth mesh cycle. Generally the T.E. of the approach cases are greater than that of recess cases, and the triple contact zones do not appear symmetrical about the pitch point. This is because,

3. The handover regions (of the double zone) are significantly expanded and the expansion rates for the approach and the recess cases are significantly different. Figure 8.5.16 shows the detailed variations of the contact ratio and the width of the handover regions against load at temperatures of $-40°C$, $23°C$ and $160°C$.

(a) Contact ratio vs. input load at $-40°C$, $23°C$ and $160°C$.

(b) The handover regions vs. input load at $-40°C$ (when contact ratio ≤ 2).

(c) The handover regions vs. input load at $23°C$ (when contact ratio ≤ 2).
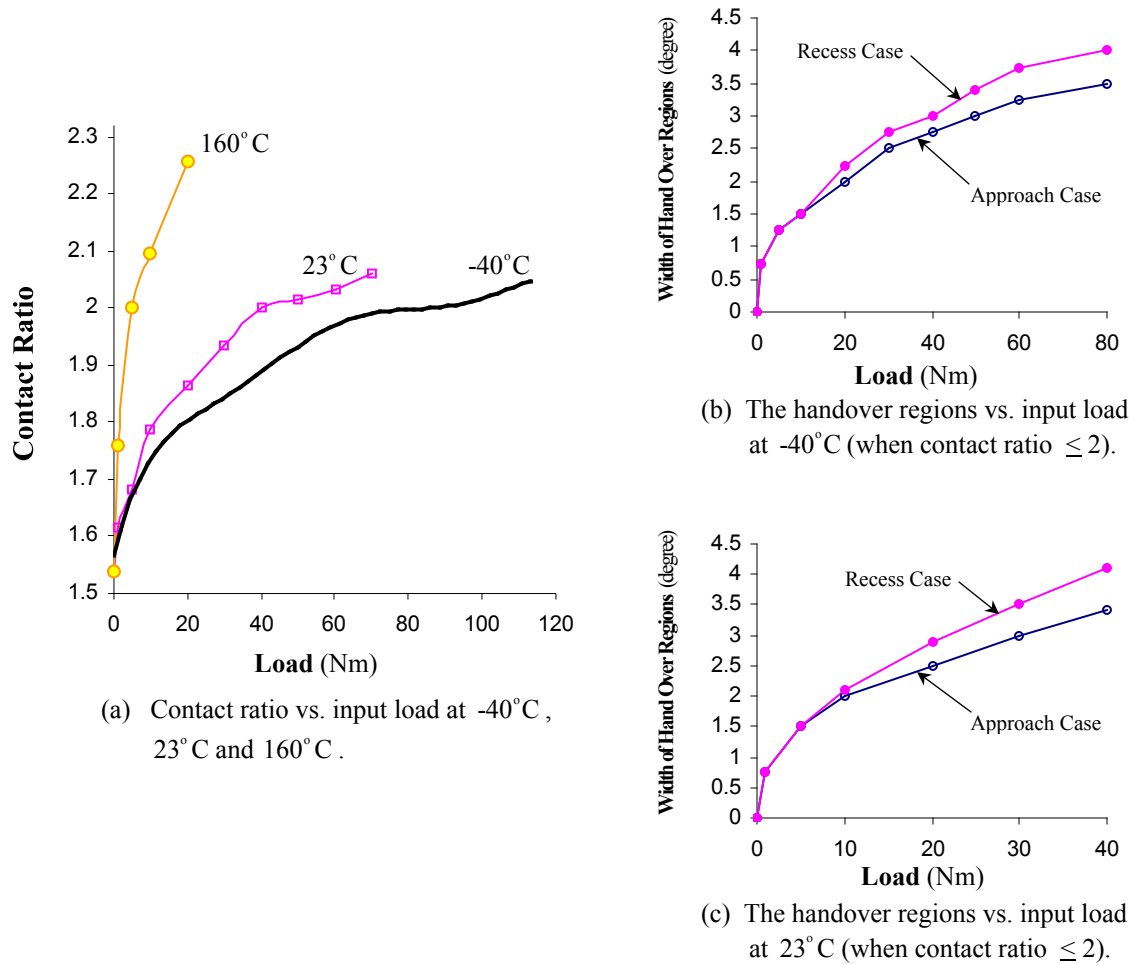
Figure 8.5. 16 Detailed variations of the contact ratio and the width of handover regions against load at temperature of $-40°C$, $23°C$ and $160°C$ (the handover regions vs. input load at $160°C$ is not shown, as more calculations with light loads were required).

8.5.2 T.E. as Function of Temperature at Certain Input Load

If it was assumed that the input load remains steady at each temperature and the temperatures are loaded without considering the time, then the T.E. (over a complete mesh

cycle) against the temperature can be plotted in a 3D figure. Under various input load, 3D figures are produced as shown from Figure 8.5.17 to 8.5.25.
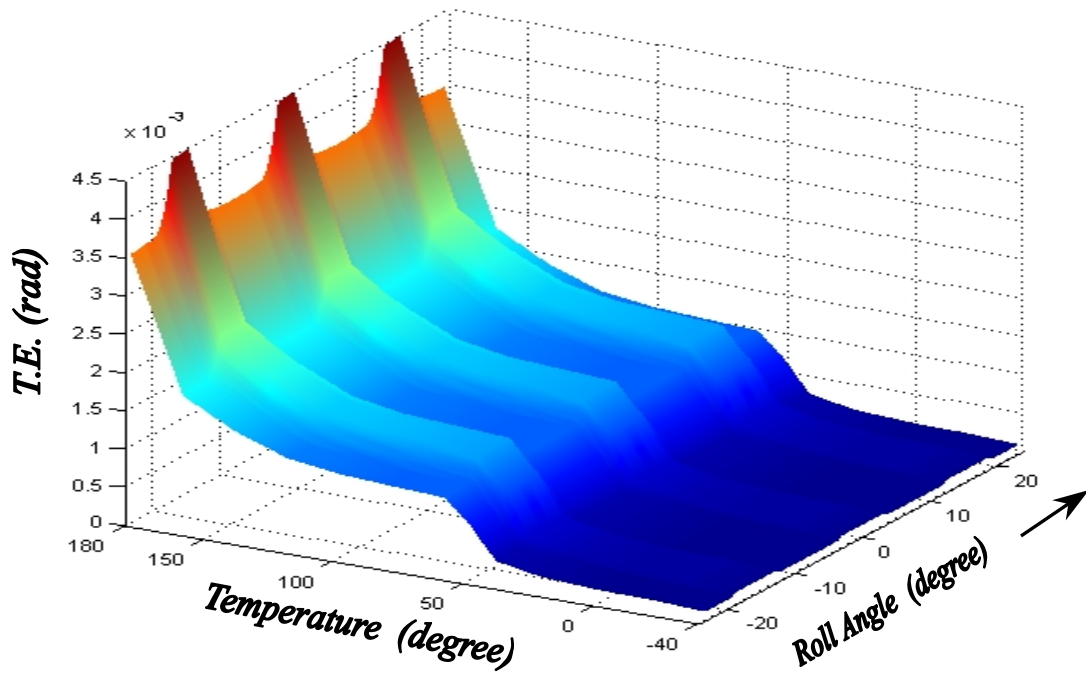
Figure 8.5. 17   Under 1 Nm input load, T.E. (over a complete mesh cycle) as
a function of full range temperature.
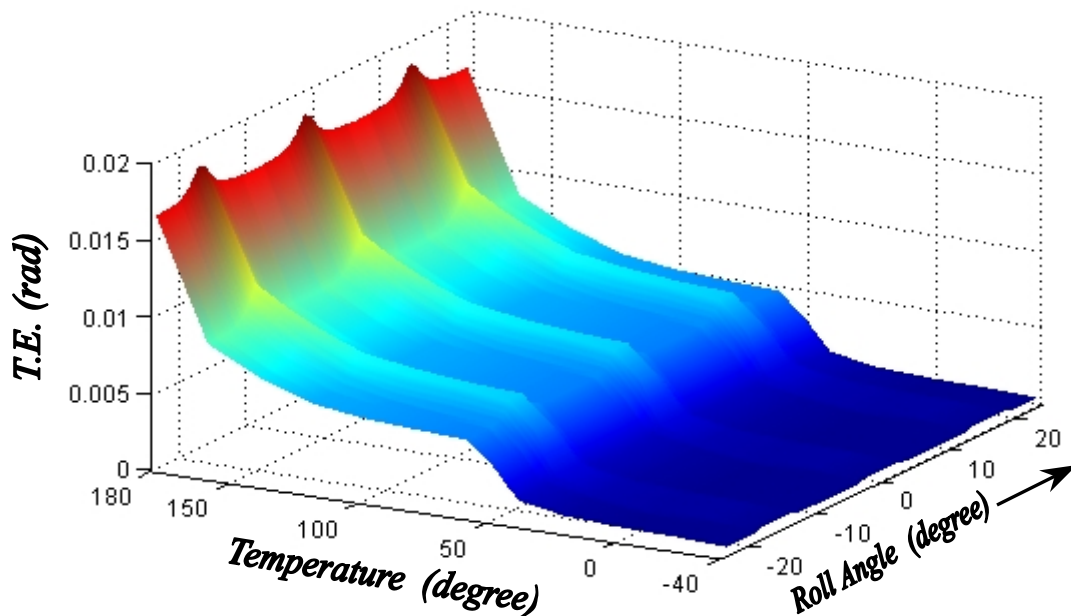
Figure 8.5. 18   Under 5 Nm input load, T.E. (over a complete mesh cycle) as a
function of full range temperature.
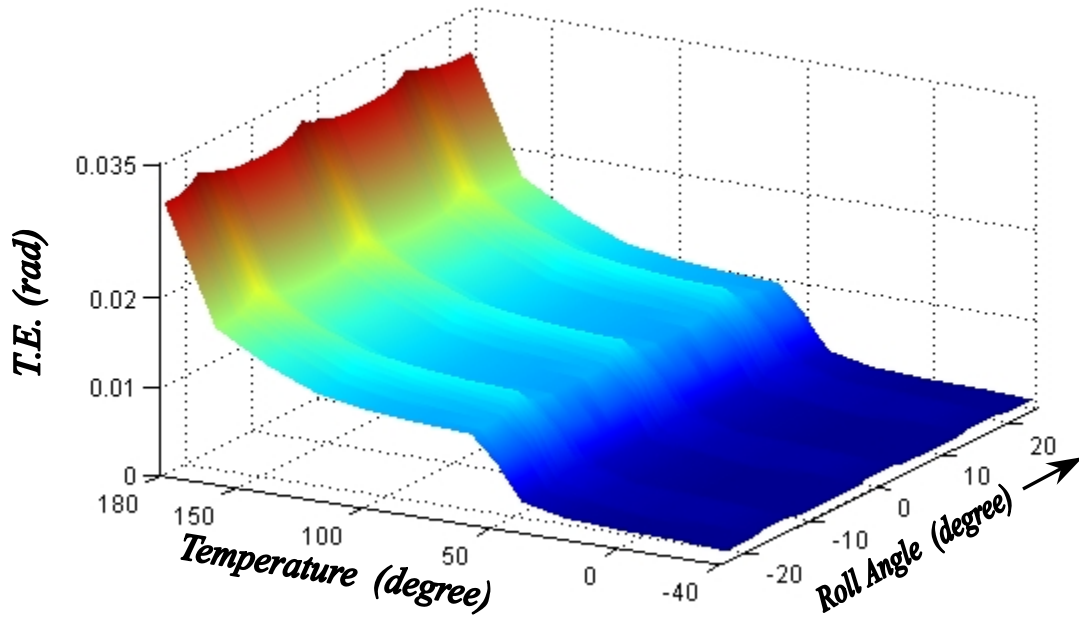
Figure 8.5. 19 Under 10 Nm input load, T.E. (over a complete mesh cycle) as a function of full range temperature.
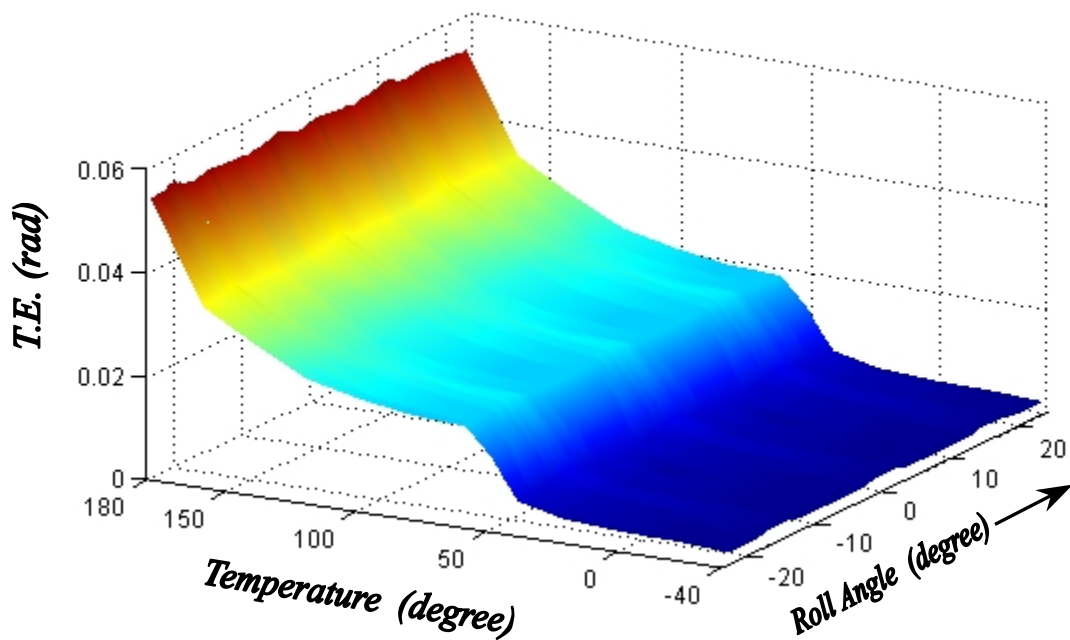
Figure 8.5. 20 Under 20 Nm input load, T.E. (over a complete mesh cycle) as a function of full range temperature.
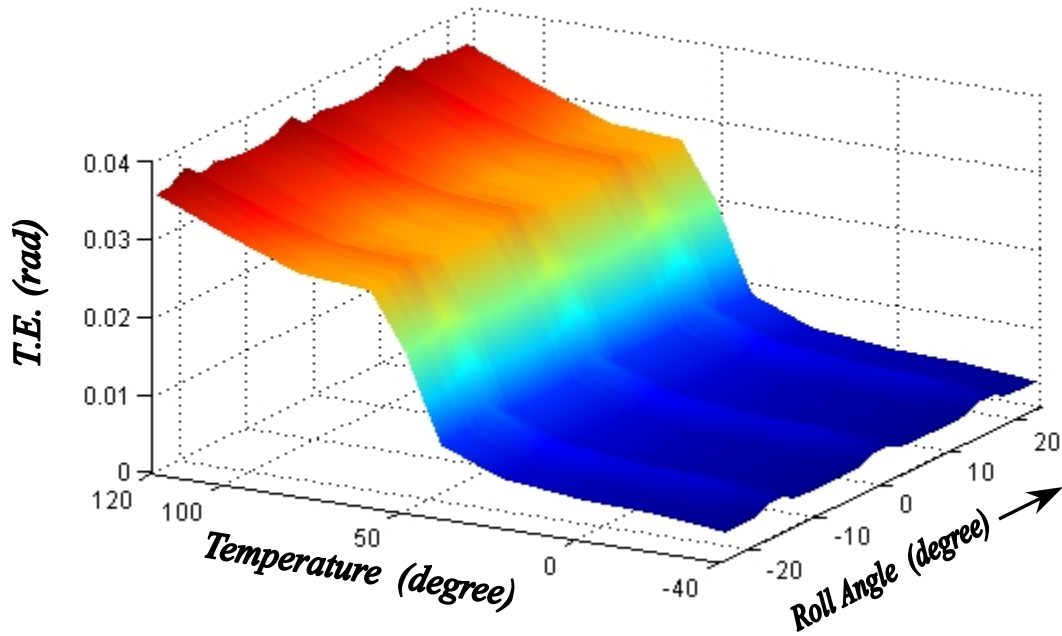
Figure 8.5. 21 Under 30 Nm input load, T.E. (over a complete mesh cycle) as a function of temperature (from $-40^{\circ}C$ to $120^{\circ}C$).
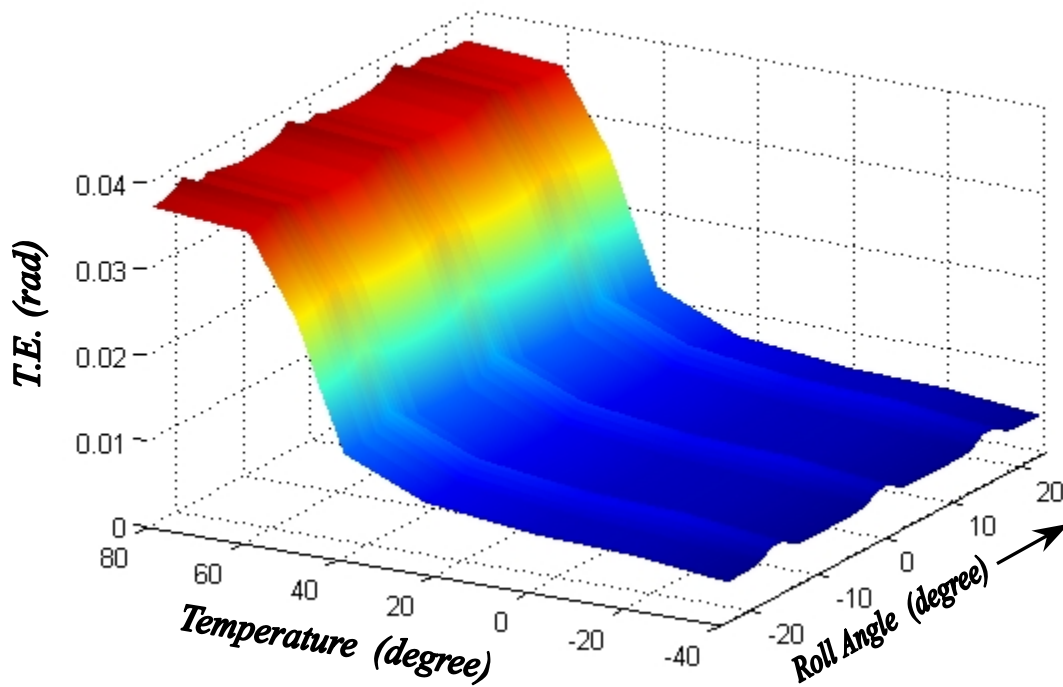
Figure 8.5. 22 Under 40 Nm input load, T.E. (over a complete mesh cycle) as a function of temperature (from $-40^{\circ}C$ to $80^{\circ}C$).
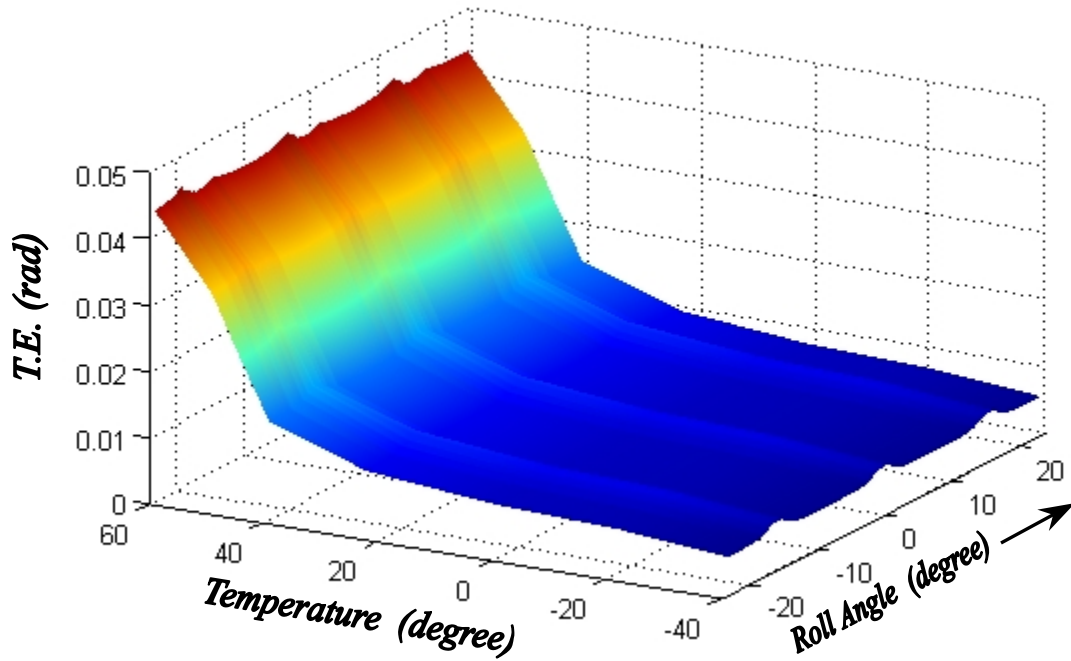
Figure 8.5. 23   Under 50 Nm input load, T.E. (over a complete mesh cycle) as a function of temperature (from $-40^{\circ}C$ to $60^{\circ}C$).
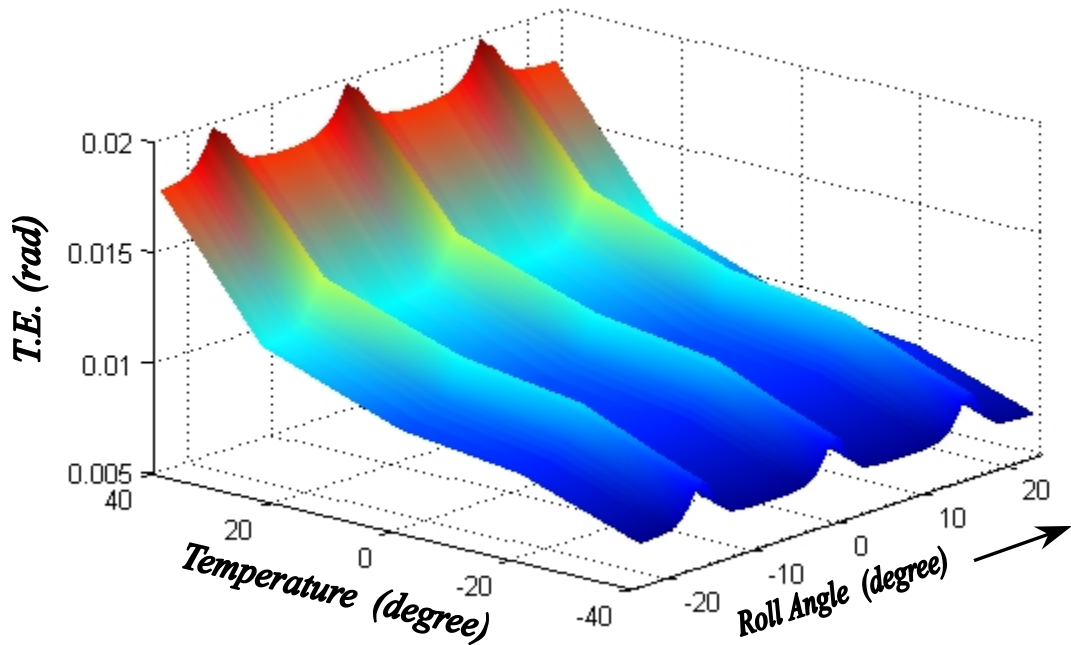
Figure 8.5. 24   Under 60 Nm input load, T.E. (over a complete mesh cycle) as a function of temperature (from $-40^{\circ}C$ to $40^{\circ}C$).
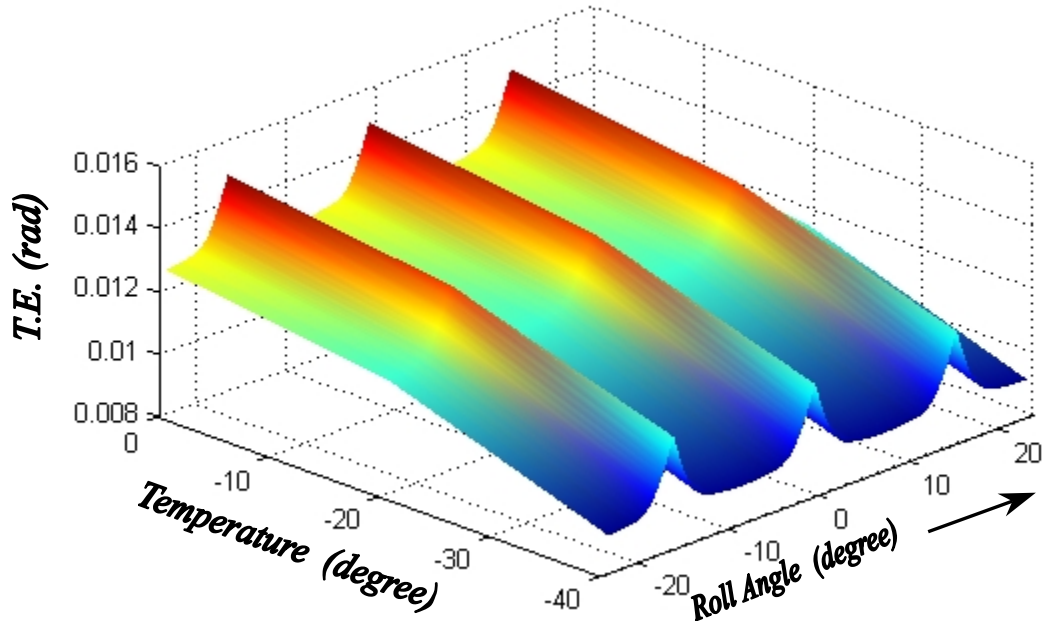
Figure 8.5. 25   Under 80 Nm input load, T.E. (over a complete mesh cycle) as
a function of temperature (from $-40^{\circ}C$ to $0^{\circ}C$).

The results show two rapid changes (in most cases) in the region of $45^{\circ}C$ to $50^{\circ}C$ and the
region over $150^{\circ}C$. This characteristic shows the dependence on the material properties
(Figure 8.3.2).

8.5.3   The Comparison with Metallic Gears

With the different materials (aluminium and nylon), the analysis has produced two groups
of T.E. curves under the same boundary and load conditions as shown in Figure 8.5.26.

The T.E. results presented in Figure 8.5.26 (a) and (b) are significantly different in both the
amplitude (absolute value) and the curve shape (relative value).   The main interesting
features of the comparison is the curve shape (relative value), so Figure 8.5.26 (a) and (b)
are compared together to produce Figure 8.5.27.

(a) Aluminum gears in mesh.

(b) Nylon (PA6) gears in mesh (temperature is at -40°C).
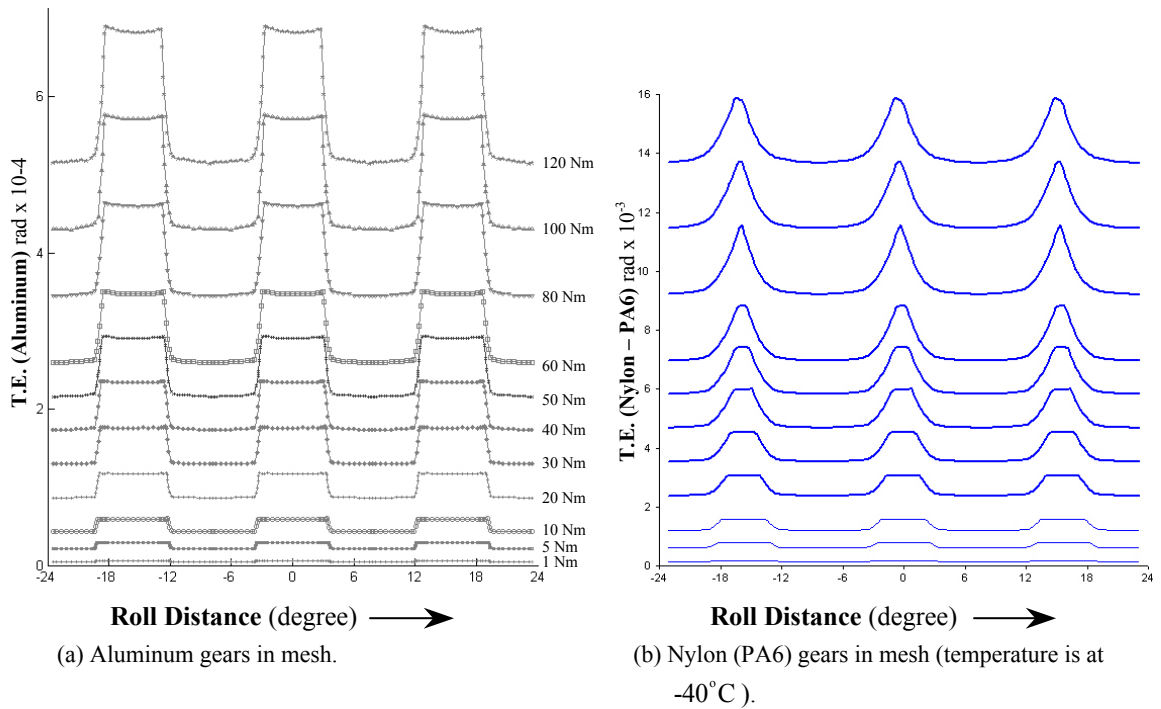
Figure 8.5. 26   T.E. of aluminium gears and nylon gears in mesh (each pair with the same boundary and load conditions.
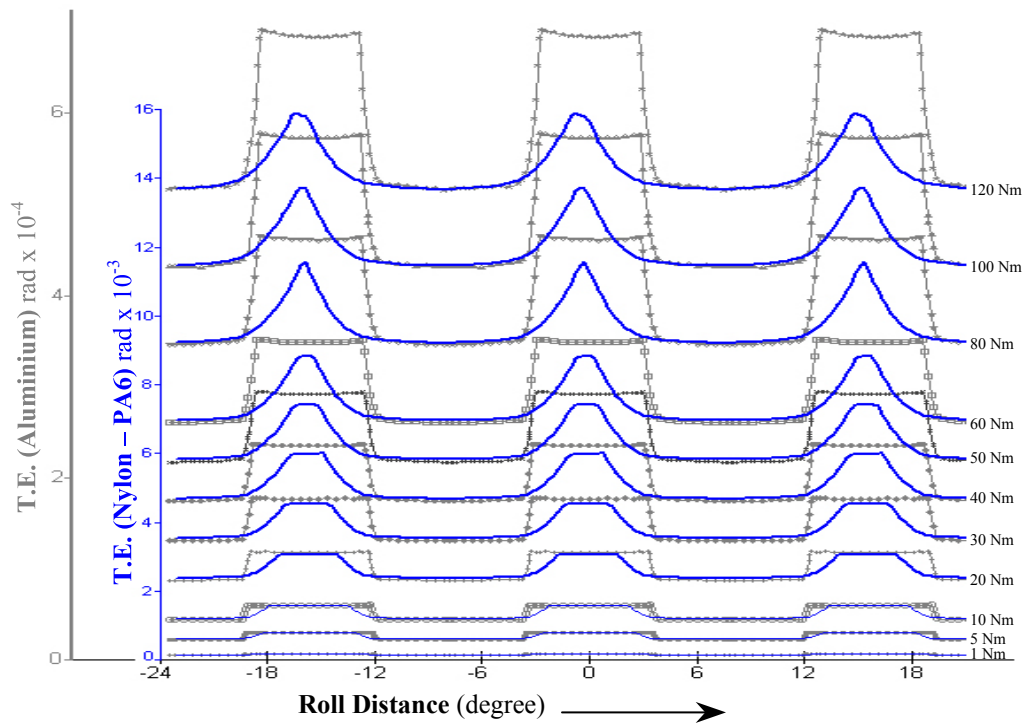
Figure 8.5. 27   The comparisons when the nylon gear pair is at temperature -40°C.

Similarly, results can be shown for $23°C$ and $160°C$ as illustrated in Figure 8.5.28 and 8.5.29.
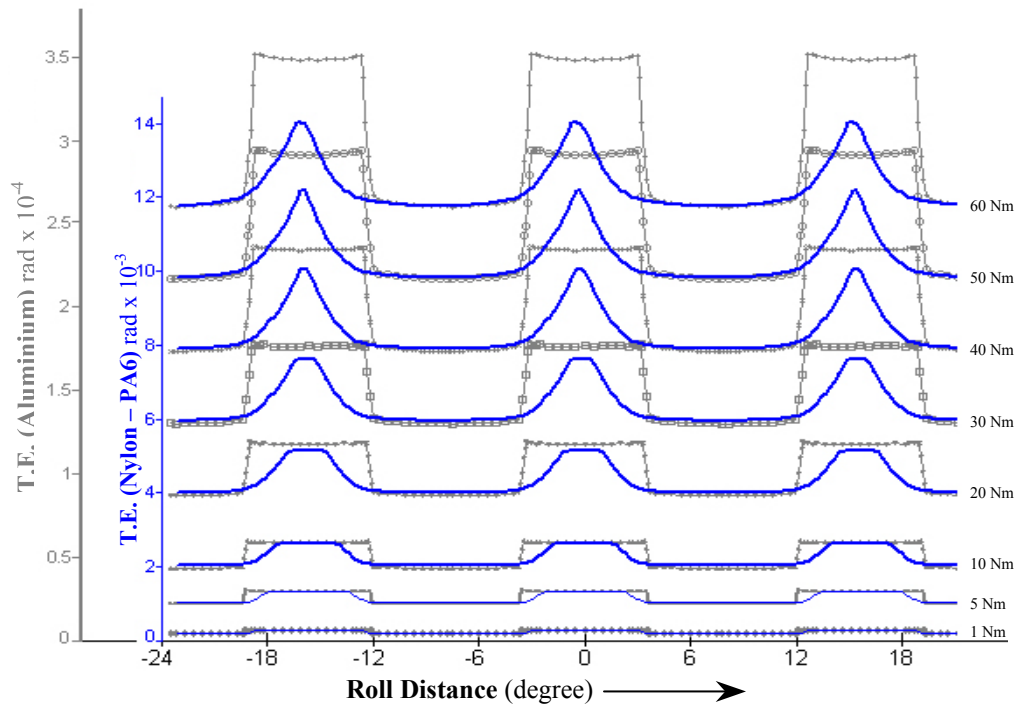
Figure 8.5. 28   The comparisons when the nylon gear pair is at temperature $23°C$.
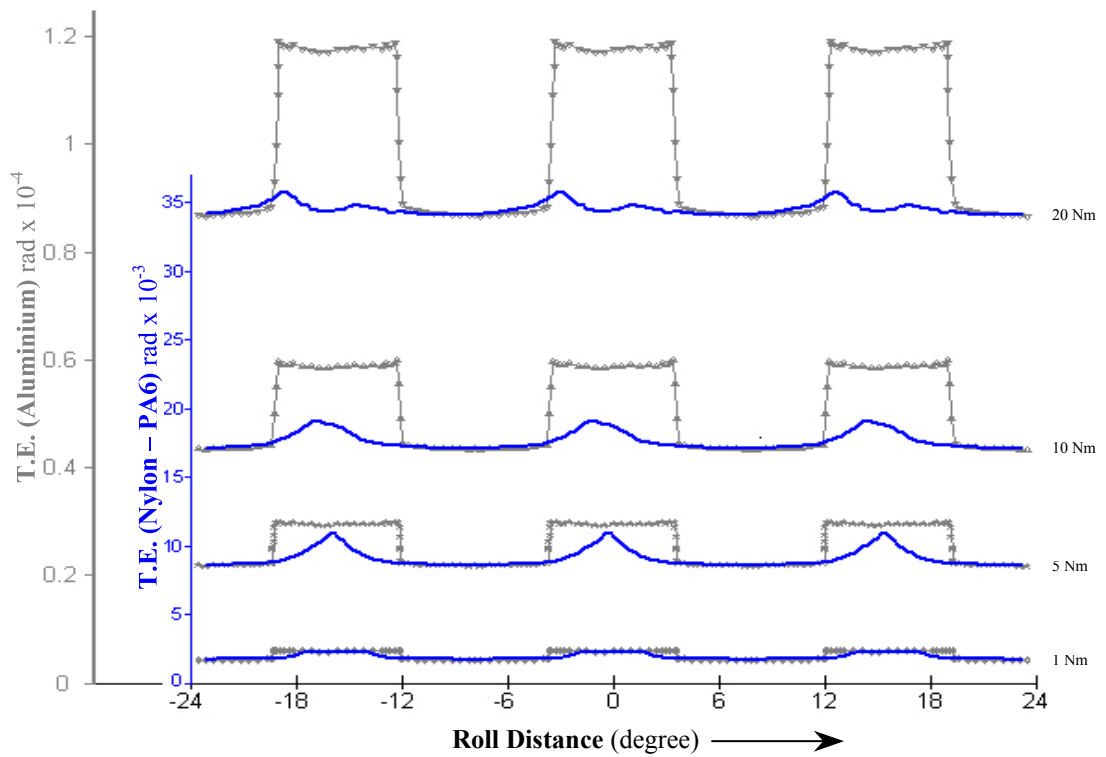
Figure 8.5. 29   The comparisons when the nylon gear pair is at temperature $160°C$.

By the observation of the comparison figures above, the following conclusions can be given,

1. When the input load tends to be very light, the T.E. curves of metallic and non-metallic gears tend to have the same shape (relative values).

2. The curve shape mainly changes (by varying material property) in the low stiffness region (single contact zone), as observed by the expansion of the handover regions (when contact ratio ≤ 2) or the handover regions plus the triple contact zone (when contact ratio > 2).

3. Double zone curve shape changes only when the triple contact zone is significantly expanded (heavy load, high temperature).

8.6   The Combined Torsional Mesh Stiffness

The combined torsional mesh stiffness under various input loads will present obvious different behaviours over the mesh cycle. The most complicated changes will occur in the lower stiffness regions including the single contact zone, the handover regions and the triple contact zone – which in most cases is still with lower stiffness, as shown in Figure 8.6.1 and 8.6.2.

It can be seen, that before the single zone disappears (contact ratio $\leq$ 2) the major variations of the stiffness are in the higher amplitude and the expansion of the handover regions that cause a minor stiffness curve phase change over the periodical mesh cycles. After the triple contact takes place, the double zone stiffness rises slowly, while the stiffness of the triple zone and handover regions are still increasing rapidly with input load and this fast change causes a major phase decrease over the periodical mesh cycle. Under extreme conditions such as the temperature reaching 180°C, the flexibility of the gears allows the triple contact to occur very early on. The triple zone stiffness and its width increases with the input load, meanwhile the increase in the double zone stiffness continues after the triple contact occurs. The stiffness curve tends to be smoothed quickly with the increasing load as shown in Figure 8.6.3.
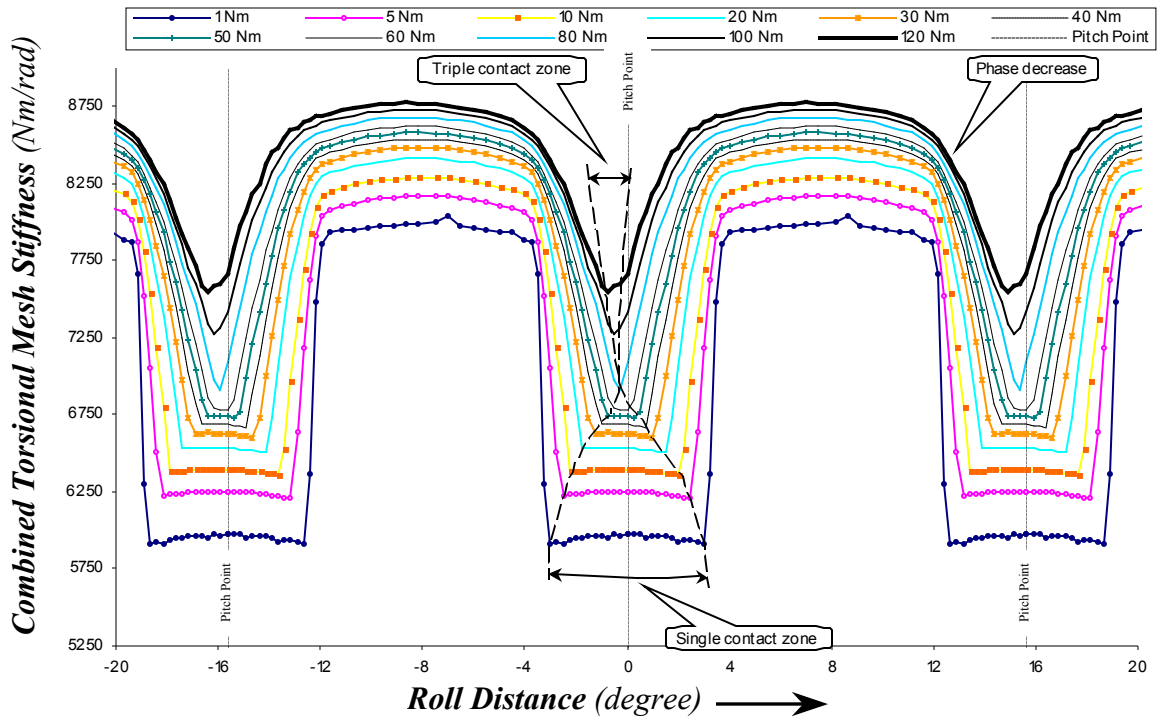
Figure 8.6. 1   The combined torsional mesh stiffness under various input loads, temperature $-40^{\circ}C$, Nylon (PA 6).
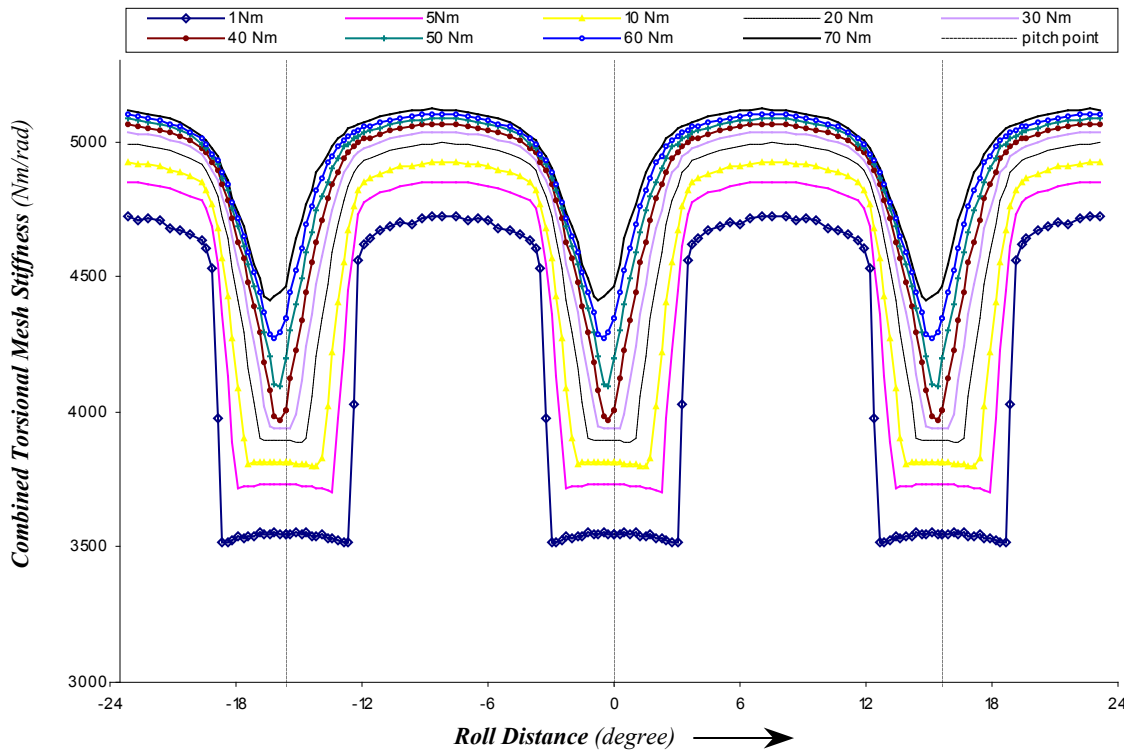
Figure 8.6. 2   The combined torsional mesh stiffness under various input loads, temperature $23^{\circ}C$, Nylon (PA 6).

209
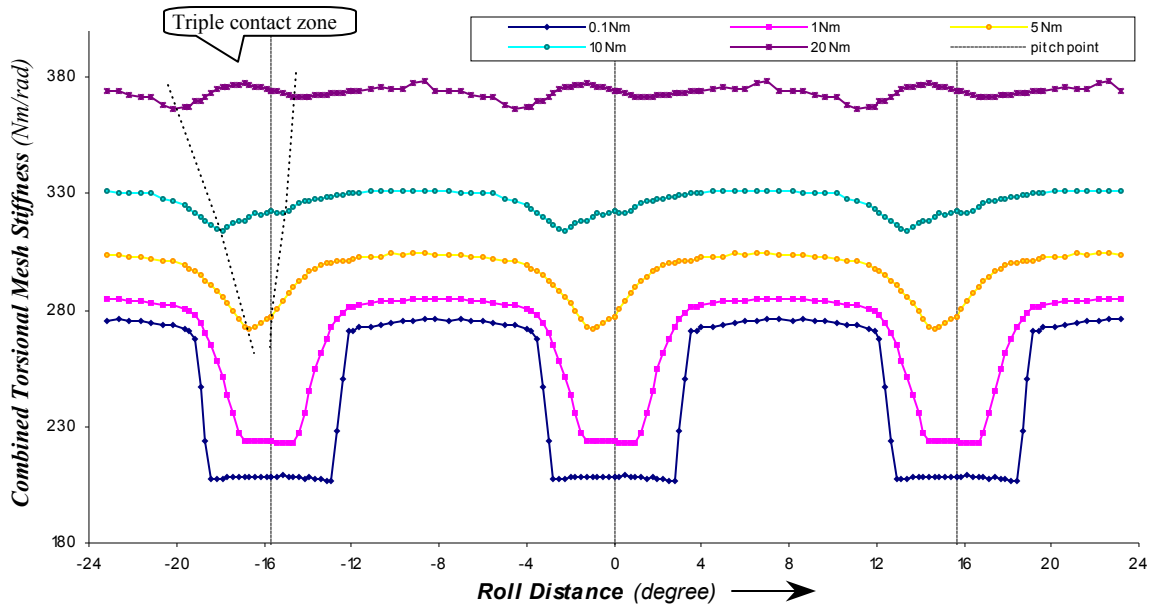
Figure 8.6. 3   The combined torsional mesh stiffness under various input loads, temperature $180^{\circ}C$, Nylon (PA 6).

Discussions above have mainly shown the variations of the combined torsional mesh stiffness against the input loads at different temperatures. For the variations of the combined torsional mesh stiffness against the temperatures at different input loads, the details are given as shown in Figure 8.6.4 to 8.6.11.
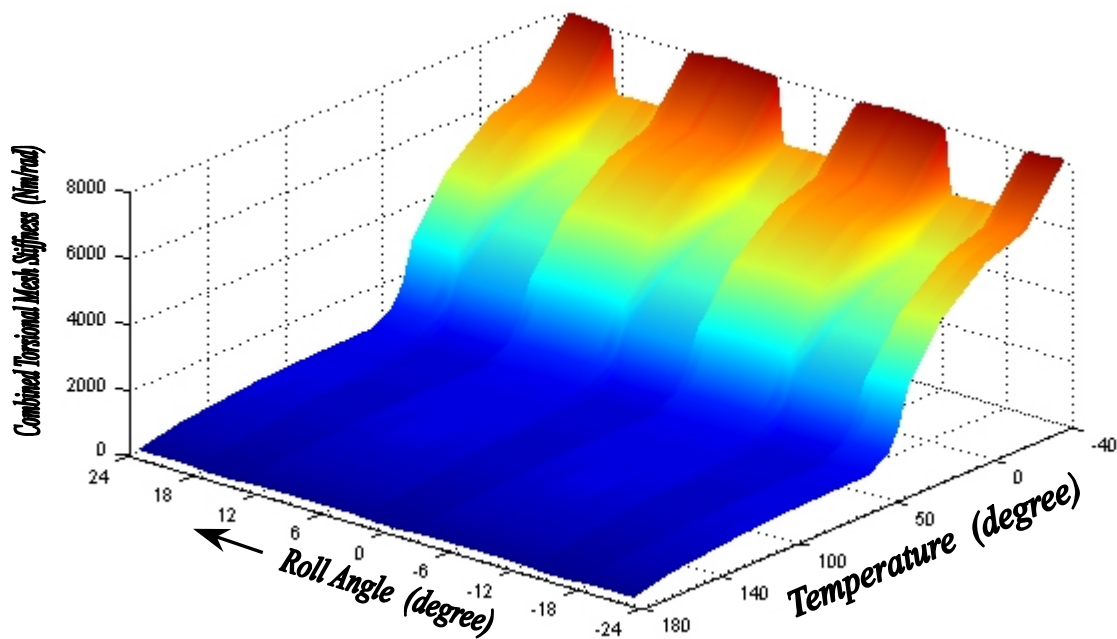
Figure 8.6. 4   Combined torsional mesh stiffness under 1 Nm input load against the full range temperature, Nylon (PA 6).

210
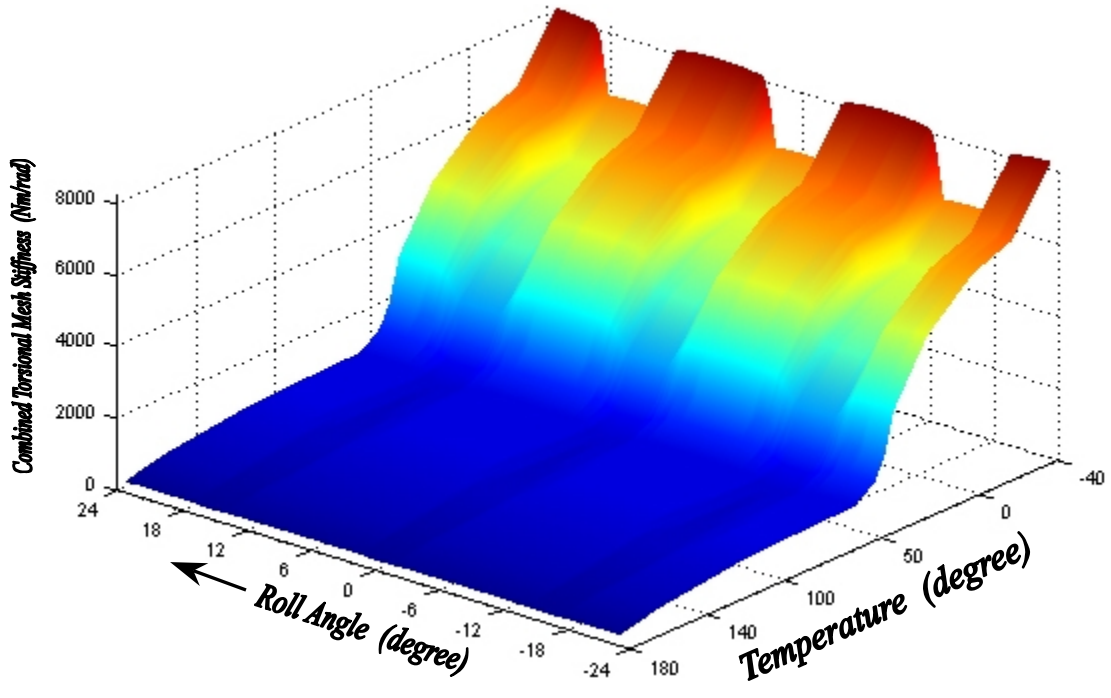
Figure 8.6. 5 Combined torsional mesh stiffness under 5 Nm input load against the full range temperature, Nylon (PA 6).
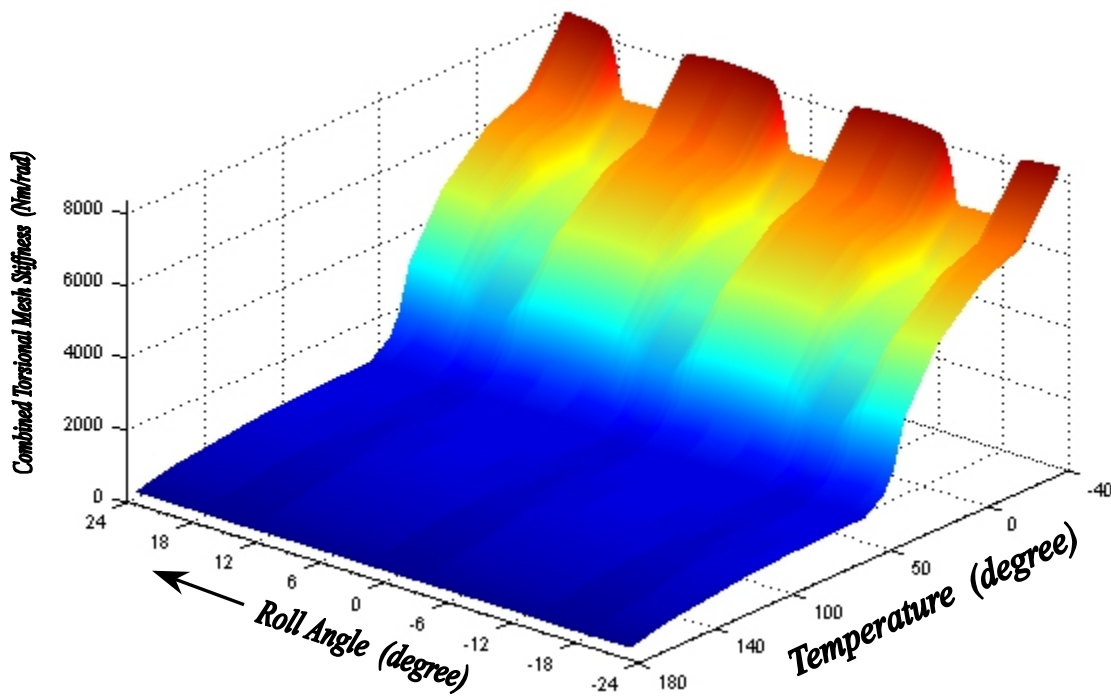
Figure 8.6. 6 Combined torsional mesh stiffness under 10 Nm input load against the full range temperature, Nylon (PA 6).
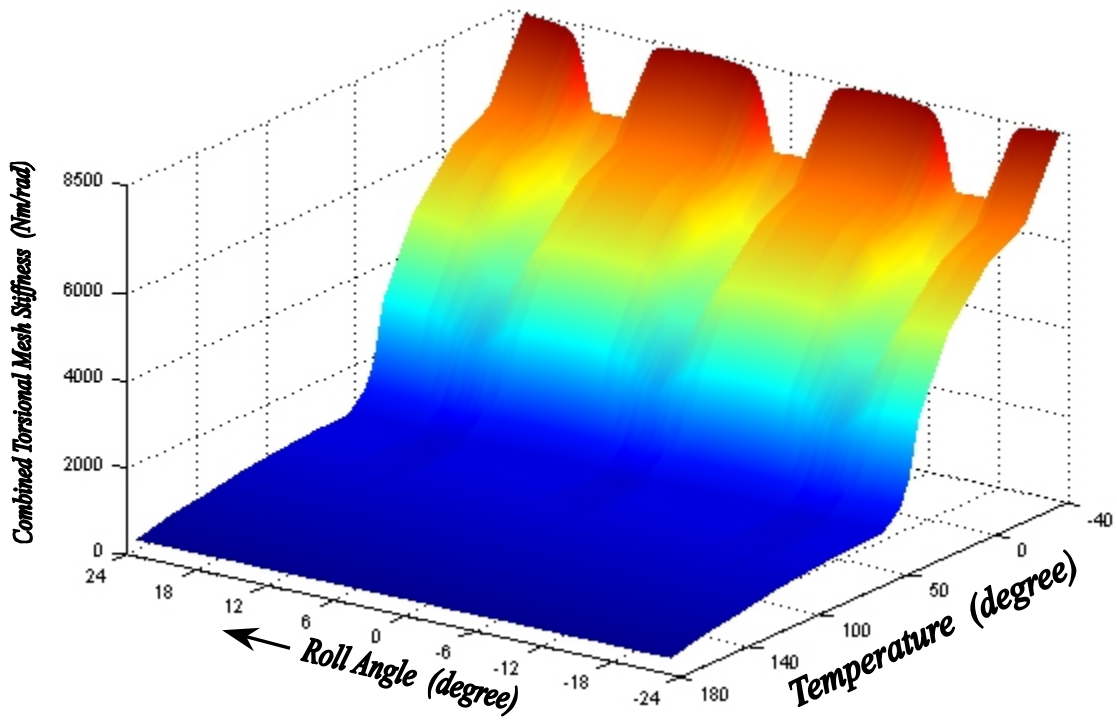
Figure 8.6. 7 Combined torsional mesh stiffness under 20 Nm input load against the full range temperature, Nylon (PA 6).
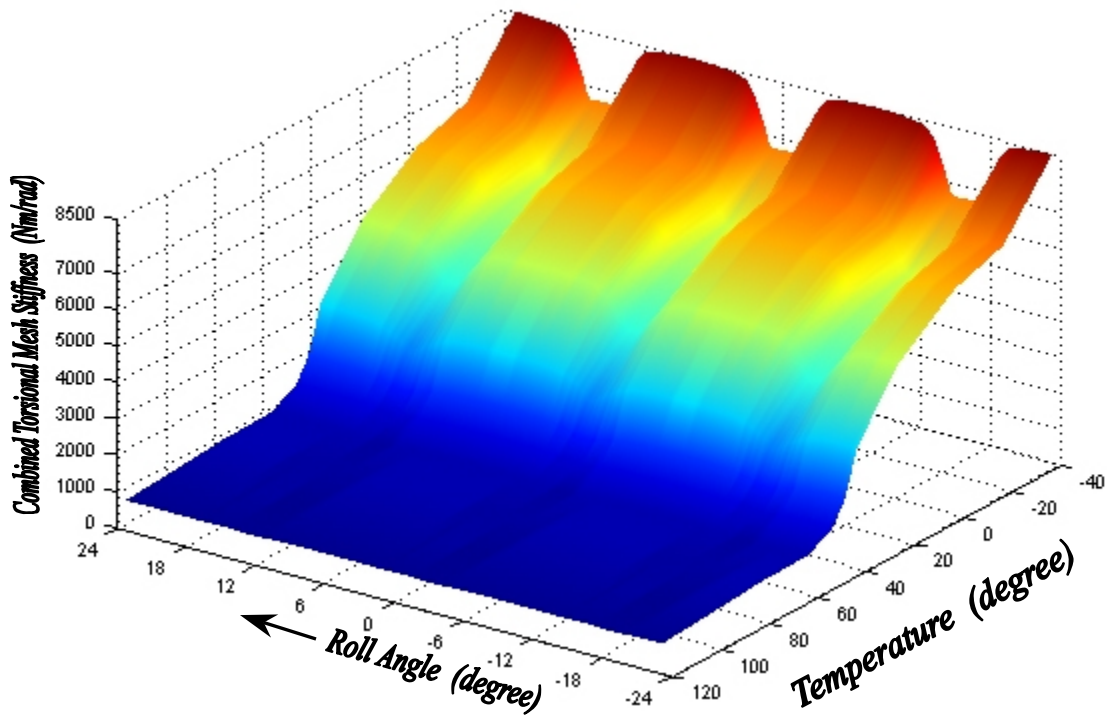
Figure 8.6. 8 Combined torsional mesh stiffness under 30 Nm input load against temperature from -40°C to 120°C, Nylon (PA 6).
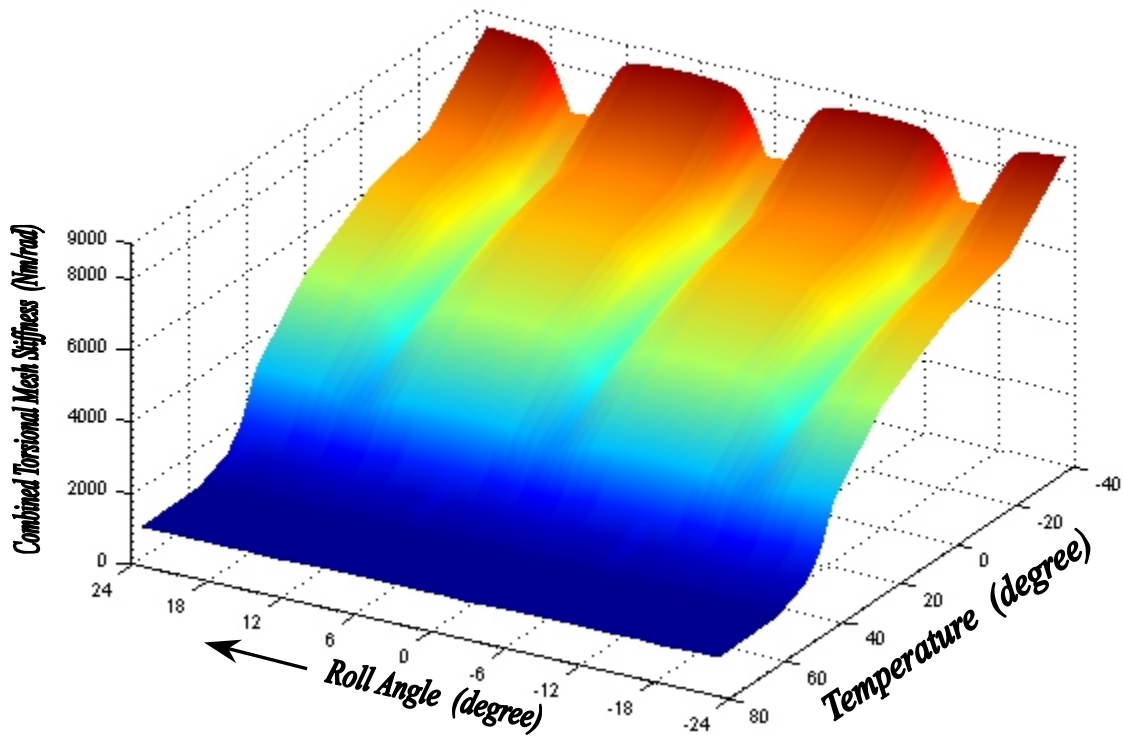
Figure 8.6. 9   Combined torsional mesh stiffness under 40 Nm input load against temperature from -40°C to 80°C, Nylon (PA 6).
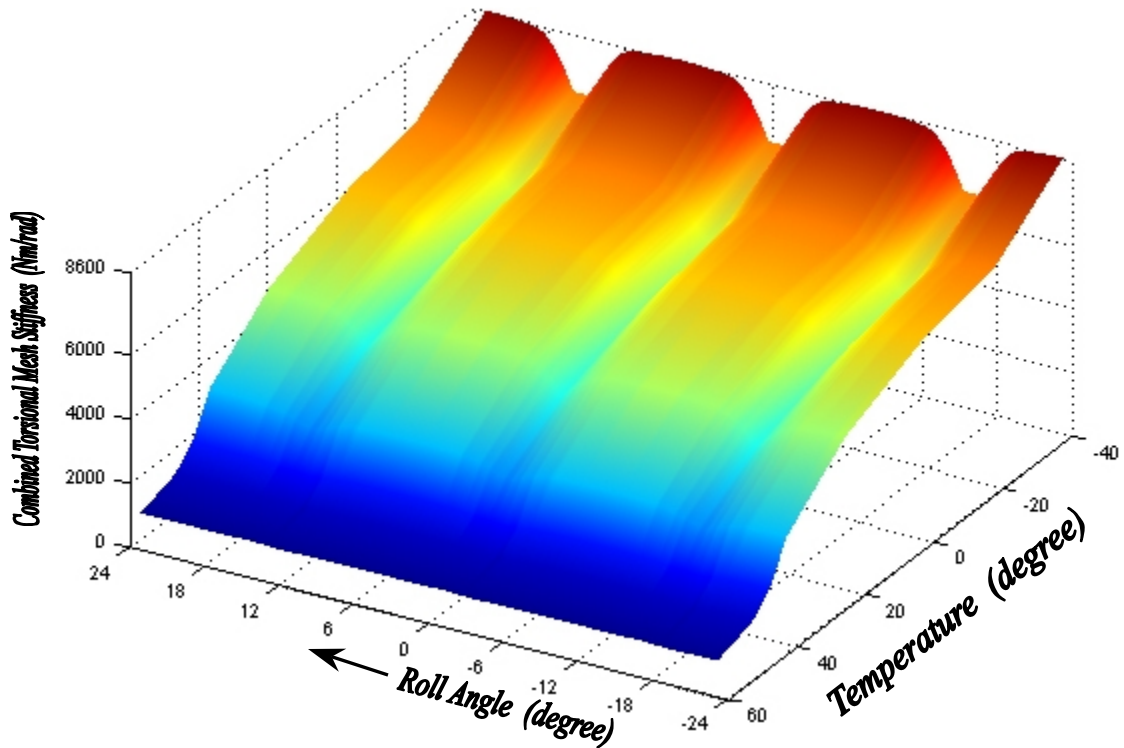
Figure 8.6. 10   Combined torsional mesh stiffness under 50 Nm input load against temperature from -40°C to 60°C, Nylon (PA 6).
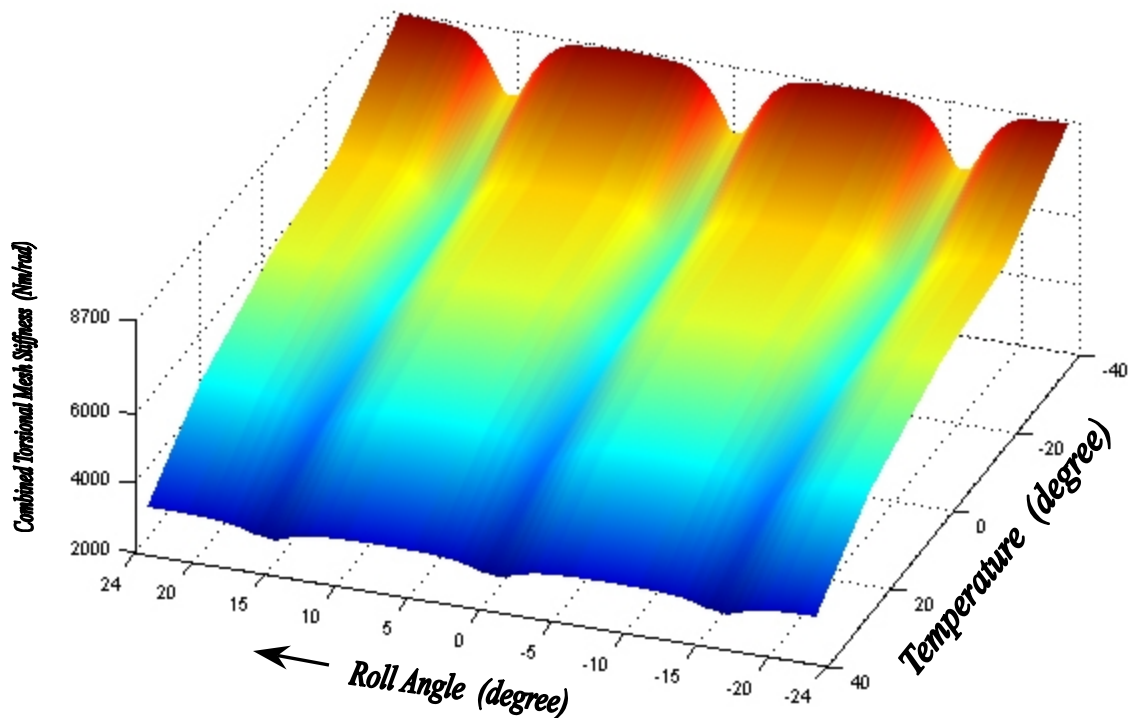
Figure 8.6. 11   Combined torsional mesh stiffness under 60 Nm load against temperature from -40°C to 40°C, Nylon (PA 6).

It can be seen that the combined torsional mesh stiffness drops with the temperature increases from -40°C to 40°C. When the temperature is higher than 40°C, the combined torsional mesh stiffness becomes relatively stable (drops much slower with temperature increase). The results indicate that this characteristic does not rely on whether the triple contact has occurred. For example, when the input load is 1 Nm, no triple contact occurs through the temperature range, while when the input load is 60 Nm, the triple contact occurs before the temperature reaches 0°C.

The behaviours of the combined torsional mesh stiffness have shown (one of) the reason why non-metallic gears run smoother than metallic gears. However, when non-metallic gears run quiet and smooth this doesn't mean the gears are under good running condition. It is likely that triple contact has taken place, and consequently this will result in excessive wear – the most significant factor to the service life.

8.7   Load Sharing Ratio

In low contact ratio (it normally is between 1.3 to 1.6) non-metallic spur gears, the load is transmitted by one pair and two pairs of teeth alternately when the combination of input

214

load and the temperature is within a limited range, otherwise, two pairs and three pairs of teeth will transmit the load alternatively.

Due to the material flexibility, the deformed teeth will be rotating (about the tooth roots), bending, shearing and the tooth flanks becoming flattened at the points of contact. These factors can easily become significant, altering the load variation outside the normal path of contact. Triple contact with low contact ratio gears is caused by a significant amount of contact outside the normal path. Theoretically any contact outside the normal path on involute spur gears will present premature contact (or corner contact). For the special case of the triple contact, increasing either the input load or the temperature or both can quickly increase the percentage of total load on the teeth with premature contact, and the triple zone can rapidly expand. The curves of tooth load sharing ratio can clearly show these complex variations from the tooth running in, to running out of contact.

8.7.1 Load Sharing Ratio as Function of Input Load at Each Temperature

It has been shown that tooth load sharing ratio is dependent on the input load (Chapter 7) for metallic gears in mesh, but for non-metallic gears, the variations can be dramatic and there will be a very limited common curve of the load sharing ratio (only when the single contact zone exists). At each of the fourteen different temperatures, the load share against various input loads is given as shown from Figure 8.7.1 to 8.7.14.
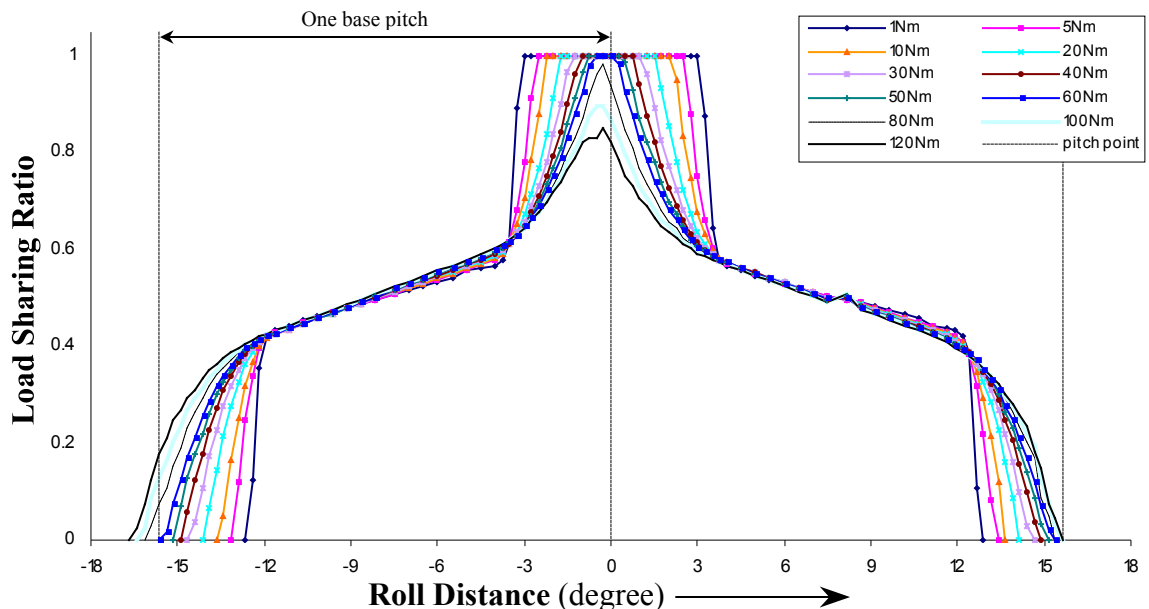
Figure 8.7. 1   The load-sharing ratio against input loads at temperature -40°C , Nylon (PA 6).

215
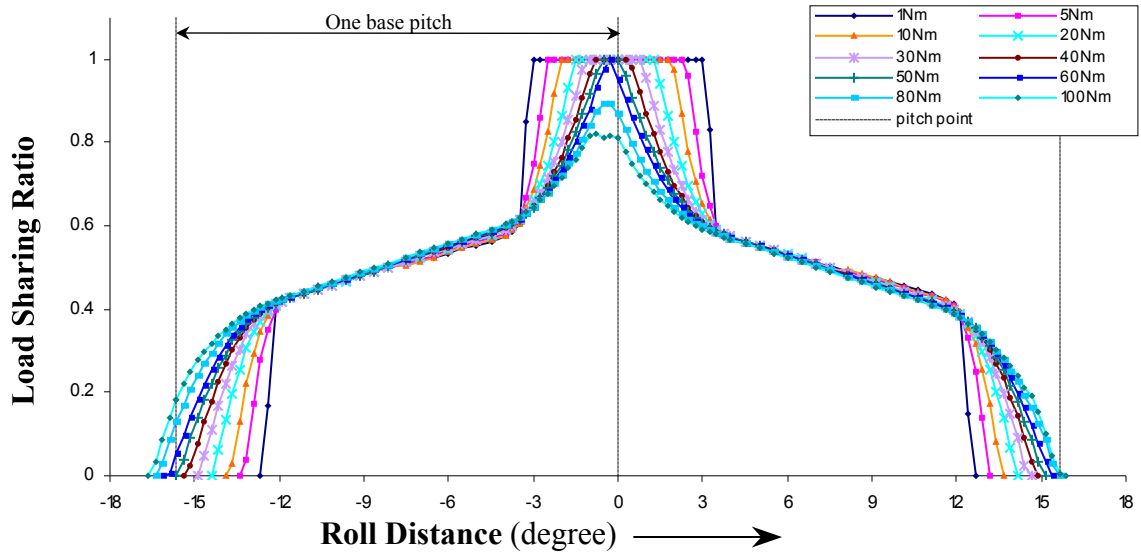
Figure 8.7. 2 The load-sharing ratio against input loads at temperature -20°C, Nylon (PA 6).
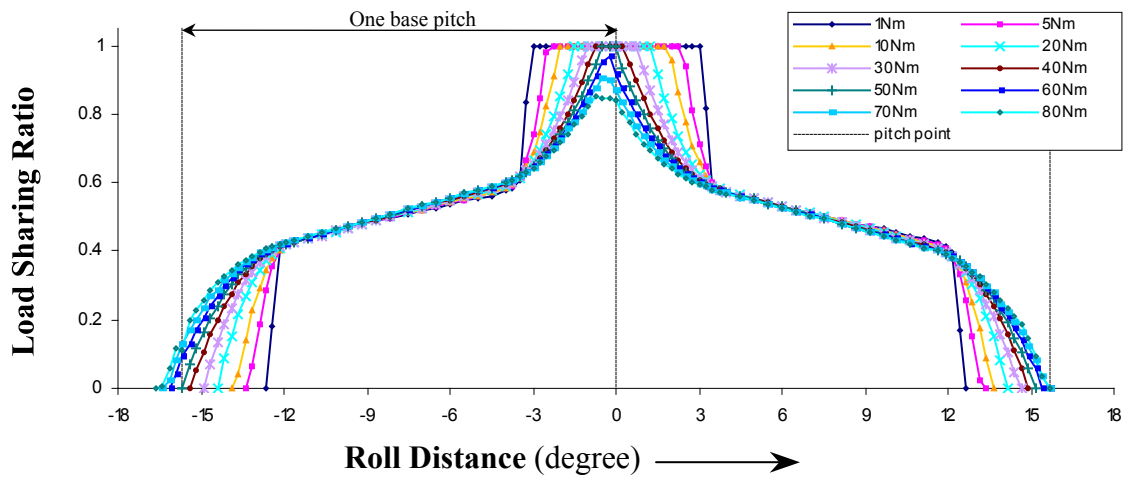
Figure 8.7. 3 The load-sharing ratio against input loads at temperature 0°C, Nylon (PA 6).
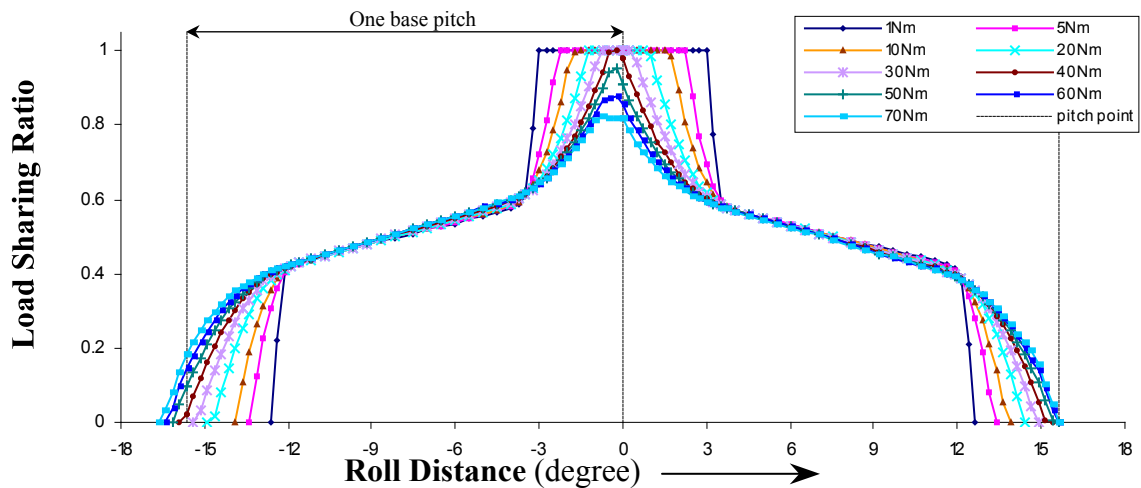
Figure 8.7. 4 The load-sharing ratio against input loads at temperature 23°C, Nylon (PA 6).

216
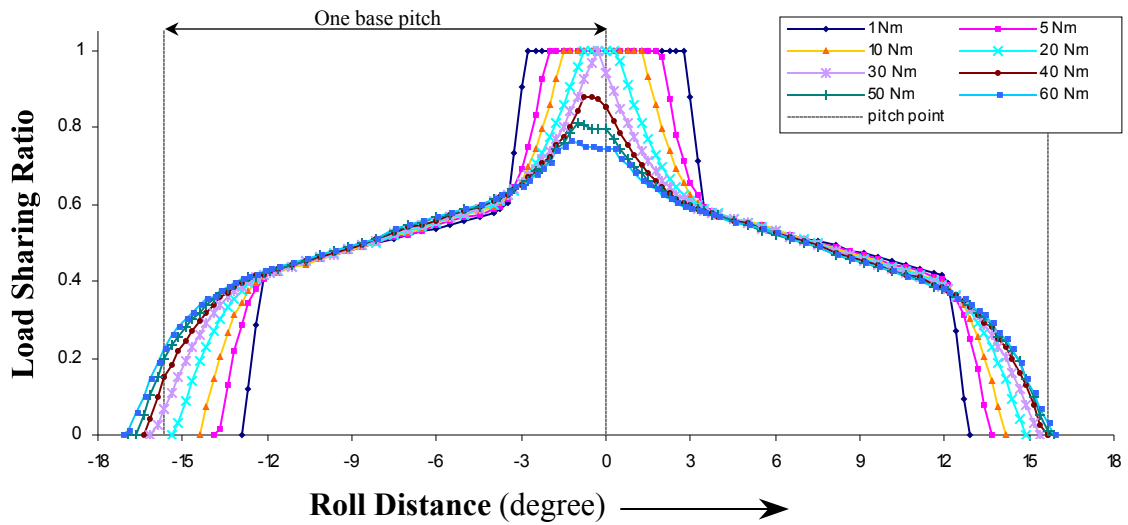
Figure 8.7. 5   The load-sharing ratio against input loads at temperature $40^{\circ}C$, Nylon (PA 6).
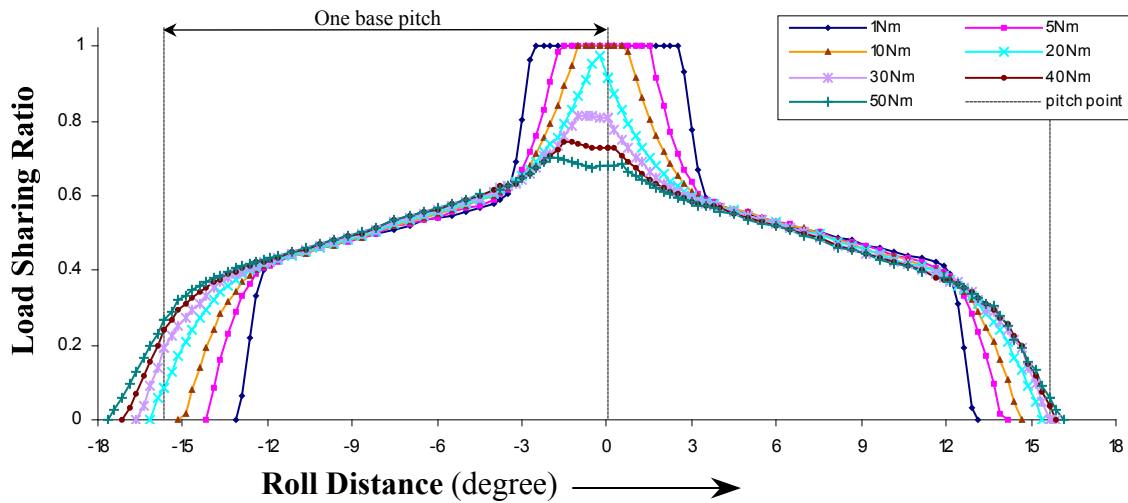
Figure 8.7. 6   The load-sharing ratio against input loads at temperature $45^{\circ}C$, Nylon (PA 6).
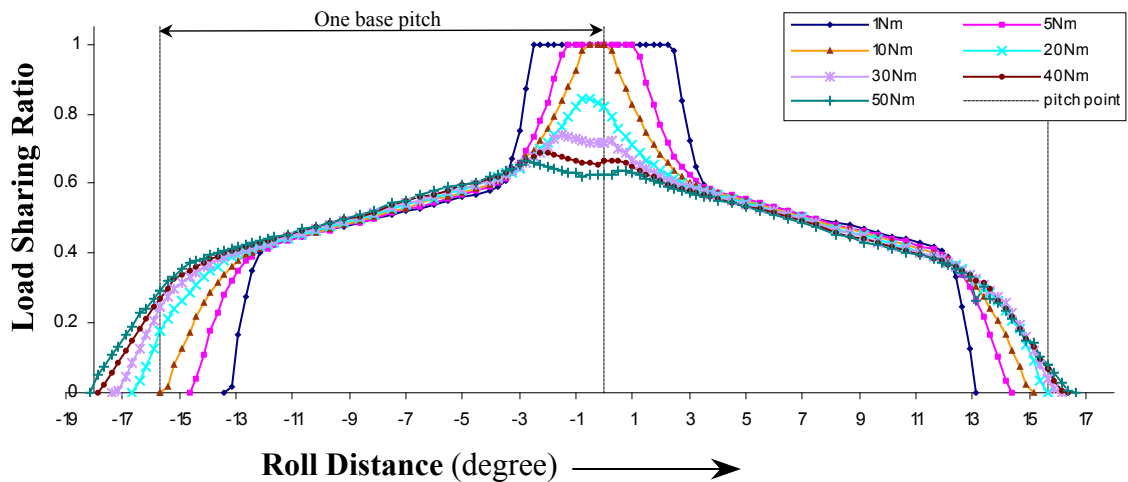
Figure 8.7. 7   The load-sharing ratio against input loads at temperature $50^{\circ}C$, Nylon (PA 6).
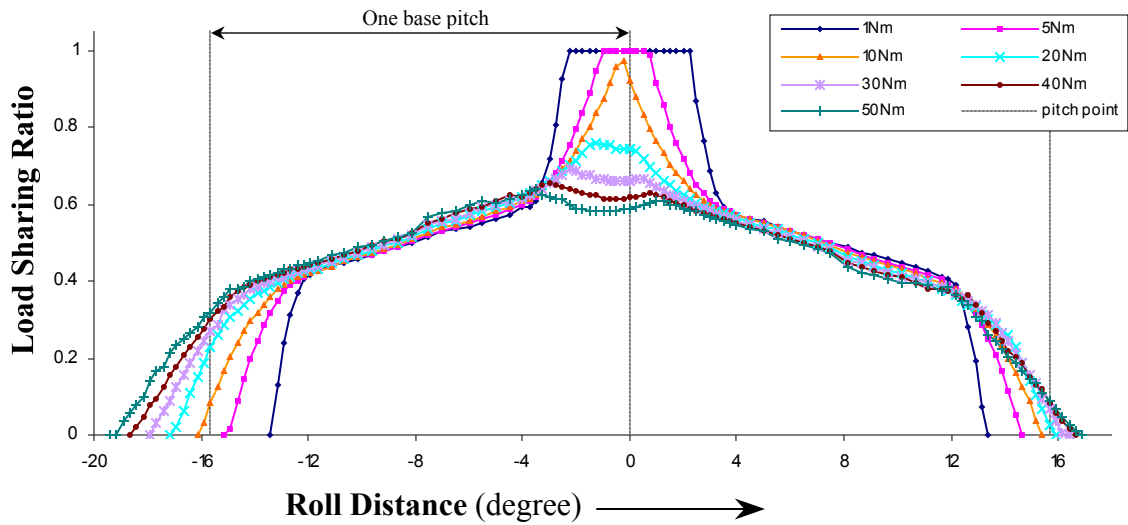
Figure 8.7. 8 The load-sharing ratio against input loads at temperature 60°C , Nylon (PA 6).
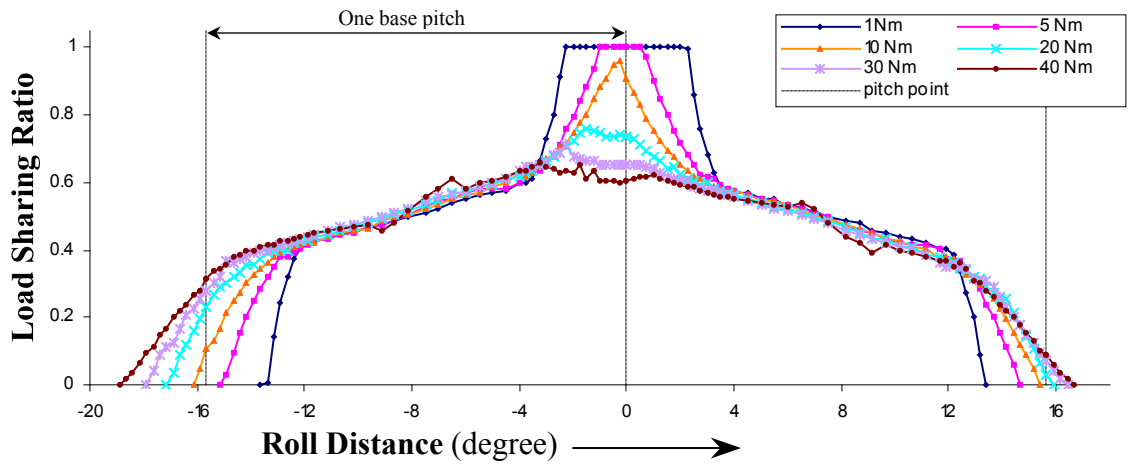
Figure 8.7. 9 The load-sharing ratio against input loads at temperature 80°C , Nylon (PA 6).
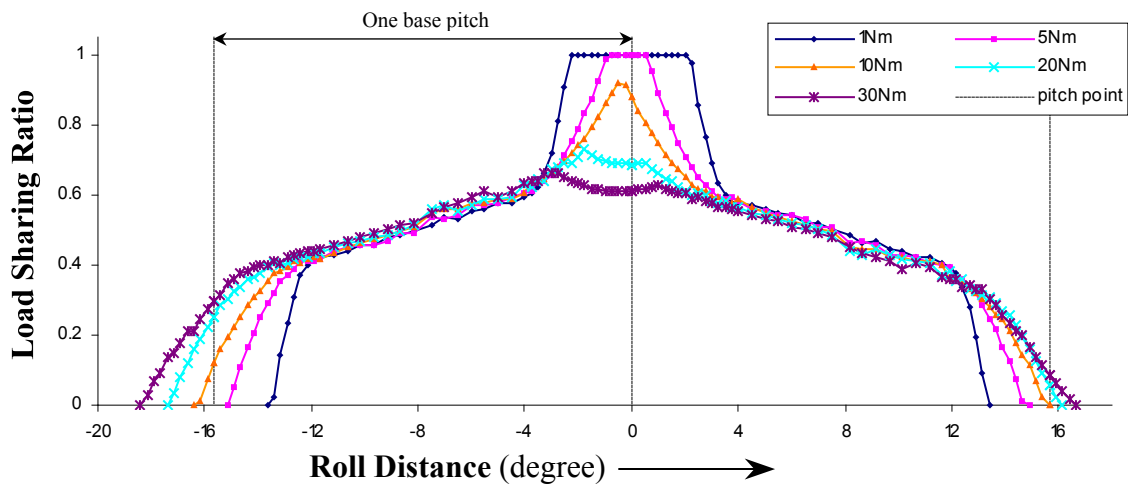
Figure 8.7. 10 The load-sharing ratio against input loads at temperature 100°C , Nylon (PA 6).
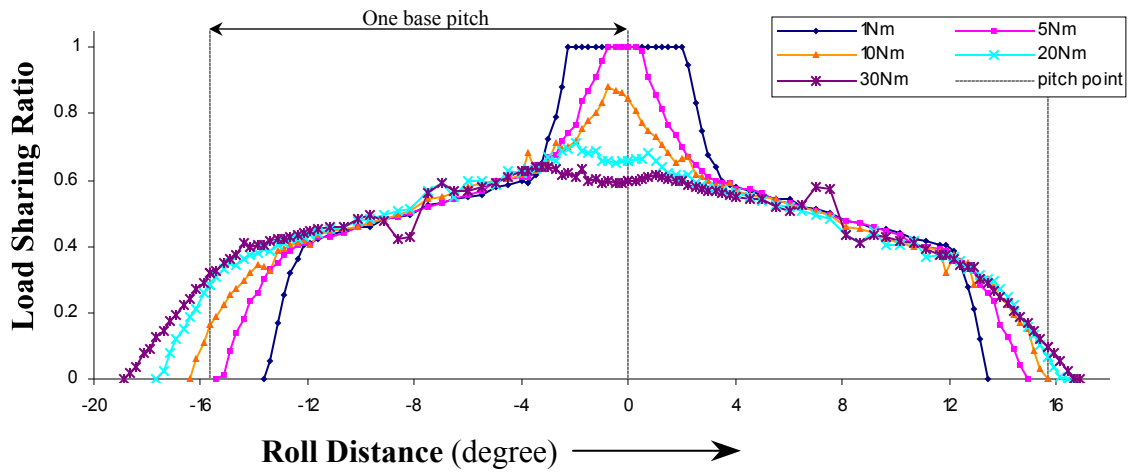
Figure 8.7. 11 The load-sharing ratio against input loads at temperature $120^\circ C$, Nylon (PA 6).
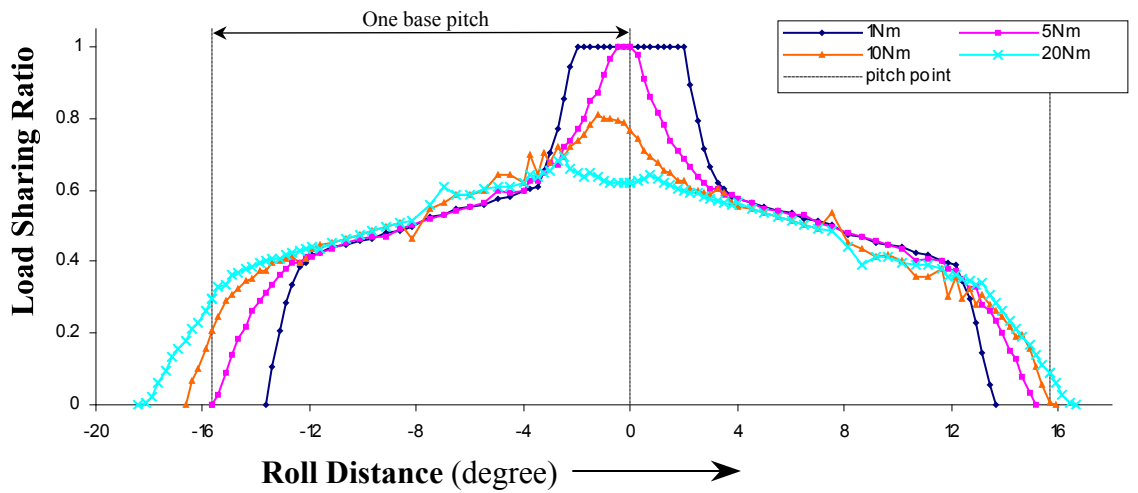
Figure 8.7. 12 The load-sharing ratio against input loads at temperature $140^\circ C$, Nylon (PA 6).
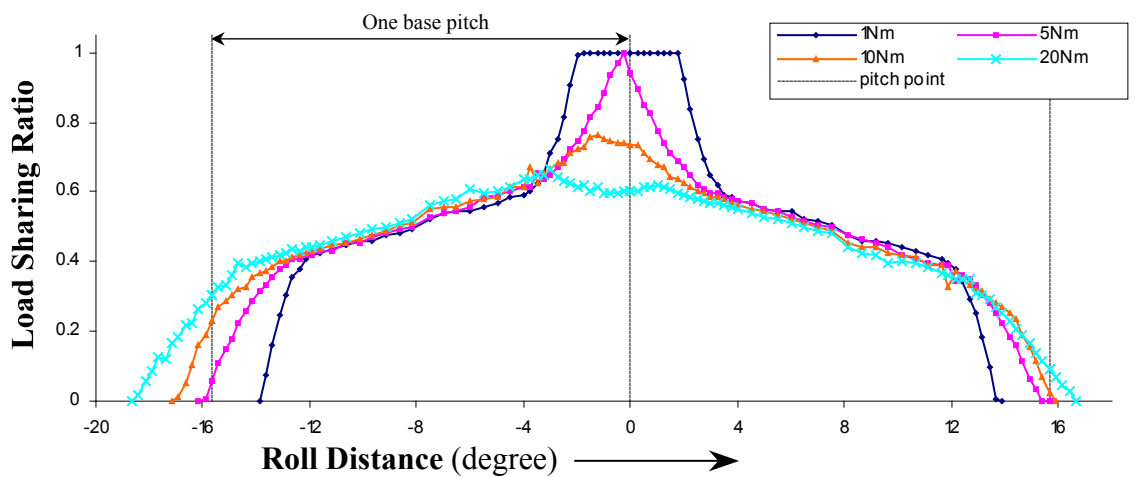
Figure 8.7. 13 The load-sharing ratio against input loads at temperature $160^\circ C$, Nylon (PA 6).
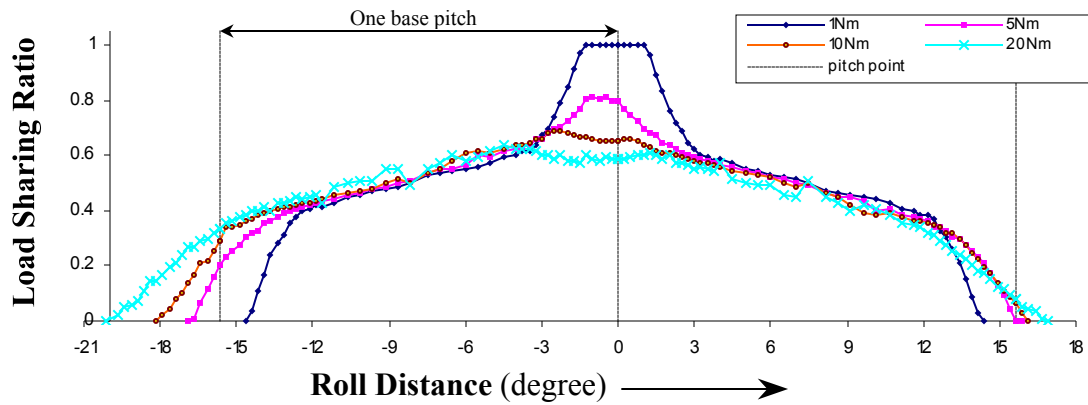
Figure 8.7. 14 The load-sharing ratio against input loads at temperature $180^{\circ}C$, Nylon (PA 6).

Results above have shown how quickly the tooth load share can change with the input loads at different temperatures. It is noted that when the curve of the load sharing ratio expands over one base pitch (it always happens at the approach case first), triple contact occurs and consequently the maximum tooth load share will be smaller than 1.

8.7.2 Load Sharing Ratio as Function of Temperature

It will be anticipated with the T.E. and the combined torsional mesh stiffness results, that the tooth load share will also be a function of temperature when the input load is stable. However, for different input loads, the temperature varying ranges are normally different. Those variations are shown in Figure 8.7.15 to 8.7.22.
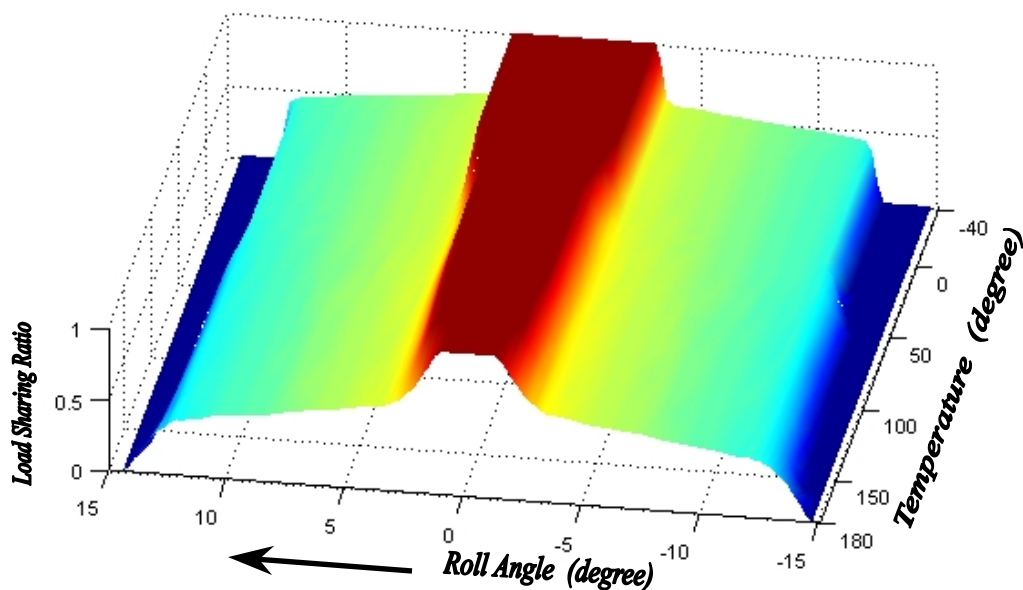
Figure 8.7. 15 Load-sharing ratio under 1 Nm input load against the full range temperature, Nylon (PA 6).
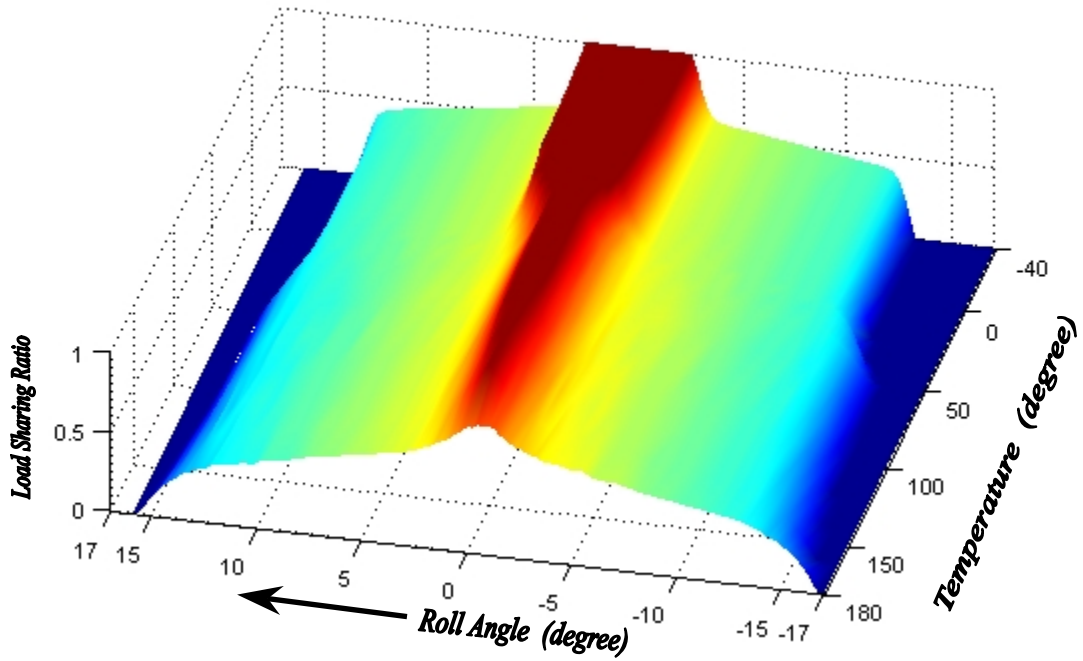
Figure 8.7. 16   Load-sharing ratio under 5 Nm input load against the full range temperature, Nylon (PA 6).
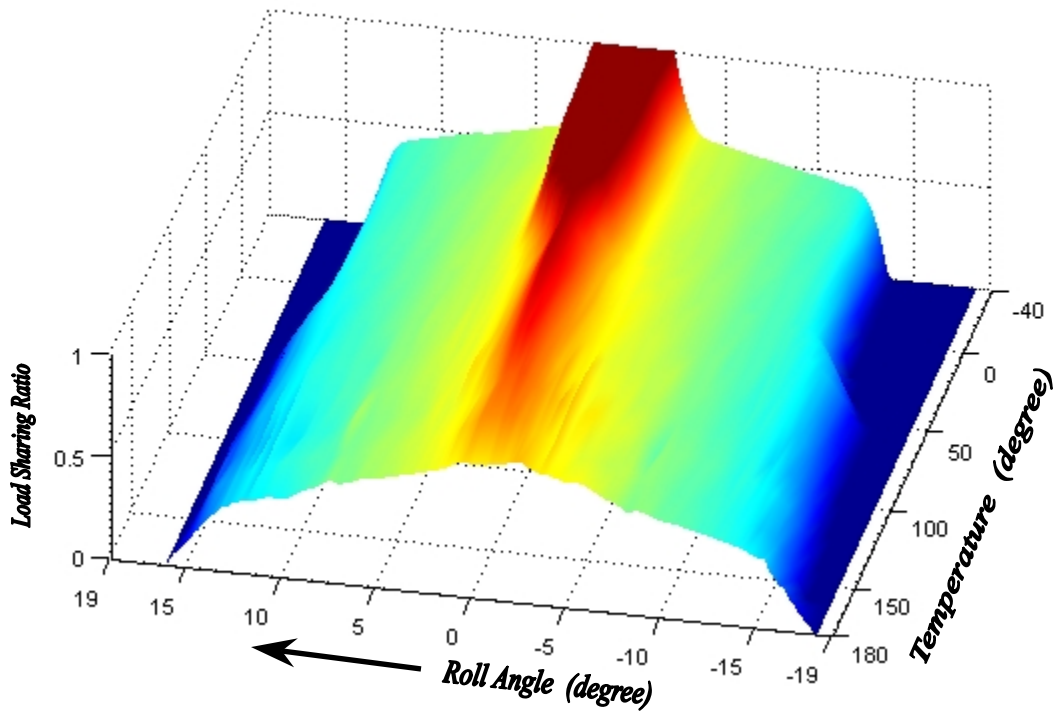
Figure 8.7. 17   Load-sharing ratio under 10 Nm input load against the full range temperature, Nylon (PA 6).
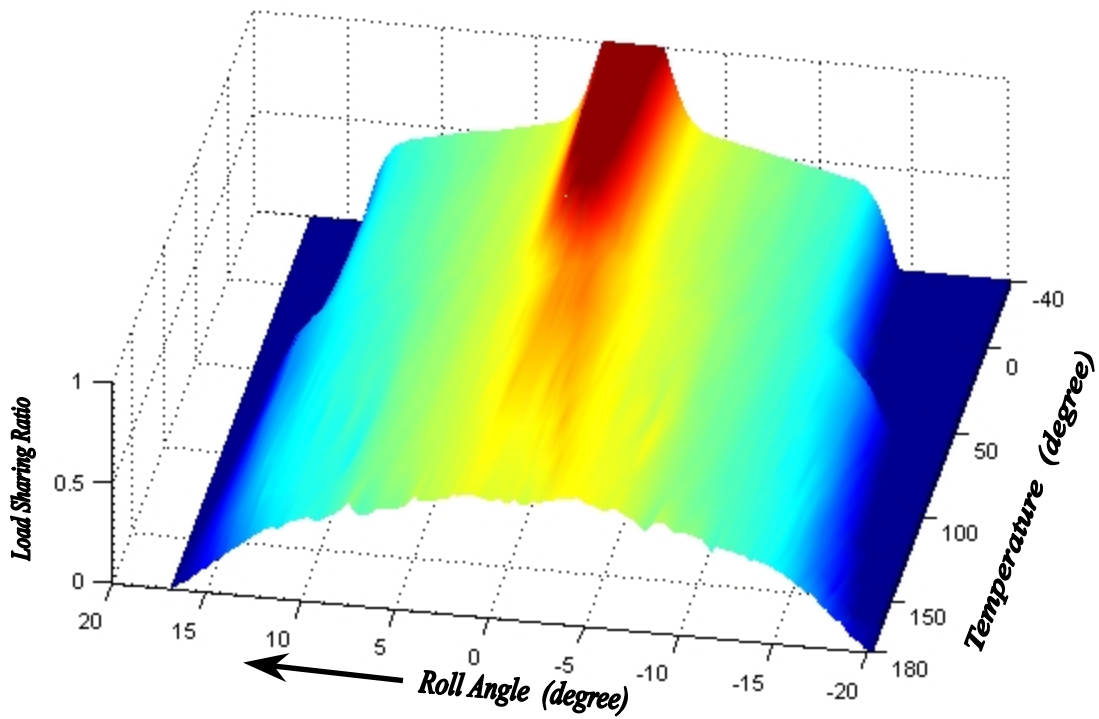
Figure 8.7. 18 Load-sharing ratio under 20 Nm input load against the full range temperature, Nylon (PA 6).
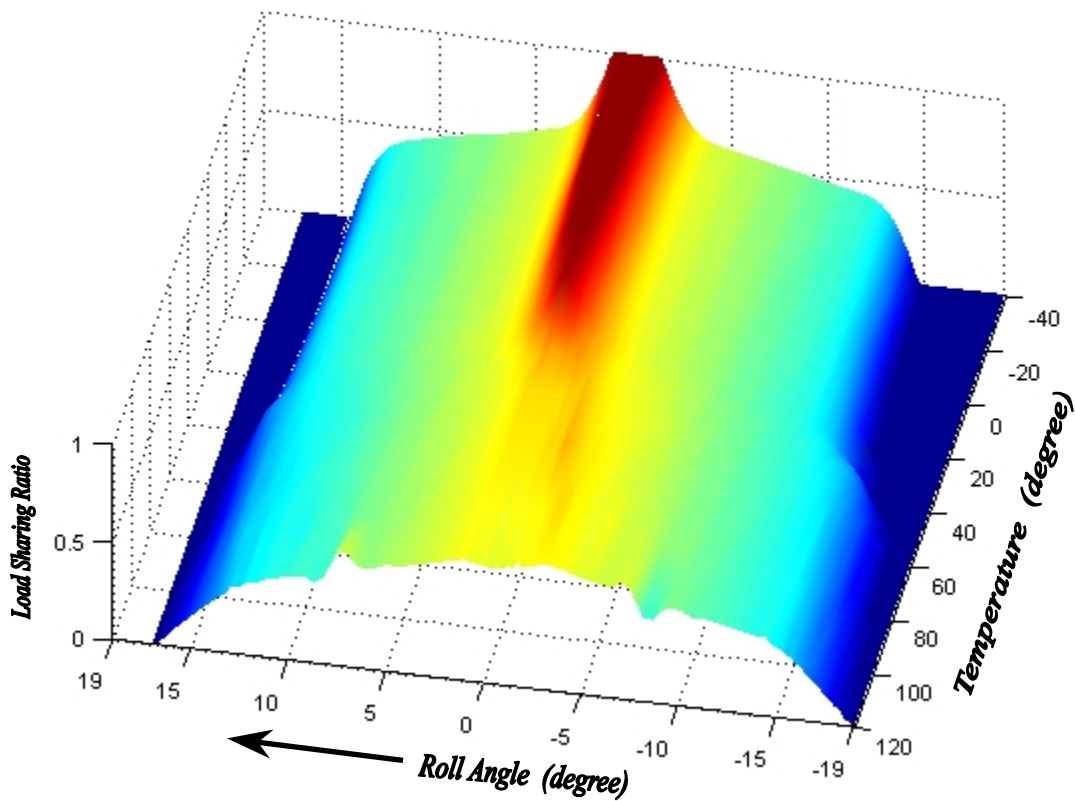
Figure 8.7. 19 Load-sharing ratio under 30 Nm input load against temperature from -40°C to 120°C , Nylon (PA 6).
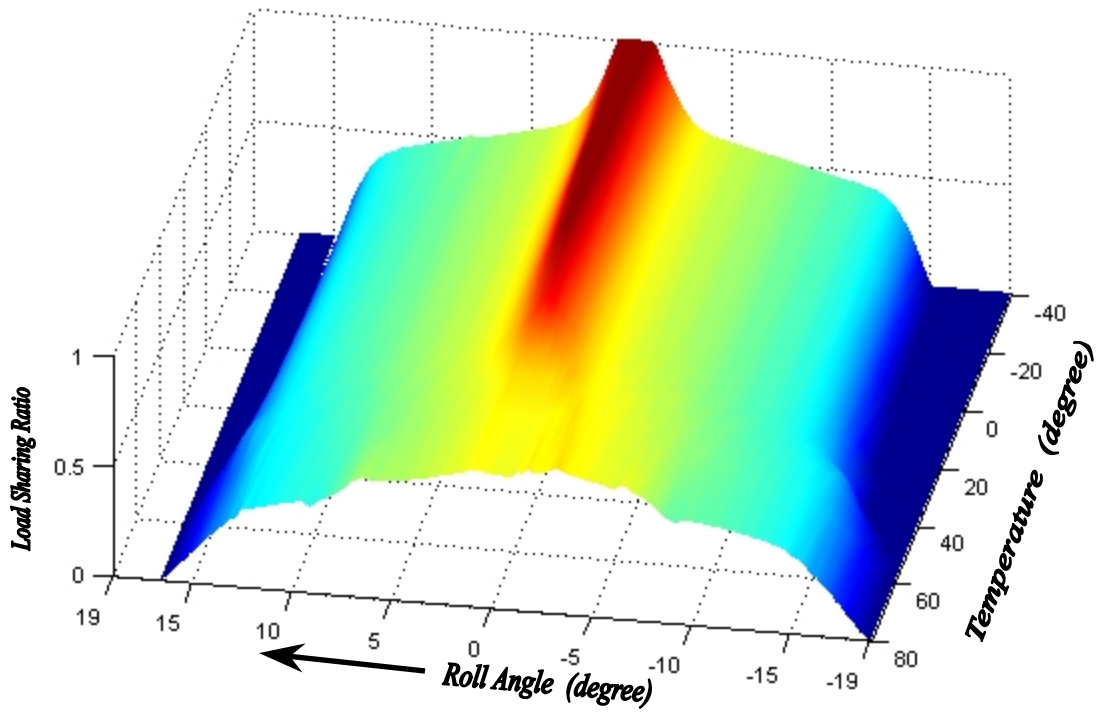
Figure 8.7. 20   Load-sharing ratio under 40 Nm input load against temperature from -40°C to 80°C , Nylon (PA 6).
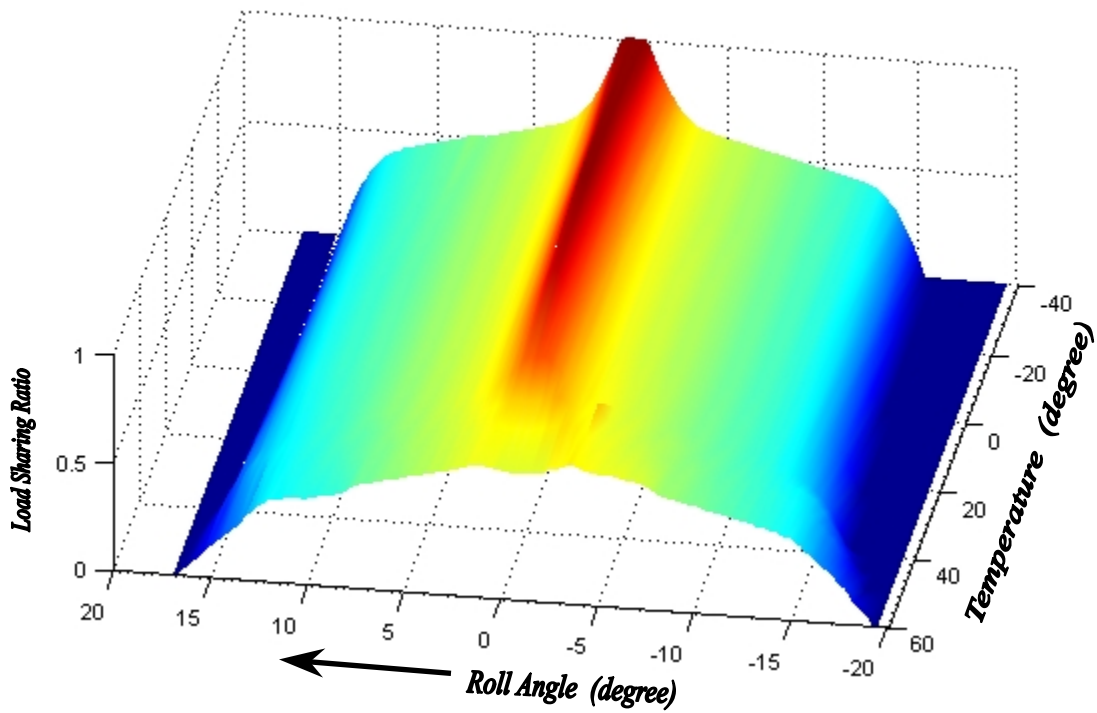
Figure 8.7. 21   Load-sharing ratio under 50 Nm input load against temperature from -40°C to 60°C , Nylon (PA 6).
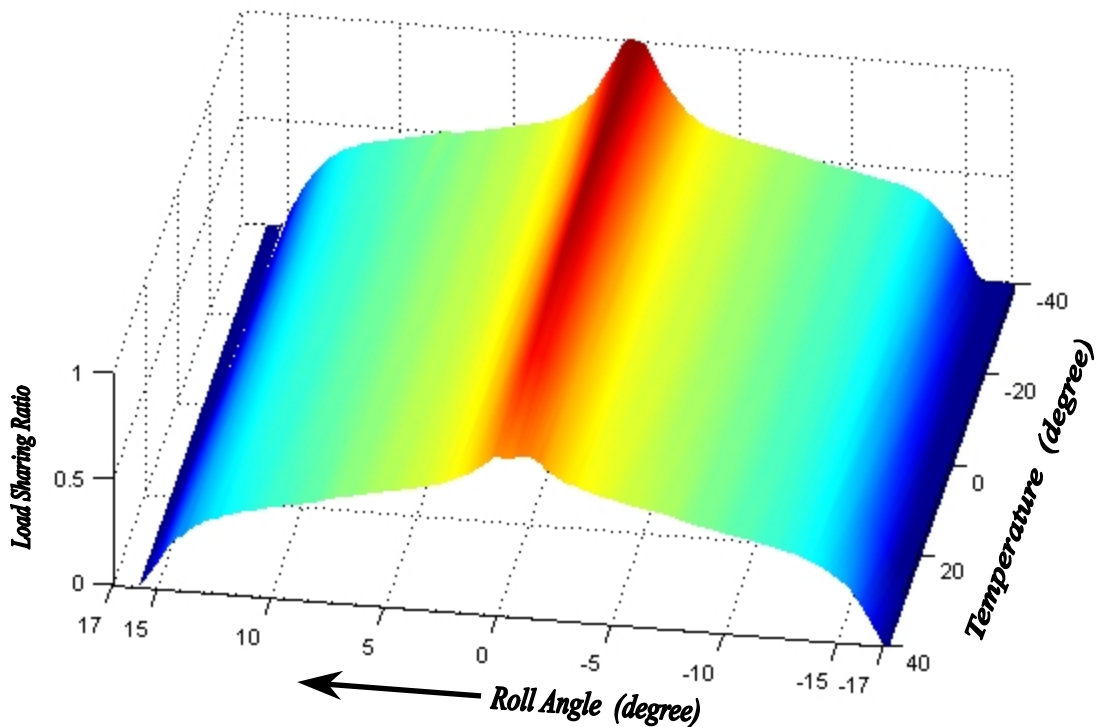
Figure 8.7. 22 Load-sharing ratio under 60 Nm input load against temperature from -40°C to 40°C, Nylon (PA 6).

Results above have shown that increasing temperature will result in tooth load sharing ratio variation in a similar way as the input torque did under a stable temperature. It is observed that the most dramatic changes occur about 50° C in most cases, and that is due to the nature of the material properties (Figure 8.3.1). The results also confirmed that within the ordinary range of temperatures, unlike the analysis for metallic gears, the behaviour of Nylon is dependent on the effects of both temperature and input torque.

8.7.3 About the Theoretical Tooth Load Share

If the gears are rigid, the tooth load-sharing ratio will not be influenced by the input load. In other words, there is only one curve of load sharing ratio for the meshing gears if they are totally rigid. For elastic gears in mesh, if the input load tends to be very light, the effect of elastic deformation can be ignored and the curve of the load sharing ratio will tend to that of the rigid gears in mesh. Theoretically, when the input load tends to zero, the curve of the load-sharing ratio will be independent of material properties, so that the metallic, non-metallic and rigid gears will all operate with theoretical tooth load share.

The research on the load-sharing ratio of involute spur gears can be found as early as the 1930's by Walker (Walker 1938). He presented the load distribution on rigid teeth as shown in Figure 8.7.23.
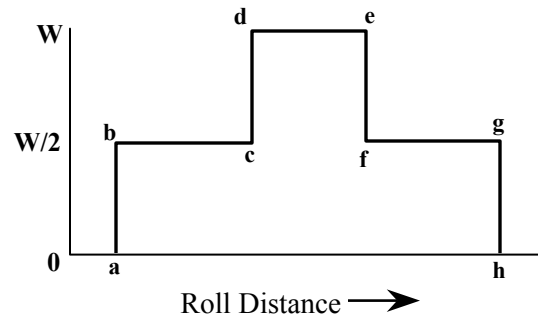
Figure 8.7. 23 The theoretical load sharing ratio (on rigid teeth).

The tooth load in the double zone bc or fg was exactly half of that in the single zone de. This figure is still predominant today, as it appears in many publications (AYEL 1984; Kuang 1992; Castro 1994; Walton 1994; Walton 1995; Sirichai 1996; Sirichai 1999; Yildirim 1999) and some important gearing handbooks (Maitra 1989; MAAG 1990). However, the proof for the load share ratio of rigid gears in mesh as shown in Figure 8.7.23 has not been found in the literature. For rigid gears in mesh, neglecting the friction at the contacts (in the double contact zone), it can be illustrated in Figure 8.7.24. The driving gear force balance equation can be given, assuming steady state conditions,

$$T - F_a \cdot r_b - F_c \cdot r_b = 0, \tag{8.1}$$

Which can be rearranged to give,

$$F_a + F_c = T / r_b. \tag{8.2}$$

Equation (8.2) shows that the sum of F_a and F_c remain constant in the double contact zone if the input load is stable. However, it seems no further information can be provided for the relation between F_a and F_c. So, Figure 8.7.23 seems to depend on the assumption of $F_a = F_c$ in the double contact zone.

The options for using FEA to prove the tooth load share of rigid gears in mesh are: (i) applying very light loads to find out the convergence curve as described in the beginning of this section and (ii) changing the modulus of elasticity to a very high value.
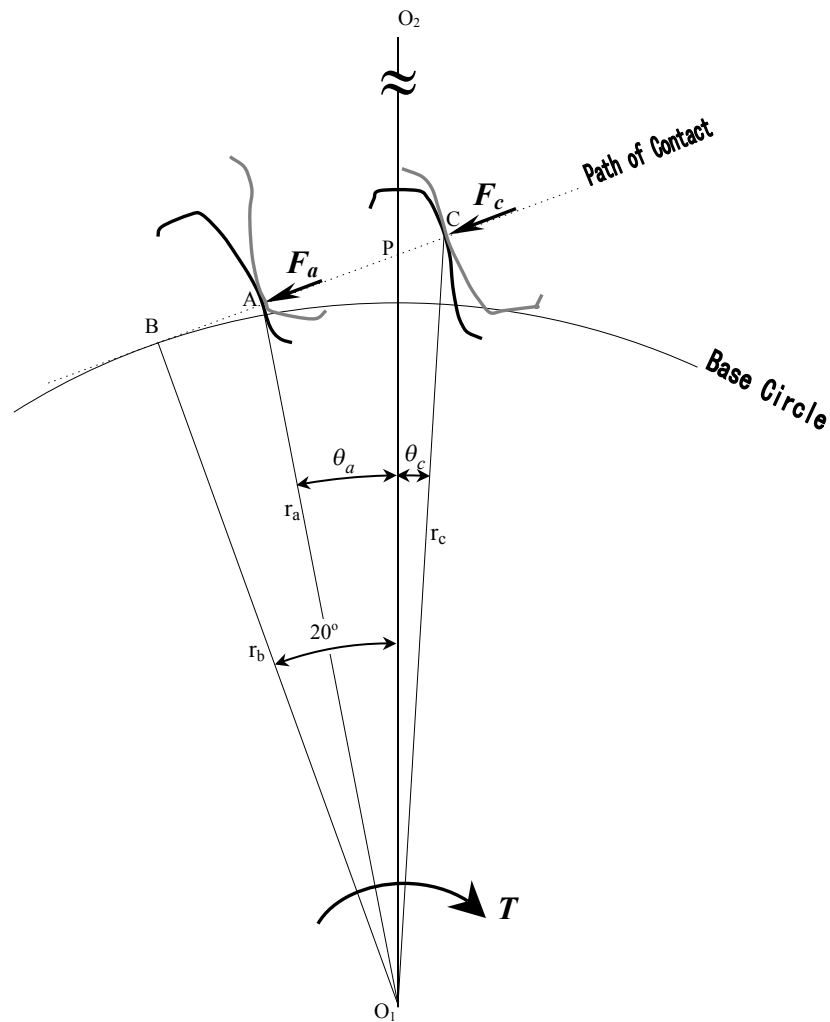
Figure 8.7. 24 Rigid gears (ratio 1:1) in mesh of double contact zone.

Firstly, the results were calculated for aluminium and nylon gears (PA 6 at 23°), both with 1 Nm input load and compared with the curve of Figure 8.7.23, as shown in Figure 8.7.25.

It can be seen, the major difference between the aluminium gears and the nylon gears are the curves in their handover regions, but they have very similar (common) double contact zones. Secondly, the input loads for the nylon gears were further decreased from 1 Nm to 0.01 Nm while the modulus changes according to Figure 8.3.1 from 23° C to 180° C were used. Results are shown in Figure 8.7.26.
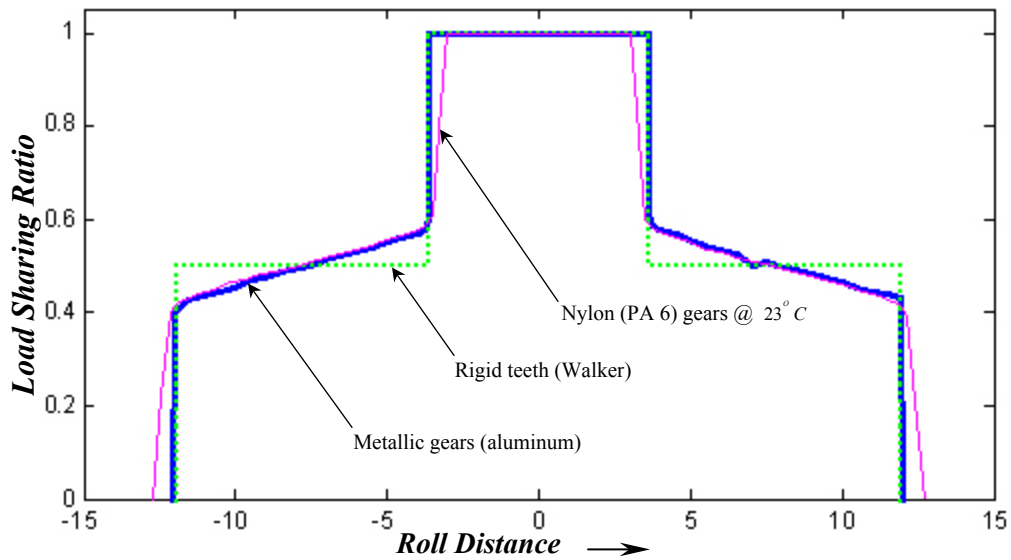
Figure 8.7. 25 With light load (1 Nm), the tooth load share of metallic and non-metallic gears are compared with that of conventional rigid teeth.
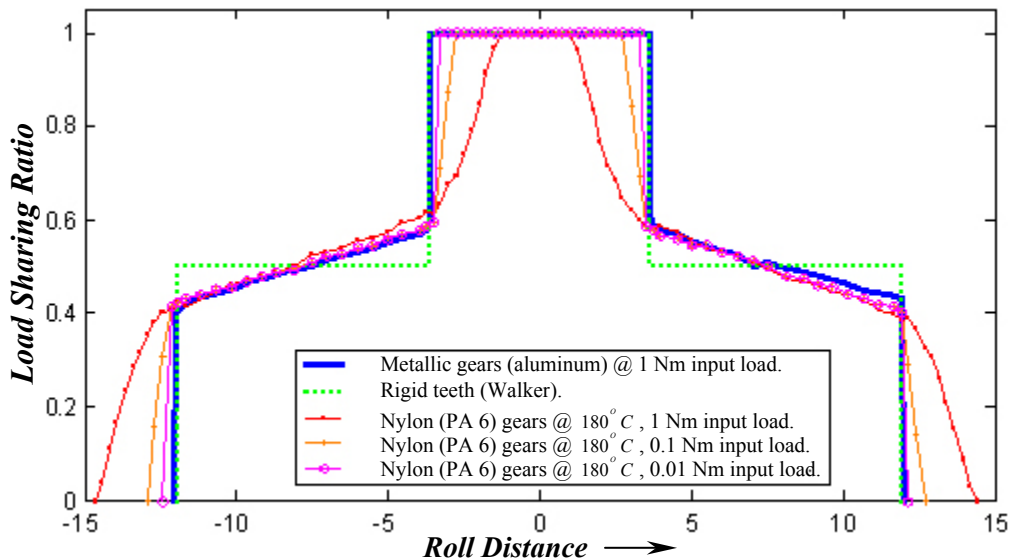
Figure 8.7. 26 The variations of the nylon gears.

These results show the difference with the curve of conventional rigid teeth in the common double contact zone compared to nylon gears with the lower modulus, but when the input load tends to the minimum, the additional difference will also tend to disappear. Finally, the result of the gears with higher modulus of elasticity (10^6 Gpa) is given and compared with that of aluminium gears (with 1 Nm input load) as shown in Figure 8.7.27.
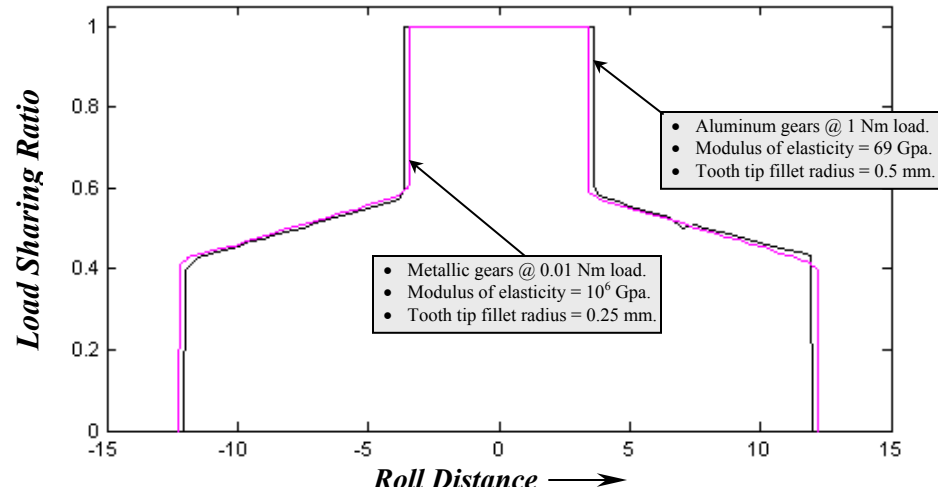
Figure 8.7. 27 The result of gears with higher modulus of elasticity.

The results above have shown that there is no possibility for the load-sharing ratio to become level over the double contact zone, so that the contact forces F_a and F_c will not tend to be equal. The magnitude of contact force seems to depend on the distance from the contact point to the hub centre, and the distance varies over the double zone almost linearly. The difference that can be observed in Figure 8.7.27 is in the contact ratio which increased from 1.536 to 1.564 due to the tooth tip fillet radius decreasing from 0.5 mm to 0.25 mm (the theoretical contact ratio 1.59 is based on the involute tooth profile without tip modification).

In conclusion, the theoretical tooth load share ratio should be produced by using FEA, if the input load were very light or the modulus of elasticity were sufficiently high and the tooth profile was of involute form. However, it can be very difficult to obtain the FEA solutions (in or near the handover regions) if, for example, there is no tooth tip fillet. More about the effects on tooth tip fillet radius can be referred to Appendix C where results of gears without tooth tip fillet are given, but the mesh density was higher than 100 thousand nodes.

Finally, a simplified theoretical tooth load share ratio can be produced, which is based on the theoretical contact ratio C_r (1.59), base pitch P_b (15.652 degree) and the assumption of the linear variations in the double zones, based on the FEA results, as shown in Figure 8.7.28.

228
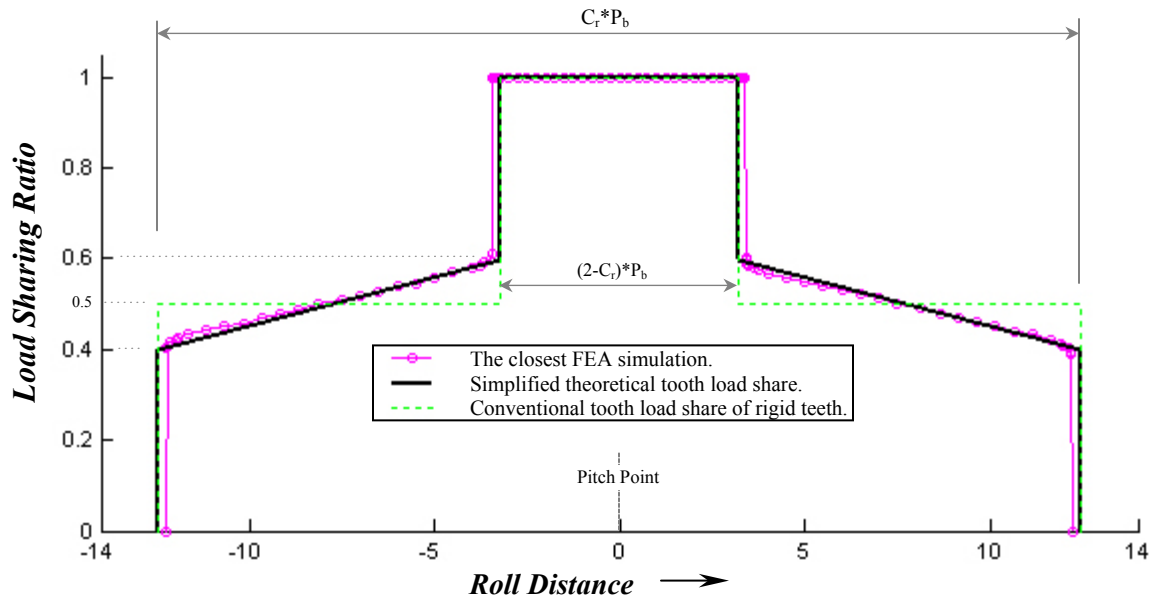
Figure 8.7. 28   The simplified theoretical tooth load share.

Actual applications may required minor FEA calculations to produce the curve of theoretical tooth load share ratio compared to the above simplified curve.

8.8   Optimal Tip Relief

The research has found that applying long tip relief can achieve a (very) low design load, and premature contact occurs when the input load is higher than the design load. In such a case, the design load will not increase significantly with a large amount of relief C_a, because the tipping has also weakened the tooth. This means over tipping (with long modification) can degrade the performance of the tooth. Nylon gears have naturally wider handover regions, higher damping and lower inertia, so long tip relief will not be considered necessary for general applications. On the other hand short type relief is very much needed to minimise the high stress that occurs at the premature contact (tooth tip) to prevent the friction coefficient increasing (see Figure 8.3.3), and consequently wear will be reduced as wear is the predominant mode of failure in the applications (Walton 1995).

The desired tipping should have the effect of model R5out12 of aluminium gears as shown in section 7.4.9. Model R5out12 has presented the longest short type relief; there is no rigid body motion when the rotation is over a complete mesh cycle. The effect of the

229

premature contact at the relief starting point S_1 (depend on the amount of C_a) is a minimum compared to other types of short relief. The more important fact is that the position S_1 only relies on the gear geometric parameters, so the S_1 of the aluminium gears is valid for the gears with different materials including nylon (PA 6). The analysis on such nylon gears has been carried out with three models with the third model being for the simulation of the commercially purchased nylon (PA 6) test gears. Tooth relief parameters of each model are listed in Table 8.1.

Parameters Model name	Ca		Ln		α (degree)
	Absolute value (mm)	Normalized value	Absolute value (mm)	Normalized value	
Model 1	0.0326	0.27	2.44	0.68	0.6
Model 2	0.0545	0.45	2.44	0.68	1.0
Model 3	0.2	1.67	2.49	0.69	

Table 8.1. Tooth relief parameters.

The form of the modified profile is the original involute curve rotated by 0.6 and 1.0 degree for model 1 and 2 respectively, and a straight line is used for model 3. More details about the test gears will be presented in the next section, and the further optimum form of the modified profile (using circular form) can be referred to Appendix E. FEA results are presented in Figure 8.8.1 to 8.8.8, with a temperature of 23° C.
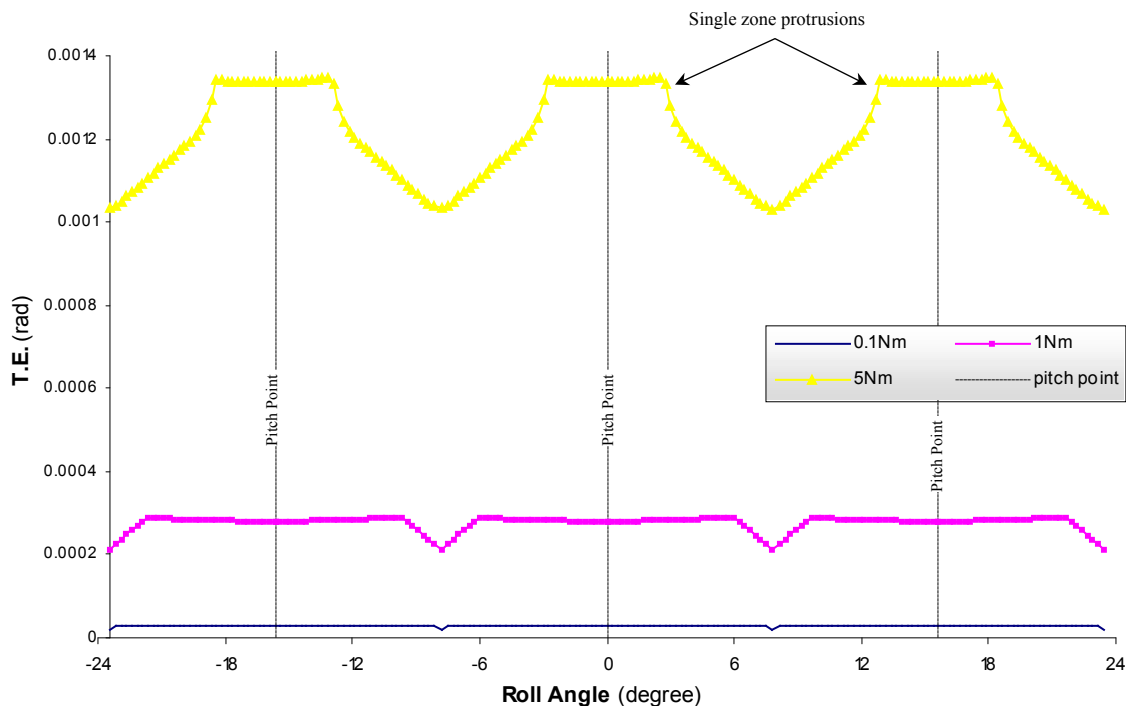
Figure 8.8. 1. The T.E. of model 1 with lighter input loads, Nylon (PA 6).
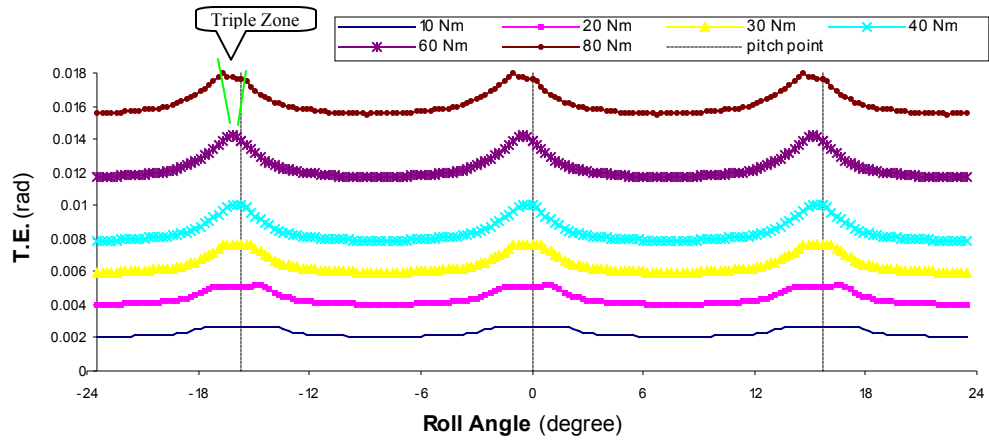
Figure 8.8. 2. The T.E. of model 1 with heavier input loads, Nylon (PA 6).
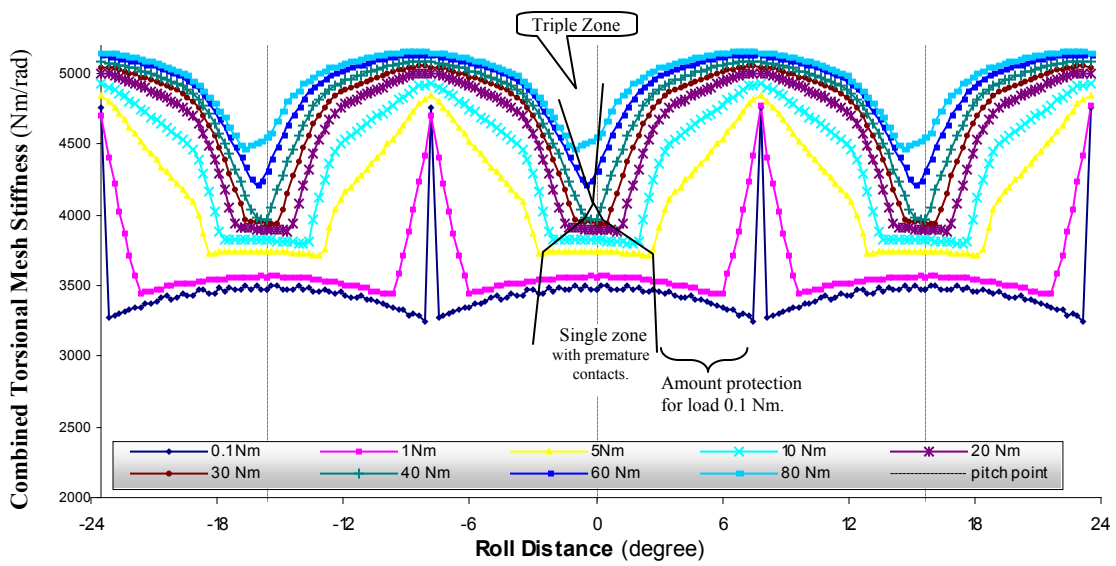
Figure 8.8. 3. The combined torsional mesh stiffness of model 1, Nylon (PA 6).
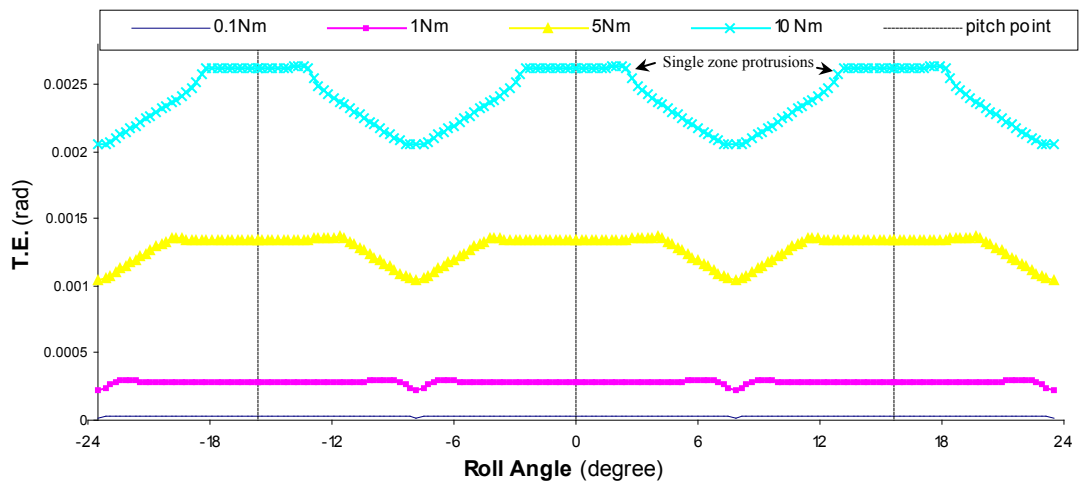
Figure 8.8. 4. The T.E. of model 2 with lighter input loads, Nylon (PA 6).

231
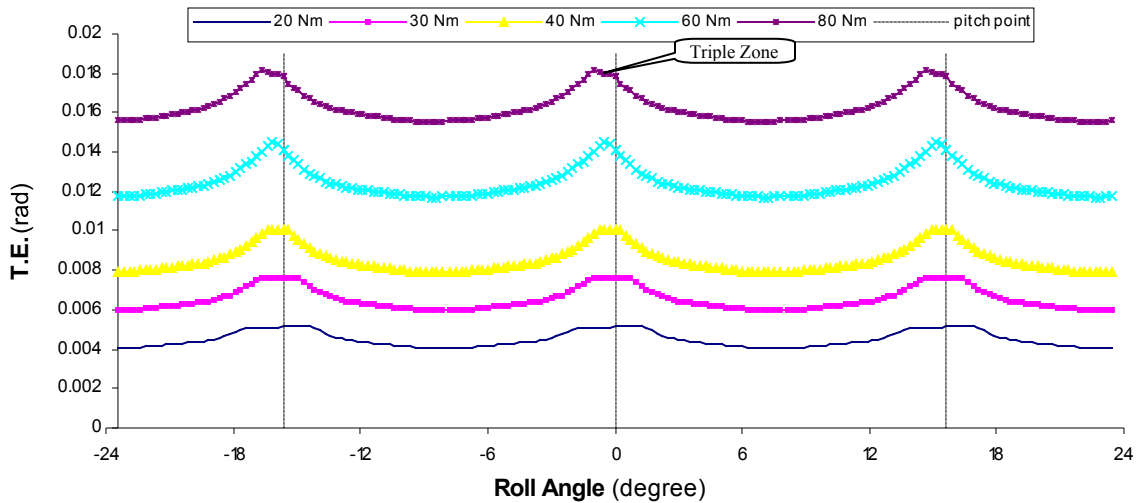
Figure 8.8. 5. The T.E. of model 2 with heavier input loads, Nylon (PA 6).
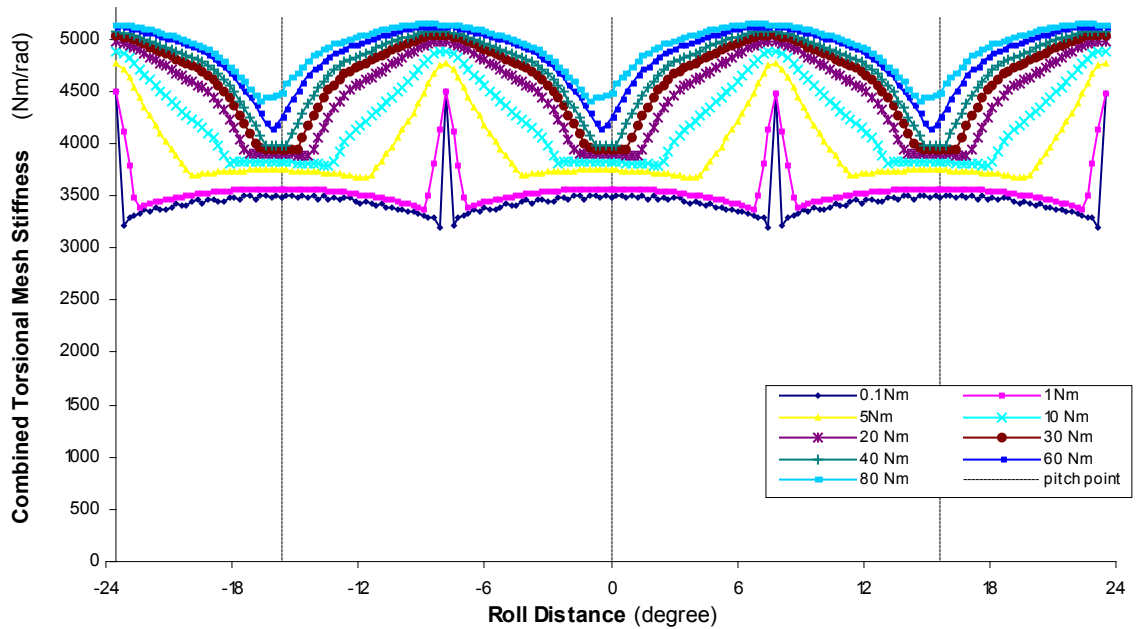
Figure 8.8. 6. The combined torsional mesh stiffness of model 2, Nylon (PA 6).

Results above have shown that the premature contacts have already occurred with the load of 5 Nm for model 1 and 10 Nm for model 2, by observing the protrusions of the T.E. curves. Even for model 2, the amount of relief is far from sufficient considering that the temperature could be higher. The amount of relief of model 3 was more than three times that of model 2 and 1.67 times the maximum allowance of current standards. With the simplest relief (straight line), model 3 presents the results as shown in Figure 8.8.7 and 8.8.8.
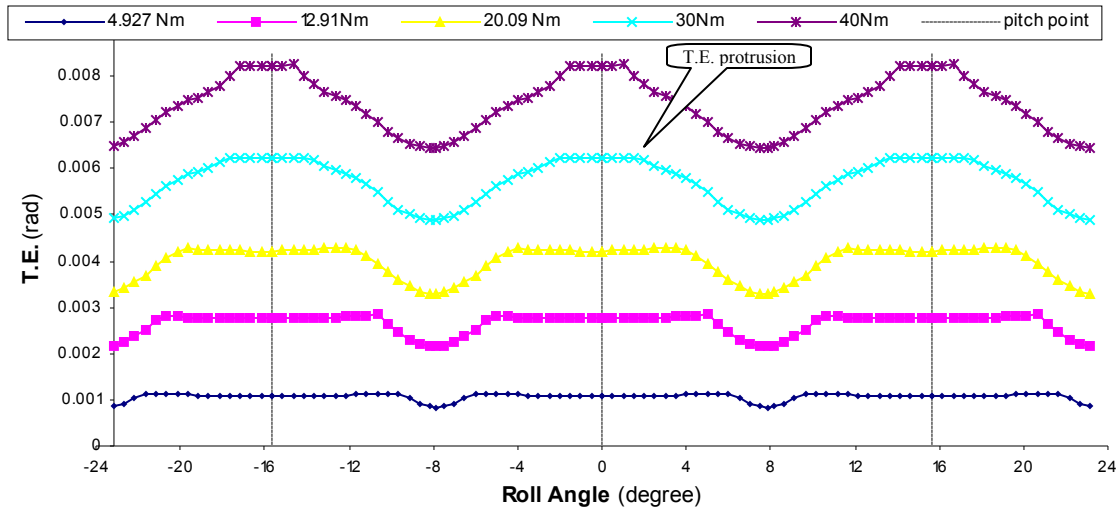
Figure 8.8. 7. The T.E. of model 3, Nylon (PA 6).
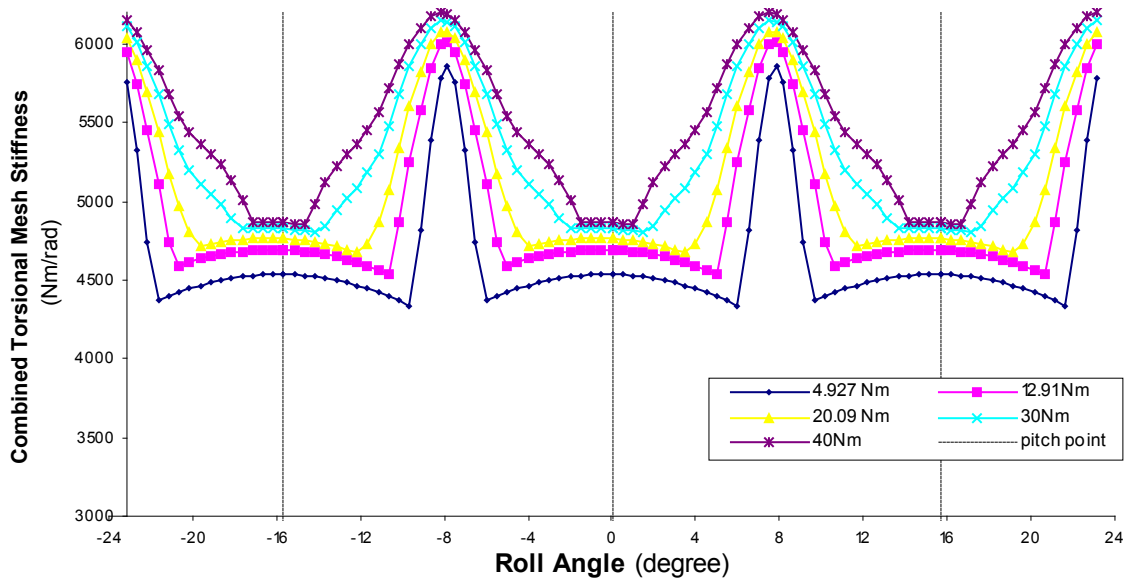
Figure 8.8. 8. The combined torsional mesh stiffness of model 3, Nylon (PA 6).

It can be seen that Model 3 has gained a wider load range, which is limited to 30 Nm at 23$^{\rm o}$ C. However, the maximum allowable load (30 Nm) can significantly decrease when the temperature is above 50$^{\rm o}$ C due to the nature of the material that has been presented in this chapter.

Model 3 was considered nearly to the limit of the amount of relief, as further increasing the amount of relief will lead to premature contact at the relief starting point becoming significant. Even if a circular form of tipping may improve the contact, the top contact (Munro 1999) may occur especially when temperature is high.

233

The benefit from the tip relief applied on the standard 20° pressure angle involute Nylon spur gears has been found to be limited by the load compared to that of metallic gears. The benefit will be further diminished considering the operating temperature influence.

8.9   Experimental Work

8.9.1   Introduction

This section presents data including previous results measured from a static test rig on aluminium gears (Sirichai 1999) and tooth profile inspections through a Higler – Optical projector (Barker 2002). All data produced for non-metallic gears were based on the commercial purchased nylon (PA 6) gears supplied by Hoffman Engineering, Perth. The nylon gears, however, were manufactured with "commercial standard" tip relief, the details and its inspections are presented in the next section.

8.9.2   Tooth Profile Inspection

Measurement of tooth profile error requires the highest accuracy possible. The traditional methods with a Hilger – Optical Projector proved to provide the highest accuracy out of the existing equipment at Curtin University of Technology, as shown in Figure 8.9.1. The optical projector works by producing a magnified silhouette of the object that can be measured or compared to a translucence master copy for a rapid gear examination, which is with the capabilities for coordinate measurements to an accuracy of 0.0001 in and angular measurements to one minute. The twenty-one data point inspection, divided the working depth into an equal number of increments, providing a sufficiently detailed analysis.

Some of the inspection results of the aluminium gears (manufactured at Curtin University and specified as in Table 4.1) are presented in Figure 8.9.2.
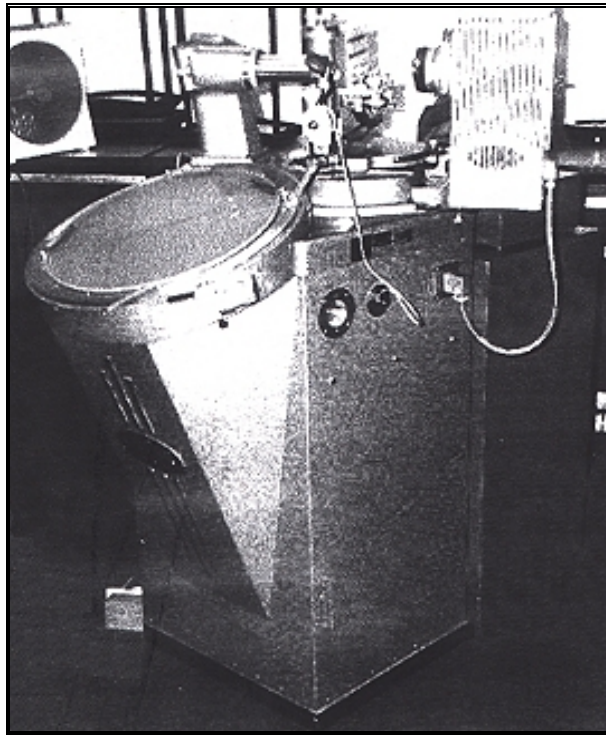
Figure 8.9 1 The Hilger – Optical Projector.
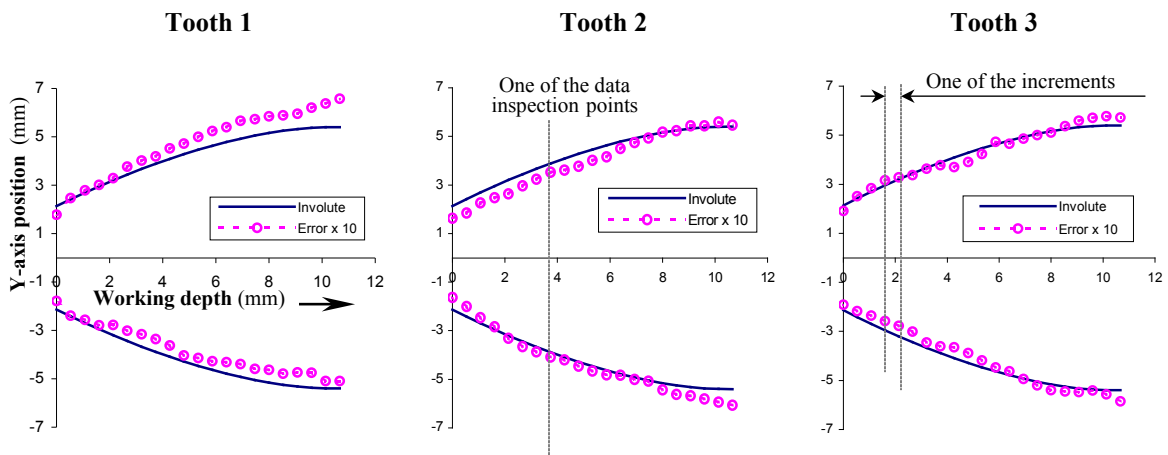
Figure 8.9 2 Comparisons of three aluminium gear teeth inspected using twenty-one data points to represent the measured profile (Error is the difference between the involute and the measured tooth profile observed in Y-axis direction).

Three typical tooth profiles have been presented, where the tooth tips are predominantly negative. The tooth tip results were partly due to the small fillet radius that may be reasonable. However, the profile error was indicated with a high level of waviness on both sides of the tooth flanks.

Except for the material property differences, the nylon gears are also specified as in Table 4.1, and a standard drawing was also provided to the manufacturer, however, the gears were obtained with a 'commercial standard' tip relief. The 'commercial standard' tip relief was given afterward by the manufacturer, as shown in Figure 8.9.3.

RACK PROFILE AS PER DIN 867(FEB 86)

Normal Module	Mn	-	25.4/DP
Pressure angle	α	-	20°
Fillet radius	pf	-	0.38 Mn
Tooth depth	hp	-	2.25 Mn
Gear addendum	hap	-	Mn
Gear dedendum	hfp	-	1.25 Mn
Pitch	P	-	π Mn

TIP RELIEF
Height δ la = 0.3 Mn
Relief Ca = 0.005 Mn.

NOTE: THIS PROFILE IS ALSO AS PER ISO 53 (1974)
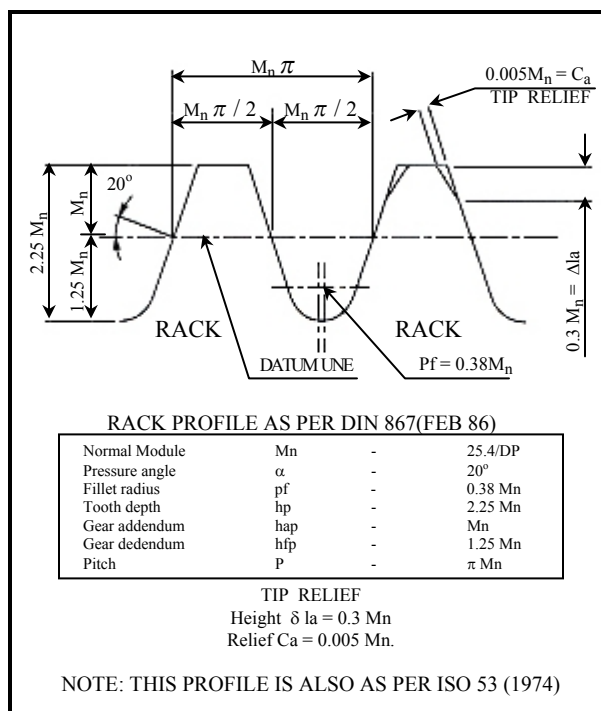
Figure 8.9 3   The manufacturer specified tip relief of the nylon gears.

The tooth profile inspections were focused on the comparisons between the true involute curve, the curve of the manufacturer specified tooth profile and the curve of the measured inspection. At each data point, errors were defined as the Y – axis position differences from the true involute curve and multiplied 10 times for clear display. Four typical inspection results of the nylon gear teeth are presented in Figure 8.9.4.

236
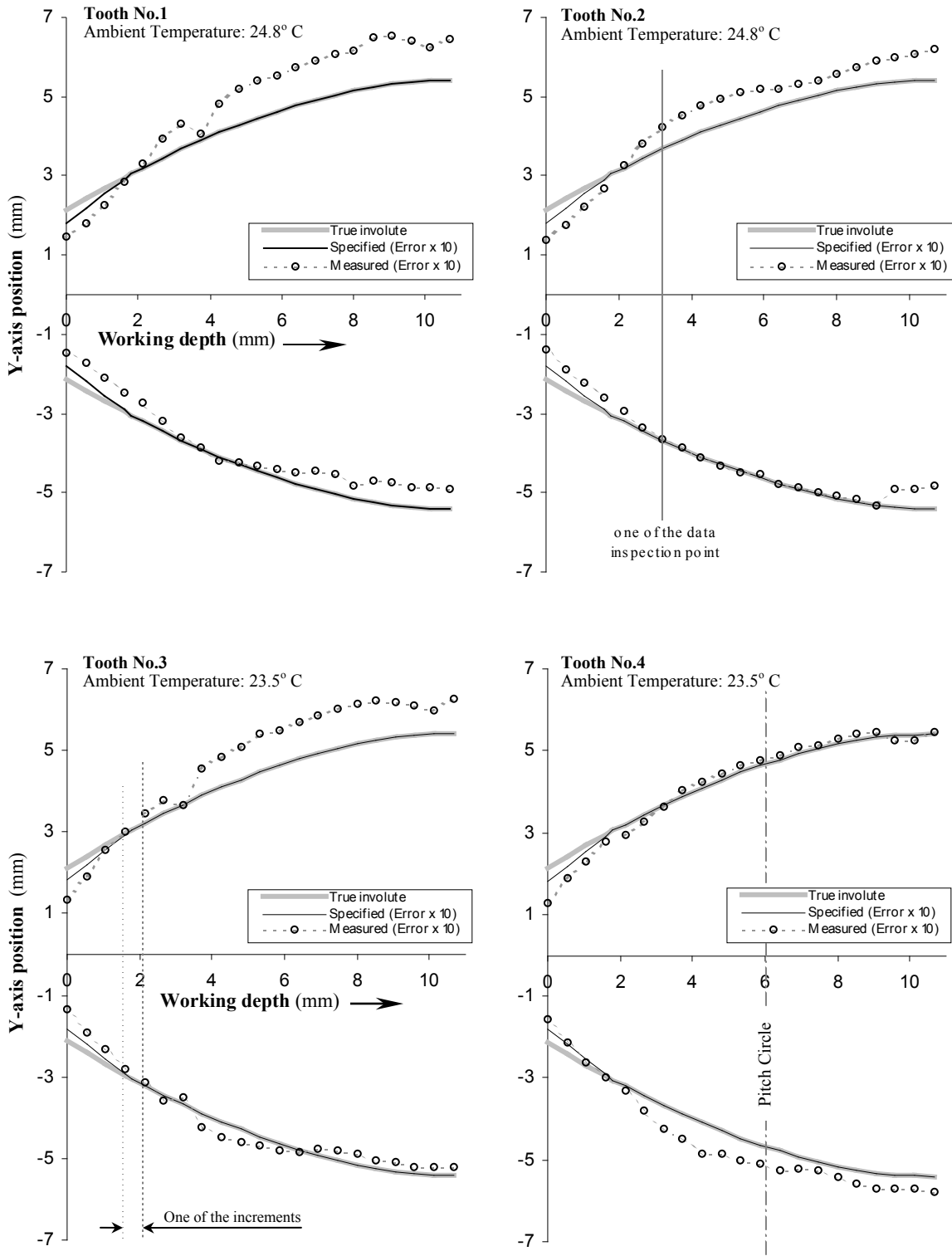
Figure 8.9 4 Comparisons of four nylon (PA 6) gear teeth inspected using twenty-one data points, the 'Error' of manufacturer and inspection results compared to the true involute.

As can be seen in Figure 8.9.4, the tooth errors are much greater than that of the aluminium gears. It is important to observe that the tip negative errors are more than twice the amount of relief C_a, which was specified by the manufacturer, and due to the actual tooth thickness at the pitch circle, the equivalent relief length L_n (same as the specified ΔL_a in Figure 8.8.3) will be greater than 0.3 M_n. These important features will be taken into account in the FEA simulations, in order to compare with the measurement of the static T.E.

8.9.3 The Measurement of Static T.E.

The measurement of static T.E. traditionally doesn't provide much detail over the mesh cycle, as for rigid structure(s) any errors will be incorporated into the total displacement, in which the elastic deformations are small. The detailed discussions have been presented in Chapter 7.

While steps have been taken to continue to improve the qualities of the test gears and the test rig assembly, the requirements for the rigidity of the shafts, bearings and the bearings supports (such as pedestals) may not have been fully realized. It has been found that the more rigid test rig will produce more accurate results, such as the test rig of the University of Huddersfield, UK, which is a few tonnes heavier than the one used in this research (as shown in Figure 8.9.5), and which has produced the classical results since Harris (Harris 1958).

The rigidity of the test rig is significant only when the test gear hub centre movements can be limited during the test. The analysis results in section 7.5 have shown that the centre distance movement of 0.005 mm will cause the measured T.E. to have a considerable error.

When gears mate with a single pair in contact, the local elastic deformation tends to occur predominantly near the contact teeth, while in the double contact zone, it will occur over the whole structure. Such a phenomenon plus the effects of other errors can cause slight variations in the centre distance especially when the support bearings are self-cantering.
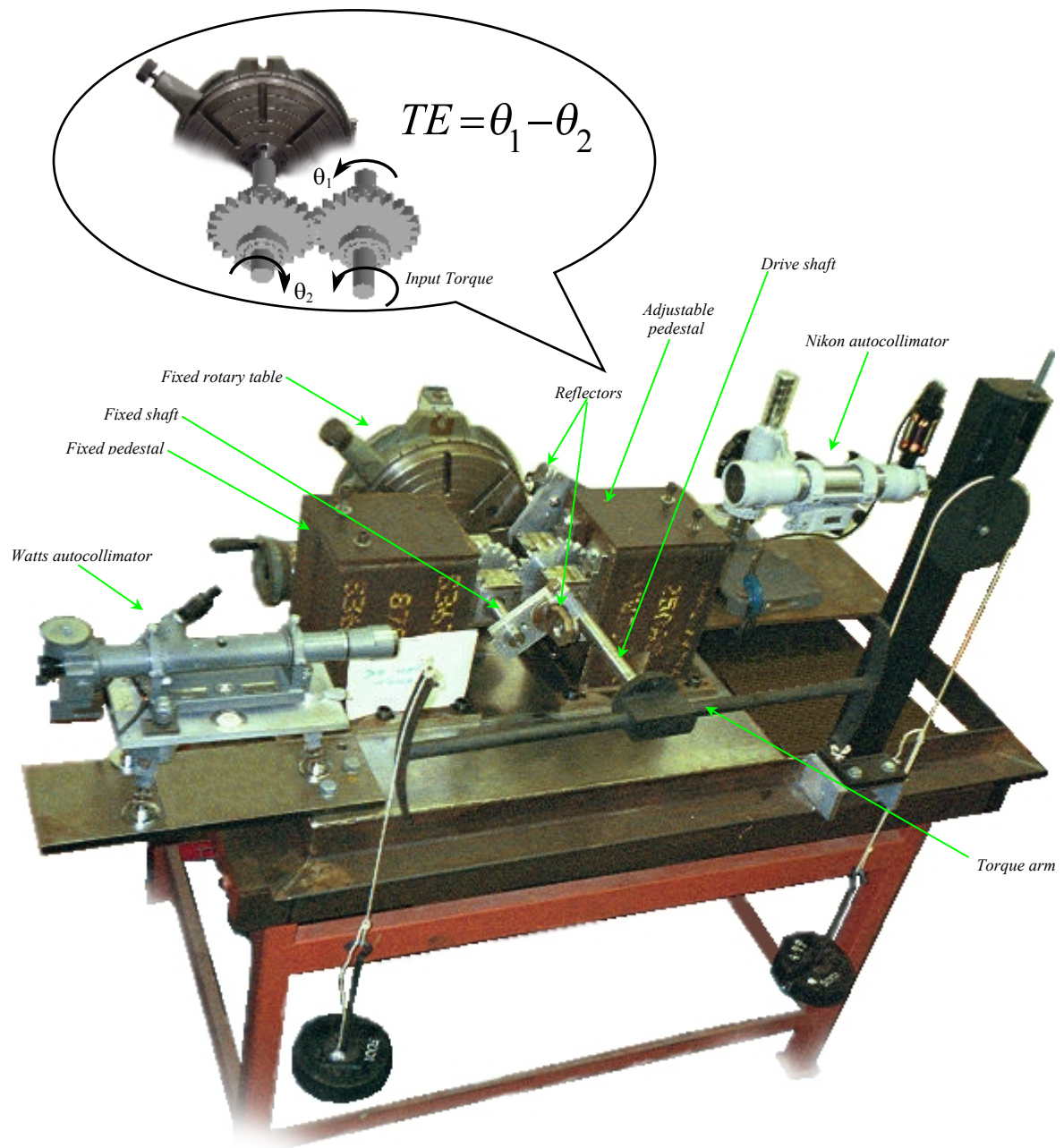
Figure 8.9 5 Illustration of the test rig components and static T.E. measurement.

The tests on the aluminium gears with the tooth profile errors as shown in Figure 8.9.2 have produced the following results: (i) *the torsional stiffness measurement*, which was carried out previously in Curtin University. It is noted that the driven gear was much stiffer than the driving gear and its hub was rigidly fixed (Sirichai 1999) as shown in Figure 8.9.6, so that the test result (as shown in Figure 8.9.6) was similar to the FEA simulated individual torsional mesh stiffness that was presented in Chapter 6.

239
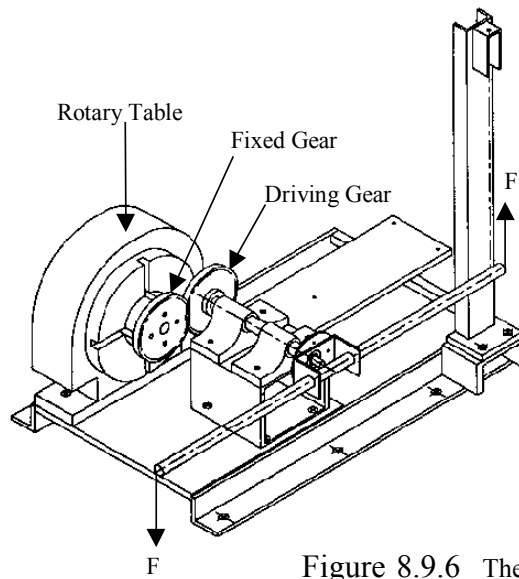
Figure 8.9.6 The torsional stiffness test rig lay out (Sirichai, 1999).
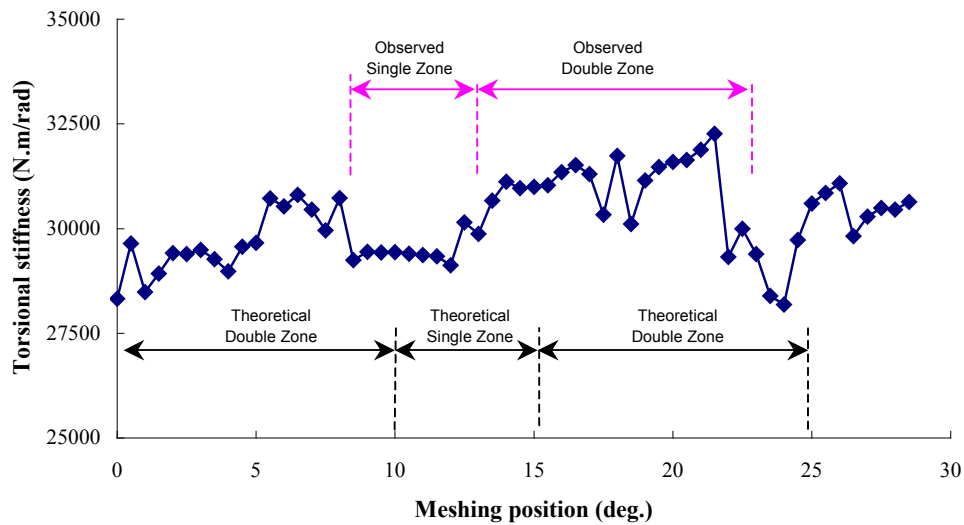
Figure 8.9 7 The torsional stiffness measurement of the aluminium gears (Sirichai, 1999).

(ii) *The static T.E. measurement,* which was carried with two identical aluminum gears on the test rig, as shown in Figure 8.9.5. The test results produced with the load 78.5 Nm are shown in Figure 8.9.7.

It can be seen that the measured T.E. did not present quality data for the research, due to the effects of the profile and testing errors which largely over ride the deformations of the gears themselves. The T.E. measured at point A, as shown in Figure 8.9.8, was due to the negative tooth (tip) profile errors and shows a similar effect of a short tip relief. It has been proven that increasing the load did not achieve an improvement in the results. Comparison

between the test (i) and (ii) will show how the rigidity changes on the gear hub can affect the tests result and it has been explained in the beginning of this section. However, the developed test rig (Figure 8.9.5) is well suitable for non-metallic gear tests.
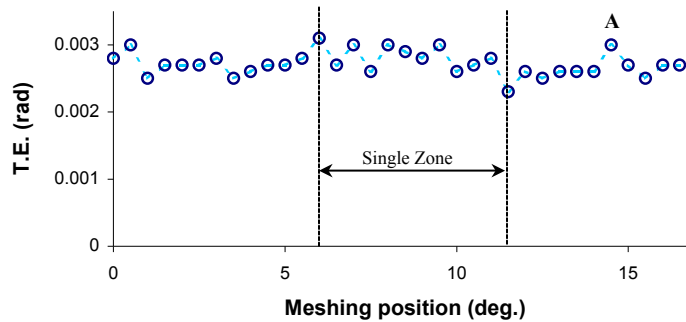
Figure 8.9 8   The static T.E. measurement of the aluminium gears (Barker 2002).

The tests on the nylon gears with the tooth profile errors as shown in Figure 8.9.4 have produced a better result compared to that of the aluminium gears, even though the profile errors are larger. This is due to the increased material flexibility; where the chaotic conditions at contact(s) have been reduced (larger contact area) and the major elastic deformations will predominantly take up the total displacement under a considerable heavier load. In order to conduct FEA modelling of the gears with the inspection measured tooth profile (Figure 8.9.4), the relief parameters have been carefully chosen, as shown in Figure 8.9.9.
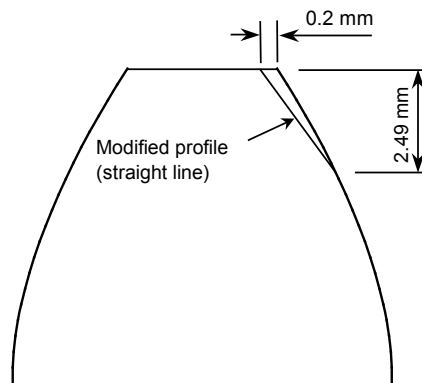
Figure 8.9 9   The tooth form to simulate the measured tooth profile.

The experimental results of static T.E. measurement under a series of input loads at temperature 20° C are shown in Figure 8.9.10, and the comparison with FEA simulation is also made, but the simulation can only be carried out with the temperature 23° C, Figure 8.3.1.
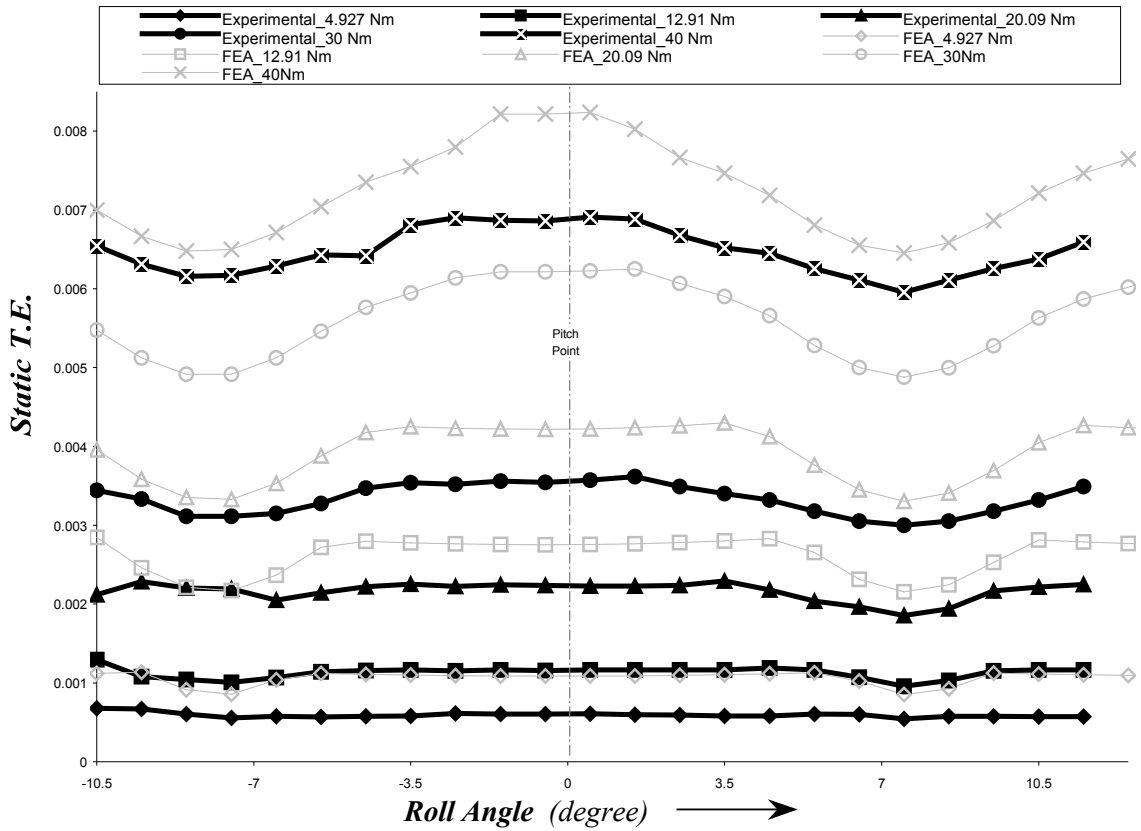
Figure 8.9 10   Experimental and numerical results.

In observation of Figure 8.9.10, the experimental data shows a stiffer material than the actual gears by their magnitude and curve shape. The error analysis at each data point was calculated by,

$$Relative\ Error = \frac{\left|T.E._{FEA} - T.E._{Exp.}\right|}{T.E._{Exp.}} \times 100. \tag{8.3}$$

Figure 8.8.11 gives an overview of the relative errors.
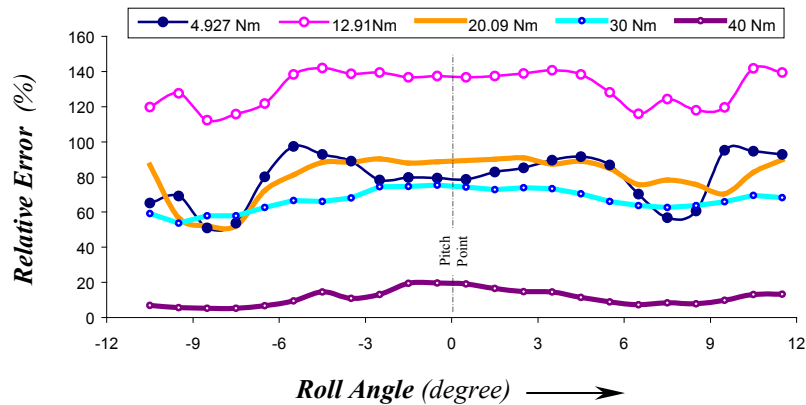
Figure 8.9 11   Relative errors between the experimental and numerical results.

242

When the input load is 40 Nm the relative errors are between 5.2 % and 19.75 %, but in most load cases the relative errors are considerable larger, between 50 % and 80 %. However, the largest errors occur when the load is 12.91 Nm, between 110 % and 140 %. In spite of the tooth profile errors, this shows the non-linear FEA modelling has not matched well to the actual material behaviours. As discussed in section 8.3, this is often the case for non-metallic gears.

The comparisons of the load – deflection behaviours of the structure produced the combined torsional deflections (T.E.) as a function of the input loads at mesh position 0.5 degree (single contact zone) and 7.5 degree (double contact zone) as shown in Figure 8.9.12, and shows the major reason for the large errors.
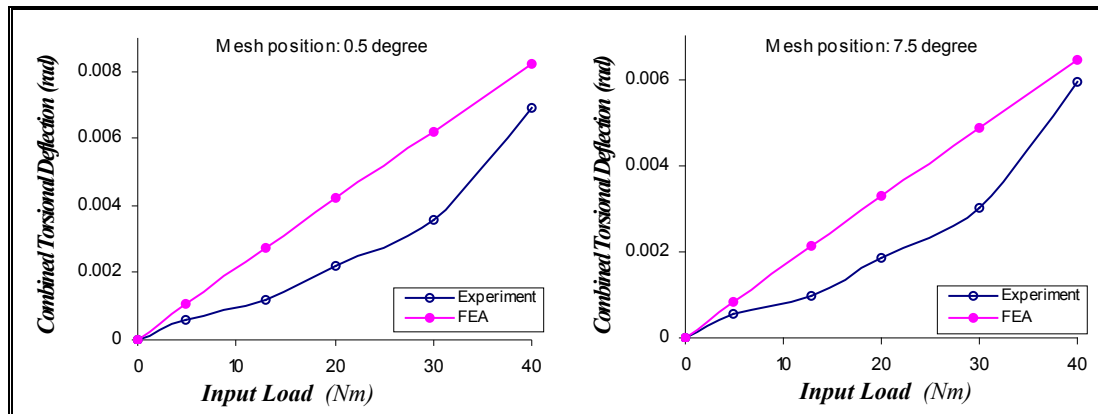
Figure 8.9 12   The deflection vs. load relationships at mesh position 0.5 and 7.5 degree.

8.10   Conclusions

This chapter has presented general finite element formulations of the change over process of the 20° pressure angle standard non-metallic (PA 6) involute spur gears in mesh. The results of the change over process have taken into account static T.E., combined torsional mesh stiffness and load sharing ratio, as solved by using the ANSYS® non-linear material MELAS option.   Those formulations, presented as functions of both input load and temperature, demonstrated the major characteristics of large tooth deflection, the triple contact caused by the large elastic deformation and the significant difference between tooth mating approach and recess cases. As a consequence of heavy load (torque, temperature or the combination), tooth load sharing can be widely expanded covering more than a

243

complete mesh cycle with more teeth come into the contact zone (triple contact) so that the gears will be running smoother (with smoother T.E. and stiffness), however, the excessive wear will then take place and subsequently reduce the gear service life.

The detailed variations of the contact ratio and the handover regions have been obtained and comparisons between the results of the metallic and the non-metallic gears have been provided. Experimental results have further confirmed the major variation trend of the static T.E.

One of the important conclusions, involving previous tests on the aluminium gears, is that the rigidity of the lateral movement constraint on the test gear hubs is most critical for a metallic gear test rig. Within normal industry manufacturing standards, there will be a considerable pitch and tooth profile error, as shown by the tooth inspections, but as long as the lateral movements can be limited, the major trend of test results will be obtained. Otherwise, there is no point to purchase expensive precision test gears.

The related error analysis also indicates several possibilities for improving the accuracy of both numerical and experimental results. In particular, it is critical for further numerical research that more realistic material properties are obtained for non-metallic materials.

Finally, the investigations of the tip relieved gears in mesh have shown that standard 20° pressure angle nylon gears have a limited range of load and temperature to prevent excessive wear. It can be expected that the power-weight ratio will not be significantly improved unless an improvement can be gained on the material properties (such as using fiber composite materials). This indicates that the application of non-metallic gears should not follow that of conventional metallic gears, and requires more efforts on the design according to its own characters. A high-pressure angle involute spur gear has been recommended by Seager (Seager 1975) because it is consistent also with low sliding speed and high tooth strength. Recent experiment work on high-pressure-angle nylon gears has achieved considerable success by Prof. D Walton, (Walton, 1995). A related FEA of high-pressure angle nylon gears can be referred in Appendix E.

CHAPTER 9

CONCLUSIONS AND FUTURE WORK

9.1   General Conclusions

This thesis has presented the development of a numerical approach for predicting the characteristics of involute spur gears in mesh for various combinations of load and temperature for metallic and non-metallic materials. The numerical models were formed over the complete mesh cycle providing detailed information of the change over process as teeth enter and leave the contact region. Various items of interest for involute spur gears were investigated including profile modifications, localised tooth cracks, and non-linear material behaviour for non-metallic gears.

The major thrust of the study has been the development of efficient and reliable numerical solution techniques using automatic mesh adaptation with contact and the element birth and death option. This included a fundamental study on the effect of plane strain and plane stress elements. The numerical approach enabled the development of a software program based on the software package ANSYS$^{®}$ to predict the effect of the gears on torsional mesh stiffness, transmission error and load sharing ratio, and provided basic information for condition monitoring and optimal gear design.

(i)   Plane strain vs. plane stress

A wide range of FEA problems are often solved with 2D assumptions because of the greatly increased computational efficiency and reduced cost. However, when the

numerical analysis involves non-linear factors such as contact, fracture or other extreme load cases, the valid 2D assumptions can be restricted to a very narrow range. A large number of FEA models and calculations were made for the investigations. The comparisons concentrated on the torsional stiffness, first maximum principal stress and stress intensity factors that were obtained under assumptions of plane stress, plane strain and 3D analysis. With the conclusion of this research, errors were found in the literature of previous research studies, especially when 2D assumptions were used with solid gears. The understanding of these results has helped to avoid large errors in the analysis.

(ii) Mesh adaptation with contact

The accuracy and the efficiency of the developed numerical models have provided the numerical results with more details of the change over process than previously obtainable, and this has proven to be an important basic tool in the numerical analysis of gears in mesh. The extension onto 3D models (using brick elements) shows great potential in analysis of all types of gears.

(iii) Element birth and death option

When the involute tooth profile modification presents a negative (or partly negative) tooth profile, the numerical solution will have instabilities. The element birth and death option has been proven to be one of the practical solution methods, which ensure the numerical results are accurately incorporated into the rigid body motion and the elastic deformation.

(iv) Handover Regions

The handover region of involute spur gears can include both the approach and recess cases, and it generally exists when gears are considered elastic. It is a key component of gear behaviour that can be found in the combined torsional mesh stiffness, transmission error, load-sharing ratio, ratio of local deformation and even in the individual torsional mesh stiffness characteristics. In particular, the handover region of the static T.E. represents the TE $_{o.p.c.}$ In previous research, the theory and evaluation methods of TE $_{o.p.c.}$ were developed mathematically (geometrical analysis), and they were found to be suitable for gears with geometrical errors. However, some confusion may arise when one attempts to apply the

theory and the methods to elastically deformed gears. The numerical evaluations presented in this thesis may be one of the alternative solutions.

(v)   Tooth profile modifications

The research on tooth profile modifications has presented the effects on the transmission error of various types of profile modifications including short, intermediate, long and excessively long profile modifications with the results illustrated using the Harris Map. The critical relief starting points S_1 and S_2 were defined as major aspects of the profile modifications. S_1 denotes the relief midway between the short and long tooth profile modifications, producing a T.E. curve (in a mesh cycle) consisting of a single zone, handover region and a point of double contact so that when the load tends to zero, the handover region disappears and the contact ratio decreases to 1. Significantly with this relief, the contact stress near the tooth tip has been minimised (Appendix D), to yield the important optimal tooth tip-relief providing improved tooth flank surface protection.

The critical relief starting point S_2 was defined for long tooth profile modifications. Relief with the starting point S_2 will produce a T.E. curve at the design load smoother than others (no protrusions), but when the input load exceeds the design load premature contact will immediately occur. On the other hand, if the relief starting point extends beyond S_2 (relief is too long) there will be constant T.E. protrusions due to rigid body motion occurring in both the single and double contact zone, and premature contact can easily occur. With the critical relief starting points S_1 and S_2, a range of long tooth profile modifications can be developed.

Further development on the tooth profile modifications included the tip-relief (short) on standard 20° pressure angle nylon gears (chapter 8) and 30° pressure angle nylon gears (Appendix). Although the optimal tip-relief was proven to be valid for non-metallic gears, the effects on 20° pressure angle nylon gears have further confirmed its disadvantages due to the excessive large deflection under high torque and temperature conditions. Applying the optimal tip-relief on 30° pressure angle nylon gears has effectively reduced the contact stress near the tooth tip so that the reduction in surface wear can be achieved, especially when a circular form was used as the modified tooth profile.

Finally, the development on tooth profile modifications involving high contact ratio gears in mesh was presented (Appendix C). The results have shown that the current standards are not well suitable for the applications of HCRG. The optimal (short) tip-relief of HCRG was found to be critical, where any other relief length above the optimal tip-relief length will result in the contact ratio decreasing below 2, hence losing (part or full of) the benefit of HCRG.

(vi)   Analysis of non-metallic gears

General finite element models of involute spur gears using non-metallic (PA 6) materials have been formulated. The models investigated the details of the standard 20° pressure angle change over regions for the static T.E., combined torsional mesh stiffness and load sharing ratio, produced by using ANSYS$^®$ non-linear material MELAS option. Those formulations, presented as functions of both input load and temperature, demonstrated the phase change of the major characteristics and the triple contact that can be caused by the large elastic deformation and the significant difference between tooth mating for the approach and recess cases. As a consequence of heavy load (torque, temperature or the combination), tooth load sharing can be widely expanded covering more than a complete mesh cycle with more teeth come into the load sharing (triple contact) so that the gears will run smoother (with smoother T.E. and stiffness). However, excessive wear may then take place which is one of the major concerns for the gear service life. Tip-relief has been found to have little effect on such a case, and the requirement for adapted gear design to such characteristics was outlined.

The related error analysis also indicated several possibilities for improving the accuracy of both numerical and experimental results. In particular, it was noted as being critical for further numerical research that more realistic material properties are obtained for non-metallic materials.

(vii) Condition monitoring gear system using high order strain measurement

Perfect involute gears in mesh along with an input shaft have been analysed. The elastic strains on the surface of the shaft near the gear hub have been found to vary in form with the transmission error over the mesh cycle. It has been recognized that the elastic strains

have more capability to reveal the details of the gear-shaft system if the measurements were obtained from both input and output shafts. This investigation has shown that the presence of a root crack changes the strain measurements on the shaft. The changes in the shaft strain appear to be larger than the curves providing changes to the T.E. due to the presence of the crack. Further studies are expected to improve the capabilities of condition monitoring and controlling transmission system noise and vibrations.

9.2 Future Work

The following areas have been noted as being worthy of further research, in the light of this thesis.

- Further numerical method investigation and study should be conducted on gears in mesh with general stress formulations over a complete mesh cycle.

- Further numerical method investigation and study should be conducted on gears in mesh under dynamic situations with and without cracked teeth, surface pitting and wear using the finite element method.

- Further numerical method investigation and study should be conducted for all types of gear mesh with and without tooth damage. This could include helical, spiral bevel and other gear tooth forms.

- Further numerical method investigation and study should be conducted on a whole gearbox with all elements in the system including the gear casing with and without tooth damage.

- Further numerical method investigation and study on non-metallic gears should be conducted including the effect of thermal expansions. This would involve the use of a coupled field analysis.

- Further experimental testing should be carried out with the aim of eliminating the lateral movement of test gear hub centres.

REFFERENCES

Aida, T. (1968). "Fundamental Research on Gear Noise and Vibration I." <u>Transaction of the Japanese Society of Mechanical Engineers</u> **34**: 2226-2264.

Aida, T. (1969). "Fundamental Research on Gear Noise and Vibration II." <u>Transaction of the Japanese Society of Mechanical Engineers</u> **35**: 2113-2119.

Aida, T., Sato, S. and **Fukuma, H.** (1967). <u>Properties of Gear Noise and Its Generating Mechanism.</u> Proceedings of the Japanese Society of Mechanical Engineers Semi-International Gearing Symposium.

Alagoz, Q., Arikan, M. A. S., Bilir, O. G. and **Parnas, L.** (2002). "3-D finite element analysis of long-fiber reinforced composite spur gears." <u>Gear Technology</u> **19(2)**: 12-19.

Alattass, M. (1994). <u>Experimental Study of Fault Influence on Vibration and Noise Measurements in a Gear Transmission Mechanism.</u> International Gearing Conference, UK.

Anderson, T. L. (1995). <u>Fracture mechanics: fundamentals and applications</u>, Boca Raton : CRC Press.

Andrei, L; Andrei, G; Epureanu, A; Oancea, N; Walton, D. (2002). "Numerical simulation and generation of curved face width gears." <u>International Journal of Machine Tools & Manufacture (UK)</u> **42(1)**: 1-6.

ANSYS (2000). User's Manual, ANSYS, Inc.

Arafa, M. H. and **Megahed, M. M.** (1999). "Evaluation of spur gear mesh compliance using the finite element method." <u>Proceedings of the Institution of Mechanical Engineers. Part C, Journal of Mechanical Engineering Science v. 213 noC6</u>: 569-79.

Arikan, M. A. S. and **Kaftanoglu, B.** (1989). "Dynamic Load and Root Stress Analysis of Spur Gears." <u>Annal of the CIRP</u> **38**: 171-174.

Arikan, M. A. S. and **Kaftanoglu, B.** (1991). <u>Dynamic Load and Contact Stress Analysis of Spur Gears.</u> Advance in Design Automation, USA.

Arikan, M. A. S. and **Tamar, M.** (1992). <u>Tooth Contact and 3-D Stress Analysis of Involute Helical Gears.</u> 6th International Power Transmission and Gearing Conference.

Arthur, P. and **Chong, K. P.** (1987). <u>Elasticity in Engineering Mechanics</u>, New York: Elsevier.

AUTODESK. (1997)., AUTODESK, USA.

AYEL, J. (1984). "Engrenages. Introduction a la Lubrification des Engrenages. La Lubrification Industrielle. Transmissions, Compressures, Turbines." <u>Collection Coloques et Seminaires 39, Paris: Ed. Technip. cap. 4</u>: 183-296, tome 1.

Babuska, I. (1988). <u>"The p- and hp- Versions Of The Finite Element Method The State Of The Art," in Finite Elements: Theory And Application</u>. Springer-Verlag, Berlin, D.L. Doyer et al. (eds).

Bahgat, B. M., Osman, M. O. M. and **Sankar, T. S.** (1981). "On the Dynamic Gear Tooth Loading as Effected by Bearing Clearances in High Speed Machinery." <u>Journal of Mechanical Design</u>: 81-DET-112.

Bahgat, B. M., Osman, M. O. M. and **Sankar, T. S.** (1983). "On the Spur-Gear Dynamic Tooth-Load under Consideration of System Elasticity and Tooth Involute Profile." <u>Journal of Mechanisms, Transmissions, and Automation in Design</u> **105(September)**: 302-309.

Bard, C., Remond, D. and **Play, D.** (1994). <u>New Transmission Error Measurement for Heavy Load Gears.</u> International Gearing Conference, UK.

Baret, C., Coccolo, G. and **Raffa, F. A.** (1994). <u>3d Stress Analysis of Spur Gears with Profile Errors and Modifications Using P-Fem Models.</u> International Gearing Conference, UK.

Barker., J (2002). "Gear tooth inspection and static transmission error test rig improvement," B. Eng. Project Report. Perth, Curtin University of Technology.

Barnett, D., Agarwal, A. and **Braun, E.** (1988). "Load sharing in high contact ratio truck transmission gearing." <u>SAE technical paper 885125</u> **2**: 252-261.

Barnett, O. W. and **Yildrim, N.** (1994). <u>Loaded Transmission Error Predictions Using a Computer Model and Its Verification.</u> International Gearing Conference, UK.

Baron, E., Favre, B. and **Mairesse, P.** (1988). <u>Analysis of Relation between Gear Noise and Transmission Error.</u> Proc. Internoise, '88.

Baumgart, J. (1992). "Investigation on the Optimization of Plastics/Steel Toothed Wheel Pairs." Gov. Res. Announc. Index (USA): 260.

Blazakis, A. and **Houser, D. R.** (1994). Finite Element and Experimental Analysis of the Effect of Thin-Rimmed Gear Geometry on Spur Gear Fillet Stresses. International Gearing Conference, UK.

Breeds, A. R. (1991). Non-metallic gears for power transmission, The University of Birmingham, U.K.

Brousseau, J., Gosselin, C. and **Cloutier, L.** (1994). Reference Point, Mesh Stiffness, and Gear Dynamic Models. International Gearing Conference, University of Newcastle, UK.

BS (1970). 436: Part 2: 1970 Specification for spur and helical gears. Part 2: basic rack form, modules and accuracy. (British Standards Institution, London).

Bushimata, T; Sakuta, H; Asai, T. (2001). "Wear of Plastic Spur Gear Made by Injection Molding." Journal of Japanese Society of Tribologists **46(11)**: 889-896.

Castro, J., Seabra, J. and **Almacinha, J.** (1994). Recent Advances in Experimental Mechanics. Experimental and analytical evaluation of the teeth load distribution in a spur gear and rack pair. Balkema, Rotterdam.

Chabert, G., Tran, T.D. and **Mathis, R.** (1974). "An Evaluation of Stresses and Deflection of Spur Gear Teeth under Strain." Journal of Engineering for Industry: 85-93.

Chen, C.-H., Wang, Y. and **Colbourne, J. R.** (1992). A General formula for Determining the Normal to the Path of Contact in Parallel-Axis Gearing. 6th International Power Transmission and Gearing Conference.

Chen, J. S., Litvin, F. L. and **Shabana, A. A.** (1994). Computerized Simulation of Meshing and Contact of Loaded Gear Drives. International Gearing Conference, UK.

Cheng, Y. and **Lim, T. C.** (1998). Dynamic Analysis of High Speed Hypoid Gears with Emphasis on Automotive Axle Noise Problem. ASME Design Engineering Technical Conference, Atlanta, GA, USA.

Cheung, Y. K. and **Zienkiewicz, O. C.** (1965). "Finite Elements in the Solution of Field Problems." Engineer **220**: 507-510.

Childs, D. B. (1980). Estimation of Seal Bearing Stiffness and Damping Parameters from Experimental Data. Second International Conference: Vibration in Rotating Machinery, IME.

Choy, F. K. and **Polyshchuk, V.** (1995). "Dynamic Analysis and Experimental Correlation of a Gear Transmission System." International Journal of Turbo and Jet Engines **12**: 269-281.

Choy, F. K., Tu, Y. K., Zakrajsek, J. J. and **Townsend, D. P.** (1991). "Effect of Gear Box Vibration and Mass Imbalance on the Dynamics of Multistage Gear Transmission." Journal of Vibration and Acoustics **113**: 333-344.

Choy, F. K., Ruan, Y. F., Tu, Y. K., Zakrajsek, J. J. and **Townsend, D. P.** (1992). "Modal Analysis of Multistage Gear Systems Coupled with Gearbox Vibrations." Journal of Mechanical Design **114**: 486-496.

Choy, F. K., Ruan, Y. F., Zakrajsek, J. J. and **Oswald, F. B.** (1993). "Modal Simulation of Gear Box Vibration with Experimental Correlation." Journal of Propulsion and Power **9(2)**: 301-306.

Choy, F. K., Polyshchuk, V., Zakrajsek, J. J., Handschuh, R. F. and **Townsend, D. P.** (1996). "Analysis of the Effects of Surface Pitting and Wear on the Vibrations of a Gear Transmission System." Tribology International **29(1)**: 77-83.

Choy, F. K., Huang, S., Zakrajsek, J. J., Handschuh, R. F. and **Townsend, D. P.** (1996). "Vibration Signature Analysis of a Faulted Gear Transmission System." Journal of Propulsion and Power **12(2)**: 289-295.

Clough, R. W. (1960). The finite element method in plane stress analysis. ASCE, Proceedings of the Second Conference on Electronic Computation.

Cook, R. D. (1989). Concepts and Applications of Finite Element Analysis, John Wiley & Sons, N.Y: 578.

Cornell, R. W. (1981). "Compliance and Stress Sensitivity of Spur Gear Teeth." Journal of Mechanical Design **103**: 447-459.

Cornell, R. W. and **Westervelt, W. W.** (1978). "Dynamic tooth loads and stressing for high contact ratio spur gears." ASME Journal of Mechanical Design **100**(1): 69-76.

Courant, R. (1943). "Variational method for the solution of problems of equilibrium and vibrations." Bulletin of the American Mathematical Society **49**: 1-23.

Coy, J. J. and **Chao, C. H.** (1982). "A Method of Selecting Grid Size to Account for Hertz Deformation in Finite Element Analysis of Spur Gears." <u>ASME Journal of Mechanical Design</u> **103**: 759-459.

Daly, K. J. and **Smith, J. D.** (1979). <u>Using Gratings in Driveline Noise Problems.</u> Proc., Noise & Vib. of Engineering and Transmissions, Cranfield.

Daniewicz, S. R., Collins, J. A. and **Houser, D. R.** (1994). "The Stress Intensity Factor and Stiffness for a Cracked Spur Gear Tooth." <u>Journal of Mechanical Design</u> **116**: 697-700.

DIN (1986). Rack profile as PER DIN 876 (FEB 86), Supplied by Hofmann Engineering, Perth.

Domininghaus, H. (1993). <u>Plastics for Engineers</u>, Bondway Publishing.

Donno, M. D. and **Litvin, F. L.** (1998). <u>Computerized Design, Generation and Simulation of Meshing of a Spiroid Worm-Gear Drive with Double-Crowned Worm.</u> 1998 ASME Design Engineering Technical Conference, Atlanta, GA, USA.

Dooner, D. B. and **Seireg, A. A.** (1998). <u>Concurrent Engineering of Toothed Bodies for Generalized Function Transmission.</u> 1998 ASME Design Engineering Technical Conference, Atlanta, GA, USA.

Drago, R. (1974). "Heavy lift helicopter brings up drive ideas." <u>Power Transmission Design</u>: 49-63.

Drago, R. J., Lenski, J. W. and **Royal, A.** (1979). <u>An Analytical Approach to the Source Reduction of Noise and Vibration in Highly Loaded Mechanical Power Transmission Systems.</u> Proceeding of the Fifth World Congress on Theory of Machines and Mechanisms.

Du, S. (1997). <u>Dynamic Modelling and Simulation of Gear Transmission Error for Gearbox Vibration Analysis</u>, Ph.D Thesis, University of New South Wales, Sydney, Australia.

Du, S.; Randall, R. B.; Kelly, D. W. (1998). "Modelling of spur gear mesh stiffness and static transmission error." <u>Proceedings of the Institution of Mechanical Engineers. Journal of Mechanical Engineering Science.</u> **212**(C4): 287-297.

Dvorak, P. (1999). "Meshless analysis breaks with FEA traditions." <u>Machine Design; Cleveland</u> **71**(23): 82-.

Elkholdy, A. H. (1985). "Tooth load sharing in high contact ratio spur gears." <u>Trans. ASME.J. of Mechanisms, Transmission and Automn in Des.</u> **107**: 11-16.

Elkholdy, A. H., Elsharkawy, A. A. and **S., Y. A.** (1998). "Effect of Meshing Tooth Stiffness and Manufacturing Error on the Analysis of Straight Bevel Gears." <u>Mechanics of Structures and Machines.</u> **21(1)**: pp 41-.

El-Saeidy Fawzi, M. A. (1991). "Effect of Tooth Backlash and Ball Bearing Deadband Clearance on Vibration Spectrum in Spur Gear Boxes." <u>Journal of Acoustical Society of America</u> **89(6)**: 2766-2773.

Enzmann, B. (1990). "Special Gearings of Plastic for Quiet Gears." <u>Antriebstechnik</u> **5**: 42-44.

Feng, P.-H. (1998). <u>Determination of Principal Curvatures and Contact Ellipse for Profile Crowned.</u> 1998 ASME Design Engineering Technical Conference, Atlanta, GA, USA.

Filiz, H. I. and **Eyercioglu, O.** (1995). "Evaluation of Gear Tooth Stresses by Finite Element Method." <u>Journal of Engineering for Industry</u> **117**: 232-239.

Forrester, B. D. (1996). <u>Advance Vibration Analysis Techniques for Fault Detection and Diagnosis in Geared Transmission System</u>, Ph.D Thesis, Swinburne University of Technology, Melbourne, Australia.

Fujio, H. (1992). <u>Laser Holographic Measurement of Tooth Flank form of Cylindrical Involute Gear: Part 2- for Helical Gear Tooth.</u> 6th International Power Transmission and Gearing Conference.

Gabbert, U. and **Graeff-Weinberg, K.** (1994). "Eine pNh-Elementformulirung für die Kontaktanalyse." <u>ZAMM74</u> **4**: 195-197.

Gargiulo, E. P. J. (1980). "A Simple Way to Estimate Bearing Stiffness." <u>Machine Design v. 70 no12 (July 9 '98) p. 132+</u>: 107-110.

Gosselin, C., Gagnon, P. and **Cloutier, L.** (1998). "Accurate Tooth Stiffness of Spiral Bevel Gear Teeth by the Finite Strip Method." <u>Journal of Mechanical Design v. 119 (Dec. '97) p. 518-21</u> **120(4)**: 599.

Gosselin, C. (1994). <u>A Review of the Current Contact Stress and Deformation formulations Compared to Finite Element Analysis.</u> International Gearing Conference, UK.

Gregory, R. W., Harris, S. L. and **Munro, R. G.** (1963). <u>Dynamic Behaviour of Spur Gears.</u> Proceedings of the Institute of Mechanical Engineers.

Gregory, R. W., Harris, S. L. and **Munro, R. G.** (1963). "A Method of Measuring Transmission Error in Spur Gear of 1:1 Ratio." J. SCI. INSTRUM. **40**: 5-9.

Gregory, R. W., Harris, S. L. and **Munro, R. G.** (1963). Torsional Motions of a Pair of Spur Gears. Proc. I. Mech. E.

Harris, S. L. (1958). Dynamic Loads on the Teeth of Spur Gears. Proc. I. Mech. E.

Hayashi, I. and **Hayashi, T.** (1979). New measuring Method of a Single Flank Transmission Error of a pair of Gears. Proc., Fifth World Congress on Theory of Machines and Mechanisms.

Hayashi, I. and **Hayashi, T.** (1981). Development of the Dynamic Measurement Method of Transmission Error of a Gear Pair. International Symposium on Gearing & Power Transmissions, Tokyo, JAPAN.

Hoff, N. H. (1956). Analysis of Structures. New York, Wiley, New York.

Houser, D. R. (1990). Research of the Ohio State University Gear Dynamics and Gear Noise Research Laboratory. First International Conference, Gearbox Noise and Vibration.

Houser, D. R., Bolze, V. M. and **Graber, J. M.** (1996). A Comparison of Predicted and Measured Dynamic and Static Transmission Error for Spur and Helical Gear Sets. 14th Intl. Modal Anal. Conf., USA.

Houser, D. R. and **Blankenship, G. W.** (1989). Methods for Measuring Gear Transmission Error under Load and At Operating Speeds., SAE Technical Paper No. 891869**:** 1-8.

Howard, I., Jia, S. and **Wang, J.** (2001). "The dynamic modelling of a spur gear in mesh including friction and a crack." Mechanical Systems and Signal Processing **15(5)**: 831-853.

Iida, H., Tamura, A. and **Yamamoto, H.** (1986). "Dynamic Characteristics of a Gear Train System with Softly Supported Shafts." Bulletin of the JSME **29(252)**: 1811-1817.

Iida, H. and **Tamura, A.** (1984). Couple Torsional-Flexural Vibration of a Shaft in a Geared System. Proceeding of the Third international Conference on Vibrations in Rotating Machinery.

Iida, H. (1980). "Coupled Torsional-Flexural Vibration of a Shaft in a Geared System of Rotors." Bulletin of the JSME **23(186)**: 2111-2117.

Inoue, K., Townsend, D. P. and **Coy, J. J.** (1992). Optimum Design of Gearbox for Low Vibration. 6th International Power Transmission and Gearing Conference, USA.

ISO/DIS (1983). 6336: 1983, Parts 1-4. (Organization for International Standardizations, Belgium).

Iwatsubo, T., Arii, S. and **Kawai, R.** (1984). "Couple Lateral-Torsional Vibration of Rotor System Trained by Gears." Bulletin of the JSME **27(224)**: 271-277.

Iwatsubo, T., Arii, S. and **Kawai, R.** (1984). The Coupled Lateral Torsional Vibration of a Geared Rotor System. Proceeding of the Third international Conference on Vibrations in Rotating Machinery.

Janover, J. S. and **Sehring, J. F.** (1989). "Finite-Element Analysis of Plastic Gear Transmission." Plast. Des. Forum **14(6)**: 69, 72, 74-75, 81.

Jia, S., Wang, J. and **Howard, I.** (2000). The Modelling of the Vibration Response of Spur Gears with Localised Teeth Crack. 13th International Congress on Condition Monitoring and Diagnostic Engineering Management, Houston, Texas, USA.

Jia, S. Howard, I. and **Wang, J.** (2001). A common formula for spur gear mesh stiffness. The JSME International Conference, Fukuoka, JAPAN.

Johnson, D. C. (1962). "Modes and Frequencies of Shafts Coupled by Straight Spur Gears." Journal of Mechanical Engineering Science **4(3)**: 241-250.

Kahraman, A. (1992). "Dynamic Analysis of Geared Rotors by Finite Elements." Journal of Mechanical Design **114(September)**: 507-514.

Kahraman, A. (1993). "Effect of Axial Vibrations on the Dynamics of a Helical Gear Pair." Journal of Vibration and Acoustics **115(1)**: 33-39.

Kahraman, A. and **Singh, R.** (1991). "Interaction between Time-Varying Mesh Stiffness and Clearance Non-Linearities in a Geared System." Journal of Sound and Vibration **146(1)**: 135-156.

Kahraman, A. and **Singh, R.** (1991). "Non-Linear Dynamics of a Geared Rotor-Bearing System with Multiple Clearances." Journal of Sound and Vibration **144(3)**: 469-506.

Kahraman, A. and **Blankenship, G. W.** (1999). "Effect of involute contact ratio on spur gear dynamics." Journal of Mechanical Design, Transactions Of the ASME [J Mech Des, Trans ASME] **121**(1): 112-118.

Kalluri, R. and **Houser, D. R.** (1998). <u>A Possible Strategy for Incorporating Edge Effects in Root Stress Estimation of Helical Gears.</u> 1998 ASME Design Engineering Technical Conference, Atlanta, GA, USA.

Kasuba, R. (1961). An Analytical and experimental Study of Dynamic Loads on Spur Gear Teeth,, University of Illinois.

Kasuba, R. (1971). "Dynamic Loads on Spur Gear Teeth by Analog Computation." <u>American Society of Mechanical Engineers</u>: 71-DE-26.

Kato, M. (1994). <u>Evaluation of Sound Power Radiated by a Gearbox.</u> 1994 International Gearing Conference, University of Newcastle, UK.

Kim, B. S. (1998). "Crack face friction effects on Mode II stress intensities for a surface-cracked coating in two-dimensional rolling contact." <u>Tribology Transactions; Park Ridge.</u> **41**(1): 35-.

Kin, V. (1992). <u>Computerized Analysis of Gear Meshing Based on Coordinate Measurement Data.</u> 6th International Power Transmission and Gearing Conference, USA.

Kishor, B. (1979). <u>Effect of Gear Errors on Non-linear Vibrations of a Gear-train System</u>. Proceedings of the Fifth World Congress on Theory of Machines and Mechanisms.

Kissling, U. L. (1994). <u>Improving Gearbox Design by Highly Integrated Calculation Programs.</u> International Gearing Conference, University of Newcastle, UK.

Kiyono, S. and **Fujii, Y.** (1981). "Analysis of Vibration of Bevel Gears." <u>Bulletin of the JSME</u> **24(188)**: 441 -446.

Kleiss, N. J. J.; Kleiss, R. E. (2000). "A practical guide for molding better plastic geared transmissions." <u>Gear Technology (USA)</u> **17(3)**: 20-25.

Kobler, H. K., Pratt, A. and **Thomson, A. M.** (1970). <u>Dynamics and Noise of Parallel Axis Gearing.</u> Proceedings of the Institute of Mechanical Engineers.

Koffi, D. and **Cuilliere, J. C.** (1995). "Study of regimes and lubrication parameters of gears of thermoplastic materials." <u>Materiaux et Techniques (Paris)</u> **83(3-4)**: 33-39.

Kowalczyk, P. (1994). "Finite-Deformation Interface formulation for Frictionless Contact Problems." <u>Communications in Numerical Methods in Engineering</u> **10**: 879-893.

Kral, S. (1991). "The Effect of Deformations of Teeth on Tribological Properties of Metal--Plastic Gearing." <u>Ropa a Uhlie (Czechoslovakia)</u> **33(10)**: 614-618.

Kuang, J. H. and **Yang, Y. T.** (1992). <u>An Estimate of Mesh Stiffness and Load Sharing Ratio of a Spur Gear Pair.</u> 6th International Power Transmission and Gearing Conference, USA.

Kubo, A. and **Kiyono, S.** (1980). "Vibration excitation of cylindrical involute gears." <u>JSME Bulletin</u> **23**(183): 1536-1543.

Kubo, A. (1992). <u>Laser Holographic Measurement of Tooth Flank form of Cylindrical Involute Gear: Part 1- Principle and Measurement of Spur Gear.</u> 6th International Power Transmission and Gearing Conference.

Kudinov, A. T. Starzhinsky, V. E.; Osipenko, S. A. (1992). "Calculation of Technological Shrinkage in Cast Toothed Gears From Thermoplastics." <u>Plasticheskie Massy (Russia)</u> **4**: 53-55.

Kurokawa, M.; Uchiyama, Y.; Nagai, S. (2000). "Tribological properties and gear performance of polyoxymethylene composites." <u>Journal of Tribology (Transactions of the ASME) (USA)</u> **122(4)**: 809-814.

Kurowski, P. (2000). "Say good-bye to defeaturing and meshing." <u>Machine Design; Cleveland; Aug 17, 2000</u> **72**(16): 71-78.

Laschet, A. and **Troeder, C.** (1984). "Torsional and Flexural Vibrations in Drive Systems: A Computer Simulation." <u>Computers in Mechanical Engineering</u> **3**: 32-43.

Lee, C., Lin, H. H., Oswald, F. B. and **Townsend, D. P.** (1991). "Influence of linear profile modification and loading conditions on the dynamic load and stress of high contact ratio spur gears." <u>Trans. ASME.J. of Mechanical Design</u> **113**: 473-480.

Lee, C. Y. and **Oden, J. T.** (1993). "Theory and approximation of quasistatic frictional contact problems." <u>Comput. Methods. Appl. Mech. Engng.</u> **106**: 407-429.

Lepi, S. M. (1998). <u>Practical guide to finite elements : a solid mechanics approach</u>, New York : Marcel Dekker.

Levy, S. (1953). "Structural analysis and influence coefficients for Delta wings." <u>J. Aero. Sci</u> **20**(7): 449-54.

Lewicki, D. (1994). <u>Improvements in Spiral-Bevel Gears to Reduce Noise and Increase Strength.</u> International Gearing Conference, University of Newcastle, UK.

Lewicki, D. G. and **Ballarini, R.** (1997). "Effect of Rim Thickness on Gear Crack Propagation Path." <u>Journal of Mechanical Design</u> **119**: 88-95.

Li, R. and **Tang, Q.** (1994). <u>Deformation numerical analysis of meshing gears and tooth profile modification</u>. 7994 International Gearing Conference, University of Newcastle, UK.

Lim, T. C. and **Singh, R.** (1990). "Vibration Transmission through Rolling Element Bearings, Part I: Bearing Stiffness formulation." <u>Journal of Sound and Vibration</u> **139(2)**: 179-199.

Lim, T. C. and **Singh, R.** (1990). "Vibration Transmission through Rolling Element Bearings, Part II: System Studies." <u>Journal of Sound and Vibration</u> **139(2)**: 201-225.

Lim, T. C. and **Singh, R.** (1991). "Vibration Transmission through Rolling Element Bearings, Part III: Geared Rotor System Studies." <u>Journal of Sound and Vibration</u> **151(1)**: 31-54.

Lim, T. C. and **Singh, R.** (1992). "Vibration Transmission through Rolling Element Bearings, Part IV: Statistical Energy Analysis." <u>Journal of Sound and Vibration</u> **153(1)**: 37-50.

Lin, H. H., Huston, R. L. and **Coy, J. J.** (1988). "On Dynamic Loads in Parallel Shaft Transmissions: Part 1." <u>Journal of Mechanisms, Transmissions, and Automation in Design</u> **110(June)**: 221-225.

Lin, H. H., Lee, C., Oswald, F. B. and **Townsend, D. P.** (1993). "Computer aided design of high contact ratio gears for minimum dynamic load and stress." <u>Trans. ASME.J. of Mechanical Design</u> **115**: 171-178.

Lin, H. H., Oswald, F. B. and **Townsend, D. P.** (1989a). <u>Dynamic Loading of Spur Gears with Linear or Parabolic Tooth Profile Modifications</u>. Proceedings of the 1989 International Power Transmission and Gearing Conference, Chicago, USA.

Lin, H. H., Oswald, F. B. and **Townsend, D. P.** (1994). "Dynamic Loading of Spur Gears with Linear or Parabolic Tooth Profile Modifications." <u>Mech. Mach. Theory</u> **29(8)**: 1115-1129.

Lin, H. H., Wang, J., Oswald, F. B. and **Coy, J. J.** (1994). "Effect of extended tooth contact on the modeling of spur gear transmissions." <u>Gear Technology</u>: 18-25.

Liou, C.-H. (1992). <u>Effect of Contact Ratio on Spur Gear Dynamic Load.</u> 6th International Power Transmission and Gearing Conference, USA.

Liou, C.-H. (1996). "Effect of Contact Ratio on Spur Gear Dynamic Load with No Tooth Profile Modifications." <u>Journal of Mechanical Design</u> **118(September)**: 439-443.

Litvin, F. L. (1989). <u>Theory of Gearing</u>, NASA Reference Publication, NASA.

Litvin, F. L., Egelja, A. M. and **De Donno, M.** (1998). "Computerized determination of singularities and envelopes to families of contact lines on gear tooth surfaces." <u>Computer Methods in Applied Mechanics and Engineering</u> **158(1/2)**: 23.

Litvin, F. L., Lu, J. and **Howkins, M.** (1998). "Computerized simulation of meshing of conventional helical involute gears and modification of geometry." <u>Mechanism and machine theory.</u> **34(1)**: 123.

Litvin, F. L., Wang, A. G. and **Handschuh, R. F.** (1998). "Computerized generation and simulation of meshing and contact of spiral bevel gears with improved geometry." <u>Computer Methods in Applied Mechanics and Engineering</u> **158(1/2)**: 35.

Litvin, F. L. and **Feng, P.-H.** (1996). "Computerized Design and Generation of Cycloidal Gearings." <u>Mech. Mach. Theory</u> **31(7)**: 891-911.

Litvin, F. L. and **Hsiao, C. L.** (1993). "Computerized Simulation of Meshing and Contact of Enveloping Gear Tooth Surfaces." <u>Computer Methods in Applied Mechanics and Engineering</u> **102**: 337-336.

Litvin, F. L. and **Lu, J.** (1993). "Computerized Simulation of Generation, Meshing and Contact of Double Circular-Arc Helical Gears." <u>Mathl. Comput. Modelling</u> **18(5)**: 31-47.

Litvin, F. L. and **Lu, J.** (1995). "Computerized Design and Generation of Double Circular-Arc Helical Gears with Low Transmission Errors." <u>Computer Methods in Applied Mechanics and Engineering</u> **127**: 57-86.

Litvin, F. L. and **Seol, I. H.** (1996). "Computerized Determination of Gear Tooth Surface as Envelope to Two Parameter Family of Surfaces." <u>Computer Methods in Applied Mechanics and Engineering</u> **138**: 213-225.

Litvin, F. L. (1995). "Computerized Design and Generation of Low-Noise Helical Gears with Modified Surface Topology." Journal of Mechanical Design **117(June)**: 254-261.

Litvin, F. L. (1996). "Application of Finite Element Analysis for Determination for Load Share, Real Contact Ratio, Precision of Motion, and Stress Analysis." Journal of Mechanical Design **118(December)**: 556-567.

Litvin, F. L. and **Kim, D. H.** (1997). "Computerized design, generation and simulation of meshing of modified involute spur gears with localized bearing contact and reduced level of transmission errors." Journal of Mechanical Design **119**: 96-100.

Lu, J., Litvin, F. L. and **Chen, J. S.** (1995). "Load Share and Finite Element Stress Analysis for Double Circular-Arc Helical Gears." Mathl. Comput. Modelling **21(10),**: 13-30.

Luscher, A. Houser, D; Snow, C. (2000). "An investigation of the geometry and transmission error of injection molded gears." Journal of Injection Molding Technology (USA) **4(4)**: 177-190.

MAAG (1990). MAAG Gear Book-Calculation and practice of gears, gear drives, toothed couplings and synchronous clutch couplings, MAAG Gear Company LTD., Zurich.

Mahalingam, S. (1968). "Couple Vibration of Gear Systems." Journal of the Royal Aeronautical Society **72**: 522-526.

Maitra, M. G. (1989). Handbook of Gear Design. New Delhi, Tata McGraw-Hill Publishing Company Limited.

Mao, K. (1993). The performance of dry running non-metallic gears, The University of Birmingham, UK.

Mark, W. D. (1992). "Elements of Gear Noise Prediction." Noise and Vibration Control Engineering: Principles and Applications, L.L. Beranek and I.L. Ver, eds., John Wiley & Sons, Inc.**:** 735-770.

Maruyama, N., Morikawa, K. and **Hitomi, N.** (1992). Gear Case Shape and Rib Distribution for Reducing Automobile Transmission Gear Noise. 6th International Power Transmission and Gearing Conference, Scottdale, Arizona, USA.

McFadden, P. D. (1985). Analysis of the Vibration of the Input Bevel Pinion in RAN Wessex Helicopter Main Rotor Gearbox Wak143 Prior to Failure., Department of Defence, Aeronautical Research Laboratory.

Moriwaki, I. (1993). "Global Local Finite Element Method (Glfem) in Gear Tooth Stress Analysis." Journal of Mechanical Design **115(December)**: 1008-1012.

Munro, R. G. (1962). The dynamic behavior of spur gears, Cambridge University.

Munro, R. G. (1997). The Use of Optical Gratings in Gear Metrology. Third International Conference on Laser Metrology and Machine Performance, UK.

Munro, R. G., Yildirim, N. and **Hall, D. M.** (1990). "Optimum profile relief and transmission error in spur gears." In Proceedings of IMechE Conference on Gearbox Noise and Vibration **paper C404/032**: 35-41.

Munro, R. G. and **Yildirim, N.** (1994). Some Measurements of Static and Dynamic Transmission Error of Spur Gears. International Gearing Conference, UK.

Munro, R. G.; Morrish., L.; Palmer, D. (1999). "Gear transmission error outside the normal path of contact due to corner and top contact." Proceedings of the Institution of Mechanical Engineers. Part C, Journal of Mechanical Engineering Science **213**(C4): 389-400.

Muthukumar, R. and **Raghavan, M. R.** (1987). "Estimation of Gear Tooth Deflection by the Finite Element Method." Mech. Mach. Theory **22**: 177-181.

Nabi, S. M., Ganesan, N. (1993). "Static Stress Analysis of Composite Spur Gears Using 3D-Finite Element and Cyclic Symmetric Approach." Composite Structures (UK) **25(1-4)**: 541-546.

Nadolski, W. and **Pielorz, A.** (1998). "The influence of variable stiffness of teeth on dynamic loads in single-gear transmission." Archive of applied mechanics = ingenieur-archiv **68(3/4)**: 185.

Nakada, T. and **Utagawa, M.** (1956). The Dynamic Loads on Gears Caused by the Varying Elasticity of the Mating Teeth of Spur Gears. The Sixth Japanese National Congress on Applied Mechanics.

Narasimhan, R. and **Rosakis, A. J.** (1988). Three Dimensional Effects Near a Crack Tip in a Ductile Three Point Bend Specimen - Part I: A Numerical Investigation. Pasadena, CA, California Institute of Technology, Division of Engineering and Applied Science.

Neriya, S. V., Bhat, R. B. and **Sankar, T. S.** (1985). "Coupled Torsional-Flexural Vibration of a Geared Shaft System Using Finite Element Analysis." <u>Shock and Vibration Bulletin</u> **55(3)**: 13-25.

Niazy, A.-S. M. (1997). "What you should know about FEA." <u>Machine Design; Cleveland</u> **69**(21): 55-58.

Niemann, G. and **Baethge, J.** (1970). "Transmission error, tooth stiffness, and noise of parallel axis gears." <u>VDI-Z</u> **Vol 2, No 4 and No 8.**

Nitu, C. and **Grecu, E.** (1997). "Plastic gears." <u>Constructia de Masini (Romania)</u> **49(11-12)**: 76-80.

Okamoto, N. (1994). <u>Creep in Connections Between Gears and Shafts.</u> 1994 International Gearing Conference, University of Newcastle, UK.

Ong, J. H. (1992). "Finite Elements for Vibration of Vehicle Transmission System." <u>Computers in Industry</u> **18**: 257-263.

Oswald, F. B. (1992). <u>Comparison of Analysis and Experiment for Gearbox Noise.</u> 6th International Power Transmission and Gearing Conference, USA.

Oswald, F. B. (1992). <u>Effect of Operations Condition on Gearbox Noise.</u> 6th International Power Transmission and Gearing Conference, Scottdale, Arizona, USA.

Oswald, F. B. (1994). <u>Influence of Gear Design Parameters on Gearbox Radiated Noise.</u> 1994 International Gearing Conference, University of Newcastle, UK.

Ozguven, H. N. and **Houser, D. R.** (1988). "Dynamic Analysis of High Speed Gears by Using Loaded Static Transmission Error." <u>Journal of Sound and Vibration</u> **125**: 71-83.

Ozguven, H. N. and **Houser, D. R.** (1988). "Mathematical Models Used in Gear Dynamics- A Review." <u>Journal of Sound and Vibration</u> **121(3)**: 383-411.

Paczelt, I.; Szabo., B.A.; Szabo, T. (1999). "Solution of Contact Problem Using the hp-Version of the Finite Element Method." <u>Computers and Mathematics with Applications</u> **38**: 49-69.

Palmer, D. and **Munro, R. G.** (1995). <u>Measurements of transmission error, vibration and noise in spur gears.</u> British Gear Association Congress, Suite45, IMEX Park, Shobnall Rd., Burton on Trent.

Panhuizen, F. (2000). "New approaches to noise reduction through the use of thermoplastics." <u>Motor Industry Research Association (MIRA), New Technology (UK)</u>: 57.

Perret-Liaudet, J. and **Sabot, J.** (1992). <u>Dynamics of Truck Gearbox.</u> 6th International Power Transmission and Gearing Conference, Scottdale, Arizona, USA.

Prasad, V. S., Dukkipati, R. V. and **Osman, M. O. M.** (1992). <u>A Group Theory for Composite Gear Trains Employing Three-Shafts.</u> 6th International Power Transmission and Gearing Conference.

Ramamurti, V. and **Rao, M. A.** (1988). "Dynamic Analysis of Spur Gear Teeth." <u>Computers and Structures</u> **29(5)**: 831-843.

Randall, R. B. (1980). <u>Advances of the Application of Cepstrum Analysis to Gearbox Diagnosis.</u> Second International Conference: Vibration in Rotating Machinery.

Randall, R. B. (1984). <u>Seperating Excitation and Structural Response Effects in Gearboxes.</u> IMECHE, Third International Conference on Vibration in Rotating Machinery.

Randall, R. B. and **Deyang, L.** (1990). <u>Hibert Transform Techniques for Torsional Vibration Analysis.</u> The Institution of Engineers Australia Vibration and Noise Conference, Australia.

Randall, R. B. and **Kelly, D. W.** (1990). <u>Analytical and Experimental Vibration Analysis of a Gearbox Casing.</u> The Institution of Engineers Australia Vibration and Noise Conference, Melbourn, Australia.

Rao, C. R. M. and **Muthuveerappan, G.** (1993). "Finite Element Modelling and Stress Analysis of Helical Gear Teeth." <u>Computers and Structures</u> **49(6)**: 1095-1106.

Rebbechi, B., Oswald, F. B. and **Townsend, D. P.** (1996). <u>Measurement of Gear Tooth Dynamic Friction.</u> Transmission and Gearing Conference, USA.

Rebbechi, B. and **Crisp, J. D. C.** (1981). <u>A New formulation of Spur-Gear Vibration.</u> International Symposium on Gearing & Power Transmissions., Tokyo.

Rebbechi, B. and **Crisp, J. D. C.** (1983). <u>The Kinetics of the Contact Point, and Oscillatory Mechanisms in Resilient.</u> The sixth world congress on theory of machines and mechanisms.

Rebbechi, B. (1992). <u>A Comparison Between Theoretical Prediction and Experimental Measurement of the Dynamic Behaviour of Spur Gears.</u> 6th International Power Transmission and Gearing Conference, USA.

Refaat, M. H. (1995). Nonlinear Finite Element Analysis of Frictional Contact Problem Using Variational Inequalities,, University of Toronto, Toronto.

Refaat, M. H. and **Meguid, S. A.** (1994a). <u>A Novel Finite Element Analysis of the General Contact Problem Using Variational Inequalities.</u> Recent Advances in Structural Mechanics ASME.

Refaat, M. H. and **Meguid, S. A.** (1995). "On the Contact Stress Analysis of Spur Gears Using Variational Inequalities." <u>Computers and Structures</u> **57(5)**: 871-882.

Regalado, I. and **Houser, D. R.** (1998). <u>Profile Modifications for Minimum Static Transmission Error in Cylindrical Gears.</u> 1998 ASME Design Engineering Technical Conference, Atlanta, GA, USA.

Remmers, E. P. (1978). "Gear Mesh Excitation Spectra for Arbitrary Tooth Spacing Errors, Load and Design Contact Ratio." <u>Journal of Mechanical Design, 100(October)</u>: 715-722.

Richard, E. D., J., Echempati, R. and **Ellis, J.** (1998). <u>Design and Stress Analysis of Gears Using the Boundary Element Method.</u> 1998 ASME Design Engineering Technical Conference, Atlanta, GA, USA.

Richards, R. R. (2001). <u>Principles of solid mechanics</u>, Boca Raton, Fla. : CRC Press, c2001.

Richardson, H. H. (1958). Static and dynamic load, stress, and deflection cycles in spur gear systems, Massachusetts Institute of Technology.

Rollinger, J. G. and **Harker, R. J.** (1967). "Instability Potential of High Speed Gearing." <u>The Journal of the Industrial Mathematics Society</u> **17**: 39-55.

Roosmalen, A. N. J. V. (1995). <u>Noise Generation Mechanism of Gear Transmissions.</u> IMechE 1995.

Rosen, M. K. and **Frint, H. K.** (1982). "Design of high contact ratio gears." <u>Journal of the American Helicopter Society</u>: 65-73.

Rosinski, J. (1992). <u>Dynamic Loads in Geared Transmission Systems in Mining Machinery</u>. Vibrations in Rotating Machinery, Proceedings of the Institute of Mechanical Engineers.

Rosinski, J., Hofmann, D. A. and **Pennell, J. A.** (1994). <u>Dynamic transmission error measurements in the time domain in high speed gears</u>. International Gearing Conference, University of Newcastle, UK.

Sabot, J. and **Perret-Liaudet, J.** (1994). <u>Computation of the Noise Radiated by a Simplified Gearbox.</u> 1994 International Gearing Conference, University of Newcastle, UK.

Seager, D. L. (1975). <u>Separation of gear teeth in approach and recess, and the likelihood of corner contact</u>. 30th Annual Meeting of American Society of Lubrication Engineers.

Seol, I. H. and **Litvin, F. L.** (1996). "Computerized Design, Generation and Simulation of Meshing and Contact of Modified Involute, Klingelnberg and Flender Type Worm-Gear Drives." <u>Journal of Mechanical Design</u> **118(December)**: 551-555.

Seol, I. H. and **Litvin, F. L.** (1996). "Computerized Design, Generation and Simulation of Meshing and Contact of Worm-Gear Drives with Improved Geometry." <u>Computer Methods in Applied Mechanics and Engineering</u> **138**: 73-103.

Sirichai, S. (1999). <u>Torsional properties of spur gears in mesh using nonlinear finite element analysis, Ph.D Thesis, Curtin University of Technology, Australia</u>.

Sirichai, y., Howard, I., Morgan, L. and **Teh, K.** (1998). <u>A finite element model of spur gears in mesh with single tooth crack</u>. ISASTI '98, -.

Sirichai, S. (1996). <u>The Measurement of Static Torsional Stiffness of Gears in Mesh.</u> Third International Symposium on Measurement Technology and Intelligent Instruments, Japan.

Sirichai, S. (1997). <u>Finite Element Analysis of Gears in Mesh</u>. Fifth International Congress on Sound and Vibration, Australia.

Smith, J. D. (1983). <u>Gears and Their Vibration</u>. USA, Marcel Dekker.

Smith, J. D. (1987). "Gear Transmission Error Accuracy with Small Rotary Encoders." <u>Journal of Mechanical Engineering Science</u> **201(c2)**: 133-5.

Smith, J. D. (1999). <u>Gear noise and vibration</u>, New York : Marcel Dekker, 1999.

Smith, R. E. (1987). <u>The Relationship of Measured Gear Noise to Measured Gear Transmission Errors.</u> American Gear Manufacturers Association.

Smith, Z.; Fletcher, M. (1997). "Shifting gears--exploiting the potential of plastics." <u>Gear Technology (USA)</u> **14(1)**: 35-39.

Solaro, M. (1993). "Criteria for the design of gears using thermoplastic materials." <u>Rev. Plast. Mod. (Spain)</u> **66(446)**: 153-157.

Stadtfeld, H. J. (1998). <u>Single Flank Test, Structure-Borne Noise Analysis and Digital Imaging of Tooth Contact.</u> 1998 ASME Design Engineering Technical Conference, Atlanta, GA, USA.

Strang, G., Fix, G. J. (1973). <u>An Analysis of the Finite Element Method</u>. Englewood Cliffs, NJ, Prentice-Hall.

Su, X. and **Houser, D. R.** (1998). <u>Calculation of Wobble From Lead Inspection Data Gear Teeth with Modifications.</u> 1998 ASME Design Engineering Technical Conference, Atlanta, GA, USA.

Sundarajan, S. and **Amin, S.** (1991). "Finite Element Analysis of Ring Gear/Casing Spline Contact." <u>Journal of Propulsion and Power</u> **7(4)**: 602-604.

Sundarajan, S. and **Young, B. G.** (1990). "Finite Element Analysis of Large Spur and Helical Gear Systems." <u>Journal of Propulsion and Power</u> **6(4)**: 451-454.

Svicarevich, P., Howard, I. and **Wang, J.** (1999). <u>The Dynamic Modelling of a Spur Gear in Mesh Including Friction</u>. Internation conference on applications of modal analysis'99, Gold Coast, Queensland, Australia.

Sweeney, P. J. and **Randall, R. B.** (1996). "Gear Transmission Error Measurement Using Phase Demodulation." <u>Journal of Mechanical Engineering Science</u> **210(3)**: 201-213.

SzabÒ, B., Babuska, I. (1991). <u>Finite Element Analysis</u>. N.Y., John Wiley & Sons, Inc.

Tavares, H. F. and **Prodonoff, V.** (1986). "A New Approach for Gearbox Modeling in Finite Element Analysis of Torsional Vibration of Gear-Branched Propulsion Systems." <u>Shock and Vibration Bulletin</u> **56(2)**: 117-125.

Terashima, K., Tukamoto, N. and **Nishida, N.** (1986). "Development of plastic gears for power transmission (Design on load carrying capacity)." <u>Bulletin of the JSME</u> **29(250)**: 1326-1329.

Terauchi, Y. and **Nagamura, K.** (1981). <u>On tooth deflection calculation and profile modification of spur gear teeth</u>. Int. Symp. on Gearing and Power Trans., Tokyo, Japan.

Terauchi, Y. and **Nagamura, K.** (1981). "Study on Deflection of Spur Gear Teeth." <u>Bulletin ofthe JSME</u> **24(188)**: 447-452.

Tessema, A. A., Walton, D and **Shippen, J** (1993). "Load sharing in Non-metallic gears." <u>KOLA ZEBATE KZ'93 Wyiwarzanie, Pomiary, eksploatacja, Poznan</u>: 221-227.

Tessema, A. A., Walton, D. (1994). <u>Flexibility effects in non-metallic gears</u>. Proc. of the 1994 Int. Gearing Conf., Newcastle upon Tyne.

Tessema, A. W., D; Weale, D. (1995). "The effect of web and flange thickness on non-metallic gear performance." <u>Gear Technology (USA)</u> **12(6)**: 30-35.

Tobe, T., Sato, K. and **Takatsu, N.** (1976). "Statistical Analysis of Dynamic Loads on Spur Gear Teeth." <u>Bulletin of the JSME</u> **19(133)**: 808-813.

Tordian, G. V. and **Geraldin, H.** (1967). <u>Dynamic Measurement of the Transmission Error in Gears.</u> Proc. JSME Semi-International Symposium.

Townsend, D. P. (1991). <u>Dudley's Gear Handbook</u>.

Townsend, D. P., Baber, B. B. and **Nagy, A.** (1979). "Evaluation of high contact ratio spur gears with profile modification." <u>NASA technical paper 1458</u>.

Tsai, Y. C. and **Chang, H. L.** (1992). <u>Reconsideration of the Logic Gear Using a General Mathematical Model of Composite Gear Profiles.</u> 6th International Power Transmission and Gearing Conference, Scotts dale, Arizona.

Tsukamoto, N. and **Terashima, K** (1986). "Development of plastic gears for power transmission (various methods of lengthening the life of plastic gears and their effect)." <u>Bulletin of the JSME</u> **29(247)**: 249-255.

Tsukamoto, N.; Marayama, H.; Terashima, K. (1990). "Fundamental Characteristics of Plastic Gears Made of Thermoplastic Resin Filled With Various Fibers." <u>JSME International Journal, Series III</u> **33(4)**: 590-596.

Tuma, J., Kubena, R. and **Nykl, V.** (1994). <u>Assessment of Gear Quality Considering the Time Domain Analysis of Noise and Vibration Signals.</u> International Gearing Conference, UK.

Umezawa, K., Ajima, T. and **Houjoh, H.** (1986). "Vibration of Three Axes Gear System." <u>Bulletin of the JSME</u> **29(249)**: 950-957.

Underhill, W. R. C., Dokainish, M. A. and **Oravas, G. E.** (1997). "A Method for Contact Problem Using Virtual Elements." <u>Computer Methods in Applied Mechanics and Engineering</u> **143**: 229-247.

Velex, P., Maatar, M. and **Octrue, M.** (1995). Loaded Transmission Error Predictions and Measurements on Spur Gears with Profile Reliefs. IMechE.

Velex, P. and **Berthe, D.** (1989). Dynamic tooth loads on geared tran. Proc. of ASME 5th Int. Power Trans. and Gearing conf., Chicago, IL.

Velinsky, S. A. (1996). "Torsional Stiffness of a Machine Drive Element with Tensile Web Structure." Mechanism and machine theory. **31(8)**: 1043.

Vijayakar, S. M., Busby, H. R. and **Houser, D. R.** (1988). "Linearization of Multibody Frictional Contact Problems." Computers and Structures **29(4)**: 569-576.

Vijayakar, S. M. and **Houser, D. R.** (1993). "Contact Analysis of Gears Using a Combined Finite Element and Surface Integral Method." Gear Technology: 26-33.

Vijayarangan, S. and **Ganesan, N.** (1994). "Static Contact Stress Analysis of a Spur Gear Tooth Using the Finite Element Method, Including Frictional Effects." Computers and Structures **51(6)**: 765-770.

Vinayak, H. and **Houser, D. R.** (1992). A Comparison of Analytical Predictions with Experiment Measurements of Transmission Error of Misaligned Loaded Gears. 6th International Power Transmission and Gearing Conference, USA.

Walford, T. L. H. and **Stone, B. J.** (1980). Some Damping and Stiffness Characteristics of Angular Contact Bearings under Oscillating Radial Load. Second International Conference: Vibration in Rotating Machinery.

Walker, H. (1938). "Gear tooth deflection and profile modification." The Engineer: 319-412 and 434-436.

Wallace, D. B. and **Seireg, A.** (1973). "Computer Simulation of Dynamic Stress, Deformation, and Fracture of Gear Teeth." Journal of Engineering for Industry: 1108-1114.

Walton, D. (1992). A new look at testing and rating non-metallic gears. 3rd World Congress on Gearing and Power Transmissions, Paris, France.

Walton, D., White, J. and **Weale, D. J.** (1998). Developments and Advancements in Plastic Gearing Technology. Society of Plastics Engineers Annual Technical Conference and Exhibition.

Walton, D. (1994). "Load Sharing in Metallic and Non-metallic Gears." Proc Instn Mech Engrs, Part C: Journal of Mechanical Engineering Science **208**: 81-87.

Walton, D. (1995). "A note on tip relief and backlash allowances in non-metallic gears." Journal of Mechanical Engineering Science **209**: 383-388.

Walton, D., Shi, Y. W. (1989). "A Comparison of Ratings for Plastic Gears." Proc. Inst. Mech. Eng. C, J. Mech. Eng. Sci. **203**: 31-38.

Wang, C. C. (1978). "Rotational Vibration with Backlash: Part 1." Journal of Mechanical Design **100**: 363-373.

Wang, C. C. (1985). "On analytical Evaluation of Gear Dynamic Factors Based on Rigid Body Dynamics." Journal of Mechanisms, Transmissions, and Automation in Design **107**: 301-311.

Wang, J., Howard, I. and **Jia, S.** (2000). FEA Analysis of Spur Gears in Mesh Using a Torsional Stiffness Approach. COMADEM, Houston, Texas, USA.

Wang, S. M. (1974). "Analysis of Non-linear Transient Motion of a Geared Torsional." Journal of Engineering for Industry **96**: 51-59.

Wang, S. M. and **Morse, I. E.** (1972). "Torsional Response of a Gear Train System." Journal of Engineering for Industry, Transactions of the ASME **94**: 583-594.

Wang, Y.-F. and **Tong, Z.-F.** (1996). "Influence of Gear Errors on Acceleration Noise From Spur Gears." J. Accoust. Soc. Am. **99(5)**: 2922-2929.

Weber, C. (1949). The deformation of loaded gears, and the effect on their load - carrying capacity, D.S.I.R. Sponsored Research (Germany), Report No. 3.

Welbourn, D. B. (1972). Forcing Frequencies Due to Gears. Vibr., in Rotating Syst. Conf.

Welbourn, D. B. (1979). Fundamental Knowledge of Gear Noise - A Survey,. Noise & Vib. of Engineering and Transmissions, Cranfield, UK.

White, J. Walton, D; Wright, NA; Kukureka, SN; Du Gard, FJ; Driver, CL; Duke, BR; Nicoll, KA (1997). An evaluation of polymer composite materials for use in mechanical power transmission drives. EUROMAT 97: 5th European Conference on Advanced Materials and Processes and Applications, Maastricht, Netherlands.

Wilcox, L. and **Coleman, W.** (1973). "Application of Finite Element to the Analysis of Gear Tooth Stresses." Journal of Engineering for Industry, Transactions of the ASME: 1139-1148.

Williams, EH; Quinn, KR (1995). "Materials for plastic gears." Mach. Des. **67(2)**: 50-52.

Wright, N. A. and **Kukureka, S. N.** (2001). Wear testing and measurement techniques for polymer composite gears. 13th International Conference on Wear of Materials, Part 2, Vancouver, BC, Canada.

Yang, D. C. H. and **Sun, Z. S.** (1985). "A rotary model for spur gear dynamics." ASME Trans., Journal of Mech., Trans., and Automation in Design **107**: 529-535.

Yau, E., Busby, H. R. and **Houser, D. R.** (1994). "A Rayleigh-Ritz Approach to Modeling Bending and Shear Deflections of Gear Teeth." Computers and Structures **50(5)**: 705-713.

Yelle, H. and **Burns, D. J.** (1981). "Calculation of contact ratios for plastic/plastic or plastic/steel spur gear pairs." Trans. Of tlie ASME.J. of Mechanical Design **103**: 528-542.

Yildirim, N. (1994). Theoretical and experimental research in high contact ratio spur gearing, Ph.D Thesis, Huddersfield University, UK.

Yildirim, N. and. **Munro, R. G.** (1999). "A new type of profile relief for high contact ratio spur gears." Proceedings of Inst. Mech Engrs, Part C **213**: 563-568.

Yildirim, N. and. **Munro, R. G.** (1999). "A systematic approach to profile relief design of low and high contact ratio spur gears." Proceedings of the Institution of Mechanical Engineers. Part C, Journal of Mechanical Engineering Science **213**(C6): 551-62.

Zakrajsek, J. J. (1990). Gear Noise, Vibration, and Diagnostic Studies at NASA Lewis Research Centre. First International Conference, Gearbox Noise and Vibration.

Zeman, J. (1957). Dynamische Zusatzkrafter in Zahnbradgetrieben. Zeitschrift des Vereines Deutscher Ingiere(99).

Zhang, H. and **Li, J.** (1992). Thermo-viscoelastic analysis of fiber reinforced plastic gears. The Second International Symposium on Composite Materials and Structures, Beijing, China, Peking University Press (China).

Zhang, T., Kohler, H. K. and **lack, G. K.** (1994). Noise Optimisation of a Double Helical Parallel Shaft Gearbox. International Gearing Conference, University of Newcastle, UK.

Zhang, T. and **Kohler, H. K.** (1994). A Gearbox Structural Optimisation Procedure for Minimising Noise Radiation. international gearing conference, Uk.

Zhang, Y. and **Fang, Z.** (1998). "Analysis of tooth contact and load distribution of helical gears with crossed axes." Mechanism and machine theory. **34(1)**: 41.

Zhang, Y. (1994). "Computerized Analysis of Meshing and Contact of Gear Real Tooth Surfaces." Journal of Mechanical Design **116(September)**: 667-682.

Zhong, Z. H. and **Mackerle, J.** (1992). "Static contact problems - A rewiew." Eng. Comput. **9**: 3-37.

Zhong-Sheng, L., Su-Huan, C. and **Tao, X.** (1993). "Derivatives of Eigenvalues for Torsional Vibration of Geared Shaft Systems." Journal of Vibration and Acoustics **115(July)**: 277-276.

APPENDIX A

LISTING OF AN APDL PROGRAM FOR THE STATIC T.E. OF INVOLUTE SPUR GEARS IN MESH

```
/GST,ON                              ! Turns graphical solution tracking on
!*
*DIM,ANG,,30                         ! Defines, ANG( ), an array parameter and its dimensions of
ANG(1)=-7.5,-7,-6.5,-6,-5.5          meshing position.  The mesh positions from –7.5 to 7.5 degree
ANG(6)=-5,-4.5,-4,-3.5,-3            cover (nearly) one base pitch – via (nearly) mid-double zone –
ANG(11)=-2.5,-2,-1.5,-1,-0.5         single zone - (nearly) mid-double zone, and which is according to
ANG(16)=0.5,1,1.5,2,2.5             the 2D model of '2dMeshedatPitch.db'
ANG(21)=3,3.5,4,4.5,5
ANG(26)=5.5,6,6.5,7,7.5
FNAM=1                               ! Set initial meshing position.
PARSAV,ALL,ANGLE_A,,                 ! Write all parameter to file.
:DOLOOP                              ! :DOLOOP of meshing position in a cyclic.
RESUME,2dMeshedatPitch,db,,0,0       ! Resumes the 2D model (in the working directory) which has pre-
!*                                   defined the material properties, element type and initial meshed,
!*                                   contact at the pitch point.
PARRES,,ANGLE_A,, ,,                 ! Replace current parameter set with all array parameter from file.
/PREP7                               ! Enter pre-processor
!*
TOQ=152.4                            ! TOQ is the input torque load (currently set to 152.4 Nm).
!*
CSYS,1
FLST,3,48,5,ORDE,2
FITEM,3,1
FITEM,3,-48
AGEN, ,P51X, , , ,ANG(%FNAM%), , , ,1
WPSTYLE,,,,,,,,,1
wpstyle,0.05,0.1,-1,1,0.003,1,2,,5       Turn the driving and driven gear with angle ANG(%FNAM%)
CSYS,4                                   and -ANG(%FNAM%) respectively.
FLST,3,48,5,ORDE,2
FITEM,3,49
FITEM,3,-96
AGEN, ,P51X, , , ,-ANG(%FNAM%), , , ,1
!*
SMRT,1                               ! Start the mesh adaptation on current model.
ESIZE,0.5,0,
FLST,5,6,5,ORDE,4
FITEM,5,24
FITEM,5,-26
FITEM,5,72
FITEM,5,-74
CM,_Y,AREA
ASEL, , , ,P51X
CM,_Y1,AREA
CHKMSH,'AREA'
CMSEL,S,_Y
!*
!*
ACLEAR,_Y1
AMESH,_Y1
!*
CMDELE,_Y
CMDELE,_Y1
```

```
CMDELE,_Y2
!*
/COM, CONTACT PAIR CREATION - START
CM,_NODECM,NODE
CM,_ELEMCM,ELEM
CM,_LINECM,LINE
CM,_AREACM,AREA
/GSAV,cwz,gsav,,temp
MP,MU,1,0.06
MAT,1
R,3
REAL,3
ET,2,169
ET,3,172
KEYOPT,3,9,0
! Generate the target surface
LSEL,S,,,258
LSEL,A,,,261
LSEL,A,,,265
CM,_TARGET,LINE
TYPE,2
NSLL,S,1
ESLN,S,0
ESURF,ALL
CMSEL,S,_ELEMCM
! Generate the contact surface
LSEL,S,,,50
LSEL,A,,,53
LSEL,A,,,56
CM,_CONTACT,LINE
TYPE,3
NSLL,S,1
ESLN,S,0
ESURF,ALL
ALLSEL
ESEL,ALL
ESEL,S,TYPE,,2
ESEL,A,TYPE,,3
ESEL,R,REAL,,3
/PSYMB,ESYS,1
/PNUM,TYPE,1
/NUM,1
EPLOT
ESEL,ALL
ESEL,S,TYPE,,2
ESEL,A,TYPE,,3
ESEL,R,REAL,,3
CMSEL,A,_NODECM
CMDEL,_NODECM
CMSEL,A,_ELEMCM
CMDEL,_ELEMCM
CMSEL,S,_LINECM
CMDEL,_LINECM
CMSEL,S,_AREACM
CMDEL,_AREACM
/GRES,cwz,gsav
CMDEL,_TARGET
CMDEL,_CONTACT
/COM, CONTACT PAIR CREATION - END
!*
FLST,2,76,1,ORDE,13
FITEM,2,4858
FITEM,2,4862
FITEM,2,-4893
FITEM,2,8219
FITEM,2,-8223
FITEM,2,8346
FITEM,2,8350
FITEM,2,-8380
FITEM,2,8863
FITEM,2,8865
FITEM,2,8869
FITEM,2,-8871
```

Generate the contact and the target elements.

Rotate the nodal coordinate of the driven gear hub nodes into the polar coordinate system which is located at the driven gear hub centre.

263

```
FITEM,2,8877
NROTAT,P51X
CSYS,1
FLST,2,76,1,ORDE,13
FITEM,2,2938
FITEM,2,2942
FITEM,2,-2973
FITEM,2,4518
FITEM,2,4522
FITEM,2,-4553
FITEM,2,4777
FITEM,2,-4780
FITEM,2,4790
FITEM,2,4795
FITEM,2,4799
FITEM,2,-4801
FITEM,2,4807
NROTAT,P51X
!*
!*
```

Rotate the nodal coordinate of the driving gear hub nodes into the global cylindrical coordinate system which is located at the driving gear hub centre.

```
FLST,2,76,1,ORDE,13
FITEM,2,2938
FITEM,2,2942
FITEM,2,-2973
FITEM,2,4518
FITEM,2,4522
FITEM,2,-4553
FITEM,2,4777
FITEM,2,-4780
FITEM,2,4790
FITEM,2,4795
FITEM,2,4799
FITEM,2,-4801
FITEM,2,4807
/GO
D,P51X, , , , , ,UX, , , , ,
!*
!*
FLST,2,76,1,ORDE,13
FITEM,2,4858
FITEM,2,4862
FITEM,2,-4893
FITEM,2,8219
FITEM,2,-8223
FITEM,2,8346
FITEM,2,8350
FITEM,2,-8380
FITEM,2,8863
FITEM,2,8865
FITEM,2,8869
FITEM,2,-8871
FITEM,2,8877
!*
/GO
D,P51X, , , , , ,ALL, , , , ,
!*
!*
```

Apply boundary conditions on driving and driven gear hub respectively.

```
FLST,2,76,1,ORDE,13
FITEM,2,2938
FITEM,2,2942
FITEM,2,-2973
FITEM,2,4518
FITEM,2,4522
FITEM,2,-4553
FITEM,2,4777
FITEM,2,-4780
FITEM,2,4790
FITEM,2,4795
FITEM,2,4799
FITEM,2,-4801
FITEM,2,4807
/GO
F,P51X,FY,-TOQ/1.14
```

Apply nodal forces on driving gear hub.

```
!*
!*
FLST,4,76,1,ORDE,13
FITEM,4,2938
FITEM,4,2942
FITEM,4,-2973
FITEM,4,4518
FITEM,4,4522
FITEM,4,-4553                                          Apply nodal coupling on driving gear hub.
FITEM,4,4777
FITEM,4,-4780
FITEM,4,4790
FITEM,4,4795
FITEM,4,4799
FITEM,4,-4801
FITEM,4,4807
CP,1,UY,P51X
FINISH                                                 ! The pre-processor finished.
!*
/SOLU                                                  ! Enter the solution.
!*
NLGEOM,1                                               ! Turn the Large-deflection key on.
NROPT,AUTO, ,                                          ! Let the program choose the Nonlinear Options (default).
LUMPM,0
EQSLV,ICCG,1.0e-6,0,                                   ! Equation solver is ICCG with its tolerance 1.0e-6.
PRECISION,0
MSAVE,0
PIVCHECK,1
SSTIF
PSTRES
TOFFST,0,
!*
TIME,1
AUTOTS,1
NSUBST,6,10,5,0                                        ! The substep is 6 within the minimum 5 and the maximum 10
KBC,0                                                  substeps.
!*
TSRES,ERASE
FINISH
/SOLU
/STATUS,SOLU
SOLVE                                                  ! Starts solving the problem.
/POST1                                                 ! Enter the postprocessor.
RSYS,1                                                 ! Turn the active coordinate system into the global cylindrical.
PRNSOL,DOF,U,Y
*CFOPEN,2D%TOQ%Nm,lis,,APPEND                          ! Open the text document '2D154.2Nm.lis' for appending.
!*CFOPEN,2Dstandard%TOQ%Nm,lis,L:\FEAResults\,APPEND   ! 'L' is network drive (optional)
*CFWRITE,,%ANG(FNAM)%,UY%FNAM%,UY('No.')               ! Write the driving gear hub master node DOF solution UY to the
*CFCLOSE                                               text file above.
SAVE,2Dstandard%TOQ%Nm%ANG(FNAM)%,DB,                  ! Save all solution in the data base (in the working directory).
!SAVE,2Dstandard%TOQ%Nm%ANG(FNAM)%,DB,L:\FEAResults\,0,0   ! ! 'L' is network drive (optional)
FINISH
FNAM=FNAM+1                                            ! Set next meshing position.
*IF,FNAM,GT,30,:ENDLOOP
PARSAV,ALL,ANGLE_A,,                                   ! Write all parameter to file.
*GO,:DOLOOP                                            ! Go back to :DOLOOP line action.
:ENDLOOP                                               ! End a do-loop when completed a cyclic mesh.
FINISH
!/CLEAR,START                                          ! Start next loop with different torque load (optional).
!/INPUT,2D_2nd,log,,, 0                                ! '2D_2nd.log' is in the working directory, otherwise the program
                                                       will stop.
```

APPENDIX B

LISTING OF AN APDL PROGRAM FOR THE STATIC T.E. OF THE NYLON GEARS IN MESH

```
/GST,ON                              ! Turns graphical solution tracking on
*DIM,ANG,,30                         ! Defines, ANG( ), an array parameter and its dimensions of
ANG(1)=-7.5,-7,-6.5,-6,-5.5          meshing position.  The mesh positions from –7.5 to 7.5 degree
ANG(6)=-5,-4.5,-4,-3.5,-3            cover (nearly) one base pitch – via (nearly) mid-double zone –
ANG(11)=-2.5,-2,-1.5,-1,-0.5         single zone - (nearly) mid-double zone, and which is according to
ANG(16)=0.5,1,1.5,2,2.5             the 2D model of 'PA6_2d.db'
ANG(21)=3,3.5,4,4.5,5
ANG(26)=5.5,6,6.5,7,7.5
FNAM=1                               ! Set initial meshing position.
PARSAV,ALL,ANGLE_A,,                 ! Write all parameter to file.
:DOLOOP                              ! :DOLOOP of meshing position in a cyclic.
RESUME,PA6_2d,db,,0,0                ! Resumes the 2D model (in the working directory) which has pre-
!*                                   defined the material properties, element type and initial meshed,
!*                                   contact at the pitch point.
PARRES,,ANGLE_A,, ,,                 ! Replace current parameter set with all array parameter from file.
/PREP7                               ! Enter pre-processor
!*
TOQ=20                               ! TOQ is the input torque load (currently set to 20 Nm).
!*
MPDATA,EX,2,,1000                    ! Using MPDATA to define the linear materials properties.
MPDATA,PRXY,2,,0.4                   Note: the linear property EX2 can not exceed the value that
!*                                   is defined below.
TB,MELA,2,1,30                       ! Using TB to define the MELA option of 30 points modulus data
TBTEMP,60                            ! at the temperature of 60 degree.
TBPT,,0.005,1.4
TBPT,,0.01,3.2
TBPT,,0.015,4.8
TBPT,,0.02,6.76
TBPT,,0.025,8.2
TBPT,,0.03,10
TBPT,,0.035,11.33
TBPT,,0.04,12.86
TBPT,,0.045,14.4
TBPT,,0.05,16
TBPT,,0.055,17.4
TBPT,,0.06,18.66
TBPT,,0.065,20
TBPT,,0.07,21.25
TBPT,,0.075,22.31
TBPT,,0.08,23.41
TBPT,,0.085,24.7
TBPT,,0.09,25.56
TBPT,,0.095,26.4
TBPT,,0.1,27.33
TBPT,,0.105,28
TBPT,,0.11,28.73
TBPT,,0.115,29.33
TBPT,,0.12,29.86
TBPT,,0.125,30.13
TBPT,,0.13,30.8
TBPT,,0.135,31.06
TBPT,,0.14,31.26
TBPT,,0.145,31.33
TBPT,,0.15,31.26
!*
FLST,3,47,5,ORDE,2
FITEM,3,48
FITEM,3,-94
```

```
AGEN, ,P51X, , , ,ANG(%FNAM%), , , ,1            ! Turn the driving gear with angle ANG(%FNAM%).
CSYS,1                                           ! Turn the active coordinate system into the global cylindrical.
FLST,3,47,5,ORDE,2
FITEM,3,1
FITEM,3,-47
AGEN, ,P51X, , , ,-ANG(%FNAM%), , , ,1           ! Turn the driven gear with angle -ANG(%FNAM%).
!*
…………………………………………………..
…………………………………………………..
…………………………………………………..
…………………………………………………..
…………………………………………………..
…………………………………………………..
…………………………………………………..
…………………………………………………..
…………………………………………………..
…………………………………………………..            The rest of the preprocessor is similar as in Appendix A.
…………………………………………………..
…………………………………………………..
…………………………………………………..
…………………………………………………..
…………………………………………………..
…………………………………………………..
…………………………………………………..
…………………………………………………..
!*
/SOLU                                           ! Enter the solution.
!*
NLGEOM,1                                         ! Turn the Large-deflection key on.
NROPT,AUTO, ,                                    ! Let the program choose the Nonlinear Options (default).
LUMPM,0
EQSLV,ICCG,1.0e-5,0,                             ! Equation solver is ICCG with its tolerance 1.0e-5.
PRECISION,0
MSAVE,0
PIVCHECK,1
SSTIF
PSTRES
TOFFST,0,
!*
TIME,1
AUTOTS,1
NSUBST,10,50,5,0                                 ! The substep is 10 within the minimum 5 and the maximum 50
KBC,0
!*
TSRES,ERASE
AUTOTS,-1.0
NEQIT,80                                         ! The number of equilibriums sets 80 for each substep.
/STATUS,SOLU
SOLVE
!*
/POST1
RSYS,1
PRNSOL,DOF,U,Y
*CFOPEN,PA6-%TOQ%Nm,lis,,APPEND
*CFWRITE,,%ANG(FNAM)%,UY%FNAM%,UY(671)
*CFCLOSE
SAVE,Pa6-2Dstandard%TOQ%Nm%ANG(FNAM)%,DB,
FINISH
FNAM=FNAM+1
*IF,FNAM,GT,30,:ENDLOOP
PARSAV,ALL,ANGLE_A,,
*GO,:DOLOOP
:ENDLOOP
FINISH
!/CLEAR,START                                    ! Start next loop with different torque load or temperature (optional).
!/INPUT,2D_2nd,log,,, 0                          ! '2D_2nd.log' is in the working directory, otherwise the program
                                                 will stop.
```

APPENDIX C
FEA OF HIGH CONTACT RATIO GEARS IN MESH

C-1 **Abstract:** High contact ratio gears have been demonstrated to provide significant advantages in decreasing tooth root and contact stresses with potential flow-on benefits for increased load carrying capacity. Previous investigations with high contact ratio gears have involved analytical, numerical and experimental aspects. Much of the earlier numerical work using FEA was limited in its usefulness due to several factors; (i) the difficulty in predicting load sharing over roll angles covering two or three teeth simultaneously in mesh, (ii) the difficulty for the analysis to obtain quality results when modeling Hertzian contact deflection simultaneously with the bending, shear and angular deflections, and (iii) the problem of primary unconstrained body motion when profile modifications were applied. This paper presents methods and results for overcoming these difficulties with recent computer hardware and software improvements. Particular developments discussed include the use of FE analysis of High Contact Ratio Gears in mesh and the results obtained when adaptive meshing and element birth and death options are used. The details of transmission error, combined torsional mesh stiffness and load sharing ratio against various input loads over a complete mesh cycle are also given. Results with various tooth profile modifications will also be presented.

C-2 **Introduction.** Previous research, (Townsend 1979; Rosen 1982; Elkholdy 1985; Barnett 1988; Lee 1991; Lin 1993; Yildirim 1999), has shown that high contact ratio gears can be designed to decrease bending stress by 20 percent and decrease contact stress by 30 percent (Drago 1974), thereby potentially enabling a higher power to weight ratio, longer service life and greater reliability.

Historically, the most significant step forward in the study of spur gears in mesh was made in 1958 by Harris (Harris 1958), with the fundamental work known as the Harris Map which has helped to provide a foundational understanding on conventional gearing (with gear contact ratios between 1.2 to 1.6). However, the Harris Map doesn't seem to automatically cover the characteristics of high contact ratio gears in mesh. Recent research (Townsend 1979; Rosen 1982; Elkholdy 1985; Barnett 1988; Lee 1991; Lin 1993; Yildirim 1999) on high contact ratio gears was based on a limited range of input loads (centered mainly on the design load). When tooth profile modifications are applied it is important to consider the effect of large and small loads on the gear behaviour. Detailed analysis on high contact ratio gears in mesh with wide range of input loads has been more difficult than the analysis on conventional low contact ratio gears for a number of reasons; (i) experimental difficulties where high contact ratio gears appear more sensitive to tooth spacing variations and other geometrical errors, (ii) mathematical models were either over complicated or used too many assumptions. With recent computing advances, numerical methods applied in the research of high contact ratio gears have become more realistic.

This paper presents results obtained by using customized ANSYS® APDL looping programs. Particular developments discussed include the use of FE analysis of high contact ratio gears in mesh and the results obtained when adaptive meshing and element birth and death options are used. The details of transmission error, combined torsional mesh stiffness and load sharing ratio against various input loads over a complete mesh cycle are given. Results with various tooth profile modifications will also be presented.

C-3   Analysis of Standard Involute Gears in Mesh. The major components of tooth deformation in a loaded involute elastic gear are: (i) tooth rotation about its root, (ii) local Hertzian contact deformation, (iii) bending displacement and (iv) shearing displacement. In particular the tooth rotation can be up to 5 to 10 times larger than the other deformation components. The complete analysis then requires FE modeling of the entire gear in mesh.

The involute tooth form of high contact ratio gears has been presented by Cornell (Cornell 1978; Cornell 1981) and it has also been used by other researchers (Lee 1991; Lin 1993). The tooth parameters used in this paper are shown in Table C-1. The FE model and its auto – mesh adaptation with contact is shown in Figure C1.

```
Gear tooth -------------------------------------------------------------------- Standard involute tooth
Material ------------------------------------------------------------------------------------ Steel
Friction coefficient ----------------------------------------------------------------------- 0.1
Number of teeth ----------------------------------------------------------------------- 32
Module M, mm (diametral pitch P, 1/in.)  ---------------------------------------- 3.18  (8)
Pressure angle, deg ------------------------------------------------------------------- 20
Addendum, mm --------------------------------------------------------------------- 1.53 * M
Face width, mm (in.) -------------------------------------------------------------- 25.4 (1.0)
Theoretical contact ratio ------------------------------------------------------------- 2.40
```

Table C-1. Tooth parameters.
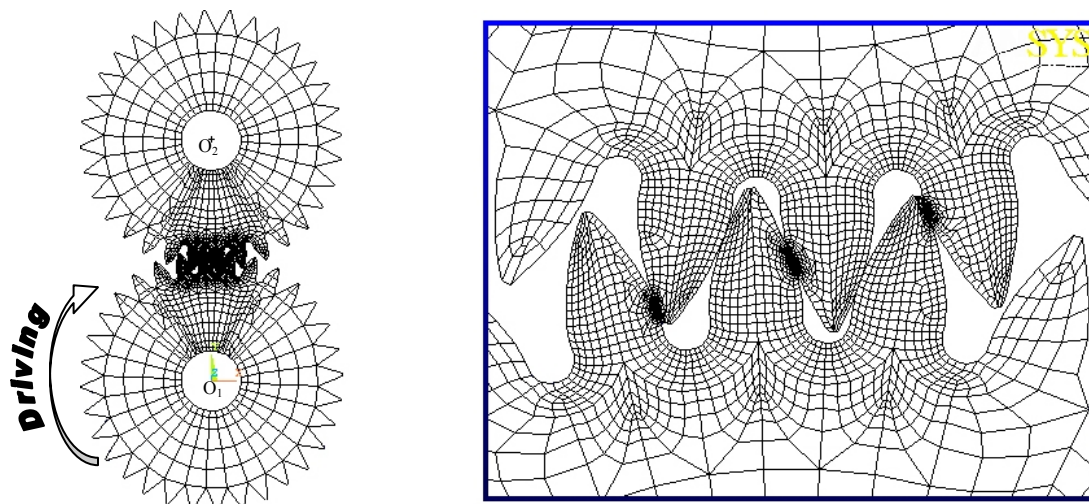
Figure C. 1 FE model of the gears in mesh (ratio 1:1) and its auto – mesh adaptation with contacts.

For a particular input load, the FEA solution for the displacement of the driving gear hub, with the driven gear restrained at its hub, was obtained for different mesh positions (about 69) over a complete mesh cycle. Results for a series of input loads can produce a map that shows the static Transmission Error (T.E.) over a complete mesh cycle as a function of input load. The same calculations can also produce the map of combined torsional mesh stiffness and load shearing ratio, as shown in Figure C2.
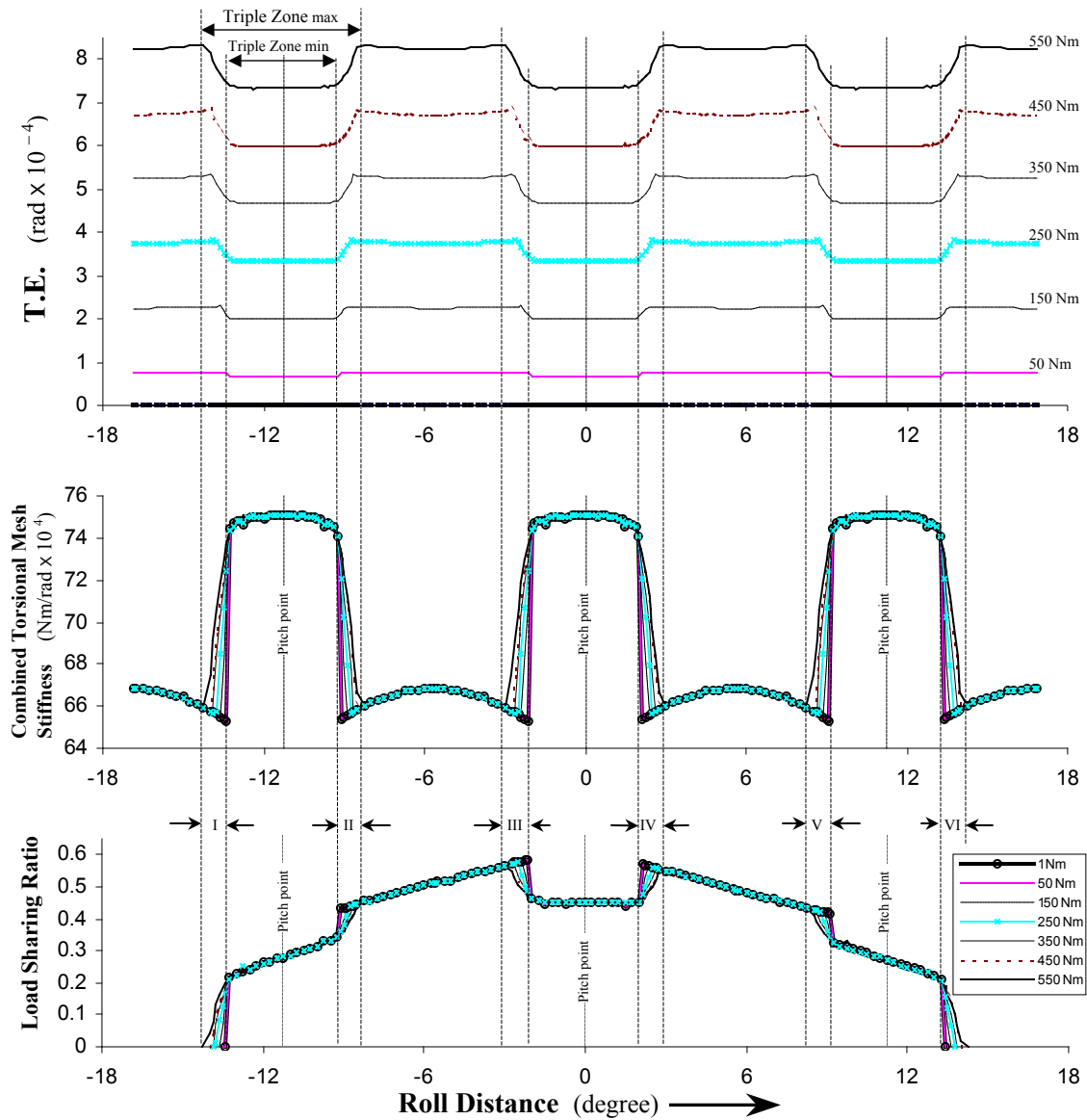
Figure C. 2 The change over process under various input loadsof the
involute gears in mesh (model 0).

Automatic mesh adaptation with contact has been known to be able to cope with the non–linearities present between contacts while avoiding the use of very large models. When the size of the elements (near the contacts) is between 0.3 to 0.5 mm, high quality results can be obtained, especially for the detailed change over region between the triple and double contact zones. As shown in Figure 2, the change over regions are denoted as regions I, III and V for the triple pair mating approach case, and regions II, IV and VI for the recess case. These regions, defined as _Handover Regions_, exist between the actual (loaded) and the theoretical (unloaded) higher stiffness zone. The higher stiffness zone is the double contact zone (when the contact ratio < 2) or the triple contact zone (when the contact ratio > 2). Generally, under a certain input load, the handover regions of approach and recess are different in their width and they vary non–linearly with input load. The expansion of handover regions will subsequently increase the contact ratio, and this can be seen in Figure C3.
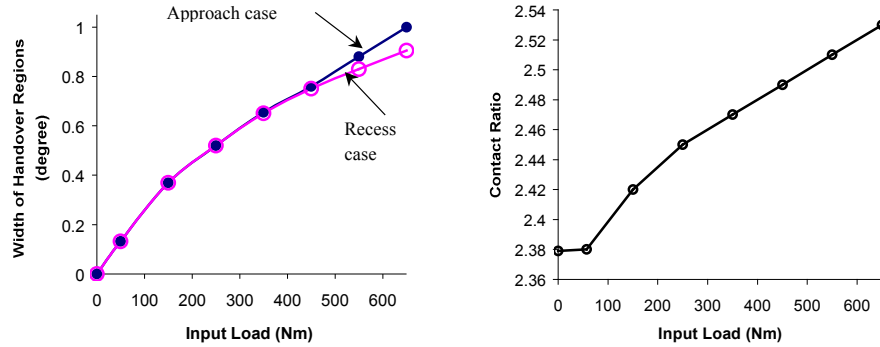
Figure C. 3 The variation of handover regions and contact ratio with a series input loads.

Previous investigation and discussion of the handover regions can be found in the work by Seager (Seager 1975), by whom the term tooth "separation" was used. Since then, researchers (Lin 1994; Munro 1999) have attempted to describe the handover region with analytical methods (geometrically), but the (T.E.) curves they produced in the handover regions were independent of the material properties.

Detailed handover region variations can be used to evaluate the amount of contact(s) outside the normal (theoretical) path that is due to the material flexibility. For the evaluation of the alignment, or geometrical errors such as manufacturing errors and wear, Munro (Munro 1999) has provided a complete theory with the calculation equations. For the general case, the evaluation of the total amount of contact(s) outside the normal path should be separated in two individual portions (approach and recess) as described above.

Because the handover regions exist when gears are loaded, tip relief is required to avoid the consequence caused by contact outside the normal path – the premature contact(s). In the past, however, researchers were required to minimise the dynamic response on the design load with long tip relief or profile modifications and the relevant research was based on the use of a limited range of input loads. Due to the meshing sensitivity of high contact ratio gears, profile modifications may also change the nature of the meshing significantly when the actual load is other than the design load, and the relevant investigations are as shown in the next section.

C-4   Analysis with Tooth Profile Modifications. The conventional amount of tip relief is as given in the existing standards such as British Standard (BS 1970) and ISO (ISO/DIS 1983), where the maximum amount of tip and flank modifications are defined as shown in Figure 4, including the parameters $C_{a\ max} = 0.02M$ and $\Delta L_{a\ max} = 0.6M$ to prevent the possibility of excess relief. Tooth profile modification of high contact ratio gears will have more effect on changing the gear transmission error (T.E.), combined torsional mesh stiffness and the shared tooth load. The existing standards applicable for high contact ratio gears should be followed with care to ensure rigid body motion leading to premature contact and large dynamic loads do not occur. The standard tip relief limitations have been chosen as reference values to normalize the amount of profile modification, for example, the amount of tip relief $C_a = 1.0$ means $^{(actual\ amount\ relief)}/C_{a\ max} = 1$.

There are different forms that can be chosen for the modified tip profile including linear and parabolic variations. The parabolic form presented by Walker (Walker 1938) attempted to remove material from the tooth tip with consideration of the effects of the

271

deformed tooth, much like that of a bent cantilever beam applied on top of the involute curve.

The modified profile form used in this research involves the original involute and relief was achieved by rotating the original curve through an angle α about the relief starting point S, as seen in Figure C4. Such relief is worthy of consideration for various reasons;
(i) the major component of the tooth displacement is the tooth rotation about its root, as described previously and (ii) it may be easier to manufacture.

The investigation involved a series of tooth-relieved models, with each model, having a particular C_a and ΔL_a combination.

Figure C. 4 Gear tooth with modified tooth profile.

In this paper, four of the models and their results will be presented. The selected models with their relief parameters are listed in Table C-2. The effects of different relief length ΔL_a on the TE, load sharing ratio and mesh stiffness are further investigated.

Parameters / Model name	Ca		ΔLa		α (degree)
	Absolute value (mm)	Normalized value	Absolute value (mm)	Normalized value	
Model 1	0.0156	0.245	0.661	0.35	1.0
Model 2	0.0108	0.17	1.558	0.82	0.3
Model 3	0.0162	0.255	2.359	1.24	0.3
Model 4	0.0174	0.274	0.928	0.49	0.8

Table C-2. Tooth relief parameters.

Model 1 is typical of a short type relief, where the relief length ΔL_a is only about one third of the standard limit. As the FEA results show in Figure C5, the relief generally results in a theoretical reduction of contact ratio with wider handover regions compared to the results illustrated in Figure C2. This model was designed to take a maximum input load of 350 Nm. Overload will cause corner contact, while the double T.E. zone will protrude upwards. On the other hand, the triple zone T.E. results also show a downward protrusion in most cases indicating that the amount of relief was too large, with premature contact occurring at the relief starting point S. So, this type of relief may only be suitable for light load designs (with limited C_a).

Model 2. The length of the modification here was 0.82 of the maximum allowable with the existing standard. On the original involute profile, segment ST_1 was one-third the length of PT_1 as shown in Figure C4. So this model was close to the one carried out by Lee and Lin (Lee 1991; Lin 1993), though the design load was 100 Nm lower due to the smaller amount of relief C_a. The most significant influence on solving this model was the length of the modification ΔL_a, which was long enough to cause rigid body (rotational) motion, which will be incorporated into the total displacement, including the T.E. in the triple contact zone. Under such conditions, the FEA solution will suffer from difficulties in attempting to

solve the primary unconstrained body motion of the driving gear, and the system matrix will become singular. One of the methods that can be used in solving such problems involves using a temporary link (or element connection) between a solid base and the driving gear to avoid the ill – conditioned system matrix. When the solution commences, (the pair of teeth are already in contact), the ANSYS[®] element birth and death option can be used to deactivate the link. Figure C6 shows the results for model 2.

The relief starting point S of model 2 remained inside the triple contact zone under both unloaded and loaded conditions, so there was a small variable (load-dependent) distance away from the HP2DTC (the highest point of second double tooth contact) (Lee 1991; Lin 1993).
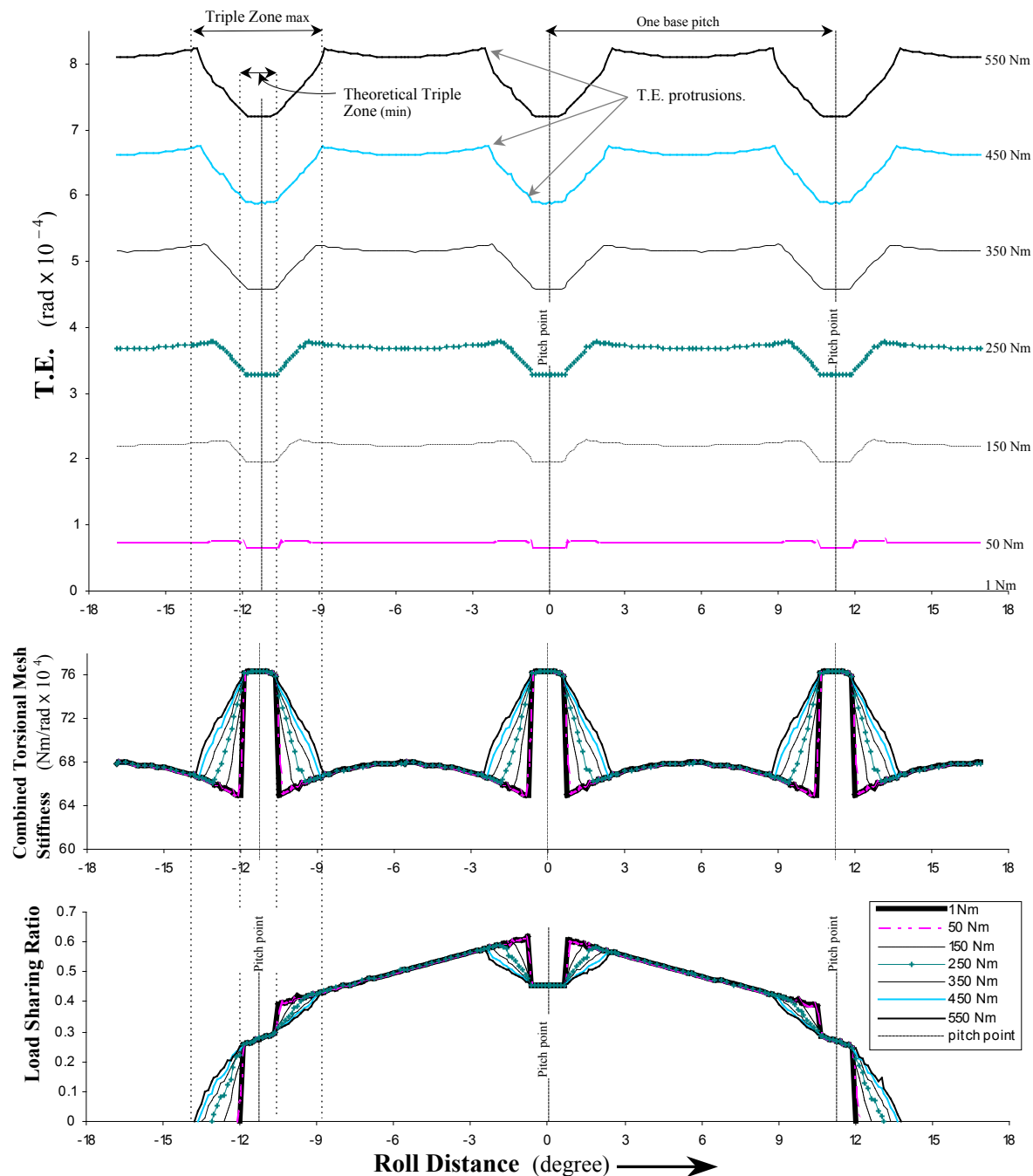
Figure C. 5 FEA results of Model 1.
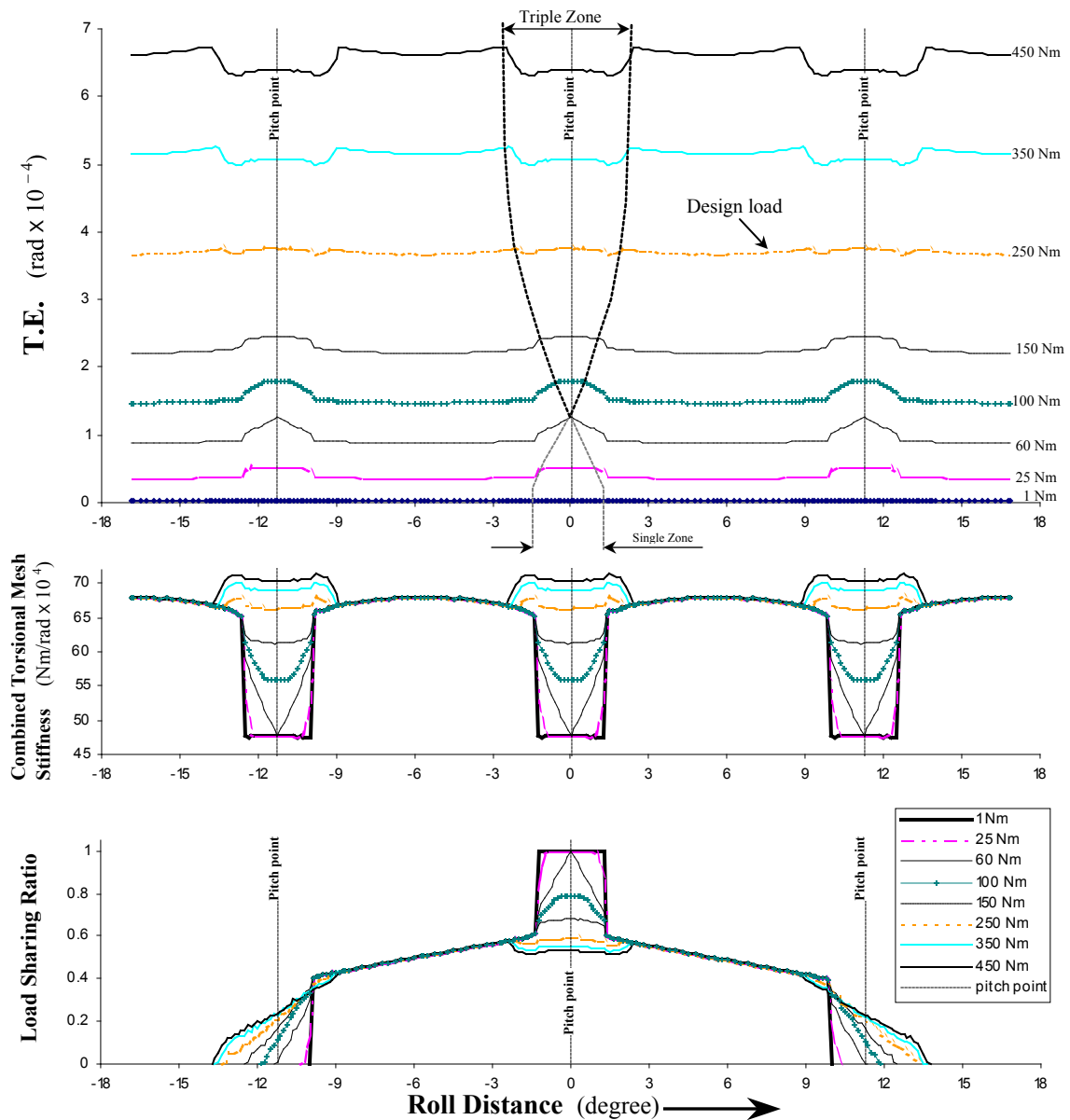
Figure C. 6 FEA results of Model 2.

The most notable variations in the results of model 2 are;

(i) Large T.E. fluctuations are present below the design load, and increasing the load will expand the triple zone with further large T.E. fluctuations.

(ii) During the loading phase (gears are expected to reach the design load) or in and out of cruise condition, gears will experience a dramatic change from LCRG to HCRG. The load sharing ratio and contact ratio variations against input load will be as shown in Figure C7 and C8 respectively.
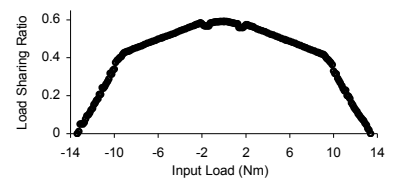
Figure C. 7 Load sharing ratio at the design load (250 Nm).
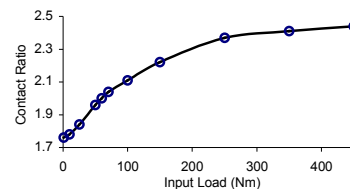
Figure C. 8 Contact ratio variations of Model 2.

274

(iii)Corner contact can still happen when the load is very light (gears operating under the cruise condition).

Model 3. The relief length here has exceeded the limit, which is 1.24 times of the maximum allowable by the current standards. Because the relief starting point S is located inside the double contact zone, (rotational) rigid body motion will be further incorporated into the part of the double zone displacement (near the double zone boundary area). Consequently no smooth T.E. curve will be found for the design load, as seen in Figure C9. In principle, this will be the same as for the tip relief situation for low contact ratio gears where the relief starting point should not be too close to the pitch point (near or inside the single zone).
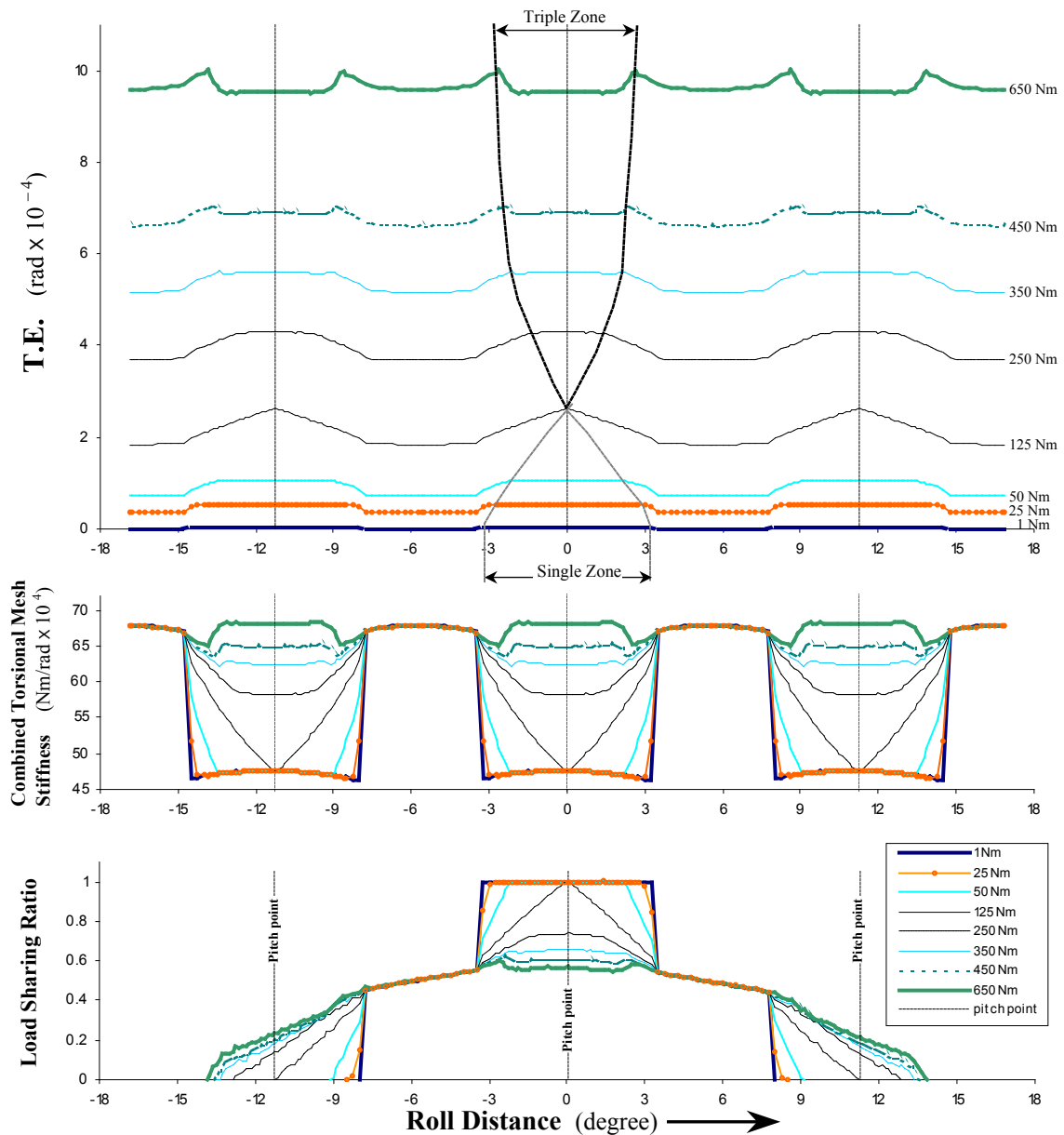
Figure C. 9 FEA results of Model 3.

On the other hand, the contact ratio will be further decreased compared to Model 2, as shown in Figure C10 and corner contact can occur when the load is very light.

Model 4. Model 4 is classified as a short type relief, because there is no rigid body (rotational) motion when the gears rotate throughout the mesh cycle. This type of relief is the longest of the short relief classifications. The critical relief parameter ΔLa was found to be (the normalized) 0.49 for this gear model. For gears with different geometrical parameters this critical relief parameter will change.
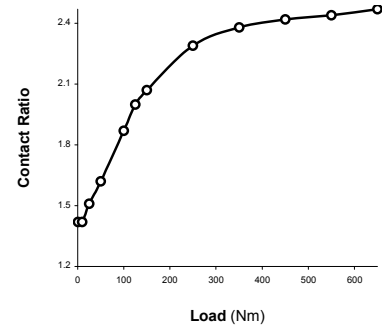
The FEA results are shown in Figure C11.

Figure C 10 Contact ratio variations of Model 3.
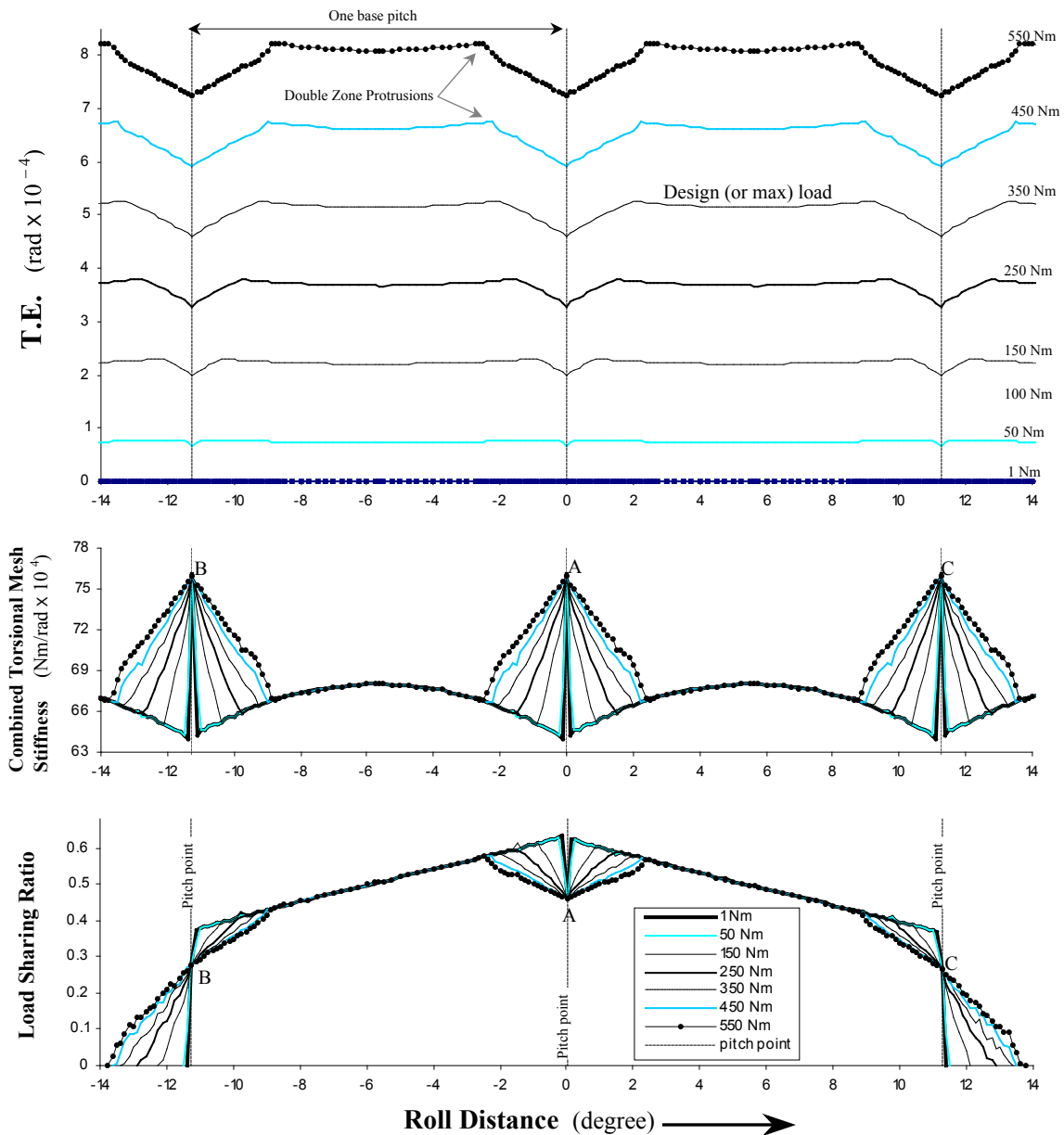
Figure C. 11 FEA results of Model 4.

276

The results of model 4 have shown that the region of triple contact can diminish to one point at the pitch point A (or B and C) when the input load tends to be very light. At the pitch point A (or B and C), the T.E. remains the value as if the gears were without tooth profile modification (pure involute) under the same load and boundary conditions, so too the combined torsional mesh stiffness and the load-sharing ratio. However, the FEA results show the minor difference in the amplitude of model 4 and model 0 (involute gears in mesh), especially in the combined torsional mesh stiffness (Figure C12). This difference was due to the different mesh density, in the numerical models as a higher mesh density was used in model 4, resulting in smaller elements which are principally stiffer.
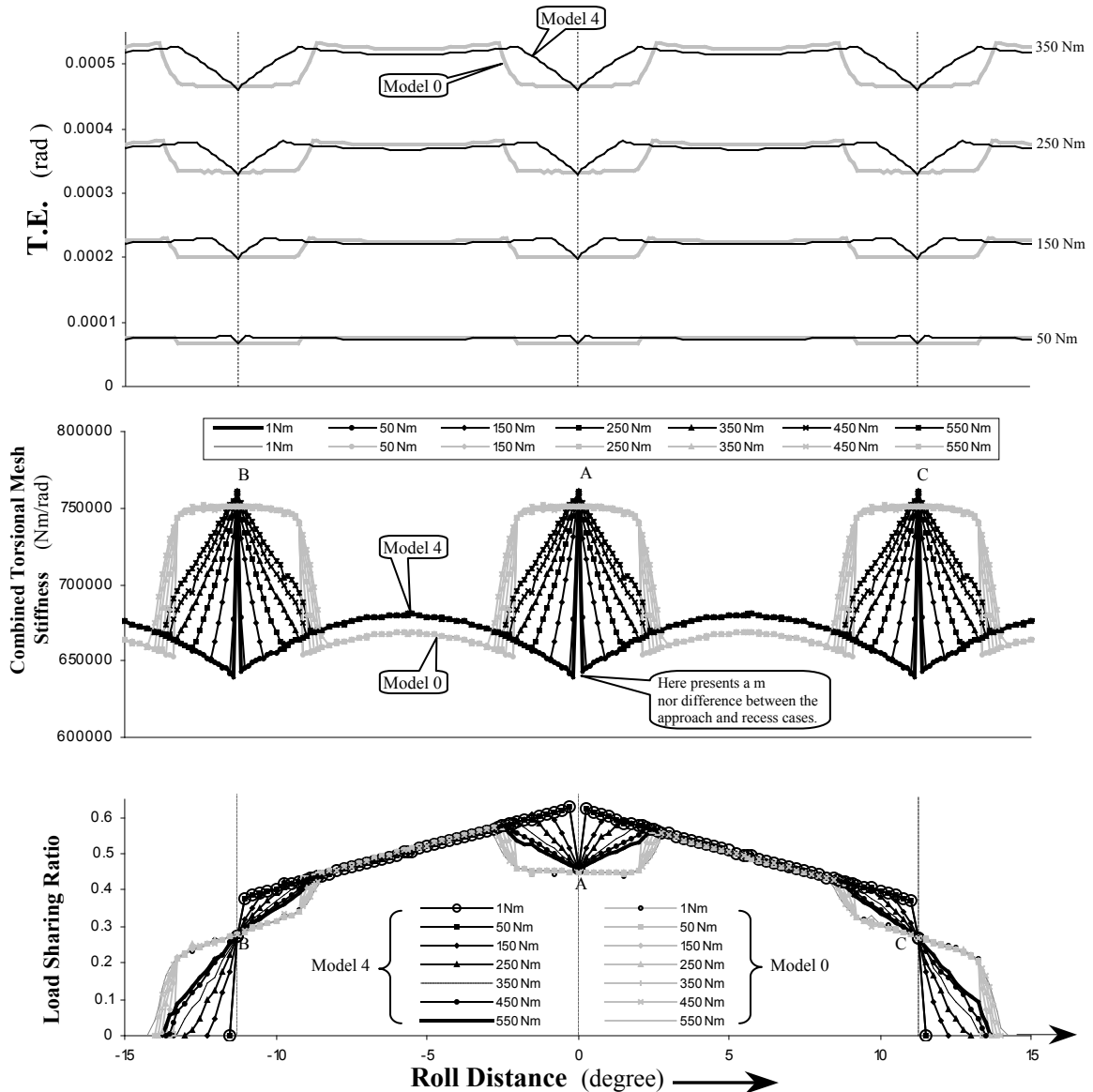
Figure C. 12 . The comparisons between model 4 and model 0.

The results also show that if the gears of Model 4 are rigid enough or the input load tends to zero, the tooth load-sharing ratio will show an exact space of a complete mesh cycle, and the contact ratio will tend towards 2. With such meshing characteristics, the consequence

277

of the (possible) premature contact at the relief starting point is minimised and the designed maximum load can be set higher, compared to Model 1. The other important characteristic of this model was that the contact ratio was always above 2, as shown in Figure C13.

C-5   Conclusions This paper has outlined methods for using FEA of high contact ratio gears in mesh, including adaptive meshing and element birth and death options. These methods have been shown to be proficient over a range of loads and teeth profile modifications, including those instances when rigid body motion is required.

Figure C. 13   Contact ratio variations of Model 4.

1.   With detailed results in the changeover process of the involute HCRG in mesh, the definition of handover region is more clearly defined. The existence of the handover region(s) presents the contact(s) outside the normal path of contact due to the material flexibility, and is one of the primary demands for tooth profile modification. Handover 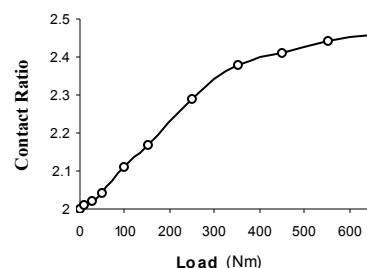regions exist in the static T.E., combined torsional mesh stiffness and load-sharing ratio. In particular, the handover region of the static T.E. represents the TE $_{o.p.c.}$ In previous research, the theory and evaluation methods of TE $_{o.p.c.}$ were developed mathematically (geometric analysis), and they are very suitable for gears with geometrical errors. However, some confusion may arise when one attempts to apply the theory and the methods to elastically deformed gears. The evaluations for the different cases should be separated. The numerical evaluations presented in this paper may be one of the alternative solutions.

2.   Four types of tooth profile modification (typical short, long, longer and optimal short) and their analysis results have been presented. The length of the tooth profile modifications was found to be the most critical relief parameter over a wide range of load. For long tooth profile modifications, if the relief length exceeds the maximum allowable by current standards, it was shown to produce a large dynamic response below the design load, and premature contact(s) may occur as the contact ratio drops below 2. Moreover, if the relief length has reached to the double contact zone, the smooth design load (T.E.) will not be achieved. Further increase in the relief length and the amount of relief, will increase the potential for flank surface scoring when the gears are operated at less than the design load. It is suggested that the relief, at least, remains within the maximum allowable by current standards (for this particular gear). However, there will be minor variations on the relief length limitation if gears take different geometrical parameters.

3.   Even if the optimal design load for minimum dynamic response can be found within the maximum allowable of current standards, one still has to be concerned for the response when the input load is lighter.

4.   The optimal relief for normal applications has been found as that which keeps the contact ratio above 2. The premature contact(s) at the tooth tip can be prevented within the designed maximum load, and at the relief starting point the possibility of premature contact (depending on the amount of relief) can be minimised. There is also a minor variation on the optimal relief for gears with different geometrical parameters. Generally, the higher the contact ratio, the shorter the optimal relief will be. The gear material properties have been found to be of no influence on this.

APPENDIX D
INVESTIGATION OF OPTIMAL TIP-RELIEF AND THE EFFECTS OF THE TOOTH PROFILE IRREGULARITIES

D-1 Introduction

High-speed gears can be excited by static T.E. resulting in high vibration levels (Walker 1938; Harris 1958; Gregory 1963; Welbourn 1979; Lin 1994). Understanding the generation of static T.E., combined torsional mesh stiffness, tooth load share and other mechanism properties over the mesh cycle with various types of tooth profile irregularities will enable further dynamic modelling to be more realistic.

HCRG (High Contact Ratio Gears) are expected to be more sensitive to irregularities in the tooth profile than LCRG (Low Contact Ratio Gears) and previous research results have proved that mainly in the dynamic response (Cornell 1978; Rosen 1982; Barnett 1988; Lee 1991; Lin 1993). However, detailed analysis of the static meshing process with HCRG has been far from sufficient and has result in many assumptions being incorporated into the dynamic models. Dynamic modelling of gear systems is often aimed at understanding the system diagnostics and condition monitoring (Du 1997; Howard 1998; Svicarevich 1999; Howard 2001), in which one of the critical stages is to have the capability of determining the difference between surface pitting and a tooth crack. Accurate knowledge of the effect and influence of tooth profile irregularities will assist this overall goal.

As part of an ongoing effort, this paper will present the analysis of FEA adaptive mesh using ANSYS® showing results of the meshing process of HCRG with and without surface pitting, tooth root crack and tooth tip fillet, in particular, the static T.E., combined torsional mesh stiffness, load sharing ratio and contact stress are presented at the design load and over a complete mesh cycle. Some results of a related LCRG are also presented so that the characteristics of HCRG are further highlighted.

D-2 Optimal Tip-relief in General Applications

Applying tip-relief to reduce the potential for gear flank surface damage and fluctuations in dynamic load and noise has been an accepted practice for many years. For general applications, short type relieves have been widely used. In order for these results to be as realistic as possible, the analysis on the effects of tooth profile pitting and root crack were carried out with a short type tooth tip-relieved gears. The analysis of short tip-relief has been presented in chapter 7, where the resulting characteristics have been shown to mainly depend on the relief length as shown by other recent publications (Yildirim 1999). However, further analysis with short type relief is still needed to determine the optimal short tip-relief for particular applications.

The involute tooth form of high contact ratio gears has been presented by Cornell (Cornell 1978; Cornell 1981) and it has also been used by other researchers (Lee 1991; Lin 1993).

The tooth parameters used in this paper are shown in Table D-1. The tooth profile of the HCRG and its related LCRG are shown in Figure D1. It can be seen, the only difference with the HCRG is the addendum of the LCRG, which is the standard 1.0 M, thus the theoretical contact ratio decreases from 2.4 to 1.71. For the comparison, there are no changes made on tooth root fillet of the LCRG (just for this section). To find out the optimal tip-relief, the analysis was carried out beginning with the LCRG, where a series of FE models were built with different C_a and ΔL_a combinations as shown in Table D-2.
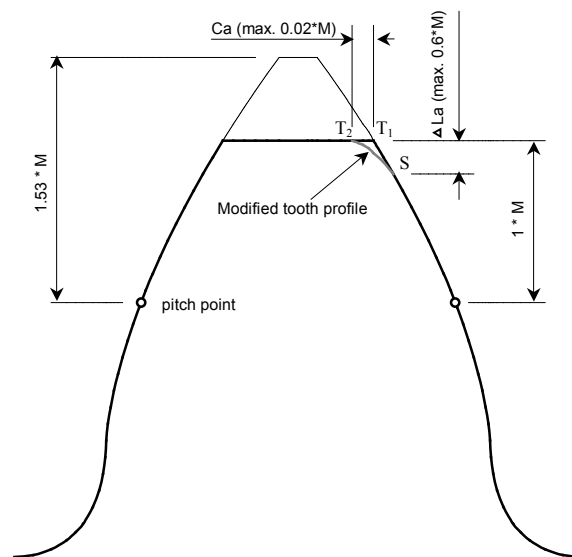

Figure D1   The tooth profile of the HCRG and its related LCRG with details of short modification.

```
Gear tooth ----------------------------------------------------------------- Standard involute tooth
Material ---------------------------------------------------------------------------------------- Steel
Friction coefficient --------------------------------------------------------------------------------0.1
Number of teeth---------------------------------------------------------------------------------- 32
Module M, mm (diametral pitch P, 1/in.) ----------------------------------------------------- 3.18 (8)
Pressure angle, deg ----------------------------------------------------------------------------- 20
Addendum, mm----------------------------------------------------------------------------------1.53 * M
Face width, mm (in.) ------------------------------------------------------------------------25.4 (1.0)
Theoretical contact ratio-------------------------------------------------------------------------- 2.40
Design load --------------------------------------------------------------------------------------350 Nm
```

Table D-1   Tooth parameters of the HCRG.

Parameters / Model name	C_a		ΔL_a	
	Absolute value (mm)	Normalized value	Absolute value (mm)	Normalized value (L_n)
Model 1	0.021	0.325	0.79	0.41
Model 2	0.023	0.360	1.05	0.55
Model 3	0.028	0.445	1.45	0.76
Model 4	0.031	0.49	1.59	0.83

Table D-2   Tooth relief parameters of the LCRG.

The standard tip-relief limitations, such as BS (1970) and ISO (ISO/DIS 1983) use $C_{a\ max.}$ = 0.02M and $\Delta L_{a\ max.}$ = 0.6M, and these have been chosen as the reference value here to normalise the modification parameters, for example the normalised relief length $L_n = \frac{actual\ relief\ length\ \Delta L_a}{max.allowable\ relief\ length\ 0.6M}$. FEA results of each model for the static T.E. and tooth contact stresses were obtained at the design load 350 Nm, as shown in Figure D2, where the results of involute (unmodified) gears are also presented. It can be seen that the T.E. of involute gears have double contact zones, handover region(s) and single contact zones. For tooth tip-relieved gears (model 1 to model 4), the single zone and the handover regions expand with the increase of the relief length ΔL_a. Meanwhile, the T.E. of double contact

280

zone will decrease; when the relief length reached to 1.59 mm (model 4), there are only single points remaining at each original double contact T.E. zone. Further increase of the relief length changes the T.E. at (or near) the middle of the double contact zone that starts to increase meaning that rigid body motion will be incorporated into the T.E. and the tip-relief will be subject to long modifications, but this will not be discussed in this paper.
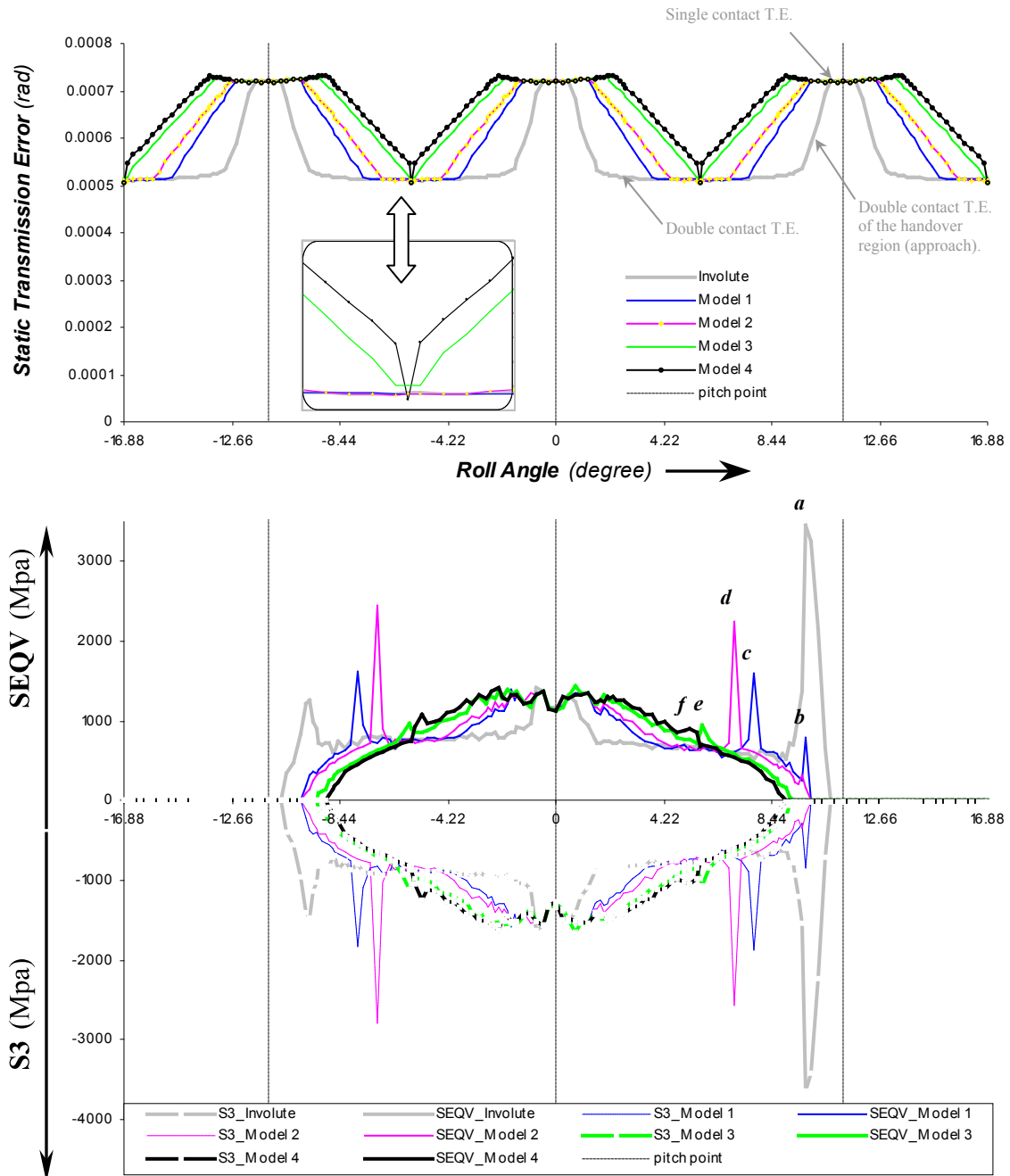

Figure D 2   FEA results of each model for the static T.E. and tooth contact stresses.

Tooth contact stresses over the mesh cycle for each model have shown dramatic changes, in particular, the peak stress values decrease when the relief length was gradually increased

from model 1 to model 4. The peak stress values of model 1, for example, show that the von Mises stress at *c* would have a value greater than that of model 2 at *d* if the amount of relief C_a were sufficient to avoid the premature contact at the tooth tip *b* (9.75 degrees). Figure D3 shows the von Mises stress of model 1 at mesh position 9.75 degrees where the tooth contact stress of MT has shown the peak value in Figure D2 at *b*. The other peak value at *c* occurred when contact was at the relief starting point.
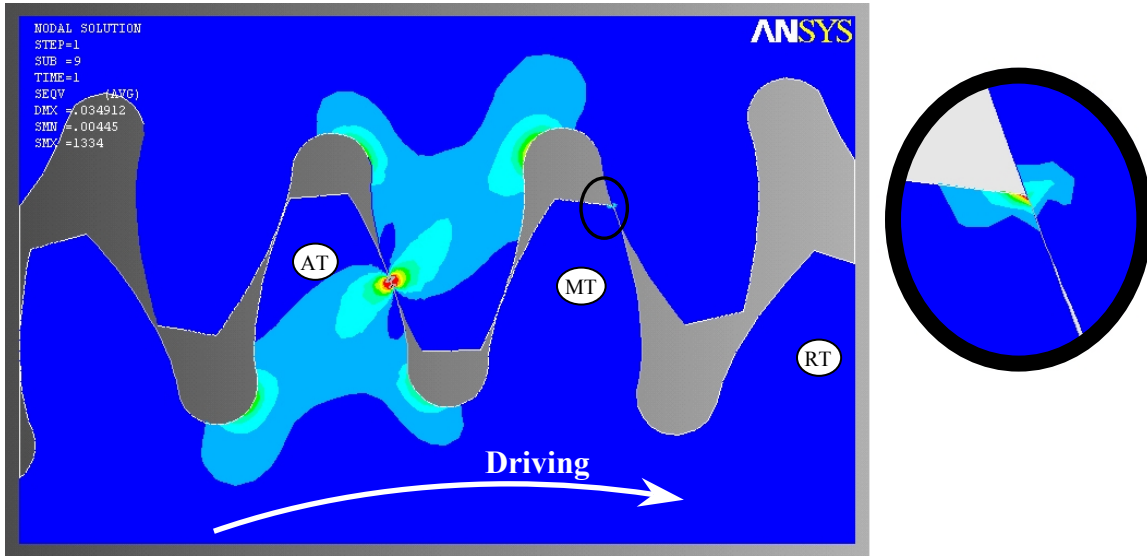

Figure D 3   The von Mises stress of model 1 at the mesh position 9.75 degrees.

> MT: mid-tooth which presents the tooth contact stresses in Figure C 15.
> AT: approach tooth.
> RT: recess tooth.
> Roll angle = 0: when MT contacts at the (un-loaded) pitch point.

The other peak values at *d*, *e* and *f* of model 2, 3 and 4 occurred when contact was at the starting points of their relief.   The maximum stress reductions have been found by model 4 due to its relief (C_a = 0.031 mm), being larger than that of the other models. However, confirmation of the optimal short tip-relief needs further analysis carried out with C_a of model 4 increasing to the maximum allowable 0.02M, which is 0.064 mm. This is shown in Figure D4.

With the maximum allowable C_a, the tooth contact stresses did not show higher values than normal particularly at the relief starting point. So, for this particular (LCRG) gear, relief length of 1.59 mm or the normalised value 0.83 will achieve an optimal performance. The possible premature contact at the relief starting point (when Ca is up to the maximum allowable) will be at a minimum compared to a relief length shorter than the normalised 0.83.

One of the characteristics of the optimal tip-relief is that the contact ratio (with gears ratio 1:1) will decrease to 1 when the input load tends to zero, as shown in Figure D5.
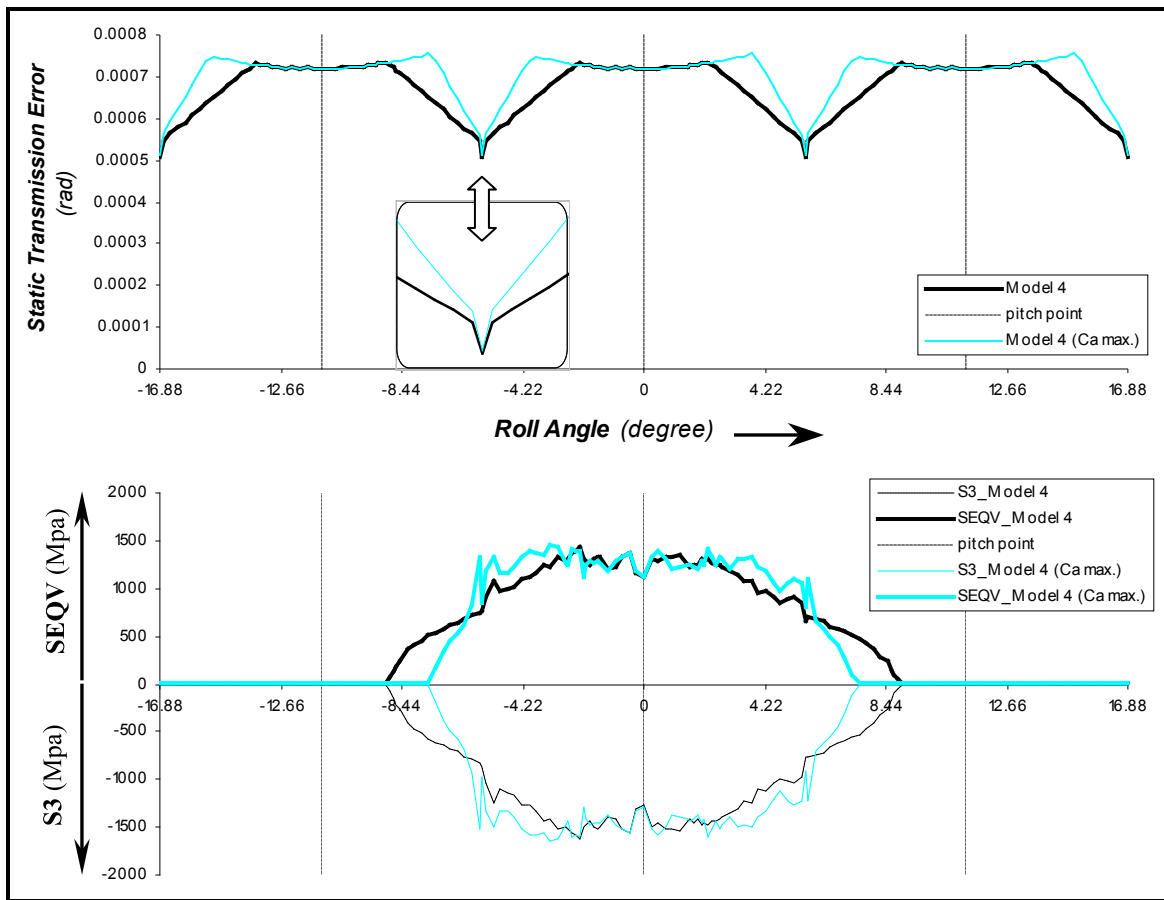
Figure D 4   T.E. and contact stresses of model 4 with the maximum relief allowable at the design load (350 Nm).

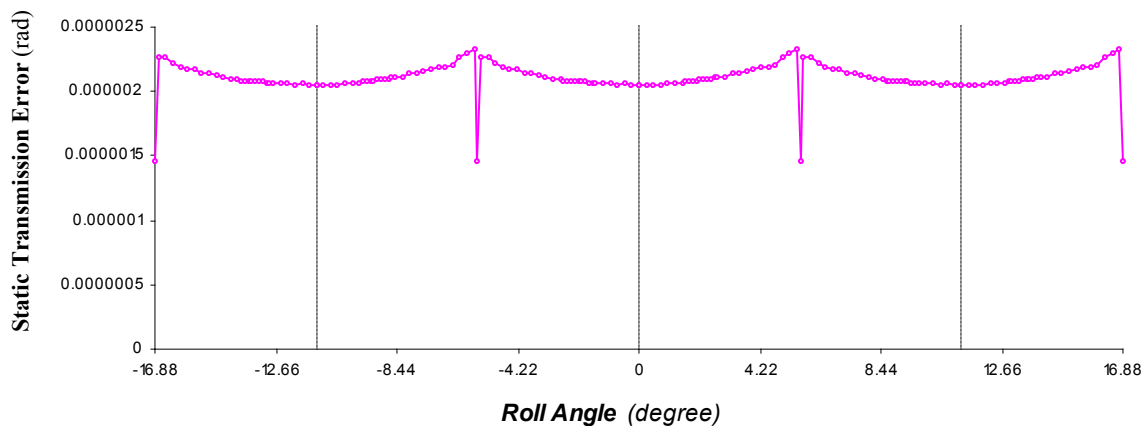Figure D 5   T.E. of model 4 with the maximum relief allowable under 1 Nm input load.

With the same procedure, the critical relief length ΔL_a for the HCRG (with the addendum 1.53M) was found to be 0.928 mm (0.49 in normalized value). One of the characteristics of the optimal tip-relief of the HCRG is that the contact ratio (with gear ratio 1:1) will decrease to 2 when the input load tends to zero.

D-3   The Analysis of Tooth Tip-relieved Gears with Crack and Pitting

The most notable tooth profile irregularities are the tooth root crack and surface pitting. The analysis is based on the Model 4 that was presented in this appendix part I, and here it is named Rfif08. Figure D6 shows the detailed features of the model, and Figure D7 gives the FEA model overview and mesh.

The crack mouth as shown was located at the middle of the tooth root fillet curve BC, and the crack length of 1mm and 2 mm was considered. Three instances of (0.1mm radius) circular pitting were simulated. The dedendum section of the drive gear is often the first to experience serious pitting damage which was represented by the pitting No. 1, however as operation continues, pitting usually progresses to the point where a considerable portion of the tooth surfaces have developed pitting, and those were represented by the pitting No. 2 and No. 3. In order to obtain detailed quality FEA solutions over the mesh cycle (s),
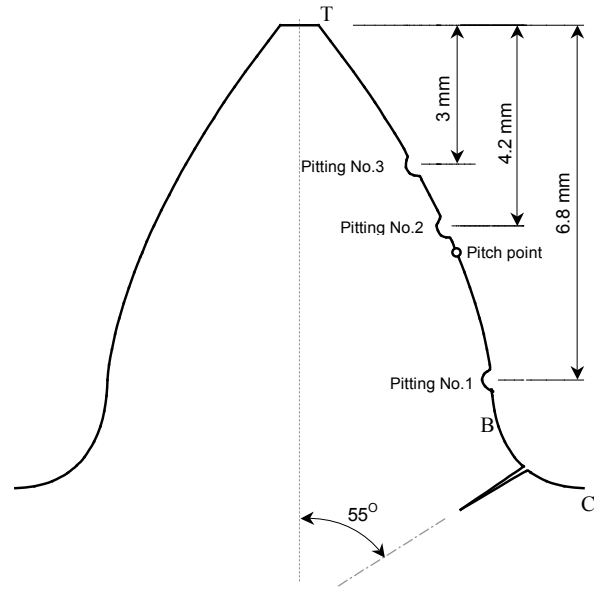

Figure D6   The detailed tooth irregularities on the tip-relieved tooth for 2D FE modeling.

adaptive mesh was used that was incorporated with the customised ANSYS® APDL looping programs, and 206 data points were produced in a complete looping to cover roll angles of three teeth. The program also output the contact stresses at each mesh position to determine the maximum vonMises (SEQV) and the minimum principal stress (S3) in the flank surface **TB** as shown in Figure D 6.
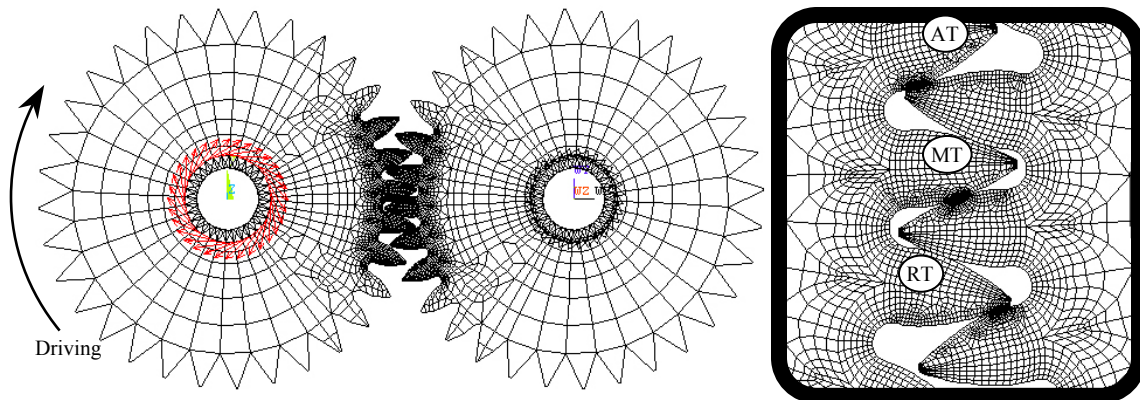

Figure D 7   Model over view and detailed adaptive mesh.

MT: mid-tooth with profile disfeaturing
AT: approach tooth
RT: recess tooth
Roll angle = 0: when MT is contacted at the pitch point (un-loaded).

D-3-1 The Effects of a Single Tooth Root Crack

The FEA results of static T.E. and combined torsional mesh stiffness are presented in Figure D8, where the results of a single tooth root crack of 1mm and 2mm are compared with that of undamaged gears. For LCRG, a tooth root crack can only cause changes to the static T.E. or combined torsional mesh stiffness in just one complete mesh cycle (Sirichai 1999; Wang 2000; Wang 2002), but for HCRG that covers the entire region from *a* to *b* (see Figure D8), which is significantly extended causing more global effect. The effect of a 1mm root crack is also significant compared to that for such a small root crack with LCRG that is usually insensitive. The maximum effects of a root crack in both cases are observed at the location *c* that is between the high stiffness (triple contact) and the low stiffness (double contact) regions in the recess case.

It is also noted that when the crack length was 2mm, small protrusions were found at mesh positions *c* and *d* in the curve of both static T.E. and combined torsional mesh stiffness. This shows that the tip-relief becomes insufficient in this case. Further study with this case has produced tooth load sharing ratio of AT, MT and RT with and without the root crack, and the contact stresses for those three teeth for the cracked gears only are shown in Figure D9.
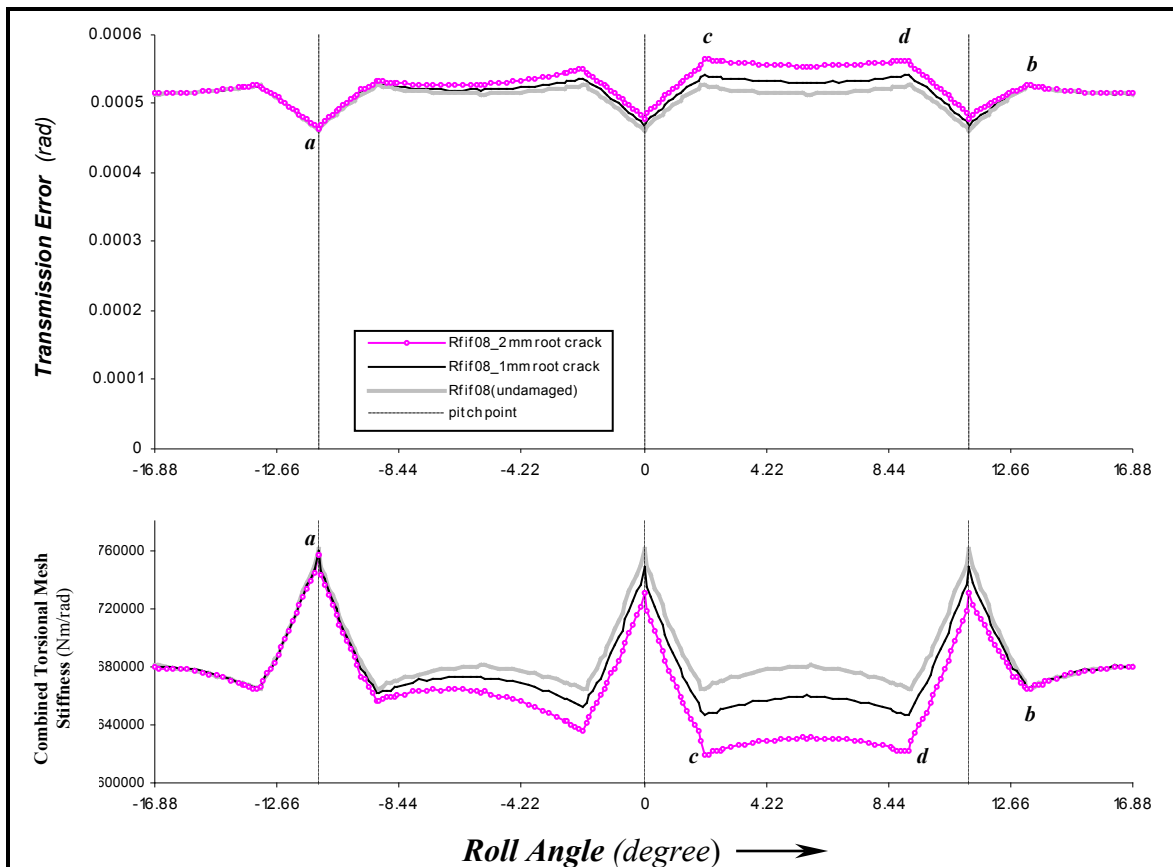

Figure D 8   Static T.E. and combined torsional mesh stiffness of tooth with a single root crack 1mm and 2mm compared with that of undamaged gears.
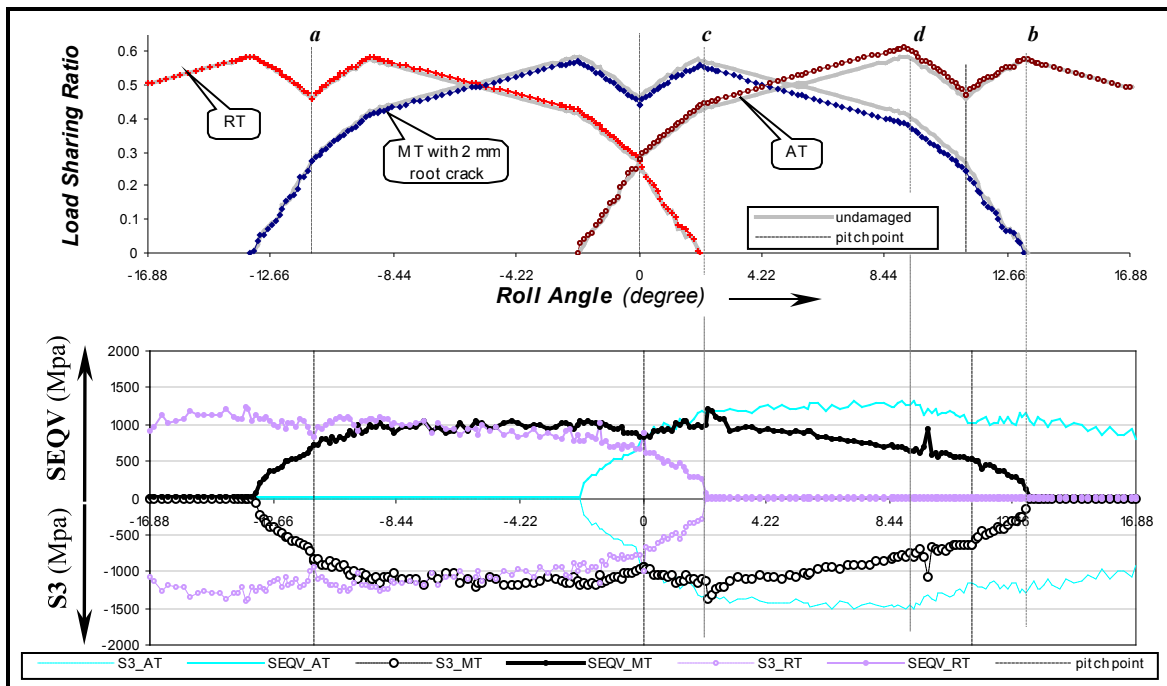
Figure D 9   Tooth load sharing and the contact stress when the tooth (MT: mid-tooth) contains a 2mm root crack.

Figure D9 has shown that the damaged tooth MT not only changes its own load-sharing ratio but also that for the neighbouring teeth RT and AT. In the affect range that is observed from *a* to *b*, teeth RT and AT tend to support the damaged tooth MT, in particular, AT takes more load from MT in the cross section (double contact zone) *cd,* and this leads to the stresses changes as shown with MT decreasing and AT increasing.

It is also noted that there are two abruptions in MT stress curves SEQV or S3 due to the insufficient tip-relief causing the premature contacts, but the stresses abruptions do not show any obvious signs that their effects have been transmitted to the neighbouring teeth. One of the abruptions, however, was not positioned at *d*, where it was expected to be.

Consider that the 2mm root crack is small, it may still enable the gears to keep running foe a long period without crack extension. Gears running under such condition will cause flank surface scoring damage, but initial pitting is most likely to occur near *c* and *d* once enough stress cycles have been built up. The position *c* is somewhere above the pitch point (depending on the input load) which is significantly different with where the conventional initial pitting that appears in the dedendum section, but contact at *d* is near the tooth tip of MT and below the pitch point of AT.

D-3-2   The Effects of Tooth Surface Pitting

Further FEA simulations were carried out when the tooth MT contains multiple pitting as shown in Figure D6 (without the tooth root crack). In the proposed rolling angle from –16.88 degree to 16.88 degree (where the rolling angle is 0 degree when the tooth MT is contacted at its pitch point), the results of static T.E., combined torsional mesh stiffness and

load sharing ratio, with and without the pitting, and the results of the contact stresses for the teeth RT, MT and AT were produced when the tooth MT contained the pitting.

All those results were aligned as shown in Figure D10. Pitting No. 1 is located in the dedendum section of the driving gear tooth MT where the initial pitting is likely to appear. This pitting has shown its wider impact on the T.E. and the combined torsional mesh stiffness than the other pitting locations. While, pitting No. 2 has shown its impact by the largest amplitude, particularly in the contact stresses. Pitting No. 2 is located where the premature contact occurs if a (2mm) root crack has occurred. Pitting No. 3 has shown more stable characteristics, and the location (addendum section) is where there is usually less chance to have pitting damage.

All the pitting locations have shown the major characteristics of localized changes to the T.E. and to the combined torsional mesh stiffness. The tooth load-sharing ratio of the tooth MT (with pitting) does affect that of its neighbouring teeth (also locally), but its stresses does not appear to affect the others. Such characteristics are significant different with that of the tooth with crack damage. Surface pitting (initial) appears to induce high frequency changes compared to a cracked tooth. Both pitting and a root crack should affect the system dynamic behaviour to excite further vibration. In particular, the large stress amplitude of the tooth with pitting will not transmit to the other teeth, but when the tooth has a root crack, the stress pattern of the damaged tooth and its neighbouring teeth are widely changed. The stress behaviours have provided the possibilities of condition monitoring gear systems using high order strain measurement (Wang 2002), because elastic strain is of the same order as stress.
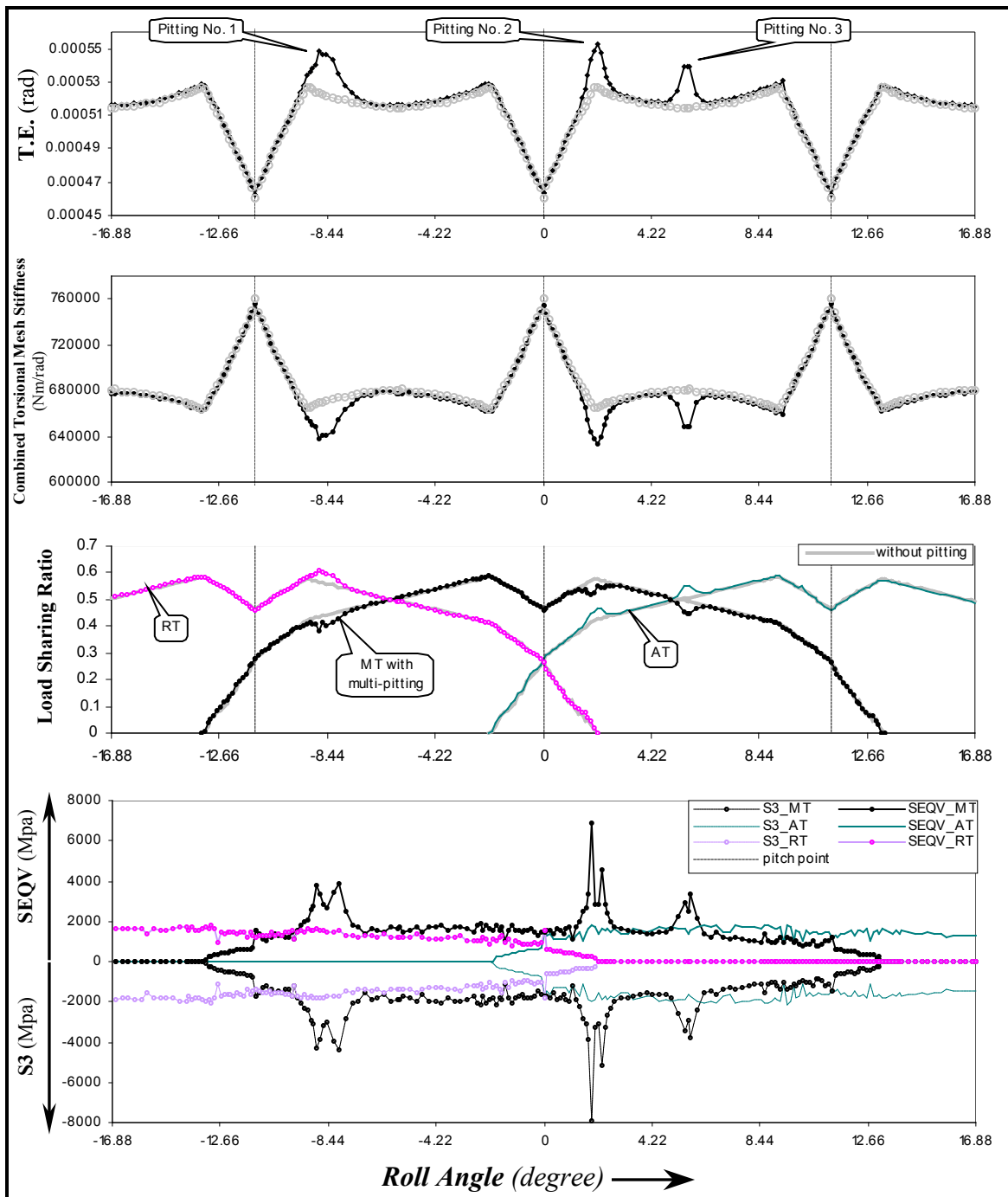
Figure D 10   The meshing process when the tooth MT presents multi-pitting.

D-3-3 3D Modelling of Surface Pitting of the LCRG and HCRG

More realistic modelling of tooth surface pitting will involve 3D FEA, in which mesh adaptation with contact(s) using brick element and symmetrical mid-plane modelling are very important for quality solutions without using huge models (mesh density was under 40,000 nodes). The detailed FE model of the HCRG with a single surface pit is shown in Figure D11.
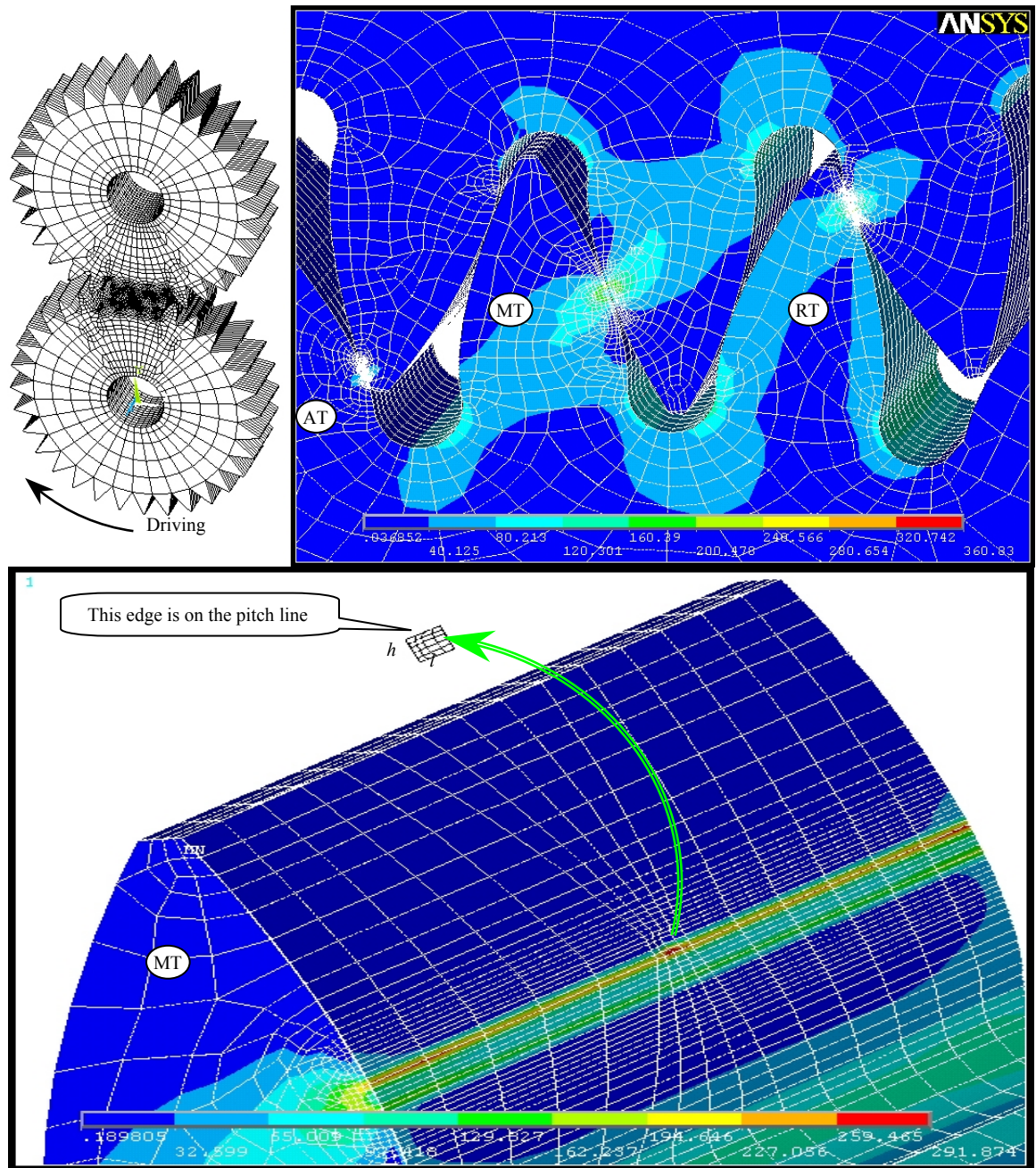
Figure D 11   3D FE model and the adaptive mesh with contact also with single pit on MT
of driving gear (the maximum depth in the pit centre is 0.1 mm).

It can be seen that a rectangular pit (*h* x *l*) was positioned just under the pitch point (or the pitch line) because the maximum tooth contact stress will be in this area for gears with optimal tip-relief.

According to Vizintin (Vizintin 2002), a 2mm x 4mm pit will cause WPC (wear – particle concentration) exceeding the critical limit, and this pit could develop fast to destructive pitting. So the FE modelling concentrated on this critical pitting and one of the analysis results is shown in Figure D12.
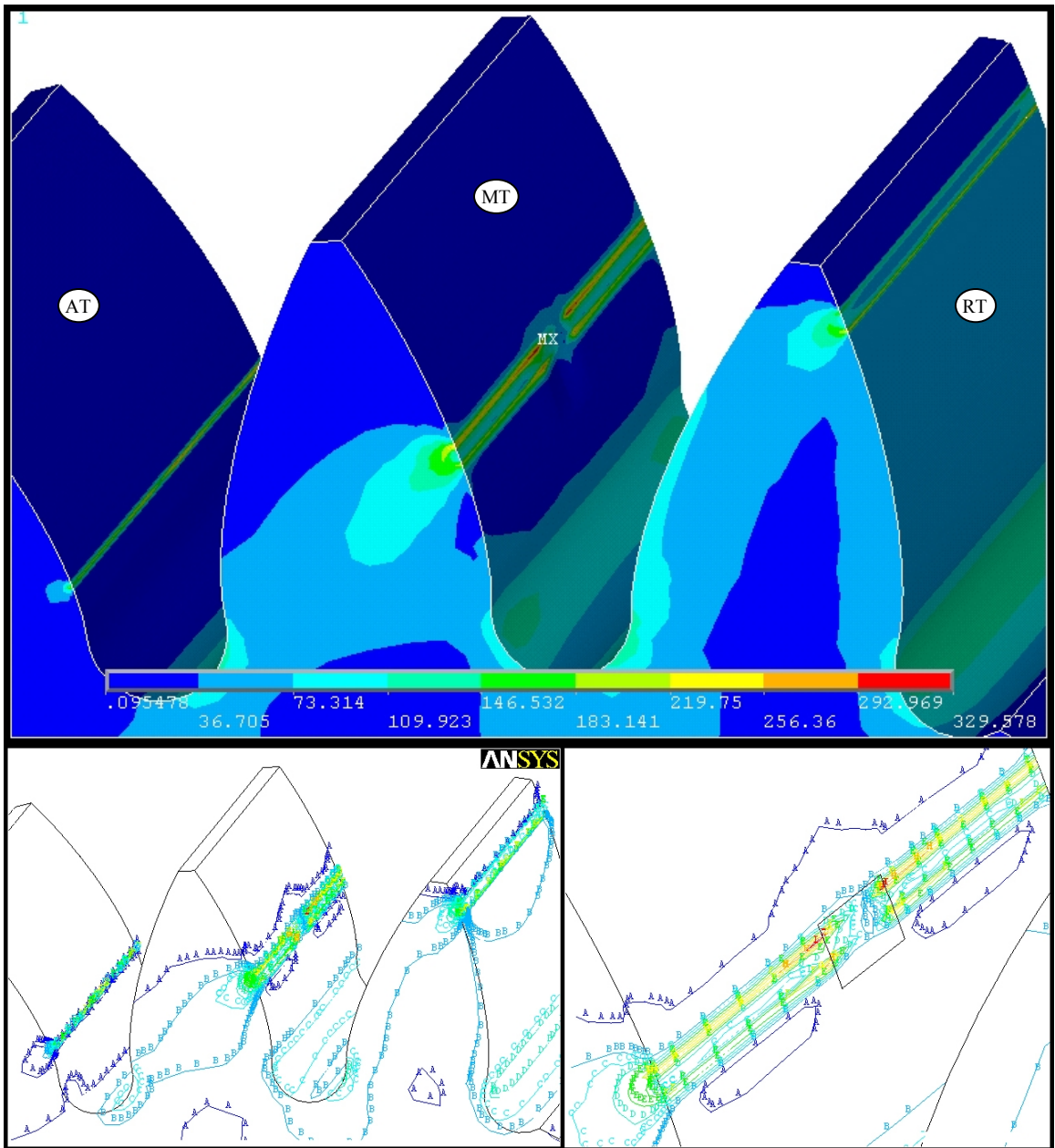
Figure D 12   The von Mises stress of the (driving) gear appeared with a critical pit (2mm x 4mm).

The static T.E. were produced by the looping programs for different mesh positions over the mesh cycle, where the pit was located in the same position (in the middle of the tooth face width and just below the pitch point) for both HCRG and LCRG. The results were also compared with that of the 2D models, as shown in Figure D13.
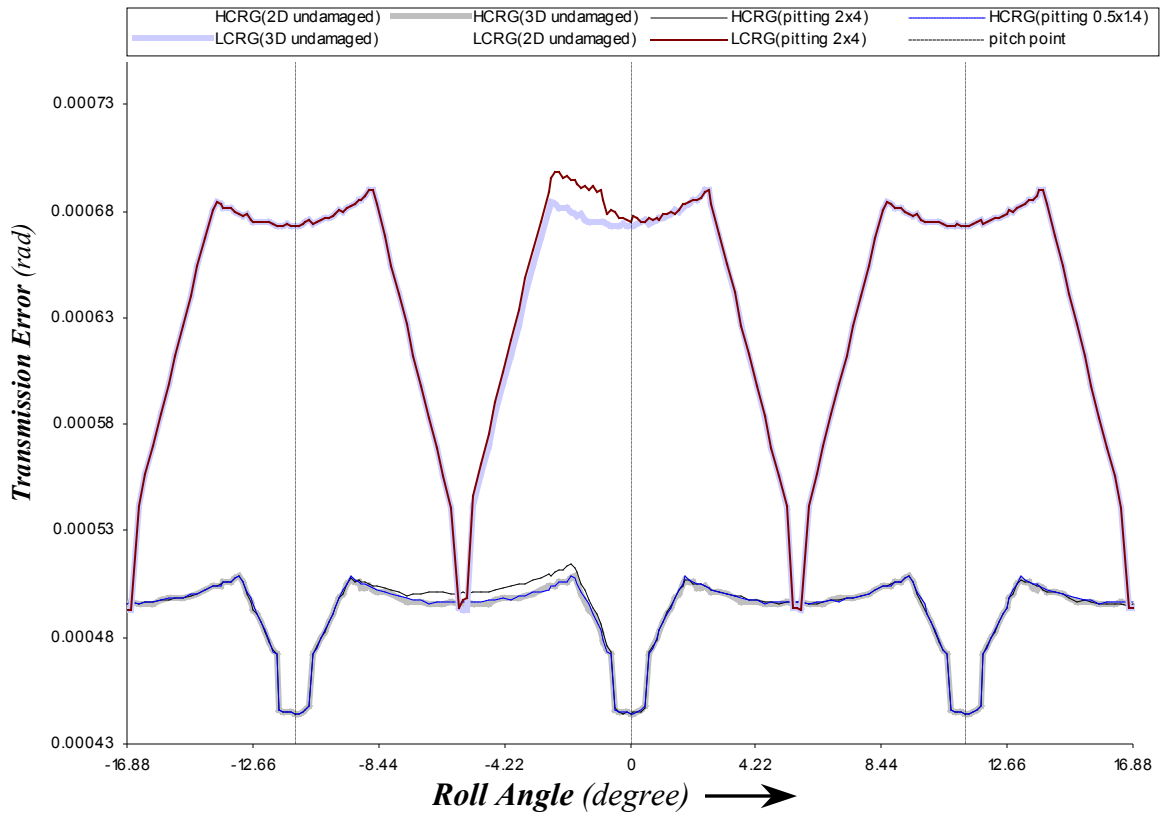
Figure D 13   Static T.E. of the HCRG and the LCRG.

It can be seen that the static T.E. has been overstated by 2D modelling compared to that of 3D modelling, however, the major difference between the 2D and the 3D FE modelling, in particular for the HCRG modelling, is the different triple contact regions and that is due to the 3D modelling having a larger contact area than the 2D's (see Figure D3 and D7). It should be noted that the HCRG with the small pitting, (0.5mm x 1.4mm) close to pitting initialisation (Vizintin 2002), hardly makes any changes to the static T.E. However the results for critical pitting size (2mm x 4mm) can cause significant change to the T.E. magnitude for the LCRG (in the half of the single contact zone) and over a wider range for the HCRG (in the complete double contact zone).

Compared to results of the single root crack damage, the following conclusions can be given,

- For the LCRG, the T.E. (and other mechanism properties) can have an abrupt change in the half of the single zone for a single critical pit, but for a root crack the change will be over the complete mesh cycle.
- For the HCRG, the single critical pit affects the T.E. over the entire double contact zone whereas the single root crack affects the T.E. over the two complete mesh cycle.

291

D-4 The Effect of Varying Tooth Tip Fillet Size

Considering the variations to tooth tip fillet radius of 0.5 mm, 0.25 mm and without the tip fillet, two FEA models, Model L and Model H were studied. Model L, with the tooth addendum 1*M, has an ideal contact ratio 1.71 (for 1:1 gear ratio) and is a conventional LCRG. Model H with the addendum increasing to 1.53*M becomes a HCRG (ideal contact ratio 2.4) that is very much the same as the model used in previous sections, where tip-relief was not applied (see Figure D14), where M is the module. The FEA solution for the transmission error has produced six results for those two models, as shown in Figure D15.
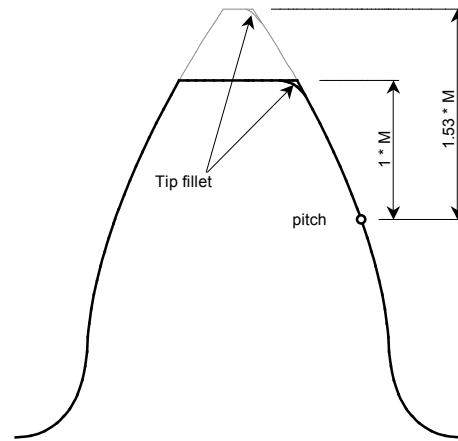
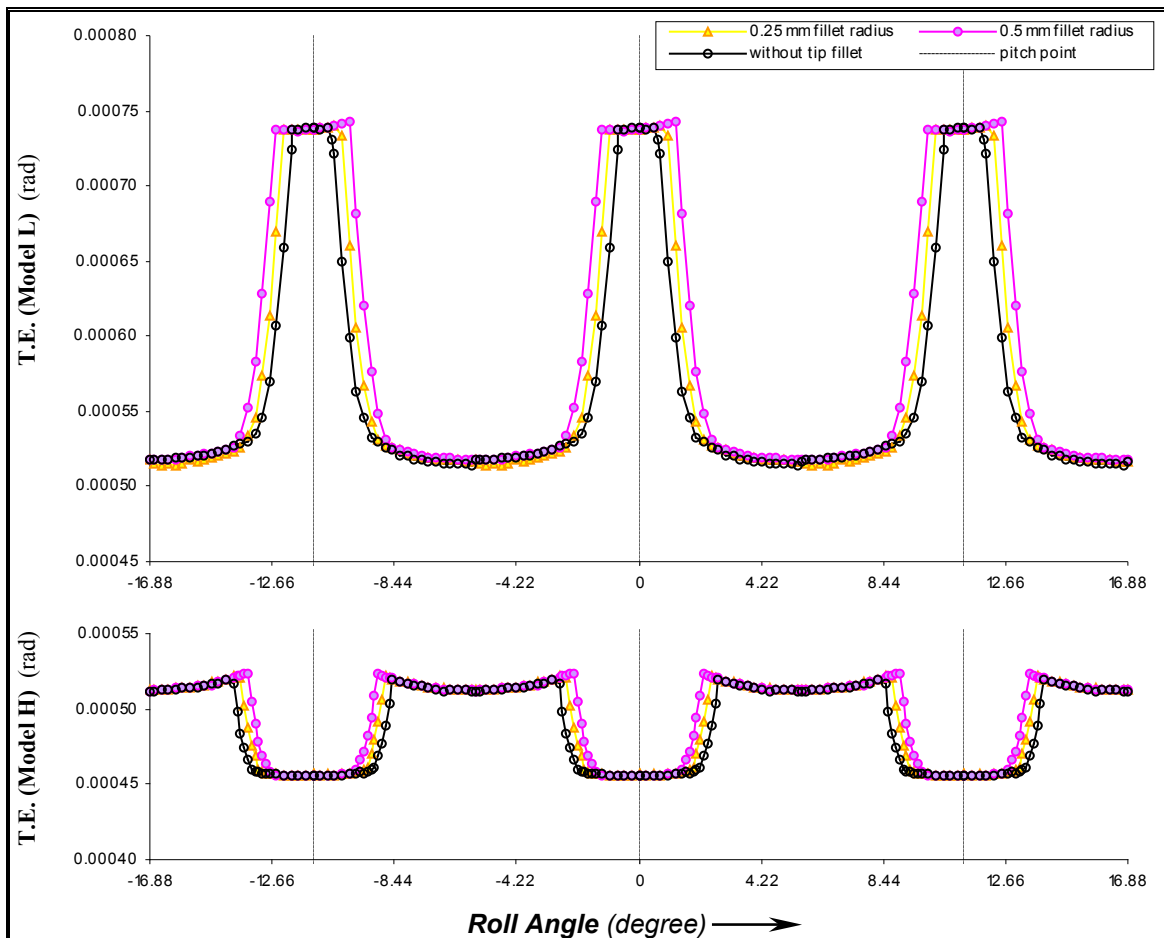Figure D14 The tooth of Model L (addendum 1*M) and Model H (addendum 1.53*M).

Figure D 15   T.E. of Model L and Model H.

292

It can be seen that even a small tip fillet can change the T.E. significantly over the mesh cycle, in particular, the contact ratio decreases when the tip fillet radius increases, as shown in Table D-3.

	Theoretical Contact Ratio (un-loaded & no tip fillet)	Loaded Contact Ratio (no tip fillet)	Loaded Contact Ratio (0.25 mm tip fillet radius)	Loaded Contact Ratio (0.5 mm tip fillet radius)
Model L	1.69	1.88	1.82	1.78
Model H	2.4	2.49	2.45	2.22
* Loaded case for all the models was the design load of 350 Nm.				

Table D-3   The contact Ratio under various conditions.

The results also show that the T.E. (relative amplitude value) decreases 70 % from LCRG to HCRG. Tooth contact stresses have also been produced over the mesh cycle under various tip fillet radius, as shown in Figure D16.
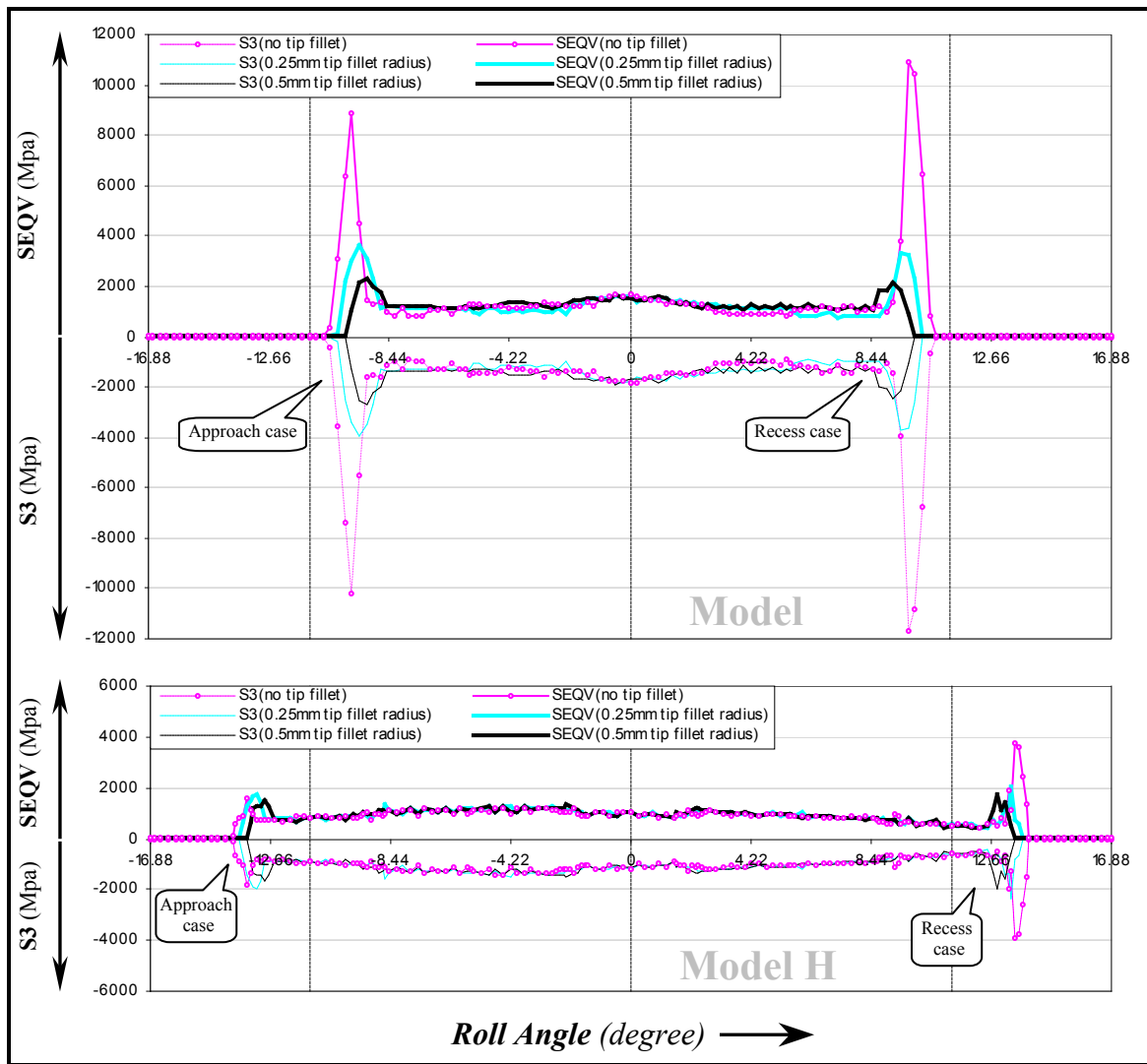

Figure D 16   Tooth contact stress variations under various tip fillet radius.(input load 350 Nm).

In the tooth contact region, away from the tooth tip, the stresses were decreased nearly 30% from LCRG to HCRG because of the tooth load reduction due to the tooth load sharing which is close to previous research results (Drago 1974). The tooth tip fillet can heavily influence the tooth contact stresses in the tooth contact approach and recess cases when tip-relief was not applied. The following points of significance were noted.

- Increasing the tooth tip fillet radius will decrease the contact stresses, but the stress decrease in the tooth approach and recess cases are not the same, as can be seen in Table D-4 and Table D-5. The fastest stress decrease is always in the tooth contact recess case (the point of highest contact stress). So, it is generally more important for the driving gear teeth to have tip-relief, but for the case of LCRG, it is important to have tip-relief on both driving and driven gear teeth due to the high contact stresses in the tooth approach case. However, the contact stresses of HCRG (Model H) in the approach case are relatively low in magnitude, and remain relatively stable when the tooth tip fillet radius change value. So, tip-relief of HCRG is not necessarily applied to the same degree on driving and driven gears. It is possible for the driven gear to have tip-relief with smaller scale than that of the driving gears, and this may help to prevent HCRG lose their contact ratio dramatically when the input load is light (below the design load) (see Part I of this appendix).

- Generally, there is about 30% difference in contact stress between LCRG and HCRG. This difference can rise up to 80% when the contact is at the tooth tip. The different matting angle between the tooth tip and flank surface should be one of the reasons along with the different tooth load share ratio. LCRG have a greater matting angle than that of HCRG and its tooth is also stronger, which makes it more important for LCRG to have tip-relief from the stress reduction point of view, and tip-relief on LCRG is also more effective than that on HCRG, as Table D-4 and D-5 have shown. Also evident is the fact that LCRG decrease the stresses faster than that of HCRG with increasing tooth tip fillet radius. Increasing gear pressure angle will have a similar influence to that of decreasing contact ratio, where the higher the pressure angle, the higher the contact stress will be when the contact is at the tooth tip, and it will be more important to have tip-relief, and the tip-relief will be more effective.

	$SEQV_{max}$ of Model L (Mpa)		$SEQV_{max}$ of Model H (Mpa)		Stress difference between the models	
	Approach	Recess	Approach	Recess	Approach	Recess
Fillet radius = 0 mm	8851.2	10940	1568.6	3593.8	82.28%	67.15%
Fillet radius = 0.25 mm	3651.5	3217.3	1706.1	2021	53.28%	37.18%
Fillet radius = 0.5 mm	2314.7	2131.7	1248	1707.7	46.08%	19.89%
Stress reduction by tip fillet (radius=0.25mm)	58.75%	70.59%	-8.77%	43.76%	-----	-----
Stress reduction by tip fillet (radius=0.5mm)	73.85%	80.51%	20.44%	52.48%	-----	-----

Table D-4   The variations with tooth tip fillet radius of maximum von Mises stress $SEQV_{max}$ in approach and recess cases and the comparison between Model L and Model H.

	$S3_{min}$ of Model L (Mpa)		$S3_{min}$ of Model H (Mpa)		Stress difference between the models	
	Approach	Recess	Approach	Recess	Approach	Recess
Fillet radius = 0 mm	-10198	-11707	-1810.7	-3720.8	82.24%	68.22%
Fillet radius = 0.25 mm	-3978.3	-3672	-1943.9	-2330.8	51.14%	36.53%
Fillet radius = 0.5 mm	-2659.2	-2425.6	-1681	-1966.4	36.79%	18.93%
Stress reduction by tip fillet (radius=0.25mm)	60.99%	68.63%	-7.36%	37.36%	-----	-----
Stress reduction by tip fillet (radius=0.5mm)	73.92%	79.28%	7.16%	47.15%	-----	-----

Table D-5   The variations with tooth tip fillet radius of the minimum principal stress $S3_{min}$ in approach and recess cases and the comparison between Model L and Model H.

D-5   Conclusions

Finite element analysis of spur gears in mesh was carried out. It has presented that the different characteristics of the LCRG and the HCRG when the tooth addendum was taken the different values. To achieve high quality solutions, the adaptive mesh was used in the customized loop programs that produced the static T.E., combined torsional mesh stiffness, load sharing ratio and contact stress over a complete mesh cycle. So that the detailed analysis can be done that including,

1. The optimal tip-relief for general applications (surface protections) was achieved by comparing the results of the gears with different tooth relief lengths particularly is the results of the contact stress over the mesh cycle. The meshing characteristics of the optimal tip-relief were presented by the variations of the static T.E. over the mesh cycle and it has clearly shown that the gears contact ratio will decrease to 1 when the load tends to zero.

2. Analysis on the tooth irregularities (surface pitting and root crack) was concentrated on the different effects between the LCRG and the HCRG. In particular the modelling for the surface pitting were carried with 2D and 3D cases. It was found that for the given tooth irregularities HCRG is less sensitive in the magnitudes than that of LCRG in most mechanism properties (such as the static T.E.), but it has a wider affected range (mesh angle) than that of LCRG over the mesh cycle.

3. In the cases of true involute tooth profile with or without tooth tip fillet, it has been found that the LCRG is more sensitive to its mechanism properties response to the load over the mesh cycle than that of the HCRG, there is 70% more response in static T.E. and 30% to 80% more response in contact stress of the LCRG than that of the HCRG. The results are also shown that the (theoretical) contact ratio decreased by any applied tip fillet and the decrease ratios are almost the same for both the LCRG and the HCRG.

It should be noted that the contact ratio of the HCRG presented in this research is sufficient high (2.4), the gear hub centre is rigidly fixed (no lateral movement) and the length of the profile modification was limited, so that the HCRG has shown its stabilities and advantages override the LCRG. Otherwise, when the contact ratio is too close to 2, the gears may become very sensitive as any errors (including wear, the lateral movement) and profile modifications (including tooth tip fillet) could cause the meshing characteristics abruptly change between that of HCRG and LCRG.

APPENDIX E
FEA OF HIGH PRESSURE ANGLE NYLON GEARS IN MESH AND THE EFFECT OF TIP RELIEF

E-1   Introduction

The previous results have shown (Chapter 8) that for the standard 20° pressure angle nylon gears there was little that could be done on the tooth profile modifications to avoid the premature contact under normal operating load conditions due to the large deformations. The premature contact(s) near the tooth tip can raise the friction coefficient and with relative high-speed movement the temperature can also be raised rapidly which generally decreases the meshing stiffness and also further modifies the friction coefficient (Domininghaus 1993). Consequently excessive wear is often a problem in the applications of standard 20° pressure angle nylon gears.

High-pressure angle involute spur gears were recommended (Seager 1975) because it is consistent also with low sliding speed and high tooth strength. Increasing the tooth strength can potentially increase the effects of the tooth profile modifications. This research will present FEA results on the standard 30° pressure angle involute spur gears (Nylon PA6) in mesh. The results of the static transmission error, combined torsional mesh stiffness, load sharing ratio and the contact stresses are presented over a complete mesh cycle for both the pure involute gear model and the (optimal) tip-relieved gear model so that the effects of an optimal tooth profile modification can be observed.

E-2   Analysis of Standard High Pressure Angle Involute Gears in Mesh.

A standard 30° pressure angle involute spur gear (nylon PA 6 at temperature 23° C) was investigated with gear parameters as given in Table E-1.

Gear tooth	Standard involute tooth
Material	Nylon (PA 6G)
Friction coefficient	0.1
Number of teeth	32
Module M	6 mm
Pressure angle, deg	30
Addendum	1 * M
Dedendum	1.25 * M
Face width	15 mm
Hub radius	15 mm
Theoretical contact ratio	1.3

Table E-1. Gear parameters.

The FE model with the gear ratio 1:1 is shown in Figure E1, where the automatic mesh adaptation with contact was incorporated into the looping program for each mesh position over the mesh cycle.
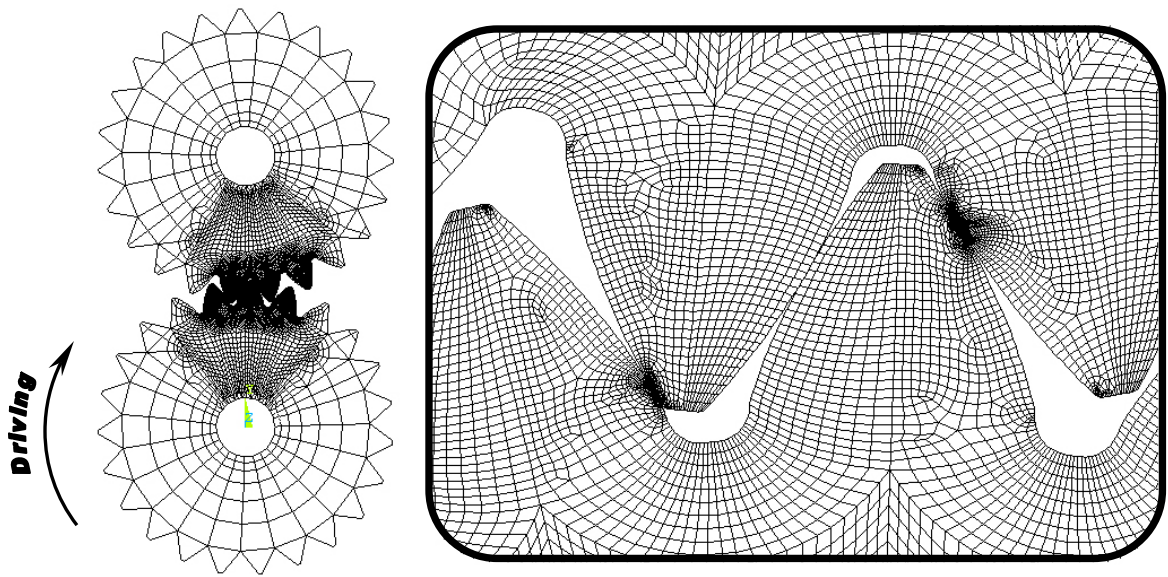
Figure E 1   FE model of the gears in mesh (ratio 1:1) and its auto – mesh adaptation with contact.

The FEA results of the T.E., combined torsional mesh stiffness and load sharing ratio under various input loads are given in Figure E2, E3 and E4 respectively.
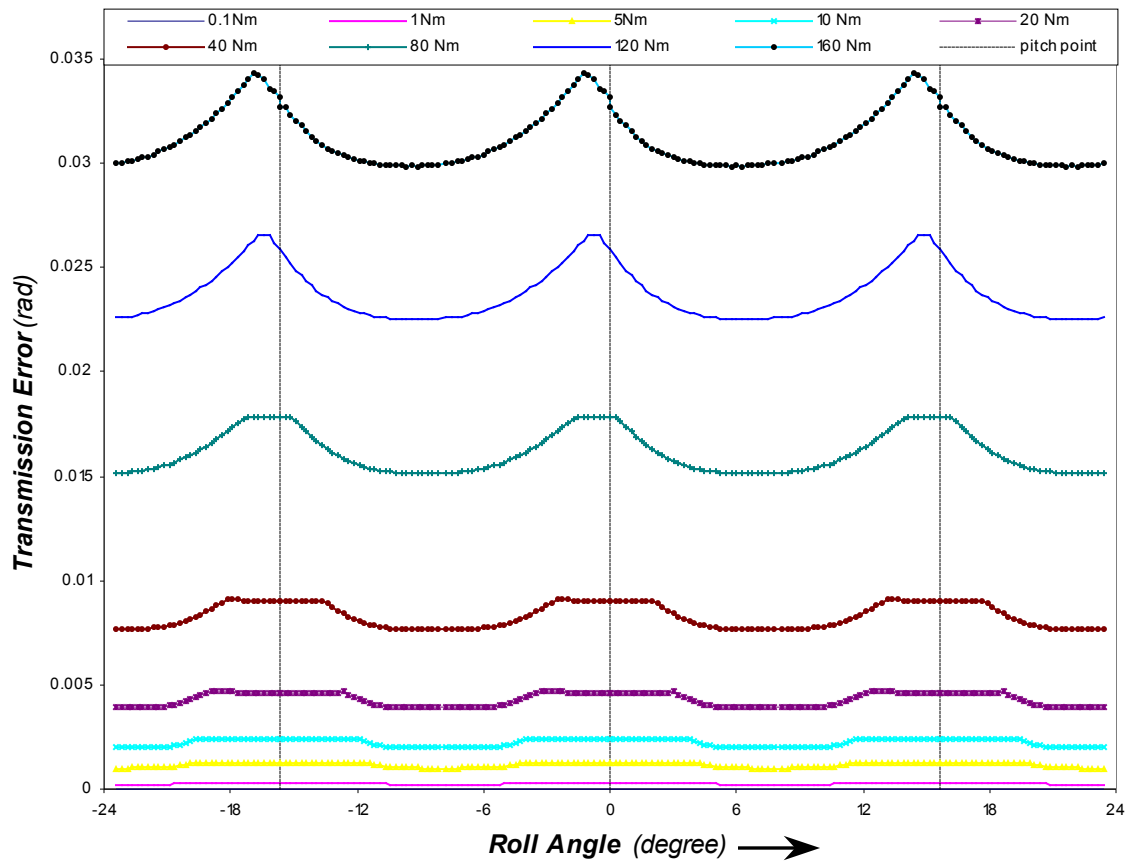

Figure E 2   T.E. of the 30° pressure angle involute spur gears in mesh under various input loads.
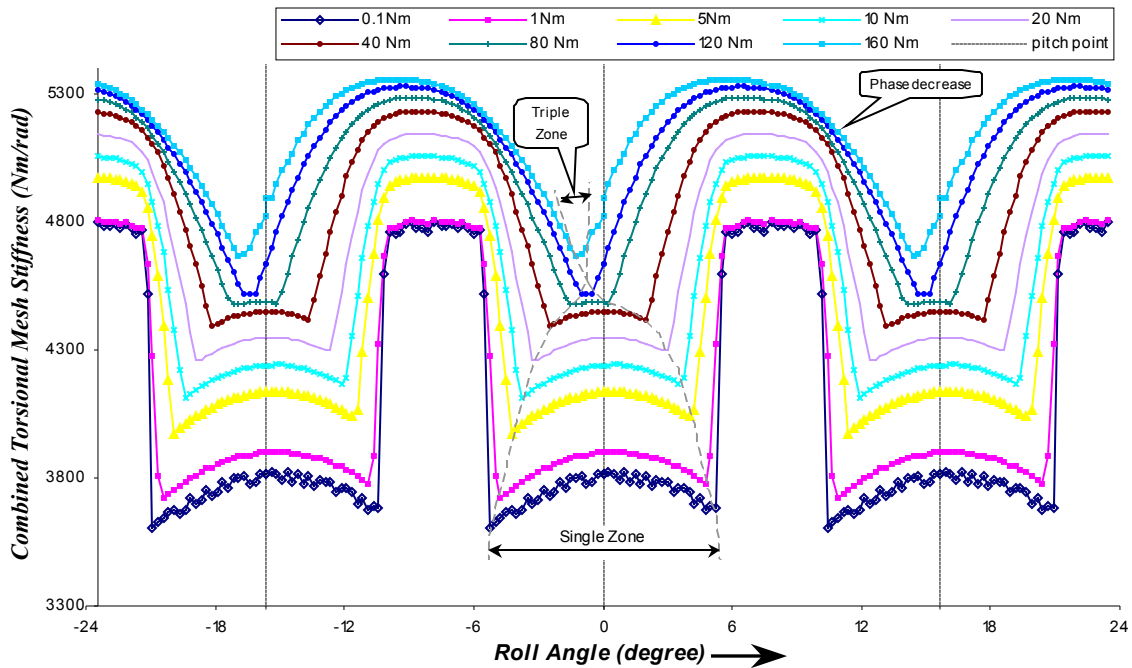
Figure E 3   Combined torsional mesh stiffness of the 30° pressure angle involute spur gears in mesh under various in put loads.
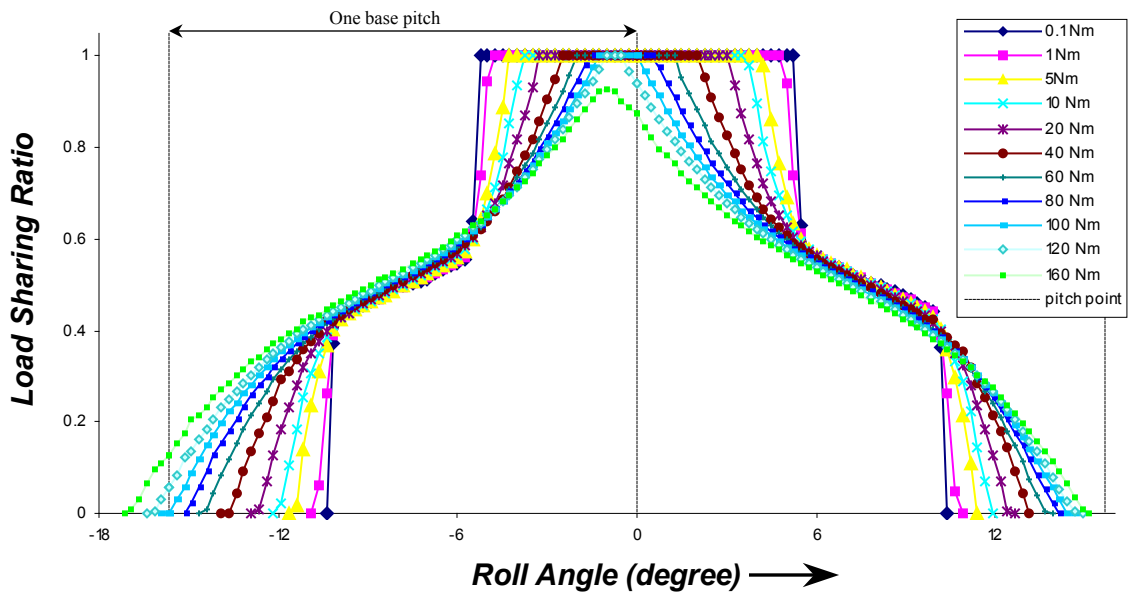
Figure E 4   Load sharing ratio of the 30° pressure angle involute spur gears in mesh under various input loads.

The results have shown that the tooth load capability is significantly increased where the triple contact can be observed when the input load is up to 160 Nm (at the temperature 23° C). A special feature is also observed particularly showing in the load-sharing ratio (Figure E4), where the curve of 120 Nm crosses over one base pitch without causing triple contact. It is known from previous analysis that the triple contact would occur here for gears with 20° pressure angle.

More detailed comparisons of these gears with the standard 20° pressure angle gears are shown in Figure E5, E6 and E7. It should be noted here that the relative T.E. of 20° pressure angle gears decrease as seen in Figure 5 at 60 Nm and 80 Nm due to the triple contact. From the load-sharing ratio (Figure E7), it can be observed that the triple contact occurred just before the load reached 50 Nm for the 20° pressure angle gears and just over 120 Nm for 30° pressure angle gears. The combined torsional mesh stiffness has shown about a 7% increase by using the high-pressure angle gears.
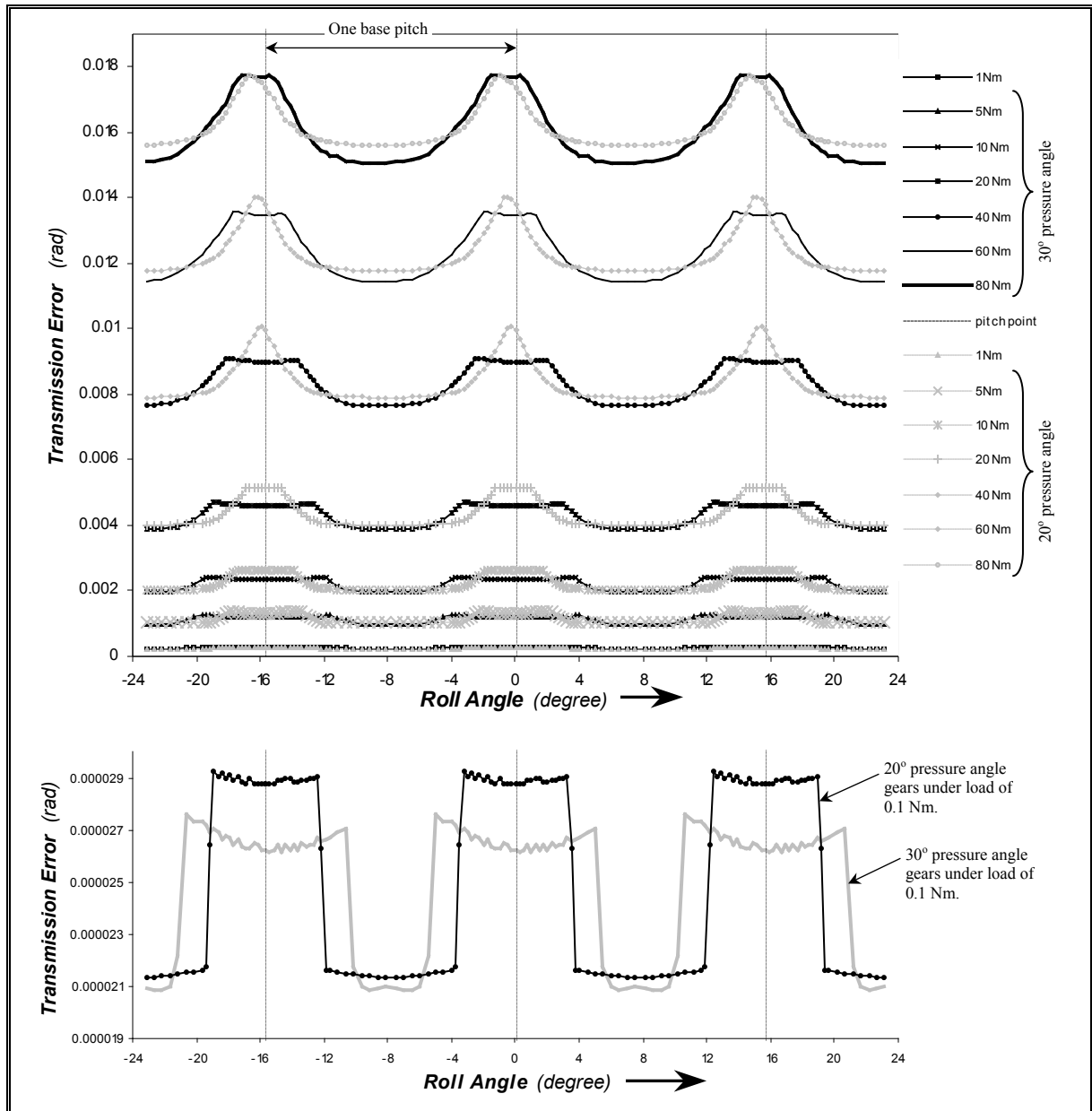
Figure E 5   T.E. Comparisons between the 30° pressure angle nylon gears and the 20° pressure angle nylon gears in mesh.
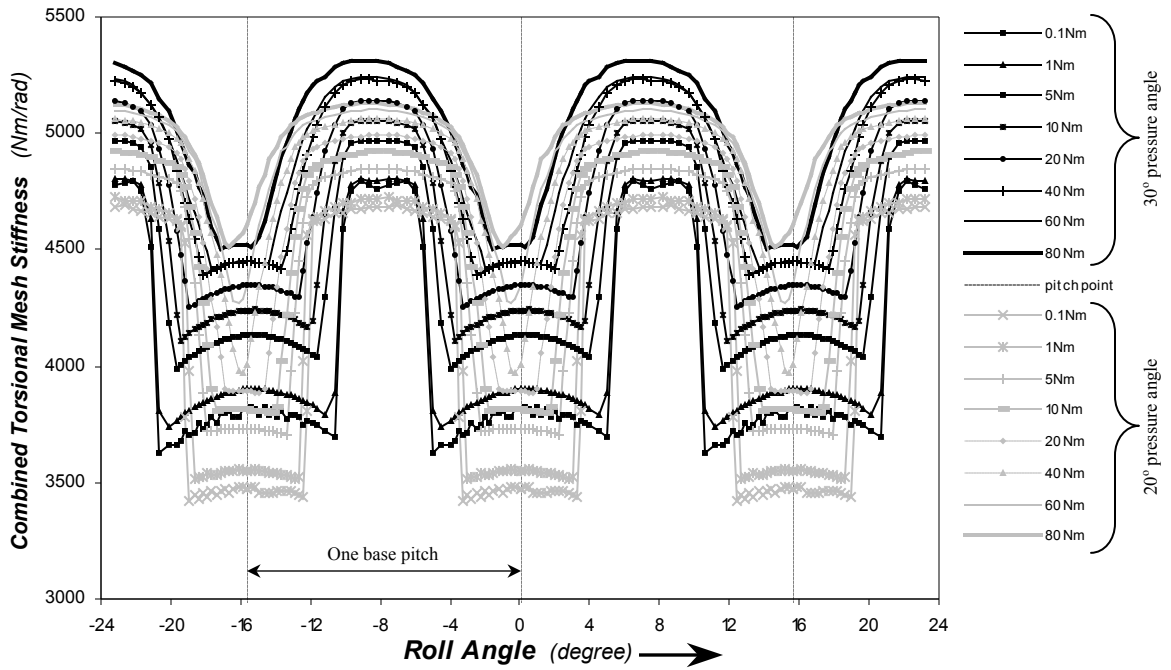
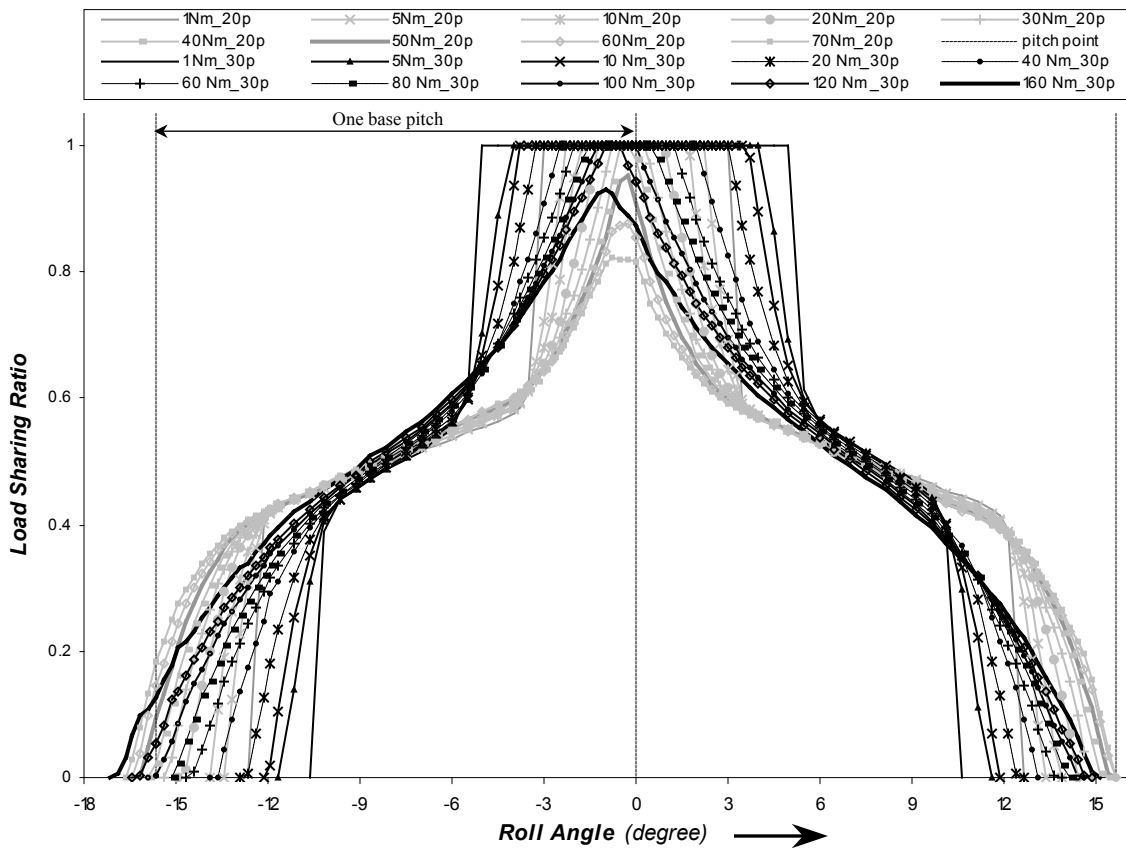Figure E 6   The comparisons of stiffness as the pressure angle changes from 20$^\text{o}$ to 30$^\text{o}$.

Figure E 7   Load sharing ratio under various input loads for 20$^\text{o}$ and 30$^\text{o}$ pressure angle gears.

During the mesh cycle, the stresses on the tooth flank surface, especially the maximum von Mises stress (SEQV) and the minimum principal stress (S3) can be determined where the contact occurs. By using FE post processing, the stress plot can be obtained as shown in Figure E8.
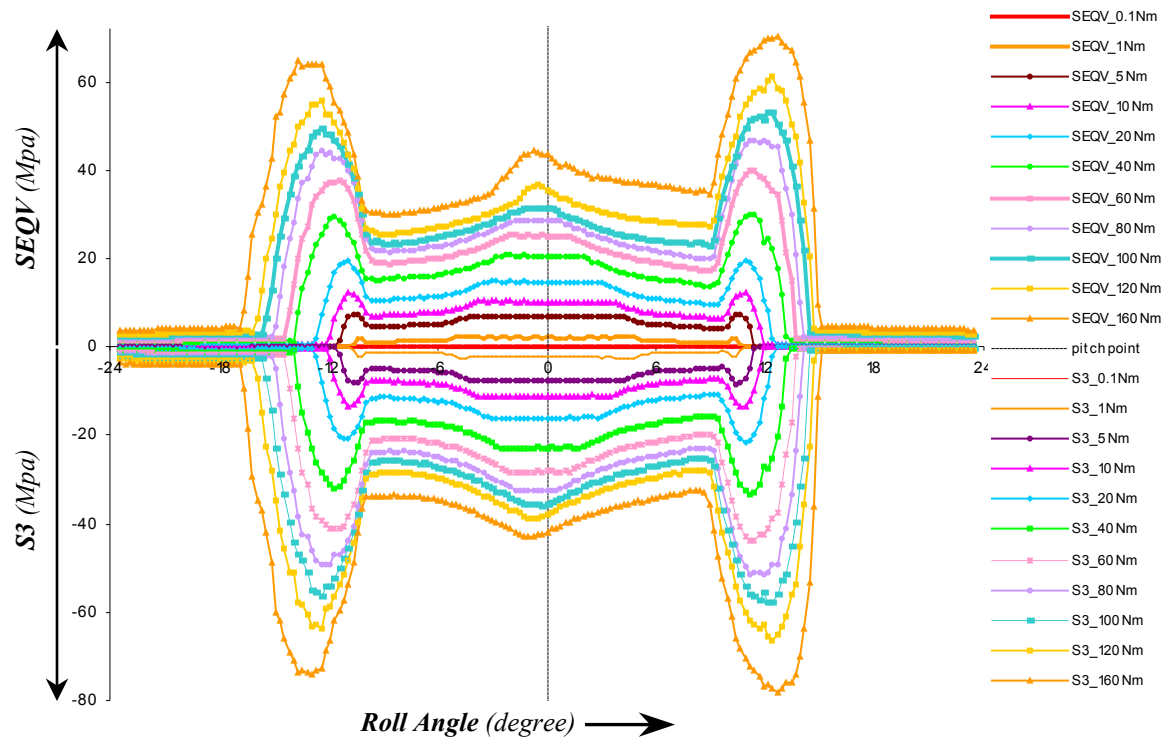

Figure E 8   The tooth (contact) stresses of the 30° pressure angle nylon gears (gear ratio 1:1) over the mesh cycle under various input loads.

It should be noted that the stresses near the tooth tip could be very high (with the load). This indicates that tip-relief may be more essential for gears with stronger teeth.

E-3   Analysis with the Optimal Tooth Profile Modifications.

The motivation for the research on the tooth profile modification of high pressure angle gears is to reduce the peak stresses as shown in Figure E8, especially when the input load is in operating range.

The principle of optimal tip-relief (in minimising the contact stress) has been presented in Appendix D. Because the tip-relief is independent of the material properties it will be valid for the application of non-metallic gears. However, increasing the gear pressure angle will change the profile of the optimal tip-relief, in which the most critical relief component ΔLa (relief length) has to be re-evaluated. The other component C_a (the amount of relief) will also need to be significantly increased due to the material flexibility. The normalization can be expressed as $\dfrac{\text{actual amount of relief } C_a}{\text{allowable } C_{a\max}\ 0.02M \text{ by current standards.}}$ and will usually have a value greater

301

than 2.0. Through a series of FE calculations with different relief lengths on the 30° pressure angle gears in mesh, the critical relief length was determined to be 1.48 mm (0.41 normalized). The tooth profile with the optimal tip-relief is illustrated in Figure E9.
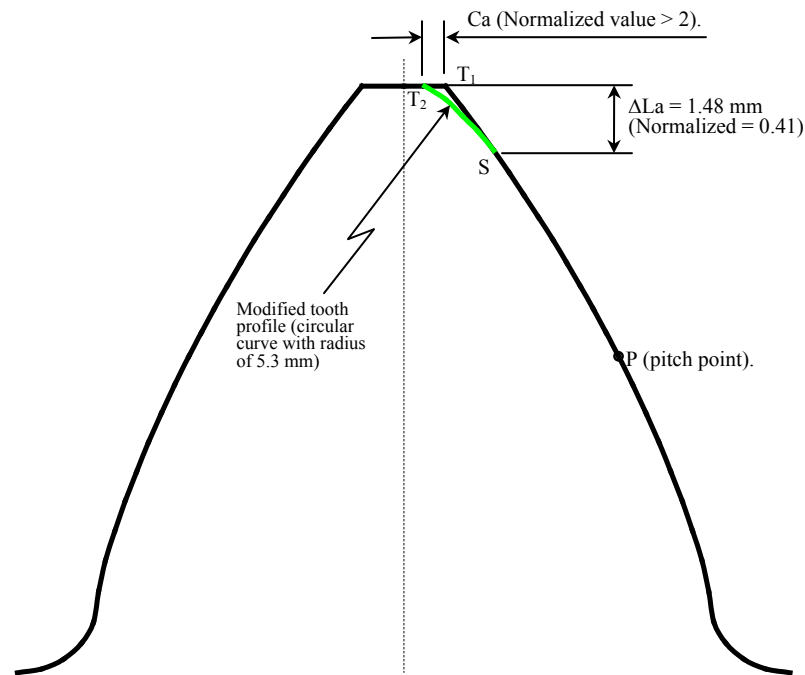

Figure E 9   Illustration of the optimal tooth tip-relief.

The use of the circular modified tooth profile can be referred to Walton (Walton 1995). The modified tooth profile ST_2 (as shown in Figure 9) is in a circular form. Once the amount of the modification C_a (or T_1T_2) is chosen (here T_1T_2 is ¼ of the tooth top land width), the minimum radius of the curve ST_2 can be found (5.3 mm) which ensures that modified tooth profile ST_2 is inside the original tooth profile (no positive materials). Thus the features of easy manufacturing and the maximum smoothness near the relief starting point (S) were achieved.

The following FEA results were considered with C_a = 0.47 mm, which is 3.92 in normalized value. The results of the static T.E., combined torsional mesh stiffness, tooth load sharing ratio and contact stresses were obtained for the temperature of 23° C, as shown in Figure E10 and the static T.E. under lighter loads is shown in Figure E11.
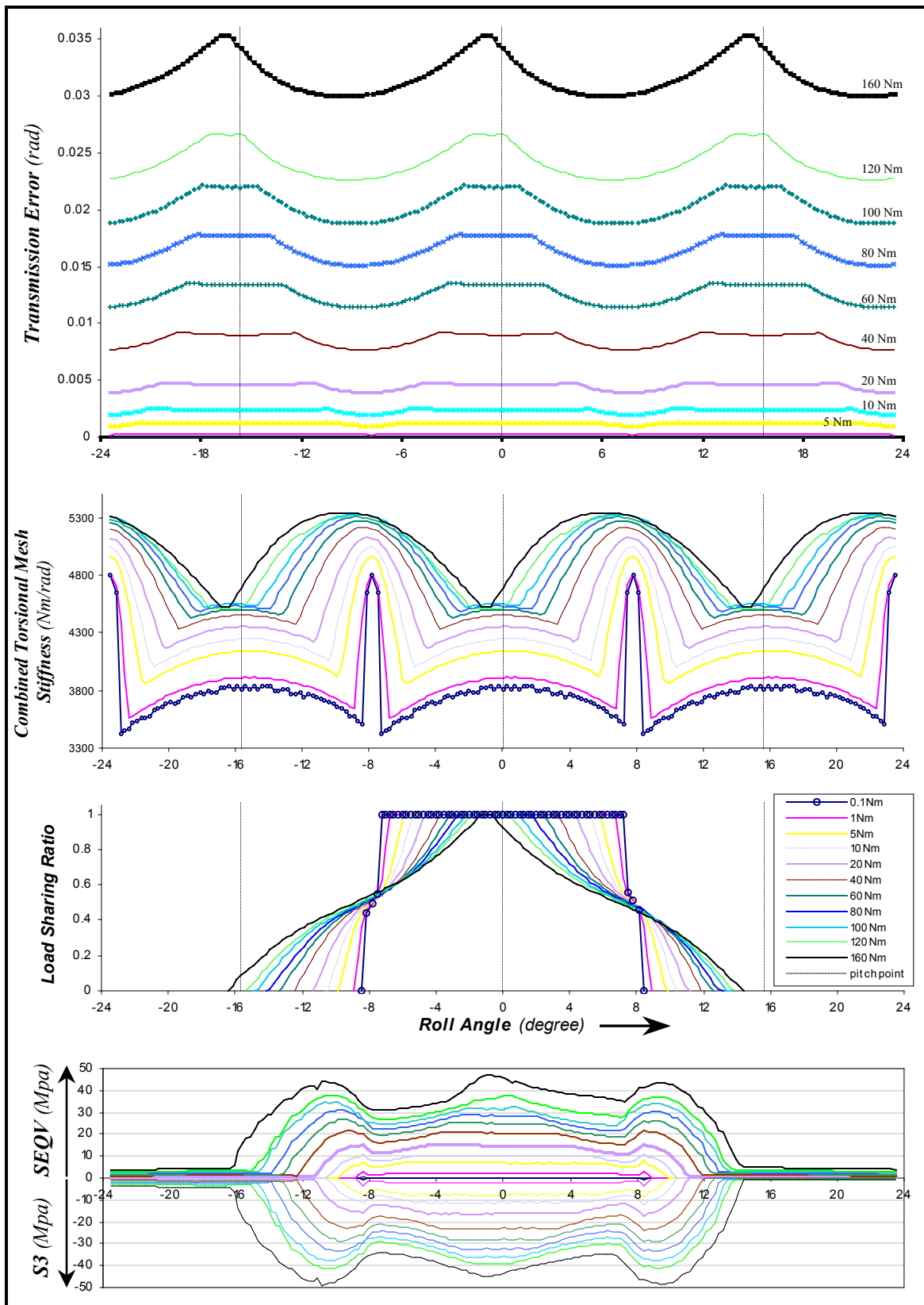
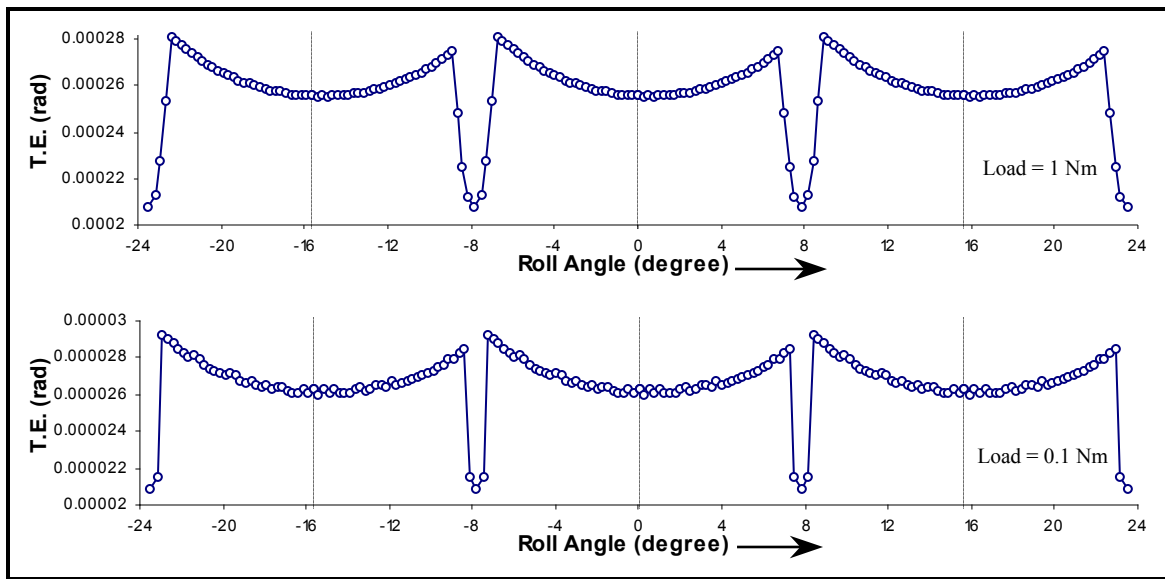Figure E 10   The change over process of the tip-relieved gears.

Figure E 11   The T.E. of the tip-relieved gears with lighter loads.

The comparisons between the tip-relieved and the unmodified (involute) gears have been made with the static T.E. shown in Figure E12, the combined torsional mesh stiffness shown in Figure E13 and the load-sharing ratio shown in Figure E14.

Figure E15 shows the stress comparisons at each input load. It should be noted that the stresses near the pitch point have remained constant in all cases. The optimal tip-relief (in current stage) is aimed at decreasing the peak stresses near the tooth tip to be close or below the constant stresses at the pitch point. These results have shown, except for the very light loads (0.1 and 1 Nm), that this primary goal has been achieved.

The optimal tip-relief not only decreases the peak stress but also shifts where the maximum stresses occur from being near the tooth tip to the relief starting point as shown in Figure E16, and this has indicated that further improvement on the optimal tip-relief may be achieved by smoothing the modified tooth profile near the relief starting point. Care must be taken here as any change made to the critical relief length could cause a big difference in the meshing characteristics, for example, if the critical relief length is shortened then the stresses at the relief starting point could rise rapidly, and if the critical relief length is extended then it could cause dynamic impact over the mesh cycle when the load is light. However, using circular profile modifications (as shown in the current results) could be one of the easiest manufacturing methods.
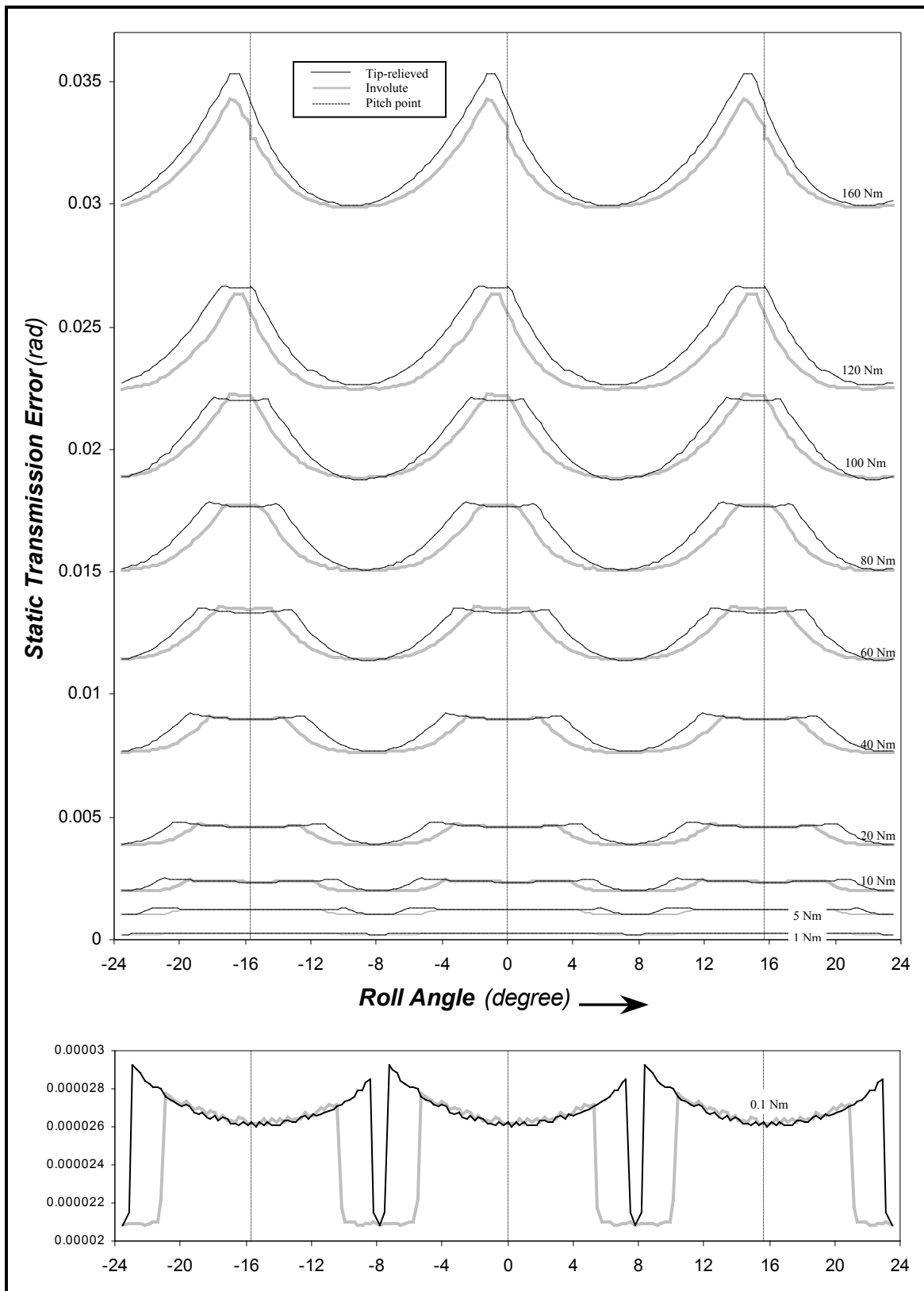
Figure E 12   Comparisons between the T.E. of the tip-relieved and the unmodified (involute) gears.
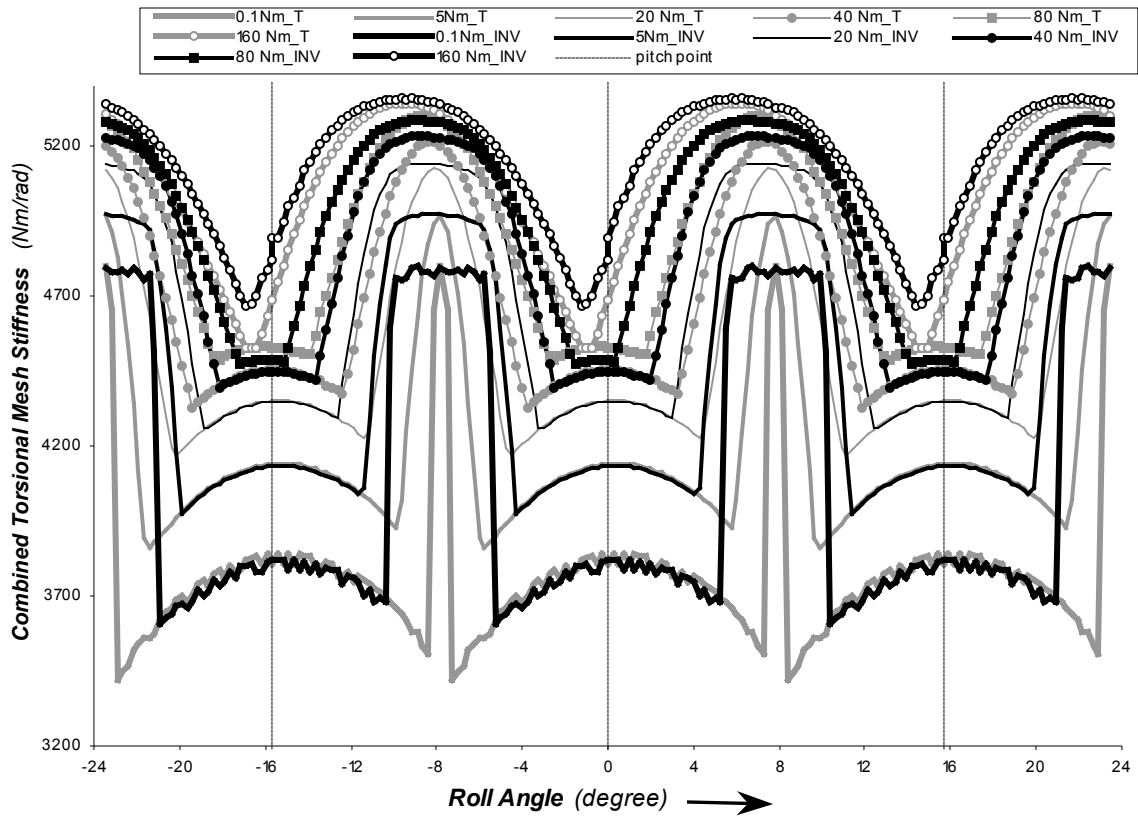
Figure E 13   Comparisons between the combined torsional mesh stiffness of the tip-relieved and the unmodified (involute) gears.
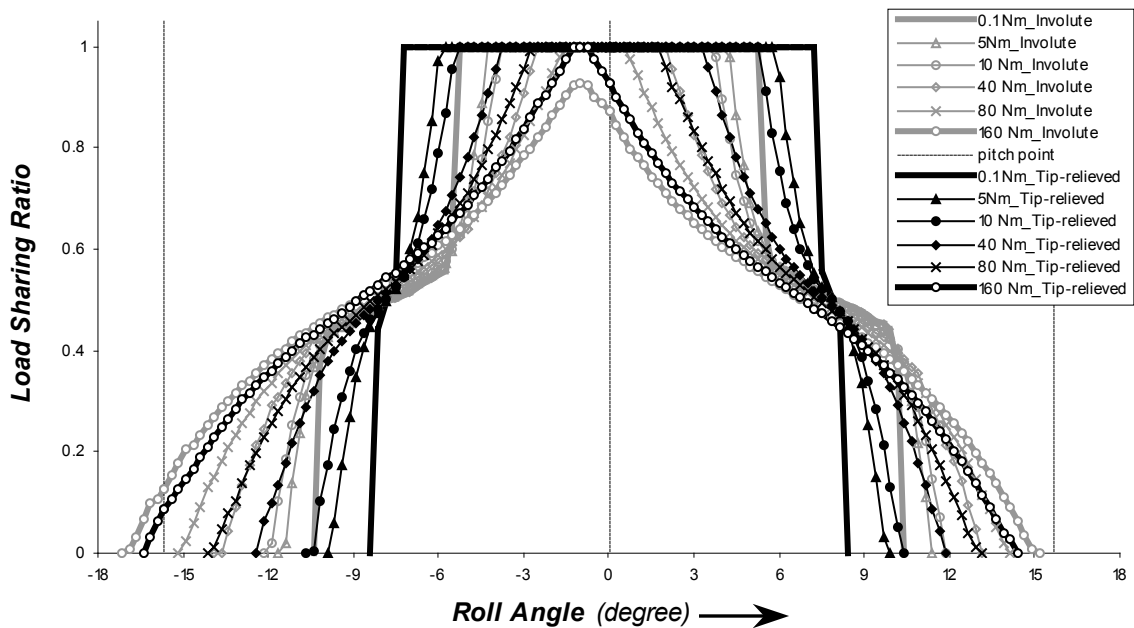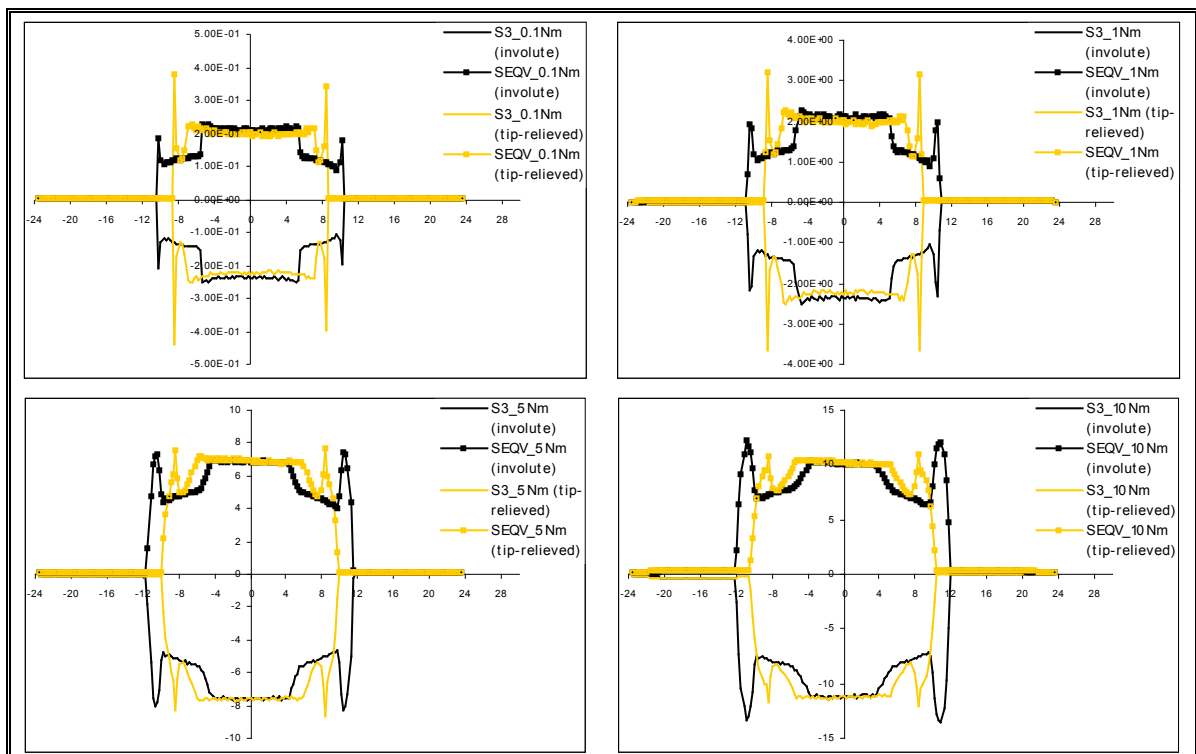

Figure E 14   Comparisons between the load-sharing ratios of the tip-relieved and the unmodified (involute) gears.

306

E-4   Conclusions.

Finite element analysis of 30° pressure angle nylon (PA 6) gears in mesh has been presented in this paper. The advantages of using the high-pressure angle for non-metallic gears were outlined by comparing with the conventional 20° pressure angle gears, especially in their static T.E., combined torsional mesh stiffness and load sharing ratio. It has been shown that high-pressure angle gears can develop high contact stresses when contact occurs at the tooth tip. In order to prevent excessive wear (relief is too short), as well as dynamic impact when load is light (relief is too long), an optimal tip-relief with a circular form was investigated. The successful achievement has been shown by the detailed comparisons between the results of the tip-relieved and the unmodified (involute) gears in mesh, especially in that the peak stresses have been successfully reduced over a wide range of the input load.
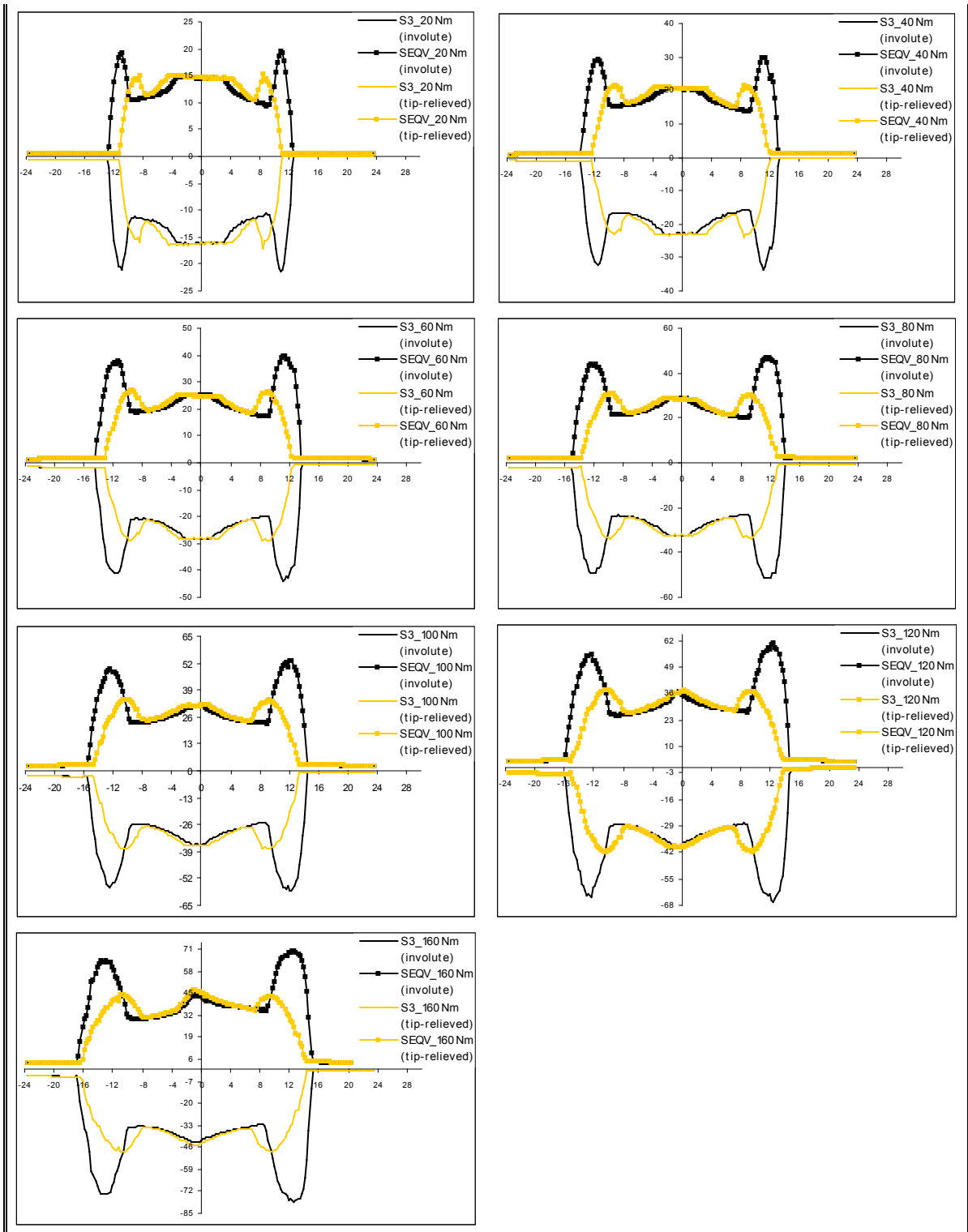
Figure E 15   The stress comparisons between the tip-relieved and the unmodified gears at each load.
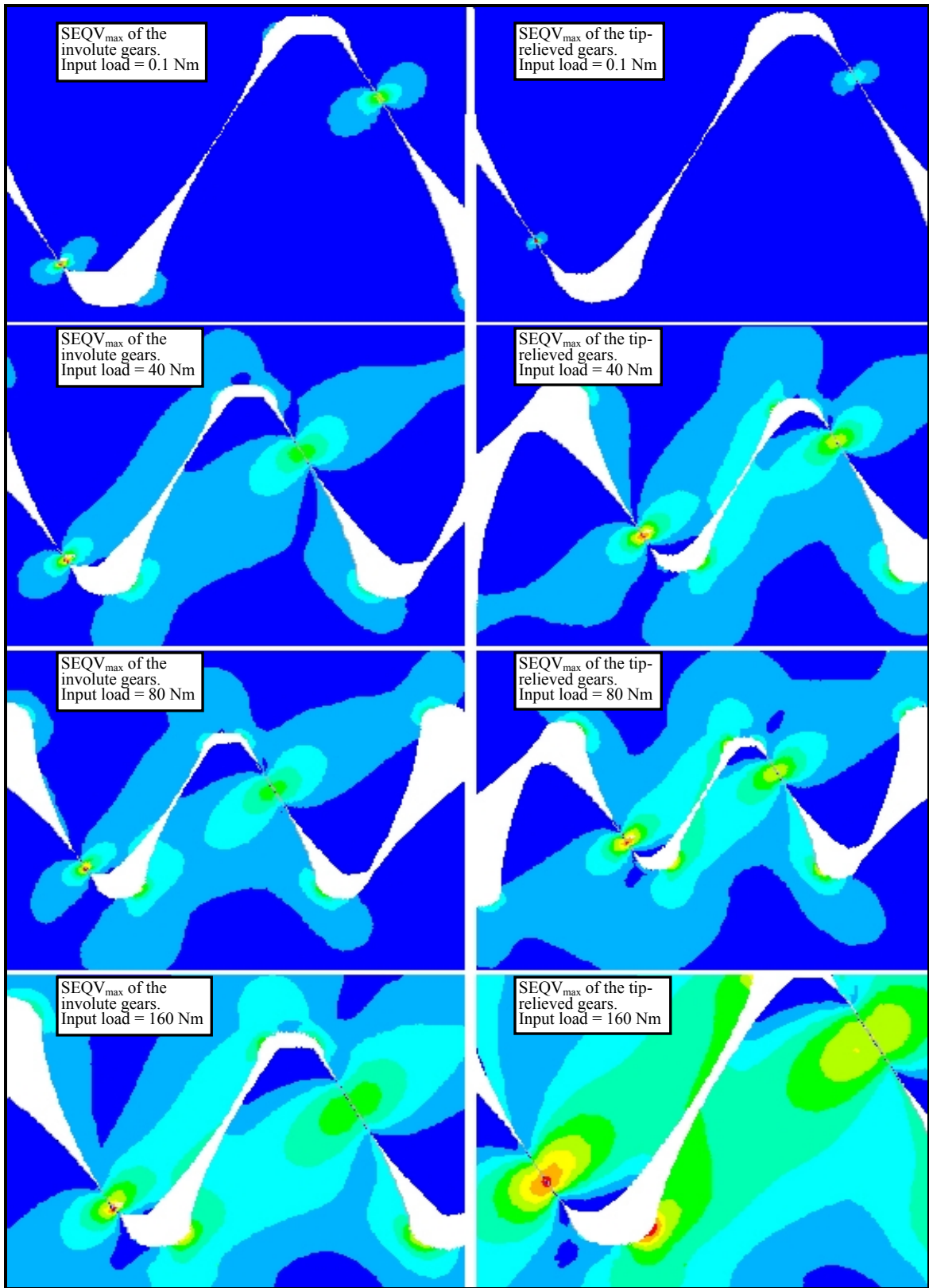
Figure E 16   The optimal tip-relief not only decreases the peak stress but also shifts the
maximum stress position from near the tooth tip to the relief starting point.